Novel tools for the implementation of synthetic biosynthesis pathways in *Rhodobacter capsulatus*

Inaugural-Dissertation

zur Erlangung des Doktorgrades

der Mathematisch-Naturwissenschaftlichen Fakultät

der Heinrich-Heine-Universität Düsseldorf

vorgelegt von

Oliver Klaus

aus Kempen (Niederrhein)

Düsseldorf, Dezember 2022

aus dem Institut für Molekulare Enzymtechnologie

der Heinrich-Heine-Universität Düsseldorf

Diese Arbeit wurde vom Europäischen Fonds für regionale Entwicklung (EFRE, Grant-Nr.: 34-EFRE-0300096) im Rahmen des CLIB-Kompetenzzentrums Biotechnologie (CKB) gefördert.

Gedruckt mit der Genehmigung der

Mathematisch-Naturwissenschaftlichen Fakultät der

Heinrich-Heine-Universität Düsseldorf

Referent: Prof. Dr. Karl-Erich Jaeger

Korreferentin: Prof. Dr. Ilka Maria Axmann

Tag der mündlichen Prüfung: 30.03.2023

Meinen Eltern und meinem Bruder

TABLE OF CONTENTS

A. CONFERENCE CONTRIBUTIONS

Klaus O*, Loeschcke A, Linke K, Hage-Hülsmann J, Troost K, Jaeger K-E, Drepper T **(2018)**: Engineering *Rhodobacter capsulatus* for the heterologous production of different terpene classes. *Annual conference of the Association for General and Applied Microbiology (VAAM).* Wolfsburg/Germany, April 2018. poster presentation

Klaus O*, Loeschcke A, Linke K, Hage-Hülsmann J, Troost K, Jaeger K-E, Drepper T **(2018)**: Heterologous production of different terpene classes using engineered *Rhodobacter capsulatus*. *Aachen Protein Engineering Symposium*, Aachen/Germany, October 2018. poster presentation

Klaus O*, Lappe A, Hilgers F, Hogenkamp F, Loeschcke A, Pietruszka J, Jaeger K-E, Drepper T **(2019)**: Photocaged IPTG derivatives for light-controlled gene expression in *Rhodobacter capsulatus*. *Annual conference of the Association for General and Applied Microbiology (VAAM).* Mainz/Germany, March 2019. poster presentation

Kruse L*, Hilgers F, **Klaus O**, Svensson V, Jaeger K.-E, Drepper T **(2020)**: Dissemination of iron-scavenging pyoverdine as a model for public good-based interspecies communication within microbial communities. *Annual conference of the Association for General and Applied Microbiology (VAAM).* Leipzig/Germany, March 2020. poster presentation

Klaus O*, Loeschcke A, Hilgers F, Hage-Hülsmann J, Troost K, Jaeger K-E, Drepper T **(2020)**: *Rhodobacter capsulatus* as a phototrophic platform organism for the synthesis of plant terpenes. *Annual conference of the Association for General and Applied Microbiology (VAAM).* Leipzig/Germany, March 2020. poster presentation

Hilgers F*, Bitzenhofer NL, **Klaus O**, Hogenkamp F, Burmeister A, Grünberger A, Pietruszka J, Jaeger K-E, Drepper T **(2022)**: Lights on and action – Optogenetic on- and off-switches for light-induced control of microbial processes. *Annual conference of the Association for General and Applied Microbiology (VAAM).* Düsseldorf/Germany, February 2022. oral presentation

* Presenting author

B. PUBLICATIONS

Hogenkamp F*, Hilgers F*, Knapp A, **Klaus O**, Bier C, Binder D, Jaeger K-E, Drepper T and Pietruszka J **(2021)**: Effect of Photocaged Isopropyl β-D-1-thiogalactopyranoside solubility on light-responsiveness of LacI-controlled expression systems in different bacteria. *ChemBioChem*, 2;22(3):539-547. doi: 10.1002/cbic.202000377.

Hilgers F*, Habash SS*, Loeschcke A, Ackermann YS, Neumann S, Heck A, **Klaus O**, Hage-Hülsmann J, Grundler FMW, Jaeger K-E, Schleker ASS, Drepper T **(2021)**: Heterologous Production of β-Caryophyllene and Evaluation of Its Activity against Plant Pathogenic Fungi. *Microorganisms*, 9(1), 168. doi: 10.3390/microorganisms9010168.

Hage-Hülsmann J*, **Klaus O*,** Linke K, Troost K, Gora L, Hilgers F, Wirtz A, Santiago-Schübel B, Loeschcke A, Jaeger K-E, Drepper T **(2021)**: Production of C_{20}, C_{30} and C_{40} terpenes in the engineered phototrophic bacterium *Rhodobacter capsulatus*. *Journal of Biotechnology*, 338:20-30. doi: 10.1016/j.jbiotec.2021.07.002.

Ölcücü G*, **Klaus O***, Jaeger K-E, Drepper T and Krauss U **(2021)**: Emerging solutions for *in vivo* biocatalyst immobilization: Tailor-made catalysts for industrial biocatalysis. *ACS Sustainable Chemistry & Engineering*, 9(27), 8919-8945. doi: 10.1021/acssuschemeng.1c02045

Hilgers F*, Hogenkamp F*, **Klaus O**, Kruse L, Loeschcke A, Bier C, Binder D, Jaeger K-E, Pietruszka J, Drepper T **(2022)**: Light-mediated control of gene expression in the anoxygenic phototrophic bacterium *Rhodobacter capsulatus* using photocaged inducers. *Frontiers in Bioengineering and Biotechnology*, 10:902059. doi: 10.3389/fbioe.2022.902059

Klaus O*, Hilgers F*, Nakielski A, Hasenklever D, Jaeger K-E, Axmann IM, Drepper T **(2022)**: Engineering phototrophic bacteria for the production of terpenoids. *Current Opinion in Biotechnology*, 77:102764. doi: 10.1016/j.copbio.2022.102764

Klaus O*, Svensson V, Jaeger K-E. Drepper T: Functionalization of polyhydroxybutyrate granules in the phototrophic bacterium *Rhodobacter capsulatus* SB1003
manuscript in preparation

Klaus O*, Lenz P*, Gensch T, Knapp F, Knapp A, Thies S, Jaeger K-E, Drepper T: Split GFP as a new system for facilitating and sensing *in vivo* protein immobilization.
manuscript in preparation

* These authors contributed equally to this work.

C. ABBREVIATIONS

ACAT	acetyl-CoA acyltransferase	**DXR**	desoxyxylulosephosphate reductase
acetyl-CoA	acetyl-coenzyme A	**EDTA**	ethylenediaminetetraacetic acid
ATP	adenosine triphosphate	**e.g**	*exempli gratia*
BC	4,5-bis(carboxymethoxy)-2-nitrobenzyl	**FPP**	farnesyl pyrophosphate
BEC	4,5-bis(ethoxycarbonylmethoxy)-2-nitrobenzyl	**GAP**	glyceraldehyde-3-phosphate
CALI	chromophore associated light inactivation	**GFP**	green fluorescent protein
cAMP	cyclic AMP	**GGPP**	geranylgeranyl pyrophosphate
CAP	catabolite activation protein	**GPP**	geranyl pyrophosphate
CatIBs	catalytically active inclusion bodies	**gRNA**	guide RNA
CDP-ME	4-diphosphocytidyl-2-methyl-D-erythritole	**HDR**	hydroxy-methyl-butenyl-diphosphate reductase
CDP-MEP	CDP-ME-2-phosphate	**HDS**	hydroxy-methyl-butenyl-diphosphate synthase
CDW	cell dry weight	**HMBPP**	(E)-4-hydroxy-3-methyl-but-2-enyl-diphosphate
CFP	cyan fluorescent protein	**HMG-CoA**	β-hydroxy-β-methylglutaryl-CoA
CMK	cytidyl-methyl kinase	**HMGR**	hydroxy-methyl-glutaryl reductase
CMS	cytidyl-methylerythritol synthase	**HMGS**	hydroxy-methyl-glutaryl synthase
CRISPR	clustered regularly interspaced short palindromic repeats	**ICM**	intracytoplasmatic membrane
CRISPRi	CRISPR interference	**IDI**	isopentenyldiphosphate isomerase
CrtE	GGPP synthase	**IOH**	isopentenol
DMAOH	dimethylallyl alcohol	**IPP**	isopentenyl diphosphate
DMAPP	dimethylallyl pyrophosphate	**IPTG**	isopropyl-β-D-thiogalactopyranoside
DNA	deoxyribonucleic acid	**IR**	infrared
DXS	1-desoxy-D-xylulose-5-phosphate synthase	**IspA**	farnesylpyrophosphate synthase
DXP	1-desoxy-D-xylulose-5-phosphate	**LacA**	galactoside transacetylase

LacI	*lac* repressor
LacY	lactose/H^+-symporter
LacZ	β-galactosidase
LOV	light oxygen voltage
MAP	2-methyl-3-pentyl-pyrrole
MBC	4-methoxy-2,2 bipyrrole-5-carboxyaldehyde
MCS	methyl-erythritol-cyclo-diphosphate synthase
Me-cPP	2-c-methyl-D-erythritol-2,4-cyclodiphosphate
MEP	2-C-methyl-D-erythritol-4-phosphate
MK	mevalonate kinase
mRNA	messenger RNA
MVA	mevalonate
MVP	mevalonate-5-phosphate
MVPP	mevalonate-5-pyrophosphate
NADPH	nicotinamide adenine dinucleotide phosphate
NP	nitropiperonyl
OrfX	PHB depolymerase
PHA	polyhydroxyalkanoate
PhaA	acetyl-CoA acetyltransferase
PhaB	acetoacetyl-CoA reductase
PhaC	polyhydroxybutyrate synthase
PHB	polyhydroxybutyrate
PigC	prodigiosin ligase
PMD	pyrophosphomevalonate decarboxylase
PMK	phosphomevalonate kinase
PS	photosensitizer
Pyr	pyruvate
RBS	ribosome binding site
RNA	ribonucleic acid
ROS	reactive oxygen species
SD	Shine-Dalgarno
UV	ultraviolet
YFP	yellow fluorescent protein

D. SUMMARY

Terpenoids represent the largest group of secondary metabolites comprising various properties and activities. Due to the enormous diversity as well as manifold applications of terpenoids, their microbial production is of growing importance for the biotechnological industry. As consequence of their complex biosyntheses, bioprocesses, and product properties, it is necessary to optimize the microbial production methods, even in already established hosts. Moreover, the evaluation and engineering of alternative new platform organisms with novel capabilities is crucial to expand the existing portfolio of producible terpenoids.

The purple non-sulfur bacterium *Rhodobacter capsulatus* has already been validated as a suitable production chassis for plant sesquiterpenes utilizing classical metabolic engineering concepts. Based on these initial results, more complex terpenoids may now be produced and a gradual control of gene expression may be beneficial. Additionally, for complex biosynthetic pathways, a compartmentalization, or stabilization of key enzymes can be beneficial reducing the accumulation of toxic intermediates, which might normally limit the cell viability and product yields. The present work aims to broaden the applicability of *R. capsulatus* as a production host for different terpene classes and to improve their biosynthesis at different cellular levels.

Hence, by [**I**] applying different metabolic engineering strategies for increased precursor availability, the sesquiterpene β-caryophyllene, the diterpene casbene, the triterpene squalene, and the tetraterpene β-carotene could successfully synthesized in *R. capsulatus*. Besides the availability of precursor molecules, [**II**] the selective control of cellular processes, e.g., *via* precise gradual control over target gene expression, was established in order to improve the efficiency of complex biosynthetic pathways. For this purpose, a broad host range P_{tac}-based vector system was implemented in *R. capsulatus* and applied in combination with photocaged IPTG derivatives with diverging water solubility to achieve light-controlled gene expression. As a proof of concept, the synthesis of the intrinsic carotenoid biosynthesis was successfully regulated by light. Subsequently, the general applicability of this light-controllable expression system was demonstrated by transfer to other industrially relevant bacterial hosts such as *Escherichia coli*, *Bacillus subtilis*, and *Pseudomonas putida.*

Immobilization of enzymes on the surface of appropriate carrier materials can lead to protein stabilization and improved substrate channeling, thereby enhancing product yields and reducing the accumulation of potentially toxic intermediates. Therefore, [**III**] granules of the biopolymer polyhydroxybutyrate (PHB) were identified as promising bioplastic material particularly suited for the *in vivo* immobilization of recombinant enzymes in bacteria. *R. capsulatus* is naturally capable to form PHB granules, which were successfully functionalized for the first time in this phototrophic bacterium by attaching the fluorescent

protein eYFP to the PHB granule surface. Since validation and optimization of *in vivo* attachment of the target protein to the biopolymer matrix is a laborious process, it would be a tremendous benefit to online-monitor and quantify this event in living cells during the production and immobilization process. To this end, [**IV**] an alternative linker for *in vivo* protein immobilization was developed in the non-native PHB producer *E. coli* combining the split GFP system and PHB technology. This new linker system offers a biosensor function that allows the *in vivo* detection of the target protein attachment to the biopolymer surface.

In this work, the heterologous terpene production in *R. capsulatus* was extended to different terpene classes and a P_{tac}-based vector system was implemented allowing light-induced gene expression and thus providing a method for the precise regulation of heterologous terpene biosynthesis. By successfully decorating PHB granules and developing a new linker/sensor system, the *in vivo* immobilization and simultaneous *in vivo* monitoring of the coupling process became possible. Hence, a cornerstone was laid for improving terpene biosynthesis in *R. capsulatus* using the PHB technology for enzyme scaffolding.

E. ZUSAMMENFASSUNG

Terpenoide stellen die größte Gruppe der Sekundärmetabolite dar und weisen eine Vielzahl an Eigenschaften und Aktivitäten auf. Aufgrund der enormen Diversität und zahlreichen Anwendungsmöglichkeiten ist deren mikrobielle Produktion von immer größer werdender Bedeutung in der biotechnologischen Industrie. Infolge der Komplexität der zugrundeliegenden Biosynthesen, Produkteigenschaften und Bioprozesse ist es erforderlich, die Herstellungsverfahren in bereits etablierten Wirten weiter zu optimieren. Darüber hinaus sind die Bewertung und Entwicklung alternativer Mikroorganismen als neue Plattformorganismen mit neuartigen Fähigkeiten von entscheidender Bedeutung für die Erweiterung des bestehenden Portfolios an herstellbaren Terpenoiden. Das Nicht-Schwefel Purpurbakterium *Rhodobacter capsulatus* wurde bereits initial auf seine Eignung als Produktionschassis für die Biosynthese pflanzlicher Sesquiterpene mit Hilfe klassischer *metabolic engineering* Konzepte evaluiert. Auf Grundlage dieser ersten Ergebnisse können nun komplexere Terpenoide produziert werden, zudem könnte eine graduelle Kontrolle der Genexpression besonders in Bezug auf komplexe Biosynthesewege von Vorteil sein. So kann beispielsweise eine Kompartimentierung oder Stabilisierung von Schlüsselenzymen die Anhäufung toxischer Intermediate verringern, die normalerweise die Zellvitalität und Produktausbeute negativ beeinflussen könnten.

Das Ziel der vorliegenden Arbeit ist es, *R. capsulatus* als Wirt für die Produktion verschiedener Terpenklassen zu etablieren und deren Biosynthese auf verschiedenen zellulären Ebenen zu verbessern. So konnten durch [**I**] die Anwendung unterschiedlicher *metabolic engineering* Strategien, mit dem Ziel einer erhöhten Verfügbarkeit von Vorstufenmolekülen, das Sesquiterpen β-Caryophyllen, das Diterpen Casben, das Triterpen Squalen und das Tetraterpen β-Caroten erfolgreich in *R. capsulatus* produziert werden. Daneben wurden [**II**] Methoden zur selektiven Steuerung zellulärer Prozesse, beispielsweise über eine präzise, schrittweise Kontrolle der Zielgenexpression etabliert, um so die Effizienz der komplexen Biosynthesewege zu verbessern. Hierfür wurde ein P_{tac}-basiertes Vektorsystem mit breitem Wirtsspektrum in *R. capsulatus* implementiert und schließlich mit *photocaged* IPTG-Varianten mit unterschiedlicher Wasserlöslichkeit eingesetzt, um eine lichtgesteuerte Genexpression zu ermöglichen. Hierdurch gelang es, die intrinsische Carotinoidbiosynthese erfolgreich durch Licht zu regulieren. Anschließend wurde durch den Transfer auf andere industriell relevante bakterielle Wirte wie *Escherichia coli, Bacillus subtilis* und *Pseudomonas putida* die allgemeine Anwendbarkeit dieses Licht-gesteuerten Expressionssystems nachgewiesen.

Die Immobilisierung von Enzymen auf der Oberfläche geeigneter Trägermaterialien kann zu einer Stabilisierung des jeweiligen Proteins und zu erleichtertem Substratfluss führen, wodurch

sich die Produktausbeute erhöht und die Akkumulation von (toxischen) Intermediaten verringert werden kann.

Daher wurden [**III**] Granula des Biopolymers Polyhydroxybutyrat (PHB) als vielversprechendes bioplastisches Material identifiziert, welches sich besonders für die *in vivo* Immobilisierung rekombinanter Enzyme in Bakterien eignet. *R. capsulatus* ist natürlicherweise in der Lage PHB-Granula zu bilden und in dieser Arbeit wurden diese Biopolymere zum ersten Mal erfolgreich in diesem phototrophen Bakterium funktionalisiert, indem das fluoreszierende Protein eYFP an die PHB-Oberfläche angelagert wurde.

Da die Validierung und Optimierung der erfolgreichen Bindung des Zielproteins and die Immobilisierungsmatrix *in vivo* ein aufwendiger Prozess ist, wäre es wünschenswert, diesen Vorgang in lebenden Zellen während des Herstellungs- und Immobilisierungsprozesses online zu überwachen und zu quantifizieren. Zu diesem Zweck wurde [**IV**] ein alternativer Linker für die *in vivo* Proteinimmobilisierung in dem nicht nativen PHB-Produzenten *E. coli* entwickelt, der das *split* GFP-System und die PHB-Technologie kombiniert. Dieses neue Linkersystem bietet eine Biosensorfunktion, die den *in vivo* Nachweis der Bindung des Zielproteins an die Biopolymeroberfläche ermöglicht.

In der vorliegenden Arbeit wurde die heterologe Terpenproduktion in *R. capsulatus* auf verschiedene Terpenklassen erweitert und ein P_{tac}-basiertes Vektorsystem implementiert, welches eine lichtinduzierte Genexpression ermöglicht und damit eine präzise Regulation der heterologen Terpenbiosynthese erlaubt. Durch die erfolgreiche Dekoration der PHB-Granula und die Entwicklung eines neuen Linker-/Sensorsystems wurde die *in vivo* Immobilisierung und gleichzeitige *in vivo* Überwachung des Kopplungsprozesses ermöglicht. Damit wurde der Grundstein für die Verbesserung der Terpenbiosynthese in *R. capsulatus* unter Verwendung der PHB-Technologie zur Immobilisierung von Enzymen gelegt.

I. INTRODUCTION

Exploring and understanding life with all its forms, colors and facets has always been the main concern of biology, the science of life. However, it is human nature to bring acquired knowledge into practice. The continuous striving for improvement drives us, it defines us, it makes us unique on planet Earth. Thus, mankind has been trying to subdue nature since the beginning of time. Fields are cultivated, animals are domesticated, and the landscape is shaped according to one`s own ideas. This process was accelerated almost 200 years ago by the industrial revolution. However, the increasing technologization of society also allows to gain detailed insights into the secrets of life. The discovery of microorganisms, the deciphering of the genetic code, the first genetic modification of an organism in the laboratory, are all milestones in life sciences and the birth of a new sub-discipline, the modern biotechnology. Learning from nature, understanding biological processes, developing further, and applying to current problems: Biotechnology has the potential to provide answers to the fundamental challenges facing humankind, such as climate change, famines, or resource scarcity. Its origins are almost as old as mankind itself. Initially still coincidental, the properties of microorganisms such as yeasts or lactic acid bacteria were used to produce high-quality food. Today, biotechnological products have become essential for a modern society. Bioactive compounds in medicines, food supplements, detergents or alternative fuels are just a few of the numerous products of this branch of industry. Enzymes as natural catalysts for the conversion of substrates into metabolites are of central importance in this context (Heux *et al*., 2015; Prasad & Roy, 2017). Therefore, it is of particular interest to increase the variability, activity, and stability of these proteins. Here, synthetic biology contributes to the development and redesign of biological systems improving enzymatic processes as well as harnessing new natural products (Böttcher & Bornscheuer, 2010; Clarke & Kitney, 2020). Moreover, controlling gene expression, e.g. by applying light as an external stimulus, allows orchestration of complex biosynthetic pathways and thus precise regulation of metabolic flux rates towards desired product formation (Binder, Frohwitter *et al*., 2016; Lalwani *et al*., 2021; Zhao *et al*., 2021).

In summary, it is possible to harness the potential of microorganisms by generating optimized cell factories for the production of proteins as wells as high-valuable secondary metabolites (Brown *et al*., 2017; Kulagina *et al*., 2021; Thak *et al*., 2020). Aim of this work was to develop different strategies to improve secondary metabolite production in the anoxygenic phototrophic bacterium *Rhodobacter capsulatus*. In the introduction, different metabolic engineering concepts for the heterologous synthesis of terpenoids, a group of valuable natural products, as well as the (light) regulation of biosynthetic pathways will be discussed. Second, engineering techniques to improve enzymatic properties will be enlightened.

I.1 Terpenoids – Applications, biosynthesis and biotechnological engineering

With up to 80,000 known compounds so far, terpenoids represent the largest group of secondary metabolites in nature (Moser & Pichler, 2019). These very heterogenous hydrocarbons are mainly produced in plants (Bergman *et al*., 2019; Pichersky & Raguso, 2018) and fulfill various functions such as defense against herbivores (Qi *et al*., 2018), as signal molecules for pollinators (Lipson Feder *et al*., 2021) or as antioxidants preventing photooxidative stress during photosynthesis (Kumar *et al*., 2020). Furthermore, terpenoids are also found in bacteria (Gozari *et al*., 2021), archaea (Matsumi *et al*., 2011), fungi (Chen & Liu, 2017; Elissawy *et al*., 2015), insects (Karlson, 1969; Quintana *et al*., 2003) and mammals (Reddy & Couvreur, 2009). Due to their enormous structure and functional diversity, terpenoids are used in numerous biotechnological applications (Tetali, 2019). Thus, they serve as fragrances (Serra, 2015) or flavors (Vespermann *et al*., 2017) and are also important components in pharmaceuticals (Ho *et al*., 2021; Kim *et al*., 2020) as well as pesticides (Sparagano *et al*., 2013). Moreover, terpenoids are used in the production of biofuels (Mewalal *et al*., 2017). Since conventional extraction of terpenoids from plant-based material is very laborious and cost-intensive, recombinant production in more-easy to handle microorganisms plays an increasingly important role (Cravens *et al*., 2019; Marienhagen & Bott, 2013).

All terpenoids are composed of different amounts of isoprene subunits (C_5) which primary leads to a subdivision into mono- (C_{10}), sesqui- (C_{15}), di- (C_{20}), tri- (C_{30}) and tetraterpenes (C_{40}) (Ruzicka, 1953). Moreover, a few examples of specialized terpenoid classes, such as hemi- (C_5) (M. Li *et al*., 2018), sester- (C_{25}) (Li & Gustafson, 2021), sesquarter- (C_{35}) (Sato, 2013) and polyterpenoids (>C_{40}) (Swiezewska & Danikiewicz, 2005) are also described in the literature. The precursor molecules of all terpenoids are the isoprene derivatives isopentenyl diphosphate (IPP) and dimethylallyl pyrophosphate (DMAPP) [see **Figure 1**]. These required precursors can be produced *via* two independent biosynthetic pathways. While most organisms only encode one of the two metabolic routes, plants are able to deploy both (Zeng & Dehesh, 2021): (**I**) The 2-C-methylerythritol 4-phosphate (MEP) pathway, which occurs in plastids, algae as well as bacteria originates from pyruvate and glyceraldehyde-3-phosphate (GAP) (Rohdich *et al*., 2002), while (**II**) the mevalonate (MVA) pathway can be found in eukaryotes and archaea with acetyl-CoA as the starting substrate (Goldstein & Brown, 1990).

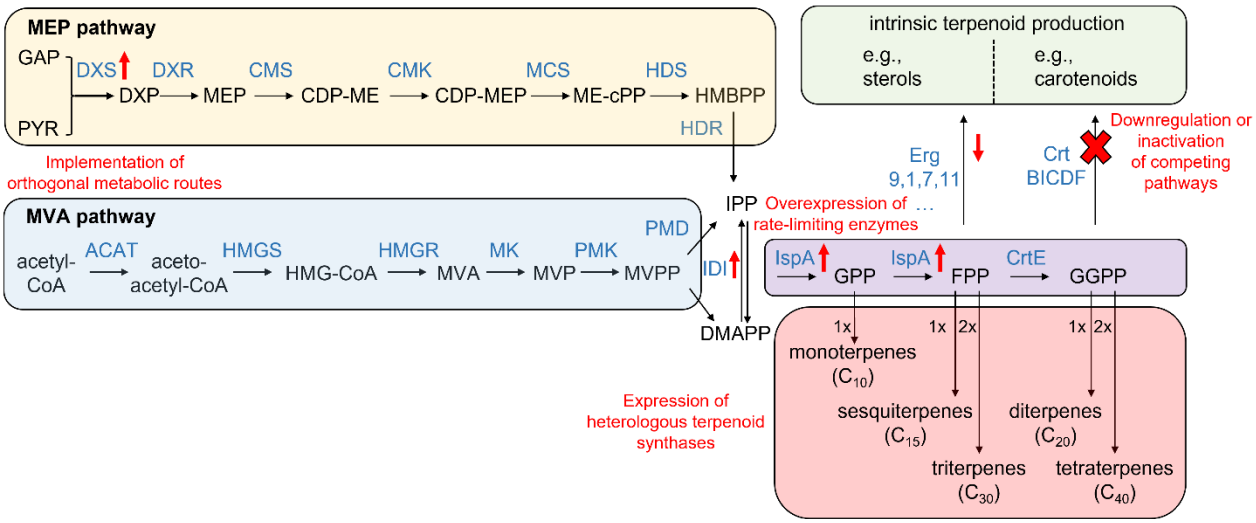

Figure 1. Schematic overview of terpenoid biosynthetic pathway and suitable metabolic engineering strategies. The MEP pathway (yellow module) originating from the substrates GAP and pyruvate consists of seven enzymatic reactions and is found in algae, bacteria, and plastids. On the opposite, the MVA pathway (blue module) is found in eukaryotes as well as archaea and comprises six steps. However, it is possible to integrate and overexpress the corresponding heterologous pathway in one organism and thus to increase the amount of precursor molecules. The end products of both metabolic pathways represent the isoprene derivatives IPP and DMAPP. These are further converted to the prenyl pyrophosphates GPP, FPP, and GGPP (purple module), the precursor of all terpenoid classes. Targeted overexpression of rate-limiting enzymes (symbolized by red ↑) can further shift the carbon flux towards the desired products. Numerous hosts naturally produce terpenes, for example carotenoids in phototrophic organisms or sterols in fungi (green module). Disruption of this intrinsic terpenoid production or downregulation of obligate metabolite biosyntheses (symbolized by red ↓) can lead to higher production of the desired prenyl pyrophosphates. The respective target terpene can finally be obtained by expression of heterologous terpenoid synthases (red module). Substrates (CDP-ME: 4-diphosphocytidyl-2-methyl-D-erythritole, CDP-MEP: CDP-ME-2-phosphate, DMAPP: dimethylallylpyrophosphate, DXP: 1-desoxy-D-xylulose-5-phosphate, FPP: farnesyl pyrophosphate, GAP: glycerinaldehyde-3-phosphate, GGPP: geranylgeranyl pyrophosphate, GPP: geranyl pyrophosphate, HMBPP: (E)-4-hydroxy-3-methyl-but-2-enyl-diphosphate, HMG-CoA: β-hydroxy-β-methylglutaryl-CoA, IPP: isopentenyl pyrophosphate, Me-cPP: 2-c-methyl-D-erythritol-2,4-cyclodiphosphate, MEP: 2-c-methyl-D-erythritol-4-phosphate, MVA: mevalonate, MVP: mevalonate-5-phosphate, MVPP: mevalonate-5-pyrophosphate, PYR: pyruvate); Enzymes (ACAT: acetyl-CoA acyltransferase, CMK: cytidyl-methyl kinase, CMS: cytidyl-methylerythritol synthase, CrtBICDF: enzymes involved in carotenoid biosynthesis, CrtE: geranylgeranyl pyrophosphate synthase, DXR: 1-desoxy-D-xylulose-5-phosphate reductase, DXS: 1-desoxy-D-xylulose-5-phosphate synthase, Erg 9,1,7,11: enzymes involved in ergosterol biosynthesis, HDR: hydroxy-methyl-butenyl-diphosphate reductase, HDS: hydroxy-methyl-butenyl-diphosphate synthase, HMGR: hydroxy-methyl-glutaryl reductase, HMGS: hydroxy-methyl-glutaryl synthase, IDI: isopentenyl diphosphate isomerase, IspA: farnesyl pyrophosphate synthase, MCS: methyl-erythritol-cyclo-diphosphate synthase, MK: mevalonate kinase, PMD: pyrophosphate-mevalonate decarboxylase, PMK: phosphate-mevalonate kinase).

Starting from IPP and DMAPP, prenyl pyrophosphates are synthesized, which form the precursor molecules of the later terpene classes. For this purpose, IPP and DMAPP are linked by a prenyl transferase *via* a head-to-tail condensation resulting in geranyl pyrophosphate (GPP) production (K. Wang, 2000). For additional elongation to farnesyl pyrophosphate (FPP) or geranylgeranyl pyrophosphate (GGPP), further molecules of IPP are linked to the existing structure (Ohnuma *et al.*, 1997). The prenyl pyrophosphates GPP, FPP, and GGPP are the

basis for the synthesis of all terpene classes. Numerous microorganisms naturally produce terpenes, such as carotenoids in phototrophs (Paniagua-Michel *et al*., 2012) or sterols in fungi (Jordá & Puig, 2020). Furthermore, the FPP synthase can be utilized as a phylogenetic marker due to its wide distribution in various groups of organisms (Cantera, 2002).

As already mentioned, the extraction of terpenoids from plant material is not very effective, thus for biotechnological applications the focus is rather on recombinant production in microorganisms (Cravens *et al*., 2019). Thus, heterologous expression of terpene synthases, often originating from plants, is employed to increase the respective efficiency using the well-established production hosts *Escherichia coli* and *Saccharomyces cerevisiae* (Liang *et al*., 2021; Paramasivan & Mutturi, 2017; Rinaldi *et al*., 2022; Ward *et al*., 2018). To generate terpenoid yields of industrial relevance, it is necessary to further optimize these hosts by metabolic engineering techniques as well as bioprocess improvement to ensure optimal carbon flux rates towards the desired products (Carsanba *et al*., 2021; Dueber *et al*., 2009; Moser & Pichler, 2019; Schempp *et al*., 2018). Different regulatory mechanisms in the corresponding metabolic pathways, such as feedback inhibition of the 1-desoxy-D-xylulose-5-phosphate synthase (DXS) by DMAPP and IPP in *E. coli* were already discovered (Banerjee *et al*., 2013). Moreover, accumulation of intermediates such as β-hydroxy-β-methylglutaryl-CoA (HMG-CoA), IPP, DMAPP and FPP are reported to cause toxic effects in bacteria (Dahl *et al*., 2013; Pitera *et al*., 2007; Sivy *et al*., 2011). Therefore, overexpression of rate-limiting enzymes of isoprenoid biosynthesis is a promising approach to enhance carbon flux and negate potential cellular inhibitory effects (Donald *et al*., 1997; Engels *et al*., 2008; H. Lim *et al*., 2020). Exemplary, in the Gram-positive bacterium *Bacillus subtilis*, plasmid-based overexpression of the entire MEP biosynthetic pathway resulted in a 20-fold increased production of the C_{30} carotenoid 4,4`-dianeurosporene (Abdallah *et al*., 2020). In addition to MEP mediated overexpression approaches, the heterologous MVA pathway has already been successfully integrated in bacteria in the pioneering work of Keasling and co-workers (Martin *et al*., 2003). Here, heterologous biosynthesis of amorpha-4,11-diene with concomitant insertion of the MVA gene cluster in *E. coli* was demonstrated. This laid the foundation for numerous further studies on heterologous terpene production in bacteria, in which the precursor supply was increased by introducing the recombinant MVA pathway (Jang *et al*., 2011; C.-L. Liu *et al*., 2019; Yang & Guo, 2014; Yang & Nie, 2016). In contrast, insertion of a functional MEP pathway in yeasts seems to be a great burden (Kirby *et al*., 2016). Since the last two enzymes IspG and IspH containing iron-sulfur cluster and hence require additional redox partners, which are not found in the cytoplasm of yeasts (Lill & Mühlenhoff, 2008), the intermediate MEcPP appears to accumulate and interrupt carbon flux within the cell (Carlsen *et al*., 2013; Partow *et al*., 2012). Furthermore, as numerous microorganisms also show a distinct intrinsic terpenoid production, it might be necessary to knockout or downregulate such

competing pathways. By replacing the promoter for controlling FFP consuming squalene synthase level with a weaker, glucose-dependent variant, it was possible to 3.4-fold enhance the production of the sesquiterpene α-santalene in *S. cerevisiae* (Scalcinati *et al*., 2012). However, indirect competition with metabolic pathways requiring carbon sources such as polyhydroxybutyrate (PHB) biosynthesis must be considered as well (Mougiakos *et al*., 2019). In the PHB deficient strain *Cupriavidus necator* H16 PHB^{-}4 (Raberg *et al*., 2014), product titers of the sesquiterpene β-farnesene up to 26.3 µM could be achieved by fed-batch processing using fructose as substrate (Milker & Holtmann, 2021). More complex terpenoids are usually highly hydrophobic, non-volatile and accumulate within a cell to partially cause membrane stress (Verwaal *et al*., 2010). Thus, this process may constrain production efficiency due to limited storage capabilities and toxic effects (C. Zhao *et al*., 2018). In *S. cerevisiae*, the triterpene squalene was observed to accumulate in peroxisomes (G.-S. Liu *et al*., 2020). For this, Wei and coworkers were able to increase squalene titers up to 11 g/L in a two-stage fed-batch fermentation by introducing the whole squalene biosynthetic pathway into peroxisomes as well as enhancing ATP, NADPH, and acetyl-CoA supply. In contrast, a heterologous approach pursued the use of hydrophobic PHB granules for the storage of lycopene in *E. coli.* Here, the terpene synthase as well as the genes required for PHB biosynthesis were heterologously expressed and lycopene was observed to attach to the granule surface *in vivo* (Y. Liu *et al*., 2020). Besides the exploitation of recombinant compartments, it is also possible to utilize cellular membranes as storage media. For example, lycopene production in *E. coli* could be increased 1.32-fold by overexpressing a heterologous *Almgs* protein from *Acholeplasma laidlawii* in combination with host genes associated with membrane biosynthesis (T. Wu *et al*., 2018).

Another possible target to improve isoprenoid biosynthesis is the terpene synthase itself, firstly through enzyme engineering, i.e., the targeted replacement of individual amino acids as well as truncation, or the addition of individual protein domains (Kschowak *et al*., 2020; Lauchli *et al*., 2013; Ronnebaum *et al*., 2021). For example, by the heterologous expression of a chimeric diterpene synthase from *Emericella variecolor* consisting of a terpene cyclase (TC) domain and a prenyl transferase (PT) domain, the tricyclic diterpene variedene could be produced in *Aspergillus oryzae* (Qin *et al*., 2016). Interestingly, a new macrocyclic ester terpene (2*E*)-α-cericerene could additionally be synthesized, suggesting that the TC domain could utilize different prenyl pyrophosphates as substrates. Finally, an exchange of the PT domain with that from another chimeric sesterterpene synthase also originated from *E. variecolor* allowed the *in vivo* production of (2*E*)-α-cericerene as the major product (Qin *et al*., 2016). Moreover, since the synthesis of a terpenoid is a multi-step enzymatic reaction, enzymes catalyzing adjacent steps in isoprenoid biosynthesis can be fused to enhance enzyme activity or reducing the accumulation of (toxic) intermediates (Albertsen *et al*., 2011;

Nogueira *et al*., 2019; Wang *et al*., 2021). Fusion of IDI and the downstream prenyl pyrophosphate synthase led to a 5.7-fold increase in carotenoid production in *E. coli* and up to 58% higher lycopene yield in *S. cerevisiae* (Kang *et al*., 2019). Here, the peculiarity was the utilization of a protein tag system with relatively short peptide pairs, allowing the construction of scaffold-free modular enzyme assemblies.

Besides the aforementioned techniques for direct optimization of cellular processes, the cultivation or production conditions may also be enhanced. This bioprocess optimization includes the selection of a suitable growth medium composition including carbon and nitrogen sources, sufficient gassing, for example with O_2 or CO_2, ideal pH value as well as temperature and precise timing of the appropriate cultivation period including an optimal start time for production (Carsanba *et al*., 2021). Gruchattka and co-workers compared the potential of metabolic networks of *E. coli* and *S. cerevisiae* to produce IPP in terms of carbon stoichiometry, energy and required redox equivalents *in silico* using elementary mode analysis. Here, they concluded that the MEP pathway can theoretically provide an almost 50% increased amount of IPP than the MVA pathway due to the different precursors and associated carbon stoichiometry. In addition, theoretical modeling revealed that supplementing glycerol in *E. coli* and ethanol in *S. cerevisiae* as carbon sources enable the highest potential product yields (Gruchattka *et al*., 2013). As an example for an *in vivo* bioprocess optimization, squalene production in the oleaginous yeast *Yarrowia lipolytica* was increased 28-fold to 502 mg/L compared to the parental strain by conventional overexpression of rate-limiting enzymes and improved cultivation processes (H. Liu *et al*., 2020). To this end, the influence of the cultivation vessel geometry was examined as well as the growth medium composition was improved by using glucose as carbon source (leading to a C/N ratio of 40:1), a regulated pH value, and PBS buffer supplemented with 1 mg/L cerulenin to inhibit competing fatty acid biosynthesis (H. Liu *et al*., 2020).

In addition to the applications already described in detail, mostly in the established hosts *E. coli* and *S. cerevisiae,* the production of terpenoids in oxygenic and anoxygenic phototrophic bacteria offers numerous new possibilities [see **Publication I**, **Chapter II.3.1**]. These groups of microorganisms naturally generate carotenoids as photoprotective agents and therefore have a strong intrinsic terpenoid production (Heck & Drepper, 2017; Lin & Pakrasi, 2019). Moreover, phototrophic growth using sun light and carbon dioxide as an energy and carbon source, respectively, offers an even more economical and ecologically friendly alternative to competing manufacturing processes (George *et al*., 2020; Jodlbauer *et al*., 2021). In addition, some bacteria are able to utilize atmospheric N_2 *via* nitrogen fixation (Bothe *et al*., 2010; Klipp *et al*., 1988; Masepohl *et al*., 2002).

The purple non-sulfur α-proteobacterium *R. capsulatus* is one of these organisms offering a highly versatile metabolism to grow either photo(hetero)trophically or chemotrophically in the

presence and absence of light, respectively (Strnad *et al*., 2010; Tabita, 1995; Weaver *et al*., 1975). Furthermore, under phototrophic conditions *R. capsulatus* generates a large intracytoplasmic membrane (Niederman, 2013). This system is formed by protrusions of the cytoplasmic membrane resulting in the generation of numerous intracytoplasmic membrane vesicles and is associated for the storage of hydrophobic metabolites and photosynthesis-associated protein complexes (Heck & Drepper, 2017). Besides these unique physiological properties, making *R. capsulatus* a promising new chassis organism for the production of plant-derived sesqui- and triterpenes (Hage-Hülsmann *et al*., 2019; Loeschcke *et al*., 2017; Troost *et al*., 2019), this bacterium is naturally capable to build up biopolymeric granules consisting of polyhydroxybutyrate (PHB) as an energy and carbon storage compound (Kranz *et al*., 1997; Mayet *et al*., 2013). These PHB granules are well-established immobilization matrices regarding enzyme scaffolding in other hosts (Dinjaski & Prieto, 2015; J. X. Wong, Ogura, *et al*., 2020), but such approaches are still missing in purple non-sulfur bacteria so far. In general, combination of heterologous terpene biosynthesis and PHB technology is conceivable in *R. capsulatus* and already established in the non-native PHB producer *E. coli* (Lee *et al*., 2014; Y. Liu *et al*., 2020).

I.2 Gene regulation – Principles and (light-mediated) control

In nature, the ability of an organism to precisely regulate cellular processes in dependence of changing environmental conditions or nutrient availability is of crucial importance. Therefore, it must be ensured that, according to the principle of economy, genetic information is only translated into physiological and morphological properties if they have an immediate benefit. Consequently, gene expression and hence the entire protein biosynthesis are subjected to precise control mechanisms. In bacteria, individual genes are assembled into gene clusters that are placed under the control of specific promoters (Jensen, 2016; Osbourn & Field, 2009). Their regulation, and thus the start of gene expression, is often determined by an external stimulus such as defined environmental conditions, e.g., temperature, pH value, oxygen availability, osmolarity or light as well as available nutrient sources represented by the presence or absence of a corresponding inducer molecule (Banerjee & Ray, 2017; Hurme & Rhen, 1998; Takano, 2016). In general, gene expression can be positively and negatively regulated (Klier *et al*., 1992; Raymondjean *et al*., 1991). Positive gene regulation is characterized by the stimulation of transcription by an activator protein that binds to its target promoter, resulting in an enhanced affinity of the RNA polymerase to the corresponding promoter region. In contrast, binding of a repressor protein to a promoter region prevents transcription during negative gene regulation.

A classic model for both regulation approaches is the well-characterized lactose utilization network from *E. coli* referred to as the *lac* operon (Jacob & Monod, 1961). In addition to the

promoter P_{lac}, the *lac* operon consists of the three genes *lacY*, *lacZ* and *lacA*: The *lac* permease (LacY) is a membrane-integrated lactose/H^+-symporter responsible for the lactose uptake into the cell (Abramson *et al*., 2004). The ingested lactose is subsequently converted by a β-galactosidase (LacZ) into the intermediates glucose, galactose and 1,6-allolactose (Juers *et al*., 2012; Lederberg, 1950), respectively, whereas non-metabolizable thiogalactosides are inactivated by a thiogalactoside transacetylase (LacA) (Marbach & Bettenbrock, 2012; Zabin *et al*., 1962). The transcription of the *lac* operon is activated under glucose depletion and derepressed by the availability of lactose (Lewis, 2013). Here, this regulation proceeds *via* the global catabolite activation protein (CAP) and the *lac* repressor protein (LacI) (Busby & Ebright, 1999; Lewis, 2005). The latter is encoded by the constitutively expressed *lacI* gene and forms a tetrameric structure (Lewis *et al*., 1996; Rutkauskas *et al*., 2009). In the absence of an inducer, LacI binds to two of three operator regions within the *lac* operon, resulting in a loop formation and consequently preventing the transcription of the *lac* genes. In the presence of an inducer molecule, its binding to LacI results in a conformational change that detaches the repressor from the operator region and allows expression of the *lac* genes (Wilson *et al*., 2007). Since metabolizing glucose instead of lactose is energetically favorable, a second control mechanism is necessary to ensure metabolization of the preferred nutrient when multiple carbon sources are available.

In case of glucose depletion, the glucose importer remains phosphorylated as the P-group would otherwise be transferred onto glucose. This in turn leads to the interaction of the phosphorylated importer and an adenylate cyclase resulting in its activation (Nelson *et al*., 1983). Thus, in the absence of intracellular glucose, cAMP molecules are produced that act as an allosteric effector for the CAP protein, which in turn enables transcriptional activation of the P_{lac} promoter (Busby & Ebright, 1999). As a result, *lac* gene expression is regulated by both (allo)lactose-mediated inactivation of the LacI repressor and activation of CAP activator protein *via* cAMP during glucose starvation [see **Figure 2**].

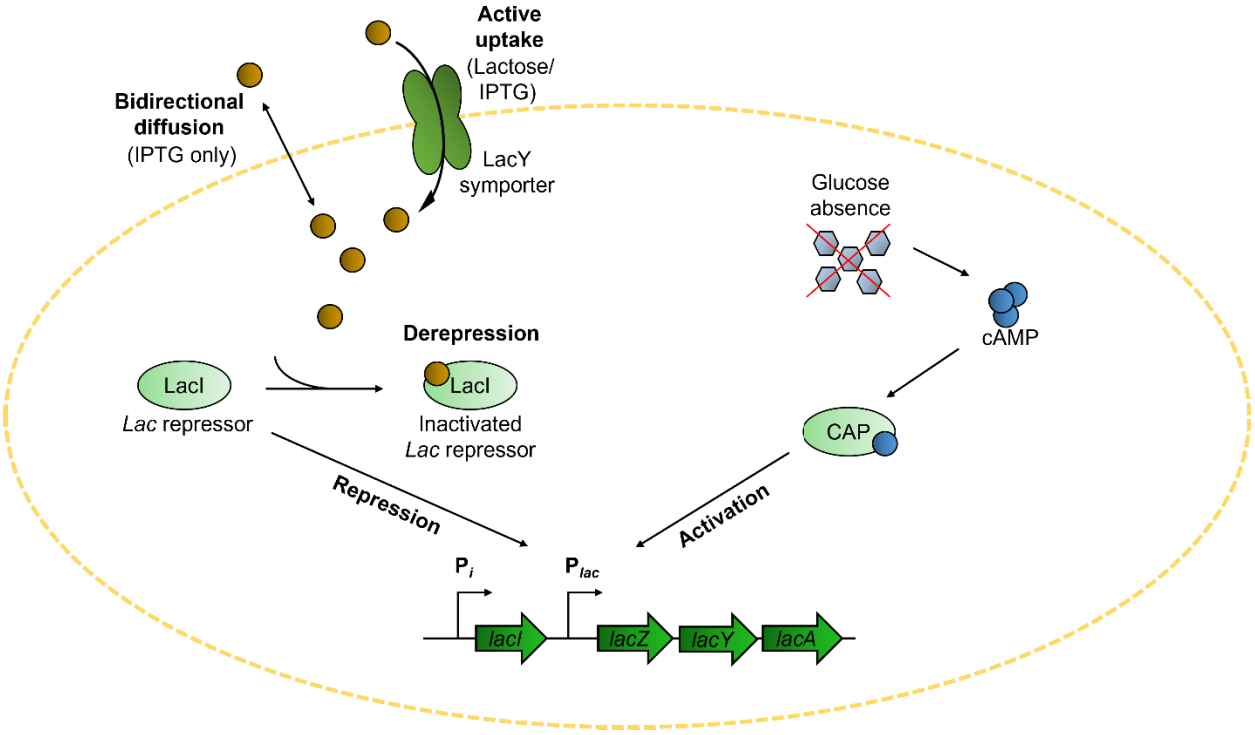

Figure 2. Schematic overview of the *E. coli lac* operon as an example of bacterial transcription regulation. In *E. coli* (the cytoplasmic membrane is depicted as yellow dashed line) the *lac* operon consists of three structural genes encoding a β-galactosidase/H^+-symporter (LacY) for the active uptake of lactose, a β-galactosidase (LacZ) for its conversion, and a galactoside transacetylase (LacA) for the inactivation of thiogalactosides. In the absence of lactose, the transcription is inhibited by the repressor LacI. Passive diffusion across the membrane only occurs for synthetic inducers such as isopropyl β-D-1-thiogalactopyranoside (IPTG). After binding of an inducer molecule, a conformational change of LacI occurs, resulting in a detachment from the promoter region. This allows transcription of the *lac* genes by the P_{lac} promoter. In addition, in the absence of glucose, cAMP molecules are produced that serve as an allosteric effector for the catabolite activation protein (CAP), which then enables activation of the P_{lac} promoter.

The availability of well-controlled expression systems is important for biotechnological processes, such as microbial heterologous production of proteins and metabolites. This allows production to be precisely adjusted to the host`s growth phase for achieving maximum product yields. For this purpose, gene expression is often initiated by adding a chemical inducer enabling the optimal control over induction of gene transcription (Cheng *et al.*, 2011; Donovan *et al.*, 1996). Further, the inducer should not cause any other undesired responses in the cell and be able to pass the cell membrane. The described *lac* operon is a well-established transcriptional regulation system for heterologous gene expression in different bacteria. Here, the non-metabolizable surrogate isopropyl β-D-1-thiogalactopyranoside (IPTG) is often utilized instead of lactose to initiate LacI derepression (Gomes *et al.*, 2020; Hu *et al.*, 2015; Lu *et al.*, 2018). In contrast to lactose, uptake of IPTG into the host organism can occur either by diffusion or active transport *via* a LacY permease. Thus, these processes are decisive for controlling intracellular inducer concentrations and for the final expression levels of target genes. Since permease-dependent inducer uptake can result in a significant heterogeneity of target gene expression, lactose permease deficient expression strains (e.g. *E. coli* Tuner

(DE3)) have to be used for gradual induction and homogeneous expression response (Binder, Probst, *et al*., 2016; Hansen *et al*., 1998). Furthermore, optogenetic switches have been developed for precise, non-invasive control of cellular processes in bacteria as well as yeasts and mammalian cells (Ankenbruck *et al*., 2018; Hartmann *et al*., 2020). For light-regulated gene expression, a chemically modified inducer molecule forms the basis, to which a photolabile protection group was fused, resulting in a so-called photocaged compound. This compound can already be added at the beginning of a cultivation process and activated at a specific time point by illumination. An example of such a photocaged compound is 6-nitropiperonal (NP)-IPTG [see **Figure 3**] (Binder *et al*., 2014; Young & Deiters, 2007). Here, the photolabile protection group is attached to two hydroxyl groups of the IPTG inhibiting its binding to LacI. Consequently, functionality can only be restored by a two-step reaction: After irradiation with UV-A light (λ_{max} = 365 nm), one of the two bonds is cleaved, resulting in two different ester intermediates. These are subsequently resolved by intracellular hydrolases into the non-toxic NP protecting group and functional IPTG (Young & Deiters, 2007).

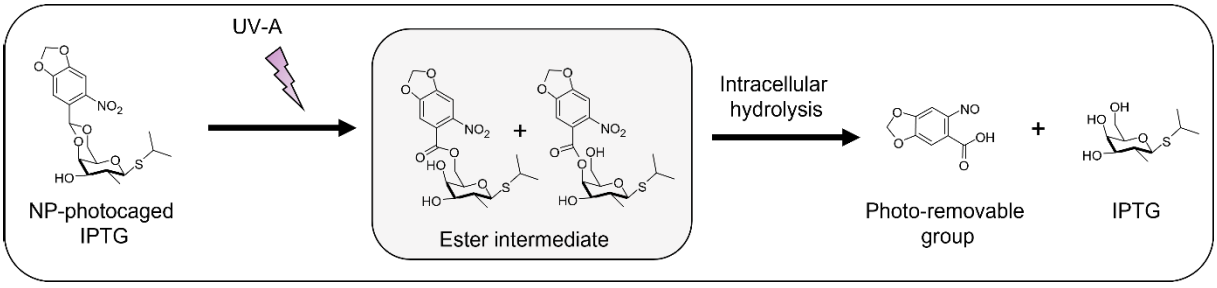

Figure 3. Light-induced release of IPTG from photocaged NP-cIPTG. The release of IPTG proceeds in two steps. After irradiation with UV-A light, two ester intermediates are formed, which are subsequently cleaved into the NP protection group and IPTG by intracellular hydrolysis.

In addition to IPTG, numerous other inducer molecules have already been combined with photolabile protection groups making them accessible for light-mediated applications in bacteria: including cAMP (Engels & Schlaeger, 1977), erythromycin (Gardner *et al*., 2011), arabinose (Binder, Bier, *et al*., 2016), salicylic acid as well as coumarin derivatives (Hogenkamp *et al*., 2022), and other carbohydrates such as glucose, galactose, rhamnose and lactose (Bier *et al*., 2016). Moreover, photolabile methionine was used in yeast to enable light-mediated repression of a *p*MET17 promoter (Kusen *et al*., 2016). Conversely, to establish an inducible system in *S. cerevisiae*, a photosensitive DMNP-EDTA chelator was utilized to facilitate light-based Cu^{2+} release in combination with a *p*CUP1 promoter (Kusen *et al*., 2017). Besides applications in yeast, approaches in other eukaryotic systems have also been pursued, such as photocaged ecdysone in human embryonic kidney (HEK) cells (W. Lin *et al*., 2002), photocaged doxycycline in tobacco leaves (Cambridge *et al*., 2006) and coumarin-caged 4-hydroxytamoxifen (P. Wong *et al*., 2017) as well as light-activated cyclofen in mouse cells (Gorka *et al*., 2018).

Furthermore, the activity of T7-RNA polymerase was set under control of a photocaged tyrosine in the active site, allowing nucleotides to reach the catalytic center only after UV-A exposure (Chou *et al*., 2010). In addition, other applications are available comprising small molecules for direct DNA or RNA interaction, such as the binding of photocaged theophylline to mRNA riboswitches (Walsh *et al*., 2014) as well as down-regulation of genes by photocaged small interfering RNAs (Q. Wang *et al*., 2021) and photocleavable groups at the 5' cap of eukaryotic mRNAs (Bollu *et al*., 2022).

Alongside the described applications, basing on chemically modified small photocaged molecules, there is another group consisting of a variety of proteins harboring light-sensitive chromophores such as photosensitive polymerases (Baumschlager *et al*., 2017), recombinases (Sheets *et al*., 2020) or photoreceptors. These photoreceptors include red and near infrared light-responsive phytochromes (Pham *et al*., 2018), light oxygen voltage (LOV)-domains responsive to blue light (Pudasaini *et al*., 2015) as well as cryptochromes (Lin & Todo, 2005; Lopez *et al*., 2021). One way to apply photoreceptors is to directly modulate gene expression by using light-dependent transcription factors or repressors respectively (Camsund *et al*., 2011; Sumi *et al*., 2019). In addition, they can be combined with effectors, such as response regulators to obtain a two-component light-dependent signaling system such as Cph8/OmpR or CcaS/CcaR (Hirose *et al*., 2008; Olshefsky *et al*., 2016; Ong & Tabor, 2018).

In contrast to photocaged compounds, those photoreceptors offer the advantage to reversibly control gene expression. However, the cofactors required for chromophore assembly must be provided by the cell.

I.3 Enzymes – Natural biocatalysts, applications and enzyme engineering

Enzymes are biochemical catalysts that accelerate the conversion of substrates into products while leaving these reactions unaltered. The substrate binds to the active site of the respective enzyme forming an enzyme-substrate complex, which is kept together either by covalent or non-covalent bonds including hydrogen and ionic bonds as well as van der Waals forces. The activation energy for conversion into the product is lowered, thereby accelerating the reaction. The majority of cellular processes are catalyzed by enzymes from protein biosynthesis to the supply of energy in metabolic pathways. A distinction is made between different types of enzymes: a large portion constitute proteins, another RNA-based ribozymes (Scott, 2007) or holoenzymes, a combination of proteins and cofactors such as inorganic ions or prosthetic groups like heme (Collins, 2006; Mowat *et al*., 2010; Nguyen, 2021). In addition to their physiological function, numerous enzymes can be used industrially as well. Due to their wide range of applications and promising characteristics, including enantio-, chemo- and regioselectivity (Jiang & Fang, 2020), enzymes are an important part of biotechnological approaches. They are either utilized directly as biotechnological compound like proteases,

lipases and amylases in laundry detergents, or their reaction products are commercialized such as amino acids and sugars (Dumorne *et al.*, 2017; Gurung *et al.*, 2013). In contrast to conventional production processes based solely on chemical reactions, enzymes are derived from renewable resources, so their use is considered particularly sustainable (Intasian *et al.*, 2021). In addition, biocatalysts are biocompatible and biodegradable, as well as in most cases non-hazardous and non-toxic (Siedentop & Rosenthal, 2022). Moreover, enzymatic reactions usually take place under mild conditions in an aqueous environment (Aschenbrenner *et al.*, 2009) and hence represents an advantage in view of environmental protection. Consequently, there is great interest in the identification of new enzymes and their biotechnological use to further broaden the product portfolio and to replace fossil-based manufacturing processes, as well as the improvement of existing biocatalysts by engineering processes (Cirino & Sun, 2008; Lancaster *et al.*, 2018; Sheldon & Pereira, 2017). For example, enzymes are generally engineered in order to improve their activity (Son & Kim, 2022), stability (e.g., pH- and temperature stability or solvent compatibility) (Bommarius & Paye, 2013; Jia *et al.*, 2012; Kohler *et al.*, 2018; Priyanka *et al.*, 2019; Tian *et al.*, 2017) as well as to achieve enhanced substrate specificity (Xie *et al.*, 2020) and selectivity (Kalkreuter *et al.*, 2021). Several engineering techniques for the optimization of enzyme properties are shown below [see **Figure 4**].

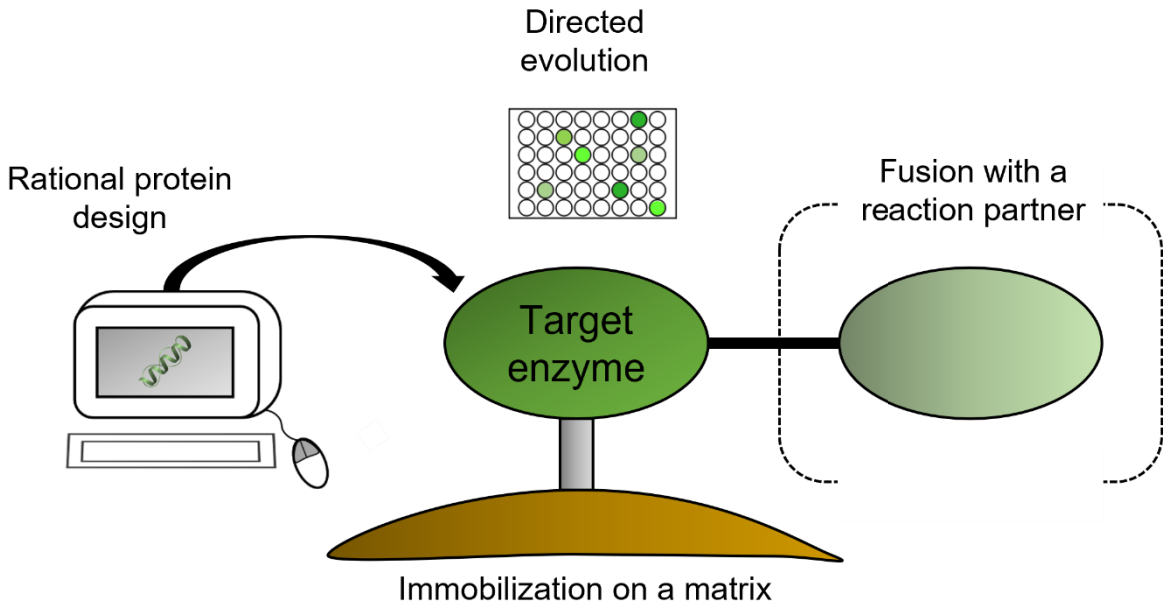

Figure 4. Strategies for enzyme engineering. The properties and functionality of an enzyme can be modified by a variety of techniques. At the molecular level, the enzyme structure can be altered either randomly by directed evolution or strategically through *in silico* assisted rational protein design. Furthermore, the target enzyme can be covalently fused to other enzymes involved in an enzymatic reaction cascade (reaction partner) to improve substrate channeling and thereby reducing the accumulation of toxic intermediates. Moreover, immobilization of enzymes to a matrix can enhance its stability as well as reusability.

Depending on available knowledge of the target enzyme in terms of sequence, structure and function, three types of strategies can be applied for enzyme engineering, namely rational protein design, directed evolution and a semi-rational approach (Ali *et al*., 2020). These principles are briefly explained below, and a current example is given in each case to illustrate the underlying methodology.

In rational protein design, individual amino acids are specifically exchanged requiring in-deep knowledge about the structure-function relation of the target enzyme (Watanabe *et al*., 2018). For example, using site saturation mutagenesis only one or few base triplets of a target gene are altered, so that the natural amino acid can be replaced by other residues at the position(s) of interest (Qu & Sun, 2022; Zheng, 2004). This method was for example applied to modify nine amino acid residues in the access tunnels for the transport of substrates, products and water to control the water entry to the active site of the cytochrome P450 monooxygenase BM3 from *Bacillus megaterium*. Here, the utilization efficiency of NAD(P)H could be improved, which is usually impaired in presence of water leading to a reduced coupling efficiency of non-natural substrates (Meng *et al*., 2022).

In contrast, directed evolution approaches do not require deeper knowledge of neither the structure nor the catalytic mechanism (Markel *et al*., 2020). In this process, iterative mutagenesis is induced e.g., *via* the use of an error-prone polymerase chain reaction to randomly mutate the nucleotide sequence of the target gene (McCullum *et al*., 2010). Subsequently, the generated protein variants can be screened for enhanced properties (Nirantar, 2021). However, this approach is very laborious and requires a selection mechanism associated to the targeted enzymatic characteristics respectively. Thus, screenings with several thousand enzyme variants are not uncommon, as reported for directed evolution of an oxidoreductase towards higher activity with more than 7,000 clones (Jiang *et al*., 2015), of an α-amylase to enhance acid stability with around 5,500 clones (Y. H. Liu *et al*., 2012) or up to 15,000 mutants of a tryptophan synthase (Xu *et al*., 2020).

In a semi-rational approach, information about the protein structure and function are available, so that promising amino acid motives can be computational preselected to significantly reduce the amount of possible protein variants (Ali *et al*., 2020). In case of three glycosyltransferases from *Vitus vinifera* the substrate binding site were mutated *in silico* and computationally analyzed regarding their interaction with different glycoside and aglycone substrates and enhanced enzymatic activity. Consequently, only six variants were generated by site-directed mutagenesis to test their predicted effects (Joshi *et al*., 2019).

Since enzymatic reactions are usually part of multistep metabolic processes, the genetic fusion of adjacent enzymes may be appropriate to facilitate substrate channeling and cofactor recycling. Moreover, it can lead to stabilization of fusion partners and increased turnover rates

through substrate channeling, as well as a reduction in the accumulation of toxic intermediates within the cell (Aalbers & Fraaije, 2019; Iturrate *et al*., 2009; Jeon *et al*., 2015; Kang *et al*., 2019). Here, the choice of a suitable linker between both enzymes plays an important role to ensure proper folding and protein stability as well as substrate channeling of charged intermediates (X. Chen *et al*., 2013; Y. Liu *et al*., 2017, 2019). As an example, a protein complex consisting of an alcohol dehydrogenase, an aldehyde dehydrogenase, and a short cation-rich, α-helix forming polypeptide linker, was used for the enzymatic reduction of acetate to ethanol (Kummer *et al*., 2021). Here, the protein folding software Rosetta` (Das & Baker, 2008) was used to determine the optimal placement of the linker to achieve ideal proximity to the active sites without simultaneously affecting the catalytic efficiency. This approach resulted in an increased amount of the desired product by 90% and a 500-fold enhanced activity compared to unfused enzyme variants (Kummer *et al*., 2021).

Another possibility is the immobilization of enzymes on a matrix for *in vitro* or *in vivo* applications (Federsel *et al*., 2021; Hyeon *et al*., 2016; S. Liu *et al*., 2021; Oliveira *et al*., 2020). These methods are often accompanied by an increased stability or improved temperature and solvent tolerance (Guzik *et al*., 2014; Matsumoto *et al*., 2019; Su *et al*., 2018). In addition, purification as well as reusability of the catalysts can be facilitated (Atiroğlu *et al*., 2021; M. Zhao *et al*., 2019). In this context, the immobilization of proteins on granules consisting of the biopolymer PHB (Dinjaski & Prieto, 2015; Tarrahi *et al*., 2020; Wong, Ogura, *et al*., 2020) is of particular importance in this thesis and will be discussed in more detail as well as compared with other *in vivo* immobilization approaches including catalytically active inclusion bodies (CatIBs) [see **Publication VI**, **Chapter II.3.1**]. PHB granules are naturally produced by numerous bacteria, such as *R. capsulatus,* as a carbon storage compound under nutrient limitation (Hahn *et al*., 1995; Kavitha *et al*., 2018; Kranz *et al*., 1997; Madison & Huisman, 1999). In addition, the biopolymer surrounded protein layer is suitable as an anchor matrix for the display of biotechnologically relevant enzymes (Peters & Rehm, 2006; Rodriguez-Abetxuko *et al*., 2020; Wong, Ogura, *et al*., 2020). However, PHB-based *in vivo* immobilization of target enzymes has not been performed in purple non-sulfur bacteria so far.

I.4 Outline of the thesis

The control of cellular processes in microorganisms and the improvement of their biotechnological applications addressing different targets within a cell is part of synthetic biology. Beginning with an optimized gene expression, obtained by adapted regulatory systems, a precise coordination of complete metabolic routes can be favorable. For instance, complex biosynthetic pathways can be adjusted by gradually inducible and non-invasive regulatory mechanisms to ensure optimal production efficiency of the bacterial host. Moreover, protein engineering techniques have the potential of tailoring various enzymatic properties.

The anoxygenic phototrophic bacterium *R. capsulatus* exhibits a highly flexible metabolism including the ability to utilize various organic compounds as electron and carbon source. Moreover, this bacterium can grow using (sun)light as energy as well as CO_2 and N_2 as carbon and nitrogen source. Besides that, *R. capsulatus* possesses a strong intrinsic tetraterpene production and has already been successfully established for the heterologous biosynthesis of sesquiterpenes as well as complex membrane proteins. In addition, it is naturally capable of producing the biopolymer PHB, a promising matrix for protein immobilization. Thus, this thesis aimed to develop new tools for the implementation of synthetic (terpenoid) biosynthesis pathways in *R. capsulatus* as host for the production of various terpene classes.

First, a general overview about the potential of phototrophic bacteria such as cyanobacteria and purple non-sulfur bacteria for terpenoid production was given in the context of the underlying metabolic engineering concepts [see **Chapter II.1.1**]. Since *R. capsulatus* was implemented in our group for the heterologous production of the sesquiterpenes valencene and patchoulol, already established metabolic engineering concepts were applied in the presented work to evaluate the general applicability of this phototrophic bacterium to produce further prominent classes of terpenoids including C_{15}, C_{20}, C_{30} and C_{40} terpenes [see **Chapter II.1.2 & Chapter II.1.3**].

In order to continue the optimization of complex bioprocesses such as terpene production, the selective control of gene expression can strongly affect the efficiency of biosynthetic pathways. For this, a broad host range P_{tac}-based vector system was developed for heterologous expression e.g., in *R. capsulatus* to achieve gradual expression control and light-mediated gene expression combined with conventional IPTG and photocaged IPTG derivates, respectively. This concept was evaluated under non-phototrophic and phototrophic conditions, followed by investigations of the adjustability of intrinsic carotenoid biosynthesis [see **Chapter II.2.1**]. Subsequently, the usage of caged inducer molecules was transferred to other industrial relevant bacterial hosts such as *E. coli*, *B. subtilis*, and *P. putida* [see **Chapter II.2.2**].

Displaying enzymes, e.g. of more complex biosynthetic pathways, onto an intracellular surface can lead to channeling substrate flux, thus enhancing conversion and hindering accumulation of (toxic) intermediates. Therefore, common methods for the *in vivo* immobilization of proteins

on different support materials were evaluated [see **Chapter II.3.1**] and PHB granules were identified as promising degradable biopolymers for enzyme immobilization and scaffolding. Thus, PHB granules were evaluated for functionalization in *R. capsulatus* for the first time, providing an alternative to already existing immobilization platforms [see **Chapter II.3.2**]. Since the detection of successfully immobilized target proteins to a matrix has been very laborious so far, the next step was the implementation of the split GFP reporter as an easily visualizable "click & play" linker module for the functionalization of those biopolymers in the non-native PHB producer *E. coli* [see **Chapter II.3.3**].

Consequently, new expression and *in vivo* immobilization techniques for Gram-negative bacteria including the alternative phototrophic production host *R. capsulatus* were developed and evaluated. The resulting production tools offer special properties for successful implementation of heterologous terpene biosynthesis.

II. RESULTS

The following section is composed of eight manuscripts, which have either been published or are about to be published in peer-reviewed journals. The presented work is based on joint publications in the context of the "*CKB – CLIB Kompetenzzentrum Biotechnologie*". In this surrounding, I would like to mention Dr. Fabienne Knapp (nèe Hilgers, Institute of Molecular Enzyme Technology, BioSC project CombiCom) for the fruitful collaboration. The own contribution to the respective manuscript is indicated on the first page of each document.

II.1 *R. capsulatus* as a platform organism for terpene production

II.1.1 Oxygenic and anoxygenic phototrophic bacteria as chassis organisms

PUBLICATION I

Engineering phototrophic bacteria for the production of terpenoids

Oliver Klaus[1]*, Fabienne Hilgers[1]*, Andreas Nakielski[2], Dennis Hasenklever[2], Karl-Erich Jaeger[1,3], Ilka Maria Axmann[2#], Thomas Drepper[1#]

[1]Institute of Molecular Enzyme Technology, Heinrich Heine University Düsseldorf, Forschungszentrum Jülich, 52425 Jülich, Germany

[2]Institute for Synthetic Microbiology, Heinrich Heine University Düsseldorf, 40225 Düsseldorf, Germany

[3]Institute of Bio- and Geosciences IBG-1: Biotechnology, Forschungszentrum Jülich GmbH, 52425 Jülich, Germany

* These authors contributed equally

[#] Corresponding authors

Status: published

Current Opinion in Biotechnology,

2022, 10, 77:102764

https://doi.org/10.1016/j.copbio.2022.102764

Own contribution:

Conceptualization, Writing parts of the manuscript – (Introduction, Terpenoid production in anoxygenic phototrophic bacteria, Effects of light on terpenoid production, Conclusion and outlook)

Available online at www.sciencedirect.com

ScienceDirect

Current Opinion in Biotechnology

Engineering phototrophic bacteria for the production of terpenoids

Oliver Klaus[1,*], Fabienne Hilgers[1,*], Andreas Nakielski[2], Dennis Hasenklever[2], Karl-Erich Jaeger[1,3], Ilka M Axmann[2] and Thomas Drepper[1]

With more than 80 000 compounds, terpenoids represent one of the largest classes of secondary metabolites naturally produced by various plants and other organisms. Owing to the tremendous structural diversity, they offer a wide range of properties relevant for biotechnological and pharmaceutical applications. In this context, heterologous terpenoid production in engineered microbial hosts represents an often cost-effective and eco-friendly way to make these valuable compounds industrially available. This review provides an overview of current strategies to employ and engineer oxygenic and anoxygenic phototrophic bacteria as alternative cell factories for sustainable terpenoid production. Besides terpenoid pathway engineering, the effects of different illumination strategies on terpenoid photoproduction are key elements in the latest studies.

Addresses
[1] Institute of Molecular Enzyme Technology, Heinrich Heine University Düsseldorf, Forschungszentrum Jülich GmbH, 52428 Jülich, Germany
[2] Institute for Synthetic Microbiology, Heinrich Heine University Düsseldorf, 40225 Düsseldorf, Germany
[3] Institute of Bio, and Geosciences IBG-1: Biotechnology, Forschungszentrum Jülich GmbH, 52428 Jülich, Germany

Corresponding authors: Ilka M Axmann (Ilka.Axmann@hhu.de), Thomas Drepper (t.drepper@fz-juelich.de)
[*] These authors contributed equally.

Current Opinion in Biotechnology 2022, **77**:102764

This review comes from a themed issue on **Pharmaceutical Biotechnology**

Edited by **Lars Regestein** and **Anita Loeschcke**

https://doi.org/10.1016/j.copbio.2022.102764

Introduction

Terpenoids, also known as isoprenoids, can be found in all kingdoms of life [1,2]. They are the largest class of plant secondary metabolites and primary constituents of essential oils in plants and flowers [3,4]. Many terpenoids have pharmacological bioactivities such as anticancer (e.g. taxol), antimalarial (artemisinin), as well as antimicrobial, anti-inflammatory [5], and anticholinesterase [6] properties suitable for treating various infections and also Alzheimer's disease. Because of the structural diversity and broad spectrum of natural functions, terpenoids further play an increasingly important role as ingredients for food, feed, cosmetics, and biofuels [7,8]. Terpenoids basically consist of one to eight isoprene units (C_5) and are accordingly subdivided into hemi- (C_5), mono- (C_{10}), sesqui- (C_{15}), di- (C_{20}), tri- (C_{30}), and tetra- (C_{40}) terpenoids [9]. The two C_5 isoprene units, isopentenyl pyrophosphate (IPP) and dimethylallyl pyrophosphate (DMAPP), are considered as the starting points of terpenoid biosynthesis, which are subsequently connected via repeated head-to-tail condensation. IPP and DMAPP can both be formed by two independent biosynthetic pathways: the 2-C-methylerythritol-4-phosphate (MEP) pathway occurs in plant plastids and algae as well as bacteria, and converts glyceraldehyde-3-phosphate (GAP) and pyruvate into IPP and DMAPP [10]. In contrast, the mevalonate (MVA) pathway uses acetyl-CoA as a precursor molecule and is mainly found in archaea and the cytosol of eukaryotes [11].

Since terpenoids are usually extracted from plant-based material, which results in considerable costs and material expenditure, the research focus is shifting to biotechnological production using versatile and accordingly engineered microbes [12–14]. In addition to the two well-established microbial production chassis *Escherichia coli* and *Saccharomyces cerevisiae* [15], phototrophic organisms offer unique benefits for sustainable production (Figure 1). Because phototrophic organisms naturally produce terpenoids such as carotenoids and other photopigments at high levels [16,17], they provide relevant building blocks for heterologous terpenoid syntheses. In addition, they form an extensive system of intracellular photosynthetic membranes (either as thylakoid membranes or intracytoplasmic membrane vesicles) that particularly suits them for hosting membrane-embedded enzymes and storage of hydrophobic compounds [18,19]. Furthermore, phototrophs can obtain energy from light and utilize atmospheric CO_2 as a carbon source, thus making them especially applicable for sustainable manufacturing concepts.

Figure 1

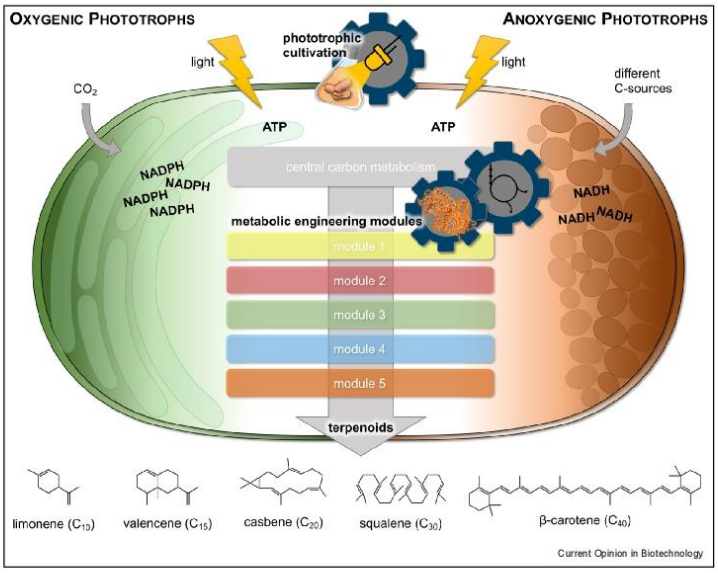

Overview of different concepts for implementing and improving terpenoid production in phototrophic bacteria. Based on the light-driven formation of energy carriers and redox equivalents as well as the central carbon metabolism, oxygenic and anoxygenic phototrophic bacteria can be engineered to produce plant terpenoids. The shown gear wheels symbolize frequently applied strategies to facilitate terpenoid formation in these hosts, including the adjustment of illumination conditions as well as the modular combination of metabolic and enzyme engineering concepts (module 1–5) that will be outlined in the following sections. The lower part of the figure shows exemplary structures for the main terpenoid classes.

In this review, we provide insights into the current state of research on terpenoid production in oxygenic and anoxygenic phototrophic bacteria, including cyanobacteria and purple nonsulfur bacteria. Furthermore, we discuss the effects of different illumination conditions on terpenoid production in phototrophic bacteria. We outline strategies on how this group of new microbial cell factories can contribute to future sustainable production and pharmaceutical applications.

Phototrophic bacteria as promising biotechnological production chassis

All phototrophic bacteria share the ability to harness light as an energy source for their metabolism and cell growth. In the last decade, they are increasingly applied as solar-powered microbial chassis to produce biofuels, recombinant proteins, and natural compounds. Photosynthetic bacteria can be subdivided into two groups, namely oxygenic and anoxygenic phototrophs, depending on their type of photosynthesis. Like plants, oxygenic phototrophs such as the cyanobacteria *Synechocystis* or *Synechococcus* harbor two light-absorbing photosystems and produce chemical energy, redox equivalents (i.e. ATP and NADPH), and molecular oxygen during photosynthesis using H_2O as an electron donor. In contrast, anoxygenic phototrophs such as the genera *Rhodobacter* and *Rhodopseudomonas*, which belong to the group of purple nonsulfur phototrophic bacteria, perform anoxygenic photosynthesis using only one photosystem and more reduced molecules than H_2O as electron donors.

Each group offers unique benefits valuable for diverse biotechnological applications. Oxygenic phototrophs generate high amounts of NADPH and thus efficiently fix CO_2 in the Calvin cycle, thereby offering efficient coupling of CO_2 reduction with bacterial photoproduction processes [20••]. Anoxygenic phototrophs exhibit a high metabolic flexibility as they prefer to grow under photoheterotrophic conditions using various organic compounds as carbon and electron sources. Therefore, anoxygenic phototrophic bacteria are particularly suited

Figure 2

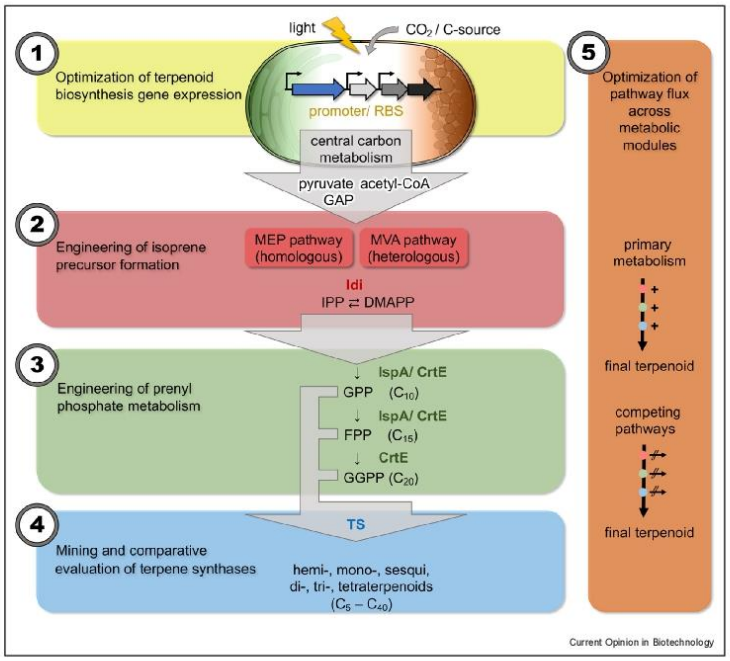

Strategies for modular terpenoid pathway engineering in photosynthetic bacteria. In most cases, modular engineering was applied to improve the precursor supply and metabolic flux of intermediates from the central carbon metabolism to the final terpenoid. These approaches also involve downregulation or elimination of competing metabolic pathways such as the biosynthesis of hopanoids, polyhydroxybutyrate, and carotenoids. GAP: glyceraldehyde 3-phosphate, MEP: 2-C-methylerythritol 4-phosphate pathway, MVA: mevalonate pathway, IPP: isopentenyl pyrophosphate, DMAPP: dimethylallyl pyrophosphate, Idi: IPP isomerase, GPP: geranyl pyrophosphate, FPP: farnesyl pyrophosphate, glyceraldehyde-3-phosphate, GGPP: geranylgeranyl pyrophosphate, IspA: FPP synthase, CrtE: geranylgeranyl pyrophosphate synthase, TS: terpene synthase.

for establishing production processes involving resource recovery from organic waste streams [21]. In addition, many anoxygenic phototrophs can grow photoautotrophically by performing light-dependent CO_2 fixation but can also switch to chemoautotrophic or chemoheterotrophic growth modes. Furthermore, oxygenic and anoxygenic phototrophic bacteria are valuable production platforms for industrially and pharmaceutically relevant terpenoids, including cycloartenol and lupeol [22], pinene [23,24••], squalene [25–27], astaxanthin [28], bisabolol [29••], β-caryophyllene [30], as well as the artemisinin precursor amorphadiene [31,32]. Similar to nonphototrophic microbial hosts, the production of terpenoids can also be optimized in phototrophic bacteria by engineering the respective biosynthetic pathways at different levels. Most commonly, various metabolic engineering strategies are applied and combined in a modular way for enhancing the precursor supply and terpenoid formation (hereafter referred to as *metabolic engineering modules*, modules 1–5, Figure 2).

Especially for phototrophic bacteria, further engineering aspects such as optimization of the illumination strategy are important to consider. In the following, metabolic engineering modules for the terpenoid production in cyanobacteria and purple nonsulfur bacteria as prominent representatives of the two groups — oxygenic and anoxygenic phototrophic bacteria — are summarized (Table 1).

Terpenoid production in oxygenic phototrophic bacteria

The cyanobacteria *Synechocystis* sp. PCC 6803, *Synechococcus elongatus* PCC 7942, and *Synechococcus* sp. PCC 7002 have emerged as very promising hosts for terpenoid production in recent years [33]. These

Table 1

Terpenoids produced by phototrophic bacteria.

					Module					
Organism		Terpenoid class	Terpenoid	Titer/specific yield[a]	1	2	3	4	5	Ref.
Aerobic phototrophs	*Synechocystis* sp. PCC 6803	Hemiterpenoid C_5	Isoprene	0.3 mg $gDCW^{-1}$	–	x	x	–	–	[39]
				0.2 mg L^{-1}	–	x	–	–	x	[52]
		Monoterpenoid C_{10}	Limonene	6.7 mg L^{-1}	–	–	x	x	x	[53]
		Sesquiterpenoid C_{15}	α-bisabolene	186 mg L^{-1}[b]	–	x	x	–	–	[38]
				22.2 mg L^{-1}	x	–	x	–	–	[34]
				179.4 mg L^{-1}[b]	–	–	–	–	–	[29••]
			α-bisabolol	96.3 mg L^{-1}[b]	–	–	–	–	–	
			Patchoulol	17.3 mg L^{-1}[b]	–	–	–	–	–	
				0.2 mg L^{-1}	–	–	–	–	–	[54]
			Valencene	17.6 mg L^{-1}	–	–	x	–	x	[35]
		Triterpenoid C_{30}	Cycloartenol	1.1 mg L^{-1}	–	–	x	–	x	[22]
			Lupeol	0.3 mg $gDCW^{-1}$	–	–	x	–	x	
			Hydroxy-/marnerol	Not quantified	–	–	x	–	x	
			2,3-oxidosqualene	1.1 mg L^{-1}	–	–	x	–	x	
			Squalene	5.1 mg L^{-1}	–	–	x	–	x	
				5.1 mg L^{-1}	–	x	x	–	x	[26]
				0.7 mg L^{-1} OD_{750}^{-1}	–	–	–	–	x	[55]
	Synechococcus elongatus PCC 7942	Hemiterpenoid C_5	Isoprene	1260 mg L^{-1}	x	x	–	x	x	[20••]
		Monoterpenoid C_{10}	Limonene	21.0 mg L^{-1}	–	x	–	–	x	[36]
				0.9 mg L^{-1} OD_{730}^{-1} d^{-1}	x	x	x	–	–	[56]
				19 mg L^{-1}	x	x	x	–	x	[40•]
		Sesquiterpenoid C_{15}	Amorphadiene	19.8 mg L^{-1}	–	x	x	–	–	[32]
			α-farnesene	5.0 mg L^{-1}	–	x	x	x	x	[57]
				4.6 mg L^{-1}	–	x	x	x	–	[58]
		Triterpenoid C_{30}	Squalene	12 mg L^{-1} OD_{730}^{-1}	x	x	x	–	x	[25]
				9.5 mg L^{-1} OD_{730}^{-1}	–	x	x	–	x	[59•]
				5 mg L^{-1} OD_{730}^{-1}	–	x	x	–	–	[32]
				1.9 mg L^{-1} OD_{730}^{-1}	–	x	x	–	x	[37]
	Synechococcus sp. PCC 7002	Monoterpenoid C_{10}	Limonene	4 mg L^{-1}	–	–	–	–	x	[41]
			Pinene	1.5 mg L^{-1}	–	–	–	–	–	[23]
		Sesquiterpenoid C_{15}	α-bisabolene	0.6 mg L^{-1}	–	–	–	–	x	[60]
		Tetraterpenoid C_{40}	Astaxanthin	3 mg $gDCW^{-1}$	–	–	–	–	–	[28]
Anaerobic phototrophs	*Rhodobacter capsulatus*	Sesquiterpenoid C_{15}	Bisabolene	9800 mg L^{-1}	x	x	x	–	x	[46••]
			β-caryophyllene	130 mg L^{-1}	–	x	x	–	–	[30]
			Patchoulol	24 mg L^{-1}	–	x	x	–	–	[49•]
			Valencene	18 mg L^{-1}	–	x	x	–	–	
		Diterpenoid C_{20}	Casbene	Minor amounts	–	x	–	–	–	[27]
		Triterpenoid C_{30}	Cycloartenol	1.1 mg L^{-1}	–	x	–	x	x	[61]
				0.3 mg L^{-1}	–	–	x	–	–	[22]
			Lupeol (oxide)	Minor amounts	–	–	x	–	–	
			2,3-oxidosqualene	0.3 mg L^{-1}	–	–	x	–	–	
			Squalene	8.24 mg L^{-1}	–	–	x	–	–	
				90 mg L^{-1}	–	x	–	x	–	[27]
			Botryococcene (C_{34})	110 mg L^{-1}	–	x	x	–	–	[44]
		Tetraterpenoid C_{40}	β-carotene	30 mg L^{-1}	–	x	–	–	–	[27]
	Rhodobacter sphaeroides	Monoterpenoid C_{10}	Pinene	0.5 mg L^{-1}	x	x	–	–	x	[24••]
		Sesquiterpenoid C_{15}	Amorphadiene	60 mg L^{-1}	–	x	–	–	–	[31]
			Farnesol	40.5 mg L^{-1}	–	–	–	x	x	[62]
				55.1 mg L^{-1}	–	–	–	–	x	[47]
		Tetraterpenoid C_{40}	β-carotene	14.9 mg $gDCW^{-1}$	x	x	–	–	x	[63]
			Lycopene	150.2 mg L^{-1}	x	–	x	–	x	[64]
		C_{59}	Coenzyme Q_{10}	185.5 mg L^{-1}	–	–	–	–	x	[47]
	Rhodopseudomonas palustris	Triterpenoid C_{30}	Squalene	23.3 mg L^{-1}	–	x	–	–	x	[51]
				15.8 mg $gDCW^{-1}$	–	x	–	–	x	[65]
		Tetraterpenoid C_{40}	Canthaxanthin	4.7 mg L^{-1}	–	–	x	–	x	[66]
			β-carotene	0.8 mg L^{-1}	–	–	x	–	x	
			Lycopene	7.2 mg L^{-1}	–	–	–	–	–	
		C_{59}	Coenzyme Q_{10}	8.2 mg $gDCW^{-1}$	–	x	x	–	x	[45]

[a] All values were rounded and converted to mg L^{-1} or mg $gDCW^{-1}$.
[b] High-density cultivation (CellDEG).

unicellular bacteria naturally produce terpenoids as part of their photosynthetic machinery, including carotenoids, hopanoids, and the phytol tail of chlorophyll [17].

In *Synechocystis* sp. PCC 6803, a linear correlation between the expression level of a heterologous bisabolene synthase and the product yield was observed, suggesting the highest possible terpenoid yield can be achieved through by optimizing the expression of the terpenoid synthase (TS). This assumption was confirmed for bisabolene production, where codon optimization and testing of different ribosome-binding sites (RBS) led to a strain with a bisabolene titer up to 7.8 mg L^{-1}, an almost 10-fold increase compared with codon optimization alone [34] (①). TS genes can be expressed using native promoters, such as P_{cpcB} for pinene production in *Synechococcus* sp. PCC 7002 [23]. Alternatively, synthetic inducible promoters, such as P_{petE} or P_{rhaT} controlling the expression through exogenous inducer molecules, can be useful, which led to the formation of α-bisabolene and valencene in *Synechocystis* sp. PCC 6803 [29••,35]. Generally, studies indicate that regardless of whether inducible or constitutive promoters are used, high TS expression is required to create a strong carbon sink and induce a metabolic 'pull' toward the target compound [36].

Moreover, overexpressing rate-limiting enzymes to enhance precursor supply represents another common metabolic engineering module (②). The overexpression of 1-deoxy-D-xylulose 5-phosphate synthase and isopentenyl-pyrophosphate isomerase genes (*dxs* and *idi*) was used in several approaches to increase titers of squalene, α-bisabolene, and isoprene, with a synergistic effect observable upon overexpression of both genes [20••,26,37,38]. Furthermore, (*E*)-4-hydroxy-3-methyl-but-2-enyl pyrophosphate synthase (IspG) was also identified as a bottleneck. Thus, increased isoprene production could be achieved through simultaneous overexpression of *dxs*, *idi*, and *ispG* [20••]. Another study introduced the heterologous MVA pathway into *Synechocystis* sp. PCC 6803, but while increasing isoprene production, the final isoprene titer was significantly lower than the titers achieved by engineering the native MEP pathway [39].

To increase farnesyl pyrophosphate (FPP) availability (③), farnesyl pyrophosphate synthase (*ispA*) from *E. coli* is commonly overexpressed, leading to improved squalene, α-bisabolene, and valencene titers in several engineered strains [26,35,37,38]. In *Synechocystis* sp. PCC 6803 and several other cyanobacteria, squalene is naturally further converted to hopanoids. Therefore, the knockout of the squalene–hopene cyclase gene (Δ*shc*) led to an accumulation of the desired squalene product, which could be further increased through other metabolic engineering modules (②, ③ & ⑤) [26]. Deletion of the squalene synthase gene (Δ*sqs*) of *Synechocystis* sp. PCC 6803 reduced the competition for FPP, leading to a 1.5-fold increased valencene product titer [35]. Afterward, the overexpression of *ispA* was combined with a CRISPRi knockdown of the native GGPP synthase *crtE* to direct metabolite flow toward FPP to increase valencene production (③ & ⑤). This strategy led to a 3.7-fold increase in production compared with the Δ*sqs* knockout strain only expressing the valencene synthase [35]. For this approach, the distribution of terpenoid precursors between the essential natural photopigments derived from GGPP and the product of interest needs to be carefully balanced to ensure high product titers while keeping the photosynthetic machinery of the cell functional.

Furthermore, the identification of an appropriate terpene synthase can be key to improve product yields [20••]. Three isoprene synthases from different plant species were compared regarding their potential for isoprene production in *S. elongatus* PCC 7942 (④), showing significant differences between their enzyme activities [20••].

To increase the metabolic flux through the terpenoid pathway (⑤), terpene synthases were fused to enzymes providing their respective prenyl pyrophosphate precursor. For example, an isoprene synthase, a limonene synthase, and a valencene synthase were fused to Idi [20••], a geranyl pyrophosphate (GPP) synthase [36] and IspA [35], respectively, resulting in improved product yields. Apart from TS selection and pathway optimization, other targets were found to extend the potential for enhancing terpenoid biosynthesis in cyanobacteria [40•,41]. The overexpression of the native essential sigma factor *rpoD* in *S. elongatus* PCC 7942 resulted in enhanced light absorption, photosynthetic efficiency, and higher carbon fixation, leading to an approximately 1.7-fold increase in specific limonene productivity [40•]. Consequently, the change of σ70 RNA polymerase-dependent gene expression groups might have a strong potential to further enhance flux through terpenoid biosynthesis [40•].

By combining metabolic engineering modules ①, ②, ④, and ⑤ for isoprene production, Gao and colleagues impressively demonstrated production of 1.26 g L^{-1} isoprene in *S. elongatus* PCC 7942 after incubation over 21 days in a photobioreactor, resulting in 65% of fixed carbon being directed toward isoprene during the stationary phase, marking the highest production using cyanobacteria to date [20••].

Terpenoid production in anoxygenic phototrophic bacteria

Anoxygenic phototrophic bacteria include purple nonsulfur, purple sulfur, green nonsulfur, and green sulfur bacteria [42]. In recent years, especially the first group

has emerged as a very promising platform to produce terpenoids with the most prominent representatives *Rhodobacter capsulatus*, *Rhodobacter sphaeroides*, and *Rhodopseudomonas palustris*. In these bacteria, the formation of photopigments and photosynthetic membranes is already induced under oxygen limitation [43]. Thus, their metabolic and morphological advantages for terpenoid production can be exploited even in the absence of light.

In *Rhodobacter* and *Rhodopseudomonas*, different heterologous and species-specific promoters were applied to express terpenoid biosynthesis genes (①). The P_{lac} promoter from *E. coli* and its variants (e.g. P_{tac} and P_{trc}) was frequently used either as constitutive (i.e. in the absence of the *lac* repressor) or inducible promoters [24••,44–47]. In addition, several strong promoters from *Rhodobacter* and other phototrophic bacteria such as P_{puf}, P_{puc}, and P_{crtE} (derived from the respective photosynthesis genes) and the promoter of the nitrogenase structural genes (P_{nif}) were broadly applied [31,46••,48]. Furthermore, a strong RBS was shown to improve the expression of pathway genes [24••].

The evaluation of modular metabolic engineering modules first focused on increasing the supply of IPP, DMAPP, and FPP not only by overproducing a set of rate-limiting enzymes of the MEP pathway (Dxs, Idi, and IspA) but also by co-expression of genes encoding all enzymes of the heterologous MVA pathway (② & ③). By differentially combining components of the isoprene and prenyl phosphate module, the heterologous production level of patchoulol, valencene, β-caryophyllene, casbene, squalene, and β-carotene could be significantly increased under phototrophic growth conditions [27,30,49•]. Similar results were achieved for α-bisabolene [46••] and amorphadiene [50], as well as squalene and botryococcene [44] when *Rhodobacter* was grown under chemoheterotrophic conditions.

In some studies, different terpene synthases were comparatively evaluated (④) to improve final terpenoid yields. For example, in the case of squalene, the activity of five different synthases was compared. By co-expression of the synthase from *Methylococcus capsulatus* with *ispA*, up to 90 mg L^{-1} squalene could be achieved [27]. Finally, the flux of intermediates across complete recombinant terpenoid pathways (⑤) was further optimized either by suppressing competing cellular pathways or by the fusion of terpene synthases with respective enzymes of the prenyl phosphate module. For example, inactivation of the polyhydroxybutyrate pathway in a *R. sphaeroides* strain expressing the MVA pathway genes resulted in an improved formation of amorphadiene [50]. To optimize the bisabolene production in *R. capsulatus*, increased NADPH availability and optimization of the central carbon metabolism by suppressing competing-side pathways in combination with promoter screening resulted in almost 10 g L^{-1} bisabolene [46••].

In most cases, however, the combination of multiple metabolic engineering modules resulted in the highest product formation. For example, pinene titers could be increased up to ~540 µg L^{-1} in *R. sphaeroides* by RBS optimization (①), overexpression of rate-limiting enzymes (② & ③), and a direct enzyme fusion consisting of a pinene synthase and a heterologous GPP synthase (⑤) [24••]. Here, all enzymes involved in the MEP pathway, namely Dxs, Dxr, IspD, IspE, IspF, IspG, IspH, and Idi were examined individually for their influence on final terpene titers, thus providing a detailed insight into flux bottlenecks in this module. In two other studies, Wang and coworkers could increase squalene and coenzyme Q_{10} (Co-Q_{10}) product titers in *R. palustris* by co-expression of *dps* and *ubiA* (for Co-Q_{10}) or *hpnD* (for squalene) with *dxs* (②). Additionally, the carotenoid and hopanoid pathways were blocked by deleting *crtB* and *shc* (⑤), resulting in improved Co-Q_{10} and squalene titers [45,51]. For further enhancing squalene synthesis, a fusion enzyme of the FPP synthase and the follow-up squalene pathway enzyme HpnD was created, to channel FPP toward the triterpene pathway and improve conversion rates (⑤).

Effects of light on terpenoid production

Besides the above-described 'classical' engineering approaches, types of illumination conditions varying in (i) intensity, (ii) applied light–dark cycles, and (iii) the emission spectrum were evaluated for improving phototropic growth and terpenoid production (Figure 3). Although some cyanobacteria are able to grow heterotrophically, photoautotrophic growth is preferred for terpenoid production as it was shown to yield higher patchoulol titers in *Synechocystis* sp. PCC 6803 compared with mixotrophic growth on glucose [54]. Therefore, optimization of illumination conditions can contribute to enhance terpenoid biosynthesis in cyanobacteria. Here, light intensity is the main factor limiting growth and terpenoid production. *Synechocystis* sp. PCC 6803 grown under high-light conditions (100 µE m^{-2} s^{-1}) reached 2-fold higher patchoulol titers than under low-light conditions (20 µE m^{-2} s^{-1}) [54]. Furthermore, applying a 12-h:12-h light–dark cycle over a 10-day cultivation had a beneficial effect on α-bisabolene productivity in *Synechocystis* sp. PCC 6803 [34].

First studies of the effect of illumination conditions on terpene production in *Rhodopseudomonas* revealed that different light intensities and light–dark cycles also influence terpenoid biosynthesis in anoxygenic phototrophic bacteria. By applying increasing light intensities for phototrophic cultivation (2000–5000 lux), it could be demonstrated that moderate- to high-light conditions

Figure 3

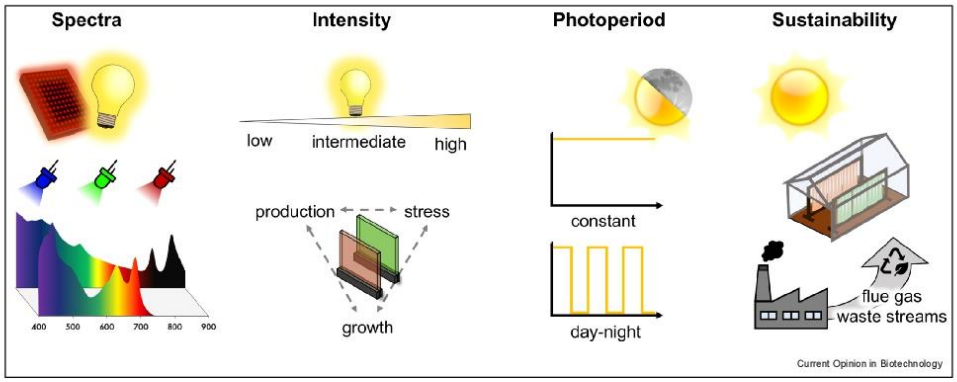

Various aspects of the applied illumination conditions, including light spectra and intensities as well as light–dark cycles, can be investigated to establish new, sustainable terpenoid photoproduction processes with phototrophic bacteria.

(i.e. 3000–4000 lux) led to elevated carotenoid levels in *Rhodopseudomonas faecalis* [67]. In addition, *Rhodopseudomonas* sp. grown under a 12-h:12-h light–dark cycle showed an increased carotenoid production, whereas the highest Co-Q_{10} levels were observed at shorter cycles (3 h:3 h) [68]. The importance of the light-emission spectrum for the biosynthesis of nonnative β-caryophyllene was initially analyzed in *R. capsulatus* [30]. Here, the use of infrared-light LED with a maximum emission wavelength of 850 nm, suitable for direct irradiation of bacteriochlorophyll *a*, instead of full-spectrum light, increased the product titer 1.5-fold.

Conclusion and outlook

In the past decade, complex metabolic engineering strategies and concepts could successfully be transferred from well-established heterotrophic microbes to phototrophic bacteria, thereby uncovering their high potential to synthesize biotechnologically and pharmaceutically relevant terpenoids. In some cases, yields were already high enough to bring terpenoids produced by phototrophic bacteria to market (e.g. the *R. sphaeroides*-based production of valencene and nootkatone by the company Isobionics, now BASF) [8]. However, when grown phototrophically, the cultivation of cyanobacteria and purple nonsulfur bacteria suffers from self-shading effects and CO_2 availability, resulting in limited cell growth or product yields. Therefore, innovative high-density cultivation systems such as the CellDEG system, which utilizes a CO_2-permeable membrane for bubble-free aeration, are promising alternative photobioreactors to further optimize illumination conditions and CO_2 supply and thereby facilitate the formation of biomass and natural compounds [29••,33,69]. In this context, it is worth mentioning that oxygenic and anoxygenic phototrophic bacteria have evolved differently to thrive under distinct illumination conditions. Thus, it can be crucial to optimize all characteristics of light (i.e. the intensity and spectrum as well as the applied light–dark cycles) to maximize individual terpenoid production capacities of the chosen production host and to identify the optimal ratio between cell growth, productivity, and light-mediated stress (Figure 3).

Recent progress in CRISPR–Cas-based genome editing and gene regulation facilitated multifactorial engineering of various phototrophic production strains. For example, dCas12-mediated CRISPRi gene knockdown was applied for enhanced pyruvate availability and squalene production in *S. elongatus* PCC 7942 [59•]. In addition, genes encoding for the competing polyhydroxybutyrate pathway were deleted in *R. sphaeroides* with CRISPR–Cas9 to improve amorphadiene production [50]. Furthermore, transposon Tn5-mediated chromosomal integration of larger gene clusters allowed more complex modifications of the terpenoid pathway [70•,71]. These synthetic biology tools, together with genome-scale modeling of metabolic networks (e.g. described in [72,73]) and ^{13}C flux analyses of the terpenoid metabolism [41,70•] will offer a deeper understanding and better control of these complex metabolic networks. Based on this progress, design–build–test–learn concepts can be applied [74] and will facilitate the development of innovative biotechnological and biomedical applications for phototrophic bacteria in the near future. For example, the efficient coupling of alternative C-sources from industrial waste streams (e.g. flue gas, organic compounds from agricultural and food waste) or

lignocellulose-derived substrates [37,42] with terpenoid production could be key for the development of sustainable and bioeconomically feasible terpenoid production processes. Here, the flexibility and robustness of such processes could be further improved by combining diverging nutrient-recovery capacities of different (phototrophic) microbes via cocultivation.

Finally, it should be noted that phototrophic bacteria of the genus *Rhodobacter* offer additional beneficial properties, including the formation of nontoxic lipopolysaccharides and the ability to colonize solid tumors, making these bacteria suitable for future biomedical applications [75]. On the other hand, cyanobacteria such as the edible *Arthrospira platensis* (spirulina) proved already-high potential for oral delivery of protein therapeutics [76]. Thus, phototrophic bacteria might be engineered as platform organisms for the *in situ* delivery of terpenoids with anticancer and other pharmaceutical activities.

Conflict of interest statement

The authors declare no conflict of interest.

Acknowledgements

This work was supported by grants from (i) the European Regional Development Fund (ERDF, 34. EFRE-0300096) within the CLIB-Kompetenzzentrum Biotechnologie (CKB) and (ii) the Bioeconomy Science Center. The scientific activities of the Bioeconomy Science Center were financially supported by the Ministry of Culture and Science of the German federal state of North Rhine-Westphalia MKW within the framework of the NRW Strategieprojekt BioSC (no. 313/323-400-00213). The authors would like to thank Dr. Achim Heck for the helpful comments on the paper.

References and recommended reading

Papers of particular interest, published within the period of review, have been highlighted as:

- • of special interest
- •• of outstanding interest

1. Gershenzon J, Dudareva N: **The function of terpene natural products in the natural world**. *Nat Chem Biol* 2007, **3**:408-414.
2. Christianson DW: **Structural and chemical biology of terpenoid cyclases**. *Chem Rev* 2017, **117**:11570-11648.
3. Pichersky E, Raguso RA: **Why do plants produce so many terpenoid compounds?** *N Phytol* 2018, **220**:692-702.
4. Cheng AX, Lou YG, Mao YB, Lu S, Wang LJ, Chen XY: **Plant terpenoids: biosynthesis and ecological functions**. *J Integr Plant Biol* 2007, **49**:179-186.
5. Miranda R de S, Jesus B da SM, Silva Luiz SR, Viana CB, Adão Malafaia CR, Figueiredo F de S, Carvalho T dos SC, Silva ML, Londero VS, Costa-Silva TA, *et al.*: **Antiinflammatory activity of natural triterpenes—An overview from 2006 to 2021**. *Phytother Res* 2022, **36**:1459-1506.
6. Min SLS, Liew SY, Chear NJY, Goh BH, Tan WN, Khaw KY: **Plant terpenoids as the promising source of cholinesterase inhibitors for anti-AD therapy**. *Biology* 2022, **11**:307.
7. Serra S: **Recent advances in the synthesis of carotenoid-derived flavours and fragrances**. *Molecules* 2015, **20**:12817-12840.
8. Schempp FM, Drummond L, Buchhaupt M, Schrader J: **Microbial cell factories for the production of terpenoid flavor and fragrance compounds**. *J Agric Food Chem* 2018, **66**:2247-2258.
9. Ruzicka L: **The isoprene rule and the biogenesis of terpenic compounds**. *Experientia* 1953, **9**:357-367.
10. Frank A, Groll M: **The methylerythritol phosphate pathway to isoprenoids**. *Chem Rev* 2017, **117**:5675-5703.
11. Lombard J, Moreira D: **Origins and early evolution of the mevalonate pathway of isoprenoid biosynthesis in the three domains of life**. *Mol Biol Evol* 2011, **28**:87-99.
12. Pham J v, Yilma MA, Feliz A, Majid MT, Maffetone N, Walker JR, Kim E, Cho HJ, Reynolds JM, Song MC, *et al.*: **A review of the microbial production of bioactive natural products and biologics**. *Front Microbiol* 2019, **10**:1404.
13. Marienhagen J, Bott M: **Metabolic engineering of microorganisms for the synthesis of plant natural products**. *J Biotechnol* 2013, **163**:166-178.
14. Cravens A, Payne J, Smolke CD: **Synthetic biology strategies for microbial biosynthesis of plant natural products**. *Nat Commun* 2019, **10**:2142.
15. Moser S, Pichler H: **Identifying and engineering the ideal microbial terpenoid production host**. *Appl Microbiol Biotechnol* 2019, **103**:5501-5516.
16. Heck A, Drepper T: **Engineering photosynthetic α-proteobacteria for the production of recombinant proteins and terpenoids**. Modern Topics in the Phototrophic Prokaryotes. Springer International Publishing; 2017:395-425.
17. Mills LA, McCormick AJ, Lea-Smith DJ: **Current knowledge and recent advances in understanding metabolism of the model cyanobacterium *Synechocystis* sp. PCC 6803**. *Biosci Rep* 2020, **40**:BSR20193325.
18. Drews G: **The Intracytoplasmic membranes of purple bacteria - Assembly of energy-transducing complexes**. *J Mol Microbiol Biotechnol* 2013, **23**:35-47.
19. Torrado A, Connabeer HM, Röttig A, Pratt N, Baylay AJ, Terry MJ, Moore CM, Bibby TS: **Directing cyanobacterial photosynthesis in a cytochrome *c* oxidase mutant using a heterologous electron sink**. *Plant Physiol* 2022,kiac203, https://doi.org/10.1093/plphys/kiac203
20. •• Gao X, Gao F, Liu D, Zhang H, Nie X, Yang C: **Engineering the methylerythritol phosphate pathway in cyanobacteria for photosynthetic isoprene production from CO_2**. *Energy Environ Sci* 2016, **9**:1400-1411.
This study combined various metabolic engineering techniques such as promoter screening, codon optimization, selection of the best performing isoprene synthase, increasing precursor supply and designing fusion proteins to reach g/L scale isoprene production in *Synechococcus elongatus* PCC 7942. By identifying metabolite bottlenecks via a ^{13}C-isotope labeling experiment, the knowledge of cyanobacterial terpenoid metabolism was considerably advanced.
21. Stephens S, Mahadevan R, Allen DG: **Engineering photosynthetic bioprocesses for sustainable chemical production: a review**. *Front Bioeng Biotechnol* 2021, **8**:610723.
22. Loeschcke A, Dienst D, Wewer V, Hage-Hülsmann J, Dietsch M, Kranz-Finger S, Hüren V, Metzger S, Urlacher VB, Gigolashvili T, *et al.*: **The photosynthetic bacteria *Rhodobacter capsulatus* and *Synechocystis* sp. PCC 6803 as new hosts for cyclic plant triterpene biosynthesis**. *PLoS One* 2017, **12**:e0189816.
23. Yang R, Zhu L, Li T, Zhu L, Ye Z, Zhang D: **Photosynthetic conversion of CO_2 into pinene using engineered *Synechococcus* sp. PCC 7002**. *Front Bioeng Biotechnol* 2021, **9**:779437.
24. •• Wu X, Ma G, Liu C, Qiu X, Min L, Kuang J, Zhu L: **Biosynthesis of pinene in purple non-sulfur photosynthetic bacteria**. *Microb Cell Fact* 2021, **20**:101.
This study evaluated the effect of overexpressing each enzyme involved in the MEP pathway separately in combination with a fusion protein consisting of a GPP synthase and a pinene synthase in *R. sphaeroides*.

25. Choi SY, Wang J-Y, Kwak HS, Lee S-M, Um Y, Kim Y, Sim SJ, Choi J, Woo HM: **Improvement of squalene production from CO_2 in *Synechococcus elongatus* PCC 7942 by metabolic engineering and scalable production in a photobioreactor**. *ACS Synth Biol* 2017, **6**:1289-1295.

26. Pattanaik B, Englund E, Nolte N, Lindberg P: **Introduction of a green algal squalene synthase enhances squalene accumulation in a strain of *Synechocystis* sp. PCC 6803**. *Metab Eng Commun* 2020, **10**:e00125.

27. Hage-Hülsmann J, Klaus O, Linke K, Troost K, Gora L, Hilgers F, Wirtz A, Santiago-Schübel B, Loeschcke A, Jaeger K-E, *et al.*: **Production of C_{20}, C_{30} and C_{40} terpenes in the engineered phototrophic bacterium *Rhodobacter capsulatus***. *J Biotechnol* 2021, **338**:20-30.

28. Hasunuma T, Takaki A, Matsuda M, Kato Y, Vavricka CJ, Kondo A: **Single-stage astaxanthin production enhances the nonmevalonate pathway and photosynthetic central metabolism in *Synechococcus* sp. PCC 7002**. *ACS Synth Biol* 2019, **8**:2701-2709.

29. •• Dienst D, Wichmann J, Mantovani O, Rodrigues JS, Lindberg P: **High density cultivation for efficient sesquiterpenoid biosynthesis in *Synechocystis* sp. PCC 6803**. *Sci Rep* 2020, **10**:5932.

This study evaluated the CellDEG system for the cultivation of cyanobacteria to high cell densities, leading to far higher product titers than achieved previously. By supplying CO_2 through a membrane instead of gas bubbles, the availability of CO_2 to the cells was considerably increased compared to flask culture. This technology has a lot of potential for future applications, as cell densities are one of the limiting factors in cyanobacterial biotechnology.

30. Hilgers F, Habash SS, Loeschcke A, Ackermann YS, Neumann S, Heck A, Klaus O, Hage-Hülsmann J, Grundler FMW, Jaeger K-E, *et al.*: **Heterologous production of β-caryophyllene and evaluation of its activity against plant pathogenic fungi**. *Microorganisms* 2021, **9**:168.

31. Orsi E, Folch PL, Monje-López VT, Fernhout BM, Turcato A, Kengen SWM, Eggink G, Weusthuis RA: **Characterization of heterotrophic growth and sesquiterpene production by *Rhodobacter sphaeroides* on a defined medium**. *J Ind Microbiol Biotechnol* 2019, **46**:1179-1190.

32. Choi SY, Lee HJ, Choi J, Kim J, Sim SJ, Um Y, Kim Y, Lee TS, Keasling JD, Woo HM: **Photosynthetic conversion of CO_2 to farnesyl diphosphate-derived phytochemicals (amorpha-4,11-diene and squalene) by engineered cyanobacteria**. *Biotechnol Biofuels* 2016, **9**:202.

33. Rodrigues JS, Lindberg P: **Engineering cyanobacteria as host organisms for production of terpenes and terpenoids**. Cyanobacteria Biotechnology. Wiley; 2021:267-300.

34. Sebesta J, Peebles CAM: **Improving heterologous protein expression in *Synechocystis* sp. PCC 6803 for alpha-bisabolene production**. *Metab Eng Commun* 2020, **10**:e00117.

35. Dietsch M, Behle A, Westhoff P, Axmann IM: **Metabolic engineering of *Synechocystis* sp. PCC 6803 for the photoproduction of the sesquiterpene valencene**. *Metab Eng Commun* 2021, **13**:e00178.

36. Li M, Long B, Dai SY, Golden JW, Wang X, Yuan JS: **Altered carbon partitioning enhances CO_2 to terpene conversion in cyanobacteria**. *Biodes Res* 2022, **2022**:1-12.

37. Choi SY, Sim SJ, Ko SC, Son J, Lee JS, Lee HJ, Chang WS, Woo HM: **Scalable cultivation of engineered cyanobacteria for squalene production from industrial flue gas in a closed photobioreactor**. *J Agric Food Chem* 2020, **68**:10050-10055.

38. Rodrigues JS, Lindberg P: **Metabolic engineering of *Synechocystis* sp. PCC 6803 for improved bisabolene production**. *Metab Eng Commun* 2021, **12**:e00159.

39. Bentley FK, Zurbriggen A, Melis A: **Heterologous expression of the mevalonic acid pathway in cyanobacteria enhances endogenous carbon partitioning to isoprene**. *Mol Plant* 2014, **7**:71-86.

40. • Shinde S, Singapuri S, Jiang Z, Long B, Wilcox D, Klatt C, Jones JA, Yuan JS, Wang X: **Thermodynamics contributes to high limonene productivity in cyanobacteria**. *Metab Eng Commun* 2022, **14**:e00193.

This study combined various metabolic engineering techniques such as promoter and RBS screening, increasing precursor supply, heterologous expression of bicarbonate transporters and overexpression of sigma factors to increase production of limonene in *Synechococcus elongatus* PCC 7942.

41. Newman DM, Sake CL, Metcalf AJ, Davies FK, Boyle NR, Boyle N: **Characterizing photosynthetic biofuel production: Isotopically non-stationary ^{13}C metabolic flux analysis (INST-13 CMFA) on limonene producing *Synechococcus* sp. PCC 7002**. *bioRxiv* 2022, **10**, https://doi.org/10.1101/2022.03.30.486112

42. George DM, Vincent AS, Mackey HR: **An overview of anoxygenic phototrophic bacteria and their applications in environmental biotechnology for sustainable Resource recovery**. *Biotechnol Rep* 2020, **28**:e00563.

43. Drews G, Golecki JR: **Structure, molecular organization, and biosynthesis of membranes of purple bacteria**. Anoxygenic Photosynthetic Bacteria. Kluwer Academic Publishers; 1995:231-257.

44. Khan NE, Nybo SE, Chappell J, Curtis WR: **Triterpene hydrocarbon production engineered into a metabolically versatile host — *Rhodobacter capsulatus***. *Biotechnol Bioeng* 2015, **112**:1523-1532.

45. Xu W, Ma X, Yao J, Wang D, Li W, Liu Li, Shao L, Wang Y: **Increasing coenzyme Q_{10} yield from *Rhodopseudomonas palustris* by expressing rate-limiting enzymes and blocking carotenoid and hopanoid pathways**. *Lett Appl Microbiol* 2021, **73**:88-95.

46. •• Zhang Y, Song X, Lai Y, Mo Q, Yuan J: **High-yielding terpene-based biofuel production in *Rhodobacter capsulatus***. *ACS Synth Biol* 2021, **10**:1545-1552.

This study combined various of metabolic engineering techniques such as promotor screening, enhanced NADPH availability, precursor supply, the introduction of the MVA pathway, and suppression of competing pathways with a two-phase fed-batch fermentation to reach g/L scale bisabolene production in *R. capsulatus*.

47. Xu M, Wu H, Shen P, Jiang X, Chen X, Lin J, Huang J, Qi F: **Enhancement of NADPH availability for coproduction of coenzyme Q_{10} and farnesol from *Rhodobacter sphaeroides***. *J Ind Microbiol Biotechnol* 2020, **47**:263-274.

48. Loeschcke A, Hage-Hülsmann J, Troost K, Wewer V, Jaeger K-E, Drepper T: **Heterologous production of plant terpenes in the photosynthetic bacterium *Rhodobacter capsulatus***. *Methods Mol Biol* 2022, **2379**:125-154.

49. • Troost K, Loeschcke A, Hilgers F, Özgür AY, Weber TM, Santiago-Schübel B, Svensson V, Hage-Hülsmann J, Habash SS, Grundler FMW, *et al.*: **Engineered *Rhodobacter capsulatus* as a phototrophic platform organism for the synthesis of plant sesquiterpenoids**. *Front Microbiol* 2019, **10**:1998.

This study established *R. capsulatus* as a producer for different heterologous sesquiterpenes based on a modular metabolic engineering concept including overexpression of rate-limiting enzymes, MVA pathway introduction and a strong oxygen-sensitive promotor.

50. Orsi E, Mougiakos I, Post W, Beekwilder J, Dompè M, Eggink G, van der Oost J, Kengen SWM, Weusthuis RA: **Growth-uncoupled isoprenoid synthesis in *Rhodobacter sphaeroides***. *Biotechnol Biofuels* 2020, **13**:123.

51. Xu W, Wang D, Fan J, Zhang L, Ma X, Yao J, Wang Y: **Improving squalene production by blocking the competitive branched pathways and expressing rate-limiting enzymes in *Rhodopseudomonas palustris***. *Biotechnol Appl Biochem* 2021,1-7, https://doi.org/10.1002/bab.2222

52. Zhou J, Yang F, Zhang F, Meng H, Zhang Y, Li Y: **Impairing photorespiration increases photosynthetic conversion of CO_2 to isoprene in engineered cyanobacteria**. *Bioresour Bioprocess* 2021, **8**:42.

53. Lin P-C, Saha R, Zhang F, Pakrasi HB: **Metabolic engineering of the pentose phosphate pathway for enhanced limonene**

production in the cyanobacterium *Synechocystis* sp. PCC 6803. *Sci Rep* 2017, **7**:17503.

54. Herold RA, Bryan SJ: **Engineered terpenoid production in *Synechocystis* sp. PCC 6803 under different growth conditions**. *bioRxiv* 2020, https://doi.org/10.1101/2020.08.19.256149

55. Englund E, Pattanaik B, Ubhayasekera SJK, Stensjö K, Bergquist J, Lindberg P: **Production of squalene in *Synechocystis* sp. PCC 6803**. *PLoS One* 2014, **9**:e90270.

56. Wang X, Liu W, Xin C, Zheng Y, Cheng Y, Sun S, Li R, Zhu X-G, Dai SY, Rentzepis PM, *et al.*: **Enhanced limonene production in cyanobacteria reveals photosynthesis limitations**. *PNAS* 2016, **113**:14225-14230.

57. Lee HJ, Choi J, Woo HM: **Biocontainment of engineered *Synechococcus elongatus* PCC 7942 for photosynthetic production of α-farnesene from CO_2**. *J Agric Food Chem* 2021, **69**:698-703.

58. Lee HJ, Lee J, Lee S-M, Um Y, Kim Y, Sim SJ, Choi J, Woo HM: **Direct conversion of CO_2 to α-farnesene using metabolically engineered *Synechococcus elongatus* PCC 7942**. *J Agric Food Chem* 2017, **65**:10424-10428.

59. • Choi SY, Woo HM: **CRISPRi-dCas12a: a dCas12a-mediated CRISPR interference for repression of multiple genes and metabolic engineering in cyanobacteria**. *ACS Synth Biol* 2020, **9**:2351-2361.

This study combined various metabolic engineering techniques such as increasing precursor supply, designing fusion proteins and suppressing competing pathways via the newly established CRISPRi dCas12a technique to increase squalene production in *Synechococcus elongatus* PCC 7942.

60. Davies FK, Work VH, Beliaev AS, Posewitz MC: **Engineering limonene and bisabolene production in wild type and a glycogen-deficient mutant of *Synechococcus* sp. PCC 7002**. *Front Bioeng Biotechnol* 2014, **2**:21.

61. Hage-Hülsmann J, Metzger S, Wewer V, Buechel F, Troost K, Thies S, Loeschcke A, Jaeger K-E, Drepper T: **Biosynthesis of cycloartenol by expression of plant and bacterial oxidosqualene cyclases in engineered *Rhodobacter capsulatus***. *J Biotechnol* 2019, **306**:100014.

62. Chen X, Jiang X, Xu M, Zhang M, Huang R, Huang J, Qi F: **Co-production of farnesol and coenzyme Q_{10} from metabolically engineered *Rhodobacter sphaeroides***. *Microb Cell Fact* 2019, **18**:98.

63. Qiang S, Su AP, Li Y, Chen Z, Hu CY, Meng YH: **Elevated β-carotene synthesis by the engineered *Rhodobacter sphaeroides* with enhanced CrtY expression**. *J Agric Food Chem* 2019, **67**:9560-9568.

64. Qu Y, Su A, Li Y, Meng Y, Chen Z: **Manipulation of the regulatory genes *ppsR* and *prrA* in *Rhodobacter sphaeroides* enhances lycopene production**. *J Agric Food Chem* 2021, **69**:4134-4143.

65. Xu W, Chai C, Shao L, Yao J, Wang Y: **Metabolic engineering of *Rhodopseudomonas palustris* for squalene production**. *J Ind Microbiol Biotechnol* 2016, **43**:719-725.

66. Giraud E, Hannibal L, Chaintreuil C, Fardoux J, Verméglio A: **Synthesis of carotenoids of industrial interest in the photosynthetic bacterium *Rhodopseudomonas palustris*: bioengineering and growth conditions**. *Methods Mol Biol* 2018, **1852**:211-220.

67. Saejung C, Ampornpat W: **Production and nutritional performance of carotenoid-producing photosynthetic bacterium *Rhodopseudomonas faecalis* PA2 grown in domestic wastewater intended for animal feed production**. *Waste Biomass Valorization* 2019, **10**:299-310.

68. Zhi R, Yang A, Zhang G, Zhu Y, Meng F, Li X: **Effects of light-dark cycles on photosynthetic bacteria wastewater treatment and valuable substances production**. *Bioresour Technol* 2019, **274**:496-501.

69. Bähr L, Wüstenberg A, Ehwald R: **Two-tier vessel for photoautotrophic high-density cultures**. *J Appl Phycol* 2016, **28**:783-793.

70. • Orsi E, Beekwilder J, van Gelder D, van Houwelingen A, Eggink G, Kengen SWM, Weusthuis RA: **Functional replacement of isoprenoid pathways in *Rhodobacter sphaeroides***. *Microb Biotechnol* 2020, **13**:1082-1093.

This study evaluated the influence of a complete replacement of the MEP pathway by the heterologous MVA pathway on sesquiterpenoid production and carbon flux in *R. sphaeroides*. Insertion of the MVA gene cluster was carried out using a Tn5 transposon system.

71. Loeschcke A, Markert A, Wilhelm S, Wirtz A, Rosenau F, Jaeger K-E, Drepper T: **TREX: a universal tool for the transfer and expression of biosynthetic pathways in bacteria**. *ACS Synth Biol* 2013, **2**:22-33.

72. Englund E, Shabestary K, Hudson EP, Lindberg P: **Systematic overexpression study to find target enzymes enhancing production of terpenes in *Synechocystis* PCC 6803, using isoprene as a model compound**. *Metab Eng* 2018, **49**:164-177.

73. Imam S, Noguera DR, Donohue TJ: **Global insights into energetic and metabolic networks in *Rhodobacter sphaeroides***. *BMC Syst Biol* 2013, **7**:89.

74. Orsi E, Beekwilder J, Eggink G, Kengen SWM, Weusthuis RA: **The transition of *Rhodobacter sphaeroides* into a microbial cell factory**. *Biotechnol Bioeng* 2021, **118**:531-541.

75. Peters L, Weidenfeld I, Klemm U, Loeschcke A, Weihmann R, Jaeger K-E, Drepper T, Ntziachristos V, Stiel AC: **Phototrophic purple bacteria as optoacoustic *in vivo* reporters of macrophage activity**. *Nat Commun* 2019, **10**:1191.

76. Jester BW, Zhao H, Gewe M, Adame T, Perruzza L, Bolick DT, Agosti J, Khuong N, Kuestner R, Gamble C, *et al.*: **Development of spirulina for the manufacture and oral delivery of protein therapeutics**. *Nat Biotechnol* 2022, **40**:956-964, https://doi.org/10.1038/s41587-022-01249-7

II.1.2 *R. capsulatus* as a host for the production of various terpene classes in the context of metabolic engineering strategies

PUBLICATION II

Production of C_{20}, C_{30} and C_{40} terpenes in the engineered phototrophic bacterium *Rhodobacter capsulatus*

Jennifer Hage-Hülsmann[1]*, **Oliver Klaus**[1]*, Karl Linke[1], Katrin Troost[1], Lukas Gora[1], Fabienne Hilgers[1], Astrid Wirtz[2], Beatrix Santiago-Schübel[3], Anita Loeschcke[1], Karl-Erich Jaeger[1,2], Thomas Drepper[1#]

[1]Institute of Molecular Enzyme Technology, Heinrich Heine University Düsseldorf, Forschungszentrum Jülich, 52425 Jülich, Germany
[2]Institute of Bio- and Geosciences IBG-1: Biotechnology, Forschungszentrum Jülich GmbH, 52425 Jülich, Germany
[3]Central Division of Analytical Chemistry ZEA-3: Analytic/Biospec, Forschungszentrum Jülich, 52425 Jülich, Germany

* These authors contributed equally
# Corresponding authors

Status: published

Journal of Biotechnology,
2021, 09,10, 338:20-30
https://doi.org/10.1021/j.jbiotec.2021.07.002

Own contribution:
Designing and performing experiments, plasmid construction, analyzing data, editing manuscript

Journal of Biotechnology 338 (2021) 20–30

Contents lists available at ScienceDirect

Journal of Biotechnology

journal homepage: www.elsevier.com/locate/jbiotec

Production of C20, C30 and C40 terpenes in the engineered phototrophic bacterium *Rhodobacter capsulatus*

Jennifer Hage-Hülsmann [a,d,1], Oliver Klaus [a,1], Karl Linke [a], Katrin Troost [a], Lukas Gora [a], Fabienne Hilgers [a,e], Astrid Wirtz [b], Beatrix Santiago-Schübel [c], Anita Loeschcke [a,d,e,*], Karl-Erich Jaeger [a,b,d,e], Thomas Drepper [a,d,e,*]

[a] Institute of Molecular Enzyme Technology, Heinrich Heine University Düsseldorf, Forschungszentrum Jülich, Jülich, Germany
[b] Institute of Bio- and Geosciences IBG-1, Forschungszentrum Jülich, Jülich, Germany
[c] Central Division of Analytical Chemistry ZEA-3: Analytik/Biospec, Forschungszentrum Jülich, Jülich, Germany
[d] Cluster of Excellence on Plant Sciences (CEPLAS), Germany
[e] Bioeconomy Science Center (BioSC), Forschungszentrum Jülich, Jülich, Germany

ARTICLE INFO

Keywords:
Rhodobacter capsulatus
Engineering biosynthesis of terpenes
Diterpene casbene
Triterpene squalene
Squalene synthases
Tetraterpene β-carotene

ABSTRACT

Terpenes constitute one of the largest groups of secondary metabolites that are used, for example, as food-additives, fragrances or pharmaceuticals. Due to the formation of an intracytoplasmic membrane system and an efficient intrinsic tetraterpene pathway, the phototrophic α-proteobacterium *Rhodobacter capsulatus* offers favorable properties for the production of hydrophobic terpenes. However, research efforts have largely focused on sesquiterpene production. Recently, we have developed modular tools allowing to engineer the biosynthesis of terpene precursors. These tools were now applied to boost the biosynthesis of the diterpene casbene, the triterpene squalene and the tetraterpene β-carotene in *R. capsulatus* SB1003. Selected enzymes of the intrinsic isoprenoid pathway and the heterologous mevalonate (MVA) pathway were co-expressed together with the respective terpene synthases in various combinations. Remarkably, co-expression of genes *ispA*, *idi* and *dxs* enhanced the synthesis of casbene and β-carotene. In contrast, co-expression of precursor biosynthetic genes with the squalene synthase from *Arabidopsis thaliana* reduced squalene titers. Therefore, we further employed four alternative pro- and eukaryotic squalene synthases. Here, the synthase from *Methylococcus capsulatus* enabled highest product levels of 90 mg/L squalene upon co-expression with *ispA*. In summary, we demonstrate the applicability of *R. capsulatus* for the heterologous production of diverse terpene classes and provide relevant insights for further development of such platforms.

1. Introduction

Terpenes are one of the largest groups of secondary metabolites that are ubiquitously present in organisms of all kingdoms of life (Chen et al., 2011; Dickschat, 2016; Schmidt-Dannert, 2014). A multitude of plant terpenes are applicable as ingredients in drugs, cosmetics or food products because they exhibit diverse relevant properties including antibiotic and antioxidant activities, a pleasant color, fragrance or flavor (Efferth, 2017; Mahizan et al., 2019; Schempp et al., 2018; Wołosik et al., 2013). Since the chemical synthesis of many terpenes is economically unfeasible and the extraction from their natural sources cannot be realized in a sustainable way, biotechnological approaches represent a promising strategy for accessing these compounds (Marienhagen and Bott, 2013; Schempp et al., 2018).

Terpenes are biosynthesized from the C5 isoprene building blocks isopentenyl pyrophosphate (IPP) and dimethylallyl pyrophosphate (DMAPP), and classified as hemi- (C5), mono- (C10), sesqui- (C15), di- (C20), tri-(C30) and tetraterpenes (C40). The isoprene precursor scaffolds IPP and DMAPP are generated *via* the mevalonate (MVA) pathway, which uses acetyl-CoA as substrate, or the 2-*C*-methyl-D-erythritol 4-

* Corresponding authors at: Institute of Molecular Enzyme Technology, Heinrich Heine University Düsseldorf, Forschungszentrum Jülich, Jülich, Germany.
E-mail addresses: j.hage-huelsmann@fz-juelich.de (J. Hage-Hülsmann), o.klaus@fz-juelich.de (O. Klaus), karllinke89@gmail.com (K. Linke), katrin.troost@gmx.de (K. Troost), LukasFJ@web.de (L. Gora), f.hilgers@fz-juelich.de (F. Hilgers), a.wirtz@fz-juelich.de (A. Wirtz), b.santiago-schuebel@fz-juelich.de (B. Santiago-Schübel), a.loeschcke@fz-juelich.de (A. Loeschcke), karl-erich.jaeger@fz-juelich.de (K.-E. Jaeger), t.drepper@fz-juelich.de (T. Drepper).
[1] Equally contributed.

https://doi.org/10.1016/j.jbiotec.2021.07.002
Received 3 December 2020; Received in revised form 28 June 2021; Accepted 1 July 2021
Available online 5 July 2021

phosphate (MEP) pathway (also referred to as DXP pathway), which uses glyceraldehylde-3-phosphate (GAP) and pyruvate. While the MVA pathway occurs in all eukaryotes and is less abundant in prokaryotes, the MEP pathway is predominant in bacteria as well as in plastids of green algae and plants (Frank and Groll, 2017; Lombard and Moreira, 2011). IPP and DMAPP are used as substrates for a series of condensation steps to yield geranyl pyrophosphate GPP (C10), farnesyl pyrophosphate FPP (C15) and geranylgeranyl pyrophosphate GGPP (C20). GPP can be converted to monoterpenoids, FPP to sesqui- and triterpenoids, and GGPP to di- and tetraterpenoids by respective terpene synthase enzymes.

Key factors for successful heterologous production of terpenes in bacteria are a suitable host organism and the employed terpene synthase enzyme. Specifically, the bacterial host should provide a sufficient precursor supply and an appropriate storage capacity for potentially toxic compounds (Cravens et al., 2019; Das et al., 2007; Schempp et al., 2018). To further optimize terpene production *via* metabolic engineering, molecular genetic tools need to be established for the applied host system. In addition, terpene synthase enzymes from diverse origin were reported to often differ significantly in their performance for a recombinant biosynthesis approach and thus represent a critical determinant of success (Beekwilder et al., 2014; Qiao et al., 2019; Troost et al., 2019). Efforts in microbial terpene production have long focused on the use of established workhorses such as *E. coli* and yeast, but more recently, also alternative host organisms of the class of phototrophic bacteria are receiving increased attention (Moser and Pichler, 2019; Schempp et al., 2018). An established representative of this group is the Gram-negative facultative phototrophic non-sulfur purple α-proteobacterium *Rhodobacter capsulatus*. This bacterium possesses the MEP pathway to yield IPP and DMAPP, which are converted into each other by the IPP isomerase Idi. The FPP synthase IspA catalyzes the elongation *via* GPP to FPP, which is then further elongated by GGPP synthase CrtE, providing the C20 scaffold GGPP as substrate for the phytoene synthase and the following biosynthetic steps to form the *Rhodobacter*-specific carotenoids spheroidene and spheroidenone (see Fig. 1). Under phototrophic growth conditions, *R. capsulatus* generates an intracytoplasmic membrane system (ICM) from invaginations of the cytoplasmic membrane (Chory et al., 1984). Besides its function of housing the photosynthesis apparatus including the photopigments bacteriochlorophyll *a* and the carotenoids, the ICM offers a storage space for heterologously produced enzymes and compounds, thus possibly enabling the bacterium to sustain increased accumulation of hydrophobic products. The applicability of *Rhodobacter* species for heterologous terpene production has been shown for several examples including sesqui-, tri- and tetraterpenes (Beekwilder et al., 2014; Hage-Hülsmann et al., 2019; Khan et al., 2015; Loeschcke et al., 2017, 2013; Orsi et al., 2019; Troost et al., 2019).

For sesquiterpenes, it was shown that the production capacity of *Rhodobacter* can be increased by strengthening the elongation of prenyl phosphates by co-expression of FPP synthase along with a sesquiterpene synthase. Further, terpene production can be enhanced by increased synthesis of isoprene units *via* the intrinsic MEP pathway by co-expression of DxS (1-deoxy-D-xylulose 5-phosphate synthase) and Idi.

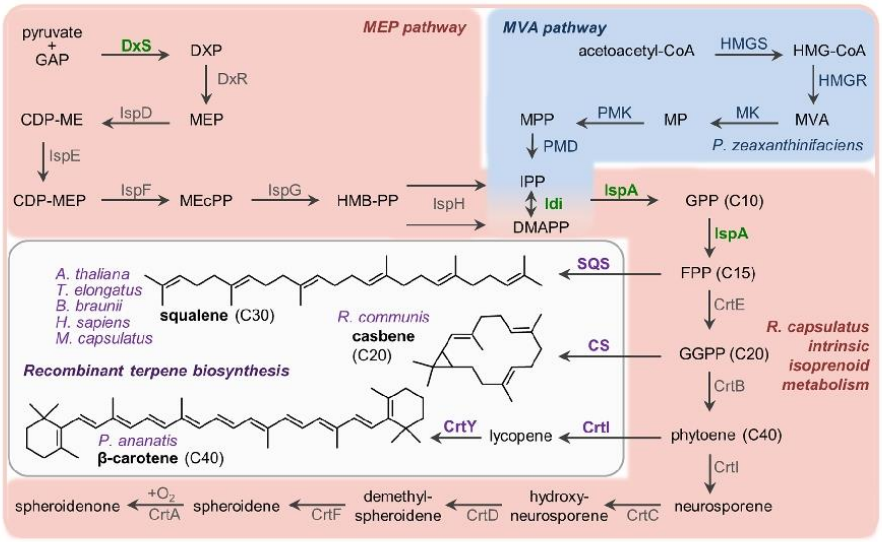

Fig. 1. Engineering concept for production of different terpenes in *R. capsulatus*. In the *R. capsulatus* intrinsic isoprenoid metabolism (red), the MEP pathway provides C5 isoprene building blocks IPP and DMAPP, which are elongated and converted to C40 carotenoids. Recombinant terpene biosynthesis (gray box) is implemented by expression of heterologous enzymes (purple): SQS: squalene synthase (originating from different organisms) for conversion of FPP to squalene; CS: casbene synthase from *R. communis* for conversion of GGPP to casbene; CrtI and CrtY: phytoene desaturase and lycopene cyclase from *P. ananatis* for the conversion of phytoene to β-carotene. To enhance terpene production, the DXP synthase and IPP isomerase (DxS and Idi from *R. sphaeroides*), as well as FPP synthase (IspA from *R. capsulatus*) of the intrinsic isoprenoid metabolism were additionally co-expressed (highlighted in green). Furthermore, an alternative route to build isoprene precursors from central metabolism *via* mevalonate was installed (blue) by expression of the MVA pathway genes from *P. zeaxanthinifaciens*. **Metabolites**: GAP, glyceraldehylde-3-phosphate; DXP, 1-deoxy-D-xylulose 5-phosphate; CDP-ME, 4-diphosphocytidyl-2-*C*-methyl-D-erythritol; CDP-MEP, CDP-ME 2-phosphate; MEcPP, 2-*C*-methyl-D-erythritol-2,4-cyclodiphosphate; HMBPP, 1-hydroxy-2-methyl-2-(*E*)-butenyl 4-diphosphate; HMG-CoA, (*S*)-3-hydroxy-3-methylglutaryl-CoA; MP, phosphomevalonate; MPP, diphosphomevalonate. **Further enzymes**: DxR, DXP reductoisomerase; IspD, MEP cytidylyltransferase; IspE, CDP-ME kinase; IspF, MEcPP synthase; IspG, HMBPP synthase; IspH, HMBPP reductase; HMGS, HMG-CoA synthase; HMGR, HMG-CoA reductase; MK, mevalonate-5-kinase; PMK, MP kinase; PMD, MPP decarboxylase; CrtB, phytoene synthase; CrtI, phytoene desaturase; CrtC, hydroxyneurosporene synthase; CrtD, hydroxyneurosporene desaturase; CrtF, demethyl-spheroidene *O*-methyltransferase; CrtA, spheroidene monooxygenase.

Moreover, the introduction of the MVA pathway, which does not naturally occur in this host, was demonstrated to enhance terpene production. Such measures have enabled successful sesquiterpene production in *Rhodobacter* (Beekwilder et al., 2014; Orsi et al., 2019; Troost et al., 2019). Two *Rhodobacter* species, namely *R. capsulatus* and *R. sphaeroides* have raised particular interest as microbial cell factories (Heck and Drepper, 2017; Orsi et al., 2021) and the latter is industrially applied for the production of the sesquiterpenes valencene and nootkatone marketed by Isobionics (now BASF). The heterologous biosynthesis of other classes of terpenes in *Rhodobacter* species is, however, less explored.

In the present study, we thus aimed to focus on the production of representatives of C20, C30 and C40 terpenes, namely casbene, squalene and β-carotene, in *R. capsulatus* SB1003. Hence, we employed the casbene synthase *Rc*CS from the castor bean shrub *Ricinus communis* (Mau and West, 1994), the squalene synthase SQS1 from the small flowering plant thale cress *Arabidopsis thaliana* (Busquets et al., 2008), and the phytoene desaturase CrtI together with lycopene cyclase CrtY of the proteobacterium *Pantoea ananatis* (Misawa et al., 1990). We further evaluated metabolic engineering strategies, which were recently established for sesquiterpene production in *R. capsulatus* by implementing co-expression of precursor biosynthetic genes *ispA*, *dxs*, and *idi* of the intrinsic isoprenoid metabolism and all genes of the MVA pathway (Troost et al., 2019), for optimizing the production of di-, tri- and tetraterpenes. The here presented data demonstrate that the metabolic engineering approach could successfully be transferred resulting in an enhanced production of casbene and β-carotene. Surprisingly, squalene production could not be improved when the *A. thaliana* synthase was employed. We therefore tested four alternative squalene synthases from the thermophilic cyanobacterium *Thermosynechococcus elongatus*, the green colonial microalga *Botryococcus braunii*, the Gram-negative methanotroph *Methylococcus capsulatus*, and *Homo sapiens*, finding highest production by the latter two in an engineered background. Therefore, the modular metabolic engineering approaches applied in this study enabled us to identify genetic setups that resulted in improved product titers of the target terpenes and demonstrate applicability of *R. capsulatus* as a platform organism for di-, tri-, and tetraterpene production.

2. Materials and methods

2.1. Bacterial strains and cultivation conditions

Escherichia coli strains DH5α (Hanahan, 1983) and S17-1 (Simon et al., 1983) were used for cloning and conjugational transfer (Klipp et al., 1988) of DNA into *Rhodobacter capsulatus*. *E. coli* cells were cultivated in LB medium (Luria/ Miller, Carl Roth: 10 g/L tryptone, 5 g/L yeast extract, 10 g/L sodium chloride) under constant shaking or on LB agar plates containing 1.5 % agar (*w/v*, Bacto agar, Difco) at 37 °C. Kanamycin was added to a final concentration of 50 µg/mL. *R.capsulatus* strains SB1003 (Strnad et al., 2010) and SB1003-MVA (Troost et al., 2019), which carries the MVA gene cluster (*mvaA-idi-hsc-mvk-pmk-mvd*) of *P. zeaxanthinifaciens*, were cultivated phototrophically on PY (peptone-yeast) agar plates (10 g/L Bacto peptone, 0.5 g/L Bacto yeast extract and 20 g/L Select Agar) or in liquid RCV minimal medium (1 mL/L 20 % $MgSO_4$ (*w/v*), 1 mL/L 7.5 % $CaCl_2$ (*w/v*), 2 mL/L 1% EDTA (*w/v*), 2.4 mL/L 0.5 % $FeSO_4$ (*w/v*) supplemented with 2 mL/L 37 % HCl, 1 mL/L 0.1 % thiamine (*w/v*), 1 mL/L trace element solution [0.4 g/L $MnSO_4$(x1 H_2O), 0.7 g/L H_3BO_3, 0.01 g/L $Cu(NO_3)_2$(x3 H_2O), 0.06 g/L $ZnSO_4$(x7 H_2O), 0.02 g/L $NaMoO_4$(x2 H_2O)]; pH 6.8) at 30 °C under anaerobic phototrophic conditions (bulb light, 2500 lx). For incubation of agar plates, anaerobic conditions were implemented by using airtight cultivation containers and gas packs to deplete atmospheric oxygen (Microbiology Anaerocult A system, Merck KgaA, Darmstadt, Germany). Liquid cultivations were performed in Hungate glass tubes, which can be capped airtight with a septum and a screw cap.

2.2. Construction of expression vectors

The di-, tri- and tetraterpene biosynthetic genes were obtained by gene synthesis (Eurofins Genomics, Ebersberg, Germany) with optimized codon-usage for expression in *R. capsulatus* (Supplementary Table S1) and were designated as follows. We used casbene synthase (encoded by *RcCS*) from *Ricinus communis* (NCBI Protein XP_002513340.1) (Mau and West, 1994) for casbene biosynthesis. Phytoene desaturase was used together with lycopene cyclase, encoded by *crtY-crtI* from *Pantoea ananatis* (NCBI Protein P21687.1 and P21685.1) (Misawa et al., 1990) for β-carotene synthesis. Different squalene synthases were selected for biosynthesis of the triterpene. We used the squalene synthase 1 (SQS1) from *Arabidopsis thaliana* (At4g34640; NCBI Protein NP_195190.1) (Busquets et al., 2008), as in our previous studies (Loeschcke et al., 2017). For *Bb*SQS, we used a version of the squalene synthase from *Botryococcus braunii* (GenBank Protein AAF20201.1), which was employed to install squalene synthesis in *R. capsulatus* before (Khan et al., 2015) with a truncation of 26 amino acids at the C-terminus, which was previously shown to facilitate enhanced expression in *E. coli* (Okada et al., 2000). We used *Te*SQS from *Thermosynechococcus elongates* BP1 (NCBI Reference Sequence: NP_681887.1), which has shown high *in vitro* activity and was functionally expressed in *E. coli* (Katabami et al., 2015; Lee and Poulter, 2008). A truncated version of the human squalene synthase (NCBI Reference AAH09251.1) was employed as *Hs*SQS, with deletion of the N-terminal 30 amino acids and the C-terminal 47 amino acids, based on previous reports (Katabami et al., 2015; Thompson et al., 1998). The squalene synthase *Mc*SQS from *Methylococcus capsulatus* str. Bath (NCBI Protein CAA71097.1) was used because it was reported to be expressed as a soluble protein (Ohtake et al., 2014). During gene synthesis, restriction endonuclease recognition sites, and homologous vector sequences were added at the 5′ or 3′ ends, as appropriate for cloning.

All terpene biosynthetic genes were cloned into the expression vector pRhon5Hi-2 (Troost et al., 2019) carrying the host-specific P_{nif} promotor (NCBI Genbank Accession MG208548). Vectors pRhon5Hi-2-Rc*CS* and pRhon5Hi-2-crtY-crtI were constructed by cloning the synthetic gene *RcCS* or the *crtY-crtI* cassette as *Nde*I/*Hind*III fragments into vector pRhon5Hi-2. To this end, *crtY-crtI* was amplified *via* PCR, adding the restriction sites to the ends by use of appropriate primers, while *RcCS* was obtained with *Nde*I/*Hind*III sites *via* gene synthesis. The gene *ispA* (*R. capsulatus* SB1003) was amplified *via* PCR using genomic DNA as template, introducing *Hind*III and *Xho*I sites with the primers. The cassette *ispA-dxs-idi* (*dxs* and *idi* from *R. sphaeroides* 2.4.1) was obtained as *Hind*III/*Xho*I-fragment by hydrolysis of vector pRhon5Hi-2-CnVS-ispA-dxs-idi (Troost et al., 2019). These genes and gene cassettes were used to construct vectors pRhon5Hi-2-RcCS-ispA and pRhon5Hi-2-RcCS-ispA-dxs-idi, as well as pRhon5Hi-2-crtY-crtI-ispA and pRhon5Hi-2-crtY-crtI-ispA-dxs-idi. Construction of pRhon5Hi-2- SQS1 was previously described (Loeschcke et al., 2017). It was used as template to amplify SQS1 with appropriate primers adding the necessary restriction sites to clone the gene as an *Xba*I/*Hind*III fragment in vectors pRhon5Hi-2-CnVS-ispA and pRhon5Hi-2-CnVS-ispA-dxs-idi (Troost et al., 2019), thereby replacing the gene *CnVS* with SQS1 to generate expression vectors pRhon5Hi-2-SQS1-ispA and pRhon5Hi2-SQS1-ispA-dxs-idi. The analogous constructs carrying the squalene synthase genes of other organisms were likewise constructed, with the difference that the 5′ end and 3′ end extensions were added during gene synthesis, so that the appropriate sequences could be readily excised without additional PCR. Relevant gene sequences on each construct were verified by sequencing performed by Eurofins Genomics (Ebersberg, Germany). All oligonucleotide primers, plasmids and strains used in this study are listed in Supplementary Table S2.

2.3. Heterologous expression of terpene biosynthesis genes in *R. capsulatus*

For introduction of terpene biosynthesis genes in *R. capsulatus*, respective pRhon5Hi-2-based vectors were transferred to the host *via* conjugation as previously described (Klipp et al., 1988). Exconjugants were subsequently selected and further cultivated on PY agar, containing 25 µg/mL kanamycin and 25 µg/mL rifampicin. For heterologous expression of terpene biosynthesis genes, cultivation was conducted in liquid RCV medium with 4 g/L malate containing 25 µg/mL kanamycin under anaerobic phototrophic conditions (bulb light, 2500 lx) in 15 mL Hungate tubes at 30 °C. Pre-cultures of 15 mL RCV medium containing 0.1 % $(NH_4)_2SO_4$ were inoculated and incubated for 72 h. Expression cultures were inoculated from pre-cultures to an initial OD_{660nm} of 0.05 in RCV medium containing 0.1 % serine as sole nitrogen source. The omission of ammonium together with implementation of anaerobic conditions ensured derepression of the P_{nif} promoter and target protein expression (Troost et al., 2019). A culture volume of 15 mL medium was used for squalene and β-carotene production cultures. For analysis of casbene production, 14 mL cultures were overlayed with 0.5 mL *n*-dodecane. Cultures were incubated for 2 days (48 h), until an OD_{660nm} of ~2-3 was reached before sampling and product analysis. For analysis of squalene and β-carotene, samples of cells corresponding to OD_{660nm} = 7.5 in 1 mL (i.e. approximately 3 mL of the cultures, depending on the specific cell density) were harvested by centrifugation (10 min, 1800 g, 4 °C), the medium was discarded, and pellets stored at -20 °C. All cultivations were conducted at least as triplicates and, for verification, repeated in independent experimental runs.

2.4. Sampling and GC analysis of casbene

After 48 h of cultivation, expression cultures in Hungate tubes with *n*-dodecane were incubated in a Multitron Standard incubation shaker (Infors HT) for additional 24 h at 30 °C in horizontal position under constant shaking at 130 rpm for further extraction of casbene from expression cultures. Thereafter, 100 µL of the *n*-dodecane layer were harvested for GC analysis. Casbene amounts could not be determined quantitatively because an authentic reference was missing. Instead, relative production levels were estimated in GC-FID analyses from areas of peaks which exclusively occurred in samples from *Rc*CS expression cultures and were absent in those of the *R. capsulatus* wildtype SB1003 or SB1003-MVA. The gas chromatograph *6890 N* (Agilent) equipped with an Agilent (5%-Phenyl)-methylsiloxane *HP*-5 column (30 m length, 0.32 mm inside diameter, 0.25 µm film thickness) was used for splitless injection of 2 µL sample volumes, using helium as carrier gas. The injector temperature was set to 240 °C and the FID to 250 °C. The oven temperature was held at 100 °C for 5 min, then ramped to 180 °C at 10 °C/min, finally to 300 °C at 20 °C/min. Signals were detected using a flame ionization detector (FID), and peak areas obtained at a retention time of 15.91 min were evaluated. GC-MS analysis was employed for corroboration of casbene (272 g/mol) accumulation in the *n*-dodecane layer. To this end, 1 µL was injected directly into a Trace GC Ultra gas chromatograph coupled to an ITQ 900 mass spectrometer (Thermo Scientific). Separation was achieved in a capillary (30 m length, 0.25 mm diameter) with a 0.25 µm film of FS-5 supreme (CS Chromatographie Service). Split mode with a split ratio of 10 was used for the injector with the inlet temperature set to 250 °C. The oven was programmed to start at 100 °C and a 1 min hold, after which temperature increased to 300 °C at a rate of 5 °C/min. Helium was used as carrier gas at a flow rate of 1 mL/min. MS data were collected from 50 to 650 *m/z* during the temperature ramp. The MS spectrum of a peak, which occurred at 29-30 min in the extracted ion chromatogram (EIC) of 272 *m/z*, was found to match previously published casbene spectra (King et al., 2014; Luo et al., 2016).

2.5. Preparation of whole cell extracts for analysis of squalene and β-carotene

Extraction of squalene from pelleted cells from *R. capsulatus* expression cultures was performed by addition of 2 mL acetone. The samples were vortexed, incubated at 50 °C and 600 rpm for 15 min and cell debris was finally separated from acetone by centrifugation (3 min, 2900 *g*, 22 °C). The acetone supernatants were transferred into fresh tubes and supplemented with 1.5 mL of 1 M NaCl solution and mixed. Afterwards, 1.8 mL *n*-hexane was added and samples were extracted for 30 s by mixing with a test tube shaker. Phase separation was reached by centrifugation (1 min, 2900 *g*, 22 °C). Finally, the *n*-hexane organic phases were transferred into fresh reaction tubes and dried using a vacuum centrifugation (20 min, 30 °C).

2.6. HPLC analysis of squalene

Dried *R. capsulatus* cell extracts were solved in 150 µL methanol-acetonitrile mixture (1:1) and used for analysis of produced squalene *via* HPLC-UV/Vis with an LC-2010 HT system (Shimadzu). Reversed phase chromatography was performed with a Kinetex C18 column (75 mm x 4.6 mm, 2.6 µm, Phenomenex) and a respective guard column. Chromatograms were recorded at 202 nm. Sample volumes of 10 µL were injected and the separation occurred with a flow rate of 1 mL/min and at an oven temperature of 35 °C. The mobile phase consisted of acetonitrile (A), methanol (B) and 2-propanol (C). Starting conditions of 14 min analyses were 80/20 (%A/B), followed by a gradient to solvent compositions of 76/19/5 (%A/B/C), then to 72/18/10 (%A/B/C), and to 56/14/30 (%A/B/C), that were reached after 2.5 min, 4.25 min and 6.00 min, respectively. The last was held for 3 min, before returning to starting conditions within 0.5 min. Those were maintained for 4.5 min for re-equilibration. Squalene amounts were quantified by calibration with a commercial authentic reference (Sigma-Aldrich). To account for extraction losses, titers in the cultures were determined *via* calibration curves generated by addition of defined amounts of authentic squalene to cell pellets of the *R. capsulatus* wildtype, and analysis of squalene signals after the same extraction procedure as applied for samples from expression cultures.

2.7. HPLC analysis of β-carotene

Dried *R. capsulatus* cell extracts were solved in 150 µL pure ethanol (p.a.) and analyzed by HPLC-PDA using an LC10Ai system (Shimadzu) equipped with the SPD-M10Avp photodiode array detector (PDA). A C30 reversed phase HPLC column (250 × 4.6 mm, 5 µm, YMC-Europe GmbH, Dinslaken, Germany) with a guard column filled with the same material (20 mm × 4.0 mm) was used for chromatography at 30 °C column oven temperature and 1 mL/min solvent flow rate. The mobile phase consisted of methanol (A), ethyl acetate (B) and acetonitrile containing 0.1 % formic acid (C). Starting conditions of 39 min analysis runs were 15/15/70 (%A/B/C) for 4 min, followed by a gradient to 10/70/20 (%A/B/C) in 15 min. This proportion was maintained for 14 min, before returning to starting conditions within 1 min which was maintained for re-equilibration for 5 min. Chromatograms were recorded at 450 nm, and absorbance spectra (from 350−550 nm) of peaks were extracted from PDA-data. Detected signals were analyzed in comparison with authentic references of carotenoids that were expected to result from heterologous gene expression, i.e. neurosporene (Standard from CaroteNature, Münsingen, Switzerland; 24.6 min), lycopene (Standard from DHI, Hørsholm, Denmark; 32 min) and β-carotene (Sigma-Aldrich; 18.5 min). Titers of β-carotene in cell cultures were estimated based on a calibration curve generated by addition of defined amounts of authentic β-carotene to cell pellets of the *R. capsulatus* wildtype, and analysis of β-carotene signals after the same extraction procedure as applied for samples from expression cultures. The signal attributed to all-*trans* β-carotene (18.5 min) was used for integration and additional signals

putatively assigned to geometrical *cis* isomers (Bononi et al., 2002; Schierle et al., 2004) were ignored for quantification as the ratio of all-*trans* to *cis* isomers was similar in all samples. Intrinsic spheroidene was identified based on the relative retention time (26.8 min) and known absorbance properties (Britton, 1995).

2.8. Analysis of Rhodobacter capsulatus pigmentation and dry cell weight

R. capsulatus pigmentation was determined by UV-Vis spectrophotometry. To this end, cell material equivalent to 1 mL with an optical density of 1 at a wavelength of 660 nm was harvested. Cell pellets were dispersed in 50 µL H_2O and cells were disrupted by adding 1 mL ethanol (p.a.). For a better cell disruption, samples were incubated for 5 min at 40 °C shaking (800 rpm). Afterwards, cell debris was pelleted by centrifugation (2 min, max. speed, 22 °C). Absorption of the ethanol samples at 455 nm was determined in a UV-Vis spectrophotometer (Thermo Scientific) as a measure of spheroidene levels.

The correlation of dry cell weight (DCW) of photoheterotrophically grown *R. capsulatus* in RCV medium to measured optical cell density at 660 nm, was determined by harvesting differently concentrated 1 mL samples of liquid cultures of the wildtype strain *R. capsulatus* SB1003 with optical densities at 660 nm of 0.5, 1.0, 1.5, 2.0 and 2.5. After centrifugation (10 min, 1100 *g*, 22 °C), supernatants were discarded and cell pellets were stored overnight at -20 °C before pellets were dried for 24 h in a freeze dryer (Lyovac GT2, Steris). The sample tubes were weighed before and after collection of cells to measure cell weight, enabling determination of a correlation of 1 mL $OD_{660nm} = 1$ with 0.6 mgDCW.

3. Results

3.1. Engineering concepts for the production of C20, C30 and C40 terpenes in R. capsulatus

In order to analyze if the recently developed tools for modular engineering of sesquiterpenoid synthesis in *R. capsulatus* (Troost et al., 2019) can be transferred to the phototrophic production of C20, C30 and C40 terpenes, we used the diterpene casbene, the triterpene squalene and the tetraterpene β-carotene as showcase targets (Fig. 1). The C20 diterpene casbene is produced in *Euphorbiaceae* (Dueber et al., 1978). The compound is known to exhibit antifungal activity (Moesta and West, 1985) and represents the precursor of further pharmacologically active diterpenes (Le et al., 2009) which accumulate in the plants (Liao et al., 2009). The casbene synthase *Rc*CS from castor bean *Ricinus communis* was chosen for expression in *R. capsulatus* to catalyze the cyclization of GGPP to casbene, since it could be functionally expressed in microorganisms before (Reiling et al., 2004). The C40 tetraterpene β-carotene is likewise derived from GGPP and occurs in microorganisms, fungi and plants (Avalos and Limón, 2015; Sandmann, 1994). This pigment is of interest for its antioxidant properties and provitamin A function (Britton et al., 2008), and is utilized as food colorant in livestock industry to enhance the color of e.g. salmon or egg yolk (Bauernfeind, 1981; Mortensen, 2006). We have previously identified the phytoene desaturase CrtI and lycopene cyclase CrtY of the bacterium *Pantoea ananatis* (Misawa et al., 1990) as suitable for the heterologous carotenoid biosynthesis in *Rhodobacter* (Loeschcke et al., 2013), where they can implement conversion of the intrinsic GGPP condensation product phytoene to β-carotene. Squalene belongs to the group of C30 triterpenes and occurs as biosynthetic product in various microorganisms including fungi, all plants and animals (Xu et al., 2016). The compound is applied e.g. in cosmetics (Huang et al., 2009), and is discussed for applications in the pharmaceutical and biofuel sector (Fox, 2009; Reddy and Couvreur, 2009; Yoshida et al., 2012). In addition, squalene is the central precursor of valuable cyclic triterpenes as, for example, cycloartenol and lupeol (Thimmappa et al., 2014). We selected the squalene synthase SQS1 of *Arabidopsis thaliana* (Busquets et al., 2008), which we employed in our previous studies (Hage-Hülsmann et al., 2019; Loeschcke et al., 2017) for successful conversion of FPP to squalene in *R. capsulatus*. The squalene titers we previously obtained under microaerobic (i.e. non-phototrophic) conditions in the wildtype strain SB1003 were relatively low (~8 mg/L) (Loeschcke et al., 2017). We thus aimed to analyze the transferability of the engineering strategies which prove successful for sesquiterpene synthesis in our previous study (Troost et al., 2019).

Accordingly, the FPP synthase IspA from *R. capsulatus* was co-expressed to enhance the prenyl phosphate elongation. Furthermore, the enzymes DxS and Idi (from *R. sphaeroides*) of the MEP pathway were co-expressed in addition to the intrinsic enzymes in order to increase the abundance of IPP and DMAPP. Finally, the isoprenoid biosynthesis pathway *via* mevalonate of *Paracoccus zeaxanthinifaciens* (Hiimbelin et al., 2002) was installed as an alternative route to C5 precursors of terpenoid biosynthesis. For gene expression in *R. capsulatus*, we used the host-specific P_{nif} promoter, which enables strong induction under anaerobic conditions with serine as sole nitrogen source in the medium (Troost et al., 2019). Codon usage adapted terpene biosynthesis genes were thus cloned in the vector pRhon5Hi-2 together with *ispA* or the cassette *ispA-dxs-idi* (Supplementary Table S1). These constructs were used for expression in the wildtype strain SB1003 as well as the recombinant strain SB1003-MVA, which carries the MVA gene cluster in the chromosome under control of P_{nif} (Troost et al., 2019).

3.2. Heterologous biosynthesis of GGPP-derived casbene and β-carotene

In order to evaluate the applicability of the modular *R. capsulatus* engineering approach for production of the diterpene casbene, the expression vectors pRhon5Hi-2-*Rc*CS, pRhon5Hi-2-*Rc*CS-ispA and pRhon5Hi-2-*Rc*CS-ispA-dxs-idi harboring the casbene synthase from *R. communis* and MEP pathway genes were transferred into the strains *R. capsulatus* SB1003 (wildtype) and SB1003-MVA (strain with recombinant MVA pathway). After photoheterotrophic cultivation in the presence of *n*-dodecane for two days, samples of the solvent were prepared for analyses by gas chromatography and flame ionization detection (GC-FID). Since casbene is not commercially available as a reference substance, we first compared obtained chromatograms of the wildtype strain SB1003 and SB1003-MVA with samples of respective *Rc*CS expression strains, which exhibited a distinct additional signal. Relative quantification of the putative casbene signal was conducted on the basis of measured peak areas (Fig. 2A, left panel). GC coupled with mass spectrometric detection was employed to corroborate accumulation of a compound with a mass spectrum corresponding to previously reported analyses of casbene (King et al., 2014; Luo et al., 2016) (Fig. 2A, right panel). Co-expression of *ispA* as well as *ispA-dxs-idi* in strain SB1003 resulted in a 1.7- and 2.3-fold increased casbene titer, demonstrating the applicability of our previously established engineering tools (Troost et al., 2019) also for diterpene production in *R. capsulatus*. The presence of the MVA pathway showed no effect on casbene levels (SB1003-MVA + *RcCS*), or even a drastic decrease of the casbene levels when *ispA* or *ispA-dxs-idi* were additionally co-expressed. In these strains, enhanced stress levels may increase the risk of plasmid instability, but since the result was confirmed in independent experimental runs, plasmid rearrangement effects appear rather unlikely. Therefore, we speculate metabolic effects to be the reason for the low product levels in SB1003-MVA under co-expression of the FPP synthase and MEP pathway genes.

To evaluate the engineering concepts for tetraterpene production, vectors pRhon5Hi-2-crtY-crtI, pRhon5Hi-2-crtY-crtI-ispA and pRhon5Hi-2-crtY-crtI-ispA-dxs-idi were employed for β-carotene synthesis in *R. capsulatus* strains SB1003 and SB1003-MVA. After 2 days of photoheterotrophic cultivation, carotenoids were extracted from cells and subsequently analyzed (Fig. 2B, left panel). Using HPLC coupled with a photo diode array detector, produced β-carotene was quantified with an authentic reference for calibration. The expression of the carotenoid biosynthesis genes from *P. ananatis* alone and in combination with *ispA* in

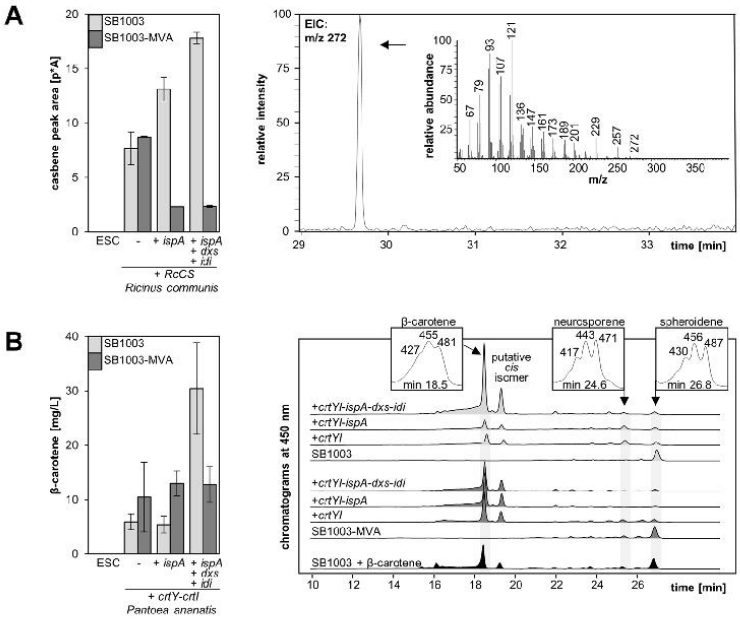

Fig. 2. Production of casbene and β-carotene in *R. capsulatus*. Production of the non-native di- and tetraterpenes was implemented by pRhon5Hi-2-based expression of casbene synthase (*Rc*CS) from *R. communis* or phytoene desaturase (CrtI) and lycopene cyclase (CrtY) from *P. ananatis* in *R. capsulatus* SB1003 (light gray) under photoheterotrophic cultivation conditions. The co-expressed genes *ispA* (from *R. capsulatus*), *dxs* and *idi* (from *R. sphaeroides*) are localized on the respective expression vectors in synthetic operons. The MVA gene cluster from *P. zeaxanthinifaciens* was co-expressed by use of strain SB1003-MVA (dark gray). **(A)** Casbene accumulation in an overlaid *n*-dodecane phase was quantified as relative peak areas by GC-FID (left) and verified by GC–MS analysis (right). **(B)** β-carotene production was analyzed by HPLC-PDA using an authentic reference for calibration and calculation of product titers based on the signal attributed to all-*trans* β-carotene. Putative *cis* isomers were ignored for quantification. HPLC chromatograms (recorded at 450 nm) are representative of replicate experiments (min. triplicate), with specific absorption spectra extracted from PDA data at the indicated retention times of β-carotene, neurosporene and spheroidene. Results in the bar diagrams represent means of independent replicate cultivations (min. triplicate) with the respective standard deviations. ESC, empty strain control.

strain SB1003 resulted in similar titers of about 5 mg/L β-carotene. In this strain, the co-expression of *ispA-dxs-idi*, however, led to a significant increase to 30 mg/L. Co-expression of the MVA pathway genes had a positive effect, with mean titers roughly doubled yielding ~10 mg/L compared to the wildtype strain expressing CrtI and CrtY. This level remained basically unchanged when *ispA* or *ispA-dxs-idi* were additionally co-expressed in SB1003-MVA. In none of the strains, the intermediate lycopene was detected. Specific yields of β-carotene are summarized in the Supplementary Table S3.

HPLC-traces moreover revealed that in the engineered strains, the intrinsic carotenoid biosynthesis was significantly altered by implementation of β-carotene production (Fig. 2B, right panel). The amounts of spheroidene, which accumulates as main carotenoid in the bacterium under anaerobic conditions, were reduced upon expression of CrtI and CrtY from *P. ananatis*. Interestingly, this effect did not seem to be compensated when precursor biosynthetic genes were co-expressed. We further observed that especially cells expressing only CrtI and CrtY produced traces of neurosporene, an intermediate in spheroidene biosynthesis. Nevertheless, heterologous terpene biosynthesis did not affect phototrophic growth of *R. capsulatus* for any of the terpene production setups, as cell densities were all in the same range at the time of sampling (see Fig. S1). In summary, we could demonstrate the biosynthesis of casbene and moderate production of β-carotene as proof of concept. For both, co-expression of the recombinant biosynthetic genes with *ispA-dxs-idi* led to best results in the wildtype background, while use of strain SB1003-MVA yielded rather inconclusive results.

3.3. Heterologous biosynthesis of the FPP-derived triterpene squalene

To test if squalene production could be likewise optimized in *R. capsulatus* by the modular engineering approach, squalene synthase 1 (SQS1) from *A. thaliana*, here referred to as *At*SQS, was introduced into strains SB1003 and SB1003-MVA *via* the vectors pRhon5Hi-2-SQS1, pRhon5Hi-2-SQS1-ispA and pRhon5Hi-2-SQS1-ispA-dxs-idi. Cells were harvested after two days of photoheterotrophic cultivation for extraction and analysis by HPLC-UV, using an authentic reference for calibration and determination of squalene titers (Fig. 3, top panel). Squalene titers of around 65 mg/L were reached by expressing the synthase alone in *R. capsulatus* SB1003. Surprisingly, each metabolic engineering approach – co-expression of *ispA*, *ispA-dxs-idi*, the MVA cluster, or their combination – reduced titers to a minimum of around 12 mg/L (*R. capsulatus* SB1003-MVA harboring pRhon5Hi-2-SQS1-ispA-dxs-idi).

To test, if product levels could be enhanced by applying our engineering tools when squalene synthases from other organisms are employed, we chose respective enzymes from four different organisms, namely the thermophilic cyanobacterium *Thermosynechococcus elongatus* (*Te*SQS), the green colonial microalga *Botryococcus braunii* (*Bb*SQS), the Gram-negative methanotroph *Methylococcus capsulatus* (*Mc*SQS), and *Homo sapiens* (*Hs*SQS). These were selected as promising candidates for having been functionally expressed in prokaryotes previously, or exhibiting high *in vitro* activities (Katabami et al., 2015; Khan et al., 2015; Lee and Poulter, 2008; Ohtake et al., 2014; Okada et al., 2000; Thompson et al., 1998). Based on previous reports, full length sequences or truncated versions were employed as detailed in the Methods Section and in Supplementary Table S1. The genes were cloned in the pRhon5Hi-2-based expression vectors for co-expression of precursor biosynthetic genes and squalene analysis according to the above described experiments.

In comparison to the initially tested *At*SQS, expression of *Te*SQS and *Bb*SQS in *R. capsulatus* SB1003 led to much lower titers (around 20 mg/L), while *Hs*SQS and *Mc*SQS enabled titers in a similar range with 43 and 71 mg/L. This observation indicates that the analyzed synthases might exhibit differences regarding their functional expression, stability, or activity. Remarkably, very different patterns of product titers were observed upon co-expression of precursor biosynthetic genes for every synthase, again demonstrating a benefit of the modular engineering toolset. While product titers could not be enhanced by co-expression of precursor biosynthetic genes in the case of *Bb*SQS, the low product levels obtained with *TeSQS*

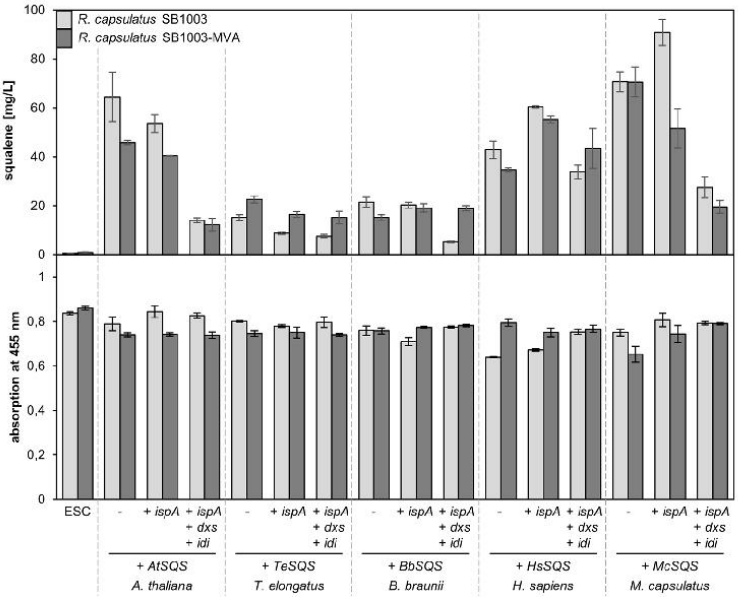

Fig. 3. Production of squalene in *R. capsulatus*. Production was implemented by pRhon5Hi-2-based expression of squalene synthases from *A. thaliana* (*At*), *T. elongatus* (*Te*), *B. braunii* (*Bb*), *H. sapiens* (*Hs*) and *M. capsulatus* (*Mc*) in *R. capsulatus* SB1003. The genes *ispA* (from *R. capsulatus*), *dxs* and *idi* (from *R. sphaeroides*) were co-expressed on the vector in synthetic operons. The MVA gene cluster from *P. zeaxanthinifaciens* was co-expressed by use of strain SB1003-MVA. After photoheterotrophic cultivation, squalene production was analyzed by HPLC-UV analysis using an authentic reference for calibration and calculation of product titers (mg/L, upper panel). Absorption at 455 nm in whole cell EtOH extracts (lower panel) is shown as a measure of spheroidene production. Results represent means of independent triplicate cultivations with the respective standard deviations. ESC, empty strain control.

could be increased by use of the strain SB1003-MVA (providing 23 mg/L). Squalene accumulation obtained with *Hs*SQS or *Mc*SQS was increased by co-expression of *ispA* in strain SB1003, yielding 61 mg/L and the overall highest squalene titer of 90 mg/L, respectively, within this comparative experiment. Specific yields of squalene are summarized in the Supplementary Table S3. Taken together, our studies thus showed that with *R. capsulatus* (i) casbene biosynthesis is generally possible, (ii) moderate β-carotene titers can be reached, and (iii) very different squalene levels - from moderate to substantial maximal titers - were obtained with five different synthases in diverse engineering setups. We therefore chose the latter case to investigate if intrinsic carotenoid levels differed in the set of squalene production strains during phototrophic growth. We first compared the strains SB1003 and SB1003-MVA and, remarkably, did not observe an increase in the signal of the intrinsic carotenoids upon introduction of the MVA pathway. Interestingly, carotenoid-specific absorption of ethanol extracts was also largely unaffected by squalene production in comparison to the empty strain controls (Fig. 3, bottom panel). Hence, our results indicate that squalene production did not consume significant amounts of cellular isoprenoids at the expense of intrinsic carotenoid biosynthesis, but the intrinsic metabolism was capable of compensating for additional FPP consumption to some extent. Moreover, we did not observe strong effects on cell growth (Fig. S2). In summary, our toolkits previously established for the heterologous biosynthesis of sesquiterpenoids (Troost et al., 2019) proved suitable to implement the biosynthesis of di-, tri- and tetraterpenes. The different effects of individual combinations of engineering modules (Table 1) highlight the value of easy-to-apply genetic setups allowing to identify optimal production conditions.

4. Discussion

This study clearly demonstrates the applicability of *R. capsulatus* as an alternative phototrophic production host for di-, tri-, and tetraterpenes using casbene, squalene and β-carotene as model compounds. In addition, we show the effects of metabolic engineering and use of different terpene biosynthetic enzymes on terpene production .

Table 1
Genetic setups for the highest terpene levels in *R. capsulatus* within our studies.

	Test case (synthase / product)	Setup resulting in highest product level (strain / co-expressed genes on pRhon5Hi-2)	Reference
	*Pc*PS / patchoulol	SB1003-MVA / *ispA-dxs-idi*	(Troost et al., 2019)
C15	*Cs*VS / valencene	SB1003-MVA / *ispA-dxs-idi*	(Troost et al., 2019)
	*Cn*VS / valencene	SB1003-MVA / *ispA*	(Troost et al., 2019)
C20	*Rc*CS / casbene	SB1003 / *ispA-dxs-idi*	This study
	*At*SQS / squalene	SB1003 / -	This study
	*Te*SQS / squalene	SB1003-MVA / -	This study
C30	*Bb*SQS / squalene	SB1003 / -	This study
	*Hs*SQS / squalene	SB1003 / *ispA*	This study
	*Mc*SQS / squalene	SB1003 / *ispA*	This study
C40	CrtYI / β-carotene	SB1003 / *ispA-dxs-idi*	This study

The beneficial effects of enhancing the precursor synthesis in the isoprenoid anabolic pathway for terpenoid production are well-known (Moser and Pichler, 2019). Likewise, the necessity of fine-tuning due to feedback and feedforward inhibitory effects within the biosynthetic pathway has been discussed (Dahl et al., 2013; Hage-Hülsmann et al., 2019; Park et al., 2017; Troost et al., 2019). For casbene and β-carotene production, co-expression of terpene biosynthetic enzymes from *R. communis* and *P. ananatis*, respectively, with IspA, DxS and Idi was most successful in our study. The same biosynthetic module also led to best results in our previous study on heterologous sesquiterpene biosynthesis in the host (Troost et al., 2019), when combined with the additional expression of the MVA pathway (Table 1). However, in the present study, strengthening the intrinsic isoprenoid metabolism of *R. capsulatus* at the steps of DXP synthase, IPP isomerase and FPP synthase was more effective than the implementation of the MVA pathway or combinations of both. This might indicate an interaction between the

MEP and MVA pathway, as recently discussed for *R. sphaeroides* (Orsi et al., 2020), but the exact mechanisms and factors influencing it remain to be elucidated.

For squalene production, we used five different synthase genes from all kingdoms, whose expression resulted in diverse initial product titers and further produced differential results upon co-expression of precursor biosynthetic genes. While co-expression of the MVA pathway genes was not beneficial for product titers in most cases, and the *ispA-dxs-idi* cassette either had no effect or reduced the production level in every case, co-expression of *ispA* enhanced squalene levels when squalene synthases from *H. sapiens* or *M. capsulatus* were used. These enzymes also showed relatively high initial product titers when expressed alone. Therefore, accumulation of IPP or FPP, which has been reported to exert inhibitory effects on human FPP synthase (Barnard and Popják, 1981; Park et al., 2017), may be avoided due to more efficient conversion to squalene. However, the *A. thaliana* synthase likewise produced a high initial titer, but all engineering approaches led to reduced product levels. This may indicate that further enzyme properties affecting substrate inhibition, which is known for the squalene synthase from yeast (Zhang et al., 1993), are likely additionally relevant. In this context, it is worth underlining that application of the same engineering toolkit for the production of the sesquiterpenes patchoulol and valencene in *R. capsulatus* revealed that strain SB1003-MVA (Table 1), which facilitates the co-expression of the MVA pathway genes, was the best production strain (Troost et al., 2019). This observation thus underpins the value of the modular engineering concept which can help to further develop *Rhodobacter* as a versatile platform organism for the production of diverse terpene classes, allowing individual adaptation in order to meet the requirements of the respective recombinant terpene pathway.

In general, terpene compounds are of high commercial interest. Thus, diverse microbial production systems have been established for their biosynthesis (Kallscheuer et al., 2018; Moser and Pichler, 2019). *Rhodobacter* species have been identified as suitable hosts for sesquiterpene production (Beekwilder et al., 2014; Orsi et al., 2019; Troost et al., 2019) and are applied in industrial processes by Isobionics (now BASF) (Schempp et al., 2018). Since the biosynthesis of other classes of terpenes in these bacteria is less established, we aimed to explore di-, tri-, and tetraterpene synthesis, choosing the above mentioned compounds casbene, squalene and β-carotene as examples. Generally, the heterologous microbial biosynthesis of the plant diterpene casbene and derivatives thereof, which exhibit promising therapeutic effects, has been established in the context of academic and industrial research (e.g. by the company Evolva). Here, maximal production above 100 mg/L was reached in *S. cerevisiae*, aided by metabolic engineering (Callari et al., 2018; Kirby et al., 2010; Wong et al., 2018). Recombinant casbene biosynthesis with titers of ~ 30 µg/L (normalized to a cell density of 1) has also been shown in *E. coli* (Reiling et al., 2004). Due to the absence of a commercial reference, accurate quantification of the product is thus far not possible *via* a straightforward calibration curve, and estimations have relied on the use of other terpenes like α-gurjunene, cembrene or in-house produced extracts. We demonstrate here for the first time applicability of the α-proteobacterium *R. capsulatus* as phototrophic production platform for this plant natural product. Further studies including accurate product quantification are still necessary for assessment of the prokaryotic host in comparison to the well-performing yeast systems, regarding casbene production.

In contrast to casbene, the tetraterpene β-carotene is an established component of various commercial products, marketed by diverse companies including BASF and DSM (Saini and Keum, 2019). While large parts of the required demand are manufactured by chemical synthesis, microbial production of natural β-carotene is gaining importance. Aside from the use of microalgae and other microbes (Dufossé, 2017; Qiang et al., 2019; Wichuk et al., 2014; Yuan and Alper, 2019), both, *S. cerevisiae* and *E. coli*–based host systems have been established, reaching titers at gram scale with the prokaryote after engineering precursor biosynthesis and optimizing fermentation conditions (López et al., 2019; Yang and Guo, 2014). We have now demonstrated that *R. capsulatus* can accumulate 30 mg/L (15 mg/g DCW) β-carotene, which is identical to the recently described yield that could be gained in the closely related *R. sphaeroides* (Qiang et al., 2019), but notably without bioprocess optimization.

Like β-carotene, the triterpene squalene is used in diverse commercial products, for which deep-sea shark liver oil has represented the major source (Gohil et al., 2019). Obtaining the compound from wild-type or engineered microorganisms in economically attractive processes can offer a paradigm change and refrainment from this practice. Very promising studies showed high-level squalene accumulation in natural producers like marine eukaryotic Thraustochytrids (Aasen et al., 2016). In addition, squalene biosynthesis has been engineered in established microbial workhorses, which offer advantages in e.g., growth rates, high-density fermentation and amenability to genetic modifications. Here, squalene titers over 2 g/L have been demonstrated for metabolically engineered *S. cerevisiae* under optimized conditions (Han et al., 2018). *E. coli*-based production reached 230 mg/L squalene upon co-expression of precursor biosynthetic genes (Katabami et al., 2015). In this study, human SQS produced higher titers than the *T. elongatus* enzyme. In contrast, *T. elongatus* SQS was superior to the human synthase for triterpene biosynthesis in *S. cerevisiae* (Qiao et al., 2019). Squalene production has also been established in *R. capsulatus* before, using SQS enzymes from *B. braunii* (Khan et al., 2015). Here, engineering of the MEP pathway led to ca. 14 mg/g DCW with glucose supplementation. In our previous study, expression of *A. thaliana* SQS1 and cultivation under non-phototrophic, microaerobic conditions led to titers of 8 mg/L squalene (Loeschcke et al., 2017). Compared to that, cultivation under photoheterotrophic conditions in the present study enhanced the titer by an order of magnitude. Generally, comparability of product levels obtained in different studies is limited due to variation of multiple parameters, e.g. in the expression system or cultivation regime. By the direct comparison in this study, we identified the SQS from *M. capsulatus*, which was previously only characterized *in vitro*, as most suitable for high-level triterpene production in *R. capsulatus* (maximal titer 90 mg/L, maximal specific yield 58 mg/g DCW), along with the enzymes from *A. thaliana*, and *H. sapiens*, while *B. braunii* and *T. elongatus* SQS enabled only minor product titers. Altogether, here demonstrated product titers are promising but potential industrial applicability remains to be elucidated in further research to assess e.g., bioprocess optimization.

Heterologous production of the named amounts of β-carotene and squalene had different effects on the intrinsic carotenoid production of *R. capsulatus*. Expression of CrtI and CrtY from *P. ananatis* effectively redirected isoprenoid biosynthesis to β-carotene and led to a drastic decrease in the intrinsic carotenoid spheroidene. This indicates that the desaturase CrtI of *P. ananatis* (Misawa et al., 1990) exhibits higher catalytic activity than the intrinsic CrtI of *R. capsulatus* (Armstrong et al., 1989), or has higher affinity to the substrate phytoene. Furthermore, *P. ananatis* CrtI can use neurosporene as substrate for conversion to lycopene by one further desaturation (Hunter et al., 1994), competing with the intrinsic neurosporene hydroxylase CrtC. In addition, substrate inhibition or feedback inhibition loops by products might not apply for the recombinant enzymes. In this context, it remains to be elucidated why low amounts of neurosporene and not lycopene were found to accumulate in strains expressing β-carotene biosynthetic enzymes. Interestingly, no obvious impairment of photoheterotrophic growth was observed for *crtY-crtI* expressing strains, suggesting that β-carotene was functionally incorporated in photosynthetic complexes, as previously shown for closely related *R. sphaeroides* (Hunter et al., 1994). Biosynthesis of squalene, which led to significantly higher product levels, only had a minor impact on *R. capsulatus* carotenoid production, showing that the intrinsic metabolism was capable of compensating for the associated enhanced consumption of isoprene units. On the other hand, it was interesting to note that co-expression of the MVA pathway did not raise spheroidene levels strongly. Since the implementation of this

pathway can lead to significant elevation of heterologous terpene product levels (Beekwilder et al., 2014; Troost et al., 2019), this may indicate a strict regulation system governing the accumulation of intrinsic tetraterpenes.

In the light of urgently required ecologically friendly technologies for building a sustainable bio-based economy, a paradigm change in the chemical industries is aspired. Since phototrophic hosts can utilize CO_2 for the synthesis of valuable compounds and – in contrast to plants – do not compete for arable land or drinking water, their use as alternative hosts promises sustainable terpene production processes (Frigaard, 2016; Heck and Drepper, 2017; Schempp et al., 2018), and has already been adopted by industry in some cases (Dufossé, 2017). For the here addressed compounds, the research interest in phototrophic host systems is documented by e.g., green alga *Chlamydomonas*-based biosynthesis of casbene (Lauersen et al., 2018), microalga *Dunaliella*- and proteobacterium *R. sphaeroides*-based production of β-carotene (Bonnefond et al., 2017; Qiang et al., 2019), and cyanobacteria- or proteobacterium *R. capsulatus*-based synthesis of squalene (Khan et al., 2015; Loeschcke et al., 2017). Our study contributes to this portfolio, demonstrating the biosynthesis of these C20, C30 and C40 terpenes in *R. capsulatus*, and moreover provides insightful case studies using metabolic engineering and recombinant enzymes.

CRediT authorship contribution statement

Jennifer Hage-Hülsmann: Data curation, Writing - original draft. **Oliver Klaus:** Investigation, Methodology, Data curation. **Karl Linke:** Methodology. **Katrin Troost:** Methodology. **Lukas Gora:** Methodology. **Fabienne Hilgers:** Methodology. **Astrid Wirtz:** Methodology. **Beatrix Santiago-Schübel:** Methodology. **Anita Loeschcke:** Data curation, Writing - review & editing, Visualization, Supervision. **Karl-Erich Jaeger:** Conceptualization, Writing - review & editing. **Thomas Drepper:** Conceptualization, Writing - review & editing, Supervision.

Declaration of Competing Interest

The authors report no declarations of interest.

Acknowledgements

JHH was funded by the Deutsche Forschungsgemeinschaft *via*CEPLAS - Cluster of Excellence on Plant Science (EXC1028). The work of OK was funded by the state of North Rhine Westphalia (NRW) and the European Regional Development Fund (EFRE), Project "CLIB-Kompetenzzentrum Biotechnologie (CKB)"34.EFRE-0300096. KT, FH and AL were funded by the Ministry of Culture and Science of the German State of North Rhine-Westphalia through NRW Strategieprojekt BioSC (No. 313/323-400-00213). The authors thankfully acknowledge Dr. Nadine Katzke and Esther Knieps-Grünhagen for valuable discussions on terpene biosynthesis in *R. capsulatus*, GC and HPLC analysis.

Appendix A. Supplementary data

Supplementary material related to this article can be found, in the online version, at doi:https://doi.org/10.1016/j.jbiotec.2021.07.002.

References

Aasen, I.M., Ertesvåg, H., Heggeset, T.M.B., Liu, B., Brautaset, T., Vadstein, O., Ellingsen, T.E., 2016. Thraustochytrids as production organisms for docosahexaenoic acid (DHA), squalene, and carotenoids. Appl. Microbiol. Biotechnol. 100, 4309–4321. https://doi.org/10.1007/s00253-016-7498-4.

Armstrong, G.A., Alberti, M., Leach, F., Hearst, J.E., 1989. Nucleotide sequence, organization, and nature of the protein products of the carotenoid biosynthesis gene cluster of *Rhodobacter capsulatus*. Mol. Gen. Genet. 216, 254–268. https://doi.org/10.1007/BF00334364.

Avalos, J., Limón, M.C., 2015. Biological roles of fungal carotenoids. Curr. Genet. 61, 309–324. https://doi.org/10.1007/s00294-014-0454-x.

Barnard, G.F., Popják, G., 1981. Human liver prenyltransferase and its characterization. Biochim. Biophys. Acta 661, 87–99. https://doi.org/10.1016/0005-2744(81)90086-3.

Bauernfeind, J.C., 1981. Carotenoids as Colorants and Vitamin A Precursors, Technological and Nutritional Applications (Ed.). Academic Press.

Beekwilder, J., van Houwelingen, A., Cankar, K., van Dijk, A.D.J., de Jong, R.M., Stoopen, G., Bouwmeester, H., Achkar, J., Sonke, T., Bosch, D., 2014. Valencene synthase from the heartwood of Nootka cypress (*Callitropsis nootkatensis*) for biotechnological production of valencene. Plant Biotechnol. J. 12, 174–182. https://doi.org/10.1111/pbi.12124.

Bonnefond, H., Moelants, N., Talec, A., Mayzaud, P., Bernard, O., Sciandra, A., 2017. Coupling and uncoupling of triglyceride and beta-carotene production by *Dunaliella salina* under nitrogen limitation and starvation. Biotechnol. Biofuels 10, 25. https://doi.org/10.1186/s13068-017-0713-4.

Bononi, M., Commissati, I., Lubian, E., Fossati, A., Tateo, F., 2002. A simplified method for the HPLC resolution of α-carotene and β-carotene (*trans* and *cis*) isomers. Anal. Bioanal. Chem. 372, 401–403. https://doi.org/10.1007/s00216-001-1144-3.

Britton, G., 1995. UV/VIS spectroscopy. In: Britton, G., Liaaen-Jensen, S., Pfander, H. (Eds.), Carotenoids. Birkhäuser, Basel, pp. 13–62.

Britton, G., Liaaen-Jensen, S., Pfander, H., 2008. Carotenoids Volume 4: Natural Functions (Eds.). Birkhäuser, Basel.

Busquets, A., Keim, V., Closa, M., del Arco, A., Boronat, A., Arró, M., Ferrer, A., 2008. *Arabidopsis thaliana* contains a single gene encoding squalene synthase. Plant Mol. Biol. 67, 25–36. https://doi.org/10.1007/s11103-008-9299-3.

Callari, R., Meier, Y., Ravasio, D., Heider, H., 2018. Dynamic control of *ERG20* and *ERG9* expression for improved casbene production in *Saccharomyces cerevisiae*. Front. Bioeng. Biotechnol. 6, 160. https://doi.org/10.3389/fbioe.2018.00160.

Chen, F., Tholl, D., Bohlmann, J., Pichersky, E., 2011. The family of terpene synthases in plants: a mid-size family of genes for specialized metabolism that is highly diversified throughout the kingdom. Plant J. 66, 212–229. https://doi.org/10.1111/j.1365-313X.2011.04520.x.

Chory, J., Donohue, T.J., Varga, A.R., Staehelin, L.A., Kaplan, S., 1984. Induction of the photosynthetic membranes of *Rhodopseudomonas sphaeroides*: biochemical and morphological studies. J. Bacteriol. 159, 540–554.

Cravens, A., Payne, J., Smolke, C.D., 2019. Synthetic biology strategies for microbial biosynthesis of plant natural products. Nat. Commun. 10, 2142. https://doi.org/10.1038/s41467-019-09848-w.

Dahl, R.H., Zhang, F., Alonso-Gutierrez, J., Baidoo, E., Batth, T.S., Redding-Johanson, A. M., Petzold, C.J., Mukhopadhyay, A., Lee, T.S., Adams, P.D., Keasling, J.D., 2013. Engineering dynamic pathway regulation using stress-response promoters. Nat. Biotechnol. 31, 1039–1046. https://doi.org/10.1038/nbt.2689.

Das, A., Yoon, S.-H., Lee, S.-H., Kim, J.-Y., Oh, D.-K., Kim, S.-W., 2007. An update on microbial carotenoid production: application of recent metabolic engineering tools. Appl. Microbiol. Biotechnol. 77, 505–512. https://doi.org/10.1007/s00253-007-1206-3.

Dickschat, J.S., 2016. Bacterial terpene cyclases. Nat. Prod. Res. 33, 87–110. https://doi.org/10.1039/c5np00102a.

Dueber, M.T., Adolf, W., West, C.A., 1978. Biosynthesis of the diterpene phytoalexin casbene: partial purification and characterization of casbene synthetase from *Ricinis communis*. Plant Physiol. 62, 598–603. https://doi.org/10.1104/pp.62.4.598.

Dufossé, L., 2017. Current carotenoid production using microorganisms. In: Singh, O. (Ed.), Bio-Pigmentation and Biotechnological Implementations. Wiley & Sons, pp. 87–106. https://doi.org/10.1002/9781119166191.ch4.

Efferth, T., 2017. From ancient herb to modern drug: *Artemisia annua* and artemisinin for cancer therapy. Semin. Cancer Biol. 46, 65–83. https://doi.org/10.1016/j.semcancer.2017.02.009.

Fox, C.B., 2009. Squalene emulsions for parenteral vaccine and drug delivery. Molecules 14, 3286–3312. https://doi.org/10.3390/molecules14093286.

Frank, A., Groll, M., 2017. The methylerythritol phosphate pathway to isoprenoids. Chem. Rev. 117, 5675–5703. https://doi.org/10.1021/acs.chemrev.6b00537.

Frigaard, N.U., 2016. Biotechnology of anoxygenic phototrophic bacteria. Adv. Biochem. Eng. Biotechnol. 156, 139–154. https://doi.org/10.1007/10_2015_5006.

Gohil, N., Bhattacharjee, G., Khambhati, K., Braddick, D., Singh, V., 2019. Engineering strategies in microorganisms for the enhanced production of squalene: advances, challenges and opportunities. Front. Bioeng. Biotechnol. 7, 50. https://doi.org/10.3389/fbioe.2019.00050.

Hage-Hülsmann, J., Metzger, S., Wewer, V., Buechel, F., Troost, K., Thies, S., Loeschcke, A., Jaeger, K.-E., Drepper, T., 2019. Biosynthesis of cycloartenol by expression of plant and bacterial oxidosqualene cyclases in engineered *Rhodobacter capsulatus*. J. Biotechnol. X 4, 100014. https://doi.org/10.1016/j.btecx.2020.100014.

Han, J.Y., Seo, S.H., Song, J.M., Lee, H., Choi, E.-S., 2018. High-level recombinant production of squalene using selected *Saccharomyces cerevisiae* strains. J. Ind. Microbiol. Biotechnol. 45, 239–251. https://doi.org/10.1007/s10295-018-2018-4.

Hanahan, D., 1983. Studies on transformation of *Escherichia coli* with plasmids. J. Mol. Biol. 166, 557–580. https://doi.org/10.1016/S0022-2836(83)80284-8.

Heck, A., Drepper, T., 2017. Engineering photosynthetic α-proteobacteria for the production of recombinant proteins and terpenoids. In: Hallenbeck, P.C., Cham, S.I. P. (Eds.), Modern Topics in the Phototrophic Prokaryotes: Environmental and Applied Aspects. Springer International Publishing, pp. 395–425, 395–425.

Huang, Z.-R., Lin, Y.-K., Fang, J.-Y., 2009. Biological and pharmacological activities of squalene and related compounds: potential uses in cosmetic dermatology. Molecules 14, 540–554. https://doi.org/10.3390/molecules14010540.

Hümbelin, M., Thomas, A., Lin, J., Li, J., Jore, J., Berry, A., 2002. Genetics of isoprenoid biosynthesis in *Paracoccus zeaxanthinifaciens*. Gene 297, 129–139. https://doi.org/10.1016/S0378-1119(02)00877-6.

Hunter, C.N., Hundle, B.S., Hearst, J.E., Lang, H.P., Gardiner, A.T., Takaichi, S., Cogdell, R.J., 1994. Introduction of new carotenoids into the bacterial photosynthetic apparatus by combining the carotenoid biosynthetic pathways of *Erwinia herbicola* and *Rhodobacter sphaeroides*. J. Bacteriol. 176, 3692–3697. https://doi.org/10.1128/jb.176.12.3692-3697.1994.

Kallscheuer, N., Classen, T., Drepper, T., Marienhagen, J., 2018. Production of plant metabolites with applications in the food industry using engineered microorganisms. Curr. Opin. Biotechnol. 56, 7–17. https://doi.org/10.1016/j.copbio.2018.07.008.

Katabami, A., Li, L., Iwasaki, M., Furubayashi, M., Saito, K., Umeno, D., 2015. Production of squalene by squalene synthases and their truncated mutants in *Escherichia coli*. J. Biosci. Bioeng. 119, 165–171. https://doi.org/10.1016/j.jbiosc.2014.07.013.

Khan, N.E., Nybo, S.E., Chappell, J., Curtis, W.R., 2015. Triterpene hydrocarbon production engineered into a metabolically versatile host - *Rhodobacter capsulatus*. Biotechnol. Bioeng. 112, 1523–1532. https://doi.org/10.1002/bit.25573.

King, A.J., Brown, G.D., Gilday, A.D., Larson, T.R., Graham, I.A., 2014. Production of bioactive diterpenoids in the *Euphorbiaceae* depends on evolutionarily conserved gene clusters. Plant Cell 26, 3286–3298. https://doi.org/10.1105/tpc.114.129668.

Kirby, J., Nishimoto, M., Park, J.G., Withers, S.T., Nowroozi, F., Behrendt, D., Rutledge, E.J.G., Fortman, J.L., Johnson, H.E., Anderson, J.V., Keasling, J.D., 2010. Cloning of casbene and neocembrene synthases from Euphorbiaceae plants and expression in *Saccharomyces cerevisiae*. Phytochemistry 71, 1466–1473. https://doi.org/10.1016/j.phytochem.2010.06.001.

Klipp, W., Masepohl, B., Pühler, A., 1988. Identification and mapping of nitrogen fixation genes of *Rhodobacter capsulatus*: duplication of a *nifA-nifB* region. J. Bacteriol. 170, 693–699. https://doi.org/10.1128/jb.170.2.693-699.1988.

Lauersen, K.J., Wichmann, J., Baier, T., Kampranis, S.C., Pateraki, I., Møller, B.L., Kruse, O., 2018. Phototrophic production of heterologous diterpenoids and a hydroxy-functionalized derivative from *Chlamydomonas reinhardtii*. Metab. Eng. 49, 116–127. https://doi.org/10.1016/j.ymben.2018.07.005.

Le, T.T.T., Gardner, J., Hoang-Le, D., Schmidt, C.W., MacDonald, K.P., Lambley, E., Schroder, W.A., Ogbourne, S.M., Suhrbier, A., 2009. Immunostimulatory cancer chemotherapy using local ingenol-3-angelate and synergy with immunotherapies. Vaccine 27, 3053–3062. https://doi.org/10.1016/j.vaccine.2009.03.025.

Lee, S., Poulter, C.D., 2008. Cloning, solubilization, and characterization of squalene synthase from *Thermosynechococcus elongatus* BP-1. J. Bacteriol. 190, 3808–3816. https://doi.org/10.1128/JB.01939-07.

Liao, S.-G., Chen, H.-D., Yue, J.-M., 2009. Plant orthoesters. Chem. Rev. 109, 1092–1140. https://doi.org/10.1021/cr0782832.

Loeschcke, A., Markert, A., Wilhelm, S., Wirtz, A., Rosenau, F., Jaeger, K.-E., Drepper, T., 2013. TREX: a universal tool for the transfer and expression of biosynthetic pathways in bacteria. ACS Synth. Biol. 2, 22–33. https://doi.org/10.1021/sb3000657.

Loeschcke, A., Dienst, D., Wewer, V., Hage-Hülsmann, J., Dietsch, M., Kranz-Finger, S., Hüren, V., Metzger, S., Urlacher, V.B., Gigolashvili, T., Kopriva, S., Axmann, I.M., Drepper, T., Jaeger, K.-E., 2017. The photosynthetic bacteria *Rhodobacter capsulatus* and *Synechocystis* sp. PCC 6803 as new hosts for cyclic plant triterpene biosynthesis. PLoS One 12, e0189816. https://doi.org/10.1371/journal.pone.0189816.

Lombard, J., Moreira, D., 2011. Origins and early evolution of the mevalonate pathway of isoprenoid biosynthesis in the three domains of life. Mol. Biol. Evol. 28, 87–99. https://doi.org/10.1093/molbev/msq177.

López, J., Cataldo, V.F., Peña, M., Saa, P.A., Saitua, F., Ibaceta, M., Agosin, E., 2019. Build your bioprocess on a solid strain—β-carotene production in recombinant *Saccharomyces cerevisiae*. Front. Bioeng. Biotechnol. 7, 171. https://doi.org/10.3389/fbioe.2019.00171.

Luo, D., Callari, R., Hamberger, B., Wubshet, S.G., Nielsen, M.T., Andersen-Ranberg, J., Hallström, B.M., Cozzi, F., Heider, H., Møller, B.L., Staerk, D., Hamberger, B., 2016. Oxidation and cyclization of casbene in the biosynthesis of *Euphorbia* factors from mature seeds of *Euphorbia lathyris* L. Proc. Natl. Acad. Sci. U.S.A. 113, E5082–E5089. https://doi.org/10.1073/pnas.1607504113.

Mahizan, N.A., Yang, S.-K., Moo, C.-L., Song, A.A.-L., Chong, C.-M., Chong, C.-W., Abushelaibi, A., Lim, S.-H.E., Lai, K.-S., 2019. Terpene derivatives as a potential agent against antimicrobial resistance (AMR) pathogens. Molecules 24, 2631. https://doi.org/10.3390/molecules24142631.

Marienhagen, J., Bott, M., 2013. Metabolic engineering of microorganisms for the synthesis of plant natural products. J. Biotechnol. 163, 166–178. https://doi.org/10.1016/j.jbiotec.2012.06.001.

Mau, C.J.D., West, C.A., 1994. Cloning of casbene synthase cDNA: evidence for conserved structural features among terpenoid cyclases in plants. Proc. Natl. Acad. Sci. U.S.A. 91, 8497–8501. https://doi.org/10.1073/pnas.91.18.8497.

Misawa, N., Nakagawa, M., Kobayashi, K., Yamano, S., Izawa, Y., Nakamura, K., Harashima, K., 1990. Elucidation of the *Erwinia uredovora* carotenoid biosynthetic pathway by functional analysis of gene products expressed in *Escherichia coli*. J. Bacteriol. 172, 6704–6712. https://doi.org/10.1128/jb.172.12.6704-6712.1990.

Moesta, P., West, C., 1985. Casbene synthetase: regulation of phytoalexin biosynthesis in *Ricinus communis* L. seedlings. Purification of casbene synthetase and regulation of its biosynthesis during elicitation. Arch. Biochem. Biophys. 238, 325–333. https://doi.org/10.1016/0003-9861(85)90171-7.

Mortensen, A., 2006. Carotenoids and other pigments as natural colorants. Pure Appl. Chem. 78, 1477–1491. https://doi.org/10.1351/pac200678081477.

Moser, S., Pichler, H., 2019. Identifying and engineering the ideal microbial terpenoid production host. Appl. Microbiol. Biotechnol. 103, 5501–5516. https://doi.org/10.1007/s00253-019-09892-y.

Ohtake, K., Saito, N., Shibuya, S., Kobayashi, W., Amano, R., Hirai, T., Sasaki, S., Nakano, C., Hoshino, T., 2014. Biochemical characterization of the water-soluble squalene synthase from *Methylococcus capsulatus* and the functional analyses of its two DXXD(E)D motifs and the highly conserved aromatic amino acid residues. FEBS J. 281, 5479–5497. https://doi.org/10.1111/febs.13090.

Okada, S., Devarenne, T.P., Chappell, J., 2000. Molecular characterization of squalene synthase from the green microalga *Botryococcus braunii*. Race B. Arch. Biochem. Biophys. 373, 307–317. https://doi.org/10.1006/abbi.1999.1568.

Onsi, E., Folch, P.L., Monje-López, V.T., Fernhout, B.M., Turcato, A., Kengen, S.W.M., Eggink, G., Weusthuis, R.A., 2019. Characterization of heterotrophic growth and sesquiterpene production by *Rhodobacter sphaeroides* on a defined medium. J. Ind. Microbiol. Biotechnol. 46, 1179–1190. https://doi.org/10.1007/s10295-019-02201-6.

Onsi, E., Beekwilder, J., van Gelder, D., van Houwelingen, A., Eggink, G., Kengen, S.W. M., Weusthuis, R.A., 2020. Functional replacement of isoprenoid pathways in *Rhodobacter sphaeroides*. Microb. Biotechnol. 13, 1082–1093. https://doi.org/10.1111/1751-7915.13562.

Onsi, E., Beekwilder, J., Eggink, G., Kengen, S.W.M., Weusthuis, R.A., 2021. The transition of *Rhodobacter sphaeroides* into a microbial cell factory. Biotechnol. Bioeng. 118, 531–541. https://doi.org/10.1002/bit.27593.

Park, J., Zielinski, M., Magder, A., Tsantrizos, Y.S., Berghuis, A.M., 2017. Human farnesyl pyrophosphate synthase is allosterically inhibited by its own product. Nat. Commun. 8, 14132. https://doi.org/10.1038/ncomms14132.

Qiang, S., Su, A.P., Li, Y., Chen, Z., Hu, C.Y., Meng, Y.H., 2019. Elevated *β*-carotene synthesis by the engineered *Rhodobacter sphaeroides* with enhanced CrtY expression. J. Agric. Food Chem. 67, 9560–9568. https://doi.org/10.1021/acs.jafc.9b02597.

Qiao, W., Zhou, Z., Liang, Q., Mosongo, I., Li, C., Zhang, Y., 2019. Improving lupeol production in yeast by recruiting pathway genes from different organisms. Sci. Rep. 9, 2992. https://doi.org/10.1038/s41598-019-39497-4.

Reddy, L.H., Couvreur, P., 2009. Squalene: a natural triterpene for use in disease management and therapy. Adv. Drug Deliv. Rev. 61, 1412–1426. https://doi.org/10.1016/j.addr.2009.09.005.

Reiling, K.K., Yoshikuni, Y., Martin, V.J.J., Newman, J., Bohlmann, J., Keasling, J.D., 2004. Mono and diterpene production in *Escherichia coli*. Biotechnol. Bioeng. 87, 200–212. https://doi.org/10.1002/bit.20128.

Saini, R.K., Keum, Y.-S., 2019. Microbial platforms to produce commercially vital carotenoids at industrial scale: an updated review of critical issues. J. Ind. Microbiol. Biotechnol. 46, 657–674. https://doi.org/10.1007/s10295-018-2104-7.

Sandmann, G., 1994. Carotenoid biosynthesis in microorganisms and plants. Eur. J. Biochem. 223, 7–24. https://doi.org/10.1111/j.1432-1033.1994.tb18961.x.

Schempp, F.M., Drummond, L., Buchhaupt, M., Schrader, J., 2018. Microbial cell factories for the production of terpenoid flavor and fragrance compounds. J. Agric. Food Chem. 66, 2247–2258. https://doi.org/10.1021/acs.jafc.7b00473.

Schierle, J., Pietsch, B., Ceresa, A., Fizet, C., Waysek, E.H., 2004. Method for the determination of β-carotene in supplements and raw materials by reversed-phase liquid chromatography: single laboratory validation. J. AOAC Int. 87, 1070–1082.

Schmidt-Dannert, C., 2014. Biosynthesis of terpenoid natural products in fungi. In: Schrader, J., Bohlmann, J. (Eds.), Biotechnology of Isoprenoids. Advances in Biochemical Engineering/Biotechnology. Springer, Cham, pp. 19–61. https://doi.org/10.1007/10_2014_283.

Simon, R., Priefer, U., Pühler, A., 1983. A broad host range mobilization system for *in vivo* genetic engineering: transposon mutagenesis in Gram negative bacteria. Nat. Biotechnol. 1, 784–791. https://doi.org/10.1038/nbt1183-784.

Strnad, H., Lapidus, A., Paces, J., Ulbrich, P., Vlcek, C., Paces, V., Haselkorn, R., 2010. Complete genome sequence of the photosynthetic purple nonsulfur bacterium *Rhodobacter capsulatus* SB 1003. J. Bacteriol. 192, 3545–3546. https://doi.org/10.1128/JB.00366-10.

Thimmappa, R., Geisler, K., Louveau, T., O'Maille, P., Osbourn, A., 2014. Triterpene biosynthesis in plants. Annu. Rev. Plant Biol. 65, 225–257. https://doi.org/10.1146/annurev-arplant-050312-120229.

Thompson, J.F., Danley, D.E., Mazzalupo, S., Milos, P.M., Lira, M.E., Harwood Jr, H.J., 1998. Truncation of human squalene synthase yields active, crystallizable protein. Arch. Biochem. Biophys. 350, 283–290. https://doi.org/10.1006/abbi.1997.0502.

Troost, K., Loeschcke, A., Hilgers, F., Özgür, A.Y., Weber, T.M., Santiago-Schübel, B., Svensson, V., Hage-Hülsmann, J., Habash, S.S., Grundler, F.M.W., Schleker, A.S.S., Jaeger, K.-E., Drepper, T., 2019. Engineered *Rhodobacter capsulatus* as a phototrophic platform organism for the synthesis of plant sesquiterpenoids. Front. Microbiol. 10, 1998. https://doi.org/10.3389/fmicb.2019.01998.

Wichuk, K., Brynjólfsson, S., Fu, W., 2014. Biotechnological production of value-added carotenoids from microalgae: emerging technology and prospects. Bioengineered 5, 204–208. https://doi.org/10.4161/bioe.28720.

Wołosik, K., Knaś, M., Zalewska, A., Niczyporuk, M., Przystupa, A.W., 2013. The importance and perspective of plant-based squalene in cosmetology. J. Cosmet. Sci. 64, 59–66.

Wong, J., de Rond, T., D'Espaux, L., van der Horst, C., Dev, I., Rios-Solis, L., Kirby, J., Scheller, H., Keasling, J., 2018. High-titer production of lathyrane diterpenoids from sugar by engineered *Saccharomyces cerevisiae*. Metab. Eng. 45, 142–148. https://doi.org/10.1016/j.ymben.2017.12.007.

Xu, W., Ma, X., Wang, Y., 2016. Production of squalene by microbes: an update. World J. Microbiol. Biotechnol. 32, 195. https://doi.org/10.1007/s11274-016-2155-8.

Yang, J., Guo, L., 2014. Biosynthesis of β-carotene in engineered *E. coli* using the MEP and MVA pathways. Microb. Cell Fact. 13, 160. https://doi.org/10.1186/s12934-014-0160-x.

Yoshida, M., Tanabe, Y., Yonezawa, N., Watanabe, M.M., 2012. Energy innovation potential of oleaginous microalgae. Biofules 3, 761–781. https://doi.org/10.4155/bfs.12.63.

Yuan, S.-F., Alper, H.S., 2019. Metabolic engineering of microbial cell factories for production of nutraceuticals. Microb. Cell Fact. 18, 46. https://doi.org/10.1186/s12934-019-1096-y.

Zhang, D., Jennings, S.M., Robinson, G.W., Poulter, C.D., 1993. Yeast squalene synthase: expression, purification, and characterization of soluble recombinant enzyme. Arch. Biochem. Biophys. 304, 133–143. https://doi.org/10.1006/abbi.1993.1331.

Supporting information

Production of C20, C30 and C40 terpenes in the engineered phototrophic bacterium *Rhodobacter capsulatus*

Jennifer Hage-Hülsmann[a,d,*], Oliver Klaus[a,*], Karl Linke[a], Katrin Troost[a], Lukas Gora[a], Fabienne Hilgers[a,e], Astrid Wirtz[b], Beatrix Santiago-Schübel[c], Anita Loeschcke[a,e,†], Karl-Erich Jaeger[a,b,d,e], Thomas Drepper[a,d,e,†]

[a] Institute of Molecular Enzyme Technology, Heinrich Heine University Düsseldorf, Forschungszentrum Jülich, Jülich, Germany

[b] Institute of Bio- and Geosciences IBG-1, Forschungszentrum Jülich, Jülich, Germany

[c] Central Division of Analytical Chemistry ZEA-3: Analytik/Biospec, Forschungszentrum Jülich, Jülich, Germany

[d] Cluster of Excellence on Plant Sciences (CEPLAS)

[e] Bioeconomy Science Center (BioSC), Forschungszentrum Jülich, Jülich, Germany

*equally contributed
† corresponding authors

Content **page**

Table S1. Sequences of terpene biosynthetic genes. Protein sequences that were used to design codon usage adapted genes are indicated with Genbank ID. Full length sequences were used unless truncations are specified. The start and stop codon of every gene is marked in bold.

Rc*CS from *Ricinus communis **[NCBI Protein XP_002513340.1]** **ATG**GCCCTGCCCTCGGCCGCGATGCAAAGCAACCCGGAAAAGCTGAACCTGTTCCACCGC CTGTCCAGCCTGCCCACCACCTCGCTTGAGTATGGGAATAATCGCTTCCCGTTCTTTTCG TCGTCGGCCAAATCGCACTTCAAGAAGCCGACGCAGGCGTGCCTTTCGTCGACGACCCAT CAGGAAGTGCGCCCGCTGGCCTATTTCCCCCCCACCGTCTGGGGGAACCGGTTCGCGTCG CTTACCTTCAACCCGTCGGAGTTCGAAAGCTATGACGAACGGGTGATCGTGCTGAAGAAG AAGGTCAAGGATATCCTGATCTCCTCGACCTCGGATTCGGTGGAGACCGTCATCCTGATC GACCTTCTTTGCCGCCTGGGCGTCAGCTATCATTTCGAAAACGATATCGAGGAACTGCTG TCGAAGATCTTCAACTCCCAGCCGGACCTTGTGGACGAAAAAGAGTGCGACCTGTACACC GCGGCGATCGTCTTCCGCGTCTTCCGCCAACATGGCTTCAAGATGTCGTCGGACGTCTTT TCGAAATTCAAAGATTCCGACGGCAAGTTCAAAGAGTCGCTGCGCGGCGACGCGAAGGGC ATGCTGTCCCTGTTTGAAGCGTCGCATCTGAGCGTGCATGGCGAAGACATCCTTGAGGAA GCGTTCGCCTTCACCAAAGATTATCTGCAATCGTCGGCGGTCGAGCTGTTCCCCAACCTG AAGCGGCATATCACCAACGCGCTGGAGCAGCCGTTCCATTCGGGCGTCCCCCGCCTGGAG GCGCGCAAGTTCATCGACCTGTACGAAGCCGATATCGAGTGCCGGAACGAGACCCTGCTG GAATTTGCCAAGCTGGATTATAACCGCGTGCAGCTGCTGCATCAGCAAGAGCTGTGCCAG TTCTCGAAGTGGTGGAAGGATCTGAACCTGGCCTCGGACATCCCGTACGCCCGGGATCGG ATGGCGGAGATCTTCTTCTGGGCGGTCGCGATGTACTTCGAGCCCGATTATGCGCACACC CGCATGATCATCGCCAAAGTGGTGCTGCTTATCAGCCTGATCGACGACACCATCGACGCC TATGCCACCATGGAGGAAACCCATATCCTGGCGGAAGCGGTCGCCCGCTGGGACATGTCG TGCCTGGAGAAGCTGCCGGACTATATGAAAGTGATCTCACAAGCTGCTGCTGAACACGTTC TCGGAGTTCGAGAAGGAGCTTACCGCCGAAGGGAAATCCTACTCGGTCAAGTATGGGCGG GAGGCGTTCCAGGAGCTGGTGCGCGGCTACTATCTTGAAGCCGTCTGGCGGGACGAGGGC AAGATCCCCTCGTTCGATGACTACCTGTACAACGGCTCGATGACCACCGGGCTGCCGCTG GTGAGCACCGCCTCGTTCATGGGCGTGCAGGAAATCACCGGCCTGAACGAATTCCAGTGG CTGGAAACCAATCCCAAACTGTCGTACGCCTCGGGGGCGTTCATCCGGCTGGTCAACGAC CTGACGTCCCATGTGACGGAACAGCAGCGCGGGCACGTGGCGTCCTGCATCGATTGCTAC ATGAACCAGCACGGGGTCTCGAAAGACGAAGCGGTGAAAATCCTGCAGAAGATGGCCACC GATTGCTGGAAGGAAATCAACGAGGAGTGCATGCGGCAGTCGCAGGTGTCGGTGGGGCAC CTGATGCGGATCGTGAACCTGGCGCGCCTTACCGACGTCTCGTACAAGTATGGCGATGGC TACACGGATTCGCAGCAGCTGAAACAGTTCGTGAAGGGCCTGTTCGTGGATCCGATCAGC ATCAAGCTTT**GA**
CrtY and CrtI from *Pantoea ananatis* **[NCBI Protein P21687.1 and P21685.1]** The intergenic sequence between *crtY* and *crtI* is the original sequence of the *crt* gene cluster from *Pantoea ananatis* (shown in blue) **ATG**CAACCCCATTACGACCTGATCCTTGTGGGGGCCGGGCTTGCGAACGGCCTTATCGCG CTGCGGCTCCAGCAGCAGCAACCCGATATGCGGATCCTCCTTATCGACGCCGCCCCGCAG GCGGGCGGGAACCATACGTGGTCCTTCCACCACGATGACCTCACGGAATCGCAACACCGG TGGATTGCCCCCCTGGTCGTCCATCATTGGCCGGATTATCAGGTCCGCTTCCCGACGCGC CGGCGCAAGCTGAACTCCGGCTATTTCTGCATCACGTCCCAGCGGTTTGCCGAAGTGCTC CAGCGGCAGTTCGGGCCGCACCTTTGGATGGACACGGCGGTCGCCGAGGTGAACGCGGAG TCCGTCCGGCTCAAGAAGGGCCAGGTGATCGGCGCGCGGGCCGTCATCGATGGGCGGGGC TACGCGGGGAACAGCGCCCTGTCGGTGGGCTTTCAGGCCTTCATCGGCCAGGAATGGCGG CTTTCGCACCCCCATGGGCTCTCCTCCCCCATCATCATGGATGCGACCGTCGATCAGCAA AACGGGTATCGCTTTGTGTACAGCCTGCCGCTTTCCCCGACCCGGCTCCTCATCGAGGAT ACCCACTACATCGATAACGCGACGCTCGACCCGGAATGCGCGCGGGCAAAACATCTGCGAT TATGCGGCCCAACAGGGGTGGCAGCTTCAGACGCTGCTGCGGGAAGAGCAAGGCGCCCTC CCGATCACGCTGTCCGGGAACGCGGACGCCTTTTGGCAGCAGCGCCCCCTGGCCTGTTCG GGGCTCCGGGCGGGGCTGTTCCATCCCACCACCGGCTATTCCCTGCCCCTGGCGGTCGCC GTGGCGGATCGCCTCTCCGCGCTCGACGTCTTTACCTCCGCGAGCATCCATCATGCGATC ACCCATTTTGCGCGCGAGCGCTGGCAGCAGCAGGGCTTTTTCCGCATGCTGAACCGCATG CTGTTTCTCGCGGGGCCCGCGGACTCCCGCTGGCGGGTCATGCAGCGGTTTTACGGCCTC CCCGAGGACCTCATCGCGCGCTTTTATGCGGGGAAGCTCACCCTGACCGACCGGCTCCGG ATCCTGTCCGGCAAGCCGCCCGTGCCCGTCCTCGCGGCGCTCCAAGCGATCATGACCACG CATCGG**TGA**AGAGCGACTAC**ATG**AAGCCTACTACCGTCATCGGGGCCGGCTTTGGCGGCC TGGCCCTGGCCATCCGGTTGCAAGCCGCGGGTATCCCGGTGCTTCTGCTTGAGCAACGCG ACAAGCCGGGCGGCCGGGCCTACGTCTATGAAGACCAGGGGTTCACCTTCGATGCGGGCC CCACCGTCATCACCGACCCCAGCGCGATCGAGGAGCTGTTCGCCCTGGCCGGCAAGCAGC TTAAAGAGTACGTCGACGTGCTGCCGGTCACCCCCTTCTATCGGCTGTGCTGGGAGTCGG GTAAAGTGTTCAACTACGACAATGACCAGACCCGGCTTGAGGCGCAGATCCAGCAGTTCA ACCCCCGCGACGTCGAGGGGTATCGGCAGTTCCTGGATTACTCCCGCGCCGTGTTCAAGG AGGGCTACCTCAAGCTCGGGACGGTGCCGTTCCTCAGCTTTCGTGATATGCTCCGGGCCG CCCCCCAGCTTGCCAAACTTCAGGCCTGGCGTTCCGTGTACAGCAAGGTCGCCAGCTACA TCGAAGATGAGCATCTGCGCCAGGCCTTTTCCTTTCACAGCCTGCTTGTCGGGGGGAACC CCTTCGCCACCAGCTCCATCTATACGCTGATTCACGCCCTGGAACGGGAATGGGGCGTGT GGTTTCCCCGCGGGGGCACCGGCGCCCTCGTCCAGGGTATGATTAAGCTGTTCCAGGACC

TGGGGGGCGAGGTCGTGCTCAATGCGCGTGTCTCGCACATGGAGACCACGGGTAACAAGA
TCGAGGCGGTGCATCTCGAAGATGGGCGCCGTTTTCTGACCCAAGCGGTGGCGTCCAACG
CCGACGTGGTGCATACCTATCGCGACCTGCTCTCGCAGCACCCCGCGGCGGTGAAGCAGT
CCAATAAGCTGCAGACGAAGCGCATGAGCAATTCCCTGTTCGTGCTCTACTTCGGGCTCA
ACCATCATCATGACCAGCTTGCGCATCATACCGTGTGCTTTGGCCCGCGGTATCGCGAAC
TGATCGATGAGATCTTCAACCATGACGGCCTTGCCGAAGATTTTTCCCTCTACCTGCATG
CGCCGTGGGTGACCGACTCCAGCCTGGCGCCCGAGGGGTGCGGCAGCTATTACGTGCTCG
CGCCGGTGCCGCATCTTGGCACCGCGAACCTTGACTGGACCGTGGAAGGGCCTAAGTTGC
GCGACCGCATCTTCGCGTATCTTGAACAGCATTATATGCCCGGCCTTCGGAGCCAGCTGG
TCACCCATCGGATGTTCACCCCGTTCGACTTCCGCGACCAGCTTAACGCCTACCATGGCT
CCGCGTTCTCCGTGGAACCCGTGCTTACCCAGTCGGCGTGGTTCCGGCCGCATAATCGCG
ACAAGACCATCACGAACCTTTATCTGGTGGGCGCCGGCACCCACCCGGGCGCCGGCATCC
CCGGCGTGATCGGCTCCGCGAAGGCGACGGCCGGGCTTATGCTTGAAGACCTGATT**TGA**

SQS1 from *Arabidopsis thaliana*
[NCBI Protein NP_195190.1]

ATGGGCAGCCTGGGCACCATGCTGCGCTATCCGGATGATATCTATCCGCTGCTGAAAATG
AAACGCGCGATCGAAAAAGCGGAAAAACAGATCCCGCCGGAACCGCATTGGGGCTTCTGC
TATAGCATGCTGCATAAAGTGAGCCGCAGCTTCAGCCTGGTGATCCAGCAGCTGAACACC
GAACTGCGCAACGCGGTGTGCGTGTTCTATCTGGTGCTGCGCGCGCTGGATACCGTGGAA
GATGATACCAGCATCCCGACCGATGAAAAAGTGCCGATCCTGATCGCGTTCCATCGCCAT
ATCTATGATACCGATTGGCATTATAGCTGCGGCACCAAAGAATATAAAATCCTGATGGAT
CAGTTCCATCATGTGAGCGCGGCGTTCCTGGAACTGGAAAAAGGCTATCAGGAAGCGATC
GAAGAAATCACCCGCCGCATGGGCGCGGCATGGCGAAATTCATCTGCCAGGAAGTGGAA
ACCGTGGATGATTATGATGAATATTGCCATTATGTGGCGGGCCTGGTGGGCCTGGGCCTG
AGCAAACTGTTCCTGGCGGCGGGCAGCGAAGTGCTGACCCCGGATTGGGAAGCGATCAGC
AACAGCATGGGCCTGTTCCTGCAGAAAACCAACATCATCCGCGATTATCTGGAAGATATC
AACGAAATCCCGAAAAGCCGCATGTTCTGGCCGCGCGAAATCTGGGGCAAATATGCGGAT
AAACTGGAAGATCTGAAATATGAAGAAAACACCAACAAAAGCGTGCAGTGCCTGAACGAA
ATGGTGACCAACGCGCTGATGCATATCGAAGATTGCCTGAAATATATGGTGAGCCTGCGC
GATCCGAGCATCTTCCGCTTCTGCGCGATCCCGCAGATCATGGCGATCGGCACCCTGGCG
CTGTGCTATAACAACGAACAGGTGTTCCGCGGCGTGGTGAAACTGCGCCGCGGCCTGACC
GCGAAAGTGATCGATCGCACCAAAACCATGGCGGATGTGTATGGCGCGTTCTATGATTTC
AGCTGCATGCTGAAAACCAAAGTGGATAAAAACGATCCGAACGCGAGCAAAACCCTGAAC
CGCCTGGAAGCGGTGCAGAAACTGTGCCGCGATGCGGGCGTGCTGCAGAACCGCAAAAGC
TATGTGAACGATAAAGGCCAGCCGAACAGCGTGTTCATCATCATGGTGGTGATCCTGCTG
GCGATCGTGTTCGCGTATCTGCGCGCGAAC**TAA**

Te*SQS from *Thermosynechococcus elongatus
[NCBI Protein NP_681887.1]

ATGCGCGTGGGCGTGAACCCGCCGATGATCCAGATGGTGCTGGAAAACCCGGTGAGCGTG
AAAGATGCGGAATGCTTCTGCCAGGAAATCCTGCCGCAGGTGAGCCGCACCTTCGCGCTG
AGCATCCGCTTCCTGCCGGGCAACCTGGGCCGCGCGGTGCTGGTGGCGTATCTGATCTGC
CGCATCGCGGATACCGTGGAAGATGATCCGGTGGCGAGCATCGCGGCGAAAACCGCGCTG
CTGGATCATCTGCTGCAGTGCTTCGATAGCCCGGCGCTGGCGAACAGCTATGGCGAAACC
GCGCGCGGCGTGCAGGGCGAACCGGCGCATGTGCAGCTGGTGAAACATACCGGCATCGTG
TTCACCCTGTATCGCAGCCTGCCGCGCACCAGCCAGCAGCATGTGCAGCGCTGGGTGAGC
GAAATGGTGCATGGCATGAAAAAATTCATCAACCTGTATCCGAACGGCATCCGCATCCAG
ACCCTGGCGGAATATAAAGAATATTGCTATTATGTGGCGGGCACCGTGGGCTATCTGCTG
ACCGATCTGTGGCATGAACATAGCCCGAGCATCGGCGCGGATGAATATCAGGTGCTGCTG
AAACGCTGCGCGGCGTTCGGCGAAGCGCTGCAGACCGTGAACATCCTGAAAGATATCGCG
TGGGATGCGGAACATGAAAACAGCATCTATATCCCGAACGAAAGCCTGATCCTGCAGGGC
AGCAGCCATCAGACCCTGCTGAGCGCGGAACATCTGCAGCAGAACCATGCGGCGATCAAA
GAACTGATCGCGCTGGCGTGGCATGATCTGGATGAAGCGCAGGCGTATCTGCTGAGCGTG
CCGAAGCGGCGATCCCGATCCGCCTGTTCTGCGTGCTGCCGCTGCTGTTCGCGTATGCG
ACCCTGCGCGAACTGACCCATAGCACCGCGATGCTGCAGCCGGGCGGCGGCGTGAAAATC
AGCCGCGCGGAAGTGAAAAGCCTGATGGTGATGGGCCCGCTGAGCATCCTGAGCAACCAT
GGCCTGCGCTGGCTGATCGGCCAGGTGCGCCAGAAACCGTTCATCCTGGGCGGCCTG**TAA**

Bb*SQS from *Botryococcus braunii
[NCBI Protein AAF20201.1 with 26 amino acid truncation at the C-terminus]

ATGGGCATGCTGCGCTGGGGCGTGGAAAGCCTGCAGAACCCGGATGAACTGATCCCGGTG
CTGCGCATGATCTATGCGGATAAATTCGGCAAAATCAAACCGAAAGATGAAGATCGCGGC
TTCTGCTATGAAATCCTGAACCTGGTGAGCCGCAGCTTCGCGATCGTGATCCAGCAGCTG
CCGGCGCAGCTGCGCGATCCGGTGTGCATCTTCTATCTGGTGCTGCGCGCGCTGGATACC
GTGGAAGATGATATGAAAATCGCGGCGACCACCAAAATCCCGCTGCTGCGCGATTTCTAT
GAAAAAATCAGGCGATCGCAGCTTCCGCATGACCGCGGGCGATCAGAAAGATTATATCCGC
CTGCTGGATCAGTATCCGAAAGTGACCAGCGTGTTCCTGAAACTGACCCCGCGCGAACAG
GAAATCATCGCGGATATCACCAAACGCATGGGCAACGGCATGGCGGATTTCGTGCATAAA
GGCGTGCCGGATACCGTGGGCGATTATGATCTGTATTGCCATTATGTGGCGGGCGTGGTG
GGCCTGGGCCTGAGCCAGCTGTTCGTGGCGAGCGGCCTGCAGAGCCCGAGCCTGACCCGC
AGCGAAGATCTGAGCAACCATATGGGCCTGTTCCTGCAGAAAACCAACATCATCCGCGAT
TATTTCGAAGATATCAACGAACTGCCGGCGCCGCGCATGTTCTGGCCGCGCGAAATCTGG
GGCAAATATGCGAACAACCTGGCGGAATTCAAAGATCCGGCGAACAAAGCGGCGGCGATG
TGCTGCCTGAACGAAATGGTGACCGATGCGCTGCGCCATGCGGTGTATTGCCTGCAGTAT
ATGAGCATGATCGAAGATCCGCAGATCTTCAACTTCTGCGCGATCCCGCAGACCATGGCG

TTCGGCACCCTGAGCCTGTGCTATAACAACTATACCATCTTCACCGGCCCGAAAGCGGCG
GTGAAACTGCGCCGCGGCACCACCGCGAAACTGATGTATACCAGCAACAACATGTTCGCG
ATGTATCGCCATTTCCTGAACTTCGCGGAAAAACTGGAAGTGCGCTGCAACACCGAAACC
AGCGAAGATCCGAGCGTGACCACCACCCTGGAACATCTGCATAAAATCAAAGCGGCGTGC
AAAGCGGGCCTGGCGCGCACCAAAGATGATACCTTCGATGAACTGCGCAGCCGCCTGCTG
GCGCTGACCGGCGGCAGCTTCTATCTGGCGTGGACCTATAACTTCCTGGATCTGCGCGGC
CCGGGCGATCTGCCGACCTTCCTGAGCGTGACCCAGCATTGGTGG**TGA**

Hs*SQS from *Homo sapiens
[NCBI Protein AAH09251.1 with 30 amino acid truncation at the N-terminus and 47 amino acid truncation at the C-terminus]

ATGGATCAGGATAGCCTGAGCAGCAGCCTGAAAACCTGCTATCGCTATCTGAACCAGACC
AGCCGCAGCTTCGCGGCGGTGATCCAGGCGCTGGATGGCGAAATGCGCAACGCGGTGTGC
ATCTTCTATCTGGTGCTGCGCGCGCTGGATACCCTGGAAGATGATATGACCATCAGCGTG
GAAAAAAAAGTGCCGCTGCTGCATAACTTCCATAGCTTCCTGTATCAGCCGGATTGGCGC
TTCATGGAAAGCAAAGAAAAAGATCGCCAGGTGCTGGAAGATTTCCCGACCATCAGCCTG
GAATTCCGCAACCTGGCGGAAAAATATCAGACCGTGATCGCGGATATCTGCCGCCGCATG
GGCATCGGCATGGCGGAATTCCTGGATAAACATGTGACCAGCGAACAGGAATGGGATAAA
TATTGCCATTATGTGGCGGGCCTGGTGGGCATCGGCCTGAGCCGCCTGTTCAGCGCGAGC
GAATTCGAAGATCCGCTGGTGGGCGAAGATACCGAACGCGCGAACAGCATGGGCCTGTTC
CTGCAGAAAACCAACATCATCCGCGATTATCTGGAAGATCAGCAGGGCGGCCGCGAATTC
TGGCCGCAGGAAGTGTGGAGCCGCTATGTGAAAAAACTGGGCGATTTCGCGAAACCGGAA
AACATCGATCTGGCGGTGCAGTGCCTGAACGAACTGATCACCAACGCGCTGCATCATATC
CCGGATGTGATCACCTATCTGAGCCGCCTGCGCAACCAGAGCGTGTTCAACTTCTGCGCG
ATCCCGCAGGTGATGGCGATCGCGACCCTGGCGGCGTGCTATAACAACCAGCAGGTGTTC
AAAGGCGCGGTGAAAATCCGCAAAGGCCAGGCGGTGACCCTGATGATGGATGCGACCAAC
ATGCCGGCGGTGAAAGCGATCATCTATCAGTATATGGAAGAAATCTATCATCGCATCCCG
GATAGCGATCCGAGCAGCAGCAAAACCCGCCAGATCATCAGCACCATCCGCACCCAGAAC
TGA

Mc*SQS from *Methylococcus capsulatus
[NCBI Protein CAA71097.1]

ATGAGCGGCACCCCGCCGAGCCAGCCGGCGCGCCATGAACATCTGAGCGATGATGAATTC
CAGGCGCATTTCCTGGATGGCGTGAGCCGCACCTTCGCGCTGACCATCCCGCGCCTGCCG
GAAGGCCTGGCGCGCCCGGTGAGCAACGGCTATCTGCTGTGCCGCATCGTGGATACCATC
GAAGATGAAGTGGCGCTGACCAGCACCCAGAAACGCCGCTATTGCGAACATTTCGCGCGC
GTGGTGGCGGGCACCGCGCCGGCGGCGCCGCTGGCGGATGAACTGTTCCCGCTGCTGAGC
GATCAGACCCTGGCGGCGGAACGCGAACTGATCGCGGCGATCCCGCGCGTGATCAGCATC
ACCCATGGCTTCGCGGCGCCGCAGCAGGAAGCGCTGGCGGAATGCGTGGCGACCATGAGC
CGCGGCATGGCGGAATTCCAGGATAAAGATCTGCGCCATGGCCTGGAAGATCTGCGCCAG
ATGGGCGATTATTGCTATTATGTGGCGGGCGTGGTGGGCGAAATGCTGACCCGCCTGTTC
TGCCATTATAGCCCGGAAATCGCGGCGCATCGCAGCCGCCTGATGGAACTGGCGTGCCCG
TTCGGCCAGGGCCTGCAGATGACCAACATCCTGAAAGATCTGTGGGATGATCATGCGCGC
GGCGTGTGCTGGCTGCCGCAGGAAGTGTTCACCGAATGCGGCTTCAGCCTGACCGAACTG
CGCCCGCATCATGCGAACCCGGATTTCGTGCGCGGCTTCGAACGCCTGATCGGCGTGGCG
CATGCGCATCTGCGCAACGCGCTGGAATATACCCTGCTGATCCCGCGCCATGAAACCGGC
ATCCGCGAATTCTGCCTGTGGGCGCTGGGCATGGCGGTGCTGACCCTGCGCAAAATCCAT
CGCCATCCGTATTTCAGCGATAGCGCGCAGGTGAAAATCACCCGCCAGGCGGTGAAAGCG
ACCATCGTGACCAGCCGCCTGACCCGCGGCAGCGATACCCTGCTGAAAGCGACCTTCCGC
CTGGCGGGCCTGGGCCTGCCGGCGGCGGTGCCGGCGGCGGTGCTGCAGCCGCGCCCGATC
GATATC**TGA**

Table S2. Oligonucleotides, plasmids and strains used in this study. Endonuclease restriction sites are underlined.

Oligonucleotides		
Name	**Application**	**Nucleotide sequence (5'→3')**
Cloning of *crtY-crtI* into pRhon5Hi-2 for β-carotene biosynthesis		
NdeI_crtI/Y Fw	PCR of *crtY-crtI*	ATATCATATGCAACCCCATTACGACCTGA
HindIII_crtI/Y rv	PCR of *crtY-crtI*	GATCAAGCTTTCAAATCAGGTCTTCAAGCATAAGC
Cloning of *SQS1* into pRhon5Hi-2 for squalene biosynthesis		
At-SQS-fw	PCR of *SQS1* (*A. thaliana*)	GCACCTGGCCGTCTAGAAATAATTTTGTTTAAC
At-SQS-rev	PCR of *SQS1* (*A. thaliana*)	TTTAAAAGCTTTACGTATCTTAAGTTAGTTCGCGCGCAG
Cloning of *ispA* into pRhon5Hi-2-RcCS and pRhon5Hi-2-crtY-crtI		
HindIII_ispA R.c. fw	PCR of *ispA* (*R. capsulatus*)	ATTAAGCTTTGAAAGAAGGAGATATAATGTTTTCCGAACGTTTG
XhoI_ispA R.c. rv	PCR of *ispA* (*R. capsulatus*)	ATATACTCGAGATATAACGCGTTCACTTGTCGCGTTCGATCAC
Plasmids		
Name		**Characteristics / Reference**
Plasmids used for cloning		
pRhon5Hi-2		pBBR22b backbone (pBBR1 ori & mob, pET22b MCS), Km^R,(pBSL15 *aphII*), P_{nif} (from *R. capsulatus*) (Troost et al., 2019)
pRhon5Hi-2-CnVS-ispA		pRhon5Hi-2, CnVS (*C. nootkatensis*), *ispA* (*R. capsulatus*) (Troost et al., 2019)
pRhon5Hi-2-CnVS-ispA-dxs-idi		pRhon5Hi-2-CnVS-ispA, *dxs*, *idi* (*R. sphaeroides*) (Troost et al., 2019)
Plasmids for casbene biosynthesis		
pRhon5Hi-2-RcCS		pRhon5Hi-2, RcCS (*R. communis*)
pRhon5Hi-2-RcCS -ispA		pRhon5Hi-2-RcCS, *ispA* (*R. capsulatus*)
pRhon5Hi-2-RcCS -ispA-dxs-idi		pRhon5Hi-2-RcCS-ispA, *dxs*, *idi* (*R. sphaeroides*)
Plasmids for β-carotene biosynthesis		
pRhon5Hi-2-crtY-crtI		pRhon5Hi-2, crtY-crtI (*P. ananatis*)
pRhon5Hi-2-crtY-crtI-ispA		pRhon5Hi-2-crtY-crtI, *ispA* (*R. capsulatus*)
pRhon5Hi-2-crtY-crtI-ispA-dxs-idi		pRhon5Hi-2-crtY-crtI-ispA, *dxs*, *idi* (*R. sphaeroides*)
Plasmids for squalene biosynthesis		
pRhon5Hi-2-SQS1		pRhon5Hi-2 carrying SQS1 (*A. thaliana*) (Loeschcke et al., 2017)
pRhon5Hi-2-SQS1-ispA		pRhon5Hi-2-SQS1, *ispA* (*R. capsulatus*)
pRhon5Hi-2-SQS1-ispA-dxs-idi		pRhon5Hi-2-SQS1-ispA, *dxs*, *idi* (*R. sphaeroides*)
Strains		
Name		**Characteristics or application / Reference**
Escherichia coli		
E. coli DH5α		Used for plasmid amplification / cloning (Hanahan, 1983)
E. coli S17-1		Used for conjugational plasmid transfer (Simon et al., 1983)
Rhodobacter capsulatus		
R. capsulatus SB1003		Wildtype strain, Rif^R (Strnad et al., 2010)
R. capsulatus SB1003-MVA		Strain SB1003 carrying the MVA gene cluster from *P. zeaxanthinifaciens* under control of P_{nif}, Rif^R/Gm^R (Troost et al., 2019)

Table S3. Specific β-carotene and squalene yields in *R. capsulatus*. Specific yields of β-carotene (upon expression of CrtY and CrtI of *P. ananatis*), and squalene (upon expression of SQS of different organisms: *At*, *A. thaliana*; *Bb*, *B. braunii*; *Te*, *T. elongatus*; *Hs*, *H. sapiens*; *Mc*, *M. capsulatus*) were calculated based on reached cell densities at the time point of cell harvesting for product analysis and a correlation of OD_{660nm} = 1 with 0.6 mgDCW (dry cell weight). Coloration indicates higher (darker) and lower (lighter) values for β-carotene (orange) and squalene (green). Co-expression of isoprenoid precursor biosynthetic genes *ispA* (of *R. capsulatus*), *dxs* and *idi* (of *R. sphaeroides*) and the MVA gene cluster (of *P. zeaxanthinifaciens*) is specified.

***Rhodobacter capsulatus* strain**	**specific yield [mg/gDCW]**					
	β-carotene (*crtY-crtI*)	**squalene** (SQS)				
		At	*Bb*	*Te*	*Hs*	*Mc*
SB1003	3.11 ± 0.92	46.44 ± 5.45	14.44 ± 1.23	10.00 ± 0.82	25.11 ± 2.20	39.33 ± 1.09
SB1003 *+ispA*	2.83 ± 1.01	41.11 ± 2.45	12.67 ± 0.72	5.56 ± 0.31	34.44 ± 0.83	57.78 ± 4.43
SB1003 *+ispA-dxs-idi*	15.06 ± 4.39	9.33 ± 0.47	3.22 ± 0.16	4.67 ± 0.47	19.56 ± 1.81	17.56 ± 2.20
SB1003-MVA	5.67 ± 3.73	28.33 ± 0.54	9.22 ± 0.57	13.33 ± 0.94	22.67 ± 0.47	40.89 ± 4.76
SB1003-MVA *+ispA*	7.39 ± 1.78	24.11 ± 0.16	11.67 ± 0.98	9.78 ± 0.63	35 ± 0.94	32,56 ± 6.53
SB1003-MVA *+ispA-dxs-idi*	7.22 ± 1.93	7.33 ± 1.52	11.44 ± 0.68	9.22 ± 1.66	27.00 ± 4.77	11.78 ± 1.37

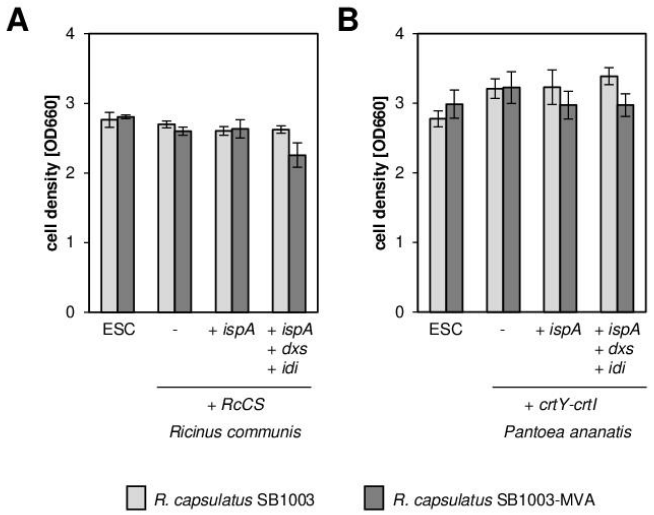

Fig. S1. Final cell densities of *R. capsulatus* casbene and β-carotene production cultures. Cell densities of *R. capsulatus* strains SB1003 (light gray) or SB1003-MVA (dark gray) with pRhon5Hi-2-based expression vectors carrying *RcCS* (from *R. communis*) or *crtY-crtI* (from *P. ananatis*) alone or in combination with *ispA* or *ispA-dxs-idi*, were analyzed, using empty strain controls (ESC) as a reference. To this end, the absorption of 1 mL diluted cell samples was measured at 660 nm at the time points of sampling for analysis of product accumulation, i.e. after 48 h of cultivation at 30 °C under anaerobic conditions in the light in RCV medium with serine. Data represent mean values of three independent cultivations with the respective standard deviations.

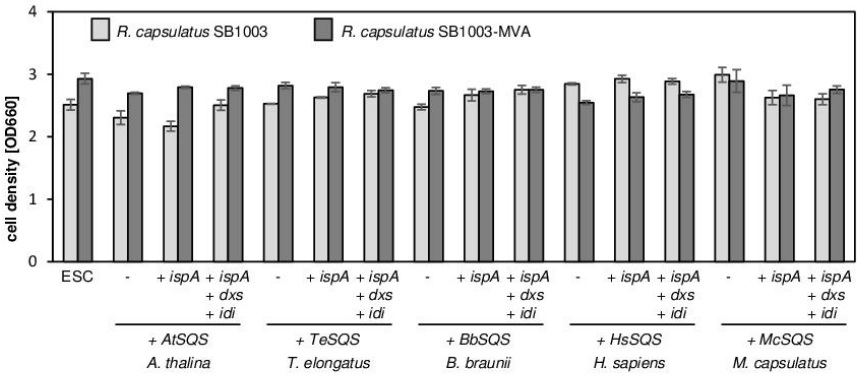

Fig. S2. Final cell densities of *R. capsulatus* squalene production cultures. Cell densities of *R. capsulatus* strains SB1003 (light gray) or SB1003-MVA (dark gray) with pRhon5Hi-2-based expression vectors carrying squalene synthases (SQS) from *A. thaliana* (*At*), *T. elongatus* (*Te*), *B. braunii* (*Bb*), *H. sapiens* (*Hs*) or *M. capsulatus* (*Mc*) alone or in combination with *ispA* or *ispA-dxs-idi*, were analyzed, using empty strain controls (ESC) as a reference. To this end, the absorption of 1 mL diluted cell samples was measured at 660 nm at the time points of sampling for analysis of product accumulation, i.e. after 48 h of cultivation at 30 °C under anaerobic conditions in the light in RCV medium with serine. Data represent mean values of three independent cultivations with the respective standard deviations.

II.1.3 Evaluation of the *R. capsulatus* terpenoid production chassis for the synthesis of β-caryophyllene

PUBLICATION III

Heterologous production of β-caryophyllene and its activity against plant pathogenic fungi

Fabienne Hilgers[1]*, Samer S Habash[2]*, Anita Loeschcke[1], Yannic S Ackermann[1], Stefan Neumann[2], Achim Heck[1], **Oliver Klaus**[1], Jennifer Hage-Hülsmann[1], Florian M W Grundler[2], Karl-Erich Jaeger[1,3], A Sylvia S Schleker[2#], Thomas Drepper[1#]

[1]Institute of Molecular Enzyme Technology, Heinrich Heine University Düsseldorf, Forschungszentrum Jülich, 52425 Jülich, Germany

[2]INRES-Molecular Phytomedicine, University of Bonn, 53115 Bonn, Germany

[3]Institute of Bio- and Geosciences IBG-1: Biotechnology, Forschungszentrum Jülich GmbH, 52425 Jülich, Germany

* These authors contributed equally

[#] Corresponding authors

Status: published

Microorganisms,

2021, 01,14, 9(1):168

https://doi.org/10.3390/microorganisms9010168

Own contribution:

Designing and performing *in vivo* experiments, analyzing data, editing manuscript

microorganisms

MDPI

Article

Heterologous Production of β-Caryophyllene and Evaluation of Its Activity against Plant Pathogenic Fungi

Fabienne Hilgers [1,†], Samer S. Habash [2,†], Anita Loeschcke [1], Yannic Sebastian Ackermann [1], Stefan Neumann [2], Achim Heck [3], Oliver Klaus [1], Jennifer Hage-Hülsmann [1], Florian M. W. Grundler [2], Karl-Erich Jaeger [1,3], A. Sylvia S. Schleker [2,*] and Thomas Drepper [1,*]

1 Institute of Molecular Enzyme Technology, Heinrich-Heine-University Düsseldorf, Forschungszentrum Jülich, Wilhelm-Johnen-Straße, 52428 Jülich, Germany; f.hilgers@fz-juelich.de (F.H.); a.loeschcke@fz-juelich.de (A.L.); y.ackermann@fz-juelich.de (Y.S.A.); o.klaus@fz-juelich.de (O.K.); j.hage-huelsmann@fz-juelich.de (J.H.-H.); karl-erich.jaeger@fz-juelich.de (K.-E.J.)

2 INRES—Molecular Phytomedicine, University of Bonn, Karlrobert-Kreiten-Str. 13, 53115 Bonn, Germany; samer@uni-bonn.de (S.S.H.); sneuman1@uni-bonn.de (S.N.); grundler@uni-bonn.de (F.M.W.G.)

3 Institute of Bio- and Geosciences (IBG-1: Biotechnology) Forschungszentrum Jülich, Wilhelm-Johnen-Straße, 52428 Jülich, Germany; a.heck@fz-juelich.de

* Correspondence: sylvia.schleker@uni-bonn.de (A.S.S.S.); t.drepper@fz-juelich.de (T.D.)

† These authors contributed equally to this work.

Abstract: Terpenoids constitute one of the largest and most diverse groups within the class of secondary metabolites, comprising over 80,000 compounds. They not only exhibit important functions in plant physiology but also have commercial potential in the biotechnological, pharmaceutical, and agricultural sectors due to their promising properties, including various bioactivities against pathogens, inflammations, and cancer. In this work, we therefore aimed to implement the plant sesquiterpenoid pathway leading to β-caryophyllene in the heterologous host *Rhodobacter capsulatus* and achieved a maximum production of 139 ± 31 mg L^{-1} culture. As this sesquiterpene offers various beneficial anti-phytopathogenic activities, we evaluated the bioactivity of β-caryophyllene and its oxygenated derivative β-caryophyllene oxide against different phytopathogenic fungi. Here, both compounds significantly inhibited the growth of *Sclerotinia sclerotiorum* and *Fusarium oxysporum* by up to 40%, while growth of *Alternaria brassicicola* was only slightly affected, and *Phoma lingam* and *Rhizoctonia solani* were unaffected. At the same time, the compounds showed a promising low inhibitory profile for a variety of plant growth-promoting bacteria at suitable compound concentrations. Our observations thus give a first indication that β-caryophyllene and β-caryophyllene oxide are promising natural agents, which might be applicable for the management of certain plant pathogenic fungi in agricultural crop production.

Keywords: terpenoids; sesquiterpene production; *Rhodobacter capsulatus*; β-caryophyllene; bioactivity; phytopathogens; plant pathogenic fungi; plant growth-promoting bacteria

Citation: Hilgers, F.; Habash, S.S.; Loeschcke, A.; Ackermann, Y.S.; Neumann, S.; Heck, A.; Klaus, O.; Hage-Hülsmann, J.; Grundler, F.M.W.; Jaeger, K.-E.; et al. Heterologous Production of β-Caryophyllene and Evaluation of Its Activity against Plant Pathogenic Fungi. *Microorganisms* **2021**, *9*, 168. https://doi.org/10.3390/microorganisms9010168

Received: 10 December 2020
Accepted: 10 January 2021
Published: 14 January 2021

1. Introduction

Among secondary metabolites, terpenoids including the class of sesquiterpenoids represent one of the largest and most diverse groups with over 80,000 known compounds, mostly isolated from plants [1–4]. Based on their number of carbon atoms, they can be divided into the subclasses of hemi- (C_5), mono- (C_{10}), sesqui- (C_{15}), di- (C_{20}), tri- (C_{30}), tetra- (C_{40}) and polyterpenes (>C_{40}) [5,6]. In general, the terpenoid synthesis starts from the two isoprene intermediates isopentenyl pyrophosphate (IPP) and dimethylallyl pyrophosphate (DMAPP), which are provided either by the mevalonate (MVA) pathway or by the 1-deoxy-D-xylulose 5-phosphate (DXP) pathway, also known as the 2-C-methyl-D-erythritol 4-phosphate (MEP) pathway. While the MVA pathway uses acetyl-Coenzyme A (acetyl-CoA) as a substrate and is predominantly found in eukaryotes (e.g., mammals, plants,

and fungi), archaea and a few bacteria [7], the DXP pathway starts from glyceraldehyde-3-phosphate (GAP) and pyruvate and primarily occurs in bacteria, cyanobacteria, and green algae [8]. Starting from IPP and DMAPP, the elongation of linear prenyl pyrophosphates is catalyzed by prenyltransferases via head-to-tail condensations and results in C_{10} geranyl pyrophosphate (GPP), C_{15} farnesyl pyrophosphate (FPP), and C_{20} geranylgeranyl pyrophosphate (GGPP). Finally, GPP is used as a precursor molecule for the synthesis of monoterpenoids, FPP for sesqui- and triterpenoid production, and GGPP for di- and tetraterpenoid biosynthesis. Terpenes exhibit manifold functions in plant physiology and development, including photoprotection (carotenoids), communication (e.g., pinene), or repellant activity against predators and parasites (e.g., verbenone, β-caryophyllene) [9–11]. Furthermore, terpenes are of commercial interest for the pharmaceutical sector due to their various bioactivities suitable for the treatment of pathogen infections, inflammation, or cancer [12,13]. For example, the sesquiterpene farnesol shows inhibitory effects against antibiotic-resistant *Staphylococci*, not only inhibiting the growth of planktonic cells in free suspension but also suppressing biofilm formation of *Staphylococcus aureus*, *Staphylococcus epidermidis*, and *Burkholderia pseudomallei* [14–17]. In the past, these compounds were exclusively obtained from essential oils of natural plant sources, requiring complex and time-consuming downstream processing. β-caryophyllene, for example, was extracted from *Cannabis sativa* [18], clove basil, *Ocimum gratissimum* [19], or representatives of the plant genus *Cordia*, such as *Cordia verbenaceae* [20]. However, the application of microorganisms as heterologous hosts allows the establishment of alternative, cost-effective, and sustainable biotechnological production processes [21–26]. As the efficiency of such processes strongly depends on the achieved production titers, metabolic engineering of the applied hosts together with the optimization of the respective secondary metabolite pathways has gained more attention in the recent past [1,27–31]. So far, terpenoids were mostly produced in the heterologous hosts *Escherichia coli* and *Saccharomyces cerevisiae* [32–36]. However, in recent studies, the terpene production in less common microbes such as phototrophs has also been established and optimized, as for example documented by the *Rhodobacter*-based production of β-farnesene, nootkatone, valencene, and amorphadiene [23,37–40], or the production of various terpenes in cyanobacteria [41].

The phototrophic non-sulfur α-proteobacteria of the genus *Rhodobacter* feature some unique physiological properties, making them interesting microbial hosts for heterologous terpene production: (i) the cell membrane is commonly considered to be a critical determinant in terpenoid production since it can function as a storage compartment for the involved enzymes and metabolites [42,43]. In this context, *Rhodobacter* seems to be particularly suited for terpene production since the bacterium can form an extended intracytoplasmic membrane system (ICM), thereby providing a naturally enlarged reservoir for membrane-bound enzymes and terpenes [44,45]. (ii) As these phototrophic bacteria produce the carotenoids spheroidene and spheroidenone using the DXP pathway [46,47], they further offer a robust and effective isoprenoid metabolism that can be engineered for efficient terpenoid production. (iii) *Rhodobacter* species enable photo(hetero)tropic growth in low-cost minimal media at relatively high growth rates, allowing the utilization of sunlight as an energy source for sustainable cultivation and production processes. Recent studies could demonstrate that engineering the isoprenoid precursor biosynthesis can lead to a strong increase of sesqui- and triterpenoid formation in *R. capsulatus* [39,48,49] and *R. sphaeroides* [38,40,50–52]. In particular, the co-expression of a terpene synthase with the FPP synthase IspA, and/or enzymes constituting the heterologous MVA pathway, resulted in enhanced production of the corresponding plant terpenoids.

A major problem in agricultural crop production is the large number of plant-damaging animals such as insects, mites, and nematodes or pathogens including viruses, bacteria, and fungi, some of which lead to high economic losses of around 60% globally [53]. One of the most widely distributed and destructive pathogens of plants causing white mold disease in more than 400 host plants all over the world is the fungus *Sclerotinia sclerotiorum* (Lib.) de Bary [54]. Another devastating example of fungal diseases is the plant vascular wilt

caused by the *Fusarium* species [55]. Other fungal pathogens such as *Phoma lingam* [56,57], *Alternaria brassicicola* [58], and *Rhizoctonia solani* [59,60] also cause major yield reduction in important crops. To control these pathogens and due to the rapidly growing world population and the resulting increase of food consumption, farmers are using synthetic and biological substances as fertilizers, pesticides, or growth regulators side by side with the cultivation of resistant or tolerant plant varieties [61–64]. Each of these methods has its limitations, but so far, the use of pesticides is the most convenient and commonly used method. Nevertheless, these can have numerous severe side effects on the environment, including the soil [65]. The soil is inhabited by an enormous diversity of organisms that are important players in maintaining a functional ecosystem and that comprise microorganisms with beneficial properties for plant development and health. For that reason, effective and sustainable alternatives are needed. Firstly, plants, as a part of a complex ecosystem, can produce enormous amounts of secondary metabolites for their survival and maintenance. Phenolics and terpenes are examples of metabolites that are produced by plants and act as antimicrobial agents and feeding deterrents [66–72]. The presence of a wide range of terpenes encouraged their use as nature-inspired plant protection agents in agriculture or their use for drug development. One of the commonly stress-associated terpenes is the sesquiterpene β-caryophyllene [73–75]. As mentioned in the previous section, various studies showed that β-caryophyllene exhibits diverse biological activities against many organisms. From a plant protection perspective β-caryophyllene was reported to promote plant growth, to induce plant defense genes, to attract entomopathogenic nematodes, and to be active against certain plant pathogenic bacteria and fungi [76–80].

In this study, we therefore aimed to use the modular co-expression of DXP/MVA genes in combination with the strictly controlled P_{nif} promoter to reconstitute the pathway of the plant sesquiterpene β-caryophyllene in *R. capsulatus* and to optimize the production under phototrophic growth conditions. For heterologous sesquiterpene production, the β-caryophyllene synthase QHS1 from *Artemisia annua* was used. Since this terpene offers a variety of beneficial bioactivities, we further evaluated the potential use of β-caryophyllene and its oxygenated derivative β-caryophyllene oxide as nature-derived fungicides. To this end, the bioactivity of β-caryophyllene/oxide against both representative plant growth-promoting bacteria and phytopathogenic fungi was investigated.

2. Materials and Methods

2.1. Bacterial Strains and Cultivation Conditions

The *Escherichia coli* strain DH5α and strain S17-1 were used for cloning and conjugation of plasmid DNA [81,82]. *E. coli* cells were cultivated at 37 °C using LB agar plates or liquid medium (Luria/Miller, Carl Roth®, Karlsruhe, Germany), containing kanamycin (25 μg mL^{-1}) when appropriate. *R. capsulatus* SB1003 [83] and SB1003-MVA [39], encompassing the chromosomally located genes *mvaA*, *idi*, *hsc*, *mvk*, *pmk* and *mvd* (also designated as MVA gene cluster) from *Paracoccus zeaxanthinifaciens*, were used for plant terpene production. All *R. capsulatus* strains used in this study were either cultivated on PY agar plates [84] containing 2% (*w*/*v*) Select Agar (Thermo Fisher Scientific, Waltham, MA, USA) or in RCV liquid medium [85] at 30 °C. Both media were supplemented with rifampicin (25 μg mL^{-1}). For cultivation of the recombinant *Rhodobacter* strain SB1003-MVA, gentamicin (4 μg mL^{-1}) was further added to the medium. If not stated otherwise, photoheterotrophic cultivation was conducted under anaerobic conditions and permanent illumination with bulb light (2500 lx), as described previously [39]. All bacterial strains and plasmids used in this study are listed in Table S1 (Supplementary Materials). All strains for bioactivity and minimum inhibitory concentration (MIC) evaluation are listed in the respective results section.

2.2. Construction of Expression Vectors

The expression vectors used in this study are based on the pRhon5Hi-2 vector carrying the promoter of the *nifH* gene for heterologous gene expression [39]. The sequence of β-caryophyllene synthase QHS1 from *A. annua* (UniProt: Q8SA63) was used to generate

an appropriate synthetic gene whose DNA sequence is suitable for the codon-usage of *R. capsulatus*. For DNA sequence adaptation, the Codon Optimization Tool by IDT Integrated DNA Technologies and the Graphical Codon Usage Analyzer tool were used [86]. The 1.7-kb *QHS1* gene was obtained from Eurofins Genomics. The synthetic DNA fragment was flanked by appropriate restriction endonuclease recognition sequences (*Xba*I/*Hin*dIII). The final sequence of the synthetic DNA fragment is shown in the Supplementary Materials. For the construction, the *Xba*I/*Hin*dIII hydrolyzed *QHS1* fragment was inserted into likewise hydrolyzed pRhon5Hi-2 as well as a variant, providing the additional isoprenoid biosynthetic gene *ispA*. Thereby, the expression vectors pRhon5Hi-2-QHS1 and pRhon5Hi-2-QHS1-ispA were constructed, carrying the terpene synthase gene immediately downstream of the P_{nif} promoter of the vector. Correct nucleotide sequences of all constructs were confirmed by Sanger sequencing (Eurofins Genomics, Ebersberg, Germany). The *QHS1* expression vectors are summarized in Table S1 (Supplementary Materials).

2.3. Cultivation of R. capsulatus for Heterologous Terpene Production

For the expression of the heterologous terpene biosynthetic genes, respective pRhon5Hi-2-based plasmids were transferred to cells of different *R. capsulatus* strains via conjugational transfer employing *E. coli* S17-1 as donor [84]. Thereafter, transconjugants were selected and further cultivated on PY agar containing kanamycin (25 μg mL^{-1}) and rifampicin (25 μg mL^{-1}). Subsequently, *Rhodobacter* cells were cultivated in airtight 4.5 mL screw neck vials (Macherey-Nagel, Düren, Germany) or airtight 15 mL hungate tubes [87] in liquid RCV medium containing kanamycin (25 μg mL^{-1}) and rifampicin (25 μg mL^{-1}). Precultures were cultivated in 15 mL RCV medium containing 0.1% $(NH_4)_2SO_4$ inoculated with cells from a freshly grown PY agar plate and incubated for 48 h at 30 °C and with bulb light illumination. Expression cultures were inoculated from precultures to an optical density at 660 nm of 0.05 in 4.5 mL or 15 mL RCV medium containing 0.1% serine as an exclusive nitrogen source. Subsequently, cells were incubated at 30 °C under permanent illumination with bulb light (3.6 mW cm^{-2} at 850 nm) or IR light (5.6 mW cm^{-2} at 850 nm) for 3–5 days. For microaerobic expression cultures, cells were cultivated in 20–60 mL RCV medium containing 0.1% serine in 100 mL flasks at 30 °C and 130 rpm in the dark. The absence of ammonium and the cultivation under oxygen-limited conditions led to the induction of the P_{nif}-dependent target gene expression. For the extraction of the produced sesquiterpenes, the cultures were overlaid with 150 μL or 500 μL *n*-dodecane, respectively, during inoculation [88].

2.4. Extraction, GC Analysis and Quantification of Sesquiterpenes

Basically, analysis of produced sesquiterpenes was conducted as described in Troost et al., 2019 [39]. In the following, the procedure is briefly described. To facilitate terpene extraction into the organic phase (*n*-dodecane) after cultivation, screw neck vials or hungate tubes were incubated in a horizontal position under permanent shaking (130 rpm, 30 °C, 24 h, in the dark) using a Multitron Standard incubation shaker (Infors HT). The *n*-dodecane samples were analyzed by gas chromatography (GC) using the Agilent *6890N* gas chromatograph equipped with a (5%-phenyl)-methylpolysiloxane *HP-5* column (length, 30 m; inside diameter, 0.32 mm; film thickness, 0.25 μm; Agilent Technologies) and a flame ionization detector (FID). The temperatures of the injector and FID were set to 240 and 300 °C, respectively. The GC was loaded with a 4-μL sample of each *n*-dodecane layer using a split ratio of 100:1 with helium as carrier gas. The following column temperatures were used during analysis: (i) 100 °C for 5 min, (ii) increased of temperature with a heating rate of 10 °C per min up to 180 °C, (iii) increased of temperature with a heating rate of 20 °C per min up to 300 °C. The signal of β-caryophyllene produced in *R. capsulatus* was verified by comparison of its retention times to a corresponding reference (β-caryophyllene from Sigma Aldrich, product number: 22075, retention time: 10.13 min). In order to determine the final product titers, the transfer efficiency from producing cells into the *n*-dodecane phase was determined as described in Supplementary Method section "Analysis of *n*-dodecane-

mediated β-caryophyllene extraction from phototrophically grown *R. capsulatus*". In brief, accumulated terpenes were extracted from cell lysates using *n*-dodecane. Subsequently, products were quantified using calibration curves of the reference compound, taking into account the specific transfer efficiencies of β-caryophyllene.

2.5. Effect of β-Caryophyllene and β-Caryophyllene Oxide on Plant Pathogenic Fungi

Isolates of the plant pathogenic fungi *P. lingam*, *S. sclerotiorum* and *A. brassicicola* were obtained from the Leibniz-Institut DSMZ (Deutsche Sammlung von Mikroorganismen und Zellkulturen GmbH, Braunschweig, Germany), while isolates of *F. oxysporum*, *R. solani* were obtained from the INRES, Plant Diseases and Plant Protection, University of Bonn. All isolates were sub-cultured on potato dextrose agar (PDA) at 24 °C and were used in this study to evaluate the bioactivity of the compounds on hyphal growth.

To test the bioactivities of β-caryophyllene and β-caryophyllene oxide, compounds were dissolved in a mixture of DMSO and Tween 20 (ratio of 1:2) to prepare differently concentrated stock solutions. These were mixed with PDA to gain the final concentrations 62.5, 125, and 250 µg mL^{-1} and to prepare PDA agar plates with terpenoids. The final DMSO and Tween 20 concentrations were always 1% (*v*/*v*) and 0.5% (*v*/*v*), respectively. Fungal discs with a diameter of 0.5 cm were cut from the culture media of freshly grown agar plates without terpenoids and placed upside down in the middle of PDA plates containing the chemicals. PDA plates with 0.5% (*v*/*v*) DMSO and 1% (*v*/*v*) Tween 20 alone were used as control. All plates were incubated for 7 days at 24 °C. Subsequently, the diameter of the fungal colony was measured, and the percentage of growth inhibition compared to the solvent control was calculated. Differences between the treatments were statistically analyzed using SigmaPlot software by one-way analysis of variance (ANOVA) and multiple comparisons for significance were performed at ($p < 0.05$) using the Holm-Sidak method.

2.6. Determination of the Minimum Inhibitory Concentration (MIC) of β-Caryophyllene and β-Caryophyllene Oxide in Liquid Cultures of Bacteria

The minimum inhibitory concentration of β-caryophyllene and β-caryophyllene was determined according to reference [89]. For the precultures, 10 mL Müller Hinton (MH) medium (Merck, Germany) was first inoculated in 100 mL flasks with four single bacterial colonies. For *R. capsulatus*, RCV was used. The liquid cultures were incubated for 18 h at 130 rpm and 37 °C (*R. capsulatus* at 30 °C). For the main cultures, MH or RCV medium was supplemented with differently concentrated stock solutions of β-caryophyllene and β-caryophyllene oxide in a mixture of DMSO and Tween 20 (ratio 1:2) to gain final concentrations of 62.5, 125, and 250 µg mL^{-1}. All bacterial cultures were adjusted to a cell density corresponding to an optical density at 625 nm of 0.1 and then diluted 50-fold with medium for *B. subtilis*, *P. putida*, *P. fluorescens*, *R. rhizogenes* and *P. polymyxa* and 2-fold for *R. capsulatus*. For the inoculation of 96-well microtiter plates (Greiner Bio-One GmbH, Frickenhausen, Germany), 50 µL MH medium with the corresponding concentration of the substance to be tested and the solvent controls were mixed with 50 µL of previously diluted bacterial culture, resulting in an end optical density at 625 nm of 0.001 and 0.025, respectively. The solvent control contained 1% (*v*/*v*) Tween 20 and 0.5% (*v*/*v*) DMSO. After inoculation, the microtiter plates (MTPs) were first shaken in a SpectraMax i3x (Molecular Devices, San Jose, CA, USA) plate photometer for 20 s to mix the solution and then incubated for 20 h at 37 °C. *R. capsulatus* was incubated at 30 °C and 300 rpm. For subsequent determination of the MICs, the optical density of cell cultures was determined at 625 nm in a plate photometer. The MIC was defined based on the European Committee on Antimicrobial Susceptibility Testing (EUCAST) guidelines as the compound concentration at which an optical density at 625 nm minus the background absorbance equals 0 [90].

3. Results

In the past, terpenoids were exclusively obtained from natural plant sources, e.g., by extracting them from essential oils, requiring a complex and time-consuming downstream

processing. The heterologous production of sesquiterpenes in a suitable microbial host, however, bears many benefits. For example, it offers the possibility to solely produce a desired compound so that it can be rather easily purified without the need of removing closely related constituents [21,34]. Thus, we here aimed to reconstitute the plant sesquiterpene pathway of β-caryophyllene in *R. capsulatus* and optimize the production under phototrophic growth conditions. Since many sesquiterpenoids exhibit promising antimicrobial activities, the antifungal efficacy of β-caryophyllene and its oxidized form against phytopathogenic fungi were evaluated.

3.1. Establishment of β-Caryophyllene Production in R. capsulatus via Overexpression of Isoprenoid Precursor Genes

Recently, we described the heterologous synthesis of the plant sesquiterpenoids valencene and patchoulol in the phototrophic bacterium *R. capsulatus* and its modular improvement by engineering the biosynthesis of the central precursor FPP [39]. To evaluate if *R. capsulatus* and the modular engineering principle can analogously be applied for the synthesis of the plant-derived sesquiterpene β-caryophyllene, we expressed the gene encoding β-caryophyllene synthase QHS1 from *A. annua* in the bacterial host. To this end, the expression vectors pRhon5Hi-2-QHS1 and pRhon5Hi-2-QHS1-ispA, carrying an additional copy of the intrinsic FPP synthase gene *ispA*, were transferred to the *R. capsulatus* wild type strain SB1003 and strain SB1003-MVA. The latter strain additionally contains the chromosomally integrated MVA pathway genes derived from *Paracoccus zeaxanthinifaciens* and thus offers a second isoprenoid biosynthesis pathway. To compare the β-caryophyllene production in all *Rhodobacter* strains grown under phototrophic conditions, cells were incubated in the absence of molecular oxygen and ammonium under constant bulb light illumination. Terpene accumulation was determined in the late stationary growth phase by analyzing *n*-dodecane samples via GC-FID measurements. The increase of β-caryophyllene production in tested *R. capsulatus* strains is shown in Figure 1 as relative values using *R. capsulatus* SB1003 solely carrying the plasmid-encoded *QHS1* gene as reference strain.

As shown in Figure 1, the expression of the β-caryophyllene synthase gene *QHS1* in *R. capsulatus* strain SB1003 led to a measurable production of β-caryophyllene. Remarkably, the co-expression of *QHS1* and *ispA* in the *R. capsulatus* strain SB1003 as well as *QHS1* expression in the engineered SB1003-MVA strain did not result in increased β-caryophyllene synthesis. However, concerted expression of *QHS1* and *ispA* in *R. capsulatus* SB1003-MVA led to a considerable increase of sesquiterpenoid production of about 300% in comparison to the reference strain.

3.2. Optimization of β-Caryophyllene Production in R. capsulatus via Modification of Cultivation Conditions

In the above-described experiments, we could demonstrate that modular engineering of the isoprenoid biosynthesis can also be applied to improve β-caryophyllene production in *R. capsulatus*. Next, we analyzed whether the modification of cultivation conditions including a prolonged cultivation time or the change of illumination parameters can further improve the product yield in the better-performing strain SB1003-MVA. First, β-caryophyllene accumulation was comparatively analyzed over five days in photoheterotrophically-grown cultures of *R. capsulatus* strain SB1003-MVA carrying pRhon5Hi-2-QHS1 or pRhon5Hi-2-QHS1-ispA. Product formation was determined by analyzing the overlaid *n*-dodecane samples via GC-FID measurements (Figure 2, blue bars).

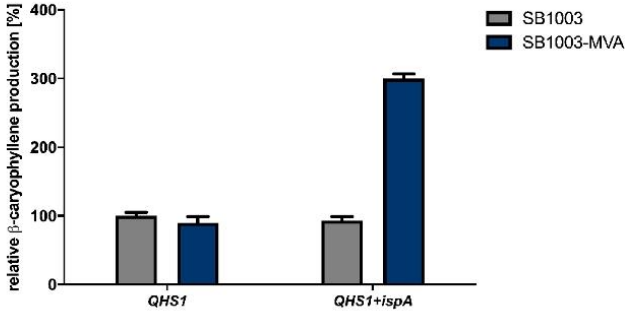

Figure 1. Heterologous β-caryophyllene production in the *R. capsulatus* strains SB1003 and SB1003-MVA. The β-caryophyllene synthase gene *QHS1* from *A. annua* was expressed in *R. capsulatus* SB1003 wild type (grey bars) and SB1003-MVA (blue bars), which additionally carries the MVA gene cluster from *P. zeaxanthinifaciens* to enable a second isoprenoid biosynthesis route. Moreover, the *ispA* gene encoding the *R. capsulatus* FPP synthase was co-expressed on the same plasmid to further enhance sesquiterpene production titers. Product formation was determined in cell cultures after three days of photoheterotrophic cultivation (gas-tight hungate tubes, 30 °C) under ammonium depletion and constant illumination with bulb light (3.6 mW cm^{-2} at 850 nm). The produced β-caryophyllene was sampled in overlaid *n*-dodecane phases for GC-FID analysis. The increase of β-caryophyllene production in engineered *R. capsulatus* strains is shown as relative values. To this end, the *R. capsulatus* SB1003 carrying the plasmid-encoded *QHS1* gene was used as a reference strain. Values are means of three independent biological replicates ($n = 3$) and error bars indicate the respective standard deviations.

The highest product levels could be detected after three days of cultivation, where cells have typically reached the beginning of the stationary growth phase. The elongation of the cultivation time did not show increased product accumulation so that all further production experiments were carried out for three days. Under standard phototrophic conditions, conventional light bulbs are used for the illumination of *R. capsulatus* cells [39,49]. This conventional light source offers a broad emission spectrum with a relatively high proportion in the infrared (IR) light range (>750 nm; 3.6 mW cm^{-2} at 850 nm) suitable for excitation of bacteriochlorophyll *a* (BChl *a*) exhibiting excitation maxima at 800 and 860 nm (Figure S6, Supplementary Materials, Reference [91]). To improve the illumination conditions for sesquiterpene production under phototrophic conditions, we subsequently analyzed if the use of (i) alternative cultivation vessels offering a better light penetration of cell cultures by a more favorable surface-area-to-volume ratio (Table S2, Supplementary Materials) or (ii) a customized IR-LED array (5.6 mW cm^{-2} at 850 nm) suitable for specific excitation of the photopigment BChl *a* with high light intensities can help to increase product formation.

To investigate the influence of illumination conditions on the heterologous production of β-caryophyllene, the strain SB1003-MVA carrying the expression vector pRhon5Hi-2-QHS1-ispA was cultivated over three days under photoheterotrophic conditions and constant illumination with bulb light or IR light in an ammonium-depleted medium in screw neck vials. As shown in Figure 2, the change of cultivation vessel geometry resulted only in a slight increase of β-caryophyllene production of *R. capsulatus* SB1003-MVA (pRhon5Hi-2-QHS1-ispA), whereas high irradiation with IR light led to a 1.9-fold increase of the final product accumulation. These results indicate that the applied illumination conditions should be taken into account to reach high product yields when *R. capsulatus* is used as an alternative terpene production host. This assumption is further supported by the observation that product levels were much lower in *R. capsulatus* SB1003-MVA (pRhon5Hi-2-QHS1-ispA) cultures that have been grown under non-phototrophic, i.e., microaerobic conditions (Figure 2, green bars). For non-phototrophic cultivation, *R. capsulatus* SB1003-MVA (pRhon5Hi-2-QHS1-ispA) was grown in 100 mL, unbaffled shake flasks containing different volumes of medium in the dark to implement different aeration conditions

(green bars). Those conditions could lead to the formation of β-caryophyllene oxide, the oxygenated derivative of β-caryophyllene. As previously described, a filling volume of 60 mL is most suitable for the induction of intrinsic terpene formation and P_{nif}-mediated target gene expression in *R. capsulatus* [39], which is corroborated by the observed β-caryophyllene production levels. Nevertheless, only a quarter of the product yield could be achieved under microaerobic, non-phototrophic growth conditions when compared to the corresponding values of phototrophically grown cells (*R. capsulatus* SB1003-MVA, pRhon5Hi-2-QHS1-ispA, 3 days, bulb light), and only traces of the oxygenated derivative were detectable (data not shown). However, to fully understand the effects of varying cultivation conditions on β-caryophyllene production, further experiments have to be performed in future studies.

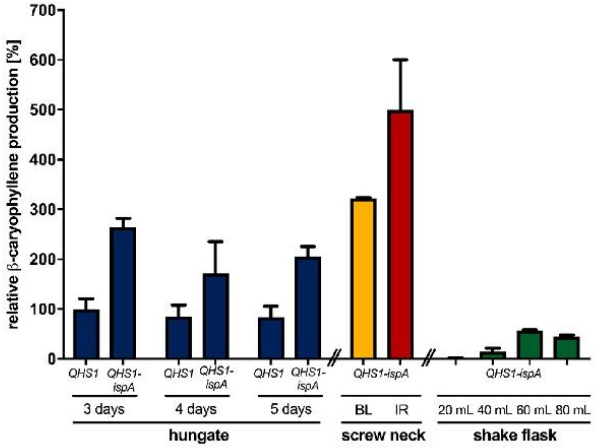

Figure 2. Heterologous β-caryophyllene production in the *R. capsulatus* strain SB1003-MVA with dependence on the cultivation time and illumination conditions. The β-caryophyllene accumulation was determined in *R. capsulatus QHS1* expression strains SB1003-MVA (pRhon5Hi-2-QHS1) and SB1003-MVA (pRhon5Hi-2-QHS1-ispA). First, product formation was determined in cell cultures after three, four, and five days of photoheterotrophic cultivation in 15 mL hungate tubes using standard illumination conditions (bulb lights, 3.6 mW cm^{-2} at 850 nm) and RCV medium supplemented with 0.1% serine. Blue bars represent the results of this experiment. Second, illumination conditions were changed by cultivating *R. capsulatus* strain SB1003-MVA (pRhon5Hi-2-QHS1-ispA) for three days under photoheterotrophic conditions using either constant illumination with bulb lights (BL; 3.6 mW cm^{-2} at 850 nm, yellow bar) or IR-emitting diodes (IR; 5.6 mW cm^{-2} at 850 nm, red bar). Here, 4.5-mL screw neck vials were used to improve light penetration due to a more favorable surface-area-to-volume ratio of this cultivation vessel. For non-phototrophic cultivation, the same strain was grown in 100-mL, unbaffled shake flasks containing different volumes of serine-supplemented RCV medium (shake flask, green bars). In all cultures, the produced β-caryophyllene was sampled in overlaid *n*-dodecane phases for GC-FID analysis. The increase of β-caryophyllene production is shown as relative values using *R. capsulatus* SB1003-MVA carrying the QHS1 expression plasmid pRhon5Hi-2-QHS1 as a reference strain. Values are the means of three independent biological replicates ($n = 3$) and the error bars indicate the respective standard deviations.

To accurately determine the final product titers, we analyzed (i) the individual transfer efficiency of β-caryophyllene from intact cells into the *n*-dodecane phase, (ii) the effect of the ICM, which is formed by *R. capsulatus* cells under phototrophic conditions, on sesquiterpenoid extraction, (iii) the differences in terpene transfer efficiencies when comparing single and repeated *n*-dodecane extraction, and finally (iv) the effect of the presence and absence

of organic solvent on the final product titers (Supplementary Method section "Analysis of *n*-dodecane-mediated β-caryophyllene extraction from phototrophically grown *R. capsulatus*"). Finally, we were able to determine a product titer of 90 ± 19 mg L^{-1} β-caryophyllene for *R. capsulatus* SB1003-MVA with pRhon5Hi-2-QHS1-ispA after 3 days of cultivation in hungate tubes under bulb light. This titer could be further increased by using IR light and screw neck vials for cultivation, reaching a final product titer of 139 ± 31 mg L^{-1}. Based on these values and the reached cell densities, the respective productivities were further calculated (Table S3, Supplementary Materials).

In summary, we showed that *R. capsulatus* can efficiently synthesize the sesquiterpene β-caryophyllene. Furthermore, the modular adaptation of precursor gene expression under phototrophic growth conditions as well as the adjustment of cultivation conditions resulted in an increased sesquiterpenoid formation.

3.3. Evaluation of Bioactivities of β-Caryophyllene and β-Caryophyllene Oxide against Different Phytopathogenic Organisms

The agricultural industry is affected by a dwindling number of effective antimicrobial substances. On the other hand, farmers have to control plant pathogenic organisms without damaging non-target organisms. As β-caryophyllene and β-caryophyllene oxide offer a variety of beneficial bioactivities [70,79,92–95], we evaluated the potential use of those two sesquiterpenes as a nature-derived fungicide. To this end, we analyzed the activity against different phytopathogenic fungi, as well as various plant growth-promoting bacteria (PGPB).

3.3.1. Bioactivities of β-Caryophyllene and β-Caryophyllene Oxide against Phytopathogenic Fungi

We investigated the bioactivity of β-caryophyllene and β-caryophyllene oxide, which can be formed spontaneously by uncatalyzed processes [96,97], against the plant pathogenic fungi *S. sclerotiorum*, *F. oxysporum*, *A. brassicicola*, *P. lingam*, and *R. solani*. This analysis would additionally reveal whether the compound's oxygenation influences potential antifungal properties. Therefore, PDA agar plates were supplemented with increasing concentrations of both compounds, fungal discs were transferred onto these plates and fungal growth was determined. Evaluation revealed that the degree of growth inhibition due to direct terpene exposure varied depending on the compound and the fungus (Figure 3).

Both compounds inhibited the hyphal growth of *S. sclerotiorum* when compared to the solvent control. The inhibition reached up to 30% when the fungus was exposed to β-caryophyllene, while it was up to 40% when the fungus was cultivated on medium containing β-caryophyllene oxide. The effect against *F. oxysporum* was less pronounced. Around 20% inhibition was observed when the fungus was cultivated on the β-caryophyllene-supplemented medium, while it was around 30% in the case of β-caryophyllene oxide. Finally, the presence of β-caryophyllene in the growth medium slightly inhibited the growth of *A. brassicicola* while inhibition was higher and reached a maximum of 10% when β-caryophyllene oxide was used. No significant effect of both compounds was observed against *P. lingam* and *R. solani* (Figure S7, Supplementary Materials). Our results thus reveal that β-caryophyllene and its oxidized form possess antifungal activity against certain phytopathogenic fungi and that β-caryophyllene oxide tends to be more effective in inhibiting fungal growth.

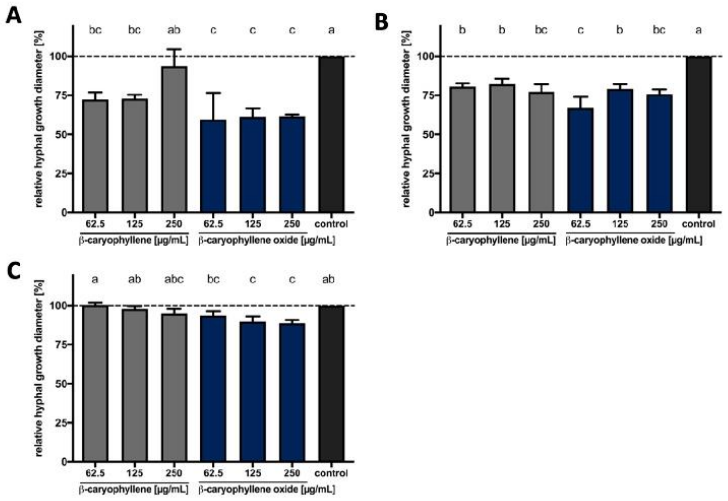

Figure 3. The effect of β-caryophyllene and β-caryophyllene oxide on the hyphal growth of plant pathogenic fungi. The effect of β-caryophyllene and β-caryophyllene oxide against *S. sclerotiorum* (**A**), *F. oxysporum* (**B**) and *A. brassicicola* (**C**). Final concentrations of 62.5 µg mL^{-1}, 125 µg mL^{-1}, and 250 µg mL^{-1} of β-caryophyllene (grey bars) and β-caryophyllene oxide (blue bars) in PDA growth medium were used. Medium mixed with the solvents DMSO and Tween 20 (final concentrations, 0.5% and 1% *v*/*v*, respectively) was used as the control (black bars). An equally sized disk with fungal mycelium was placed in the center of each plate and incubated for seven days at 24 °C. Subsequently, the diameter of each fungal colony was measured, and the relative growth compared to the solvent control was calculated. Each bar represents the mean ± standard deviation of three independent biological measurements with three technical replicates each ($n = 9$). Different letters on the top of the bars indicate significant differences between the treatments based on ANOVA and Holm-Sidak post-hoc method ($p < 0.05$), while the same letters represent no significant differences.

3.3.2. Antimicrobial Activities against Plant Growth-Promoting Bacteria

As the previous investigations showed antifungal properties against several phytopathogenic fungi, the use of the sesquiterpenoids as natural compound-based plant protection products could be considered. To investigate potential toxic off-target effects on bacteria that promote plant growth, we next examined whether the addition of β-caryophyllene/oxide affects the growth of bacteria at concentrations used in the hyphal growth assay. For this purpose, the growth of representatives of the plant growth-promoting bacteria (PGPB) group [98–100], including the two diazotrophic bacteria *Rhizobium rhizogenes* and *Rhodobacter capsulatus* [101,102], the two bacilli *Bacillus subtilis* [103,104] and *Paenibacillus polymyxa* [105], as well as the pseudomonads *Pseudomonas fluorescens* [104] and *Pseudomonas putida* [106] was analyzed in presence of β-caryophyllene and β-caryophyllene oxide. Both compounds were added to diluted bacterial cultures in increasing concentrations. After overnight incubation, the MICs were determined according to the respective optical density of the cell cultures (Figure 4).

The bacteria *R. rhizogenes*, *R. capsulatus*, *B. subtilis*, and *P. polymyxa* did not show reduced cell growth in comparison to the solvent control upon the addition of the two terpenes β-caryophyllene and β-caryophyllene oxide (Figure 4A–D). These bacteria showed an increase in growth, which could be explained by the metabolization of the terpenes. For *P. putida*, no effect of β-caryophyllene oxide was detected compared to the solvent control (Figure 4F). β-caryophyllene showed an influence on *P. putida*, which was concentration independent since all tested concentrations led to comparable cell growth. The cell densi-

ties were about 40% lower compared to the solvent control. This effect was also observed for *P. fluorescens*, where the two terpenes reduced growth by up to 40% (Figure 4E).

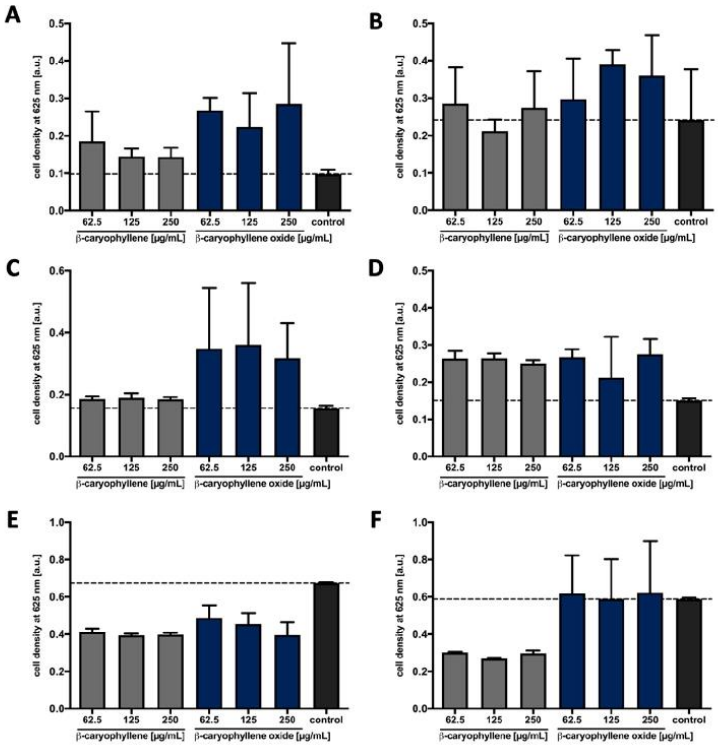

Figure 4. The influence of β-caryophyllene and β-caryophyllene oxide on the growth of plant growth-promoting bacteria. Final concentrations of 62.5 µg mL^{-1}, 125 µg mL^{-1} and 250 µg mL^{-1} of β-caryophyllene (grey bars) and β-caryophyllene oxide (blue bars) were added to cultures of *R. rhizogenes* (**A**), *R. capsulatus* (**B**), *B. subtilis* (**C**), *P. polymyxa* (**D**), *P. fluorescens* (**E**) and *P. putida* (**F**) in 100 µL MH medium (*R. capsulatus* in RCV medium) in MTPs. The final solvent concentration was 1% (*v*/*v*) Tween 20 and 0.5% (*v*/*v*) DMSO. To determine the influence of the terpenes on the growth of the bacteria, the cells were incubated stationary for 20 h at 37 °C (*R. capsulatus* at 30 °C) and the cell density was measured at 625 nm using a plate photometer. The solvent control (control, black bars) was MH or RCV medium containing 1% (*v*/*v*) Tween 20 and 0.5% (*v*/*v*) DMSO. Values are means of three independent biological replicates ($n = 3$) and error bars indicate the respective standard deviations.

In summary, for β-caryophyllene and β-caryophyllene oxide, no MIC could be determined for any of the tested PGPB, but a reduction of cell growth could be observed for both Pseudomonads. As a diverse group of different representative soil bacteria was tested, the results nevertheless indicate that β-caryophyllene and β-caryophyllene oxide do not exhibit strong broad-spectrum antibacterial activities at concentrations which considerably inhibit the hyphal growth of *S. sclerotiorum* and *F. oxysporum* (63 µg mL^{-1}).

4. Discussion

The management of plant pathogens in the process of crop production is crucial, no matter whether organic, integrated, or conventional farming practices are applied.

For many decades, synthetic pesticides were considered the fastest and most effective pest and pathogen control method. Recently, due to the rise of public health concerns about pesticide toxicity and harm to the environment, many of these effective chemicals were banned, thereby markedly limiting the options for plant protection. Therefore, it is important to find environmentally safe and sustainable natural products to control pathogens and thus ensure yield and food quality. In this context, plant metabolites are a rich source of bioactive compounds explorable for the use of preventing and controlling plant pathogenic microbes. In the last decade, several studies investigated terpenoids as potential antiphytopathogenic compounds [67,71,76,77,107,108]. β-caryophyllene is a natural bicyclic sesquiterpene that is a constituent of many essential oils. Many studies showed that these essential oils, which are containing β-caryophyllene as one of the main ingredients, are active against plant pathogens [109–111]. For example, methanol extracts from *Artemisia annua* leaves, one of the common β-caryophyllene producers, strongly inhibit the growth of the plant pathogenic fungi *F. oxysporum* and *Fusarium solani* [79]. In another study, the essential oil from *Murraya paniculata* leaves showed inhibitory activities on the mycelial growth of *S. sclerotiorum*, a fungus that poses a high risk to several crops. The gas chromatography analysis of the essential oil composition introduced β-caryophyllene as one of the main constituents (23.8%) [109]. Furthermore, essential oils from *Piper aduncum*, which also has β-caryophyllene as one of its main constituents (7.2%), inhibited the mycelial growth of the fungus *S. sclerotiorum* [110]. As a second alternative or complementary means for plant protection, there is also a multitude of important and useful microorganisms that support plant growth, which are called plant growth-promoting bacteria and plant growth-promoting fungi (PGPF). To offset the negative effects of chemical substances or make their use superfluous, more and more PGPB are now being used in agriculture [112]. Microorganisms can fulfill different functions in this process. *Bacillus subtilis*, for example, accumulates at the root system during the germination of various plants and prevents competing harmful fungi from spreading [103]. Diazotrophic organisms can supply plants with biologically available nitrogen by fixing atmospheric dinitrogen, thus making it available to the plants [113]. When fighting phytopathogens, it is important to consider and ideally avoid negative off-target effects on the above-mentioned beneficial microorganisms. Corresponding tests are therefore now frequently included in the first evaluation of antimicrobial activities.

So far, no studies were investigating the effect of pure β-caryophyllene and β-caryophyllene oxide against a selection of phytopathogenic fungi aiming to determine and compare the potential antifungal properties of the two compounds and species-specific differences in sensitivity. In our current study, we show the potential of sustainable production of β-caryophyllene in the heterologous host *Rhodobacter capsulatus* and the species-specific promoting or inhibitory effects for selected plant growth-promoting bacteria for both of the tested sesquiterpenoids at appropriate compound concentrations. Furthermore, we tested the bioactivities of both β-caryophyllene and β-caryophyllene oxide against several plant pathogenic fungi and showed that both substances were active against certain fungi. Interestingly, the oxidized form tended to be even more effective, and additionally has a more beneficial activity profile concerning the PGPB. These results are supported by previous reports which are introducing β-caryophyllene as a bioactive compound in its purified form [79] and as a component of several essential oils [109,110]. The purified β-caryophyllene showed a MIC of 130 µg mL^{-1} for *F. oxysporum* [79], which is below the maximal concentration tested in this study. However, our plate-based approach is not completely comparable with the method used for MIC determination in liquid medium. According to our results, the inhibitory effect of the hyphal growth was different depending on the tested fungus. Such a difference is dependent on the fungal species and frequently described by previous studies showing that the novel fungicide 3-[5-(4-chlorophenyl)-2,3-dimethyl-3-isoxazolidinyl] pyridine (SYP-Z048) affected several pathogenic fungi in different ways [114]. Overall, our current results demonstrate that both β-caryophyllene and β-caryophyllene oxide exhibit bioactivity against plant pathogenic fungi and therefore

could be suitable as potential fungicides in agriculture as, in contrast to many broad-spectrum pesticides, they do not harm many species of plant growth-promoting bacteria. However, despite the sesquiterpenes being natural compounds, which are often associated with non-harmful ecotoxicological profiles, effects against *Pseudomonas* species were corroborated and will need to be taken into account. So far, there is only limited information about the individual activities of terpenes against plant pathogens and the underlying molecular mechanisms. To be able to explain the differences we observed in the activity of the two terpenes against the different organisms and to get more data on the activity spectrum, our investigations need to be extended by including more target and non-target organisms. In addition, the respective modes of action on the molecular level have to be determined. Besides additional plant pathogens, this not only includes analyzing further plant growth-promoting bacteria, but it must be tested if plant growth-promoting fungi react sensitively to the terpenes, as indicated by a previous promising study [80]. In particular, fungi of the genus *Trichoderma*, which are said to have many advantageous properties for plants, could be investigated more closely [115,116].

To be able to provide appropriate quantities of an active antifungal substance, the heterologous production of promising sesquiterpenes in a suitable microbial host bears various benefits, such as the possibility to solely produce the desired compound without complex downstream processing and in high amounts. Therefore, we established the biosynthesis of the plant sesquiterpene β-caryophyllene in the heterologous production host *R. capsulatus* under phototrophic and non-phototrophic conditions. For this purpose, the intrinsic isoprenoid biosynthesis pathway was optimized in terms of its precursor supply. In particular, the P_{nif}-based co-expression of *ispA* and the genetically integrated MVA pathway resulted in a substantial increase in sesquiterpenoid production of around 300%. These results are in agreement with previous studies, where engineering of isoprenoid precursor supply was a valuable tool to increase the terpenoid production in *Rhodobacter* [38,40,48] and other bacterial hosts [23,117–125]. Also, we were able to increase the terpene production level further by changing the cultivation conditions from bulb light in a 14 mL hungate tube to IR light in a 4.5 mL screw neck vial, achieving a final β-caryophyllene titer of 139.29 ± 31.35 mg L^{-1} and a specific productivity of 1.30 ± 0.32 mg g^{-1} dry cells h^{-1}. In recent studies, production titers around 220 mg L^{-1} [126] and specific productivities of 1.15 mg g^{-1} dry cells h^{-1} [127] were achieved in *E. coli*. Thus, we attained yields comparable to the current literature and successfully established *R. capsulatus* as a heterologous host for the production of β-caryophyllene. Furthermore, the β-caryophyllene yields achieved in *R. capsulatus* could be sufficient to use this host as a microbial system for in situ agent delivery. In the future, sesquiterpenoid producing *R. capsulatus* might thus be applicable as cell extracts with biocontrol activities for plant protection or as engineered antiphytopathogenic PGPB that can be added as live cultures to soils contained in vertical farming.

Supplementary Materials: The following are available online at https://www.mdpi.com/2076-2607/9/1/168/s1. Figure S1: Transfer efficiency of the β-caryophyllene reference compound from cultivation medium into the *n*-dodecane phase in the presence of intact *R. capsulatus* cells in hungate and screw neck vials, Figure S2: Transfer efficiency of the β-caryophyllene reference compound from cultivation medium into the *n*-dodecane phase in the presence of intact and disrupted *R. capsulatus* cells, Figure S3: Extraction efficiency of the β-caryophyllene reference compound from cultivation medium in the presence of disrupted and intact *R. capsulatus* cells by repeatedly using *n*-dodecane as organic solvent over four days, Figure S4: Comparison of relative β-caryophyllene formation in *R. capsulatus* production strains cultivated with and without an *n*-dodecane layer, Figure S5: Quantification of extracted β-caryophyllene via a calibration curve of β-caryophyllene reference signals in GC-FID analyses, Figure S6: Emission range of different light sources and the absorption spectrum of phototrophically cultivated *R. capsulatus* cells [128], Figure S7: Effect of β-caryophyllene and β-caryophyllene oxide on the hyphal growth of plant pathogenic fungi, Table S1: Bacterial strains and plasmids used in this study, Table S2: Cultivation vessel specifications, Table S3: Productivities of β-caryophyllene in *R. capsulatus* SB1003 cultures.

Author Contributions: Conceptualization, T.D., A.L., K.-E.J., A.S.S.S., F.M.W.G.; methodology, F.H., Y.S.A., J.H.-H., A.H., S.S.H.; validation, F.H., S.S.H.; formal analysis, S.S.H., F.H.; investigation, F.H., S.S.H., Y.S.A., S.N., O.K.; writing—original draft preparation, F.H., S.S.H.; writing—review and editing, T.D., A.S.S.S., A.L., K.-E.J., F.M.W.G.; visualization, F.H.; supervision, T.D., A.L., A.S.S.S.; project administration, A.L., T.D., A.S.S.S., K.-E.J., F.M.W.G.; funding acquisition, A.L., T.D., A.S.S.S., K.-E.J., F.M.W.G. All authors have read and agreed to the published version of the manuscript.

Funding: The work was supported by grants from the Bioeconomy Science Center, and the European Regional Development Fund (ERDF: 34.EFRE-0300096) within the project CLIB-Kompetenzzentrum Biotechnologie CKB). The scientific activities of the Bioeconomy Science Center were financially supported by the Ministry of Innovation, Science and Research of the German federal state of North Rhine-Westphalia MIWF within the framework of the NRW Strategieprojekt BioSC (No. 313/323-400-00213).

Institutional Review Board Statement: Not applicable.

Informed Consent Statement: Not applicable.

Data Availability Statement: The datasets generated and/or analyzed during the current study are available from the corresponding authors on reasonable request.

Acknowledgments: The authors would like to thank Olaf Cladders, Edwin Thiemann, Volker Neu, and Helmut Guenther from Vossloh-Schwabe Lighting Solutions GmbH & Co. KG (Kamp-Lintfort, Germany) for their time, efforts and tremendous expertise in the LED array development thereby making the "illumination project" possible.

Conflicts of Interest: The authors declare no conflict of interest. The funders had no role in the design of the study, in the collection, analyzes, or interpretation of data, in the writing of the manuscript, or in the decision to publish the results.

References

1. Bian, G.; Deng, Z.; Liu, T. Strategies for terpenoid overproduction and new terpenoid discovery. *Curr. Opin. Biotechnol.* **2017**, *48*, 234–241. [CrossRef] [PubMed]
2. Christianson, D.W. Structural and Chemical Biology of Terpenoid Cyclases. *Chem. Rev.* **2017**, *117*, 11570–11648. [CrossRef] [PubMed]
3. Pemberton, T.A.; Chen, M.; Harris, G.G.; Chou, W.K.W.; Duan, L.; Köksal, M.; Genshaft, A.S.; Cane, D.E.; Christianson, D.W. Exploring the Influence of Domain Architecture on the Catalytic Function of Diterpene Synthases. *Biochemistry* **2017**, *56*, 2010–2023. [CrossRef] [PubMed]
4. Wink, M. Modes of Action of Herbal Medicines and Plant Secondary Metabolites. *Medicines* **2015**, *2*, 251–286. [CrossRef]
5. Ruzicka, L. The isoprene rule and the biogenesis of terpenic compounds. *Experientia* **1953**, *9*, 357–367. [CrossRef]
6. Croteau, R.; Kutchan, T.M.; Lewis, N.G. Secondary Metabolites. *Biochem. Mol. Biol. Plants* **2000**, *7*, 1250–1318.
7. Boucher, Y.; Doolittle, W.F. The role of lateral gene transfer in the evolution of isoprenoid biosynthesis pathways. *Mol. Microbiol.* **2000**, *37*, 703–716. [CrossRef]
8. Frank, A.; Groll, M. The Methylerythritol Phosphate Pathway to Isoprenoids. *Chem. Rev.* **2017**, *117*, 5675–5703. [CrossRef]
9. Langenheim, J.H. Higher plant terpenoids: A phytocentric overview of their ecological roles. *J. Chem. Ecol.* **1994**, *20*, 1223–1280. [CrossRef]
10. Gershenzon, J.; Dudareva, N. The function of terpene natural products in the natural world. *Nat. Chem. Biol.* **2007**, *3*, 408–414. [CrossRef]
11. Pichersky, E.; Raguso, R.A. Why do plants produce so many terpenoid compounds? *New Phytol.* **2018**, *220*, 692–702. [CrossRef] [PubMed]
12. Efferth, T. From ancient herb to modern drug: *Artemisia annua* and artemisinin for cancer therapy. *Semin. Cancer Biol.* **2017**, *46*, 65–83. [CrossRef] [PubMed]
13. Mahizan, N.A.; Yang, S.-K.; Moo, C.-L.; Song, A.A.-L.; Chong, C.-M.; Chong, C.-W.; Abushelaibi, A.; Lim, S.-H.E.; Lai, K.-S. Terpene Derivatives as a Potential Agent against Antimicrobial Resistance (AMR) Pathogens. *Molecules* **2019**, *24*, 2631. [CrossRef] [PubMed]
14. Walencka, E.; Rozalska, S.; Wysokinska, H.; Rozalski, M.; Kuzma, L.; Rozalska, B. Salvipisone and aethiopinone from *Salvia sclarea* hairy roots modulate staphylococcal antibiotic resistance and express anti-biofilm activity. *Planta Med.* **2007**, *73*, 545–551. [CrossRef] [PubMed]
15. Jabra-Rizk, M.A.; Meiller, T.F.; James, C.E.; Shirtliff, M.E. Effect of farnesol on *Staphylococcus aureus* biofilm formation and antimicrobial susceptibility. *Antimicrob. Agents Chemother.* **2006**, *50*, 1463–1469. [CrossRef] [PubMed]
16. Gomes, F.I.A.; Teixeira, P.; Azeredo, J.; Oliveira, R. Effect of farnesol on planktonic and biofilm cells of *Staphylococcus epidermidis*. *Curr. Microbiol.* **2009**, *59*, 118–122. [CrossRef] [PubMed]

17. Castelo-Branco, D.S.C.M.; Riello, G.B.; Vasconcelos, D.C.; Guedes, G.M.M.; Serpa, R.; Bandeira, T.J.P.G.; Monteiro, A.J.; Cordeiro, R.A.; Rocha, M.F.G.; Sidrim, J.J.C.; et al. Farnesol increases the susceptibility of *Burkholderia pseudomallei* biofilm to antimicrobials used to treat melioidosis. *J. Appl. Microbiol.* **2016**, *120*, 600–606. [CrossRef]
18. Malingre, T.; Hendriks, H.; Batterman, S.; Bos, R.; Visser, J. The Essential Oil of *Cannabis sativa*. *Planta Med.* **1975**, *28*, 56–61. [CrossRef]
19. De Vasconcelos Silva, M.; Craveiro, A.; Abreu Matos, F.; Machado, M.I.; Alencar, J. Chemical variation during daytime of constituents of the essential oil of *Ocimum gratissimum* leaves. *Fitoterapia* **1999**, *70*, 32–34. [CrossRef]
20. Matias, E.F.F.; Alves, E.F.; Silva, M.K.N.; Carvalho, V.R.A.; Figueredo, F.G.; Ferreira, J.V.A.; Coutinho, H.D.M.; Silva, J.M.F.L.; Ribeiro-Filho, J.; Costa, J.G.M. Seasonal variation, chemical composition and biological activity of the essential oil of *Cordia verbenacea* DC (*Boraginaceae*) and the sabinene. *Ind. Crops Prod.* **2016**, *87*, 45–53. [CrossRef]
21. Marienhagen, J.; Bott, M. Metabolic engineering of microorganisms for the synthesis of plant natural products. *J. Biotechnol.* **2013**, *163*, 166–178. [CrossRef]
22. Kallscheuer, N.; Classen, T.; Drepper, T.; Marienhagen, J. Production of plant metabolites with applications in the food industry using engineered microorganisms. *Curr. Opin. Biotechnol.* **2019**, *56*, 7–17. [CrossRef]
23. Schempp, F.M.; Drummond, L.; Buchhaupt, M.; Schrader, J. Microbial Cell Factories for the Production of Terpenoid Flavor and Fragrance Compounds. *J. Agric. Food Chem.* **2018**, *66*, 2247–2258. [CrossRef] [PubMed]
24. Pham, J.V.; Yilma, M.A.; Feliz, A.; Majid, M.T.; Maffetone, N.; Walker, J.R.; Kim, E.; Cho, H.J.; Reynolds, J.M.; Song, M.C.; et al. A Review of the Microbial Production of Bioactive Natural Products and Biologics. *Front. Microbiol.* **2019**, *10*, 1–27.
25. Cravens, A.; Payne, J.; Smolke, C.D. Synthetic biology strategies for microbial biosynthesis of plant natural products. *Nat. Commun.* **2019**, *10*, 2142.
26. Sgobba, E.; Wendisch, V.F. Synthetic microbial consortia for small molecule production. *Curr. Opin. Biotechnol.* **2020**, *62*, 72–79. [CrossRef] [PubMed]
27. Kirby, J.; Keasling, J.D. Metabolic engineering of microorganisms for isoprenoid production. *Nat. Prod. Rep.* **2008**, *25*, 656–661. [PubMed]
28. Mitchell, W. Natural products from synthetic biology. *Curr. Opin. Chem. Biol.* **2011**, *15*, 505–515. [CrossRef] [PubMed]
29. Chen, Y.; Zhou, Y.J.; Siewers, V.; Nielsen, J. Enabling technologies to advance microbial isoprenoid production. *Adv. Biochem. Eng. Biotechnol.* **2015**, *148*, 143–160.
30. Wong, J.; Rios-Solis, L.; Keasling, J.D. Microbial Production of Isoprenoids. In *Consequences of Microbial Interactions with Hydrocarbons, Oils, and Lipids: Production of Fuels and Chemicals*; Lee, S.Y., Ed.; Springer International Publishing: Cham, Switzerland, 2016; pp. 1–24. ISBN 978-3-319-31421-1.
31. Helfrich, E.J.N.; Lin, G.-M.; Voigt, C.A.; Clardy, J. Bacterial terpene biosynthesis: Challenges and opportunities for pathway engineering. *Beilstein J. Org. Chem.* **2019**, *15*, 2889–2906.
32. Chemler, J.A.; Koffas, M.A.G. Metabolic engineering for plant natural product biosynthesis in microbes. *Curr. Opin. Biotechnol.* **2008**, *19*, 597–605. [CrossRef] [PubMed]
33. Paddon, C.J.; Westfall, P.J.; Pitera, D.J.; Benjamin, K.; Fisher, K.; McPhee, D.; Leavell, M.D.; Tai, A.; Main, A.; Eng, D.; et al. High-level semi-synthetic production of the potent antimalarial artemisinin. *Nature* **2013**, *496*, 528–532. [CrossRef] [PubMed]
34. Atanasov, A.G.; Waltenberger, B.; Pferschy-Wenzig, E.-M.M.; Linder, T.; Wawrosch, C.; Uhrin, P.; Temml, V.; Wang, L.; Schwaiger, S.; Heiss, E.H.; et al. Discovery and resupply of pharmacologically active plant-derived natural products: A review. *Biotechnol. Adv.* **2015**, *33*, 1582–1614. [CrossRef]
35. Zhang, C.; Hong, K. Production of Terpenoids by Synthetic Biology Approaches. *Front. Bioeng. Biotechnol.* **2020**, *8*, 347. [CrossRef] [PubMed]
36. Yu, Y.; Rasool, A.; Liu, H.; Lv, B.; Chang, P.; Song, H.; Wang, Y.; Li, C. Engineering *Saccharomyces cerevisiae* for high yield production of α-amyrin via synergistic remodeling of α-amyrin synthase and expanding the storage pool. *Metab. Eng.* **2020**, *62*, 72–83. [CrossRef]
37. Bauer, K.; Garbe, D.; Surburg, H. *Common Fragrance and Flavor Materials*; Wiley-VCH: Weinheim, Germany, 2001.
38. Beekwilder, J.; van Houwelingen, A.; Cankar, K.; van Dijk, A.D.J.; de Jong, R.M.; Stoopen, G.; Bouwmeester, H.; Achkar, J.; Sonke, T.; Bosch, D. Valencene synthase from the heartwood of Nootka cypress (*Callitropsis nootkatensis*) for biotechnological production of valencene. *Plant Biotechnol. J.* **2014**, *12*, 174–182. [CrossRef]
39. Troost, K.; Loeschcke, A.; Hilgers, F.; Özgür, A.Y.; Weber, T.M.; Santiago-Schübel, B.; Svensson, V.; Hage-Hülsmann, J.; Habash, S.S.; Grundler, F.M.W.; et al. Engineered *Rhodobacter capsulatus* as a Phototrophic Platform Organism for the Synthesis of Plant Sesquiterpenoids. *Front. Microbiol.* **2019**, *10*, 1998. [CrossRef]
40. Orsi, E.; Folch, P.L.; Monje-López, V.T.; Fernhout, B.M.; Turcato, A.; Kengen, S.W.M.; Eggink, G.; Weusthuis, R.A. Characterization of heterotrophic growth and sesquiterpene production by *Rhodobacter sphaeroides* on a defined medium. *J. Ind. Microbiol. Biotechnol.* **2019**, *46*, 1179–1190. [CrossRef]
41. Lin, P.-C.; Pakrasi, H.B. Engineering cyanobacteria for production of terpenoids. *Planta* **2019**, *249*, 145–154. [CrossRef]
42. Das, A.; Yoon, S.-H.; Lee, S.-H.; Kim, J.-Y.; Oh, D.-K.; Kim, S.-W. An update on microbial carotenoid production: Application of recent metabolic engineering tools. *Appl. Microbiol. Biotechnol.* **2007**, *77*, 505–512. [CrossRef]
43. Arendt, P.; Miettinen, K.; Pollier, J.; De Rycke, R.; Callewaert, N.; Goossens, A. An endoplasmic reticulum-engineered yeast platform for overproduction of triterpenoids. *Metab. Eng.* **2017**, *40*, 165–175. [CrossRef] [PubMed]

44. Tucker, J.D.; Siebert, C.A.; Escalante, M.; Adams, P.G.; Olsen, J.D.; Otto, C.; Stokes, D.L.; Hunter, C.N. Membrane invagination in *Rhodobacter sphaeroides* is initiated at curved regions of the cytoplasmic membrane, then forms both budded and fully detached spherical vesicles. *Mol. Microbiol.* **2010**, *76*, 833–847. [CrossRef] [PubMed]
45. Drews, G. The intracytoplasmic membranes of purple bacteria—Assembly of energy-transducing complexes. *J. Mol. Microbiol. Biotechnol.* **2013**, *23*, 35–47. [CrossRef] [PubMed]
46. Armstrong, G.A.; Alberti, M.; Leach, F.; Hearst, J.E. Nucleotide sequence, organization, and nature of the protein products of the carotenoid biosynthesis gene cluster of *Rhodobacter capsulatus*. *Mol. Gen. Genet. MGG* **1989**, *216*, 254–268. [CrossRef]
47. Armstrong, G.A. Genetics of eubacterial carotenoid biosynthesis: A colorful tale. *Annu. Rev. Microbiol.* **1997**, *51*, 629–659. [CrossRef]
48. Khan, N.E.; Nybo, S.E.; Chappell, J.; Curtis, W.R. Triterpene hydrocarbon production engineered into a metabolically versatile host—*Rhodobacter capsulatus*. *Biotechnol. Bioeng.* **2015**, *112*, 1523–1532. [CrossRef]
49. Loeschcke, A.; Dienst, D.; Wewer, V.; Hage-Hülsmann, J.; Dietsch, M.; Kranz-Finger, S.; Hüren, V.; Metzger, S.; Urlacher, V.B.; Gigolashvili, T.; et al. The photosynthetic bacteria *Rhodobacter capsulatus* and *Synechocystis* sp. PCC 6803 as new hosts for cyclic plant triterpene biosynthesis. *PLoS ONE* **2017**, *12*, e0189816. [CrossRef]
50. Orsi, E.; Beekwilder, J.; Peek, S.; Eggink, G.; Kengen, S.W.M.; Weusthuis, R.A. Metabolic flux ratio analysis by parallel 13C labeling of isoprenoid biosynthesis in *Rhodobacter sphaeroides*. *Metab. Eng.* **2020**, *57*, 228–238. [CrossRef]
51. Orsi, E.; Mougiakos, I.; Post, W.; Beekwilder, J.; Dompè, M.; Eggink, G.; Van Der Oost, J.; Kengen, S.W.M.; Weusthuis, R.A. Growth-uncoupled isoprenoid synthesis in *Rhodobacter sphaeroides*. *Biotechnol. Biofuels* **2020**, *13*. [CrossRef]
52. Orsi, E.; Beekwilder, J.; van Gelder, D.; van Houwelingen, A.; Eggink, G.; Kengen, S.W.M.; Weusthuis, R.A. Functional replacement of isoprenoid pathways in *Rhodobacter sphaeroides*. *Microb. Biotechnol.* **2020**, *13*, 1082–1093. [CrossRef]
53. Oerke, E.-C. Crop losses to pests. *J. Agric. Sci.* **2006**, *144*, 31–43. [CrossRef]
54. Bolton, M.D.; Thomma, B.P.H.J.; Nelson, B.D. *Sclerotinia sclerotiorum* (Lib.) de Bary: Biology and molecular traits of a cosmopolitan pathogen. *Mol. Plant Pathol.* **2006**, *7*, 1–16. [CrossRef] [PubMed]
55. Okungbowa, F.I.; Shittu, H.O. *Fusarium* wilts: An overview. *Environ. Res. J.* **2012**, *6*, 83–102.
56. West, J.S.; Kharbanda, P.D.; Barbetti, M.J.; Fitt, B.D.L. Epidemiology and management of *Leptosphaeria maculans* (phoma stem canker) on oilseed rape in Australia, Canada and Europe. *Plant Pathol.* **2001**, *50*, 10–27. [CrossRef]
57. Fitt, B.D.L.; Brun, H.; Barbetti, M.J.; Rimmer, S.R. World-Wide Importance of Phoma Stem Canker (*Leptosphaeria maculans* and *L. biglobosa*) on Oilseed Rape (*Brassica napus*). *Eur. J. Plant Pathol.* **2006**, *114*, 3–15. [CrossRef]
58. Singh, H.K.; Singh, R.B.; Kumar, P.; Singh, M.; Yadav, J.K.; Singh, P.K.; Chauhan, M.P.; Shakywar, R.C.; Maurya, K.N.; Priyanka, B.S.; et al. *Alternaria* blight of rapeseed mustard–A Review. *J. Environ. Biol.* **2017**, *38*, 1405–1420. [CrossRef]
59. Verma, P.R. Biology and control of *Rhizoctonia solani* on rapeseed: A Review. *Phytoprotection* **2005**, *77*, 99–111. [CrossRef]
60. Paulitz, T.C.; Okubara, P.A.; Schillinger, W.F. First Report of Damping-Off of Canola Caused by *Rhizoctonia solani* AG 2-1 in Washington State. *Plant Dis.* **2006**, *90*, 829. [CrossRef]
61. Bridge, J. Nematode management in sustainable and subsistence agriculture. *Annu. Rev. Phytopathol.* **1996**, *34*, 201–225. [CrossRef]
62. Heydari, A.; Pessarakli, M. A Review on Biological Control of Fungal Plant Pathogens Using Microbial Antagonists. *J. Biol. Sci.* **2010**, *10*, 273–290. [CrossRef]
63. Habash, S.; Al-Banna, L. Phosphonate fertilizers suppressed root knot nematodes *Meloidogyne javanica* and *M. incognita*. *J. Nematol.* **2011**, *43*, 95–100. [PubMed]
64. Timper, P. Conserving and enhancing biological control of nematodes. *J. Nematol.* **2014**, *46*, 75–89. [PubMed]
65. Lu, C.; Tian, H. Global nitrogen and phosphorus fertilizer use for agriculture production in the past half century: Shifted hot spots and nutrient imbalance. *Earth Syst. Sci. Data* **2017**, *9*, 181–192. [CrossRef]
66. Cheng, A.-X.; Xiang, C.-Y.; Li, J.-X.; Yang, C.-Q.; Hu, W.-L.; Wang, L.-J.; Lou, Y.-G.; Chen, X.-Y. The rice (E)-β-caryophyllene synthase (OsTPS3) accounts for the major inducible volatile sesquiterpenes. *Phytochemistry* **2007**, *68*, 1632–1641. [CrossRef] [PubMed]
67. Echeverrigaray, S.; Zacaria, J.; Beltrão, R. Nematicidal Activity of Monoterpenoids against the Root-Knot Nematode *Meloidogyne incognita*. *Phytopathology* **2010**, *100*, 199–203. [CrossRef]
68. Zengin, H.; Baysal, A.H. Antibacterial and antioxidant activity of essential oil terpenes against pathogenic and spoilage-forming bacteria and cell structure-activity relationships evaluated by SEM microscopy. *Molecules* **2014**, *19*, 17773–17798. [CrossRef]
69. Dambolena, J.S.; Zunino, M.P.; Herrera, J.M.; Pizzolitto, R.P.; Areco, V.A.; Zygadlo, J.A. Terpenes: Natural Products for Controlling Insects of Importance to Human Health—A Structure-Activity Relationship Study. *Psyche A J. Entomol.* **2016**, *2016*, 1–17. [CrossRef]
70. Araniti, F.; Sánchez-Moreiras, A.M.; Graña, E.; Reigosa, M.J.; Abenavoli, M.R. Terpenoid trans -caryophyllene inhibits weed germination and induces plant water status alteration and oxidative damage in adult *Arabidopsis*. *Plant Biol.* **2017**, *19*, 79–89. [CrossRef]
71. Pungartnik, C. Antifungal Potential of Terpenes from *Spondias Purpurea* L. Leaf Extract against *Moniliophthora perniciosa* that causes Witches Broom Disease of *Theobroma cacao*. *Int. J. Complement. Altern. Med.* **2017**, *7*. [CrossRef]
72. Habash, S.S.; Könen, P.P.; Loeschcke, A.; Wüst, M.; Jaeger, K.-E.; Drepper, T.; Grundler, F.M.W.; Schleker, A.S.S. The Plant Sesquiterpene Nootkatone Efficiently Reduces *Heterodera schachtii* Parasitism by Activating Plant Defense. *Int. J. Mol. Sci.* **2020**, *21*, 9627. [CrossRef]

73. Kigathi, R.N.; Unsicker, S.B.; Reichelt, M.; Kesselmeier, J.; Gershenzon, J.; Weisser, W.W. Emission of Volatile Organic Compounds After Herbivory from *Trifolium pratense* (L.) Under Laboratory and Field Conditions. *J. Chem. Ecol.* **2009**, *35*, 1335–1348. [CrossRef] [PubMed]
74. Pazouki, L.; Kanagendran, A.; Li, S.; Kännaste, A.; Rajabi Memari, H.; Bichele, R.; Niinemets, Ü. Mono- and sesquiterpene release from tomato (*Solanum lycopersicum*) leaves upon mild and severe heat stress and through recovery: From gene expression to emission responses. *Environ. Exp. Bot.* **2016**, *132*, 1–15. [CrossRef] [PubMed]
75. Muchlinski, A.; Chen, X.; Lovell, J.T.; Köllner, T.G.; Pelot, K.A.; Zerbe, P.; Ruggiero, M.; Callaway, L.; Laliberte, S.; Chen, F.; et al. Biosynthesis and Emission of Stress-Induced Volatile Terpenes in Roots and Leaves of Switchgrass (*Panicum virgatum* L.). *Front. Plant Sci.* **2019**, *10*, 1144. [CrossRef] [PubMed]
76. Huang, M.; Sanchez-Moreiras, A.M.; Abel, C.; Sohrabi, R.; Lee, S.; Gershenzon, J.; Tholl, D. The major volatile organic compound emitted from *Arabidopsis thaliana* flowers, the sesquiterpene (E)-β-caryophyllene, is a defense against a bacterial pathogen. *New Phytol.* **2012**, *193*, 997–1008. [CrossRef] [PubMed]
77. Rasmann, S.; Köllner, T.G.; Degenhardt, J.; Hiltpold, I.; Toepfer, S.; Kuhlmann, U.; Gershenzon, J.; Turlings, T.C.J. Recruitment of entomopathogenic nematodes by insect-damaged maize roots. *Nature* **2005**, *434*, 732–737. [CrossRef]
78. Degenhardt, J.; Hiltpold, I.; Kollner, T.G.; Frey, M.; Gierl, A.; Gershenzon, J.; Hibbard, B.E.; Ellersieck, M.R.; Turlings, T.C.J. Restoring a maize root signal that attracts insect-killing nematodes to control a major pest. *Proc. Natl. Acad. Sci. USA* **2009**, *106*, 13213–13218. [CrossRef]
79. Ma, Y.-N.; Chen, C.-J.; Li, Q.-Q.; Xu, F.-R.; Cheng, Y.-X.; Dong, X. Monitoring Antifungal Agents of *Artemisia annua* against *Fusarium oxysporum* and *Fusarium solani*, Associated with *Panax notoginseng* Root-Rot Disease. *Molecules* **2019**, *24*, 213. [CrossRef]
80. Yamagiwa, Y.; Inagaki, Y.; Ichinose, Y.; Toyoda, K.; Hyakumachi, M.; Shiraishi, T. *Talaromyces wortmannii* FS2 emits β-caryophyllene, which promotes plant growth and induces resistance. *J. Gen. Plant. Pathol.* **2011**, *77*, 336–341. [CrossRef]
81. Hanahan, D. Studies on transformation of *Escherichia coli* with plasmids. *J. Mol. Biol.* **1983**, *166*, 557–580. [CrossRef]
82. Simon, R.; Priefer, U.; Pühler, A. A Broad Host Range Mobilization System for In Vivo Genetic Engineering: Transposon Mutagenesis in Gram Negative Bacteria. *Bio/Technology* **1983**, *1*, 784–791. [CrossRef]
83. Strnad, H.; Lapidus, A.; Paces, J.; Ulbrich, P.; Vlcek, C.; Paces, V.; Haselkorn, R. Complete genome sequence of the photosynthetic purple nonsulfur bacterium *Rhodobacter capsulatus* SB1003. *J. Bacteriol.* **2010**, *192*, 3545–3546. [CrossRef] [PubMed]
84. Klipp, W.; Masepohl, B.; Pühler, A. Identification and mapping of nitrogen fixation genes of *Rhodobacter capsulatus*: Duplication of a nifA-nifB region. *J. Bacteriol.* **1988**, *170*, 693–699. [CrossRef] [PubMed]
85. Weaver, P.F.; Wall, J.D.; Gest, H. Characterization of *Rhodopseudomonas capsulata*. *Arch. Microbiol.* **1975**, *105*, 207–216. [CrossRef] [PubMed]
86. Fuhrmann, M.; Hausherr, A.; Ferbitz, L.; Schödl, T.; Heitzer, M.; Hegemann, P. Monitoring dynamic expression of nuclear genes in *Chlamydomonas reinhardtii* by using a synthetic luciferase reporter gene. *Plant Mol. Biol.* **2004**, *55*, 869–881. [CrossRef] [PubMed]
87. Hungate, R.E. *Chapter IV A Roll Tube Method for Cultivation of Strict Anaerobes*; Norris, J.R., Ribbons, D.W.B.T.-M., Eds.; Academic Press: Cambridge, MA, USA, 1969; Volume 3, pp. 117–132.
88. Rodriguez, S.; Kirby, J.; Denby, C.M.; Keasling, J.D. Production and quantification of sesquiterpenes in *Saccharomyces cerevisiae*, including extraction, detection and quantification of terpene products and key related metabolites. *Nat. Protoc.* **2014**, *9*, 1980–1996. [CrossRef]
89. Wiegand, I.; Hilpert, K.; Hancock, R.E.W. Agar and broth dilution methods to determine the minimal inhibitory concentration (MIC) of antimicrobial substances. *Nat. Protoc.* **2008**, *3*, 163–175. [CrossRef]
90. European Committee for Antimicrobial Susceptibility Testing (EUCAST) of the European Society of Clinical Microbiology and Infectious Diseases (ESCMID). Determination of minimum inhibitory concentrations (MICs) of antibacterial agents by broth dilution. *Clin. Microbiol. Infect.* **2003**, *9*, ix–xv. [CrossRef]
91. Kim, S.; Jahandar, M.; Jeong, J.H.; Lim, D.C. Recent Progress in Solar Cell Technology for Low-Light Indoor Applications. *Curr. Altern. Energy* **2019**, *3*, 3–17. [CrossRef]
92. Ruberto, G.; Baratta, M.T. Antioxidant activity of selected essential oil components in two lipid model systems. *Food Chem.* **2000**, *69*, 167–174. [CrossRef]
93. Medeiros, R.; Passos, G.F.; Vitor, C.E.; Koepp, J.; Mazzuco, T.L.; Pianowski, L.F.; Campos, M.M.; Calixto, J.B. Effect of two active compounds obtained from the essential oil of *Cordia verbenacea* on the acute inflammatory responses elicited by LPS in the rat paw. *Br. J. Pharmacol.* **2007**, *151*, 618–627. [CrossRef]
94. Fidyt, K.; Fiedorowicz, A.; Strządała, L.; Szumny, A. β-caryophyllene and β-caryophyllene oxide-natural compounds of anticancer and analgesic properties. *Cancer Med.* **2016**, *5*, 3007–3017. [CrossRef] [PubMed]
95. Paula-Freire, L.I.G.; Andersen, M.L.; Gama, V.S.; Molska, G.R.; Carlini, E.L.A. The oral administration of trans-caryophyllene attenuates acute and chronic pain in mice. *Phytomedicine* **2014**, *21*, 356–362. [CrossRef] [PubMed]
96. Sköld, M.; Karlberg, A.-T.; Matura, M.; Börje, A. The fragrance chemical β-caryophyllene—Air oxidation and skin sensitization. *Food Chem. Toxicol.* **2006**, *44*, 538–545. [CrossRef] [PubMed]
97. Steenackers, B.; Neirinckx, A.; De Cooman, L.; Hermans, I.; De Vos, D. The strained sesquiterpene β-caryophyllene as a probe for the solvent-assisted epoxidation mechanism. *ChemPhysChem* **2014**, *15*, 966–973. [CrossRef]
98. De Souza, R.; Ambrosini, A.; Passaglia, L.M.P. Plant growth-promoting bacteria as inoculants in agricultural soils. *Genet. Mol. Biol.* **2015**, *38*, 1678–4685. [CrossRef]

99. Nath Yadav, A. Plant Growth Promoting Bacteria: Biodiversity and Multifunctional Attributes for Sustainable Agriculture. *Adv. Biotechnol. Microbiol.* **2017**, *5*. [CrossRef]
100. Singh, V.K.; Singh, A.K.; Singh, P.P.; Kumar, A. Interaction of plant growth promoting bacteria with tomato under abiotic stress: A review. *Agric. Ecosyst. Environ.* **2018**, *267*, 129–140. [CrossRef]
101. Çakmakçi, R.; Dönmez, F.; Aydin, A.; Şahin, F. Growth promotion of plants by plant growth-promoting rhizobacteria under greenhouse and two different field soil conditions. *Soil Biol. Biochem.* **2006**, *38*, 1482–1487. [CrossRef]
102. Çakmakçi, R.; Dönmez, M.F.; Erdoğan, Ü. The effect of plant growth promoting rhizobacteria on Barley seedling growth, nutrient uptake, some soil properties, and bacterial counts. *Turk. J. Agric. For.* **2007**, *31*, 189–199.
103. Lahlali, R.; Peng, G.; Gossen, B.D.; McGregor, L.; Yu, F.Q.; Hynes, R.K.; Hwang, S.F.; McDonald, M.R.; Boyetchko, S.M. Evidence that the Biofungicide Serenade (*Bacillus subtilis*) Suppresses Clubroot on Canola via Antibiosis and Induced Host Resistance. *Phytopathology* **2012**, *103*, 245–254. [CrossRef]
104. Berg, G. Plant-microbe interactions promoting plant growth and health: Perspectives for controlled use of microorganisms in agriculture. *Appl. Microbiol. Biotechnol.* **2009**, *84*, 11–18. [CrossRef] [PubMed]
105. El-Howeity, M.A.; Asfour, M.M. Response of some varieties of canola plant (*Brassica napus* L.) cultivated in a newly reclaimed desert to plant growth promoting rhizobacteria and mineral nitrogen fertilizer. *Ann. Agric. Sci.* **2012**, *57*, 129–136. [CrossRef]
106. Bertrand, H.; Nalin, R.; Bally, R.; Cleyet-Marel, J.-C. Isolation and identification of the most efficient plant growth-promoting bacteria associated with canola (*Brassica napus*). *Biol. Fertil. Soils* **2001**, *33*, 152–156. [CrossRef]
107. Ntalli, N.; Ferrari, F.; Giannakou, I.O.; Menkissoglu-Spiroudi, U. Synergistic and antagonistic interactions of terpenes against *Meloidogyne incognita* and the nematicidal activity of essential oils from seven plants indigenous to Greece. *Pest. Manag. Sci.* **2011**, *67*, 341–351. [CrossRef] [PubMed]
108. Jiménez-Reyes, M.F.; Carrasco, H.; Olea, A.F.; Silva-Moreno, E. Natural Compounds: A Sustainable Alternative to the Phytopathogens Control. *J. Chil. Chem. Soc.* **2019**, *64*, 4459–4465. [CrossRef]
109. Da Silva, F.; Alves, C.; Oliveira Filho, J.; Vieira, T.; Crotti, A.E.; Miranda, M. Chemical constituents of essential oil from *Murraya paniculata* leaves and its application to in vitro biological control of the fungus *Sclerotinia sclerotiorum*. *Food Sci. Technol.* **2019**, *39*. [CrossRef]
110. Valadares, A.C.F.; Alves, C.C.F.; Alves, J.M.; de Deus, I.P.B.; de Oliveira Fi, J.G.; Dos Santos, T.C.L.; Dias, H.J.; Crotti, A.E.M.; Miranda, M.L.D. Essential oils from *Piper aduncum* inflorescences and leaves: Chemical composition and antifungal activity against *Sclerotinia sclerotiorum*. *An. Acad. Bras. Cienc.* **2018**, *90*, 2691–2699. [CrossRef]
111. Yang, C.; Yang, C.; Gao, X.; Jiang, Y.; Sun, B.; Gao, F.; Yang, S. Synergy between methylerythritol phosphate pathway and mevalonate pathway for isoprene production in *Escherichia coli* Synergy between methylerythritol phosphate pathway and mevalonate pathway for isoprene production in *Escherichia coli*. *Metab. Eng.* **2016**, *37*, 79–91. [CrossRef]
112. Syed, S.; Prasad Tollamadugu, N.V.K.V. Chapter 16—Role of Plant Growth-Promoting Microorganisms as a Tool for Environmental Sustainability. In *Recent Developments in Applied Microbiology and Biochemistry*; Buddolla, V., Ed.; Academic Press: Cambridge, MA, USA, 2019; pp. 209–222. ISBN 978-0-12-816328-3.
113. Dobbelaere, S.; Vanderleyden, J.; Okon, Y. Plant Growth-Promoting Effects of Diazotrophs in the Rhizosphere. *CRC Crit. Rev. Plant Sci.* **2003**, *22*, 107–149. [CrossRef]
114. Chen, F.; Han, P.; Liu, P.; Si, N.; Liu, J.; Liu, X. Activity of the novel fungicide SYP-Z048 against plant pathogens. *Sci. Rep.* **2014**, *4*, 6473. [CrossRef]
115. Guzmán-Guzmán, P.; Porras-Troncoso, M.D.; Olmedo-Monfil, V.; Herrera-Estrella, A. *Trichoderma* Species: Versatile Plant Symbionts. *Phytopathology* **2018**, *109*, 6–16. [CrossRef] [PubMed]
116. Finkel, O.M.; Castrillo, G.; Herrera Paredes, S.; Salas González, I.; Dangl, J.L. Understanding and exploiting plant beneficial microbes. *Curr. Opin. Plant. Biol.* **2017**, *38*, 155–163. [CrossRef] [PubMed]
117. Anthony, J.R.; Anthony, L.C.; Nowroozi, F.; Kwon, G.; Newman, J.D.; Keasling, J.D. Optimization of the mevalonate-based isoprenoid biosynthetic pathway in *Escherichia coli* for production of the anti-malarial drug precursor amorpha-4,11-diene. *Metab. Eng.* **2009**, *11*, 13–19. [CrossRef] [PubMed]
118. Ajikumar, P.K.; Xiao, W.-H.; Tyo, K.E.J.; Wang, Y.; Simeon, F.; Leonard, E.; Mucha, O.; Phon, T.H.; Pfeifer, B.; Stephanopoulos, G. Isoprenoid Pathway Optimization for Taxol Precursor Overproduction in *Escherichia coli*. *Science (80-)* **2010**, *330*, 70–74. [CrossRef]
119. Henke, N.; Wichmann, J.; Baier, T.; Frohwitter, J.; Lauersen, K.; Risse, J.; Peters-Wendisch, P.; Kruse, O.; Wendisch, V. Patchoulol Production with Metabolically Engineered *Corynebacterium glutamicum*. *Genes* **2018**, *9*, 219. [CrossRef]
120. Frohwitter, J.; Heider, S.A.E.; Peters-Wendisch, P.; Beekwilder, J.; Wendisch, V.F. Production of the sesquiterpene (+)-valencene by metabolically engineered *Corynebacterium glutamicum*. *J. Biotechnol.* **2014**, *191*, 205–213. [CrossRef]
121. Chen, H.; Zhu, C.; Zhu, M.; Xiong, J.; Ma, H.; Zhuo, M.; Li, S. High production of valencene in *Saccharomyces cerevisiae* through metabolic engineering. *Microb. Cell Fact.* **2019**, *18*, 195.
122. Westfall, P.J.; Pitera, D.J.; Lenihan, J.R.; Eng, D.; Woolard, F.X.; Regentin, R.; Horning, T.; Tsuruta, H.; Melis, D.J.; Owens, A.; et al. Production of amorphadiene in yeast, and its conversion to dihydroartemisinic acid, precursor to the antimalarial agent artemisinin. *Proc. Natl. Acad. Sci. USA* **2012**, *109*, E111–E118.
123. Englund, E.; Shabestary, K.; Hudson, E.P.; Lindberg, P. Systematic overexpression study to find target enzymes enhancing production of terpenes in *Synechocystis* PCC 6803, using isoprene as a model compound. *Metab. Eng.* **2018**, *49*, 164–177. [CrossRef]

124. Bentley, F.K.; Zurbriggen, A.; Melis, A. Heterologous expression of the mevalonic acid pathway in cyanobacteria enhances endogenous carbon partitioning to isoprene. *Mol. Plant.* **2014**, *7*, 71–86. [CrossRef]
125. Krieg, T.; Sydow, A.; Faust, S.; Huth, I.; Holtmann, D. CO_2 to Terpenes: Autotrophic and Electroautotrophic α-Humulene Production with *Cupriavidus necator*. *Angew. Chem. Int. Ed.* **2018**, *57*, 1879–1882. [CrossRef] [PubMed]
126. Yang, J.; Li, Z.; Guo, L.; Du, J.; Bae, H.-J. Biosynthesis of β-caryophyllene, a novel terpene-based high-density biofuel precursor, using engineered *Escherichia coli*. *Renew. Energy* **2016**, *99*, 216–223. [CrossRef]
127. Yang, J.; Nie, Q. Engineering *Escherichia coli* to convert acetic acid to β-caryophyllene. *Microb. Cell Fact.* **2016**, *15*, 74. [CrossRef] [PubMed]
128. Hogenkamp, F.; Hilgers, F.; Knapp, A.; Klaus, O.; Bier, C.; Binder, D.; Jaeger, K.-E.; Drepper, T.; Pietruszka, J. Effect of Photocaged Isopropyl β-D-1-Thiogalactopyranoside Solubility on Light-Responsiveness of LacI-controlled Expression Systems in Different Bacteria. *ChemBioChem* **2020**. [CrossRef] [PubMed]

Supplementary Materials

Heterologous Production of β-Caryophyllene and Evaluation of its Activity against Plant Pathogenic Fungi

Table of contents

1. Supplementary methods

Bacterial strains and plasmids

All bacterial strains, plasmids and oligonucleotides used in this study are listed in Table S1.

Table S1. Bacterial strains and plasmids used in this study.

Strains, plasmids	Relevant features or description	References
	Strains	
***E. coli* DH5α**	*F- Φ80lacZΔM15 Δ(lacZYA-argF) U169 recA1 endA1 hsdR17 phoA supE44 thi-1 gyrA96 relA1 deoR*	[81]
***E. coli* S17-1**	Ec294::[RP4-2 (Tc^R::Mu)(Km^R::Tn7)] *recA, thi, pro, hsdR- hsdM+* Tp^R Sm^R	[82]
***R. capsulatus* SB1003**	Wild-type, Rif^R	[83]
***R. capsulatus* SB1003-MVA**	SB1003-derivative, carrying the chromosomally intergrated MVA cluster from *Paracoccus zeaxanthinifaciens*, Rif^R, Gm^R	[39]
	Plasmids	
pRhon5Hi-2	pBBR1mcs (basic vector, rep mob Cm^R), pET22b (MCS, pelB), pBSL15 (aphII), P_{nif}	[39]
pRhon5Hi-2-QHS1	pRhon5Hi-2 with P_{nif} *QHS1*	This study
pRhon5Hi-2-QHS1-ispA	pRhon5Hi-2 with P_{nif} *QHS1-ispA*	This study

Analysis of *n*-dodecane-mediated β-caryophyllene extraction from phototrophically grown *R. capsulatus*.

The extraction of sesquiterpenoids from microbial cell cultures is mostly performed *via* a two-phase cultivation using an *n*-dodecane layer ($^1/_{30}$ of the culture volume) as solvent phase which is added prior to cultivation [88]. In analogy to our prior work [39], we performed the extraction and quantification of β-caryophyllene as described in the Materials and Methods section.

To quantify the final product titers, a calibration curve was generated using a pure β-caryophyllene reference from Sigma Aldrich. However, the correlation of signals from *n*-dodecane extracted samples with the reference signals does not take into account extraction efficiencies of β-caryophyllene when using *n*-dodecane as organic solvent. It can be assumed that, in dependence of its specific properties, it only diffuses to a certain extent into the *n*-dodecane layer. In addition, terpenes that are produced in the cytoplasm of *R. capsulatus* can additionally be retained by the intracytoplasmic membrane system thereby further affecting the transfer into the organic phase. Therefore, the transfer efficiency of β-caryophyllene from cultivation medium into *n*-dodecane in the presence of intact and disrupted *R. capsulatus* cells was first determined for both hungate and screw neck vials. For this purpose, the reference compound was first mixed with 14 mL or 4.5 mL of phototrophically grown *R. capsulatus* SB1003 cells (cultivation parameters: anaerobic growth, 30 °C, approx. up to OD_{660nm} = 2.5) in appropriate amounts (β-caryophyllene: 71.4 mg L^{-1} and 881.4 mg L^{-1}, respectively). For this purpose, 11.48 µL or 51.7 µL β-caryophyllene, which is an oil, was added as a 10-fold dilution in diethyl ether. After addition, the cultures were sealed and vortexed for 1 min. Subsequently, the reference substance was extracted using *n*-dodecane as described. The transfer efficiency was determined via GC analysis by comparing peak areas of the specific signals from appropriately diluted solutions to samples that had undergone extraction (**Figure S1**).

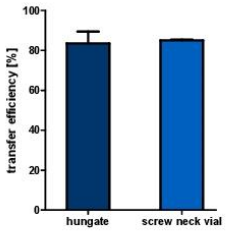

Figure S1. Transfer efficiency of the β-caryophyllene reference compound from cultivation medium into the *n*-dodecane phase in the presence of intact *R. capsulatus* cells in hungate (dark blue) and screw neck vials (light blue). For extraction, 71.4 mg L^{-1} or 881.4 mg L^{-1} β-caryophyllene were added to 14 mL or 4.5 mL cell culture (OD_{660nm} = 2.5), respectively. For details, see text above. Values are means of triplicate measurements. Error bars indicate the respective standard deviations.

By using intact *R. capsulatus* cells, a transfer efficiency of around 85% could be determined for both the hungate and the screw neck vial. Thus, it could be shown that there are some methodological losses, which have to be considered for product quantification. To moreover analyze if putative interaction of intracellularly produced sesquiterpenoids with the *Rhodobacter* ICM can further decrease product transfer, the experiment was repeated using disrupted cells. However, as the transfer efficiencies were nearly equal for the hungate and the screw neck vial, all further experiments were only performed for the hungate cultivation. First, equally cultivated *R. capsulatus* wildtype cells (OD_{660nm} = 2.5) were disrupted using a ball mill (3 × 10 min, 30 Hz, Mixer Mill MM 400, Retsch GmbH, Germany) and subsequently mixed with the same amount of reference compound as described previously. Extraction

and quantification were performed as described for intact cell samples and signals were subsequently compared to those of the non-extracted reference compounds (**Figure S2**).

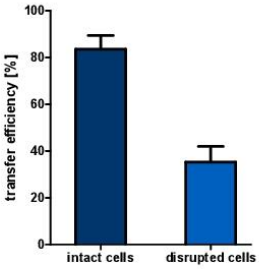

Figure S2. Transfer efficiency of the β-caryophyllene reference compound from cultivation medium into the *n*-dodecane phase in the presence of intact (dark blue) and disrupted (light blue) *R. capsulatus* cells. For extraction, 71.4 mg L^{-1} β-caryophyllene were added to 14 mL cell lysate (OD660nm = 2.5). For further details, see text above. Values are means of triplicate measurements. Error bars indicate the respective standard deviations.

It could be seen, that disrupted cells lead to a strong decrease of the extraction efficiency (35%) in comparison to the previous measurement using intact cells (85%), suggesting that this hydrophobic terpenoid (log*P* = 5.35; values were calculated using the ALOGPS2.1 online tool described by Tetko *et al.* 2005; doi:10.1007/s10822-005-8694-y) is strongly attached to the intracytoplasmic membrane system. Hence, for calculating the final production titers, the individual transfer efficiency for disrupted cell cultures (here termed c_t *or* 'transfer efficiency coefficient', factor: 1.6474) was taken into account.

Besides the above described negative effect of cellular components on the extraction efficiency, we further analyzed, if repeated *n*-dodecane-dependent sesquiterpenoid extraction should be considered for an optimal estimation of the overall production titers. Thus, an experiment with repeated sesquiterpenoid extractions from disrupted wildtype cultures that were mixed with the reference compound as described above was performed over four days (**Figure S3**). For quantitative analysis of β-caryophyllene, a calibration curve with the authentic reference compound ranging from 0.5 to 4 mg mL^{-1} *n*-dodecane, were used (slope: 382.16; see also depicted below in **Figure S5**).

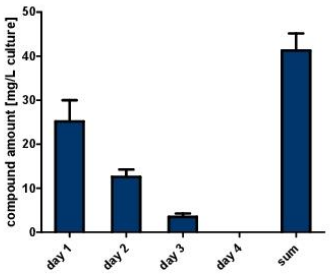

Figure S3. Extraction efficiency of the β-caryophyllene reference compound from cultivation medium in the presence of disrupted (dark blue) and intact (light blue) *R. capsulatus* cells by repeatedly using *n*-dodecane as organic solvent over four days. See text above for details. For repeated extraction, 71.4 mg L^{-1} β-caryophyllene were added to 14 mL cell lysate (OD660nm = 2.5). Subsequently, 500 µL *n*-dodecane was used for a 24 h extraction period over a total duration of four days. Single extraction procedures were repeated four times and the sesquiterpenoid concentration of each fraction was analyzed via GC. Values are means of triplicate measurements. Error bars indicate the respective standard deviations.

The overall extraction efficiency was increased by repeated extraction to 39% for disrupted cells in comparison to the amount determined after the first extraction. Therefore, it has also to be taken into account by which factor the quantification on day 1 underestimates product titers (here termed c_{ex} *or* 'coefficient for repeated extraction'; factor: 1.3897) in order to calculate the final product titers.

Finally, we analyzed if the presence of an *n*-dodecane layer positively or negatively affects the β-caryophyllene formation in *R. capsulatus* cells during cultivation. Therefore, an experiment with repeated sesquiterpene extraction out of production cultures that had been cultivated (3 days) with and without an *n*-dodecane layer before extraction was performed over four days (**Figure S4**). For the analysis of the β-caryophyllene producing *R. capsulatus* cultures grown without a solvent layer, equal amounts of *n*-dodecane were added after cultivation and prior to the extraction procedure.

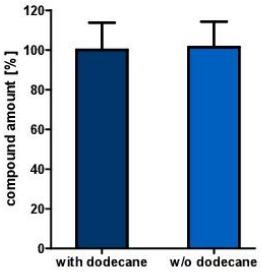

Figure S4. Comparison of relative β-caryophyllene formation in *R. capsulatus* production strains cultivated with (dark blue) and without an *n*-dodecane layer (light blue). Data was normalized to the amount of sesquiterpene extracted from cultures with *n*-dodecane. See text above for details. For *R. capsulatus* cultures containing the *n*-dodecane layer, 500 µL of the solvent was added before cultivation. In contrast, the same amount of solvent was added to cultures without *n*-dodecane after the cultivation. Compounds were extracted and analyzed as described above. Values are means of triplicate measurements. Error bars indicate the respective standard deviations.

Almost no changes of β-caryophyllene formation could be observed in the absence of the *n*-dodecane layer. Hence, the *n*-dodecane layer can alternatively be added after cultivation of the *Rhodobacter* production strains prior to the extraction procedure without any product losses. However, it must be considered that an addition of the organic solvent after cultivation is only reasonable for non-volatile terpenoids, as otherwise the product loss could be excessively high.

In summary, product titers of *R. capsulatus* β-caryophyllene production cultures were determined by analysis of *n*-dodecane extraction samples from disrupted cells. To this end, *R. capsulatus* strains were cultivated without the solvent, disrupted and then extracted one time with *n*-dodecane. Using the calibration curves obtained with reference compounds (**Figure S5**) and taking into account the cultivation parameters v and r_D, as well as the above described results on losses of this procedure (**Figure S2** and **S3**), equation 1 was used for calculating the final β-caryophyllene titers. The dodecane volume ratio r_D represents the ratio of the dodecane volume which was used for the calibration curve (1 mL) to the dodecane volume which was used as a solvent layer during extraction of the production cultures.

$$\text{compound amount}\left[\frac{mg}{L\ culture}\right] = \frac{pa}{s*v*r_D} * 1000\ mL * c_t * c_{ex} \quad (1)$$

$\boldsymbol{pa} = \boldsymbol{peak\ area\ [pA*s]}$
$\boldsymbol{s} = \boldsymbol{slope\ of\ calibration\ curve}$
$v = culture\ volume\ [mL]$
$r_D = dodecane\ volume\ ratio$
$c_t = transfer\ efficiency\ coefficient$
$c_{ex} = coefficient\ for\ repeated\ extraction$

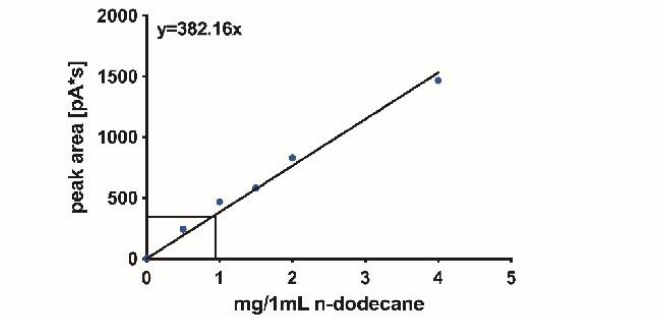

Figure S5. Quantification of extracted β-caryophyllene *via* a calibration curve of β-caryophyllene reference signals in GC-FID analyses. The signal intensities of the authentic reference compound, which were measured as peak areas [pA*s], were correlated to compound quantities [mg] in 1 mL solvent in different concentrations. Mean values of detected signals of *n*-dodecane extraction samples from disrupted cells of the best *R. capsulatus* production strain (SB1003-MVA with pRhon5Hi-2-QHS1-ispA) are indicated (black lines from Y-axis to calibration line). As the extracts from *R. capsulatus* cultures were prepared with *n*-dodecane volumes of 500 µL for hungate cultures and 150 µL for screw neck vials, the extracted amount of biosynthetic product [mg] could be calculated from the linear equations in consideration of the respective solvent amount. These data were used for calculation of product levels in cultures, taking the used culture volume, and factors r_D, c_t and c_{ex} into account, as described above.

2. Supplementary data

Emission range of used light sources and *in vivo* absorption spectrum of phototrophically grown *R. capsulatus* culture

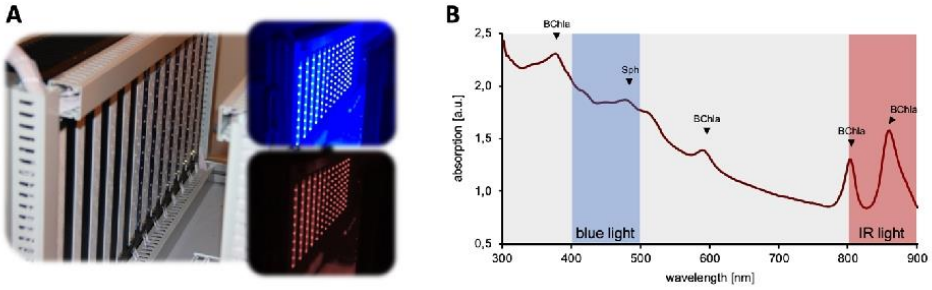

Figure S6. Emission range of different light sources and the absorption spectrum of phototrophically cultivated *R. capsulatus* cells. To illuminate phototrophic cell cultures of *R. capsulatus* more specifically, a custom-made LED panel (**A**) was developed by Vossloh-Schwabe Lighting Solutions GmbH & Co. KG (Kamp-Lintfort, Germany). Each LED array, carries 130 IR (λ_{max}= 850 nm, max. 5.6 mW cm^{-2}) and 130 blue-light LEDs (λ_{max} = 455 nm, 4.0 mW cm^{-2}) on a joint area of 1950 cm^2 (697 x 280 mm), suitable for specific excitation of photopigments spheroidene (indicated as Sph) and bacteriochlorophyll *a* (BChl *a*). In addition, the array offers 63 UV-A LEDs (λ_{max}= 364 nm, max. 7.6 mW cm^{-2}) in a separate area of 900 cm^2 (361 × 250 mm), suitable for applying photocaged inducers (see for example [128]) for future optogenetic approaches with *R. capsulatus*. Light intensity quantifications were conducted using a Thermal Power Sensor (S302C, Thorlabs Inc, USA). The emission maxima for the following light sources are shown in (**B**): (i) Blue LEDs emit blue light at around 450 nm (blue area) and (ii) IR LEDs emit light at around 850 nm (light red area). Additionally, a whole-cell absorption spectrum of a *R. capsulatus* culture is shown (dark red line). The three peaks at around 480 nm represent the carotenoid spheroidene, while the peaks at 380 nm, 600 nm, 800 nm and 860 nm represent BChl *a*.

Specifications of cultivation vessels for anaerobic growth of *R. capsulatus* cultures.

Table S2. Cultivation vessel specifications.

Cultivation vessel	Hungate	Screw neck vial
Vessel Specification	Hungate tube (Bellco Glass)	Screw neck vial N13, clear (MN)
Total volume	16.5 mL	4.5 mL
Working volume	15 mL	4.2 mL
Glass type	Type 1 class B borosilicate glass, transmission > 90% at 850 nm	Type 1 borosilicate glass (FIOLAX®), transmission > 90% at 850 nm
Wall thickness	1.05 mm	0.95 mm
Lateral surface area	~ 60.3 cm^2	~ 18.5 cm^2
Surface-to-volume-ratio	4.02 cm^{-1}	4.40 cm^{-1}

Productivities of β-caryophyllene in *R. capsulatus* SB1003 cultures.

Table S3. Production titers of β-caryophyllene in *R. capsulatus* SB1003 cultures.

Compound	**β-caryophyllene**	
Rhodobacter capsulatus strain	SB1003-MVA/pRhon5Hi-2-QHS1-ispA	
Cultivation vessel	Hungate tube	Screw neck vial
Titer at below defined time point (mg L^{-1} culture)	90.39 ± 18.61 mg L^{-1}	139.29 ± 31.35 mg L^{-1}
Time point of highest titer (h)	72 h	72 h
OD at the time point of highest titer (660 nm)	2.79 ± 0.09	2.50 ± 0.06
Cell mass at the time point of highest product titer (gDCW L^{-1} culture)	1.67 ± 0.05 gDCW L^{-1}	1.50 ± 0.04 gDCW L^{-1}
Volumetric productivity (mg L^{-1} h^{-1})[1]	1.26 ± 0.26 mg L^{-1} h^{-1}	1.93 ±0.44 mg L^{-1} h^{-1}
Specific yield at above defined time point (mg $gDCW^{-1}$)	54.01 ± 9.64 mg $gDCW^{-1}$	93.41 ±23.40 mg $gDCW^{-1}$
Specific productivity (mg $gDCW^{-1}$ h^{-1})[1]	0.75 ± 0.13 mg $gDCW^{-1}$ h^{-1}	1.30 ±0.32 mg $gDCW^{-1}$ h^{-1}

[1] Productivities per hour were calculated based on product levels that were present at the time points when highest titers were reached and are thus not necessarily maximal productivities.

Codon optimized DNA sequence of β-caryophyllene synthase QHS1 from *A. annua* for expression in *R. capsulatus*.

The shown sequence encompasses the QHS1 gene referring to the mRNA sequence published in GenBank: AF472361.1, encoding the QHS1 protein (UniProtKB - Q8SA63). At the 5'-end, the synthetic DNA fragment carries a short sequence derived from pET22b (between the *Xba*I and *Nde*I sites) harboring the corresponding ribosome binding site (RBS).

*Xba*I **RBS** Nde*I*/**Start**

TCTAGAAATAATTTTGTTTAACTTTAAG**AAGGAG**ATATACAT**ATG**AGCGTGAAAGAAGAAAAAGTGATC
CGCCCGATCGTGCATTTCCCGCCGAGCGTGTGGGCGGATCAGTTCCTGATCTTCGATGATAAACAGGCGG
AACAGGCGAACGTGGAACAGGTGGTGAACGAACTGCGCGAAGATGTGCGCAAAGATCTGGTGAGCAGC
CTGGATGTGCAGACCGAACATACCAACCTGCTGAAACTGATCGATGCGATCCAGCGCCTGGGCATCGCG
TATCATTTCGAAGAAGAAATCGAACAGGCGCTGCAGCATATCTATGATACCTATGGCGATGATTGGAAA
GGCCGCAGCCCGAGCCTGTGGTTCCGCATCCTGCGCCAGCAGGGCTTCTATGTGAGCTGCGATATCTTCA
AAAACTATAAAAAAGAAGATGGCAGCTTCAAAGAAAGCCTGACCAACGATGTGGAAGGCCTGCTGGAA
CTGTATGAAGCGACCTATCTGCGCGTGCAGGGCGAAGGCGTGCTGGATGATGCGCTGGTGTTCACCCGCA
CCTGCCTGGAAAAAATCGCGAAAGATCTGGTGCATACCAACCCGACCCTGAGCACCTATATCCAGGAAG
CGCTGAAACAGCCGCTGCATAAACGCCTGACCCGCCTGGAAGCGCTGCGCTATATCCCGATGTATGAAC
AGCAGGCGAGCCATAACGAAAGCCTGCTGAAACTGGCGAAACTGGGCTTCAACCTGCTGCAGAGCCTGC
ATCGCAAAGAACTGAGCGAAGTGAGCCGCTGGTGGAAAGGCCTGGATGTGCCGAACAACCTGCCGTAT
GCGCGCGATCGCATGGTGGAATGCTATTTCTGGGCGCTGGGCGTGTATTTCGAACCGAAATATAGCCAGG
CGCGCATCTTCCTGGCGAAAGTGATCAGCCTGGCGACCGTGCTGGATGATACCTATGATGCGTATGGCAC
CTATGAAGAACTGAAAATCTTCACCGAAGCGATCCAGCGCTGGAGCATCACCTGCATCGATATGCTGCC
GGAATATCTGAAACTGCTGTATCAGGGCGTGCTGGATATCTATATCGAAATGGAAGAAATCATGGGCAA
AGAAGGCAAAGCGCATCATCTGAGCTATGCGAAAGAAAGCATGAAAGAGTTCATCCGCAGCTATATGAT
GGAAGCGAAATGGGCGAACGAAGGCTATGTGCCGACCGCGGAAGAACACATGAGCGTGGCGTTCGTGA
GCAGCGGCTATAGCATGCTGGCGACCACCTGCTTCGTGGGCATGGGCGATATCGTGACCGATGAAGCGTT
CAAATGGGCGCTGACCAAACCGCCGATCATCAAAGCGAGCTGCGCGATCGCGCGCCTGATGGATGATAT
CCATAGCCAGAAAGAAGAAAAAGAACGCATCCATGTGGCGAGCAGCGTGGAAAGCTATATGAAACAGT
ATGATGTGACCGAAGAACATGTGCTGAAAGTGTTCAACAAAAAAATCGAAGATGCGTGGAAAGATATC
ACCCGCGAAAGCCTGGTGCGCAAAGATATCCCGATGCCGCTGATGATGCGCGTGATCAACCTGGCGCAG
GTGATGGATGTGCTGTATAAACATAAAGATGGCTTCACCAACGTGGGCGAAGAACTGAAAGATCATATC
AAAAGCCTGCTGGTGCATCCGATCCCGATC**TGA**AAGCTT

Stop *Hind*III

Bioactivities of β-caryophyllene and β-caryophyllene oxide against phytopathogenic fungi

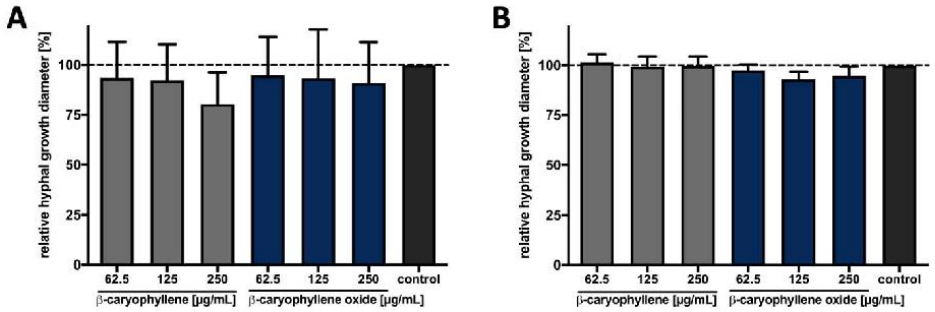

Figure S7. Effect of β-caryophyllene and β-caryophyllene oxide on the hyphal growth of plant pathogenic fungi. Effect of β-caryophyllene and β-caryophyllene oxide against A) *P. lingam* and B) *R. solani*. Final concentration of 62.5 µg mL^{-1}, 125 µg mL^{-1} and µg mL^{-1} of β-caryophyllene (gray bars) and β-caryophyllene oxide (blue bars) in PDA growth medium were used. Medium mixed with the solvents DMSO and Tween 20 (final concentrations, 0.5% and 1% *v/v*, respectively) was used as control. Fungal mycelium was placed in the center of each plate and incubated for 7 days at 24 °C. Subsequently, the diameter of the fungal colony was measured, and the relative growth percentage was calculated. Each bar represents the mean ± standard deviation of 3 independent biological replicates ($n = 9$). No significant differences based on ANOVA test ($P < 0.05$).

References

39. Troost, K.; Loeschcke, A.; Hilgers, F.; Özgür, A.Y.; Weber, T.M.; Santiago-Schübel, B.; Svensson, V.; Hage-Hülsmann, J.; Habash, S.S.; Grundler, F.M.W.; et al. Engineered *Rhodobacter capsulatus* as a Phototrophic Platform Organism for the Synthesis of Plant Sesquiterpenoids. *Front. Microbiol.* **2019**, *10*, 1998.
81. Hanahan, D. Studies on transformation of *Escherichia coli* with plasmids. *J. Mol. Biol.* **1983**, *166*, 557–580.
82. Simon, R.; Priefer, U.; Pühler, A. A Broad Host Range Mobilization System for *In Vivo* Genetic Engineering: Transposon Mutagenesis in Gram Negative Bacteria. *Bio/Technology* **1983**, *1*, 784–791.
83. Strnad, H.; Lapidus, A.; Paces, J.; Ulbrich, P.; Vlcek, C.; Paces, V.; Haselkorn, R. Complete genome sequence of the photosynthetic purple nonsulfur bacterium *Rhodobacter capsulatus* SB1003. *J. Bacteriol.* **2010**, *192*, 3545–3546.
88. Rodriguez, S.; Kirby, J.; Denby, C.M.; Keasling, J.D. Production and quantification of sesquiterpenes in *Saccharomyces cerevisiae*, including extraction, detection and quantification of terpene products and key related metabolites. *Nat. Protoc.* **2014**, *9*, 1980–1996.
128 Hogenkamp, F.; Hilgers, F.; Knapp, A.; Klaus, O.; Bier, C.; Binder, D.; Jaeger, K.-E.; Drepper, T.; Pietruszka, J. Effect of Photocaged Isopropyl β-D-1-Thiogalactopyranoside Solubility on Light-Responsiveness of LacI-controlled Expression Systems in Different Bacteria. *ChemBioChem* **2020**, doi:10.1002/cbic.202000377.

II.2 Light-mediated control of gene expression

II.2.1 Light-controlled gene expression in *R. capsulatus* to regulate intrinsic terpene biosynthesis

PUBLICATION IV

Light-mediated control of gene expression in the anoxygenic phototrophic bacterium *Rhodobacter capsulatus* using photocaged inducers

Fabienne Hilgers[1]*, Fabian Hogenkamp[2]*, **Oliver Klaus**[1], Luzie Kruse[1], Anita Loeschcke[1], Claus Bier[2], Dennis Binder[1], Karl-Erich Jaeger[1,3], Thomas Drepper[1#] and Jörg Pietruszka[2,3#]

[1]Institute of Molecular Enzyme Technology, Heinrich Heine University Düsseldorf, Forschungszentrum Jülich, 52425 Jülich, Germany

[2]Institute of Bioorganic Chemistry, Heinrich Heine University Düsseldorf, Forschungszentrum Jülich, 52425 Jülich, Germany

[3]Institute of Bio- and Geosciences IBG-1: Biotechnology, Forschungszentrum Jülich GmbH, 52425 Jülich, Germany

* These authors contributed equally

Corresponding authors

Status: published

Frontiers in Bioengineering and Biotechnology,

2022, 09, 30, 10:902959

https://doi.org/10.3389/fbioe.2022.902059

Own contribution:

Designing and performing experiments, plasmid construction, analyzing data, writing parts of the manuscript

frontiers | Frontiers in Bioengineering and Biotechnology

TYPE Original Research
PUBLISHED 30 September 2022
DOI 10.3389/fbioe.2022.902059

OPEN ACCESS

EDITED BY
Pasquale Stano,
University of Salento, Italy

REVIEWED BY
Klaas Jan Hellingwerf,
University of Amsterdam, Netherlands
Armin Baumschlager,
ETH Zürich, Switzerland

*CORRESPONDENCE
Jörg Pietruszka,
j.pietruszka@fz-juelich.de
Thomas Drepper,
t.drepper@fz-juelich.de

†These authors have contributed equally to this work

SPECIALTY SECTION
This article was submitted to Synthetic Biology,
a section of the journal
Frontiers in Bioengineering and Biotechnology

RECEIVED 22 March 2022
ACCEPTED 07 September 2022
PUBLISHED 30 September 2022

CITATION
Hilgers F, Hogenkamp F, Klaus O, Kruse L, Loeschcke A, Bier C, Binder D, Jaeger K-E, Pietruszka J and Drepper T (2022), Light-mediated control of gene expression in the anoxygenic phototrophic bacterium Rhodobacter capsulatus using photocaged inducers. *Front. Bioeng. Biotechnol.* 10:902059. doi: 10.3389/fbioe.2022.902059

Light-mediated control of gene expression in the anoxygenic phototrophic bacterium *Rhodobacter capsulatus* using photocaged inducers

Fabienne Hilgers[1†], Fabian Hogenkamp[2†], Oliver Klaus[1], Luzie Kruse[1], Anita Loeschcke[1], Claus Bier[2], Dennis Binder[1], Karl-Erich Jaeger[1,3], Jörg Pietruszka[2,3]* and Thomas Drepper[1]*

[1]Institute of Molecular Enzyme Technology, Heinrich Heine University Düsseldorf at Forschungszentrum Jülich, Jülich, Germany, [2]Institute of Bioorganic Chemistry, Heinrich Heine University Düsseldorf at Forschungszentrum Jülich, Jülich, Germany, [3]Institute of Bio- and Geosciences: Biotechnology (IBG-1), Forschungszentrum Jülich, Jülich, Germany

Photocaged inducer molecules, especially photocaged isopropyl-β-D-1-thiogalactopyranoside (cIPTG), are well-established optochemical tools for light-regulated gene expression and have been intensively applied in *Escherichia coli* and other bacteria including *Corynebacterium glutamicum, Pseudomonas putida* or *Bacillus subtilis*. In this study, we aimed to implement a light-mediated on-switch for target gene expression in the facultative anoxygenic phototroph *Rhodobacter capsulatus* by using different cIPTG variants under both phototrophic and non-phototrophic cultivation conditions. We could demonstrate that especially 6-nitropiperonyl-(NP)-cIPTG can be applied for light-mediated induction of target gene expression in this facultative phototrophic bacterium. Furthermore, we successfully applied the optochemical approach to induce the intrinsic carotenoid biosynthesis to showcase engineering of a cellular function. Photocaged IPTG thus represents a light-responsive tool, which offers various promising properties suitable for future applications in biology and biotechnology including automated multi-factorial control of cellular functions as well as optimization of production processes.

KEYWORDS

caged compounds, light-controlled gene expression, optogenetics, purple non-sulfur photosynthetic bacteria, *Rhodobacter capsulatus*

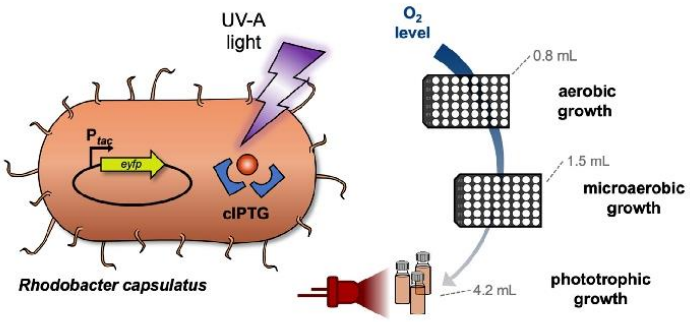

GRAPHICAL ABSTRACT

Introduction

In the field of optogenetics, the application of light offers various advantageous properties such as non-invasive control with high spatiotemporal resolution (Deiters, 2009; Drepper et al., 2011; Brieke et al., 2012; Gardner and Deiters, 2012; Bardhan and Deiters, 2019; Baumschlager and Khammash, 2021). In this context, photo-labile protecting groups are useful for controlling a multitude of cellular processes including cell signaling (Liu et al., 2017; Bardhan and Deiters, 2019; Kolarski et al., 2019) or gene expression (Young and Deiters, 2007; Gardner et al., 2011; Binder et al., 2014; Bier et al., 2016; Kusen et al., 2016; Hogenkamp et al., 2022). For light-regulated gene expression, especially photocaged isopropyl-β-D-1-thiogalactopyranoside (cIPTG) was applied, e.g., for automated optimization of heterologous gene expression in *Escherichia coli* using a high-throughput screening system (Wandrey et al., 2016). The growth medium can be supplemented with photocaged IPTG, which remains non-functional, until a light-pulse releases the inducer from its caging group so that it can induce expression of target genes under control of a *lac* (or *lac*-type) promoter by specific interaction with the LacI repressor. Photocaged IPTG has further been utilized to control gene expression in the Gram-positive bacteria *Corynebacterium glutamicum* (Binder et al., 2016; Burmeister et al., 2021) and *Bacillus subtilis* as well as the Gram-negative bacterium *Pseudomonas putida* (Hogenkamp et al., 2021). However, the applicability of photocaged inducer molecules for light-mediated control of bio(techno)logical processes has not been studied so far in phototrophic bacteria, since the individual emission spectra of applied light sources might hamper the separation of photosynthetic from optochemical control processes. In this study, we thus evaluated if photocaged IPTG can be used to implement non-invasive light control for target gene expression in the facultative anaerobic phototroph *R. capsulatus*.

R. capsulatus is a metabolically versatile bacterium that is able to grow either under phototrophic conditions (i.e., in the absence of oxygen and presence of light) by performing anoxygenic photosynthesis or under chemotrophic conditions (in the presence of an electron acceptor, e.g., molecular oxygen) (Stoppani et al., 1955; Tabita, 1995; Strnad et al., 2010). Upon reduction of oxygen tension, *R. capsulatus* starts to form an intracytoplasmic membrane (ICM) system, which harbors the photosynthesis apparatus (Drews and Oelze, 1981; Wu and Bauer, 2008; Tucker et al., 2010; Drews, 2013). Since this ICM system can function as a naturally enlarged storage compartment for membrane-embedded enzymes and metabolites, the phototrophic lifestyle renders novel approaches possible where *R. capsulatus* is applied as an alternative host for the production of otherwise difficult-to-express membrane proteins as well as hydrophobic secondary metabolites such as plant-derived terpenoids (Khan et al., 2015; Loeschcke et al., 2017; Hage-Hülsmann et al., 2019; Troost et al., 2019; Hilgers et al., 2021; Klaus et al., 2022).

Phototrophic growth offers robust and relatively fast cell division of *R. capsulatus* cells, as the broad emission spectrum of bulb light or natural daylight is suitable for the excitation of all photopigments, namely the carotenoids spheroidene (λ^{abs}_{max} = 454, 478, 509 nm) and spheroidenone (λ^{abs}_{max} = 500 nm) as well as bacteriochlorophyll *a* (BChl *a*, λ^{abs}_{max} = 800 and 860 nm) (Obeid et al., 2009; Boran et al., 2010; Katzke et al., 2010; Elkahlout et al., 2019). In the presented study, we evaluated whether optochemical induction of gene expression can be established under non-phototrophic and phototrophic growth conditions by using UV-A light-responsive cIPTG. For phototrophic cultivation of *R. capsulatus* cells, cell suspensions were illuminated using near infrared (NIR) light-emitting LEDs

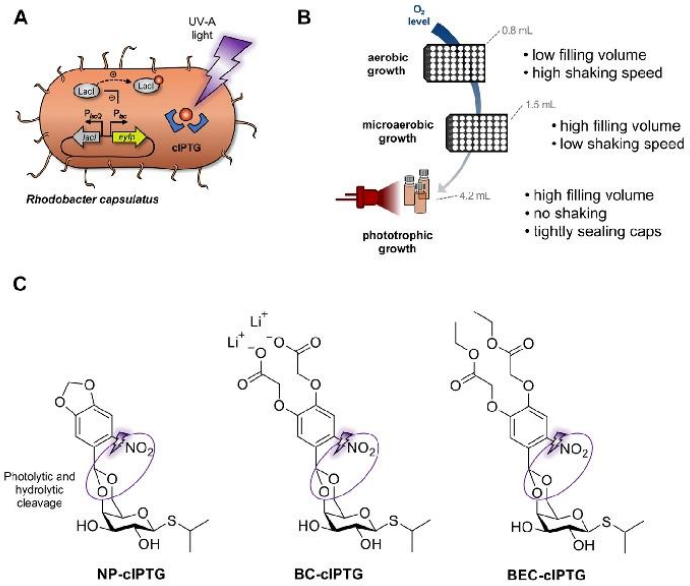

FIGURE 1
Establishment of optochemical control over gene expression in *R. capsulatus* under non-phototrophic and phototrophic growth conditions. **(A)** Light-controlled expression of the reporter gene *eyfp* in *R. capsulatus* using photocaged IPTG (cIPTG; red circle with blue frames). Upon illumination with UV-A light (purple flash symbol), the protection group is cleaved off, the previously inactive IPTG molecule is released and induces LacI/P_{tac}-mediated *eyfp* expression. **(B)** For analyzing light-dependent control of gene expression, *R. capsulatus* cells were either cultivated under non-phototrophic conditions (i.e., aerobic or microaerobic conditions in Round Well Plates with filling volumes of 0.8 and 1.5 mL, respectively) or anaerobic, phototrophic growth conditions using NIR light LED as sole light source (red LED diodes; λ_{max} = 850 nm, small scale screw neck vials). **(C)** Photocaged IPTG variants NP-cIPTG, BC-cIPTG and BEC-cIPTG used in this study as well as the respective cleavage sites addressed by photolysis and subsequent enzymatic hydrolysis (purple circles).

(λ_{max} = 850 nm) instead of commonly used broad-spectrum bulb light to avoid unintended activation of the optochemical on-switch (Figure 1A).

Since the formation of the ICM system might function as natural, hydrophobic diffusion barrier, which could affect the uptake of caged inducer molecules under phototrophic growth conditions, we additionally evaluated the applicability of the three differentially soluble cIPTG variants 6-nitropiperonyl photocaged IPTG (NP-cIPTG), 4,5-bis(carboxymethoxy)-2-nitrobenzyl photocaged IPTG (BC-cIPTG) and 4,5-bis(ethoxycarbonylmethoxy)-2-nitrobenzyl photocaged IPTG (BEC-cIPTG) (Hogenkamp et al., 2021) for this optochemical approach (Figure 1). While the well-established NP-cIPTG shows a low solubility in the cultivation medium resulting in the formation of an emulsion, BC-cIPTG offers an approximately 200-fold higher water-solubility. In contrast, BEC-cIPTG exhibits low water-solubility but offers hydrophobic side chains that might enhance its ICM-permeability. The original water solubility of IPTG is restored *via* the uncaging process, leading to a dissolution of the emulsion-like mixture after UV-A illumination.

As those photocaged molecules strongly differ in hydrophobicity and water-solubility, we wanted to compare their general usability for light-controlled gene expression in *R. capsulatus* under phototrophic (formation of high ICM levels) and non-phototrophic (moderate to low ICM formation) conditions. In summary, we could demonstrate that photocaged inducer molecules and especially NP-cIPTG can be applied for light-mediated control over gene expression in the phototrophic bacterium *R. capsulatus*. Furthermore, we successfully applied this optochemical approach to control the intrinsic carotenoid pathway to showcase engineering of secondary metabolite biosynthesis. This optochemical on-switch thus offers various promising properties suitable for biotechnological applications in phototrophic hosts including automated bioprocess engineering approaches under defined light conditions.

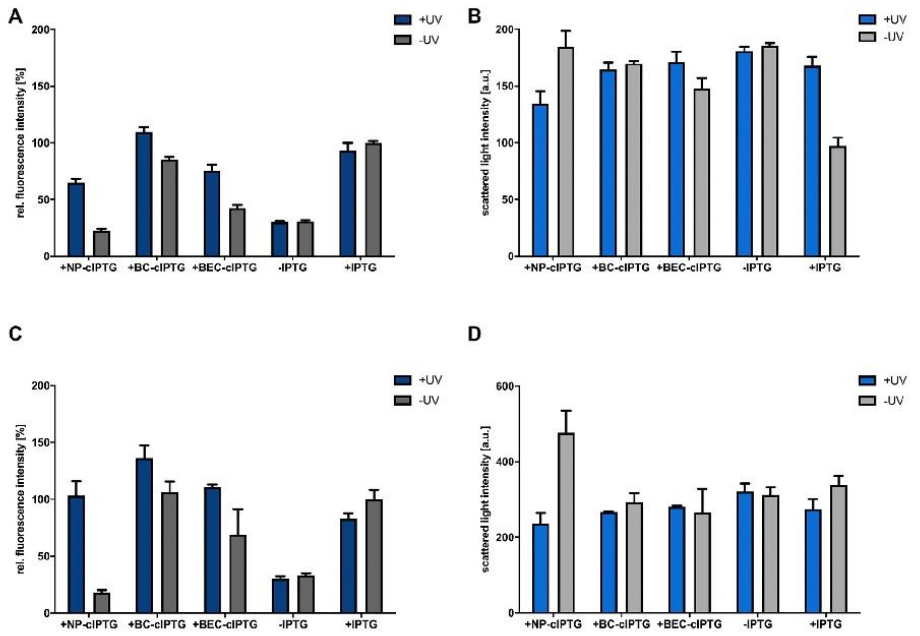

FIGURE 2
Application of cIPTG derivatives for light-mediated control of gene expression in *R. capsulatus* under non-phototrophic conditions. Light-controlled *eyfp* reporter gene expression and corresponding cell densities in aerobically **(A,B)** and microaerobically **(C,D)** grown *R. capsulatus* SB1003 cultures carrying pRholHi-2-eYFP using the three cIPTG derivatives NP-, BC- and BEC-cIPTG. Biomass-normalized eYFP *in vivo* fluorescence (λ_{ex} = 508 nm, λ_{em} = 532 nm) and cell growth represented by the scattered light intensity (λ = 620 nm) of cultures supplemented with 1 mM of each cIPTG variant is shown in relation to a control culture (1 mM IPTG) after 48 h of cultivation (RCV medium, 30°C; for aerobic cultures 800 rpm and 800 µL filling volume and for microaerobic cultures 400 rpm and 1,500 µL filling volume). Induction of reporter gene expression was performed after 9 h *via* UV-A light exposure at 365 nm (~1 mW/cm^2) for 30 min or the addition of 1 mM IPTG. **(B,D)**. Values are means of individual biological triplicates. Error bars indicate the respective standard deviations.

Results

cIPTG-mediated light control of gene expression in *R. capsulatus* under non-phototrophic conditions

In order to establish a cIPTG-based optochemical control of gene expression in the facultative phototrophic organism *R. capsulatus*, we first constructed the expression plasmid pRholHi-2-eYFP containing the repressor gene *lacI* and the LacI-controlled P_{tac} promoter originating from the shuttle vector pEKEx2 (Eikmanns et al., 1991) (Supplementary Table S1) as well as the downstream located *eyfp* reporter gene, whose expression was first analyzed in *R. capsulatus* under aerobic and microaerobic conditions (i.e., low and intermediate induction of ICM formation) in the dark. Since we performed small scale cultivation of *R. capsulatus* in the BioLector microbioreactor for the first time, the filling volume of the Round Well Plates as well as the shaking frequencies were experimentally determined to adjust the aeration of cultures during non-phototrophic growth (Figure 1B; Supplementary Figure S1). To this end, the *R. capsulatus* strain carrying the corresponding *eyfp* expression vector pRholHi-2-eYFP was cultivated in the dark without the addition of IPTG but with varying filling volumes and shaking frequencies (800 µL and 800 rpm, 1,000 µL or 1,500 µL and 400 rpm) for 48 h at 30°C. In these cultures, bacterial growth (scattered light intensity, Supplementary Figure S1A) and the dissolved oxygen tension (DOT; Supplementary Figure S1B) were online-monitored. Sufficient conditions for aerobic and microaerobic growth were found to be 800 µL filling volume and 800 rpm shaking frequency or 1,500 µL and 400 rpm, respectively. To evaluate the functionality and inducibility of the LacI/P_{tac} promoter

system in *R. capsulatus* under non-phototrophic growth conditions, IPTG was added at increasing concentrations (0–10 mM) to the medium after 9 h of cultivation (early logarithmic growth phase) and reporter gene expression was analyzed by detecting the specific eYFP fluorescence (Supplementary Figures S2A,B). The results showed a comparatively high *eyfp* expression for IPTG concentrations of 1 mM and above; thus, 1 mM was chosen as sufficient inducer concentration in all further experiments. To evaluate, whether cIPTG derivatives can be applied for light-controlled gene expression in *R. capsulatus* under non-phototrophic conditions, we analyzed the induction response of NP-cIPTG, BC-cIPTG and BEC-cIPTG in comparison to IPTG for the strain *R. capsulatus* SB1003/pRholHi-2-eYFP in the absence and presence of UV-A light (λ_{max} = 365 nm, 1 mW/cm^2, 30 min). Both experiments revealed considerable induction levels for all three cIPTG derivatives leading to induction levels of at least 70% and up to nearly 150% in comparison to IPTG (Figures 2A,C). The corresponding measurements of the respective cell densities (Figures 2B,D) further revealed that cell growth was slightly affected by the respective photolysis products or UV-A light exposure under aerobic conditions and considerably less influenced under microaerobic conditions. This can also be confirmed by the growth curves and fluorescence measurements (Supplementary Figures S4A,B, S5).

However, only NP-cIPTG showed a reasonably low induction level under light exclusion for aerobic and microaerobic cultivation conditions over 48 h in RCV medium at 30°C, whereas the use of BC-cIPTG and BEC-cIPTG led to high illumination-independent fluorescence signals. In order to analyze, if the *Rhodobacter* cultivation medium is responsible for the observed instability effect, the light-independent cleavage of IPTG was analyzed in a control experiment using the well-established strain *E. coli* Tuner (DE3) (Binder et al., 2014). To this end, we measured the induction of *eyfp* reporter gene expression upon addition of cIPTG variants, which were previously incubated either in LB or RCV medium (Supplementary Figure S4C). These data show that no auto-hydrolysis was observed for any cIPTG derivative in sole RCV or LB medium and thus could give a first hint that host specific enzymes or metabolites might be involved in the light-independent hydrolysis of BC- and BEC-cIPTG at least under aerobic and microaerobic growth conditions. We therefore identified the non-toxic and functional NP-cIPTG as the most promising candidate for light-controlled induction of gene expression in *R. capsulatus* under non-phototrophic conditions.

In a next step, we evaluated the applicability of cIPTG as an optochemical on-switch under phototrophic conditions, where additional bottlenecks may arise such as permanent illumination necessary for photosynthesis and the extensive formation of ICM that might function as additional cellular diffusion barriers.

Light-mediated induction of gene expression in *R. capsulatus* under anaerobic, phototrophic growth conditions

In the laboratory, phototrophic *R. capsulatus* cultures are typically grown in sealed hungate tubes under constant illumination with bulb light to ensure both a strict oxygen exclusion and optimal light conditions. First, we analyzed whether illumination of cultures, which is essential for phototrophic growth, already leads to unwanted uncaging effects. For this purpose, we used 1,2-dimethoxy-4-nitrobenzene (DMNB) as a molecular UV-A light detector suitable for the analysis of nitrobenzyl-based photouncaging processes (Pelliccioli and Wirz, 2002; Nakayama et al., 2011; Brieke et al., 2012). Under UV-A light exposure, the DMNB molecule undergoes a photoconversion into 2-methoxy-5-nitrophenolate (MNP) accompanied by a precisely detectable increase of absorption at λ_{max} = 422 nm (Supplementary Figures S7A–C) (Van Riel et al., 1981; Zhang et al., 1999). To detect undesired uncaging processes induced by different light sources applicable for phototrophic cultivation of *R. capsulatus* cells (Kaschner et al., 2014; Peters et al., 2019; Hilgers et al., 2021), the DMNB solution was exposed for 48 h either to bulb light (broad emission spectrum with high NIR light and low UV light components) or NIR light (monochromatic, λ_{max} = 850 nm). Additionally, a dark control and samples with increasing UV-A light exposure times from 30 to 90 min were performed (Supplementary Figure S7D).

Interestingly, analysis of photochemical MNP formation at 422 nm after 24 and 48 h revealed that exposure to bulb light leads to absorption values comparable to samples that were irradiated by UV-A light for 30 min. Thus, bulb light is not applicable as a light source for the phototrophic cultivation of *R. capsulatus* if cIPTG is intended to be used as an optochemical on-switch. In contrast, NIR light at 850 nm (i.e., the absorption maximum of the photopigment BChl a) seems to be a promising alternative light source, as even after 48 h no photoconversion of DMNB could be detected in comparison to the dark control. To determine, which NIR light intensities are needed for efficient phototrophic growth of *R. capsulatus,* cells were cultivated with NIR light of increasing intensities ranging from 0.5 mW/cm^2 up to 5.1 mW/cm^2 using a custom-made NIR light LED panel (Hilgers et al., 2021) and analyzed the growth behavior (Supplementary Figure S8). The data revealed that both too high and too low NIR light intensities have a negative effect on phototrophic growth due to insufficient energy supply or adverse cultivation temperatures. However, illumination properties of NIR LED panels could be appropriately adjusted for phototrophic growth of *R. capsulatus*: An NIR-light intensity of 1.7 mW/cm^2 led to similar cell densities as

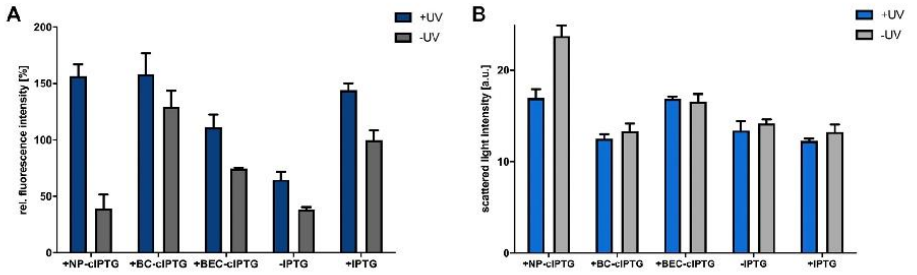

FIGURE 3
Application of cIPTG derivatives for light-controlled induction of gene expression in phototrophically grown *R. capsulatus* cells. Light-controlled *eyfp* reporter gene expression **(A)** and corresponding cell densities **(B)** of phototrophically grown *R. capsulatus* SB1003 cells carrying pRholHi-2-eYFP using the cIPTG derivatives NP-, BC- and BEC-cIPTG. Biomass-normalized eYFP *in vivo* fluorescence (λ_{ex} = 508 nm, λ_{em} = 532 nm) and cell growth represented by the scattered light intensity of cultures supplemented with 1 mM of each cIPTG variant are shown in relation to a control culture (1 mM IPTG) after 48 h of cultivation [30°C, screw neck vials, constant NIR light illumination (λ_{max} = 850 nm, 1.7 mW/cm^2)]. Induction of reporter gene expression was performed after 6 h *via* UV-A light exposure (365 nm; ~2 mW/cm^2) for 30 min. Values are means of individual biological triplicates. Error bars indicate the respective standard deviations.

compared to bulb light irradiation without exceeding the optimal growth temperature. It is worth mentioning that an altered color could be observed for *R. capsulatus* cultures grown under NIR light illumination, which might indicate an adaptation of photopigment synthesis or accumulation.

Next, we analyzed whether photocleavable cIPTG derivatives can be applied for UV-A light-dependent control of gene expression in phototrophically growing *R. capsulatus* cells. To this end, the strain *R. capsulatus* SB1003 carrying the plasmid pRholHi-2-eYFP was cultivated under constant NIR light illumination and reporter gene expression in cIPTG-supplemented cultures was induced after 6 h (early logarithmic growth phase) with 30 min of UV-A light (365 nm; ~2 mW/cm^2). Resulting eYFP fluorescence signals were analyzed when cells reached the stationary growth phase (48 h). As shown in Figure 3A, UV-A light-induced uncaging of the cIPTG derivatives NP- and BC-cIPTG resulted in even higher *eyfp* expression levels as in the control experiment, where conventional IPTG was added to UV-A exposed cultures, while the expression strength of BEC-cIPTG was slightly lower. Remarkably, changing the water solubility and thus the hydrophobicity of cIPTG did not result in improved *eyfp* expression levels under phototrophic growth conditions. Based on the approximately similar fluorescence signals observed after IPTG and NP-cIPTG induction under aerobic, microaerobic, and phototrophic conditions, it can thus be concluded that the putative IPTG diffusion barrier formed by ICM do not exert a significant influence on NP-cIPTG uptake. In addition, as previously observed in cultures that have been grown under aerobic and microaerobic conditions, BC-cIPTG and BEC-cIPTG were not stable during phototrophic cultivation, resulting in almost equally high induction levels in the control (−UV) as compared to the UV-A light exposed cultures (+UV). In contrast, NP-cIPTG showed sufficient stability and neglectable toxicity under phototrophic growth conditions (Figure 3; Supplementary Figures S4,S6).

Further it should be noted that the cell density-normalized eYFP fluorescence under phototrophic conditions is significantly higher than under aerobic or microaerobic conditions (Supplementary Figure S2). Similar results were obtained in the study of Katzke and co-workers, where the protein yield of the T7 expression strain *R. capsulatus* B10S-T7 was superior under phototrophic growth conditions (Katzke et al., 2010). This observation further supports the assumption that an increased energy availability during phototrophic growth might facilitate efficient synthesis of heterologous proteins in *R. capsulatus*. In this context, it is worth mentioning that phototrophically cultivated *R. capsulatus* cells showed an increased eYFP fluorescence in the presence and absence of conventional IPTG, when cultures were additionally illuminated with UV-A light. This observation might indicate that UV-A light illumination, although it was only briefly applied in an early phase of cell cultivation, can also lead to an excitation of the photopigment BChl *a* in the Soret band (Happ et al., 2005; Xin et al., 2007). This might further boost photosynthesis and thereby facilitate energy-demanding processes including *eyfp* over-expression if applied NIR light exposure is not sufficient for full BChl *a* excitation.

Additionally, phototrophically grown cultures without supplemented IPTG exhibited a high basal *eyfp* expression level (Figures 2, 3; Supplementary Figures S2A–C). Since wild-type control cultures without an expression plasmid did not show

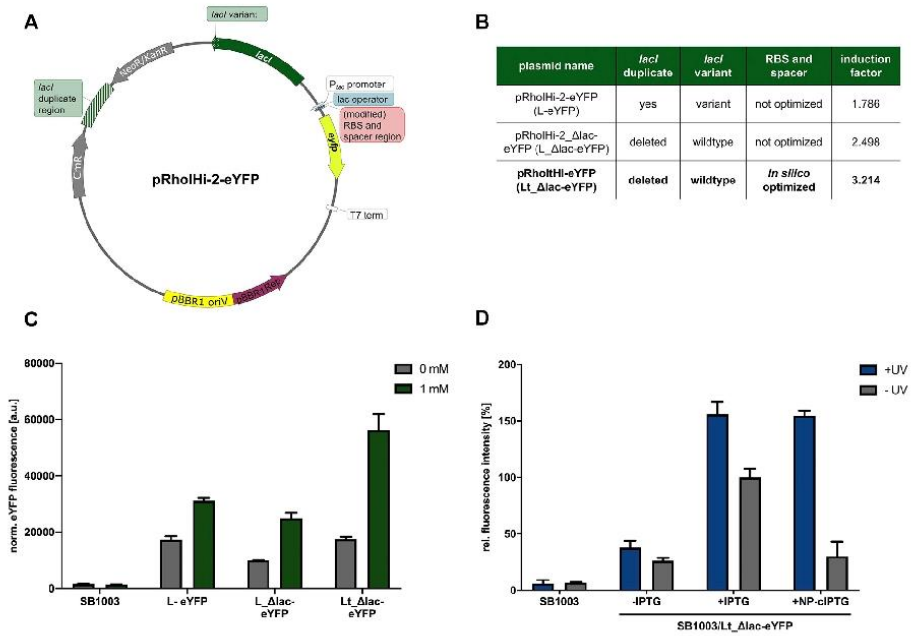

plasmid name	*lacI* duplicate	*lacI* variant	RBS and spacer	induction factor
pRholHi-2-eYFP (L-eYFP)	yes	variant	not optimized	1.786
pRholHi-2_Δlac-eYFP (L_Δlac-eYFP)	deleted	wildtype	not optimized	2.498
pRholtHI-eYFP (Lt_Δlac-eYFP)	**deleted**	**wildtype**	***In silico* optimized**	3.214

FIGURE 4
Optimization of expression plasmid pRholHi-2-eYFP. To improve the properties of the expression plasmid pRholHi-2-eYFP **(A)** several engineering steps were conducted **(A,B)**. First, a defective *lacI* gene (*lacI* variant) was exchanged by the corresponding wildtype *lacI* gene from *E. coli* K12. Secondly, a 519-bp *lacI*-homologous DNA fragment approximately 1.5 kb upstream of the *lacI* gene was deleted (*lacI* duplicate region). Additionally, the ribosome binding site (RBS) consisting of the Shine-Dalgarno (SD) sequence, and its corresponding downstream spacer was replaced by an *in silico* optimized version. The induction factors of the respective expression systems were calculated as the ratio of the normalized eYFP fluorescence values of induced and non-induced cultures. **(C)** After construction, the three plasmid variants were evaluated regarding their resulting basal expression levels and induction factors in phototrophically grown *R. capsulatus* SB1003 cultures. Biomass-normalized eYFP *in vivo* fluorescence (λ_{ex} = 508 nm, λ_{em} = 532 nm) of cultures supplemented with 1 mM IPTG is shown in comparison to uninduced cultures and the *R. capsulatus* wildtype control strain after 48 h of cultivation (30°C, screw neck vials, NIR light: λ_{max} = 850 nm, 1.7 mW/cm^2). Induction of reporter gene expression was performed after 6 h. **(D)** Light-controlled *eyfp* reporter gene expression in phototrophically grown *R. capsulatus* SB1003 cells carrying the best performing expression plasmid pRholtHi-eYFP using NP-cIPTG. Biomass-normalized eYFP *in vivo* fluorescence (λ_{ex} = 508 nm, λ_{em} = 532 nm) of cultures supplemented with 1 mM NP-cIPTG is shown in relation to a 1 mM IPTG and a *R. capsulatus* wildtype control after 48 h of cultivation (30°C, screw neck vials, NIR light: λ_{max} = 850 nm, 1.7 mW/cm^2). Induction of reporter gene expression was performed after 6 h *via* UV-A light exposure (365 nm; ~2 mW/cm^2, 30 min). Values are means of individual biological triplicates. Error bars indicate the respective standard deviations.

significantly increased fluorescence levels, the promoter system appears to be affected by high basal expression, possibly caused by an insufficient amount of the LacI repressor. As noted in previous studies, increasing the level of LacI has been shown to be extremely valuable for reducing basal expression and thereby increasing the tightness of an expression system (Dubendorf and Studier, 1991; Studier, 1991).

The data presented so far can be summarized as follows: 1) the *eyfp* expression experiments clearly demonstrated that NP-cIPTG can be used as an optochemical on-switch for light-dependent induction of heterologous gene expression in *R. capsulatus*. 2) Neither constant illumination with NIR light, which is required for photosynthesis, nor the formation of ICM negatively affected the function of light-responsive cIPTG. Hence, this optochemical switch can be used for the facultative phototrophic bacterium under both non-phototrophic and phototrophic growth conditions.

Optimization of pRholHi-2-eYFP

As mentioned above, phototrophically grown *R. capsulatus* cultures exhibited a high basal *eyfp* expression level under uninduced conditions (Figure 3). Therefore, we next analyzed if

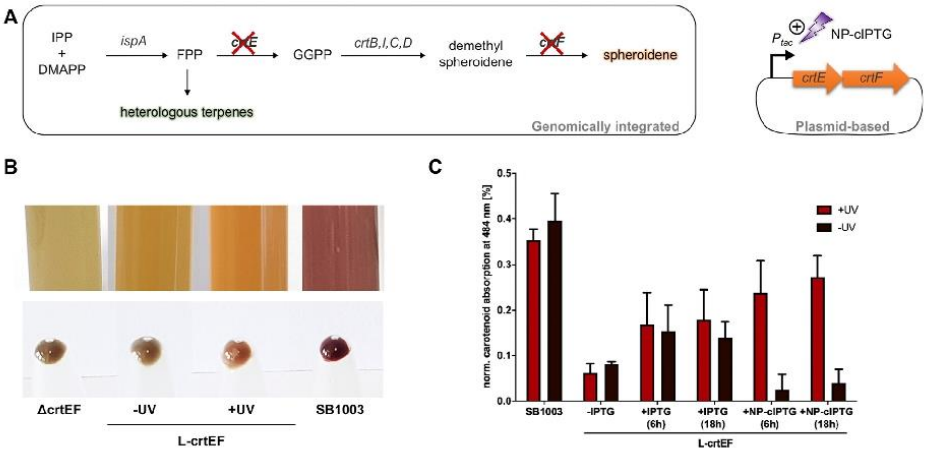

FIGURE 5
Light-controlled induction of carotenoid production in phototrophically grown *R. capsulatus* SB1003 *ΔcrtEF* cells carrying pRholtHi-crtE-crtF. **(A)** Intrinsic carotenoid synthesis of *R. capsulatus* starting from the terpene C_5 building blocks IPP and DMAPP. Deletion of genes encoding the relevant carotenoid pathway enzymes CrtE and CrtF results in a carotenoid-deficient strain (Hage-Hülsmann et al., 2019). The genes *crtE* and *crtF* were cloned in a plasmid and placed under control of the P_{tac} promoter to facilitate IPTG-based control. Light-mediated induction of *crt* gene expression was achieved by using NP-cIPTG. IPP, isopentenyl pyrophosphate; DMAPP, dimethylallyl pyrophosphate; FPP, farnesyl pyrophosphate; IspA, FPP synthase; GGPP, geranylgeranyl pyrophosphate; CrtE, GGPP synthase; CrtB, phytoene synthase; CrtI, phytoene desaturase; CrtC, hydroxyneurosporene synthase; CrtD, hydroxyneurosporene desaturase; CrtF, demethylspheroidene O-methyltransferase. **(B)** Pigmentation of phototrophically grown *R. capsulatus* strains SB1003 *ΔcrtEF* (ΔcrtEF), SB1003 *ΔcrtEF*/pRholtHi-crtE-crtF supplemented with 1 mM NP-cIPTG under non-illuminated (-UV, L-crtEF) or UV-A illuminated conditions (+UV, L-crtEF) and SB1003 wildtype strain (SB1003). Besides liquid cultures, cell pellets corresponding to an optical density at 660 nm of 2.5 are shown. **(C)** Carotenoid absorption at 484 nm of *R. capsulatus* SB1003 *ΔcrtEF*/pRholtHi-crtE-crtF (L-crtEF) cultures supplemented with 1 mM NP-cIPTG (+NP-cIPTG + UV and -UV) are shown in comparison to the respective absorption of extracts from *R. capsulatus* SB1003 wildtype (SB1003) cells. In addition, cell cultures supplemented with 1 mM IPTG (positive control, +IPTG) or without IPTG (negative control, -IPTG) were likewise analyzed after 48 h of phototrophic cultivation [RCV medium, 30°C, screw neck vials, NIR light (λ_{max} = 850 nm, 1.7 mW/cm²)]. *R. capsulatus* SB1003 *ΔcrtEF* cultures were used to determine the background absorption at 484 nm and thus corresponding values were subtracted from all other values. Induction was performed after a cultivation time of six or 18 h *via* UV-A light exposure at 365 nm (~2 mW/cm²) for 30 min. Values are means of individual biological triplicates. Error bars indicate the respective standard deviations.

the expression properties of the LacI/P_{tac} system can be further improved. In a recent publication, it was shown that the well-known shuttle vector pEKEx-2 (Eikmanns et al., 1991), which was used for isolating the *lacI*^{q}-P_{tac}-lacO fragment in this work, showed likewise high basal target gene expression in uninduced *C. glutamicum* cultures (Bakkes et al., 2020). The authors proved that this plasmid features two unfavorable parts (Figure 4), which might hamper tight LacI-mediated gene expression and plasmid stability. Firstly, the nucleotide sequence of the repressor gene *lacI* revealed a deviation from the original *E. coli* K12 sequence at the 3′-end resulting in a substitution and elongation of the last 19 amino acid residues of LacI (starting from amino acid residue 341), which might lead to decreased repressor activity. Secondly, the plasmid backbone harbors a duplicated DNA sequence upstream of the *lacI* gene that corresponds to a correct LacI C-terminal coding sequence, which might lead to plasmid instability due to homologous recombination. After reconstitution of the original *lacI* sequence, leaky target gene expression could be significantly decreased (Bakkes et al., 2020). Following these recent findings, we replaced the likewise occurring wrong *lacI* gene variant on pRholHi-2-eYFP (in Figure 4 designated as L-eYFP) accordingly by an intact *lacI* and deleted the DNA duplicate region (519 bp) approximately 1.5 kb upstream of the *lacI* gene in the plasmid backbone (pRholHi-2_Δlac-eYFP; in Figure 5 designated as L_Δlac-eYFP). To analyze, if the *Rhodobacter* expression plasmid can be further improved, we finally implemented an *in silico* optimized ribosome binding site consisting of an optimized Shine-Dalgarno (SD) and SD-spacer sequence (pRholtHi-eYFP, in Figure 5 designated as Lt_Δlac-eYFP; for SD and spacer sequences, please see the Supplementary Material). Subsequently, LacI-controlled *eyfp* reporter gene expression in all three constructs was analyzed in *R. capsulatus* SB1003 under phototrophic conditions to evaluate the influence of those modifications on the basal expression level and induction factor of the respective expression systems (Figures 4B,C).

As already observed in the previous measurements, the expression plasmid pRholHi-2-eYFP leads to a high basal *eyfp*

reporter gene expression with an induction factor of only ~1.8 (Figures 4B,C). After reconstitution of the original *lacI* gene from *E. coli* and the deletion of the homologous *lacI* region in the plasmid backbone (pRholHi-2_Δlac-eYFP), the fluorescence level after induction was slightly decreased but the basal expression was also reduced leading to an induction factor of ~2.5. However, the *in silico* calculation of an optimized RBS for *eyfp* expression in *R. capsulatus* (pRholtHi-eYFP) finally led to a 1.8-fold increased eYFP fluorescence level when compared to pRholHi-2-eYFP and an induction factor of ~3.2. Further, the gradual inducibility of the novel plasmid variant pRholtHi-eYFP (Lt_Δlac-eYFP) was evaluated in *R. capsulatus* under both non-phototrophic and phototrophic growth conditions. For this purpose, IPTG was added to the medium at increasing concentrations (0–10 mM) after 9 h of cultivation (early logarithmic growth phase) and reporter gene expresion was analyzed by detecting the specific eYFP fluorescence (Supplementary Figures S2D–F). The optimized plasmid shows an improved induction profile with a gradual induction response. Additionally, the influence of the induction time point was evaluated under non-phototrophic and phototrophic growth conditions revealing the induction of reporter gene expression can be performed under both applied conditions in the lag, early, mid-logarithmic and late-logarithmic growth phase without having a strong influence on the growth or induction of eYFP gene expression (Supplementary Figure S3).

Further, toxicity measurements with the *R. capsulatus* SB1003 wildtype strain revealed no significant impairments of UV-A light or the photolysis products on cell growth (Supplementary Figure S6). Subsequently, this plasmid variant was used to reevaluate the cIPTG-mediated induction of *eyfp* expression in *R. capsulatus* under phototrophic conditions (Figure 4D). For this purpose, only NP-cIPTG was applied. As expected, the fluorescence intensity of cultures supplemented with IPTG and NP-cITPG after UV-A illumination was comparably high and the basal expression could be reduced (induction factor of ~5.2) in comparison to the previous measurement (Figure 3A, induction factor for NP-cIPTG ~2.9). Thus, not only the optimization of the plasmid backbone, but also the *in silico* optimization of the RBS sequence clearly increased the tightness and strength of this expression plasmid.

Optochemical control of a secondary metabolite pathway in phototrophically grown *R. capsulatus*

Finally, we applied the light switch to modulate an intrinsic biosynthetic secondary metabolite pathway of *R. capsulatus*. We chose the early enzymatic step of the carotenoid pathway as suitable target, which is responsible for the conversion of the precursor molecule farnesyl pyrophosphate (FPP). FPP is a key metabolite that is essential for the synthesis of the photopigments spheroidene and spheroidenone (belonging to the class of tetraterpenoids) and heterologous sesqui- and triterpenoids (Figure 5A) (Troost et al., 2019; Hage-Hülsmann et al., 2021; Hilgers et al., 2021).

In a mutant strain lacking the relevant carotenoid biosynthesis genes *crtE* and *crtF*, intrinsic carotenoid biosynthesis cannot be performed, which results in a distinct greenish-colored phenotype (Figure 5B, Hage-Hülsmann et al., 2019). We used this strain for light-controlled complementation of the observed mutant phenotype, by placing *crtEF* expression under LacI/P_{tac} control. For this purpose, the plasmid pRholtHi-crtE-crtF was transferred to the carotenoid deletion strain *R. capsulatus* SB1003 *ΔcrtEF* and cells were grown phototrophically for 2 days under NIR light (λ_{max} = 850 nm, 1.7 mW/cm^2). Firstly, the influence of the induction level on carotenoid production was evaluated by addition of IPTG concentrations ranging from 0 to 1 mM. Interestingly, in contrast to the eYFP reporter gene expression, increasing IPTG concentrations did not lead to gradually elevated carotenoid levels but rather to an on-or-off response possibly due to suboptimal fluxes of intermediates (Supplementary Figure S9). Nevertheless, this test system was subsequently evaluated for light-controlled regulation of carotenoid production using NP-cIPTG. Induction of the plasmid-encoded genes *crtE* and *crtF* was performed after six or 18 h *via* appropriate UV-A light exposure (30 min, λ_{max} = 365 nm, 2 mW/cm^2) or by adding IPTG at the respective time point. For quantification of the carotenoid accumulation, the absorption of the cultures containing IPTG as well as *R. capsulatus* SB1003 wildtype and SB1003 *ΔcrtEF* cultures as corresponding positive and negative controls were analyzed using a Tecan Microplate reader (Figure 5C). While *R. capsulatus* SB1003 *ΔcrtEF* cultures without induction of *crtEF* expression exhibited a similar pigmentation as observed in the control strain (ΔcrtEF) (Figure 5B), addition of IPTG resulted in a clearly visible change of the cell coloration indicating a partial complementation of the phenotype that is caused by the *crtEF* gene deletion. This observation could be verified by quantitative analysis of the corresponding carotenoid absorption (Figure 5C). In addition, optochemical induction of *crtEF* gene expression using NP-cIPTG could almost completely restore the carotenoid-deficient phenotype resulting in a pronounced carotenoid absorption level thereby demonstrating the applicability of caged inducers as light-responsive on-switches for secondary metabolite biosynthesis under phototrophic conditions. This may open up new strategies for the dynamic control of complex secondary metabolite pathways such as the terpene pathway in phototrophic bacteria, which were recently shown to be promising alternative production hosts for the sustainable production of plant terpenes (Hage-Hülsmann et al., 2019; Troost et al., 2019; Hilgers et al., 2021; Klaus et al., 2022). In this context, the optochemical control of the carotenoid

production might offer the possibility to precisely activate the carotenoid biosynthesis pathway in *R. capsulatus* cells allowing to modulate the FPP level for improving heterologous terpene production. This approach seems to be promising since an efficient terpene production requires a suitable FPP supply (Loeschcke et al., 2017; Troost et al., 2019; Hilgers et al., 2021). In near future, heterologous production of terpenes could thus be improved by performing phototrophic growth with optochemically controlled carotenoid levels to ensure an optimal supply of the FPP intermediate.

Discussion

Two aspects were considered for establishing photocaged inducers as alternative optochemical on-switches suitable for light-driven induction of gene expression in the phototroph *R. capsulatus*: 1) the general functionality of photocaged inducers including their stability during cell cultivation, their non-toxicity, and their induction efficiency and 2) specific characteristics such as the compatibility of absorption spectra of photocaged inducers and photopigments as well as the robust applicability of the light-responsive inducer molecules under diverging growth conditions.

We could show that neither the three cIPTG derivatives nor the photoproducts are toxic for *R. capsulatus* and can basically be applied for inducing LacI/P_{tac}-based target gene expression. However, only NP-cIPTG showed a sufficient stability in non-phototrophic and phototrophic *Rhodobacter* cultures when grown in the absence of UV-A light. The photoconversion of NP-cIPTG resulted in a specific activation of the P_{tac} promoter leading to a strong expression of downstream located genes irrespective of the chosen growth conditions. Remarkably, in some cases we could observe even higher induction levels when cIPTG instead of IPTG was used. These findings could be explained by an improved diffusion of the caged IPTG derivatives over the bacterial cell membrane in comparison to IPTG. Similar enhancement of photocaged inducer mediated induction of gene expression could also be observed in other bacterial expression hosts (Hogenkamp et al., 2021; Hogenkamp et al., 2022).

To retain the specific UV-A light responsiveness of cIPTG during phototrophic growth, we applied NIR light-emitting LED panels as alternative light sources. Irradiation of BChl *a* at 850 nm was shown to be sufficient for phototrophic growth thereby making the spectral range of 300–800 nm available for optochemical and optogenetic approaches. Besides the use of photocaged inducers these approaches thus may also include a variety of photoreceptors such as the well-known blue light-responsive photoreceptors of the LOV-, BLUF- or cryptochrome families (Briggs and Christie, 2002; Gomelsky and Klug, 2002; Lin and Todo, 2005; Losi and Gärtner, 2008; Drepper et al., 2011; Losi et al., 2018) or red light-sensing phytochromes (Levskaya et al., 2005; Rockwell et al., 2006; Tang et al., 2021).

Consequently, light-mediated regulation of gene expression in photosynthetic microbes using photocaged inducers opens up the possibility to optimize production of valuable secondary metabolites including terpenes. The combination of different optochemical and optogenetic switches further offers multi-factorial light-driven regulation approaches in principle allowing the gradual and dynamic control of complex biological processes with high spatial and temporal resolution. In future, this tool could thus prove valuable e.g., for automated control processes, where different light stimuli control cellular production processes in response to signals of intermediate- or product-specific biosensor in a closed-loop or microfluidic setup (Toettcher et al., 2011; Milias-Argeitis et al., 2016; Lalwani et al., 2018; Boada et al., 2020). Thus, photocaged inducers can contribute to non-invasive, light-mediated optimization of sustainable production processes in photosynthetic microbes.

Material and methods

Bacterial strains and plasmids

The *Escherichia coli* strain DH5α (Hanahan, 1983) was used for cloning and the strain S17-1 (Simon et al., 1983) for the conjugational transfer of expression plasmids. All *E. coli* strains were grown at 37°C on LB agar plates or in liquid LB medium (Luria/Miller, Carl Roth®), supplemented with kanamycin (50 μg mL^{-1}) when necessary. The *R. capsulatus* strain SB1003 (Strnad et al., 2010) was grown on PY agar plates containing 2% Select Agar (Thermo Fisher Scientific) or in RCV liquid medium containing 15 mM ammonium and supplemented with kanamycin (25 μg mL^{-1}) at 30°C. For cultivation of strain SB1003, rifampicin (25 μg mL^{-1}) was used additionally. If not stated otherwise, cultivation was conducted under anaerobic, photoheterotrophic conditions and permanent illumination with bulb light (2500 lx), as described previously (Troost et al., 2019).

All bacterial strains as well as the construction and genetic properties of plasmids used in this study are listed in Supplementary Table S1.

Cultivation of *R. capsulatus* for target gene expression

The aerobic and microaerobic expression cultures were grown in RCV + ammonium medium at 30°C using 48-well Round Well Plates® in a BioLector microbioreactor system (m2p labs, Germany) applying variable filling volumes and shaking frequencies to control dissolved oxygen tension (800, 1,000 and 1,500 μL; 800 rpm or 400 rpm, respectively).

Cultures were inoculated with an optical density of 0.1 determined at 660 nm. The cell density was measured during cultivation *via* scattered light intensity at 620 nm and the eYFP fluorescence intensities were online-monitored using a 508/532 nm filter. Heterologous and homologous gene expression was induced during early logarithmic phase (after approx. 9 h) *via* UV-A light exposure (VL-315. BL lamp, Vilber Lourmat, France; ~1 mW/cm^2, 30 min exposure) in RCV medium that was supplemented with BC-, BEC- or NP-cIPTG (1 mM) or by adding IPTG (1 mM) directly after light exposure in corresponding control cultures. In a previous study it could be demonstrated that these illumination conditions were sufficient for almost complete photoconversion of all cIPTG derivatives resulting in the full release of the active inducer molecule (Hogenkamp et al., 2021). The phototrophic expression cultures were inoculated with a starting OD_{660nm} of 0.5 in completely filled 4.2 mL screw neck vials (N13; Macherey-Nagel, Düren, Germany) using tight screw caps with a bonded septum (Macherey-Nagel, Düren, Germany) in RCV + ammonium medium at 30°C. Those were shown to be appropriate cultivation vessels for phototrophic growth in a previous study (Hilgers et al., 2021). To establish adequate environmental conditions for anoxygenic photosynthesis, cells were permanently illuminated with NIR light (850 nm, 1.7 mW/cm^2) using customized LED panels that have been described previously (Hilgers et al., 2021). The expression was induced after 6 h by UV-A light irradiation (365 nm, 2 mW/cm^2, 30 min exposure, the UV-A light LEDs are also installed on the panels) using NP-, BC-, or BEC-cIPTG (1 mM) added prior to cultivation. Due to the slightly higher distance of the vials to the LED panels during phototrophic cultivation in comparison to MTP and a possible shading effect of the increasingly colored *R. capsulatus* cells, we increased the UV-A light intensity to 2 mW/cm^2 to ensure a full uncaging of cIPTG. The same concentration of IPTG was used for corresponding control experiments. After 48 h of cultivation, *R. capsulatus* biomass and eYFP fluorescence were determined. For comparable measurements, 800 µL of each vial were transferred to one well of a Round Well Plate and further incubated at 30°C for 1.5 h in a BioLector microbioreactor system (m2p labs, Germany) (800 µL, 800 rpm) to ensure O_2-dependent eYFP chromophore maturation. After eYFP maturation was completed, the cell density was measured *via* scattered light intensity at 620 nm and the eYFP fluorescence was determined by using a 508/532 nm filter. It should be noted that the low solubility of NP-cIPTG in the cultivation medium can promote the formation of an emulsion-like solution, which can interfere with the determination of cell densities *via* the measurement of scattered light intensities in this experimental setup.

DMNB-actinometry

For the DMNB assay, 1.25 mM DMNB was dissolved in aqueous KOH solution (0.5 M) with 10% (v/v) DMSO. The alkaline DMNB solution was subsequently incubated under the same conditions applied for phototrophic growth of *R. capsulatus*. DMNB photoconversion to MNP was monitored by the increase of absorption at a wavelength of 422 nm (100 µl, Tecan Infinite M1000 Pro microplate reader). The UV-A exposure was carried out using a UV-A hand lamp (VL-315. BL 45 W, Vilber Lourmat, France; 5.4 mW/cm^2 at 365 nm for 1.5 cm distance to light source), the other light sources were used as described above.

Carotenoid production

The carotenoid complementation assay was performed using 4.2 mL screw neck vials (N13; Macherey-Nagel, Düren, Germany) for cultivation of *R. capsulatus* SB1003 *ΔcrtEF* in NP-cIPTG supplemented RCV medium containing 15 mM ammonium [starting OD_{660nm} = 0.1, 30°C, anaerobic conditions, permanent illumination with NIR light (850 nm, 1.7 mW/cm^2)]. The expression of the *crtEF* genes located on the P_{tac}-based expression vector pRholtHi-crtE-crtF was induced after six or 18 h *via* UV-A light exposure (365 nm, 2 mW/cm^2, 30 min exposure). IPTG was added at the same time points to the respective control strains. After 48 h, carotenoid accumulation was analyzed in 100 µL RCV *via* absorption measurement at 484 nm using an Infinite M1000 Pro microplate reader (Tecan Group LTD., Maennedorf, Switzerland).

For all illumination experiments, intensities of different light sources were quantified at relevant wavelengths (i.e., 365 and 850 nm) by using a Thermal Power Sensor (S302C, Thorlabs Inc., United States).

Synthesis of photocaged compounds

NP-cIPTG (Young and Deiters, 2007; Binder et al., 2014), BEC-cIPTG and BC-cIPTG (Hogenkamp et al., 2021) were synthesized as published previously.

Determination of compound purity by qNMR

The purity of the NP-cIPTG, BEC-cIPTG and BC-cIPTG was determined *via* quantitative NMR. (Methanesulfonyl)methane was utilized as internal standard for BC-cIPTG and 3,5-bis(trifluoromethyl)bromobenzene for NP-cIPTG as well as BEC-cIPTG. The spectra were measured at 20°C on a Bruker

Avance/DRX 600 spectrometer with 64 scans each and 30 µs relaxation time between each scan. The results in Supplementary Table S2 are means of triplicate measurements.

Data availability statement

The original contributions presented in the study are included in the article/Supplementary Material, further inquiries can be directed to the corresponding authors.

Author contributions

Conceptualization TD, K-EJ, and JP; methodology FHI, FHO, OK, LK, DB, and CB; validation FHI; formal analysis FHI; investigation, FHI, FHO, OK, and LK; writing–original draft preparation FHI, OK, and FHO; writing—review and editing TD, AL, K-EJ, and JP; visualization FHI; supervision TD; project administration TD, K-EJ, and JP; funding acquisition AL, TD, JP, and K-EJ. All authors have read and agreed to the published version of the manuscript.

Funding

The work was supported by grants from 1) The German Federal Ministry of Education and Research (BMBF, FKZ: 031A167A), 2) The Bioeconomy Science Center, and 3) The European Regional Development Fund (ERDF: 34. EFRE-0300096 and 34. EFRE-0300097) within the project CLIB-Kompetenzzentrum Biotechnologie (CKB). The scientific activities of the Bioeconomy Science Center were financially supported by the Ministry of Culture and Science of the German federal state of North Rhine-Westphalia within the framework of the NRW Strategieprojekt BioSC (No. 313/323-400-00213).

Conflict of interest

The authors declare that the research was conducted in the absence of any commercial or financial relationships that could be construed as a potential conflict of interest.

Publisher's note

All claims expressed in this article are solely those of the authors and do not necessarily represent those of their affiliated organizations, or those of the publisher, the editors and the reviewers. Any product that may be evaluated in this article, or claim that may be made by its manufacturer, is not guaranteed or endorsed by the publisher.

Supplementary material

The Supplementary Material for this article can be found online at: https://www.frontiersin.org/articles/10.3389/fbioe.2022.902059/full#supplementary-material

References

Bakkes, P. J., Ramp, P., Bida, A., Dohmen-Olma, D., Bott, M., and Freudl, R. (2020). Improved pEKEx2-derived expression vectors for tightly controlled production of recombinant proteins in *Corynebacterium glutamicum*. *Plasmid* 112, 102540. doi:10.1016/j.plasmid.2020.102540

Bardhan, A., and Deiters, A. (2019). Development of photolabile protecting groups and their application to the optochemical control of cell signaling. *Curr. Opin. Struct. Biol.* 57, 164–175. doi:10.1016/j.sbi.2019.03.028

Baumschlager, A., and Khammash, M. (2021). Synthetic biological approaches for optogenetics and tools for transcriptional light-control in bacteria. *Adv. Biol.* 5, 2000256. doi:10.1002/adbi.202000256

Bier, C., Binder, D., Drobietz, D., Loeschcke, A., Drepper, T., Jaeger, K.-E., et al. (2016). Photocaged carbohydrates: Versatile tools for controlling gene expression by light. *Synthesis* 49, 42–52. doi:10.1055/s-0035-1562617

Binder, D., Frohwitter, J., Mahr, R., Bier, C., Grünberger, A., Loeschcke, A., et al. (2016). Light-controlled cell factories: Employing photocaged isopropyl-β-d-thiogalactopyranoside for light-mediated optimization of *lac* promoter-based gene expression and (+)-Valencene biosynthesis in *Corynebacterium glutamicum*. *Appl. Environ. Microbiol.* 82, 6141–6149. doi:10.1128/AEM.01457-16

Binder, D., Grünberger, A., Loeschcke, A., Probst, C., Bier, C., Pietruszka, J., et al. (2014). Light-responsive control of bacterial gene expression: Precise triggering of the *lac* promoter activity using photocaged IPTG. *Integr. Biol.* 6, 755–765. doi:10.1039/C4IB00027G

Boada, Y., Vignoni, A., Picó, J., and Carbonell, P. (2020). Extended metabolic biosensor design for dynamic pathway regulation of cell factories. *iScience* 23, 101305. doi:10.1016/j.isci.2020.101305

Boran, E., Özgür, E., van der Burg, J., Yücel, M., Gündüz, U., and Eroglu, I. (2010). Biological hydrogen production by *Rhodobacter capsulatus* in solar tubular photo bioreactor. *J. Clean. Prod.* 18, S29–S35. doi:10.1016/j.jclepro.2010.03.018

Brieke, C., Rohrbach, F., Gottschalk, A., Mayer, G., and Heckel, A. (2012). Light-controlled tools. *Angew. Chem. Int. Ed.* 51, 8446–8476. doi:10.1002/anie.201202134

Briggs, W. R., and Christie, J. M. (2002). Phototropins 1 and 2: Versatile plant blue-light receptors. *Trends Plant Sci.* 7, 204–210. doi:10.1016/S1360-1385(02)02245-8

Burmeister, A., Akhtar, Q., Hollmann, L., Tenhaef, N., Hilgers, F., Hogenkamp, F., et al. (2021). Optochemical) control of synthetic microbial coculture interactions on a microcolony level. *ACS Synth. Biol.* 10, 1308–1319. doi:10.1021/acssynbio.0c00382

Deiters, A. (2009). Light activation as a method of regulating and studying gene expression. *Curr. Opin. Chem. Biol.* 13, 678–686. doi:10.1016/j.cbpa.2009.09.026

Drepper, T., Krauss, U., Meyer zu Berstenhorst, S., Pietruszka, J., and Jaeger, K.-E. (2011). Lights on and action! Controlling microbial gene expression by light. *Appl. Microbiol. Biotechnol.* 90, 23–40. doi:10.1007/s00253-011-3141-6

Drews, G., and Oelze, J. (1981). Organization and differentiation of membranes of phototrophic bacteria. *Adv. Microb. Physiol.* 22, 1–92. doi:10.1016/S0065-2911(08)60325-2

Drews, G. (2013). The intracytoplasmic membranes of purple bacteria-assembly of energy-transducing complexes. *Microb. Physiol.* 23, 35–47. doi:10.1159/000346518

Dubendorf, J. W., and Studier, F. W. (1991). Controlling basal expression in an inducible T7 expression system by blocking the target T7 promoter with *lac* repressor. *J. Mol. Biol.* 219, 45–59. doi:10.1016/0022-2836(91)90856-2

Eikmanns, B. J., Kleinertz, E., Liebl, W., and Sahm, H. (1991). A family of *Corynebacterium glutamicum/Escherichia coli* shuttle vectors for cloning, controlled gene expression, and promoter probing. *Gene* 102, 93–98. doi:10.1016/0378-1119(91)90545-M

Elkahlout, K., Sagir, E., Alipour, S., Koku, H., Gunduz, U., Eroglu, I., et al. (2019). Long-term stable hydrogen production from acetate using immobilized *Rhodobacter capsulatus* in a panel photobioreactor. *Int. J. Hydrogen Energy* 44, 18801–18810. doi:10.1016/j.ijhydene.2018.10.133

Gardner, L., and Deiters, A. (2012). Light-controlled synthetic gene circuits. *Curr. Opin. Chem. Biol.* 16, 292–299. doi:10.1016/j.cbpa.2012.04.010

Gardner, L., Zou, Y., Mara, A., Cropp, T. A., and Deiters, A. (2011). Photochemical control of bacterial signal processing using a light-activated erythromycin. *Mol. Biosyst.* 7, 2554. doi:10.1039/c1mb05166k

Gomelsky, M., and Klug, G. (2002). Bluf: A novel FAD-binding domain involved in sensory transduction in microorganisms. *Trends Biochem. Sci.* 27, 497–500. doi:10.1016/S0968-0004(02)02181-3

Hage-Hülsmann, J., Klaus, O., Linke, K., Troost, K., Gora, L., Hilgers, F., et al. (2021). Production of C20, C30 and C40 terpenes in the engineered phototrophic bacterium *Rhodobacter capsulatus*. *J. Biotechnol.* 338, 20–30. doi:10.1016/j.jbiotec.2021.07.002

Hage-Hülsmann, J., Metzger, S., Wewer, V., Buechel, F., Troost, K., Thies, S., et al. (2019). Biosynthesis of cycloartenol by expression of plant and bacterial oxidosqualene cyclases in engineered *Rhodobacter capsulatus*. *J. Biotechnol.* 4, 100014. doi:10.1016/j.btecx.2020.100014

Hanahan, D. (1983). Studies on transformation of *Escherichia coli* with plasmids. *J. Mol. Biol.* 166, 557–580. doi:10.1016/S0022-2836(83)80284-8

Happ, H. N., Braatsch, S., Broschek, V., Osterloh, L., and Klug, G. (2005). Light-dependent regulation of photosynthesis genes in *Rhodobacter sphaeroides* 2.4.1 is coordinately controlled by photosynthetic electron transport *via* the PrrBA two-component system and the photoreceptor AppA. *Mol. Microbiol.* 58, 903–914. doi:10.1111/j.1365-2958.2005.04882.x

Hilgers, F., Habash, S. S., Loeschcke, A., Ackermann, Y. S., Neumann, S., Heck, A., et al. (2021). Heterologous production of β-caryophyllene and evaluation of its activity against plant pathogenic fungi. *Microorganisms* 9, 168. doi:10.3390/microorganisms9010168

Hogenkamp, F., Hilgers, F., Bitzenhofer, N. L., Ophoven, V., Haase, M., Bier, C., et al. (2022). Optochemical control of bacterial gene expression: Novel photocaged compounds for different promoter systems. *Chembiochem*. 23, e202100467. doi:10.1002/cbic.202100467

Hogenkamp, F., Hilgers, F., Knapp, A., Klaus, O., Bier, C., Binder, D., et al. (2021). Effect of photocaged isopropyl β-d-1-thiogalactopyranoside solubility on the light responsiveness of LacI-controlled expression systems in different bacteria. *ChemBioChem* 22, 539–547. doi:10.1002/cbic.202000377

Kaschner, M., Loeschcke, A., Krause, J., Minh, B. Q., Heck, A., Endres, S., et al. (2014). Discovery of the first light-dependent protochlorophyllide oxidoreductase in anoxygenic phototrophic bacteria. *Mol. Microbiol.* 93, 1066–1078. doi:10.1111/mmi.12719

Katzke, N., Arvani, S., Bergmann, R., Circolone, F., Markert, A., Svensson, V., et al. (2010). A novel T7 RNA polymerase dependent expression system for high-level protein production in the phototrophic bacterium *Rhodobacter capsulatus*. *Protein Expr. Purif.* 69 (2), 137–146. doi:10.1016/j.pep.2009.08.008

Khan, N. E., Nybo, S. E., Chappell, J., and Curtis, W. R. (2015). Triterpene hydrocarbon production engineered into a metabolically versatile host-*Rhodobacter capsulatus*. *Biotechnol. Bioeng.* 112, 1523–1532. doi:10.1002/bit.25573

Klaus, O., Hilgers, F., Nakielski, A., Hasenklever, D., Jaeger, K.-E., Axmann, I. M., et al. (2022). Engineering phototrophic bacteria for the production of terpenoids. *Curr. Opin. Biotechnol.* 77, 102764. doi:10.1016/j.copbio.2022.102764

Kolarski, D., Sugiyama, A., Breton, G., Rakers, C., Ono, D., Schulte, A., et al. (2019). Controlling the circadian clock with high temporal resolution through photodosing. *J. Am. Chem. Soc.* 141, 15784–15791. doi:10.1021/jacs.9b05445

Kusen, P. M., Wandrey, G., Probst, C., Grünberger, A., Holz, M., Meyer zu Berstenhorst, S., et al. (2016). Optogenetic regulation of tunable gene expression in yeast using photo-labile caged methionine. *ACS Chem. Biol.* 11, 2915–2922. doi:10.1021/acschembio.6b00462

Lalwani, M. A., Zhao, E. M., and Avalos, J. L. (2018). Current and future modalities of dynamic control in metabolic engineering. *Curr. Opin. Biotechnol.* 52, 56–65. doi:10.1016/j.copbio.2018.02.007

Levskaya, A., Chevalier, A. A., Tabor, J. J., Simpson, Z. B., Lavery, L. A., Levy, M., et al. (2005). Synthetic biology: Engineering *Escherichia coli* to see light. *Nature* 438, 441–442. doi:10.1038/nature04405

Lin, C., and Todo, T. (2005). The cryptochromes. *Genome Biol.* 6, 220. doi:10.1186/gb-2005-6-5-220

Liu, J., Hemphill, J., Samanta, S., Tsang, M., and Deiters, A. (2017). Genetic code expansion in zebrafish embryos and its application to optical control of cell signaling. *J. Am. Chem. Soc.* 139, 9100–9103. doi:10.1021/jacs.7b02145

Loeschcke, A., Dienst, D., Wewer, V., Hage-Hülsmann, J., Dietsch, M., Kranz-Finger, S., et al. (2017). The photosynthetic bacteria *Rhodobacter capsulatus* and *Synechocystis sp.* PCC 6803 as new hosts for cyclic plant triterpene biosynthesis. *PLoS ONE* 12, e0189816. doi:10.1371/journal.pone.0189816

Losi, A., Gardner, K. H., and Möglich, A. (2018). Blue-light receptors for optogenetics. *Chem. Rev.* 118, 10659–10709. doi:10.1021/acs.chemrev.8b00163

Losi, A., and Gärtner, W. (2008). Bacterial bilin- and flavin-binding photoreceptors. *Photochem. Photobiol. Sci.* 7l, 1168–1178. doi:10.1039/b802472c

Milias-Argeitis, A., Rullan, M., Aoki, S. K., Buchmann, P., and Khammash, M. (2016). Automated optogenetic feedback control for precise and robust regulation of gene expression and cell growth. *Nat. Commun.* 7, 12546. doi:10.1038/ncomms12546

Nakayama, K., Heise, I., Görner, H., and Gärtner, W. (2011). Peptide release upon photoconversion of 2-nitrobenzyl compounds into nitroso derivatives. *Photochem. Photobiol.* 87, 1031–1035. doi:10.1111/j.1751-1097.2011.00957.x

Obeid, J., Magnin, J. P., Flaus, J. M., Adrot, O., Willison, J. C., and Zlatev, R. (2009). Modelling of hydrogen production in batch cultures of the photosynthetic bacterium *Rhodobacter capsulatus*. *Int. J. Hydrogen Energy* 34, 180–185. doi:10.1016/j.ijhydene.2008.09.081

Pelliccioli, A. P., and Wirz, J. (2002). Photoremovable protecting groups: Reaction mechanisms and applications. *Photochem. Photobiol. Sci.* 1, 441–458. doi:10.1039/b200777k

Peters, L., Weidenfeld, I., Klemm, U., Loeschcke, A., Weihmann, R., Jaeger, K.-E., et al. (2019). Phototrophic purple bacteria as optoacoustic *in vivo* reporters of macrophage activity. *Nat. Commun.* 10, 1191. doi:10.1038/s41467-019-09081-5

Rockwell, N. C., Su, Y.-S., and Lagarias, J. C. (2006). Phytochrome structure and signaling mechanisms. *Annu. Rev. Plant Biol.* 57, 837–858. doi:10.1146/annurev.arplant.56.032604.144208

Simon, R., Priefer, U., and Pühler, A. (1983). A broad host range mobilization system for *in vivo* genetic engineering: Transposon mutagenesis in gram-negative bacteria. *Biotechnol. (N. Y.).* 1, 784–791. doi:10.1038/nbt1183-784

Stoppani, A. O., Fuller, R. C., and Calvin, M. (1955). Carbon dioxide fixation by *Rhodopseudomonas capsulatus*. *J. Bacteriol.* 69, 491–501. doi:10.1128/jb.69.5.491-501.1955

Strnad, H., Lapidus, A., Paces, J., Ulbrich, P., Vlcek, C., Paces, V., et al. (2010). Complete genome sequence of the photosynthetic purple nonsulfur bacterium *Rhodobacter capsulatus* SB1003. *J. Bacteriol.* 192, 3545–3546. doi:10.1128/JB.00366-10

Studier, F. W. (1991). Use of bacteriophage T7 lysozyme to improve an inducible T7 expression system. *J. Mol. Biol.* 219, 37–44. doi:10.1016/0022-2836(91)90855-Z

Tabita, F. R. (1995). The biochemistry and metabolic regulation of carbon metabolism and CO2 fixation in purple bacteria. *Anoxygenic Photosynth. Bact.* Vol. 2, 885–914. doi:10.1007/0-306-47954-0_41

Tang, K., Beyer, H. M., Zurbriggen, M. D., and Gärtner, W. (2021). The red edge: Bilin-binding photoreceptors as optogenetic tools and fluorescence reporters. *Chem. Rev.* 121, 14906–14956. doi:10.1021/acs.chemrev.1c00194

Toettcher, J. E., Gong, D., Lim, W. A., and Weiner, O. D. (2011). Light-based feedback for controlling intracellular signaling dynamics. *Nat. Methods* 8, 837–839. doi:10.1038/nmeth.1700

Troost, K., Loeschcke, A., Hilgers, F., Özgür, A. Y., Weber, T. M., Santiago-Schübel, B., et al. (2019). Engineered *Rhodobacter capsulatus* as a phototrophic platform organism for the synthesis of plant sesquiterpenoids. *Front. Microbiol.* 10, 1998. doi:10.3389/fmicb.2019.01998

Tucker, J. D., Siebert, C. A., Escalante, M., Adams, P. G., Olsen, J. D., Otto, C., et al. (2010). Membrane invagination in *Rhodobacter sphaeroides* is initiated at curved regions of the cytoplasmic membrane, then forms both budded and fully detached spherical vesicles. *Mol. Microbiol.* 76, 833–847. doi:10.1111/j.1365-2958.2010.07153.x

van Riel, H. C. H. A., Lodder, G., and Havinga, E. (1981). Photochemical methoxide exchange in some nitromethoxybenzenes. The role of the nitro group in S_N2Ar^* reactions. *J. Am. Chem. Soc.* 103, 7257–7262. doi:10.1021/ja00414a036

Wandrey, G., Bier, C., Binder, D., Hoffmann, K., Jaeger, K.-E., Pietruszka, J., et al. (2016). Light-induced gene expression with photocaged IPTG for induction profiling in a high-throughput screening system. *Microb. Cell Fact.* 15, 63. doi:10.1186/s12934-016-0461-3

Wu, J., and Bauer, C. E. (2008). "RegB/RegA, A global redox-responding two-component system," in *Bacterial signal transduction: Networks and drug targets* (New York, NY: Springer New York), 131–148. doi:10.1007/978-0-387-78885-2_9

Xin, Y., Lin, S., and Blankenship, R. E. (2007). Femtosecond spectroscopy of the primary charge separation in reaction centers of *Chloroflexus aurantiacus* with selective excitation in the Q_Y and Soret bands. *J. Phys. Chem. A* 111, 9367–9373. doi:10.1021/jp073900b

Young, D. D., and Deiters, A. (2007). Photochemical activation of protein expression in bacterial cells. *Angew. Chem. Int. Ed.* 46, 4290–4292. doi:10.1002/anie.200700057

Zhang, J. Y., Esrom, H., and Boyd, I. W. (1999). UV intensity measurement of 308 nm excimer lamp using chemical actinometer. *Appl. Surf. Sci.* 138-139, 315–319. doi:10.1016/S0169-4332(98)00412-7

frontiers

Supplementary Material

Table of contents

1 Supplementary Methods

Bacterial strains and plasmids

All bacterial strains, plasmids and oligonucleotides used in this study are listed in Table S1.

Table S1: Bacterial strains, plasmids and oligonucleotides used in this study.

Strains, plasmids, oligonucleotides	Relevant features, description or sequences	References
	Strains	
***E. coli* DH5α**	*F⁻ Φ80lacZΔM15 Δ(lacZYA-argF) U169 recA1 endA1 hsdR17 phoA supE44 thi-1 gyrA96 relA1 deoR*	[1]
***E. coli* S17-1**	Ec294::[RP4-2 (Tc^R::Mu)(Km^R::Tn7)] *recA, thi, pro, hsdR⁻ hsdM⁺* Tp^R, Sm^R	[2]
***E. coli* Tuner(DE3)**	*F⁻ompT hsdS*$_B$ (r_B^- m_B^-) *gal dcm lacY1*(DE3)	Novagen, Merck KGaA
***R. capsulatus* SB1003**	Wild-type, Rif^R	[3]
R. capsulatus* SB1003 *ΔcrtEF	*ΔcrtE*, *ΔcrtF*, Rif^R,Sm^R	[4]
	Plasmids	
pRholHi-2-eYFP	pBBR1-MCS-derivative, Km^R, Cm^R, with *SmaI*/*Xho*I inserted *lacI*^{q}-P_{tac}-lacO, *eyfp*	This work
pRholHi-2_Δlac-eYFP	pRholHi-2-eYFP derivative with homologous *lacI* fragment deletion and reconstituted *E. coli lacI*	This work
pRholtHi-eYFP	pRholHi-2-eYFP derivative with homologous *lacI* fragment deletion, reconstituted *E. coli lacI* and *in silico* calculated P_{tac} RBS (i.e., Shine-Dalgarno and spacer sequence)	This work
pRholtHi-crtE-crtF	pBBR1-MCS-derivative, Km^R, Cm^R, with inserted *crtE crtF*	This work
pRhofHi-2-eYFP	pBBR1-MCS-derivative, Km^R, Cm^R, P_{fru} with *Sma*I/*Xho*I inserted *eyfp*	Troost, unpublished
pRhotHi-2-lacI-eYFP	pBBR1-MCS-derivative, Km^R, Cm^R, pBBR22b-*lacI*, P_{T7}-lacO-MCS with *Nde*I *Xho*I inserted *eyfp*	[5]
	Oligonucleotides	
1) SmaI_Ptac_eYFP_fw	Binds at the 5' end of the *lacI*$_q$ gene on pEKEX-2-eYFP plasmid, contains *Sma*I site. 5'-ATATCCCGGGCAAACATGGCCTGTCGC TTG-3'	This work
2) XhoI_Ptac_eYFP_rev	Binds at the 3' end of the *eyfp* gene on pEKEX-e-eYFP plasmid, contains *Xho*I site. 5'-ATATCTCGAGCACACTACCATCGGCGC TAC-3'	This work
3) pRholHi-dlacI _fw	Binds at the 3`end of the plasmid pRholHi-2-eYFP downstream of the redundant *lacI* region, inserts homologous regions for InFusion® cloning. 5'-CGTTGCGCAATTCCGCGAACCCCAGAGT-3'	This work
4) pRholHi-dlacI_rev	Binds at the 5`end of the plasmid pRholHi-2-eYFP upstream of the redundant *lacI* region, inserts homologous regions for InFusion® cloning. 5'-CGGAATTGCGCAACGCAATTAATGTAAG TTAG-3'	This work

5) **pRholHi_fw**	Binds at the 3' end of the plasmid pRholHi-2-eYFP downstream of the *lacI* gene variant. 5'-ATTCACCACCCTGAATTGACTCTC-3'	This work
6) **pRholHi_rev**	Binds at the 5' end of the plasmid pRholHi-2-eYFP upstream of the *lacI* gene variant. 5'-GCGAGGGCGTGCAAGATTC-3'	This work
7) **lacI_EC_fw**	Binds at the 5' end of the native *lacI* gene of *E. coli*, inserts homologous regions for InFusion® cloning. 5'-CTTGCACGCCCTCGCTCACTGCCCGCTTTC CAG-3'	This work
8) **lacI_EC_rev**	Binds at the 3' end of the native *lacI* gene of *E. coli*, inserts homologous regions for InFusion® cloning. 5'-TTCAGGGTGGTGAATGTGAAACCAGTAACG TTATACGATG-3'	This work
9) **pRholtHi_RBS_fw**	Binds at the 3' end of the plasmid pRholHi-2_Δlac-eYFP and inserts homologous regions for InFusion® cloning. 5'-ACAAGGAGGTATTCATATGACCATGATT ACGCCAAGC-3'	This work
10) **pRholtHi_RBS_rev**	Binds at the 5' end of the plasmid pRholHi-2_Δlac-eYFP and inserts homologous regions for InFusion® cloning. 5'-TGAATACCTCCTTGTGAAATTGTTATCCG CTCAC-3'	This work
11) **CrtEF_genome_fw**	Binds at the 5' end of the *crtE* gene in the *R. capsulatus* SB1003 genome, inserts homologous regions for InFusion® cloning. 5'-AGGAGGTATTTTCATATGTCTCTGG ATAAACGTATCGAG-3'	This work
12) **CrtEF_genome_rev**	Binds at the 3' end of the *crtF* gene in the *R. capsulatus* SB1003 genome, inserts homologous regions for InFusion® cloning. 5'- CTCGAATTCGGATCCTCAGCCGC GTTCGGCCTC_-3'	This work
13) **pRholtHi-crtEF_fw**	Binds at the3' end of the plasmid pRholtHi-eYFP. 5'- GGATCCGAATTCGAGCTCC-3'	This work
14) **pRholtHi-crtEF_rev**	Binds at the 5' end of the plasmid pRholtHi-eYFP. 5'- ATGAAAATACCTCCTTGTGAAATTG -3'	This work
15) **pRholtHi-crtEF-QC_fw**	Binds at the RBS of plasmid pRholtHi-crtE-crtF and inserts optimized RBS/spacer 5'- CAAGGAGGTTTCATATGTCTCTG GATAAACG -3'	This work
16) **pRholtHi-crtEF-QC_rev**	Binds at the RBS of plasmid pRholtHi-crtE-crtF and inserts optimized RBS/spacer 5'- TATGAAACCTCCTTGTGAAA TTGTTATCCG -3'	This work

All recombinant DNA techniques were carried out using *E. coli* DH5α as described by Sambrook *et al.*[6]. Construction of expression vectors were carried out using restriction and ligation cloning. The PCR fragment containing the gene for $lacI^q$ and the P_{tac} promoter was amplified from a synthetic gene construct on the shuttle vector pEKEx-2 (Eurofins Genomics, Ebersberg, Germany) with oligos 1 and 2 generating appropriate *Sma*I/*Xho*I restriction sites at

its 5'- and 3'-ends. This fragment was inserted into the likewise hydrolyzed plasmid pRhofHi-2-eYFP to build the plasmid pRholHi-2-eYFP.

For construction of the optimized pRholHi-2_Δlac-eYFP plasmid, the redundant 1.5 kb *lacI* fragment upstream of the original *lacI* gene was deleted and the *lacI* gene variant was replaced by the original *lacI* gene from *E. coli* K12. Both changes were conducted in one cloning step. For this purpose, three PCR fragments were generated: the first one encompasses the region between the deleted redundant *lacI* fragment and the original *lacI* gene of the plasmid backbone (oligos 3 and 6), the second one encompasses a native version of the *lacI* gene from *E. coli* (oligos 7 and 8) and the third one encompasses the plasmid backbone after the *lacI* gene until the redundant *lacI* region (oligos 4 and 5). Subsequently, the three fragments were assembled *via* InFusion® Cloning (Takara Bio Europe, St Germain en Laye, France).

The plasmid pRholtHi-eYFP was constructed using the pRholHi_Δlac-eYFP by changing the RBS consisting of the Shine-Dalgarno and spacer sequence upstream of the *eyfp* reporter gene. An *in silico* optimized RBS and RBS-spacer including an NdeI site prior to the start codon of *eyfp* (for sequences see chapter "DNA sequences of P_{tac} promoter regions including their RBS, RBS-spacers and/or MCS") was calculated with the Salis Lab RBS calculator (https://salislab.net/software/predict_rbs_calculator) [7]. The plasmid backbone was amplified *via* PCR using olios 9 and 10, which featured homologous regions containing the optimized RBS and reassembled *via* InFusion® Cloning (Takara Bio Europe, St Germain en Laye, France).

For the plasmid pRholtHi-crtE-crtF, the genes *crtE* and *crFE* were amplified from the genome of *R. capsulatus* SB1003 with oligos 11 and 12 generating appropriate homologous regions for InFusion® Cloning (Takara Bio Europe, St Germain en Laye, France) at their 5'- and 3'-ends. The plasmid backbone was amplified *via* PCR from the pRholtHi-eYFP using oligos 13 and 14. The PCR fragment was inserted into the amplified backbone to build the plasmid pRholtHi-crtE-crtF. Additionally, an *in silico* optimized RBS and RBS-spacer including an NdeI site prior to the start codon of *crtE* (for sequences see chapter "DNA sequence of CrtE and CrtF from *R. capsulatus* SB1003 for cIPTG-mediated expression in *R. capsulatus* cultures") was calculated with the Salis Lab RBS calculator (https://salislab.net/software/predict_rbs_calculator) [7]. The adaption of the RBS spacer was performed *via* QuikChange using oligos 15 and 16.

2 Supplementary Data

Determination of suitable cultivation parameters for aerobic and microaerobic growth of *R. capsulatus*

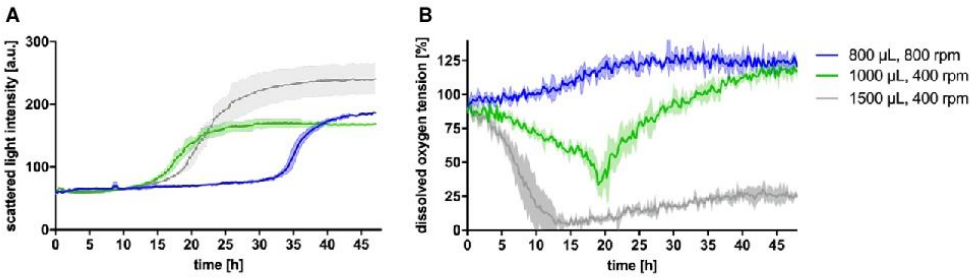

Figure S1: (**A**) Cell growth of *R. capsulatus* SB1003/pRholHi-2-eYFP expression cultures under varying filling volumes and shaking frequencies. The bacteria were grown in RCV medium for 48 h in Round Well Plates in the dark at 30 °C. To identify filling volumes and shaking frequencies that are appropriate for aerobic and microaerobic growth, the following cultivation conditions were applied: (i) 800 rpm and with 800 µL RCV medium (blue), (ii) 400 rpm and 1000 µL RCV medium (green) and (iii) 400 rpm and 1500 µL RCV medium (grey). Cell growth was analyzed by determining the scattered light intensity using a BioLector system. Values are means of individual biological triplicates. Error bars indicate the respective standard deviations. (**B**) Dissolved oxygen tension (DOT) of the same *R. capsulatus* cultures as described in A). The DOT was determined in plates with oxygen sensitive optodes during cultivation of *Rhodobacter* in the BioLector system (λ_{ex} = 520 nm, λ_{em} = 600 nm). Values are means of individual biological triplicates. Error bars indicate the respective standard deviations.

To control the oxygen level during non-phototrophic growth, the filling volume of the Round Well plate as well as the shaking frequencies were appropriately adapted so that a maximal aeration (around 100%) and a minimal aeration (< 25%) were maintained throughout the cultivation. For this purpose, bacterial growth (Figure S1A) and the dissolved oxygen tension (DOT; Figure S1B) were online-monitored using the scattered light intensity and DO optodes (m2p-labs, Germany), respectively. A filling volume of 800 µL and a shaking frequency of 800 rpm resulted in a constant oxygen tension of 100% (Figure S1B, blue line). To reduce the DOT during *R. capsulatus* cultivation, a filling volume of 1000 µL and a shaking frequency of 400 rpm were applied. However, these conditions were not sufficient for constant microaerobic growth, as the oxygen tension increased up to 100% during stationary growth phase (Figure S1B, green line). Therefore, a lager filling volume (1500 µL) at the same shaking frequency were used, which led to a strongly decreased oxygen tension of under 25% during both logarithmic and stationary growth phase (Figure S1B, grey line).

Determination of IPTG concentrations sufficient for the induction of *eyfp* reporter gene expression in *R. capsulatus* under aerobic, microaerobic and phototrophic conditions

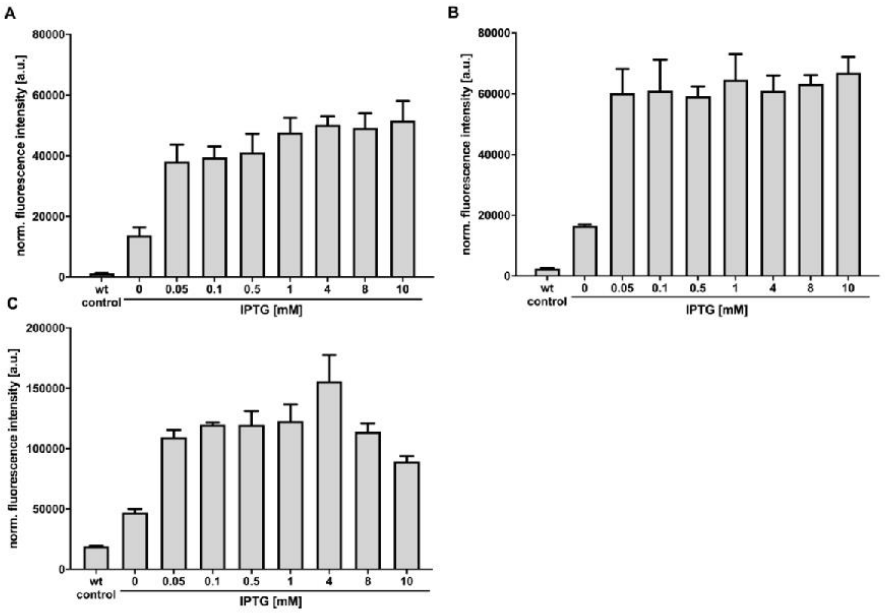

Figure S2: Relative eYFP fluorescence intensities of *R. capsulatus* SB1003/pRholHi-2-eYFP cultures grown aerobically **(A)**, microaerobically **(B)** or anaerobically **(C)** and supplemented with increasing amounts of IPTG. Aerobic and microaerobic cultures were incubated in 800 µL or 1500 µL RCV medium and a shaking frequency of 800 rpm or 400 rpm for 48 h in the dark at 30 °C. Induction of gene expression was performed after 9 h by adding IPTG at concentrations ranging from 0 to 10 mM. Phototrophic cultures were incubated in 4.2 mL RCV medium for 48 h at 30 °C under constant illumination with bulb light (2000 lx) and IPTG was added prior to culture inoculation. *In vivo* fluorescence intensities of all cultures were determined by using a BioLector system (eYFP: λ_{ex} = 508 nm, λ_{em} = 532 nm) and values were normalized to cell densities. Values are means of individual biological triplicates. Error bars indicate the respective standard deviations.

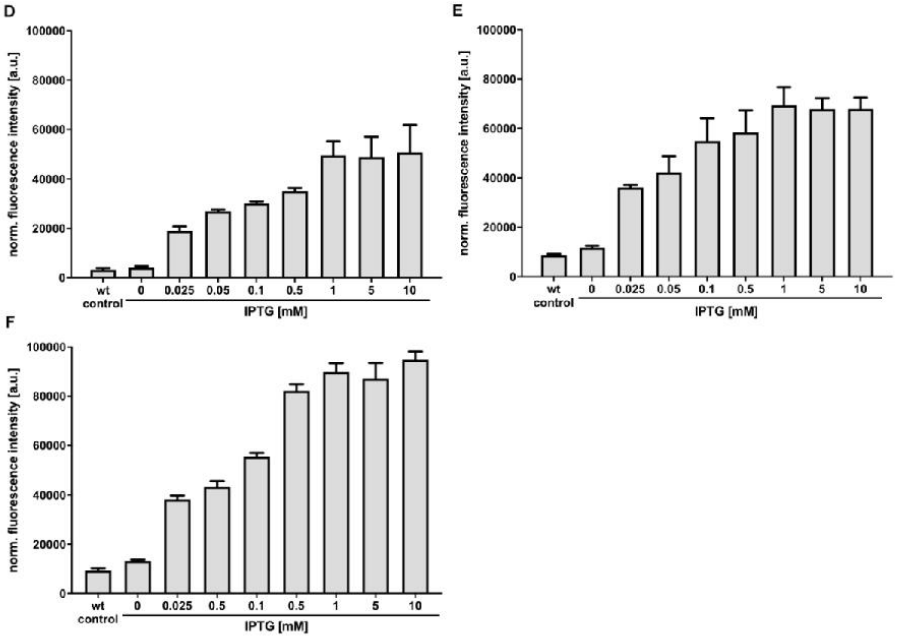

Continued figure S2: Relative eYFP fluorescence intensities of *R. capsulatus* SB1003/pRholtHi-eYFP cultures grown aerobically **(D)**, microaerobically **(E)** or anaerobically **(F)** and supplemented with increasing amounts of IPTG. Aerobic and microaerobic cultures were incubated in 800 µL or 1500 µL RCV medium and a shaking frequency of 800 rpm or 400 rpm for 48 h in the dark at 30 °C. Induction of gene expression was performed after 9 h by adding IPTG at concentrations ranging from 0 to 10 mM. Phototrophic cultures were incubated in 4.2 mL RCV medium for 48 h at 30 °C under constant illumination with bulb light (2000 lx) and IPTG was added prior to culture inoculation. *In vivo* fluorescence intensities of all cultures were determined by using a BioLector system or a Tecan Microplate reader (eYFP: λ_{ex} = 508 nm, λ_{em} = 532 nm) and values were normalized to cell densities. Values are means of individual biological triplicates. Error bars indicate the respective standard deviations.

Considerably high *eyfp* expression levels could be seen for IPTG concentrations of 1 mM and above, thus 1 mM was chosen as a sufficient inducer concentration in all further experiments. The induction profile using the optimized expression plasmid pRholtHi-eYFP shows an enhanced gradual induction in comparison to the precedent plasmid.

Influence of the induction time on the *eyfp* reporter gene expression and growth of *R. capsulatus* under microaerobic and phototrophic conditions

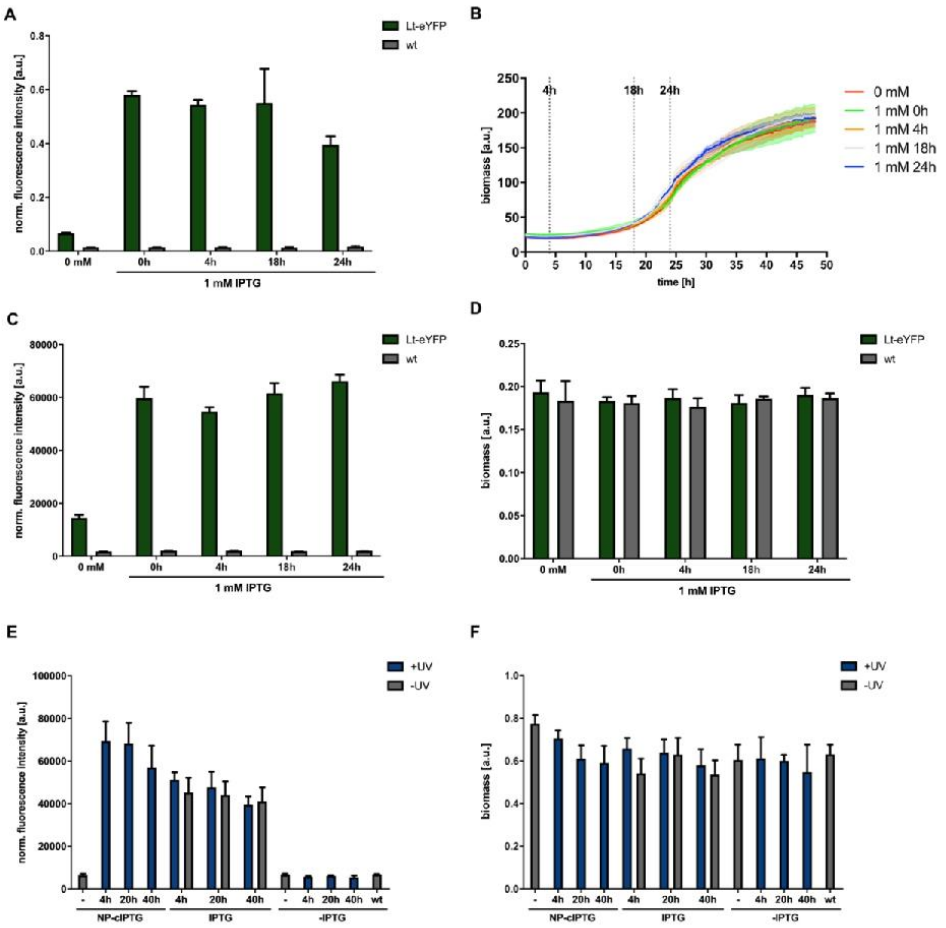

Figure S3: Effect of different induction time-points on eYFP fluorescence intensities and cell growth of *R. capsulatus* SB1003/pRholtHi-eYFP cultures grown microaerobically **(A,B)** or anaerobically **(C,D).** For induction of eYFP gene expression, IPTG was supplemented at different time points (0h, 4h = lag phase, 18 h = early logarithmic growth phase, and 24h = mid-logarithmic growth phase). Microaerobic cultures were incubated in 1500 µL RCV medium and a shaking frequency of 400 rpm for 48 h in the dark at 30 °C. Phototrophic cultures were incubated in 4.2 mL RCV medium for 48 h at 30 °C under constant illumination with bulb light (2000 lx). Additionally, the influence of increasing cell densities on NP-cIPTG uncaging was evaluated in anaerobically grown *R. capsulatus* cultures **(E,F)**. For light-induction of eYFP gene expression, growth media were supplemented with 1 mM NP-cIPTG prior cultivation and cultures were subsequently illuminated with UV-A light (365 nm, ~2 mW/cm^2) for 30 min at the given time points (4h = lag phase, 20 h = early logarithmic growth phase, and 40h = late logarithmic growth phase) or kept in the dark (-). Corresponding control cultures were supplemented with 1mM IPTG at the same time points. While cultures that were induced after both 4h and 20h have 44h for eYFP production (fluorescence measurement after 48h or 64h of the total cultivation time, respectively), the cultivation time could not be expanded accordingly

for cultures induced after 40h, because *R. capsulatus* cultures start to die after approximately 72h under the here applied cultivation conditions. For those cultures, the fluorescence measurement was conducted after 72h of the total cultivation time, corresponding to an eYFP production time of 32h. *In vivo* fluorescence intensities (eYFP: λ_{ex} = 508 nm, λ_{em} = 532 nm) and biomass of all cultures (scattered light intensity at 620 nm or absorption at 660 nm, respectively) were determined at the above stated time points by using a BioLector system or a Tecan Microplate reader and fluorescence values were normalized to cell densities. Values are means of individual biological triplicates. Error bars indicate the respective standard deviations.

The results demonstrate that the induction and uncaging works well even under higher cell densities. The slightly lower fluorescence intensity after 40h in **Fig. S5 E** is most probably due to a shorter time span from induction to the final eYFP measurement.

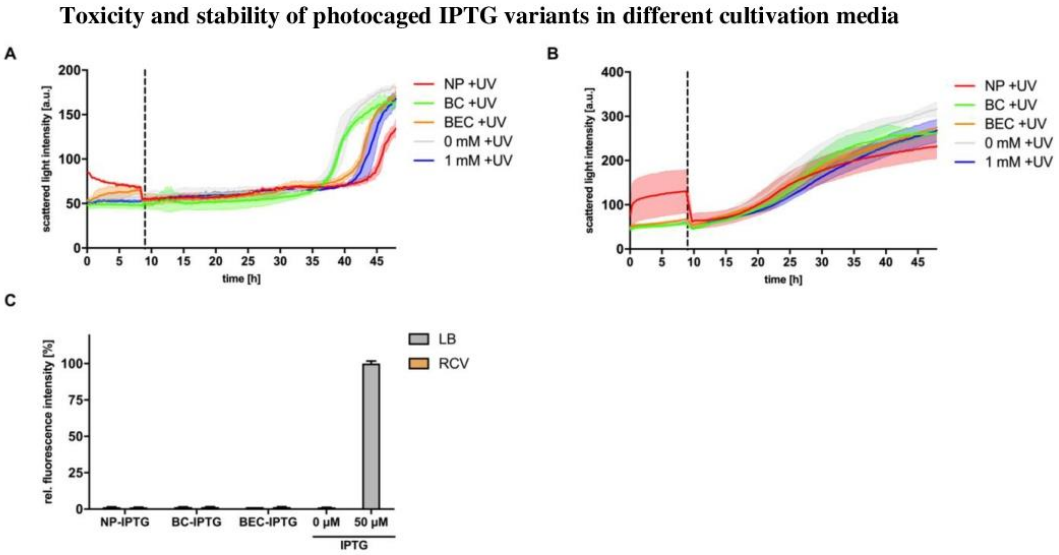

Figure S4: A-B) Growth curves of *R. capsulatus* SB1003/pRholHi-2-eYFP expression cultures in the presence of the photocaged IPTG variants compared to an uninduced (0 mM) and induced (1 mM IPTG) expression culture. Cells were grown over 48 h using a BioLector system (RCV medium supplemented with 1 mM of each caged compound, 30°C, 800 rpm and 800 µL filling volume for aerobic cultures **(A)**, 400 rpm and 1500 µL for microaerobic cultures **(B)**). Cell growth was analyzed by determining the scattered light intensity. After 9 h, formation of photoproducts was induced in cultures of *R. capsulatus via* light exposure at 365 nm (~1 mW/cm^2, indicated by dashed lines) for 30 min. The addition of IPTG was used as a control to comparatively analyze cell growth. Values are means of individual biological triplicates. Error bars indicate the respective standard deviations. **C)** eYFP *in vivo* fluorescence intensity of *E. coli* Tuner (DE3)/pRhotHi-2-lacI-eYFP expression cultures supplemented with the photocaged inducers which were previously incubated under different conditions. The three caged inducers (1 mM) were either incubated in LB (grey bars) or RCV (orange bars) medium for 48 h at 30 °C and added to the *E. coli* cultures afterwards in appropriate concentrations resulting in an end concentration of 50 µM. The *E. coli* cultures were incubated in the dark for 20 h in LB medium at 30 °C. *In vivo* stability of the photocaged IPTG variants is reflected by a low induction of reporter gene expression. As positive control, *E. coli* Tuner (DE3)/ pRhotHi-2-lacI-eYFP cultures supplemented with and without IPTG were used. *In vivo* fluorescence intensities were determined by using a BioLector system (eYFP: λ_{ex} = 508 nm, λ_{em} = 532 nm) and are shown in relation to the respective fluorescence intensities of the positive control cultures (50 µM IPTG). All values are normalized to cell-densities and are means of individual biological triplicates. Error bars indicate the respective standard deviations.

The elevated scattered light values at the beginning of the cultivation (i.e., before UV-A light exposure, Figure S4 A and B) can be attributed to the poorer water solubility of NP-cIPTG at concentrations of 1 mM, as a certain amount of these compounds initially form emulsions in the cultivation medium. Consequently, they contribute significantly more to the scattered light value than the bacterial cells that are initially still present in low numbers. However, exposure

to UV-A light dissolves these emulsions, which is reflected by the rapid decrease in the scattered light intensity after 9 h.

This control experiment with the well-established expression strain *E. coli* Tuner(DE3) [5] indicated that cIPTG instability was not detectable in sole LB or RCV medium. This gives a first hint that the instability of BC-cIPTG and BEC-cIPTG might be caused by using *R. capsulatus* as expression host, probably due to host specific enzymes or metabolism products.

Effect of UV-A light illumination on growth and *eyfp* reporter gene expression of *R. capsulatus* SB1003/pRholHi-2-eYFP cultures under aerobic and microaerobic conditions

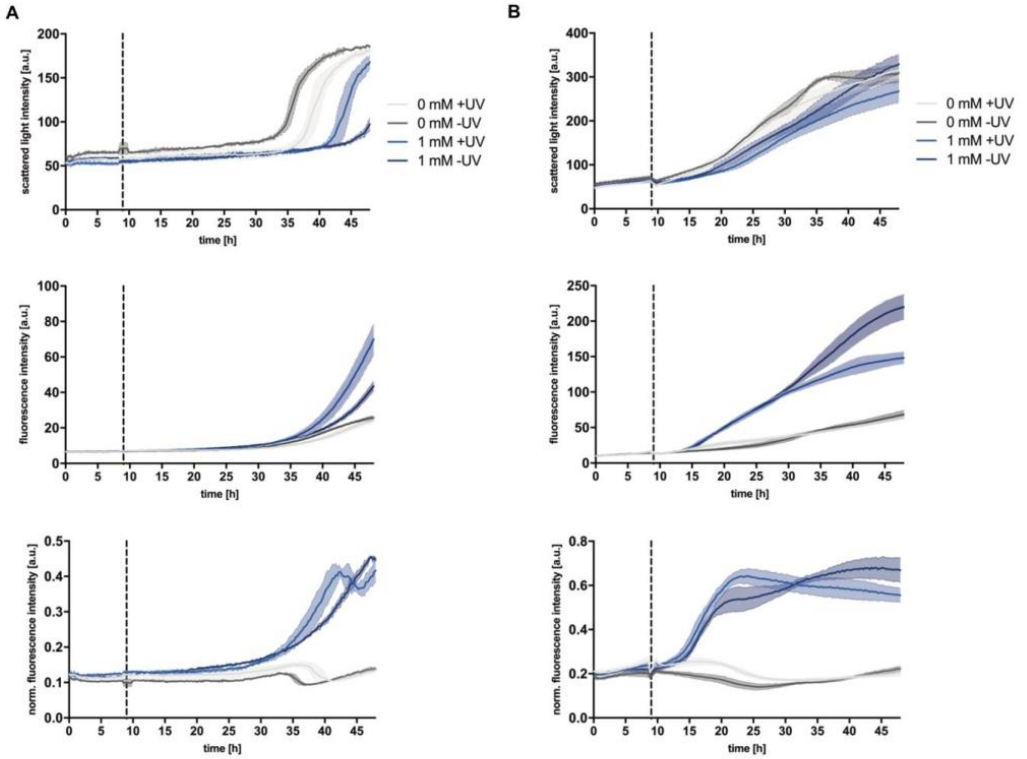

Figure S5: Cell growth and eYFP fluorescence during cultivation of *R. capsulatus* SB1003/pRholHi-2-eYFP. Cells were grown over 48 h in RCV medium at 30°C, 800 rpm and with 800 µL filling volume for aerobic conditions **(panel A)** and 400 rpm and 1500 µL for microaerobic conditions **(panel B)** using a BioLector system. Induction of eYFP gene expression was performed using 1 mM of IPTG (blue lines; uninduced grey lines). Simultaneously, cultures were incubated with (light lines) and without (dark line) UV-A light exposure at 365 nm (~1 mW/cm^2) for 30 min. The time point of induction is indicated by the dashed lines (9 h). Cell growth was analyzed by determining the scattered light intensity and the *in vivo* eYFP fluorescence intensities were measured at λ_{ex} = 508 nm, λ_{em} = 532 nm, as depicted in both center graphs in the middle, and normalized to cell densities, as shown in the bottom graphs. Values are means of individual biological triplicates. Error bars indicate the respective standard deviations.

Detailed toxicity analysis of UV-A light illumination and NP-cIPTG on growth of *R. capsulatus* SB1003 wildtype cultures under phototrophic conditions

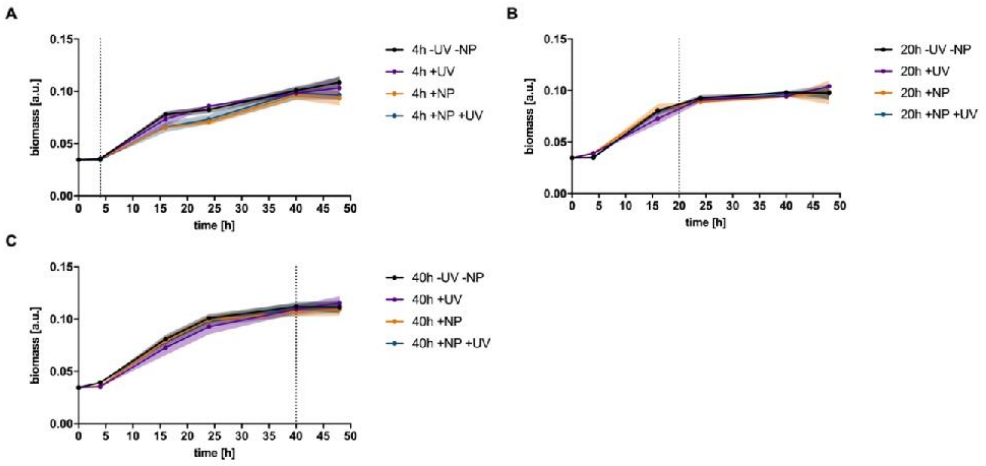

Figure S6: Cell growth during phototrophic cultivation of *R. capsulatus* SB1003 wildtype. Cells were grown over 48 h in RCV medium at 30°C in screw neck vials under NIR light (λ_{max} = 850 nm, 1.7 mW/cm^2). At the indicated time points, cultures were supplemented with photolysis product (NP) resulting in an end concentration of 1 mM (orange lines), illuminated with UV-A light at 365 nm (~2 mW/cm^2) for 30 min (purple lines). The photolysis product was generated by a complete uncaging of an NP-cIPTG solution under UV-A light. Simultaneously, cultures were incubated in the presence of UV-A light and photolysis products (blue lines). The time point of illumination and/or addition of NP-cIPTG photolysis products (4h, 20h, or 40h) are indicated by the dashed lines. *R. capsulatus* cells that have been cultivated phototrophically without UV-A exposure and addition of NP-cIPTG photoproducts were used as a corresponding control experiment (black lines). Cell growth was analyzed by determining the absorption at 660 nm using a Tecan Microplate reader. Values are means of individual biological triplicates. Error bars indicate the respective standard deviations.

DMNB-actinometry for photochemical monitoring of UV-A light exposure

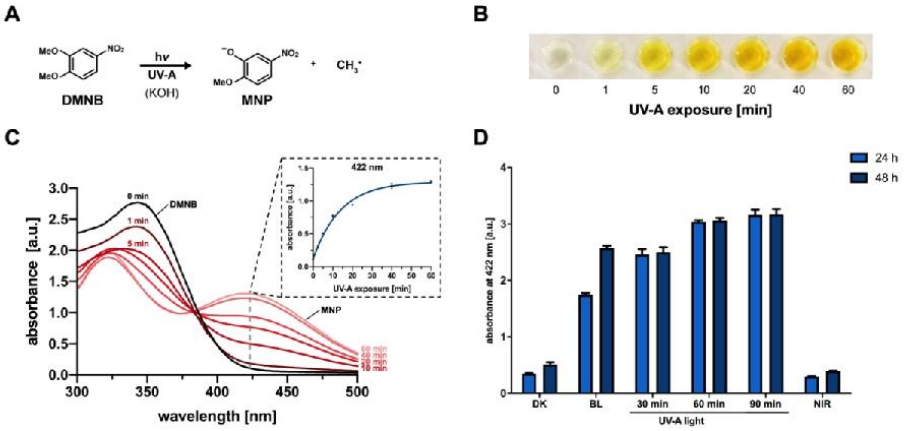

Figure S7: Photochemical monitoring of UV-A light exposure using DMNB actinometry. **(A)** Photochemical formation of 2-methoxy-5-nitrophenolate (MNP) from 1,2-dimethoxy-4-nitrobenzene (DMNB) using UV-A light in aqueous potassium hydroxide solution [8]. **(B)** Colorimetric changes of DMNB solution upon increased UV-A exposure. **(C)** Light-mediated conversion of DMNB (1.25 mM) after 0, 1, 5, 10, 20, 40 and 60 min of mid-power UV-A light exposure (5.4 mW/cm^2). The grey dashed line indicates respective maximal absorption differences of ΔA_{max}= 422 nm in the blue range; the insert shows the relation between absorbance at 422 nm and the duration of UV-A exposure. **(D)** Light-mediated formation of 2-methoxy-5-nitrophenolate (MNP) from a 1.25 mM DMNB solution in aqueous potassium hydroxide was determined spectrophotometrically *via* the increase of absorbance at 422 nm after illumination with bulb light (BL, 2500 lx) and NIR light (NIR, λ_{max} = 850 nm; 1.23 mW/cm^2) for 24 h or 48 h. DMNB photoconversion was compared to samples that have been exposed to UV-A light for 30–90 min (λ_{max} = 365 nm; 5.4 mW/cm^2) or kept unexposed (dark control, DK). Values are means of triplicate measurements. Error bars indicate the respective standard deviations.

Evaluation of NIR-light intensities for optimal phototrophic growth of *R. capsulatus* SB1003 expression cultures

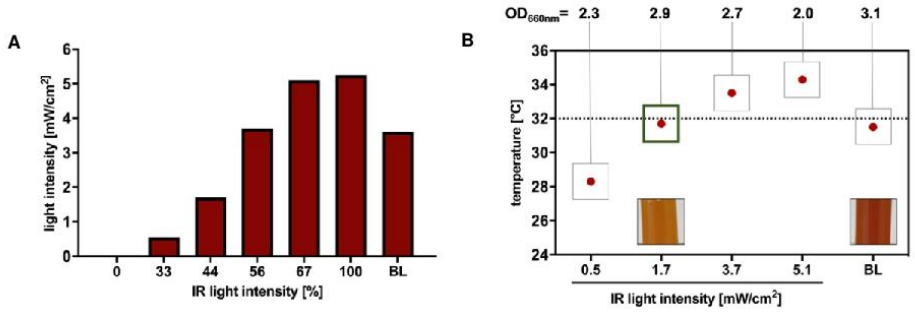

Figure S8: (**A**) Detected NIR light intensities [mW/cm^2] at λ_{max}= 850 nm of NIR panels from Vossloh-Schwabe [9] for increasing intensity settings, which can be set *via* a rotary knob with a continuous adjustment are shown in comparison to the NIR light amount of bulb light (BL) at λ_{max}= 850 nm. Light intensity quantifications were conducted using a Thermal Power Sensor (S302C, Thorlabs Inc, USA). (**B**) Medium temperature at suitable NIR light intensities after 48 h of cultivation and two pictures of corresponding *R. capsulatus* SB1003 cultures in the cultivation vessel as well as the respective optical density at 660 nm. The cultivation temperature of 33 °C should not be exceeded to avoid adverse effects on cell growth. The culture without any growth impairment and with the highest cell density is marked with a green frame and can be compared to cultures exposed with bulb light (BL).

For the determination of suitable NIR light intensities for efficient phototrophic growth of *R. capsulatus,* cells were cultivated with NIR light of increasing intensities ranging from 0.5 mW/cm^2 up to 5.1 mW/cm^2 (Figure S5 A) and analyzed with respect to their growth behavior (Figure S5 B). Screw neck vials, which were used as cultivation vessels, were placed in a distance of approx. 10 cm from each NIR panel. Adequately grown cultures without any sunken cells could only be detected for NIR light intensities of 1.7 mW/cm^2 and 3.1 mW/cm^2 represented by cell numbers corresponding to an optical density at 660 nm of 2.9 and 2.7, which are comparable to the optical density of cultures grown in bulb light (OD_{660nm}= 3.1). Lower or higher NIR light intensities led to decreased cell densities and unequally distributed cultures with sunken cells indicating a hampered cell viability. Presumably, this was on the one hand due to the insufficient exposure intensity and on the other hand due to the excessively high temperature of over 33 °C in the cultivation medium for the highest NIR light intensity. For all following experiments, an NIR light intensity of 1.7 mW/cm^2 was chosen as this condition offers an appropriate medium temperature and the highest cell density after 48 h.

Influence of increasing IPTG concentrations on the carotenoid production in NIR-illuminated *R. capsulatus* SB1003 *ΔcrtEF* cells harboring an expression plasmid carrying *crtEF* genes under P_{tac} control

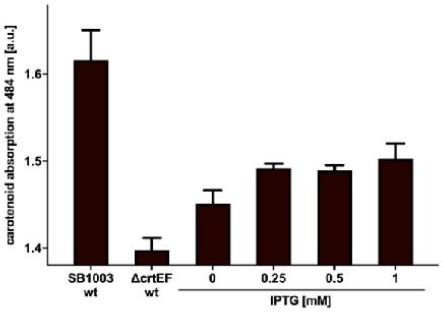

Figure S9: Carotenoid absorption at 484 nm of *R. capsulatus* SB1003 *ΔcrtEF*/ pRholtHi-crtE-crtF (L-crtEF) supplemented with IPTG concentrations ranging from 0 to 1 mM are shown in comparison to the respective absorption of *R. capsulatus* SB1003 wildtype (SB1003 wt) cell extracts. In addition, *R. capsulatus* SB1003 *ΔcrtEF* (*ΔcrtEF* wt) cultures were likewise analyzed after 48 h of phototrophic cultivation (RCV medium, 30 °C, screw neck vials, NIR light (λ_{max} = 850 nm, 1.7 mW/cm^2)). Induction was performed after a cultivation time of 6 h *via* addition of IPTG. Carotenoid absorption values are normalized to the cell densities. Values are means of individual biological triplicates. Error bars indicate the respective standard deviations.

DNA sequences of P_{tac} promoter regions including their RBS, RBS-spacers and/or MCS

pEKEx-2:

P_{tac} promoter SD lac operator

TTGACAATTAATCATCGGCTCGTATAATGTGTGGAA**TTGTGAGCGGATAACA**
ATTTCACAC**AGGAA**ACAGAATTAAAAGATATGACCATGATTACGCC**AAGCTTGC**
ATGCCTGCAGGTCGACTCTAGAGGATCCCCGGGTACCGAGCTCGAATTC

pUC18/19 MCS **BamHI**

pRholHi-2-eYFP and pRholHi-2_Δlac-eYFP:

P_{tac} promoter SD lac operator

TTGACAATTAATCATCGGCTCGTATAATGTGTGGAA**TTGTGAGCGGATAACA**
ATTTCACAC**AGGAA**ACAGAATTAAAAGAT**ATG**ACC**ATG**ATTACGCC**AAGCTTGC**
ATGCCTGCAGGTCGACTCTAGAGGATCCA**AGGAG**ATATAGAT**ATG**-*eyfp*

pUC18/19 MCS **BamHI** **optimized SD**

8 bp RBS-spacer (between Shine-Dalgarno sequence and start codon)

pRholtHi-eYFP:

P_{tac} promoter lac operator

TTGACAATTAATCATCGGCTCGTATAATGTGTGGAA**TTGTGAGCGGATAACA**
ATTTCACA**AGGAG**GTATTCAT**ATG**-*eyfp*

optimized SD **NdeI**

Optimized 8 bp RBS-spacer (between Shine-Dalgarno sequence and start codon)

DNA sequence of CrtE and CrtF from *R. capsulatus* SB1003 for cIPTG-mediated expression in *R. capsulatus* cultures

The shown sequence encompasses the *crtE* (red bases) and *crtF* gene (blue bases) referring to the mRNA sequence published in GenBank: CP001312.1, encoding the GGPP synthase CrtE and the demethylspheroidene O-methyltransferase CrtF (UniProtKB: P17060 and P17061, respectively). The sequence was optimized using a 6 bp RBS-spacer between the Shine-Dalgarno sequence and start codon.

[...]lacO **RBS** **opt. SD** **Start** *crtE*
TAACAATTTCAC**AAGGAGGTTTCATATG**TCTCTGGATAAACGTATCGAGTCGGC
GCTGGTCAAGGCGCTGTCACCCGAGGCTTTGGGTGAATCTCCGCCGTTGCTTGCC
GCCGCGCTGCCTTACGGGGTGTTTCCCGGCGGCGCGCGGATCCGGCCGACGATCC
TTGTCTCGGTCGCGCTCGCCTGTGGCGACGATTGCCCGGCGGTCACCGATGCCGC
GGCCGTGGCGCTGGAGCTGATGCATTGCGCGAGCCTCGTGCATGACGATCTGCCC
GCCTTCGACAATGCCGACATCCGGCGCGGCAAGCCGAGCCTTCACAAGGCCTATA
ATGAACCGCTTGCGGTTCTGGCGGGCGACAGCCTGCTGATCCGCGGCTTCGAAGT
GCTGGCCGATGTCGGCGCCGTCAACCCGGACCGGGCGCTGAAGCTGATCTCGAA
ACTGGGTCAGCTGTCGGGGGCGCGCGGCGGGATCTGCGCCGGTCAGGCCTGGGA
AAGCGAATCCAAGGTCGATCTGGCCGCCTATCATCAGGCGAAGACCGGGGCGCT
GTTCATTGCCGCGACCCAGATGGGGGCGATTGCGGCGGGCTACGAGGCCGAACC
CTGGTTCGATCTGGGCATGCGGATCGGCTCGGCCTTCCAGATCGCCGACGACCTG
AAAGACGCGCTGATGTCGGCCGAGGCAATGGGCAAGCCCGCCGGGCAGGACATC
GCGAACGAACGCCCGAATGCGGTCAAGACGATGGGCATCGAGGGCGCGCGCAAA
CATCTGCAAGATGTGCTGGCGGGGGCGATCGCCTCGATCCCGTCCTGCCCCGGTG
AGGCGAAGCTGGCCCAGATGGTGCAGCTTTACGCCCACAAGATCATG
Stop **Start** *crtF*
GACATCCCGGCCAGCGCCGAGAGGGGC**TGA**TC**GTG**CCGAAGGACGACCACACG
GGCGCGACGGCCGACCGGACCGCGCAGCCGACAGGAACGGGAAAGCAGCCGCT
GGTTCCGGGCCAGCCCGGGGCGGCGCCGGTGCAGCCGGGGCGGGTGAATTTCTTC
ACCCGGATCGCGCTGTCGCAACGGCTGCATGAAATCTTCGAACGCCTGCCGCTGA
TGAACCGCGTCACCCGGCGCGAGGGCGAGGCGCTCTTCGACATCGTTTCGGGCTT
CGTGCAAAGCCAGGTTCTCTTGGCGATCGTCGAATTCCGGGTGCTGCATATTCTG
GCCGGGGCCTCTTGGCCCTTGCCGCAACTGGCCGAACGCACCGGCCTGGCCGAGG
ACCGGCTGGCGGTGCTGATGCAGGCCGCCGCCGCCTTGAAGCTGGTGAAATTCCG
CCGCGGTCTGTGGCAGCTTGCCCCGCGTGGCGCCGCCTTCATCACCGTGCCAGGG
CTCGAGGCGATGGTGCGCCATCACCCCGTCCTTTACCGCGATCTGGCCGATCCGG
TGGCTTTTCTGAAAGGCGACATCGAACCCGAGCTGGCGGGCTTCTGGCCCTATGT
CTTCGGGCCGCTGGCGCAGGAAGATGCGGGGCTCGCCGAGCGCTATTCGCAGCTG
ATGGCCGACAGCCAGCGCGTCGTGGCCGATGACACCTTGCGGCTTGTCGATCTGC
GCGATGCCAAGCGGGTGATGGATGTGGGCGGCGGCACCGGGGCCTTCCTGCGCG
TCGTGGCCAAGCTTTACCCCGAGCTGCCCTTGACGCTGTTCGACCTGCCGCATGTG
CTGTCGGTGGCGGACCGCTTCAGCCCGAAGCTCGATTTCGCGCCGGGCAGCTTCC
GCGACGATCCGATCCCGCAGGGCGCCGATGTCATCACTTTGGTGCGCGTGCTGTA
TGACCATCCTGACAGCGTCGTCGAACCGCTTCTGGCCAAGGTGCATGCCGCCTTG
CCGCCGGGCGGGCGTCTGATCATCTCGGAGGCGATGGCGGGGGGCGCAAAACCC
GACCGTGCCTGCGATGTCTATTTCGCCTTCTACACGATGGCGATGAGTTCGGGGC
GCACGCGTTCCCCCGAAGAGATCAAGCAAATGCTTGAAAAAGCTGGGTTCACCA
AGGTGTCGAAACCGCGGACCCTGCGCCCCTTCATCACCTCGGTGATCGAGGCCGA
ACGCGGC**TGA**
Stop

Determination of photocaged compound purity by qNMR

Table S2: Compound purities determined by qNMR.

Compound	Purity [%]
NP-cIPTG	88.9 ± 3.4
BEC-cIPTG	90.7 ± 1.3
BC-cIPTG	79.6 ± 1.8

The spectral and (photo-)chemical properties (solubility, absorption maximum, molar extinction coefficient, uncaging quantum yield, uncaging half-life time) of the photocaged compounds NP-cIPTG, BEC-cIPTG and BC-cIPTG have been reported previously [10].

References

1. Hanahan, D. Studies on transformation of *Escherichia coli* with plasmids. *J. Mol. Biol.* **1983**, *166*, 557–580, doi:10.1016/S0022-2836(83)80284-8.

2. Simon, R.; Priefer, U.; Pühler, A. A Broad host range mobilization system for *in vivo* genetic engineering: transposon mutagenesis in gram-negative bacteria. *Bio/Technology* **1983**, *1*, 784–791, doi:10.1038/nbt1183-784.

3. Strnad, H.; Lapidus, A.; Paces, J.; Ulbrich, P.; Vlcek, C.; Paces, V.; Haselkorn, R. Complete genome sequence of the photosynthetic purple nonsulfur bacterium *Rhodobacter capsulatus* SB1003. *J. Bacteriol.* **2010**, *192*, 3545–6, doi:10.1128/JB.00366-10.

4. Hage-Hülsmann, J.; Metzger, S.; Wewer, V.; Buechel, F.; Troost, K.; Thies, S.; Loeschcke, A.; Jaeger, K.-E.; Drepper, T. Biosynthesis of cycloartenol by expression of plant and bacterial oxidosqualene cyclases in engineered *Rhodobacter capsulatus*. *J. Biotechnol.* **2019**, *4*, 100014, doi:10.1016/j.btecx.2020.100014.

5. Binder, D.; Grünberger, A.; Loeschcke, A.; Probst, C.; Bier, C.; Pietruszka, J.; Wiechert, W.; Kohlheyer, D.; Jaeger, K.-E.; Drepper, T. Light-responsive control of bacterial gene expression: precise triggering of the *lac* promoter activity using photocaged IPTG. *Integr. Biol.* **2014**, *6*, 755–765, doi:10.1039/C4IB00027G.

6. Sambrook, J.; Fritsch, E.F.; T. Maniatis *Molecular cloning : a laboratory manual.*; Cold Spring Habor Laboratory Press, New York., **1989**.

7. Salis, H. M.; Mirsky, E. A.; and Voigt, C. A. *Automated design of synthetic ribosome binding sites to control protein expression*. Nat. Biotechnol. **2009**, 27, 946–950. doi:10.1038/nbt.1568.

8. Zhang, J.-Y., Esrom, H., and Boyd, I. W. UV intensity measurement of 308 nm excimer lamp using chemical actinometer. *Appl. Surf. Sci.* **1999**;138–139, 315–319. doi:10.1016/S0169-4332(98)00412-7.

9. Hilgers, F.; Habash, S.S.; Loeschcke, A.; Ackermann, Y.S.; Neumann, S.; Heck, A.; Klaus, O.; Hage-Hülsmann, J.; Grundler, F.M.W.; Jaeger, K.-E.; Schleker, A.S.S.; Drepper, T. Heterologous production of β-caryophyllene and evaluation of its activity against plant pathogenic fungi. *Microorganisms*. **2021**;9. doi:10.3390/microorganisms9010168

10. Hogenkamp, F.; Hilgers, F.; Knapp, A.; Klaus, O.; Bier, C.; Binder, D.; Jaeger, K. E.; Drepper, T. & Pietruszka, J. Effect of photocaged isopropyl β-D-1-thiogalactopyranoside solubility on the light responsiveness of LacI-controlled expression systems in different bacteria. *ChemBioChem*. **2021**;22: 539–547. doi:10.1002/cbic.202000377

II.2.2 New expression systems for light-controlled gene expression in bacteria

PUBLICATION V

Effect of photocaged Isopropyl β-D-1-thiogalactopyranoside solubility on light-responsiveness of LacI-controlled expression systems in different bacteria

Fabian Hogenkamp[1]*, Fabienne Hilgers[2]*, Andreas Knapp[2], **Oliver Klaus**[2], Claus Bier[1], Dennis Binder[2], Karl-Erich Jaeger[2,3], Thomas Drepper[2#] and Jörg Pietruszka[1,3#]

[1]Institute of Bioorganic Chemistry, Heinrich Heine University Düsseldorf, Forschungszentrum Jülich, 52425 Jülich, Germany

[2]Institute of Molecular Enzyme Technology, Heinrich Heine University Düsseldorf, Forschungszentrum Jülich, 52425 Jülich, Germany

[3]Institute of Bio- and Geosciences IBG-1: Biotechnology, Forschungszentrum Jülich GmbH, 52425 Jülich, Germany

* These authors contributed equally

[#] Corresponding authors

Status: published

ChemBioChem,

2021, 02, 22, (3):539-547

https://doi.org/10.1002/cbic.202000377

Own contribution:

Designing and performing *in vivo* experiments, analyzing data, editing manuscript

ChemBioChem
Full Papers
doi.org/10.1002/cbic.202000377
Chemistry Europe
European Chemical Societies Publishing

Effect of Photocaged Isopropyl β-D-1-thiogalactopyranoside Solubility on the Light Responsiveness of LacI-controlled Expression Systems in Different Bacteria

Fabian Hogenkamp[+],[a] Fabienne Hilgers[+],[b] Andreas Knapp,[b] Oliver Klaus,[b] Claus Bier,[a] Dennis Binder,[b] Karl-Erich Jaeger,[b, c] Thomas Drepper,*[b] and Jörg Pietruszka*[a, c]

Photolabile protecting groups play a significant role in controlling biological functions and cellular processes in living cells and tissues, as light offers high spatiotemporal control, is non-invasive as well as easily tuneable. In the recent past, photoresponsive inducer molecules such as 6-nitropiperonyl-caged IPTG (NP-cIPTG) have been used as optochemical tools for Lac repressor-controlled microbial expression systems. To further expand the applicability of the versatile optochemical on-switch, we have investigated whether the modulation of cIPTG water solubility can improve the light responsiveness of appropriate expression systems in bacteria. To this end, we developed two new cIPTG derivatives with different hydrophobicity and demonstrated both an easy applicability for the light-mediated control of gene expression and a simple transferability of this optochemical toolbox to the biotechnologically relevant bacteria *Pseudomonas putida* and *Bacillus subtilis*. Notably, the more water-soluble cIPTG derivative proved to be particularly suitable for light-mediated gene expression in these alternative expression hosts.

Introduction

In general, optogenetics combines genetic and optical methods to allow fast control of cellular functions with high spatiotemporal resolution and in a non-invasive fashion.[1] The control over gene expression by light can basically be realised by employing genetically encoded photoreceptors or chemically photocaged (bio)molecules. Recombinant photoreceptors are typically based on light-responsive two- or one-component systems, are extensively studied and have been successfully employed as reversible photoswitches for light-mediated *in vivo* signal transduction in various biological applications.[2]

Besides the use of photoreceptors photolabile protecting groups were established as optochemical tools for a variety of diverse applications.[3] In recent years, many approaches were published, in which photocaged compounds have been used for controlling different cellular processes, ranging from cell signalling,[3b,4] over drug delivery[5] to gene expression.[6] In this context, especially 2-nitrobenzyl-photocaging groups (NB) and their derivatives such as 6-nitropiperonyl (NP) were commonly used to mediate an adequate and well-characterised UV-A light-triggered release of bioactive molecules.[3d,7] To implement caged compounds as versatile optochemical switches, a variety of photolabile protecting groups has been developed focusing on the i) redshifted absorption,[3b,8] ii) higher quantum yields[9] and iii) an improved solubility.[10] Especially for *in vivo* approaches an excellent stability towards enzymatic hydrolysis, good biocompatibility, and low overall toxicity of caged compounds (also including the photolysis products) are indispensable.[11] In addition, the extend of the caged compound's solubility could further modulate their ability to pass bacterial cell membranes either through passive processes including free diffusion and porin-based uptake or by active, membrane transporter-mediated processes.[12]

In the recent past, photoresponsive inducer molecules such as caged derivatives of doxycycline,[13] isopropyl β-D-thiogalactopyranoside (IPTG)[6a,b] or several other carbohydrates[6c,d] have been used as irreversible optochemical switches for appropriate microbial expression systems. Especially the applicability of 6-nitropiperonyl photocaged IPTG (NP-cIPTG, **1**) for bioengineering approaches using *Escherichia coli*[14] and *Corynebacterium glutamicum*[15] as production hosts could be demonstrated. However, a further expansion of the applicability in different expression hosts was for instance hindered by the low water-

[a] F. Hogenkamp,[+] Dr. C. Bier, Prof. Dr. J. Pietruszka
Institute of Bioorganic Chemistry
Heinrich Heine University Düsseldorf at Forschungszentrum Jülich
Stetternicher Forst, 52426 Jülich (Germany)
E-mail: j.pietruszka@fz-juelich.de
[b] F. Hilgers,[+] Dr. A. Knapp, O. Klaus, Dr. D. Binder, Prof. Dr. K.-E. Jaeger, Dr. T. Drepper
Institute of Molecular Enzyme Technology
Heinrich Heine University Düsseldorf at Forschungszentrum Jülich
Stetternicher Forst, 52426 Jülich (Germany)
E-mail: T.Drepper@fz-juelich.de
[c] Prof. Dr. K.-E. Jaeger, Prof. Dr. J. Pietruszka
Institute of Bio- and Geosciences (IBG-1: Biotechnology)
Forschungszentrum Jülich
Stetternicher Forst, 52426 Jülich (Germany)
[+] These authors contributed equally to this work.

Supporting information for this article is available on the WWW under https://doi.org/10.1002/cbic.202000377

ChemBioChem
Full Papers
doi.org/10.1002/cbic.202000377
Chemistry Europe
European Chemical Societies Publishing

solubility of NP-cIPTG (**1**; 0.7 mM), as appropriately high inducer concentrations were not soluble in the cultivation medium.

Derivatives of the 2-nitrobenzyl group with improved solubility in aqueous media have been applied before (Figure 1 A). Tsien and co-worker as well as Ni *et al.* conceived a 4,5-bis (carboxymethoxy)-2-nitrobenzyl protecting group (BC, **2**), which they stated to be highly water-soluble.

However, they masked the carboxylate **2** as acetoxymethyl ester **3** to facilitate diffusion across cell membranes.[12a,b] Russell *et al.* published a similar derivative **4**, but bearing an additional third carboxy group in the benzylic position, for the synthesis of photolabile tyrosine, whereby a solubility of at least 30 mM was reached.[10b] As the formation of a dioxolane is required for the protection of IPTG, previously reported α-carboxy-2-nitrobenzyl (α-CNB, **5**–**8**) photocages[10a,c,16] were not considered, because the α-carboxy-group increases solubility, but concurrently blocks the position where the dioxolane is later formed.

Based on these results the BC protecting group **2** was chosen in this work as a candidate for the synthesis of a charged, highly water-soluble photocaged IPTG derivative (Figure 1 B) and was further applied to determine the influence of the solubility and the charge on the inducer uptake through the cell membrane and the resulting expression response. In addition, the 4,5-bis(ethoxycarbonylmethoxy)-2-nitrobenzyl protecting group (BEC, **9**) harbouring lipophilic ester moieties, was selected as an alternative caging group, which might facilitate its passive diffusion across cell membranes. Afterwards, enzymatic hydrolysis of the ester moiety could lead to intracellular accumulation.[12c] To comparatively analyse the effect of caged inducer solubility on light dependent control of gene expression in bacteria, the two new cIPTG derivatives BEC-cIPTG (**10a**, derived from **9**) and BC-cIPTG (**10b**, derived from **2**) were synthesised and the maximum solubility was quantified. The photophysical properties as well as photolysis in aqueous media were characterised. Subsequently, the *in vivo* applicability of the newly synthesised compounds for light-inducible gene expression was analysed in comparison to the well-established NP-cIPTG (**1**) in *E. coli* in a time-resolved manner. Finally, we investigated whether optochemical control of gene expression can also be implemented in the alternative expression hosts *Pseudomonas putida* and *Bacillus subtilis*, which exhibit individual morphological and physiological properties. Therefore, we used the photocaged IPTG derivatives **1**, **10a**, and **10b** together with appropriate LacI repressor-controlled expression systems and comparatively evaluated their light-responsiveness.

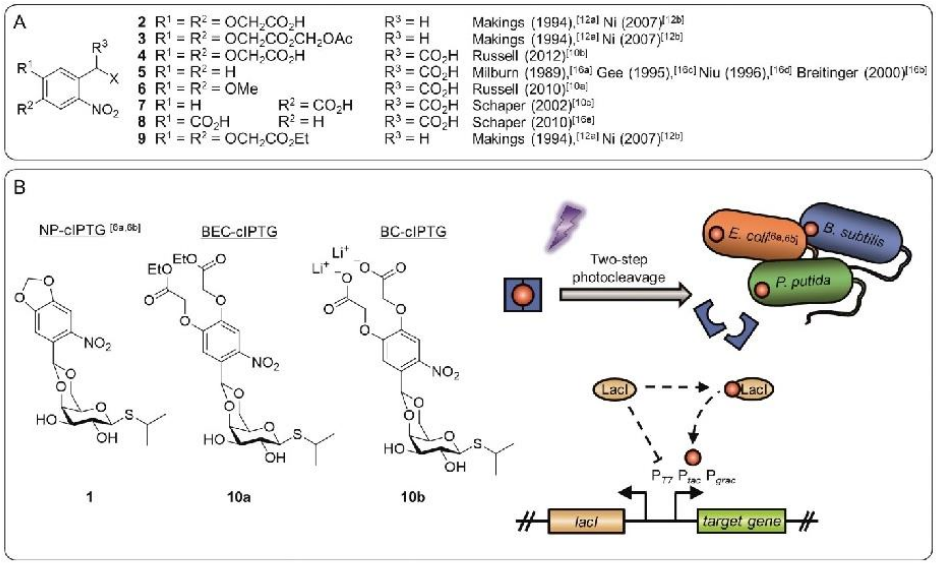

Figure 1. Photolabile protection groups and their application in this work. A) A variety of previously published photolabile protection groups with improved aqueous solubility or membrane permeability based on the NB photocaging group. B) Three photolabile protection groups were used in this work to construct the photocaged IPTG variants NP-cIPTG (**1**), BEC-cIPTG (**10a**) and BC-cIPTG (**10b**), strongly differing in their water solubility. These caged inducer molecules (red dot with blue frame) are biologically inactive; however, upon illumination with UV-A light, their activity can be restored by a two-step cleavage process. Subsequently, the IPTG binds the repressor protein LacI releasing LacI from the P_{T7}, P_{tac} or P_{grac} promoter and thus inducing gene expression. This principle was applied to analyse the effect of cIPTG solubility on the inducibility of LacI repressor-controlled target gene expression in *E. coli*, *P. putida*, and *B. subtilis*.

ChemBioChem
Full Papers
doi.org/10.1002/cbic.202000377
Chemistry Europe
European Chemical Societies Publishing

Results

Synthesis and photochemical properties of cIPTGs

The BC-cIPTG (**10b**) was synthesised in a three-step reaction (Scheme 1; yield over three steps: 24%) from 4,5-bis (ethoxycarbonylmethoxy)-2-nitrobenzaldehyde (**11**), which was obtained following the previously reported procedure by Ni *et al.* (see the Supporting Information).[12b] The 2-nitrobenzaldehyde derivative **11** was reacted with triethyl orthoformate to form the corresponding acetal **12** in 89% yield, which then was converted to BEC-cIPTG (**10a**; 45%) in a transacetalisation, as the direct acetalization was not feasible. In this step the triethyl orthoformate was preferred to the trimethyl orthoformate due to the occurrence of transesterification during the acid-catalysed reaction, which was leading towards a mixture of products. After deprotection under basic conditions the BC-cIPTG (**10b**) could be obtained in 59% yield as the corresponding lithium-salt, which promised advantageous solubility properties compared to the free-acid. NP-cIPTG (**1**) was synthesised from 6-nitropiperonal (**13**) according to literature procedures.[6a,b] The purity of BEC-cIPTG (**10a**), BC-cIPTG (**10b**) and NP-cIPTG (**1**) was determined by qNMR (Table S3 in the Supporting Information).

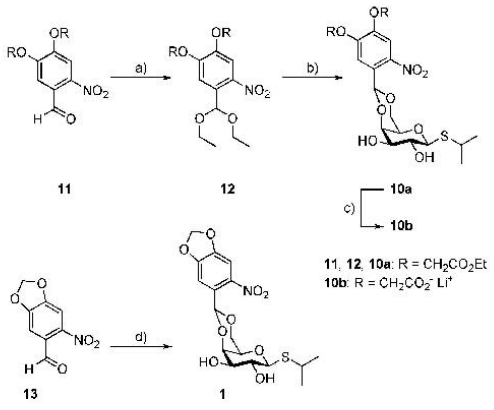

Scheme 1. Synthesis of BEC-, BC- and NP-photocaged IPTGs **10a**, **10b** and **1**: a) Triethyl orthoformate, pyridinium *p*-toluenesulfonate, ethanol, reflux, 19 h (89%); b) IPTG, *p*-toluenesulfonic acid, CH_2Cl_2, RT, 20 h (45%); c) 0.2 M LiOH (aq.), MeOH, 0 °C–RT, 1 h (59%); d) IPTG, sulfuric acid, DMSO, 0 °C–RT, 24 h (21%).

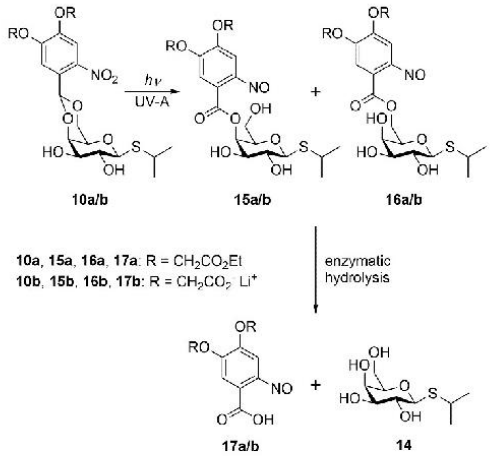

Scheme 2. Two-step release sequence after photolysis of BEC- and BC-photocaged IPTG **10a** and **10b** by irradiation with UV-A light and a subsequent enzymatic hydrolysis by a microbial esterase, as previously described.[6a,b]

Due to the structural similarity of the newly synthesised caged compounds **10a** and **10b** to the NP-cIPTG (**1**), IPTG (**14**) should be released upon UV-A light exposure in a two-step photocleavage reaction as previously described.[6a,b] In the first step the irradiation with UV-A light leads to the formation of ester intermediates **15** and **16**, which might subsequently be cleaved by a microbial esterase. The corresponding nitroso compounds **17** are formed as the photo by-product (Scheme 2).

The *in vitro* characterisation (Tables 1 and S2, Figures S1–S3) of the new photocaged compounds **10a** and **10b** showed uncaging quantum yields (Φ_u) and molar extinction coefficients (ε) in the range of previously reported caged compounds.[6d,17] The resulting photolytic efficiencies ($\varepsilon\Phi_u$) are all in the same order of magnitude. However, more importantly the uncaging half-life time of the photolytic cleavage amounts to 2.2 min for BEC-cIPTG (**10a**), 3.5 min for BC-cIPTG (**10b**), and 3.4 min for NP-cIPTG (**1**). This underlines the fast formation of the ester intermediates **15** and **16** (Figure S4, Table S2). Full photoconversion of the cIPTG variants (1 mM) by irradiation with UV-A light (375 nm, 6.4 mW cm^{-2}) was achieved in less than 30 min for **10a** and **1**. For derivative **10b** about ~5% of the starting material remained after irradiation for 30 min (Figure S15).

The BC-cIPTG (**10b**) showed a maximum solubility of 147 mM in deionised and degassed water, which is over 200 times higher than the maximum solubility of NP-cIPTG (**1**),[6b] but only ~8% of the maximum solubility of IPTG (**14**) itself (Table 1). Other previously reported photocaged carbohydrates were in the range of 4–58 mM.[6d] In contrast, the BEC-

Table 1.

Compound	λ_{max} [nm]	ε[a] [M^{-1}cm^{-1}]	$t_{0.5}$[b] [min]	s[c] [mM]	Φ_u[d]	$\varepsilon\Phi_u$[a] [M^{-1}cm^{-1}]
1[e]	241 336	1690	3.4	0.7	0.50	845
10a[e]	298	1810	2.2	<0.1	0.68	1230
10b[f]	242 340	3543	3.5	147	0.46	1630
14	204	–	–	1941	–	–

[a] ε = molar extinction coefficient at λ = 375 nm. [b] $t_{0.5}$ = uncaging half-life time. [c] *s* = solubility in deionised and degassed water. [d] Φ_u = uncaging quantum yield upon 375 nm irradiation. [e] measured in MeOH. [f] measured in sodium phosphate buffer (0.1 mM, pH 7.5).

ChemBioChem
Full Papers
doi.org/10.1002/cbic.202000377
Chemistry Europe
European Chemical Societies Publishing

cIPTG (**10a**) displayed a more than 7-times lower solubility of <0.1 mM, as expected due to the ester-protected carboxylic acids. Since the possible higher membrane permeability of BEC-cIPTG might result in an improved *in vivo* applicability, this cIPTG derivative was additionally used for further investigations.

Applicability of cIPTGs for light-controlled gene expression in bacteria

After the successful synthesis of BEC- and BC-cIPTG (**10a** and **10b**), we next analysed whether the different solubility of the cIPTG derivatives (solubility in aqueous solvents: **10b** ≫ **1** > **10a**, see Table 1) affect the inducibility of LacI repressor-controlled expression systems. The regulatory system, which originally controls the lactose consumption in *E. coli*, is one of the most often used regulation mechanisms for triggering heterologous gene expression in this host.[18] The development of different recombinant promoters (e.g., P_{tac}, P_{trc}, P_{T7}), whose activities can be tightly and gradually controlled by the concentration of the added inducer (e.g., the non-hydrolysable lactose analogue IPTG) led to its broad applicability in basic research and biotechnological production processes. Furthermore, the development of light-responsive NP-cIPTG (**1**) allowed for non-invasive light-mediated control of gene expression in *E. coli*.[6a–c] To further optimise light responsiveness of this promising optochemical on-switch in *E. coli* and to facilitate its transferability to other industrially relevant microbes, we used the following Gram-negative and -positive bacteria as appropriate model hosts offering individual morphological and physiological properties: i) *E. coli* Tuner(DE3) is a lactose permease-deficient strain and was shown to be well suited for NP-cIPTG-based light control of gene expression, because the uptake of appropriate inducers is solely dependent on passive diffusion processes. Previous studies using *E. coli* Tuner(DE3) revealed a very stringently controlled and homogeneous gene expression that gradually responded to changes of illumination time or light intensity.[6b,c,14] ii) *P. putida* KT2440 is a rod-shaped, Gram-negative soil bacterium, which offers a pronounced tolerance towards xenobiotics[19] as well as redox stress.[20] Besides its genetic accessibility and its FDA certification as a host-vector biosafety system,[21] *P. putida* exhibits an extraordinary versatile metabolism that makes it especially suited for a variety of biotechnological applications including the production of various high-value natural products and their derivatives.[22] iii) *Bacillus subtilis* DB430 is a Gram-positive bacterium commonly used as a "microbial cell factory" for high-level production and secretion of proteins for industrial applications.[23] In contrast to the Gram-negative bacteria used in this study, *B. subtilis* possesses a more rigid and thick cell wall which might act as an additional diffusion barrier for the photocaged IPTG molecules, but lacks an outer membrane. For all the here tested bacterial hosts, expression systems encompassing LacI-controlled, IPTG-inducible promoters have been successfully established in recent studies (Table S1).[6b,18, 22c, 24]

To exclude detrimental effects of the new caged inducers or UV-A light exposure on cell viability, we first analysed the growth of *E. coli*, *P. putida* and *B. subtilis* cells in the presence of the cIPTG derivatives **10a** and **10b** as well as their corresponding photoproducts in comparison to conventional IPTG (**14**). For these studies, we used inducer concentrations that were sufficient to fully induce reporter gene expression in the respective expression hosts (Figure S5). Comparative growth of all strains clearly demonstrated that UV-A light exposure (30 min, 365 nm, ~1 mW cm^{-2}) did not lead to considerable growth impairments in the presence (Figure S6) or absence (Figure S7) of IPTG (**14**) and its photocaged derivatives **1**, **10a** and **10b**. Furthermore, the stability of **1**, **10a** and **10b** were analysed by measuring the fluorescence intensity of cultures in the dark (Figure S6 A). The data clearly reveals a pronounced *in vivo* stability of the new cIPTG derivatives **10a** and **10b** over 20 h in LB medium at 30 °C.

Expression studies in E. coli: To further evaluate the applicability of the new cIPTG derivatives **10a** and **10b** in comparison to **1** in *E. coli*, we used the well-established strain *E. coli* Tuner (DE3) carrying the eYFP expression vector pRhotHi-2-lacI-EYFP.[6b,14] Initially, we could observe that, in contrast to the variants **1** and **10a** which form an emulsion-like structure at relevant concentrations in LB medium without considerable amounts of ethanol or DMSO, variant **10b** can be completely dissolved in the cultivation medium, superseding the use of additional solvents. To compare the UV-A light-induced gene expression mediated by differently soluble photocaged IPTG variants during *E. coli* cultivation, light exposure was carried out for 30 min in order to ensure sufficient photoconversion of **1**, **10a** and **10b** (Figure S4). First, the general applicability of cIPTG variants was evaluated by analysing eYFP expression in cultures that reached the stationary growth phase. As shown in Figure 2A, illumination of the already established NP-cIPTG resulted in comparable eYFP expression levels as in the control experiment, where conventional IPTG (**14**) was added. In contrast, the new water-soluble BC-cIPTG (**10b**) and the more hydrophobic BEC-cIPTG (**10a**) led to a slight decrease of reporter gene expression in this experimental setup.

To analyse the properties of the cIPTG variants in more detail, eYFP expression was subsequently online monitored during batch cultivation of *E. coli*. Illumination of BC-cIPTG (**10b**) resulted in the fastest induction response in the early logarithmic growth phase (~4–7 h after inoculation) as also indicated by a lower half-maximal responsiveness with $t_{0.5\ final}$ = 4.16 h when compared to NP-cIPTG (**1**) and BEC-cIPTG (**10a**; $t_{0.5\ final}$ = 4.41 and 4.51 h, respectively, Table S4 and Figure S8). Thus, these results give a first indication that NB caging group derivatives with improved water-solubility such as BC might slightly facilitate the overall uptake of cIPTG in *E. coli*. However, the lower final eYFP expression levels in the respective cultures point to a less efficient enzymatic release of IPTG from ester intermediates **15** and **16**, which is eventually caused by the increasing size of these photolabile protecting groups. All in all the differential solubility of tested cIPTG variants in aqueous solvents seems to play a minor role for optochemical *in vivo* applications in *E. coli*, since only marginal differences of light-controlled gene expression could be observed.

ChemBioChem
Full Papers
doi.org/10.1002/cbic.202000377
Chemistry Europe
European Chemical Societies Publishing

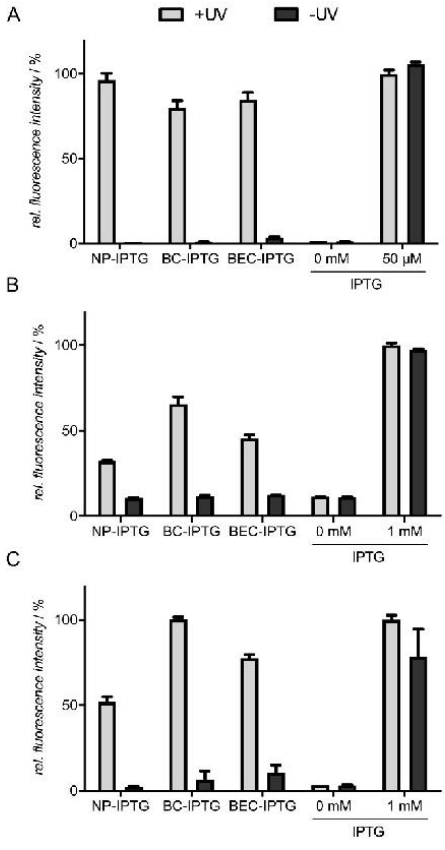

Figure 2. Light-controlled gene expression in A) *E. coli* Tuner(DE3)/pRhotHi-2-lacI-EYFP, B) *P. putida* KT2440/pVLT33-GFPmut3 and C) *B. subtilis* DB430/pHT01-sfGFP using NP-, BC-, and BEC-cIPTG. A) *In vivo* eYFP fluorescence (λ_{ex} = 508 nm, λ_{em} = 532 nm) of *E. coli* cultures supplemented with 50 µM of each cIPTG variant is shown in relation to a 50 µM IPTG (**14**) after 20 h (stationary growth phase). Induction was performed after 2.5 h by UV-A light exposure at 365 nm (~1 mW cm^{-2}) for 30 min or the addition of 50 µM **14**. B) *In vivo* GFPmut3 fluorescence (λ_{ex} = 508 nm, λ_{em} = 532 nm) of *P. putida* cultures supplemented with 1 mM of each cIPTG variant is shown in relation to a 1 mM IPTG (**14**) control after 20 h (stationary growth phase). Induction was performed after 3 h by UV-A light exposure at 365 nm (~1 mW cm^{-2}) for 30 min or the addition of 1 mM **14**. C) *In vivo* sfGFP fluorescence (λ_{ex} = 488 nm, λ_{em} = 520 nm) of cultures supplemented with 1 mM of each cIPTG variant is shown in relation to a 1 mM IPTG (**14**) control after 20 h. Induction was performed after 5 h by UV-A light exposure at 365 nm (~1 mW cm^{-2}) for 30 min or the addition of 1 mM **14**. *In vivo* fluorescence intensities were normalized to cell densities, and values are means of triplicate measurements. Error bars indicate the standard deviations.

Expression studies in P. putida: Next, we analysed whether the optochemical cIPTG/LacI system can be transferred to the Gram-negative bacterium *P. putida* KT2440 and if the solubility of the caged inducer has an effect on its *in vivo* applicability. In the following experiments, we used *P. putida* KT2440 carrying the expression vector pVLT33 harbouring a GFPmut3 gene, which is under control of the P_{tac} promoter (Table S1), and the same experimental setup as established for reference strain *E. coli* Tuner(DE3).

Because we could observe only basal induction of gene expression when 50 µM IPTG (**14**) was added to *P. putida* expression cultures (Figure S5), 1 mM of each IPTG derivative was used. As depicted in Figure 2B, the comparison of GFPmut3 fluorescence in *P. putida* cultures that reached the stationary growth phase demonstrates an induction of reporter gene expression of about 70% for BC-cIPTG (**10b**) when compared to conventional IPTG (**14**). In contrast, the use of NP- and BEC-cIPTG (**1** and **10a**) led to a lower induction response of ~50% or less. For BC-cIPTG (**10b**) the maximal responsiveness value $t_{0.5\ final}$ of 2.62 h is significantly slower than IPTG (**14**; $t_{0.5\ final}$ = 1.41 h; Figure S8 and Table S4). In summary, cIPTG constitutes an optochemical tool that can be used as an optogenetic switch for LacI-controlled expression systems in *P. putida*, but comparative expression studies revealed that modified IPTG variants **10a**, **10b** and **1** work less efficient than in *E. coli*. Remarkably, only the variant BC-cIPTG (**10b**) that offers an increased solubility in aqueous solution showed a satisfactory applicability for controlling gene expression by light. Similar to the *E. coli* Tuner(DE3), *P. putida* lacks a specific lactose permease.[30] Therefore, IPTG can only pass the cytoplasmic membrane *via* passive diffusion processes. Furthermore, in pseudomonads including *P. putida*, the outer membrane exhibits a reduced permeability as compared to *E. coli*. The uptake of small water-soluble molecules is mainly mediated by a defined set of specific porins such as OprF, which is characterised by a significantly slower diffusion rate compared to the more unspecific *E. coli* porins OmpF and OmpC.[25–26] As a consequence, the water-soluble compound **10b** could be transported over the outer membrane in a slower process.

Expression studies in B. subtilis: The Gram-positive bacterium *B. subtilis* was used as an expression host to determine the effect of inducer solubility on the uptake process, which is here solely influenced by the permeability of the cytoplasmic membrane and the surrounding cell wall. As this bacterium is not able to use lactose as a carbon source, and a lactose permease-encoding gene could not be identified in the genome,[27] the uptake of inducer molecules is most probably restricted to passive diffusion. To evaluate the cIPTG applicability, we used the *B. subtilis* DB430/pHT01-sfGFP strain, where fluorescence reporter expression is driven by the LacI-controlled P_{grac} promoter.[24b] Similar to *P. putida*, we added the respective inducer at a concentration of 1 mM to ensure full induction of recombinant gene expression (Figure S5). Remarkably, illumination of BC-cIPTG (**10b**) led to a strong and fast induction response comparable to the results obtained with IPTG (**14**; Figures 2C and S8, Table S4). In contrast, the induction with BEC-cIPTG (**10a**) led to a sfGFP expression level of around 75% in comparison to IPTG (**14**), while addition of NP-cIPTG (**1**) resulted in only 50% sfGFP fluorescence. Based on this observation, we cannot exclude that the cell wall of *B. subtilis*, which is much thicker (20–80 nm) than in Gram-negative organisms (5–10 nm),[28] is less permeable for the more hydro-

ChemBioChem
Full Papers
doi.org/10.1002/cbic.202000377
Chemistry Europe
European Chemical Societies Publishing

phobic cIPTG variants. In addition, the extremely fast responsiveness of BC-cIPTG (**10b**) in *B. subtilis* ($t_{0.5\,final}$ ~ 2.3 h), which also outperforms the respective induction response in *E. coli* ($t_{0.5\,final}$ ~ 4.3 h), might indicate an efficient catalytic cleavage of the ester intermediate after photoconversion. It should be noted that addition of BC- and BEC-cIPTG resulted in an increased basal target gene expression in non-illuminated cultures, which might be due to a slightly reduced stability of these cIPTG derivatives probably caused by a minimal catalytic release of the respective caging groups.

Analysis of expression heterogeneity: Finally, we elucidated, if the differential solubility of the applied cIPTG derivatives has an effect on the expression heterogeneity. For *E. coli* strain Tuner (DE3), we have previously proven a homogeneous induction response for both IPTG (**14**) and NP-cIPTG (**1**), which is primarily due to the absence of the permease and the resulting inducer uptake by diffusion.[6b] In contrast, for *Bacillus* species considerable expression heterogeneities are frequently described.[29] For the direct comparison of expression heterogeneity, fluorescence of the reporter proteins was determined at the single-cell level in light-exposed and non-illuminated cell cultures of *E. coli* and *B. subtilis* using flow cytometry. The results indicate that reporter gene expression was induced homogenously in *E. coli* cells irrespective of the added cIPTG variant (Figure S9 A) thereby corroborating observations from microfluidic investigations with NP-cIPTG (**1**).[6b] Similarly, the differential solubility of cIPTG variants did not affect the rate of expression heterogeneity in *B. subtilis* although it is generally more pronounced than in *E. coli* (Figure S9 B). Thus, expression heterogeneity is not provoked by a varying efficiency of inducer uptake.

Discussion

We developed the two new cIPTG derivatives **10a** and **10b** with varying hydrophobicity and aimed to analyse whether the change of cIPTG solubility affects the inducibility of LacI repressor-controlled target gene expression in *E. coli, P. putida* and *B. subtilis*. In the here presented *in vivo* studies, the derivatives are stable against spontaneous hydrolysis and did not induce elevated basal expression of target genes in the dark. In *E. coli*, only marginal differences of light-controlled gene expression could be observed for the new cIPTG variants in comparison to the well-established NP-cIPTG (**1**). Nevertheless, the increased water-solubility of derivative **10b** and its homogeneous dispersion without addition of an organic cosolvent, noticeably improves the applicability of this cIPTG derivative. The transfer to *P. putida* and *B. subtilis* clearly demonstrated that the solubility of photocaged inducer molecules is an important aspect that has to be considered for the establishment of a light-controlled expression system. Here, BC-cIPTG (**10b**), the variant that offers an increased solubility in aqueous solution, resulted in high expression levels together with a comparable or even increased induction factor in comparison to IPTG (for direct comparison of cIPTG derivatives' induction factors see Table S5). In this context it should be noted that, besides the improved solubility in microbial cultivation media, the diverging hydrophobicity of the cIPTG variants as well as the negative charge in case of BC-IPTG might additionally affect the complex processes that are involved in light-induced gene expression. These processes include i) the efficiency of photoconversion under the applied cultivation and illumination conditions, ii) the enzymatic hydrolysis of cIPTG ester intermediates by cytoplasmic, periplasmic or extracellular esterases, and iii) the individual permeability of cell membranes for cIPTG, the ester intermediates or released inducer. Thus, the individual physiological and morphological properties of the chosen microbial expression host might exhibit relevant differences such as the respective membrane composition or the ability for active inducer uptake *via* appropriate transporters. In Gram-negative bacteria, for example, the inducer has to pass two membranes, a process that occurs through i) free diffusion (both membranes), ii) passive transport processes involving unspecific or specific porins (outer membrane), and iii) active transport mechanisms that are facilitated by suitable permeases (cytoplasmic membrane). In Gram-positive bacteria, even though only one membrane needs to be passed, the surrounding cell wall is much thicker than in Gram-negative hosts and thus a distinct interaction with the differently soluble cIPTG variants might additionally influence their uptake. However, to unravel the role of individual properties of respective bacterial strains for cIPTG uptake and IPTG release, further experiments have to be performed in future studies.

In conclusion, we have constructed two new caged IPTG variants, characterised their (photo)chemical properties and demonstrated an easy applicability for the light-mediated control of gene expression in Gram-negative and Gram-positive bacteria. Because of their differential solubility, BC-, NP- and BEC-cIPTG constitute a valuable "starter set" which enables an easy access to a robust, light-responsive expression system in a broad variety of different hosts. Due to the non-invasive nature, the here presented optochemical on-switches additionally allow the external triggering of gene expression in closed biological systems thereby making, for example, anaerobic expression hosts more accessible in the near future.

Experimental Section

General remarks: All chemicals for synthesis were obtained from commercial suppliers and used without further purification unless stated otherwise. Solvents were reagent grade and were dried as well as purified by common methods. Thin-layer chromatography (TLC) was performed using pre-coated silica gel plates (Polygram® SIL G/UV, Macherey-Nagel) and components were visualised by oxidative staining or UV light. Flash chromatography was performed on silica gel (Merck silica gel 60 (0.063–0.200 μm) and solvents for flash chromatography (petroleum ether/ethyl acetate) were distilled prior to use. Optical rotation was determined at 20 °C on a Perkin Elmer Polarimeter 241 MC against sodium D-line and melting points were recorded using a Büchi melting point B-545 apparatus. The NMR spectra (^{1}H and ^{13}C) were measured at 20 °C on a Bruker Avance/DRX 600 spectrometer in deuterated solvents ($CDCl_3$, [D_6]DMSO, D_2O). The chemical shifts are given in ppm relative to the solvent (^{1}H: $CDCl_3$ = 7.26 ppm, ^{1}H: [D_6]DMSO = 3.31 ppm or ^{1}H: D_2O = 4.79 ppm/^{13}C: $CDCl_3$ = 77.16 ppm or ^{13}C: [D_6]

ChemBioChem | Full Papers doi.org/10.1002/cbic.202000377 | Chemistry Europe European Chemical Societies Publishing

DMSO = 39.52 ppm). Signals were assigned by means of H COSY, HSQC and HMBC experiments. The IR spectra were recorded with a Perkin Elmer SpectrumOne IR-spectrometer ATR (Waltham, USA). HRMS (ESI) spectra were recorded by the centrum of analytics of the Heinrich Heine University. UV/Vis absorption spectra were recorded on a Genesys 10S UV/VIS Spectrophotometer (Thermo Scientific) and uncaging experiments were performed in a quartz cuvette with the LUMOS 43® from Atlas Photonics at 375 nm. Light intensity was quantified using a Thermal Power Sensor (S302 C, Thorlabs Inc, USA) and the decay was detected by a Jasco HPLC system [column: Hyperclone 5 μ ODS (C18) 120 (Phenomenex)] combined with an UV/Vis-detector.

Synthesis of 4,5-Bis(ethoxycarbonylmethoxy)-2-nitrobenzylaldehyde diethyl acetal (12): To a solution of 4,5-bis (ethoxycarbonylmethoxy)-2-nitrobenzaldehyde (**11**) (3.00 g, 8.44 mmol) in ethanol (50 mL) triethyl orthoformate (1.88 g, 12.6 mmol, 1.50 equiv.) and pyridinium *p*-toluenesulfonate (424 mg, 1.69 mmol, 0.20 equiv.) were added and heated under reflux for 19 h. A dean-stark trap filled with molecular sieve (3 Å) was utilised for the constant removal of water. After the reaction was completed as indicated by TLC, it was washed with saturated $NaHCO_3$ solution. The aqueous phase was then extracted with CH_2Cl_2 and the combined organic phase was dried with anhydrous Na_2SO_4 and concentrated under reduced pressure. The residue was purified by flash column chromatography on SiO_2 (petroleum ether/ethyl acetate 85:15) to yield a yellow solid (3.22 g, 7.51 mmol, 89%). R_f = 0.25 (petroleum ether/ethyl acetate 80:20) m.p. 62.1 °C; ^{1}H NMR (600 MHz, [D$_6$]DMSO): δ = 1.12 (t, $^3J_{2',1''}$ = 7.1 Hz, 6 H, 2′-*H*), 1.22 (t, $^3J_{11,10 \text{ and } 11',10'}$ = 7.1 Hz, 6 H, 11-*H* and 11′-*H*), 3.50 (dq, $^2J_{1'a,1'b}$ = 9.3 Hz, $^3J_{1'a,2'}$ = 7.1 Hz, 2 H, 1′$_a$-*H*), 3.62 (dq, $^2J_{1'b,1'a}$ = 9.3 Hz, $^3J_{1'b,2'}$ = 7.1 Hz, 2 H, 1′$_b$-*H*), 4.18 (q, $^3J_{10,11 \text{ or } 10',11'}$ = 7.1 Hz, 2 H, 10-*H* or 10′-*H*), 4.19 (q, $^3J_{10,11 \text{ or } 10',11'}$ = 7.1 Hz, 2 H, 10-*H* or 10′-*H*), 4.96 (s, 2 H, 8′-*H*), 4.99 (s, 2 H, 8-*H*), 5.88 (s, 1 H, 7-*H*), 7.09 (s, 1 H, 6-*H*), 7.57 ppm (s, 1 H, 3-*H*); ^{13}C NMR (151 MHz, [D$_6$]DMSO): δ = 14.0 (*C*-11 and *C*-11′), 14.9 (*C*-2′), 60.8 (*C*-10 or *C*-10′), 60.9 (*C*-10 or *C*-10′), 65.5 (*C*-8 or *C*-8′), 65.6 (*C*-8 or *C*-8′), 97.7 (*C*-7), 110.6 (*C*-3), 111.5 (*C*-6), 127.9 (*C*-1), 141.4 (*C*-2), 146.5 (*C*-4), 150.2 (*C*-5), 168.1 (*C*-9 or *C*-9′), 168.1 ppm (*C*-9 or *C*-9′); IR (ATR-film): $\tilde{\nu}$ = 2981, 1755, 1692, 1581, 1526, 1446, 1346, 1291, 1196, 1176, 1080, 878, 796 cm^{-1}; HRMS (ESI): *m/z* calcd for $C_{19}H_{27}NO_{10}^+$: 447.1973 $[M+NH_4]^+$; found: 447.1972.

Synthesis of BEC-clPTG (10a): To a solution of 4,5-bis (ethoxycarbonylmethoxy)-2-nitrobenzylaldehyde diethyl acetal (**12**) (1.00 g, 2.33 mmol, 1.50 equiv.) in dry CH_2Cl_2 (6 mL) IPTG (370 mg, 1.55 mmol) was added. After 5 min p-TSA (11.8 mg, 0.06 mmol, 4 mol%) was added to the suspension and it was stirred at room temperature for 20 h. After the reaction was completed as indicated by TLC, a small amount of triethylamine was added and the reaction was concentrated under reduced pressure. The residue was purified by flash column chromatography on SiO_2 (petroleum ether/ethyl acetate 50:50 to 20:80) to yield a white solid (403 mg, 0.70 mmol, 45%). R_f = 0.35 (petroleum ether/ethyl acetate 20:80); m.p. 104.5 °C; [α] = −68 (c = 1.0 in $CHCl_3$); ^{1}H NMR (600 MHz, $CDCl_3$): δ = 1.31 (t, $^3J_{11,10 \text{ or } 11',10'}$ = 7.2 Hz, 6 H, 11-*H* and 11′-*H*), 1.35 (d, $^3J_{CH3\text{-}a/b,SCH}$ = 6.8 Hz, 3 H, *CH*$_3$-a or *CH*$_3$-b), 1.36 (d, $^3J_{CH3\text{-}a/b,SCH}$ = 6.8 Hz, 3 H, *CH*$_3$-a or *CH*$_3$-b), 2.56 (brs, 2 H, 2″-*OH* and 3″-*OH*), 3.25 (septet, $^3J_{SCH,CH3\text{-}a/b}$ = 6.8 Hz, 1 H, S*CH*), 3.52 (dt, $^3J_{5'',6''}$ = 1.7 Hz, $^3J_{5'',4''}$ = 1.2 Hz, 1 H, 5″-*H*), 3.64–3.70 (m, 2 H, 2″-*H* and 3″-*H*), 4.08 (dd, $^2J_{6''b,6''a}$ = 12.5 Hz, $^3J_{6''b,5''}$ = 1.7 Hz, 1 H, 6″-*H*$_b$), 4.24–4.31 (m, 6 H, 10-*H* / 10′-*H* / 4″-*H* / 6″-*H*$_a$), 4.41 (d, $^3J_{1'',2''}$ = 8.7 Hz, 1 H, 1″-*H*), 4.77 (s, 2 H, 8-*H*), 4.82 (s, 2 H, 8′-*H*), 6.21 (s, 1 H, 7-*H*), 7.35 (s, 1 H, 6-*H*), 7.54 ppm (s, 1 H, 3-*H*); ^{13}C NMR (151 MHz, $CDCl_3$): δ = 14.3 (*C*-11 or *C*-11′), 14.3 (*C*-11 or *C*-11′), 24.1 (*CH*$_3$-a or *CH*$_3$-b), 24.3 (*CH*$_3$-a or *CH*$_3$-b), 35.5 (SCH), 61.8 (*C*-10 or *C*-10′), 61.9 (*C*-10 or *C*-10′), 66.4 (*C*-8 or *C*-8′), 66.6 (*C*-8 or *C*-8′), 69.8 (*C*-6″), 70.1 (*C*-5″), 70.3 (*C*-3″), 73.9 (*C*-2″), 76.2 (*C*-4″), 85.7 (*C*-1″), 96.6 (*C*-7), 111.5 (*C*-3), 112.8 (*C*-6), 127.7 (*C*-1), 141.3 (*C*-2), 147.6 (*C*-4), 151.7 (*C*-5), 167.9 (*C*-9 or *C*-9′), 167.9 ppm (*C*-9 or *C*-9′); IR (ATR-film): $\tilde{\nu}$ = 3478, 2967, 2916, 2866, 1747, 1520, 1287, 1176, 1097, 1077, 1027, 989 cm^{-1}; UV/Vis (MeOH): λ_{max} (ε) = 298 nm (8006 dm^3 mol^{-1} cm^{-1}); HRMS (ESI): *m/z* calcd for $C_{24}H_{37}N_2O_{13}S$: 593.2011 $[M+NH_4]^+$; found: 593.2011.

Synthesis of BC-clPTG (10b): A solution of BEC-clPTG (**10a**) (200 mg, 0.35 mmol) in MeOH (3.5 mL) was cooled to 0 °C and a 0.2 M solution of LiOH (3.5 mL) was added. The reaction mixture was stirred for 1 h at room temperature. After the reaction was completed as indicated by TLC, the MeOH was evaporated under reduced pressure and the remaining solution was lyophilised overnight. The residue was suspended in THF, sonicated for 15 min and filtrated. After washing with small amounts of cold THF a white solid (107 mg, 0.21 mmol, 59%) was obtained. m.p. 190 °C (decay); [α] = −92 (c = 1.0 in H_2O); ^{1}H NMR (600 MHz, D_2O): δ = 1.29 (d, $^3J_{CH3\text{-}a,SCH}$ = 6.8 Hz, 3 H, *CH*$_3$-a), 1.31 (d, $^3J_{CH3\text{-}b,SCH}$ = 6.8 Hz, 3 H, *CH*$_3$-b), 3.26 (septet, $^3J_{SCH,CH3\text{-}a/b}$ = 6.8 Hz, 1 H, S*CH*), 3.66 (t, $^3J_{5'',6''}$ = 9.8 Hz, 1 H, 2″-*H*), 3.71–3.82 (m, 2 H, 3″-*H*, 5″-*H*), 4.18 (m, 2 H, 6″-*H*), 4.37 (d, $^3J_{4'',3''}$ = 3.6 Hz, 1 H, 4″-*H*), 4.60 (s, 2 H, 8′-*H*), 4.62 (d, $^3J_{1'',2''}$ = 9.8 Hz, 1 H, 1″-*H*), 4.67 (d, J = 2.6 Hz, 2 H, 8-*H*), 6.20 (s, 1 H, 7-*H*), 7.32 (s, 1 H, 6-*H*), 7.55 ppm (s, 1 H, 3-*H*); ^{13}C NMR (151 MHz, D_2O): δ = 22.9 (*CH*$_3$-a), 23.3 (*CH*$_3$-b), 35.0 (SCH), 67.3(C-8′), 67.4 (C-8), 69.1 (C-2″), 69.3 (C-6″), 69.6 (C-5″), 72.8 (C-3″), 76.5 (C-4″), 84.8 (C-1″), 96.4 (C-7), 109.2 (C-3), 110.8 (C-6), 126.3 (C-1), 140.0 (C-2), 147.2 (C-4), 151.5 (C-5), 175.1 (C-9), 175.4 ppm (C-9′); IR (ATR-film): $\tilde{\nu}$ = 3124, 3043, 1605, 1522, 1398, 1335, 1277, 1077, 1047, 1024, 824 cm^{-1}; UV/Vis (H_2O): λ_{max} (ε) = 245 (5008), 342 nm (3191 dm^3 mol^{-1} cm^{-1}); HRMS (ESI): *m/z* calcd for $C_{20}H_{29}N_2O_{13}S^+$: 537.1385 $[M+NH_4]^+$; found: 537.1382.

Determination of purity by qNMR: The purity of the photocaged IPTG derivatives **10a**, **10b** and **1** was determined via quantitative NMR. 3,5-bis(trifluoromethyl)bromobenzene was utilised as internal standard for **10a** as well as **1** and (methanesulfonyl)methane for **10b**. The spectra were measured at 20 °C on a Bruker Avance/DRX 600 spectrometer with 64 scans each and 30 μs relaxation time between each scan. The results in Table S3 are means of triplicate measurements.

Solubility analysis: The solubility of **10a**, **10b** and **14** was determined photometrically at 25 °C using a spectrophotometer Shimadzu UV-1800 (CPS-240A). The absorbance of a serial dilution in degassed and deionised water was measured at the absorption maximum of the respective compound. A saturated solution was measured under the same conditions. The solubility was calculated using the Beer-Lambert law.[13b]

Hydrolytic stability: For the determination of the hydrolytic stability, a 1 mM solution of the respective compound in methanol or sodium phosphate buffer (0.1 M, pH 7.5) was stored in the dark at room temperature. Samples were removed after 0 and 24 h and analysed by reversed-phase HPLC.

Quantification of uncaging half-life times: A 1 mM solution of each photocaged compound in methanol or sodium phosphate buffer (0.1 M, pH 7.5) was prepared. In a cuvette 1 mL of this solution was irradiated at room temperature using the LUMOS 43 (375 nm) for a certain time period. The sample was then analysed by reverse phase HPLC Jasco HPLC system [column: Hyperclone 5 μ ODS (C_{18}) 120 (Phenomenex)]. For each photocaged compound, the procedure was repeated for different irradiation times. The decrease of concentration was measured by an UV detector.[6d]

Determination of uncaging quantum yields: The quantum yields of **1**, **10a** and **10b** were determined by a relative method in comparison to the quantum yield of 2-nitropiperonylacetate (NPA-Ac), as this substrate shows a sufficient similarity to **1**, **10a** and **10b**. The procedure was followed as previously described in literature (Figure S4 and Table S2).[6c,30]

ChemBioChem | Full Papers doi.org/10.1002/cbic.202000377 | Chemistry Europe European Chemical Societies Publishing

Bacterial strains and plasmids: The *E. coli* strain DH5α[31] was used for all cloning procedures, while the *E. coli* strain S17-1[32] and Tuner (DE3) (Novagen) were applied for conjugation and expression studies, respectively. All *E. coli* strains, the *P. putida* strain KT2440[33] and the *B. subtilis* strain DB430[34] were grown on LB agar plates or in liquid LB medium (Luria/Miller, Carl Roth®), at 37 °C (*E. coli*) or 30 °C (*P. putida, B. subtilis*). Media were supplemented either with kanamycin (50 μg mL^{-1}), gentamicin (25 μg mL^{-1}), irgasan (25 μg mL^{-1}) or chloramphenicol (5 μg mL^{-1}), when appropriate.

All bacterial strains and plasmids used in this study are listed in Table S1, Supporting Information.

Plasmid construction: All recombinant DNA techniques were carried out as described by Sambrook *et al.*[35] For the construction of the *B. subtilis* expression vector pHT01-sfGFP, the sfGFP-encoding gene was synthesised with flanking NdeI and HindIII restriction sites (Eurofins Genomics, Germany) and subsequently cloned into pET-22(b) (Novagen, Merck). The resulting vector pET-22(b)-sfGFP was used as template for SLIC cloning[36] of a DNA fragment encompassing the *sfgfp* gene into the *B. subtilis* expression vector pHT01 (MoBiTec, Germany) using oligos 3–6 (Table S1, Supporting Information). The *P. putida* expression vector pVLT33-GFPmut3 was constructed by restriction and ligation. To this end, the *gfpmut3* gene was amplified with flanking *EcoR*I and *Xba*I restriction sites *via* PCR using oligos 1–2 (Table S1). Afterwards, the *EcoR*I/*Xba*I hydrolysed fragment was ligated into the likewise hydrolysed vector backbone pVLT33, resulting in the final expression vector pVLT33-GFPmut3. Correct nucleotide sequences of all constructs were confirmed by Sanger sequencing (Eurofins Genomics).

Cultivation conditions: All *E. coli*, *P. putida* and *B. subtilis* expression cultures were grown in 48-well Flowerplates® in a BioLector microbioreactor system (m2p labs, Germany) (800 μL LB medium, 1200 rpm, 30 °C), inoculated with an optical density at 580 nm of 0.05. During cultivation, the cell density was measured online through the scattered light intensity at 620 nm. In addition, fluorescence of eYFP and GFP variants (GFPmut3 and sfGFP) were continuously determined using a 508/532 nm and 488/520 nm filter, respectively. cIPTG variants **10a**, **10b** or NP-cIPTG (**1**) were added prior inoculation (final concentration: 50 μM for *E. coli*, 1 mM for *P. putida* and *B. subtilis;* purities of cIPTG variant after synthesis were taken into account accordingly) and expression of reporter genes was induced during the early logarithmic growth phase (after approx. 2.5 h for *E. coli*, 3 h for *P. putida* and 5 h for *B. subtilis*) *via* UV-A light exposure (VL-315.BL lamp, Vilber Lourmat, France; ~1 mW cm^{-2}, 30 min exposure) or by addition of equal amounts of conventional IPTG (**14**) after illumination.

Determination of expression heterogeneity: For measurement of the expression heterogeneity, *E. coli* and *B. subtilis* cultures were analysed on the single-cell level by flow cytometry regarding their fluorescence intensity and distribution. Expression cultures were grown as described above and were subsequently sampled as soon as they reached the late logarithmic growth phase (after 8 h for *E. coli* and after 10 h for *B. subtilis*). For this purpose, 40 μL was taken out of the Flowerplate® cultures and added to 600 μL PBS buffer (pH 7.4). Subsequently, the cells were harvested by centrifugation (2 min, 15 000 rpm – 21130×g, RT), adjusted to an optical density of 0.5 (OD_{580}) in 100 μL PBS buffer and then transferred into a 96-well microtiter plate (Greiner Bio-One GmbH, Frickenhausen, Germany). Finally, these samples were analysed with a flow cytometer (Amnis® CellStreamTM System, Luminex Corporation, Austin, USA). The individual cellular fluorescence brightness was measured using a 488-nm laser (15% intensity for *E. coli* and 5% for *B. subtilis*) for excitation and a 528/46 nm bandpass filter for detection. To exclude cell debris and cell aggregates, the cells were also analysed regarding their size (forward scatter, FSC) and granularity (side scatter, SSC). FSC was measured using an FSC laser (nm) with 80% of the laser power for *E. coli* and 50% for *B. subtilis* and a 456/51 nm bandpass filter for detection. For determination of SSC a nm-light laser with 80% of the laser power for *E. coli* and 50% for *B. subtilis* (773/56 nm bandpass filter) was used. Based on the scatter plots, bacterial cells were gated from irrelevant counts for fluorescence analysis. Flow cytometric data were evaluated with the CellStream™ Analysis Software (Merck, now Luminex Corporation).

Acknowledgements

The work was supported by grants from German Federal Ministry of Education and Research (BMBF, FKZ: 031A167A), the Bioeconomy Science Center, and the European Regional Development Fund (ERDF: 34.EFRE-0300096 and 34.EFRE-0300097) within the project CLIB-Kompetenzzentrum Biotechnologie CKB). The scientific activities of the Bioeconomy Science Center were financially supported by the Ministry of Innovation, Science and Research of the German federal state of North Rhine-Westphalia MIWF within the framework of the NRW Strategieprojekt BioSC (no. 313/323-400-00213). The authors thank Dr. Anita Loeschcke for the helpful discussion, Sonja Kubicki for the construction of the plasmid pVLT33-GFPmut3, Vera Ophoven for synthetic, and Birgit Henßen for analytical support. Open access funding enabled and organized by Projekt DEAL.

Conflict of Interest

The authors declare no conflict of interest.

Keywords: caged compounds · gene expression · optogenetics · photochemistry · synthetic biology

[1] K. Deisseroth, *Nat. Methods* **2011**, *8*, 26–29.
[2] a) R. M. Hughes, *Crit. Rev. Biochem. Mol. Biol.* **2018**, *53*, 453–474; b) Z. Liu, J. Zhang, J. Jin, Z. Geng, Q. Qi, Q. Liang, *Front. Microbiol.* **2018**, *9*, 2692; c) E. M. Zhao, Y. Zhang, J. Mehl, H. Park, M. A. Lalwani, J. E. Toettcher, J. L. Avalos, *Nature* **2018**, *555*, 683–687; d) S. R. Schmidl, F. Ekness, K. Sofjan, K. N. M. Daeffler, K. R. Brink, B. P. Landry, K. P. Gerhardt, N. Dyulgyarov, R. U. Sheth, J. J. Tabor, *Nat. Chem. Biol.* **2019**, *15*, 690–698.
[3] a) C. Brieke, F. Rohrbach, A. Gottschalk, G. Mayer, A. Heckel, *Angew. Chem. Int. Ed.* **2012**, *51*, 8446–8476; *Angew. Chem.* **2012**, *124*, 8572–8604; b) A. Bardhan, A. Deiters, *Curr. Opin. Struct. Biol.* **2019**, *57*, 164–175; c) L. Gardner, A. Deiters, *Curr. Opin. Chem. Biol.* **2012**, *16*, 292–299; d) A. Deiters, *Curr. Opin. Chem. Biol.* **2009**, *13*, 678–686; e) T. Drepper, U. Krauss, S. Meyer zu Berstenhorst, J. Pietruszka, K.-E. Jaeger, *Appl. Microbiol. Biotechnol.* **2011**, *90*, 23–40.
[4] a) J. Liu, J. Hemphill, S. Samanta, M. Tsang, A. Deiters, *J. Am. Chem. Soc.* **2017**, *139*, 9100–9103; b) D. Kolarski, A. Sugiyama, G. Breton, C. Rakers, D. Ono, A. Schulte, F. Tama, K. Itami, W. Szymanski, T. Hirota, B. L. Feringa, *J. Am. Chem. Soc.* **2019**, *141*, 15784–15791.
[5] J. M. Silva, E. Silva, R. L. Reis, *J. Control. Release* **2019**, *298*, 154–176.
[6] a) D. D. Young, A. Deiters, *Angew. Chem. Int. Ed.* **2007**, *46*, 4290–4292; *Angew. Chem.* **2007**, *119*, 4368–4370; b) D. Binder, A. Grünberger, A. Loeschcke, C. Probst, C. Bier, J. Pietruszka, W. Wiechert, D. Kohlheyer, K.-E. Jaeger, T. Drepper, *Integr. Biol.* **2014**, *6*, 755–765; c) D. Binder, C. Bier, A. Grünberger, D. Drobietz, J. Hage-Hülsmann, G. Wandrey, J. Büchs, D. Kohlheyer, A. Loeschcke, W. Wiechert, K.-E. Jaeger, J. Pietruszka, T. Drepper, *ChemBioChem* **2016**, *17*, 296–299; d) C. Bier, D. Binder, D.

ChemBioChem
Full Papers
doi.org/10.1002/cbic.202000377
Chemistry Europe
European Chemical Societies Publishing

Drobietz, A. Loeschcke, T. Drepper, K.-E. Jaeger, J. Pietruszka, *Synthesis* **2017**, *49*, 42–52; e) P. M. Kusen, G. Wandrey, V. Krewald, M. Holz, S. Meyer zu Berstenhorst, J. Büchs, J. Pietruszka, *J. Biotechnol.* **2017**, *258*, 117–125; f) P. M. Kusen, G. Wandrey, C. Probst, A. Grünberger, M. Holz, S. Meyer zu Berstenhorst, D. Kohlheyer, J. Büchs, J. Pietruszka, *ACS Chem. Biol.* **2016**, *11*, 2915–2922.

[7] J. E. T. Corrie in *Dynamic Studies in Biology: Phototriggers, Photoswitches and Caged Biomolecules*, (Eds.: M. Goeldner, R. Givens), Wiley-VCH, Weinheim, **2005**, pp. 1–94.

[8] a) A. Y. Vorobev, A. E. Moskalensky, *Comput. Struct. Biotechnol. J.* **2019**, *18*, 27–34; b) I. Aujard, C. Benbrahim, M. Gouget, O. Ruel, J.-B. Baudin, P. Neveu, L. Jullien, *Chem. Eur. J.* **2006**, *12*, 6865–6879.

[9] A. Specht, M. Goeldner, *Angew. Chem. Int. Ed.* **2004**, *43*, 2008–2012; *Angew. Chem.* **2004**, *116*, 2042–2046.

[10] a) A. G. Russell, M.-E. Ragoussi, R. Ramalho, C. W. Wharton, D. Carteau, D. M. Bassani, J. S. Snaith, *J. Org. Chem.* **2010**, *75*, 4648–4651; b) A. G. Russell, M. J. Sadler, H. J. Laidlaw, A. Gutierrez-Loriente, C. W. Wharton, D. Carteau, D. M. Bassani, J. S. Snaith, *Photochem. Photobiol. Sci.* **2012**, *11*, 556–563; c) K. Schaper, S. Mobarekeh, C. Grewer, *Eur. J. Org. Chem.* **2002**, *2002*, 1037–1046; d) M. Noguchi, M. Skwarczynski, H. Prakash, S. Hirota, T. Kimura, Y. Hayashi, Y. Kiso, *Bioorg. Med. Chem.* **2008**, *16*, 5389–5397.

[11] A. P. Pelliccioli, J. Wirz, *Photochem. Photobiol. Sci.* **2002**, *1*, 441–458.

[12] a) L. R. Makings, R. Y. Tsien, *J. Biol. Chem.* **1994**, *269*, 6282–6285; b) J. Ni, D. A. Auston, D. A. Freilich, S. Muralidharan, E. A. Sobie, J. P. Y. Kao, *J. Am. Chem. Soc.* **2007**, *129*, 5316–5317; c) K. M. Schelkle, C. Schmid, K. Yserentant, M. Bender, I. Wacker, M. Petzoldt, M. Hamburger, D.-P. Herten, R. Wombacher, R. R. Schröder, U. H. F. Bunz, *Angew. Chem. Int. Ed.* **2017**, *56*, 4724–4728; *Angew. Chem.* **2017**, *129*, 4802–4806.

[13] a) S. B. Cambridge, D. Geissler, S. Keller, B. Cürten, *Angew. Chem. Int. Ed.* **2006**, *45*, 2229–2231; *Angew. Chem.* **2006**, *118*, 2287–2289; b) S. B. Cambridge, D. Geissler, F. Calegari, K. Anastassiadis, M. T. Hasan, A. F. Stewart, W. B. Huttner, V. Hagen, T. Bonhoeffer, *Nat. Methods* **2009**, *6*, 527–531.

[14] G. Wandrey, C. Bier, D. Binder, K. Hoffmann, K.-E. Jaeger, J. Pietruszka, T. Drepper, J. Büchs, *Microb. Cell Fact.* **2016**, *15*, 1–16.

[15] D. Binder, J. Frohwitter, R. Mahr, C. Bier, A. Grünberger, A. Loeschcke, P. Peters-Wendisch, D. Kohlheyer, J. Pietruszka, J. Frunzke, K.-E. Jaeger, V. F. Wendisch, T. Drepper, *Appl. Environ. Microbiol.* **2016**, *82*, 6141–6149.

[16] a) T. Milburn, N. Matsubara, A. P. Billington, J. B. Udgaonkar, J. W. Walker, B. K. Carpenter, W. W. Webb, J. Marque, W. Denk, *Biochemistry* **1989**, *28*, 49–55; b) H.-G. A. Breitinger, R. Wieboldt, D. Ramesh, B. K. Carpenter, G. P. Hess, *Biochemistry* **2000**, *39*, 5500–5508; c) K. R. Gee, L. Niu, K. Schaper, G. P. Hess, *J. Org. Chem.* **1995**, *60*, 4260–4263; d) L. Niu, K. R. Gee, K. Schaper, G. P. Hess, *Biochemistry* **1996**, *35*, 2030–2036; e) K. Schaper, S. A. Madani Mobarekeh, P. Doro, D. Maydt, *Photochem. Photobiol.* **2010**, *86*, 1247–1254.

[17] J. E. T. Corrie, *J. Chem. Soc. Perkin Trans. 1* **1993**, 2161–2166.

[18] K. Terpe, *Appl. Microbiol. Biotechnol.* **2006**, *72*, 211–222.

[19] a) O. Simon, I. Klaiber, A. Huber, J. Pfannstiel, *J. Proteomics* **2014**, *109*, 212–227; b) Ö. Akkaya, D. R. Pérez-Pantoja, B. Calles, P. I. Nikel, V. de Lorenzo, *MBio* **2018**, *9*, e01512–18.

[20] a) M. Fernández, S. Conde, J. de la Torre, C. Molina-Santiago, J.-L. Ramos, E. Duque, *Antimicrob. Agents Chemother.* **2012**, *56*, 1001–1009; b) M. Chavarría, P. I. Nikel, D. Pérez-Pantoja, V. de Lorenzo, *Environ. Microbiol.* **2013**, *15*, 1772–1785.

[21] L. F. Kampers, R. J. Volkers, V. A. Martins dos Santos, *Microb. Biotechnol.* **2019**, *12*, 845–848.

[22] a) P. I. Nikel, V. de Lorenzo, *New Biotechnol.* **2014**, *31*, 562–571; b) T. Tiso, R. Zauter, H. Tulke, B. Leuchtle, W.-J. Li, B. Behrens, A. Wittgens, F. Rosenau, H. Hayen, L. M. Blank, *Microb. Cell Fact.* **2017**, *16*, 225; c) P. I. Nikel, V. de Lorenzo, *Metab. Eng.* **2018**, *50*, 142–155; d) E. Martínez-García, V. de Lorenzo, *Curr. Opin. Biotechnol.* **2019**, *59*, 111–121; e) A. Loeschcke, S. Thies, *Curr. Opin. Biotechnol.* **2020**, *65*, 213–224; f) M. R. Incha, M. G. Thompson, J. M. Blake-Hedges, Y. Liu, A. N. Pearson, M. Schmidt, J. W. Gin, C. J. Petzold, A. M. Deutschbauer, J. D. Keasling, *Metab. Eng. Commun.* **2020**, *10*, e00119.

[23] J. van Dijl, M. Hecker, *Microb. Cell Fact.* **2013**, *12*, 3.

[24] a) S. C. Troeschel, S. Thies, O. Link, C. I. Real, K. Knops, S. Wilhelm, F. Rosenau, K.-E. Jaeger, *J. Biotechnol.* **2012**, *161*, 71–79; b) H. D. Nguyen, T. T. P. Phan, W. Schumann, *Curr. Microbiol.* **2007**, *55*, 89–93; c) M. M. Bagdasarian, E. Amann, R. Lurz, B. Rückert, M. Bagdasarian, *Gene* **1983**, *26*, 273–282.

[25] H. Löwe, P. Sinner, A. Kremling, K. Pflüger-Grau, *Microb. Biotechnol.* **2020**, *13*, 97–106.

[26] E. Eren, J. Vijayaraghavan, J. Liu, B. R. Cheneke, D. S. Touw, B. W. Lepore, M. Indic, L. Movileanu, B. van den Berg, *PLoS Biol.* **2012**, *10*, e1001242.

[27] a) O. Krispin, R. Allmansberger, *J. Bacteriol.* **1998**, *180*, 2265–2270; b) M. Steinmetz, in *Bacillus subtilis and Other Gram-Positive Bacteria: Biochemistry, Physiology* and Molecular Genetics (Eds.: A. L. Sonenshein, J. A. Hoch, R. Losick), American Society of Microbiology, Washington, **1993**, pp. 157–170.

[28] M. R. J. Salton, K. S. Kim, in *Medical Microbiology*, 4th ed. (Ed.: S. Baron), University of Texas Medical Branch at Galveston, Galveston, **1996**, Chapter 2.

[29] a) K. M. Münch, J. Müller, S. Wienecke, S. Bergmann, S. Heyber, R. Biedendieck, R. Münch, D. Jahn, *Appl. Environ. Microbiol.* **2015**, *81*, 5976–5986; b) T. N. Ploss, E. Reilman, C. G. Monteferrante, E. L. Denham, S. Piersma, A. Lingner, J. Vehmaanperä, P. Lorenz, J. M. van Dijl, *Microb. Cell Fact.* **2016**, *15*, 57; c) D. B. Kearns, R. Losick, *Genes Dev.* **2005**, *19*, 3083–3094; d) D. Dubnau, R. Losick, *Mol. Microbiol.* **2006**, *61*, 564–572.

[30] a) F. Bley, K. Schaper, H. Görner, *Photochem. Photobiol.* **2008**, *84*, 162–171; b) B. A. M. Bier, *PhD thesis*, Heinrich Heine University Düsseldorf (Germany), **2011**.

[31] D. Hanahan, *J. Mol. Biol.* **1983**, *166*, 557–580.

[32] R. Simon, U. Priefer, A. Pühler, *Bio/Technology* **1983**, *1*, 784–791.

[33] M. Bagdasarian, R. Lurz, B. Rückert, F. C. H. Franklin, M. M. Bagdasarian, J. Frey, K. N. Timmis, *Gene* **1981**, *16*, 237–247.

[34] R. H. Doi, S.-L. Wong, F. Kawamura, *Trends Biotechnol.* **1986**, *4*, 232–235.

[35] J. Sambrook, E. F. Fritsch, T. Maniatis, *Molecular Cloning: A Laboratory Manual*, Cold Spring Harbor Laboratory Press, Cold Spring Harbor, **1989**, p. 1546.

[36] J.-Y. Jeong, H.-S. Yim, J.-Y. Ryu, H. S. Lee, J.-H. Lee, D.-S. Seen, S. G. Kang, *Appl. Environ. Microbiol.* **2012**, *78*, 5440–5443.

Manuscript received: June 12, 2020
Revised manuscript received: August 31, 2020
Accepted manuscript online: September 11, 2020
Version of record online: October 23, 2020

ChemBioChem

Supporting Information

Effect of Photocaged Isopropyl β-D-1-thiogalactopyranoside Solubility on the Light Responsiveness of LacI-controlled Expression Systems in Different Bacteria

Fabian Hogenkamp[+], Fabienne Hilgers[+], Andreas Knapp, Oliver Klaus, Claus Bier, Dennis Binder, Karl-Erich Jaeger, Thomas Drepper,* and Jörg Pietruszka*

Table of Contents

S1 Supporting methods

S1.1 Synthesis of 3,4-bis(ethoxycarbonylmethoxy)benzaldehyde (18)

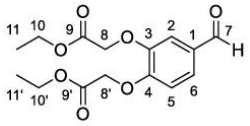

To a solution of 3,4-dihydroxybenzaldehyde (3.00 g, 21.7 mmol) in DMF (42 mL) K_2CO_3 (12.2 g, 86.9 mmol, 4.00 equiv.) was added and it was stirred for 30 min at room temperature. The reaction mixture was cooled to 0 °C and ethyl bromoacetate was added dropwise. The reaction mixture was stirred for additional 30 min at 0 °C, before it was stirred at room temperature for 16 h. The reaction was quenched by addition of water (60 mL). The aqueous phase was extracted with ethyl acetate. The organic phase was washed with saturated NaCl solution, dried with anhydrous $MgSO_4$ and concentrated under reduced pressure. The residue was purified by flash-column chromatography on SiO_2 (petroleum ether/ethyl acetate 7:3) to yield a white solid (5.88 g, 19.0 mmol, 87%). The spectroscopic data are in agreement with previously reported literature values.[1] R_f = 0.27 (petroleum ether/ethyl acetate 7:3); m.p. 55 °C, Lit.[2]: 55 - 56 °C; ^{1}H-NMR (600 MHz, $CDCl_3$): δ = 1.28 (t, $^3J_{11,10 \text{ or } 11',10'}$ = 7.2 Hz, 3 H, 11-*H* or 11′-*H*), 1.29 (t, $^3J_{11,10 \text{ or } 11',10'}$ = 7.2 Hz, 3 H, 11-*H* or 11′-*H*), 4.26 (q, $^3J_{10,11 \text{ or } 10',11'}$ = 7.2 Hz, 4 H, 10-*H* and 10´-*H*), 4.76 (s, 2 H, 8-*H*), 4.80 (s, 2 H, 8´-*H*), 6.92 (d, $^3J_{5,6}$ = 8.3 Hz, 1 H, 5-*H*), 7.37 (d, $^4J_{2,6}$ = 1.9 Hz, 1 H, 2-*H*), 7.47 (dd, $^3J_{6,5}$ = 8.3 Hz, $^4J_{6,2}$ = 1.9 Hz, 1 H, 6-*H*), 9.83 ppm (s, 1 H, 7-*H*); ^{13}C-NMR (151 MHz, $CDCl_3$): δ = 14.27 (*C*-11 and *C*-11′), 61.63 (*C*-10 or *C*-10′), 61.74 (*C*-10 or *C*-10′), 66.25 (*C*-8), 66.28 (*C*-8′), 113.05 (*C*-2), 113.66 (*C*-5), 127.00 (*C*-6), 131.14 (*C*-1), 148.39 (*C*-3), 153.17 (*C*-4), 168.16 (*C*-9′), 168.39 (*C*-9), 190.59 ppm (*C*-7); IR (ATR-film): $\tilde{\nu}$ = 2977, 1755, 1724, 1687, 1585, 1510, 1429, 1207, 1138, 1054, 1024, 671 cm^{-1}; MS (ESI, positive-ion): m/z (%): 333.2 (100) $[M+Na]^+$, 349.1 (40) $[M+K]^+$.

S1.2 Synthesis of 4,5-bis(ethoxycarbonylmethoxy)-2-nitrobenzaldehyde (11)

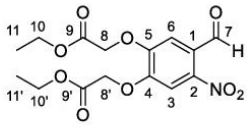

A solution of KNO_3 (2.31 g, 22.8 mmol, 1.25 equiv.) in trifluoroacetic acid (30 mL) was cooled to 0 °C and a solution of 3,4-bis(ethoxycarbonylmethoxy)benzaldehyde (**18**) (5.66 g, 18.2 mmol, 0.9 M) in trifluoroacetic acid was added dropwise. The reaction mixture was stirred for 1 h at 0 °C and for 16 h at room temperature. Then it was concentrated under reduced pressure, the residue was dissolved in ethyl acetate and washed with saturated $NaHCO_3$ and saturated NaCl solution. The organic phase was dried with anhydrous $MgSO_4$ and concentrated under reduced pressure. The residue was purified by flash-column chromatography on SiO_2 (petroleum ether/ethyl acetate 6:4) to yield a yellow solid (4.44 g, 12.5 mmol, 69%). The spectroscopic data are in agreement with previously reported literature values.[1] R_f = 0.44 (toluene/ethyl acetate 85:15); m.p. 94 °C; ^{1}H-NMR (600 MHz, $CDCl_3$): δ = 1.30 (t, $^3J_{11,10 \text{ or } 11',10'}$ = 7.2 Hz, 3 H, 11-*H* or 11′-*H*), 1.32 (t, $^3J_{11,10 \text{ or } 11',10'}$ = 7.2 Hz, 3 H, 11-*H* or 11′-*H*), 4.28 (q, $^3J_{10,11 \text{ or } 10',11'}$ = 7.2 Hz, 2 H, 10-*H* or 10′-*H*), 4.29 (q, $^3J_{10,11 \text{ or } 10',11'}$ = 7.2 Hz, 2 H, 10-*H* or 10′-*H*), 4.85 (s, 2 H, 8-*H* or 8′-*H*), 4.86 (s, 2 H, 8-*H* or 8′-*H*), 7.34 (s, 1 H, 3-*H*), 7.58 (s, 1 H, 6-*H*), 10.41 ppm (s, 1 H, 7-*H*); ^{13}C-NMR (151 MHz, $CDCl_3$): δ = 14.2 (*C*-11 or *C*-11′), 14.3 (*C*-11 or *C*-11′), 62.0 (*C*-10 or *C*-10′), 62.1 (*C*-10 or *C*-10′), 66.1 (*C*-8 or *C*-8′), 66.4 (*C*-8 or *C*-8′), 110.4 (*C*-6), 112.5 (*C*-3), 126.3 (*C*-1 or *C*-2), 144.2 (*C*-1 or *C*-2), 150.9 (*C*-4 or *C*-5), 151.9 (*C*-4 or *C*-5), 167.3 (*C*-9 or *C*-9′), 167.4 (*C*-9 or *C*-9′), 187.3 ppm (*C*-7); IR (ATR-film): $\tilde{\nu}$ = 2987, 1740, 1687, 1570, 1507, 1283, 1196, 1168, 1070, 1022, 792 cm^{-1}; MS (ESI, positive-ion): m/z (%): 378.2 (50) $[M+Na]^+$.

S1.3 Bacterial strains and plasmids

All bacterial strains, plasmids and oligonucleotides used in this study are listed in Table S1.

Table S1: Bacterial strains, plasmids and oligonucleotides used in this study.

Strains, plasmids, oligonucleotides	Relevant features, description or sequences[a]	References
	Strains	
***E. coli* DH5α**	*F⁻ Φ80lacZΔM15 Δ(lacZYA-argF) U169 recA1 endA1 hsdR17 phoA supE44 thi-1 gyrA96 relA1 deoR*	[3]
***E. coli* S17-1**	Ec294::[RP4-2 (Tc^R::Mu)(Km^R::Tn7)] *recA, thi, pro, hsdR⁻ hsdM⁺* Tp^R Sm^R	[4]
***E. coli* Tuner(DE3)**	*F⁻ompT hsdS*$_B$ (r_B^- m_B^-) *gal dcm lacY1(DE3)*	Novagen, Merck KGaA
***P. putida* KT2440**	Wild-type	[5]
***B. subtilis* DB430**	*trpC2 his nprE aprE bpf ispI*	[6]
	Plasmids	
pRhotHi-2-lacI-EYFP	pBBR1-MCS-derivative, Km^R, Cm^R, pBBR22b-*lacI*, P_{T7}-lacO-MCS with *Nde*I *Xho*I inserted *eyfp*	[7]
pVLT33	R6K, RSF1010 $lacI^q$, Kan^R, P_{tac}	[8]
pVLT33-GFPmut3	R6K, RSF1010 $lacI^q$, Kan^R, P_{tac} with *EcoR*I *Xba*I inserted *gfpmut3*	This work
pET-22(b)-sfGFP	Ap^R, *lacI*, P_{T7}-lacO-MCS with *Nde*I *Hin*dIII inserted *sfgfp*	This work
pHT01	Pgrac-lacO-MCS, *lacI*, Cm^R	MoBiTec, Germany
pHT01-sfGFP	Pgrac-lacO-MCS, *lacI*, Cm^R, *sfgfp*	This work
	Oligonucleotides	
1) EcoRI_GFP_fw	Binds at the 5' end of the *gfpmut3* gene, inserts *EcoR*I site 5'-ATATGAATTCATGGTACCAAGTAAAGGAG-3'	This work
2) XbaI_GFP_rev	Binds at the 3' end of the *gfpmut3* gene, inserts *Hind*III site 5'-ATATTCTACATTATTTGTATAGTTCATC CATGC-3'	This work
3) pHT01_fw	Amplification of pHT01 plasmid for SLIC cloning 5'- GAAGGGAATTCATATTACTTAGAGGAT ACT-3′	This work
4) pHT01_rev	Amplification of pHT01 plasmid for SLIC cloning 5'- CCTCCTTTAATTGGGAATTGTTATCCG-3'	This work
5) sfgfp_fw	Binds at the 5'end of the *sfgfp* gene for SLIC cloning 5'- GGATAACAATTCCCAATTAAAGGAGGA GATATACATATGAGCAAAGGAGAAGA-3'	This work
6) sfgfp_rev	Binds at the 3' end of the *sfgfp* gene for SLIC cloning 5'- GTATCCTCTAAGTAATATGAATTCCCTTC CAGCCGGATCTCAGTGGT-3'	This work

S2 Supporting data

S2.1 UV-Vis spectra of compounds

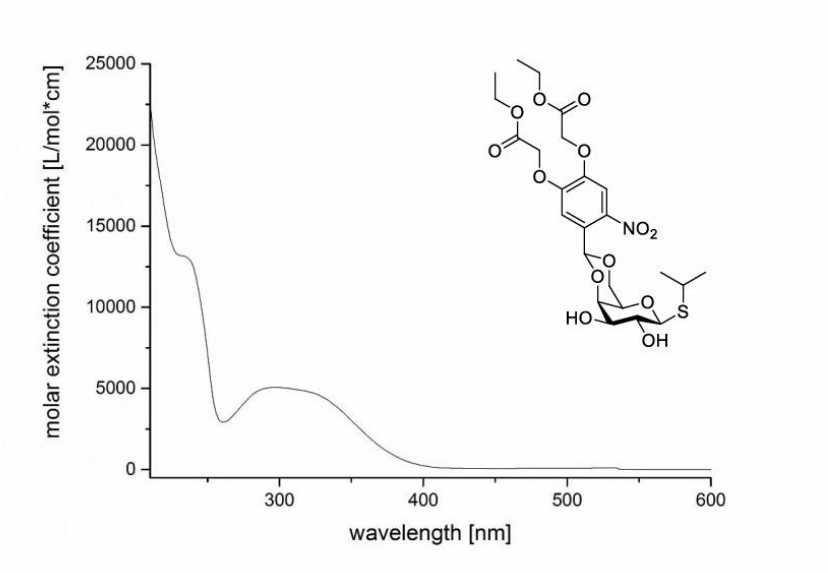

Figure S1: UV-Vis spectrum of compound **10a** (0.125 mM in MeOH, 25 °C).

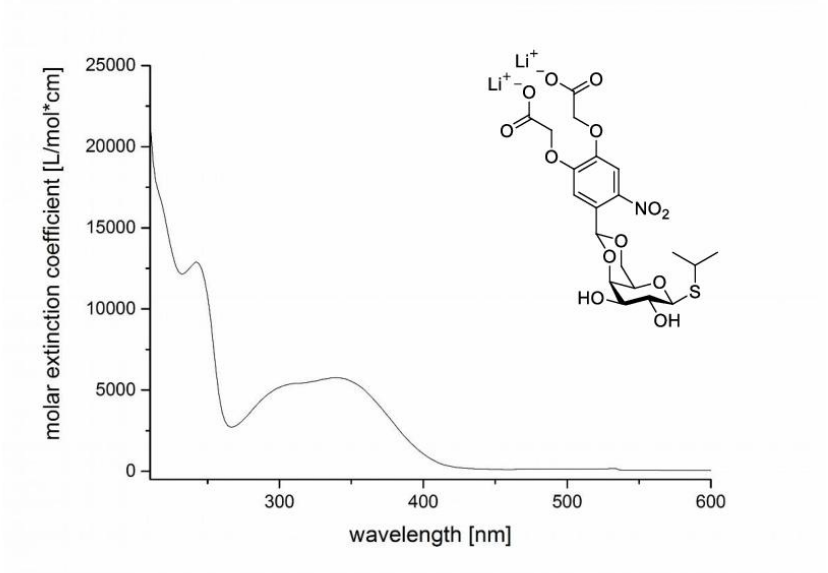

Figure S2: UV-Vis spectrum of compound **10b** [0.125 mM in sodium phosphate buffer (0.1 mM, pH 7.5), 25 °C].

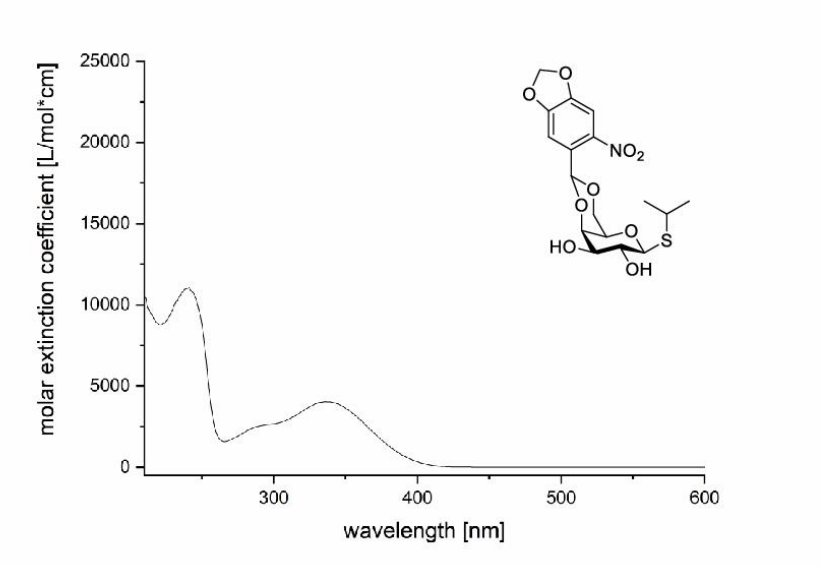

Figure S3: UV-Vis spectrum of compound **1** (0.200 mM in MeOH, 25 °C).

S2.2 Determination of uncaging half-life times

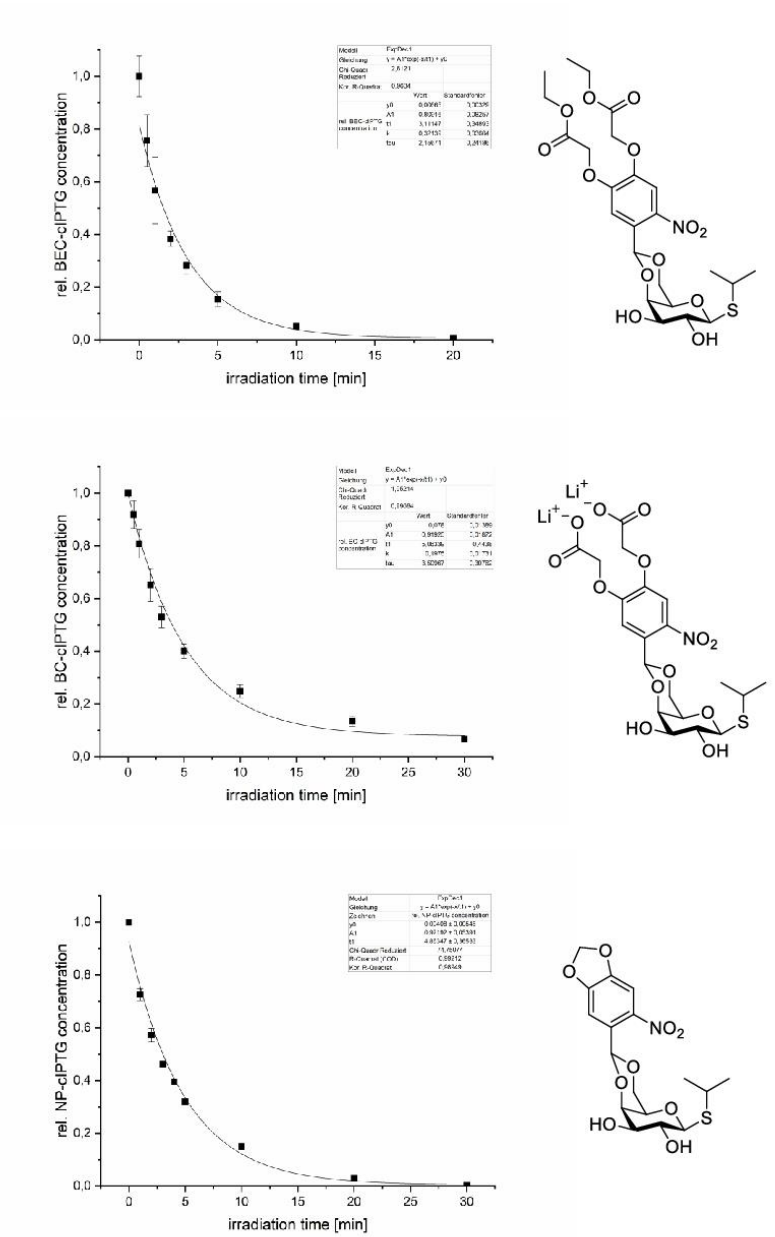

Figure S4: *In vitro* decay of caged IPTG controlled via reverse phase HPLC of compounds **10a**, **1** (1 mM in MeOH) and **10b** [1 mM in sodium phosphate buffer (0.1 mM, pH 7.5)]; 375 nm, 6.4 mW cm^{-2}, room temperature.

Table S2: Fitting parameters and uncaging half-life times $t_{0.5}$ for caged IPTG derivatives.

Inducer	y_0	A_1	t_1	k	$t_{0.5}$ [min]
BEC-cIPTG (**10a**)	0.00665	0.80916	3.11147	0.32139	2.15671
BC-cIPTG (**10b**)	0.078	0.91925	5.06339	0.1975	3.50967
NP-cIPTG (**1**)	0.00408	0.92192	4.86347	0.20561	3.3711

S2.3 Determination of purity by qNMR

Table S3: Compound purities determined by qNMR

Compound	Purity [%]
BEC-cIPTG (**10a**)	90.7 ± 1.3
BC-cIPTG (**10b**)	74.0 ± 2.5
NP-cIPTG (**1**)	80.4 ± 2.3

S2.4 Determination of IPTG concentrations sufficient for the induction of gene expression in *E. coli*, *P. putida* and *B. subtilis*

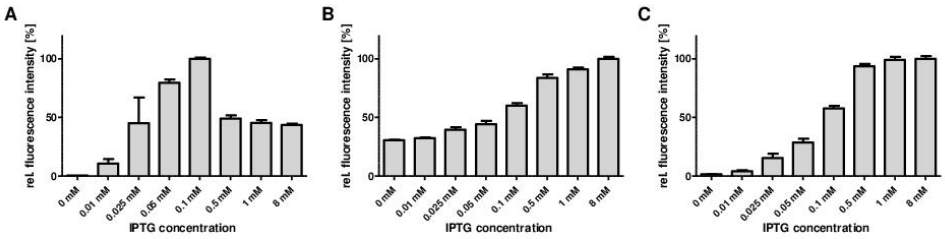

Figure S5: Relative fluorescence intensities of *E. coli* Tuner(DE3)/pRhotHi-2-lacI-eYFP (**A**), *P. putida* KT2440/pVLT33-GFPmut3 (**B**) and *B. subtilis* DB430/pHT01-sfGFP (**C**) expression cultures supplemented with increasing amounts of IPTG (**14**). Cultures were incubated in LB medium for 20 h in the dark at 30 °C. Induction of gene expression was performed after 2.5 h for *E. coli*, after 3 h for *P. putida* and after 5 h for *B. subtilis* by adding IPTG (**14**) concentrations ranging from 0 to 8 mM. *In vivo* fluorescence intensities were determined by using a BioLector system (eYFP: λex = 508 nm, λem = 532 nm, GFPmut3: λex = 508 nm, λem = 532 nm, sfGFP: λex = 488 nm, λem = 520 nm) and normalised to cell densities. Values are means of triplicate measurements. Error bars indicate the respective standard deviations.

S2.5 Stability and toxicity of novel photocaged IPTG variants

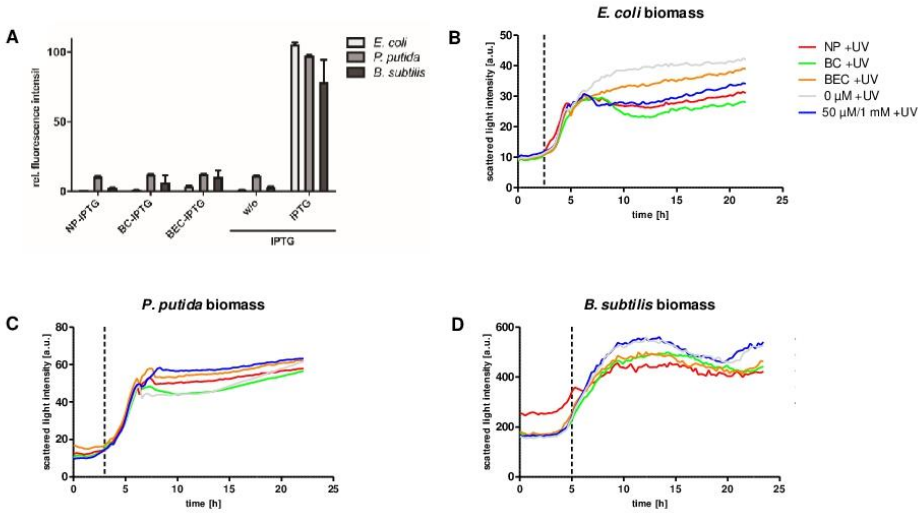

Figure S6: A) Normalised fluorescence intensity of *E. coli* Tuner(DE3)/pRhotHi-2-lacI-eYFP, *P. putida* KT2440/pVLT33-GFPmut3 and *B. subtilis* DB430/pHT01-sfGFP expression cultures (supplemented with 50 µM of each compound for *E. coli* and 1 mM for *P. putida* and *B. subtilis*). All cultures were incubated in the dark for 20 h in LB medium at 30 °C. *In vivo* stability of new photocaged IPTG variants **10a** (BEC) and **10b** (BC) is reflected by the low induction of reporter gene expression and was compared to NP-cIPTG (**1**, NP) as well as to cultures with and without IPTG (**14**). *In vivo* fluorescence intensities were determined by using a BioLector system (eYFP: λex = 508 nm, λem = 532 nm, GFPmut3: λex = 508 nm, λem = 532 nm, sfGFP: λex = 488 nm, λem = 520 nm) normalised to cell densities and are shown in relation to the respective fluorescence intensities of IPTG (**14**). Values are means of triplicate measurements. Error bars indicate the respective standard deviations. **B-D)** Growth curves of *E. coli* Tuner(DE3)/pRhotHi-2-lacI-eYFP, *P. putida* KT2440/pVLT33-GFPmut3 and *B. subtilis* DB430/pHT01-sfGFP expression cultures in the presence of novel photocaged IPTG variants **10a** (BEC) and **10b** (BC) compared to **1** (NP) as well as uninduced (0 mM) and induced (50 µM/1 mM of **14**). Cells were grown over 20 h using a BioLector system (LB medium supplemented with 50 µM of each caged compound for *E. coli* and 1 mM for *P. putida* and *B. subtilis*, 30 °C, 1200 rpm). Cell growth was analysed by determining the scattered light intensity. After 2.5, 3, and 5 h, formation of photoproducts was induced in cultures of *E. coli, P. putida* and *B. subtilis via* light exposure at 365 nm (~1 mW cm^{-2}, indicated by dashed lines) for 30 min or by the addition of conventional IPTG (**14**). Values are means of triplicate measurements.

S2.6 Effect of UV-A light illumination on cell growth and fluorescence of *E. coli*, *P. putida* and *B. subtilis* expression cultures

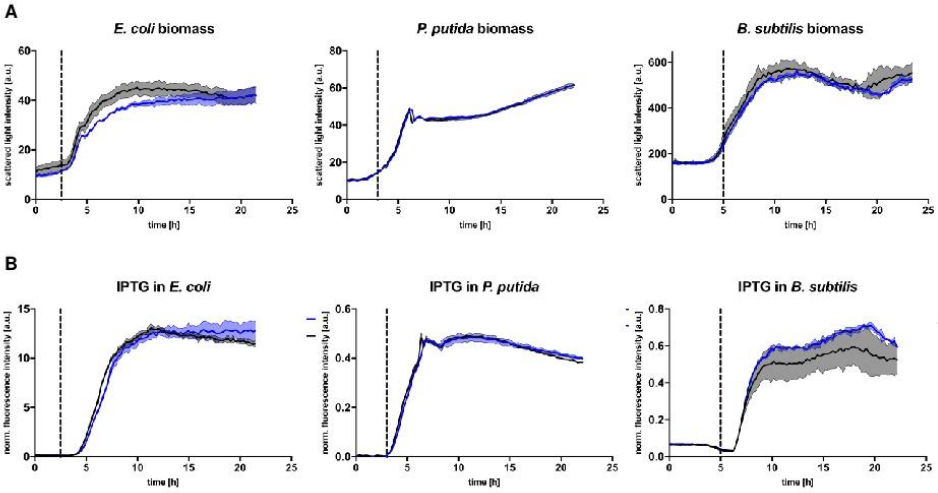

Figure S7: A) Growth curves of *E. coli* Tuner(DE3)/pRhotHi-2-lacI-eYFP, *P. putida* KT2440/pVLT33-GFPmut3 and *B. subtilis* DB430/pHT01-sfGFP expression cultures in the presence (blue line) and absence (black line) of UV-A light. Cells were grown over 20 h using a BioLector system (LB medium without inducer, 30 °C, 1200 rpm). Cell growth was analyzed by determining the scattered light intensity. After 2.5h (*E. coli*), 3 (*P. putida*), and 5 h (*B. subtilis*), cultures were exposed to UV-A light at 365 nm (~1 mW cm^{-2}, indicated by dashed lines) for 30 min. Values are means of triplicate measurements. Error bars indicate the respective standard deviations. **B)** Increase of fluorescent reporter-mediated signals during cultivation of *E. coli* Tuner(DE3)/pRhotHi-2-lacI-eYFP, *P. putida* KT2440/pVLT33-GFPmut3 and *B. subtilis* DB430/pHT01-sfGFP expression cultures with (blue line) and without (black line) UV-A exposure at 365 nm (~1 mW cm^{-2}) for 30 min; cells were grown over 20 h in LB medium at 30 °C and 1200 rpm using a BioLector system. Induction was performed using 50 µM of IPTG (**7**) for *E. coli* and 1 mM IPTG for *P. putida* and *B. subtilis*. The individual time point of induction is indicated by the dashed lines (*E. coli* 2.5 h, *P. putida* 3 h, *B. subtilis* 5 h). *In vivo* fluorescence intensities were determined by using a BioLector system (eYFP: λex = 508 nm, λem = 532 nm, GFPmut3: λex = 508 nm, λem = 532 nm, sfGFP: λex = 488 nm, λem = 520 nm) and normalised to cell densities. Values are means of triplicate measurements.

S2.7 Comparative analysis of light-responsiveness of cIPTG variants in different bacterial expression systems

In order to analyse the light-responsiveness of BC-, BEC-, and NP-cIPTG in different bacterial expression hosts, fluorescent protein expression was online monitored during batch cultivation in LB medium at 30 °C and 1200 rpm using a BioLector system (eYFP: λex = 508 nm, λem = 532 nm, GFPmut3: λex = 508 nm, λem = 532 nm, sfGFP: λex = 488 nm, λem = 520 nm). To analyse time-resolved fluorescent protein signals of *E. coli* Tuner(DE3)/pRhotHi-2-lacI-eYFP, *P. putida* KT2440/pVLT33-GFPmut3 and *B. subtilis* DB430/pHT01-sfGFP expression strains, cultures were supplemented with IPTG (**7**), BEC-cIPTG (**10a**), BC-cIPTG (**10b**), and NP-cIPTG (**1**). Induction of gene expression was performed after 2.5 h, 3 h or 5 h for *E. coli, P. putida* and *B. subtilis*, respectively, *via* UV-A light exposure at 365 nm (~1 mW cm^{-2}) for 30 min or the addition of **14**. Cell density-normalised fluorescence signal curves (Fig. S8) were plotted and fitted to a sigmoidal Boltzmann fit using GraphPad Prism 5.03 ®. The half-maximal responsiveness of each cIPTG variant was calculated from fitting parameters (Table S4) using the following standard equation for sigmoidal Boltzmann fitting:

$$y = \frac{A_1 - A_2}{1 + e^{(x - x_0)idx}} + A_2$$

Table S4: Calculation of half-maximal responsiveness $t_{0.5}$ for the lacI/P_{tac}/P_{T7}/P_{grac}-regulated systems using fitting parameters from sigmoidal Boltzmann fits. Final half-maximal responsiveness $t_{0.5}$ final was calculated as the difference of $t_{0.5}$ calc. and the induction time point t_0. ($y_{0.5}$ = fluorescence intensity at half-maximal time value, A1 = initial value, A2 = final value, x_0 = center value, dx = time constant)

Inducer	$y_{0.5}$	A1	A2	x_0	dx	$t_{0.5}$ [h] calc.	t_0 [h]	$t_{0.5}$ [h] final
***E. coli* Tuner(DE3)/pRhotHi-2-lacI-eYFP**								
NP-IPTG (1)	6.36	-0.12	12.36	6.87	1.21	6.91	2.5	4.41
BC-IPTG (10b)	5.52	-0.16	10.55	6.59	1.41	6.66	2.5	4.16
BEC-IPTG (10a)	4.36	-0.01	8.68	7.01	0.91	7.01	2.5	4.51
IPTG (14)	6.49	-0.13	12.61	6.71	0.99	6.75	3.0	3.75
***P. putida* KT2440/pVLT33-GFPmut3**								
NP-IPTG (1)	0.06	-0.01	0.10	6.37	0.78	6.58	3.0	3.58
BC-IPTG (10b)	0.15	-0.01	0.28	5.55	0.67	5.62	3.0	2.62
BEC-IPTG (10a)	0.09	0.00	0.17	5.87	0.82	5.94	3.0	2.94
IPTG (14)	0.23	0.00	0.45	4.89	0.61	4.91	3.5	1.41
***B. subtilis* DB430/pHT01-sfGFP**								
NP-IPTG (1)	0.11	0.04	0.34	7.25	0.60	6.96	5.0	1.96
BC-IPTG (10b)	0.25	0.06	0.68	7.52	0.61	7.31	5.0	2.31
BEC-IPTG (10a)	0.17	0.06	0.51	7.30	0.68	6.97	5.0	1.97
IPTG (14)	0.24	0.05	0.64	7.80	0.68	7.57	5.5	2.07

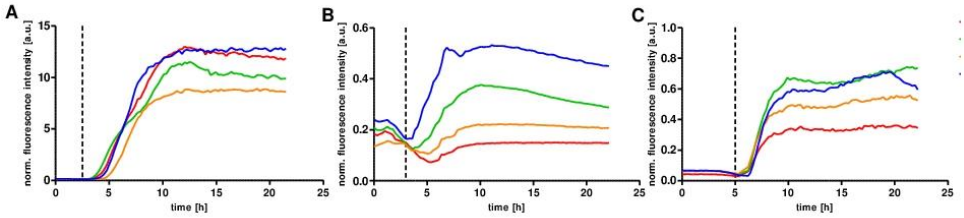

Figure S8: Normalised fluorescence protein expression profiles of *E. coli* Tuner(DE3)/pRhotHi-2-lacI-eYFP (**A**), *P. putida* KT2440/pVLT33-GFPmut3 (**B**) and *B. subtilis* DB430/pHT01-sfGFP (**C**) cultures supplemented with IPTG (**7**; blue line), BEC-cIPTG (**10a**; orange line), BC-cIPTG (**10b**; green line), and NP-cIPTG (**1**; red line) (50 µM of each compound were used for *E. coli* and 1 mM for *P. putida* and *B. subtilis*). Cells were grown over 20 h in LB medium at 30 °C and 1200 rpm using a BioLector system. Induction was performed using UV-A exposure at 365 nm (~1 mW cm^{-2}) for 30 min or respective amount of IPTG (**14**). Time of induction is indicated by dashed lines (*E. coli* 2.5 h, *P. putida* 3 h, *B. subtilis* 5 h). *In vivo* fluorescence intensities were online-monitored during cultivation (eYFP: λex = 508 nm, λem = 532 nm, GFPmut3: λex = 508 nm, λem = 532 nm, sfGFP: λex = 488 nm, λem = 520 nm) and normalised to cell densities. Values are means of triplicate measurements.

Table S5: Calculation of induction factors for IPTG and light-responsive cIPTG in *E. coli* Tuner(DE3)/pRhotHi-2-lacI-eYFP, *P. putida* KT2440/pVLT33-GFPmut3 and *B. subtilis* DB430/pHT01-sfGFP. Cultures were supplemented with IPTG (**14**), BEC-cIPTG (**10a**), BC-cIPTG (**10b**), and NP-cIPTG (**1**) in concentrations of 50 µM of each compound for *E. coli* and 1 mM for *P. putida* and *B. subtilis*. These values correspond to Figure 2 shown in the result section.

Inducer	**Induction factor**		
	E. coli	***P. putida***	***B. subtilis***
NP-cIPTG **(1)**	114.93±3.47	3.03±0.10	20.14±1.22
BC-cIPTG **(10b)**	87.57±21.15	5.47±0.12	21.80±11.94
BEC-cIPTG **(10a)**	23.45±2.36	3.62±0.20	8.20±2.67
IPTG (-UV-A)	96.80±2.56	8.65±0.14	25.62±2.21

S2.8 Heterogeneity of light-induced reporter gene expression in *E. coli* and *B. subtilis* using different cIPTG variants

Caged inducer variants **10a** (BEC), **10b** (BC) and **1** (NP) were used in comparison to conventional IPTG (**14**) to analyse the heterogeneity of reporter gene expression in *E. coli* Tuner(DE3)/pRhotHi-2-lacI-eYFP (**A, C**) and *B. subtilis* DB430/pHT01-sfGFP (**B, D**) cultures. To this end, fluorescence intensity and fluorescence distribution of 10,000 cells of a population were determined using flow cytometry when cultures reached the late logarithmic growth phase (8 h for *E. coli* and 10 h for *B. subtilis*).

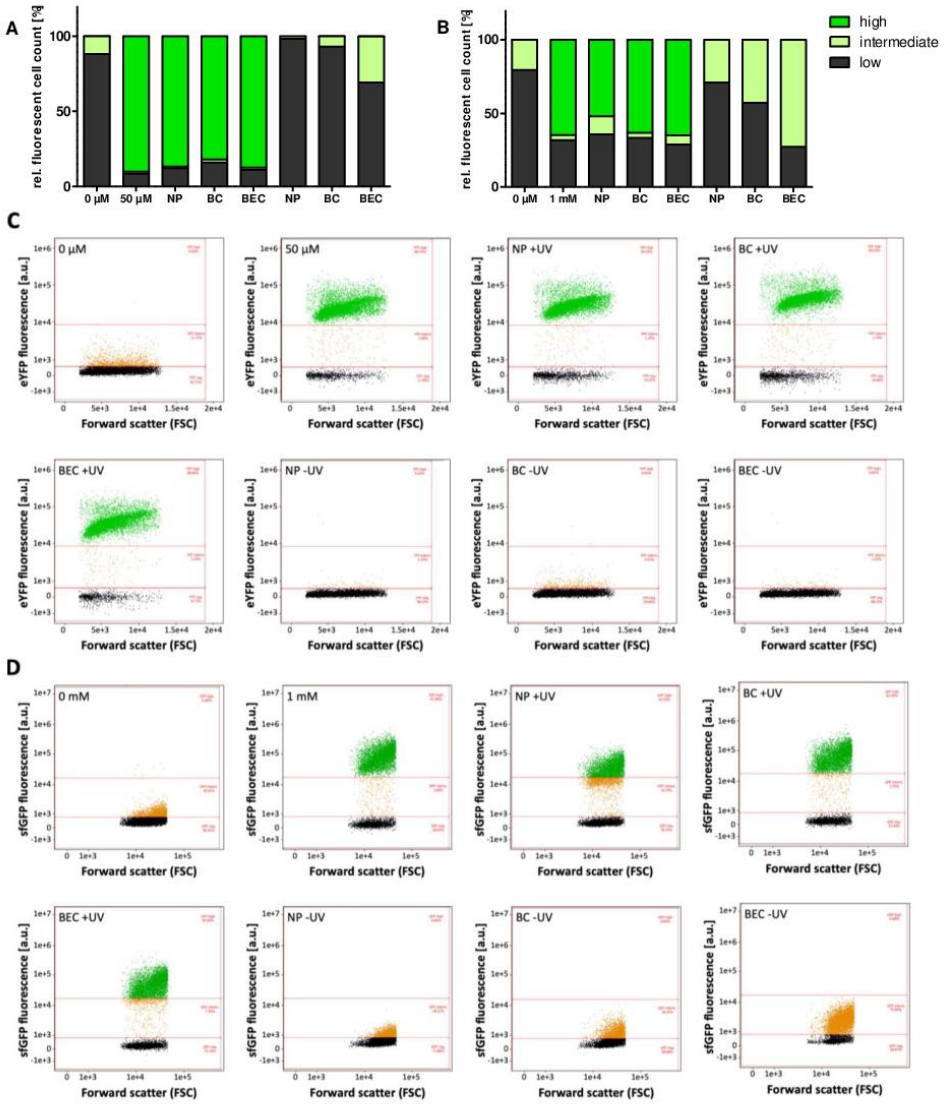

Figure S9: Single cell analysis of *E. coli* Tuner(DE3)/pRhotHi-2-lacI-eYFP (**A**) and *B. subtilis* DB430/pHT01-sfGFP (**B**) expression cultures supplemented with 50 µM of each caged compound for *E. coli* and 1 mM for *B. subtilis*. Induction was

performed after 2.5 h for *E. coli* and after 5 h for *B. subtilis* using UV-A light (30 min, ~1 mW cm^{-2}) or common IPTG (**14**). As a negative control, cells of both species were identically cultivated but kept in the dark. Culture samples were collected after late logarithmic growth phase (8 h for *E. coli* and 10 h for *B. subtilis*) and analysed using flow cytometry. The cells were gated based on FSC and SSC to exclude cell debris and accumulation of cells. The fluorescence intensities of eYFP or sfGFP were measured using a 488 nm-laser and a 528/46 nm bandpass filter and intensity values were classified into the three categories "**high**", "intermediate" **and** "**low**". All values are means of triplicate measurements. Raw data of the diagrams depicted in (**A**) and (**B**) are shown for *E. coli* Tuner(DE3)/pRhotHi-2-lacI-eYFP (**C**) and *B. subtilis* DB430/pHT01-sfGFP (**D**). Initially, the cells were gated based on their respective FSC and SSC signals to exclude cell debris and accumulation of cells. Afterwards, they were analysed regarding both their eYFP or sfGFP fluorescence intensity and their forward scatter signal (FSC). All graphs are representative examples of triplicate measurements.

S2.9 NMR spectra of compounds

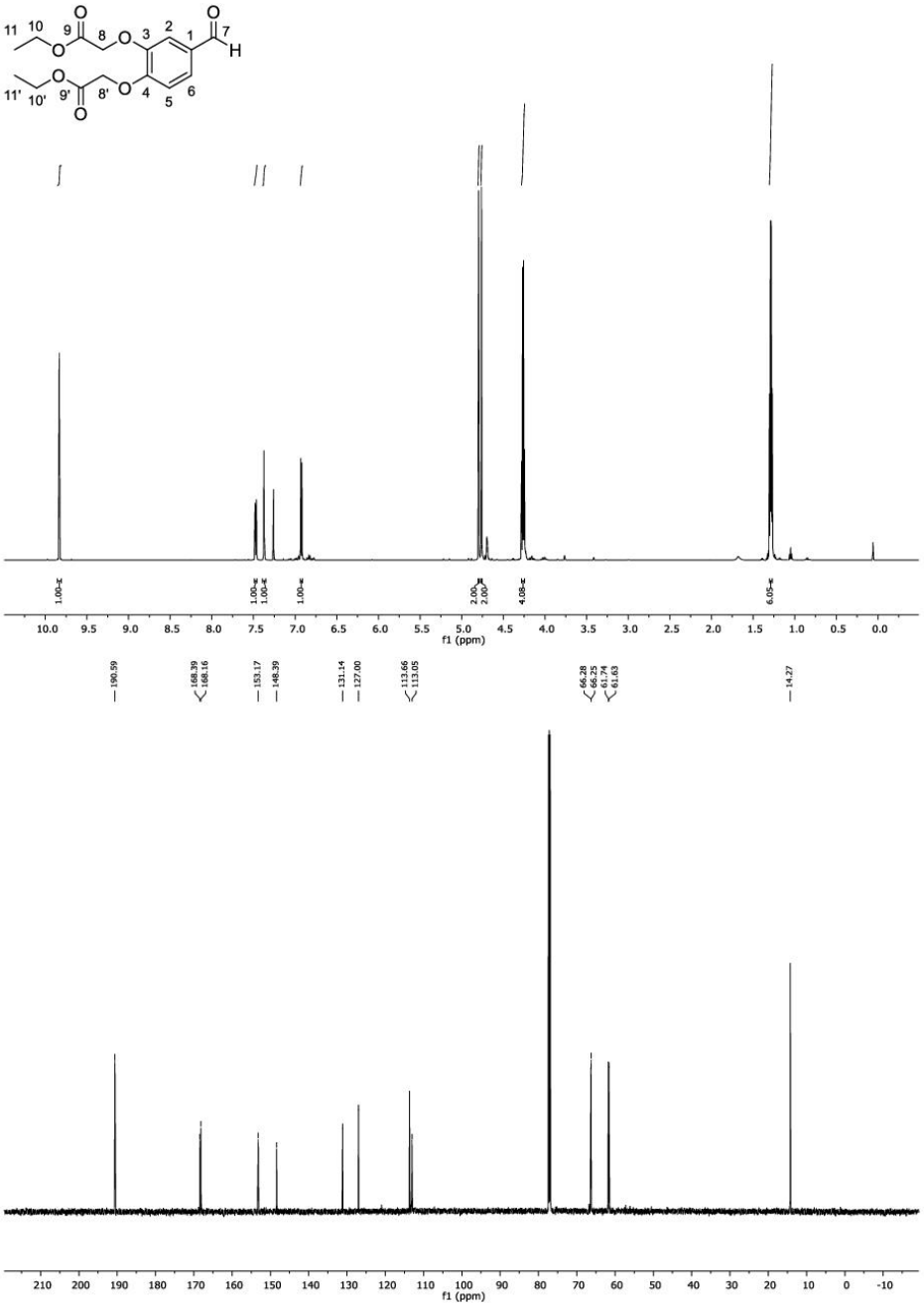

Figure S10: ^{1}H- and ^{13}C-NMR spectra of **18** in $CDCl_3$ (600 MHz/151 MHz).

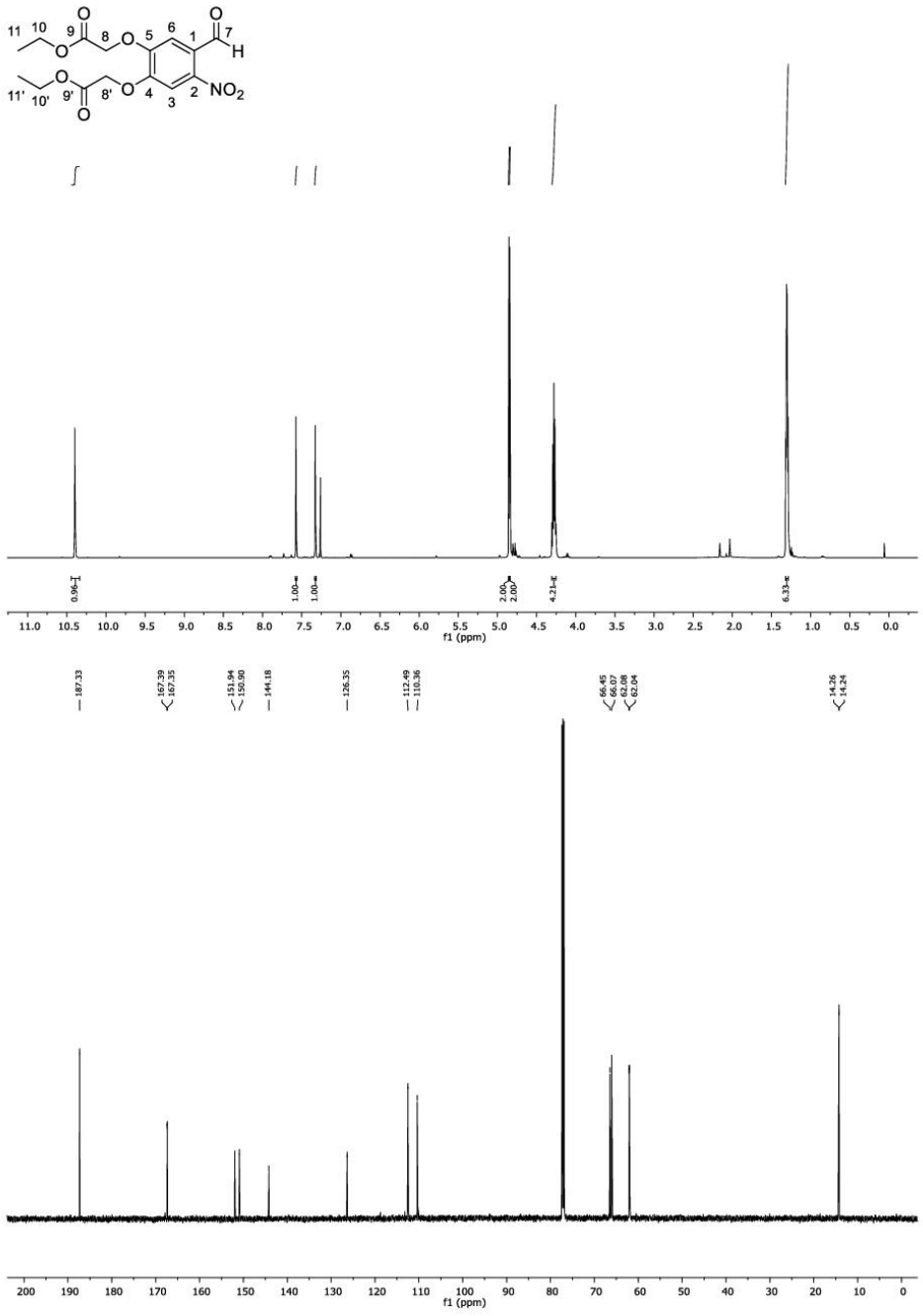

Figure S11: ^{1}H- and ^{13}C-NMR spectra of **11** in $CDCl_3$ (600 MHz/151 MHz).

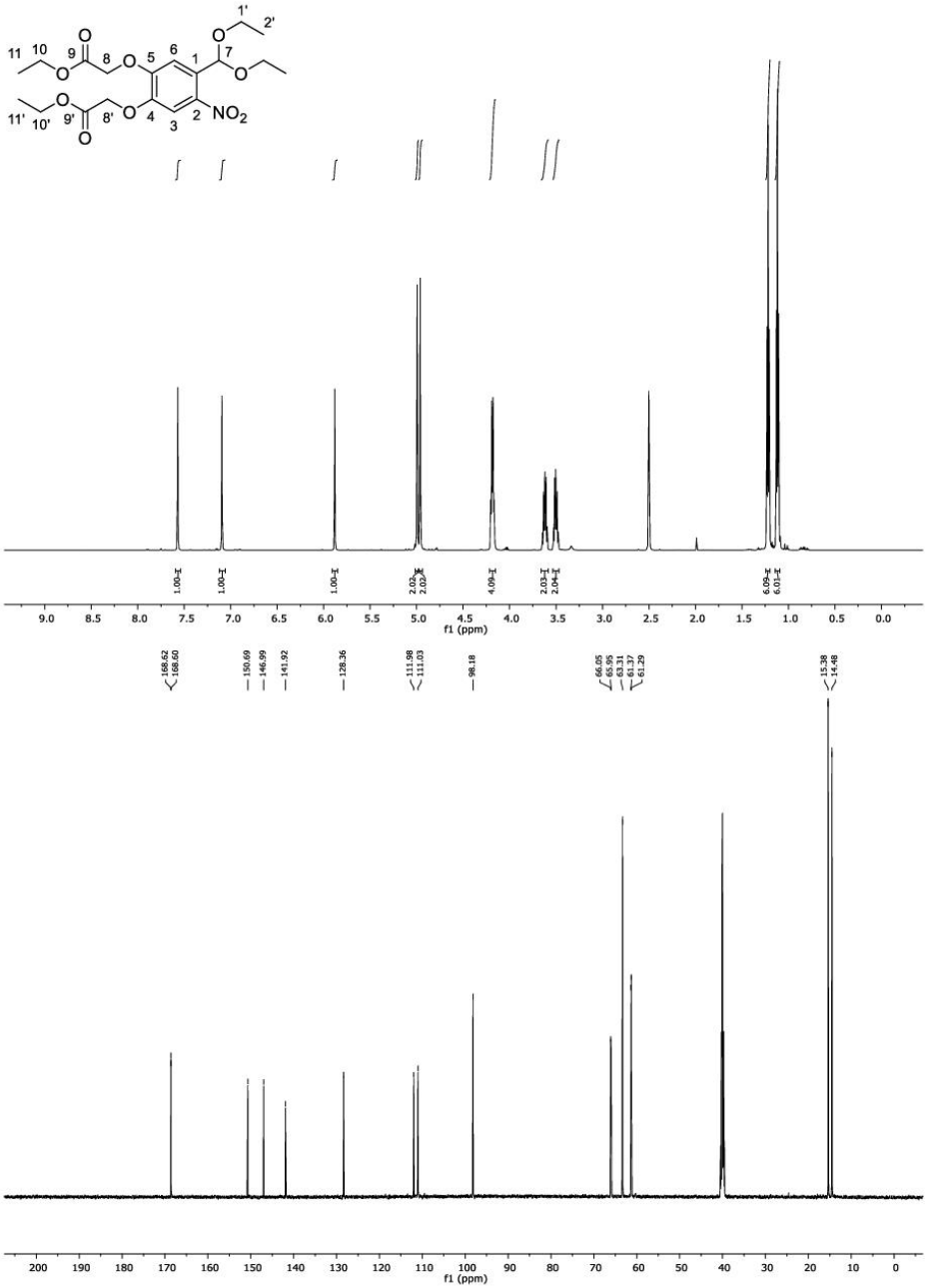

Figure S12: ^{1}H- and ^{13}C-NMR spectra of **12** in DMSO (600 MHz/151 MHz).

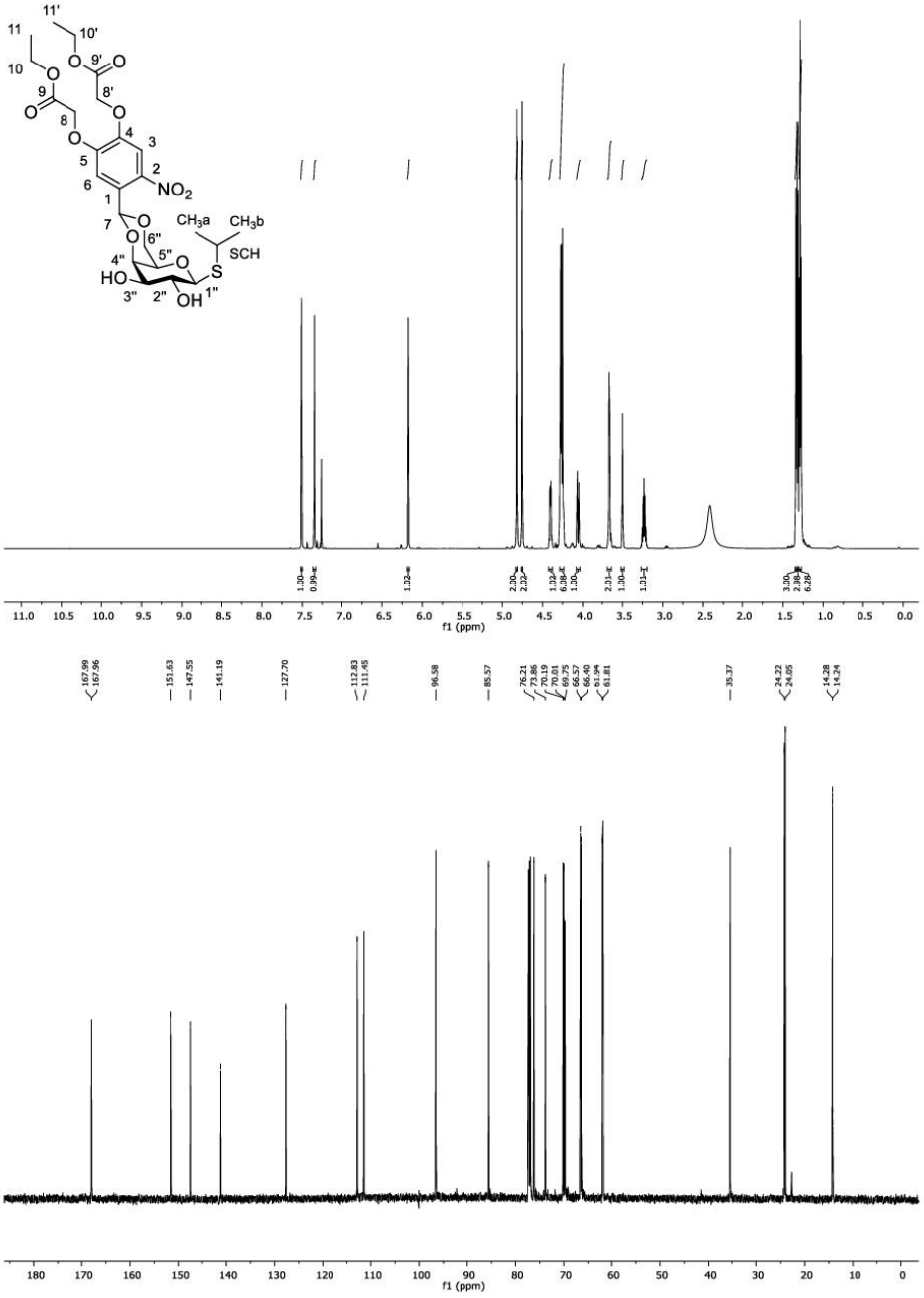

Figure S13: ^{1}H- and ^{13}C-NMR spectra of **10a** in $CDCl_3$ (600 MHz/151 MHz).

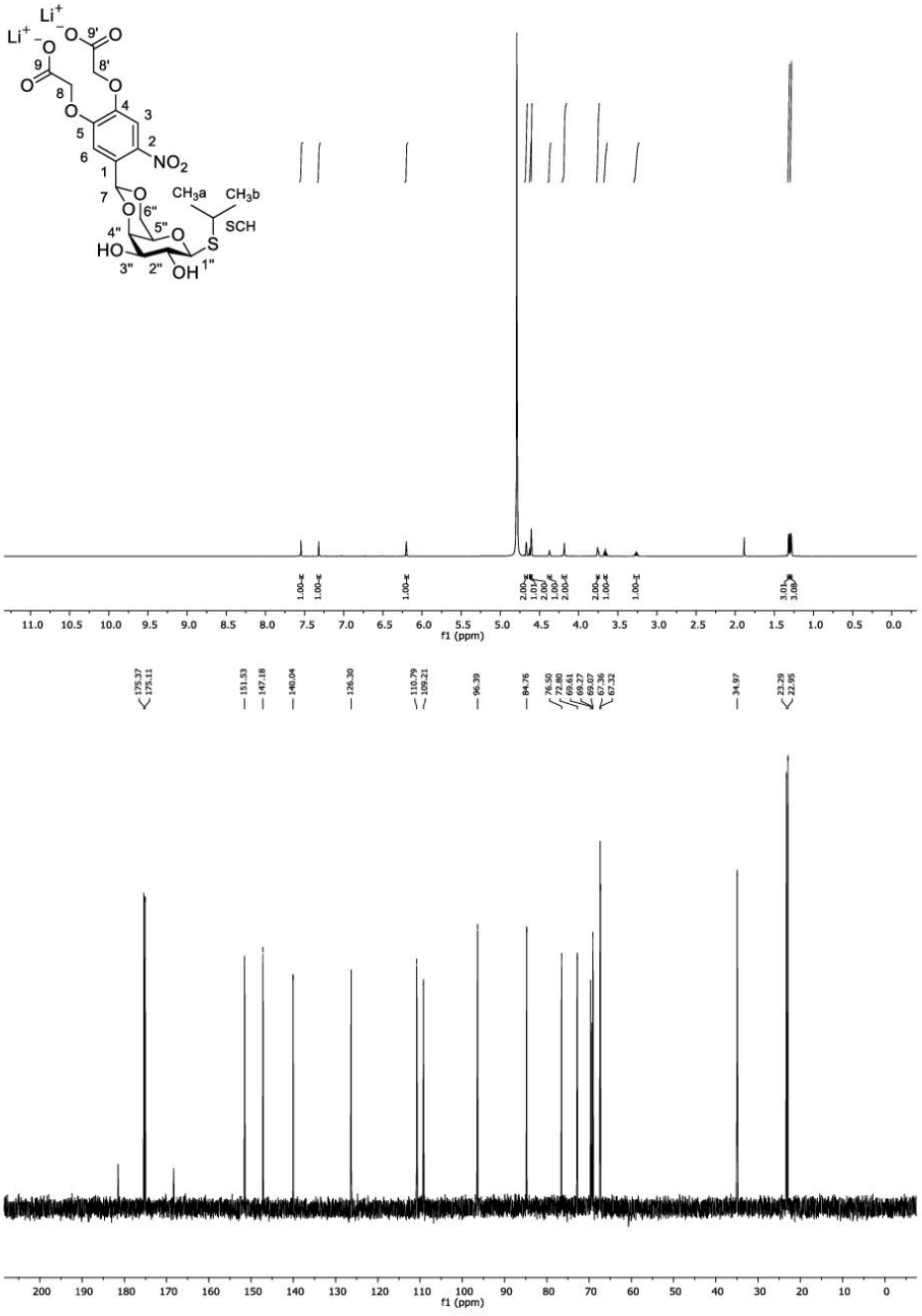

Figure S14: ^{1}H- and ^{13}C-NMR spectra of **10b** in D_2O (600 MHz/151 MHz).

S2.10 HPLC-Traces

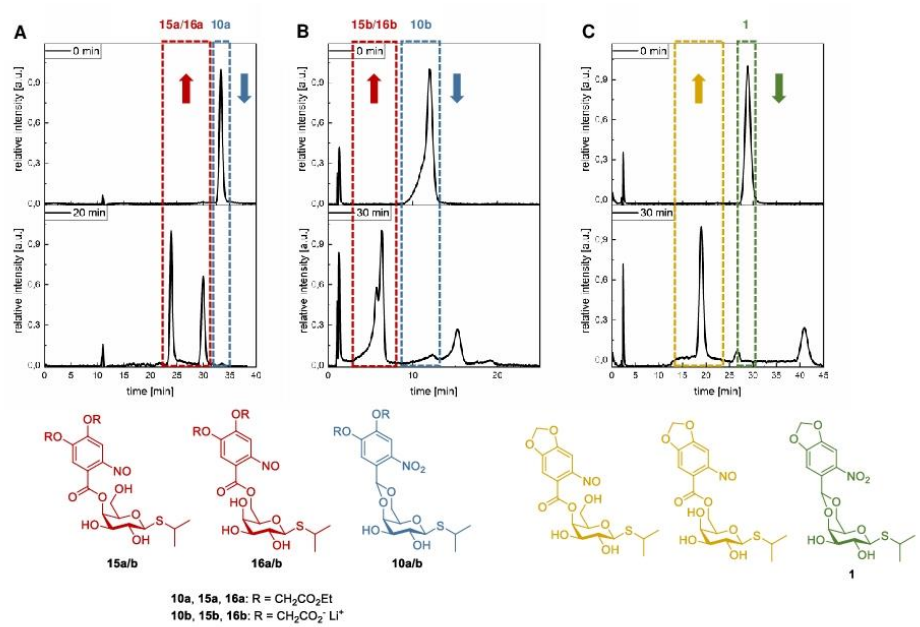

Figure S15: A) UV trace at 298 nm of the reverse phase HPLC analysis of BEC-cIPTG (**10a**) (1 mM in MeOH) before irradiation and after 20 min of irradiation (375 nm, 6.4 mW cm^{-2}, room temperature). **B**) UV trace at 340 nm of the reverse phase HPLC analysis of BC-cIPTG (**10b**) [1 mM in sodium phosphate buffer (0.1 mM, pH 7.5)] before irradiation and after 30 min of irradiation (375 nm, 6.4 mW cm^{-2}, room temperature). **C**) UV trace at 336 nm of the reverse phase HPLC analysis of NP-cIPTG (**1**) (1 mM in MeOH) before irradiation and after 30 min of irradiation (375 nm, 6.4 mW cm^{-2}, room temperature). Assignment of photoproducts for **A**), **B**) and **C**) was performed by observation of shifts in the UV-spectrum, which were in accordance to previously investigated derivatives.[9]

[1] J. Ni, D. A. Auston, D. A. Freilich, S. Muralidharan, E. A. Sobie, J. P. Y. Kao, *J. Am. Chem. Soc.* **2007**, *129*, 5316-5317.

[2] E. Brunet, M. a. T. Alonso, O. Juanes, O. Velasco, J. C. Rodríguez-Ubis, *Tetrahedron* **2001**, *57*, 3105-3116.

[3] D. Hanahan, *J. Mol. Biol.* **1983**, *166*, 557-580.

[4] R. Simon, U. Priefer, A. Pühler, *Bio/Technology* **1983**, *1*, 784-791.

[5] M. Bagdasarian, R. Lurz, B. Rückert, F. C. H. Franklin, M. M. Bagdasarian, J. Frey, K. N. Timmis, *Gene* **1981**, *16*, 237-247.

[6] R. H. Doi, S.-L. Wong, F. Kawamura, *Trends Biotechnol.* **1986**, *4*, 232-235.

[7] D. Binder, A. Grunberger, A. Loeschcke, C. Probst, C. Bier, J. Pietruszka, W. Wiechert, D. Kohlheyer, K.-E. Jaeger, T. Drepper, *Integr. Biol.* **2014**, *6*, 755-765.

[8] V. de Lorenzo, L. Eltis, B. Kessler, K. N. Timmis, *Gene* **1993**, *123*, 17-24.

[9] a) F. Bley, K. Schaper, H. Görner, *Photochem. Photobiol.* **2008**, *84*, 162-171; b) C. Bier, Heinrich Heine University Düsseldorf (Düsseldorf, Germany), **2017**.

II.3 Development of *in vivo* protein immobilization concepts

II.3.1 *In vivo* biocatalysts immobilization techniques

PUBLICATION VI

Emerging solutions for *in vivo* biocatalysts immobilization: tailor-made catalysts for industrial biocatalysis

Gizem Ölcücü[1,2*], **Oliver Klaus**[1*], Karl-Erich Jaeger[1,2],
Thomas Drepper[1#], Ulrich Krauss[1,2#]

[1]Institute of Molecular Enzyme Technology, Heinrich Heine University Düsseldorf, Forschungszentrum Jülich, 52425 Jülich, Germany
[2]Institute of Bio- and Geosciences IBG-1: Biotechnology, Forschungszentrum Jülich GmbH, 52425 Jülich, Germany

* These authors contributed equally
# Corresponding authors

Status: published

ACS Sustainable Chemistry & Engineering,
2021, 9, 27, 8919-8945
https://doi.org/10.1021/acssuschemeng.1c02045

Own contribution:
Writing parts of the manuscript – (PHA-based systems, SpyTag/-Catcher systems, comparison table, general conclusion)

ACS Sustainable Chemistry & Engineering

pubs.acs.org/journal/ascecg

Perspective

Emerging Solutions for *in Vivo* Biocatalyst Immobilization: Tailor-Made Catalysts for Industrial Biocatalysis

Gizem Ölçücü,[§] Oliver Klaus,[§] Karl-Erich Jaeger, Thomas Drepper,* and Ulrich Krauss*

Cite This: https://doi.org/10.1021/acssuschemeng.1c02045

Read Online

ACCESS | Metrics & More | Article Recommendations | Supporting Information

ABSTRACT: In industry, enzymes are often immobilized to generate more stable enzyme preparations that are easier to store, handle, and recycle for repetitive use. Traditionally, enzymes are bound to inorganic carrier materials, which requires case-to-case optimization and incurs additional labor and costs. Therefore, with the advent of rational protein design strategies as part of bottom-up synthetic biology approaches, numerous immobilization methods have been developed that enable the one-step production and immobilization of enzymes onto biogenic carrier materials often directly within the production host, which we here refer to as *in vivo* immobilization. As a result, nano- to micro-meter-sized functionalized biomaterials, or biologically produced enzyme immobilizates, are obtained that can directly be used for synthetic purposes. In this Perspective, we provide an overview over established and recently emerging *in vivo* enzyme immobilization methods, with special emphasis on their applicability for (industrial) biocatalysis. For each approach, we present fundamental working principles as well as advantages and limitations guiding future research avenues toward sustainable applications in the bioindustry.

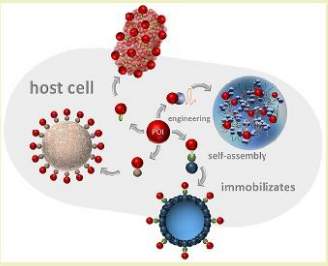

KEYWORDS: *Biocatalysis, Bioeconomy, Sustainable chemistry, Protein engineering, Synthetic biology, Enzyme immobilization*

INTRODUCTION

Industrial biocatalysis is part of a multibillion dollar industry,[1] concerned with the industrial-scale production of valuable chemical compounds such as fine chemicals, agrochemicals, and pharmaceuticals. The employed biocatalysts are enzymes, which carry out chemical reactions with exquisite efficiency and chemo-, regio-, and stereoselectivity, often not achievable with conventional chemical catalysts.[1,2] As biologically produced macromolecules, enzymes are a renewable resource and, in addition, can be regarded as sustainable and biodegradable catalysts, i.e., in contrast to rare earth or transition metal catalysts used in chemical asymmetric catalysis.[1,3] This is all the more true if the microorganism used to produce an enzyme is grown on inexpensive renewable resources, e.g., in the framework of third-generation biorefineries.[4] Likewise, enzymes as cellular constituents have evolved to optimize the biological function of their respective host organism and are generally most active and stable in an aqueous environment, at physiological temperature and pH. In contrast, industrial processes are often performed under harsh conditions, at elevated temperatures, at extreme pH values, and in the presence of organic solvents, to enable high substrate loads and product yields.[5−7] Under those conditions, however, enzymes are often unstable. While modern protein engineering methods allow the tailoring of enzymes to meet specific process requirements, the custom engineering of such tailored biocatalysts is still a time- and labor-intensive process.[1] Traditionally, enzymes have therefore been immobilized in or on inorganic and organic carrier materials, respectively, to improve their stability, while at the same time allowing easier handling and recycling in industrial settings.[8−11] This, however, increases process costs as additional materials and preparation steps are needed.[12] Furthermore, immobilization commonly results in reduced enzymatic activities as compared to the free enzymes,[13] which can be due to (partial) denaturation as a consequence of carrier attachment or diffusional limitation.[13,14] Finally, there are no truly generic immobilization techniques that work for every enzyme, so that time-consuming case-to-case optimization is needed as part of process development. Thus, in addition to the engineering of improved enzyme variants, generic, cheap, and easy to perform immobilization methods are urgently needed to further promote the use of enzymes in industrial biocatalysis, in the framework of fostering a sustainable bioeconomy.

To meet these shortcomings, a multitude of *in vivo* enzyme immobilization methods have been developed in recent years to engineer the production of solely biologically produced

Received: March 24, 2021
Revised: June 7, 2021

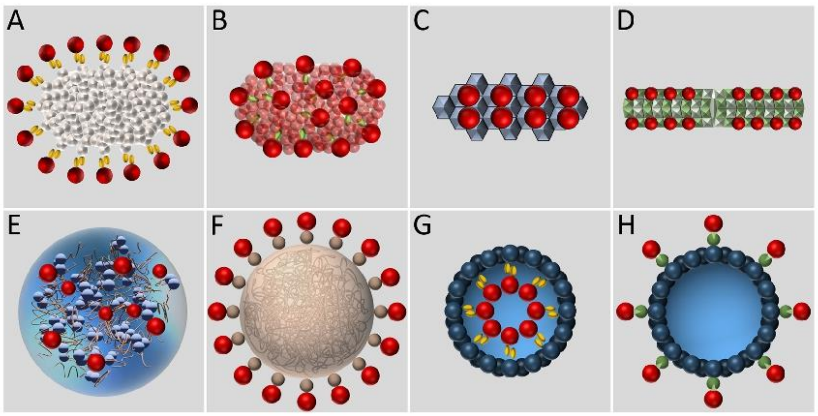

Figure 1. *In vivo* protein immobilization strategies of increasing complexity. The figure summarizes all protein immobilization principles that were considered in this Perspective. Immobilized target proteins are shown in red. (A) Inclusion body (IB) display. (B) Catalytically active inclusion bodies (CatIBs). (C) Cry3Aa crystal-based protein entrapment. (D) Forizymes. (E) Protein condensates formed by liquid−liquid phase separation (LLPS). (F) Polyhydroxyalkanoate (PHA) granule-based protein immobilization. (G) Protein encapsulation using viruslike particles (VLPs). (H) VLP-based protein display. For a better understanding, simplified schematic structures are shown, which are not drawn to scale. See Figures 2−4 for details. All abbreviations used in this Perspective are summarized in Table S1 in the Supporting Information.

enzyme immobilizates for applications in life sciences, biocatalysis, synthetic chemistry, and biomedicine.[14−24] In general, the target enzymes are engineered, e.g., by fusing them to other protein modules, which intrinsically facilitate self-assembly of the recombinant fusion protein into nano- or micro-meter-sized supramolecular structures inside (microbial) cells. This renders such *in vivo* enzyme immobilization methods very cost-effective as they enable the production of immobilized biocatalysts in one step. The insoluble nature of the resulting biocatalyst immobilizates at the same time enables efficient preparation and downstream processing, e.g., recycling from the reaction system, by centrifugation and/or filtration.

In summary, a plethora of *in vivo* methods have been developed, where different protein modules, such as aggregation or crystallization promoting tags,[17,24−27] intrinsically disordered proteins or parts thereof,[28−32] or affinity and protein−protein interaction tags, are fused to target proteins[23,33] in order to facilitate their (i) aggregation,[26,34] (ii) self-assembly,[15,35] (iii) crystal entrapment,[18,27] (iv) liquid−liquid phase separation (LLPS),[36] or (v) sequestration to cellular carrier materials[19,20,37,38] (Figure 1).

Due to the diverse nature of the different immobilization strategies, e.g., with regard to both the carrier (biogenic proteinaceous and nonproteinaceous) and the method of immobilization (surface binding/attachment, particle/crystal entrapment, or encapsulation/sequestration in compartments), it is very difficult to define decisive criteria under which the different strategies and systems can be grouped. Therefore, in the following, the different *in vivo* immobilization methods will be presented in order of increasing architectural/structural complexity of the enzyme immobilizates and the involved building principles (Figure 1). For each approach, we present fundamental working principles to illustrate the necessary engineering effort, highlight application examples to showcase applicability for biocatalysis, and summarize applicable production hosts, which are an important issue for biocatalyst production. Finally, we develop a concise overview of potential advantages and limitations for future industrial applications and research avenues.

■ DISPLAY/ENTRAPMENT OF PROTEINS ON/WITHIN INCLUSION BODIES AND PROTEIN CRYSTALS

The group of *in vivo* immobilizates, which we consider as architecturally "less" complex, includes systems that feature protein-based "carrier" materials such as conventional, inactive inclusion bodies (IBs) as the carrier for IB-display approaches,[16,39] catalytically active IBs (CatIBs),[17,25,26,40] as well as related systems that rely on target protein sequestration/encapsulation within *in vivo* produced protein crystals or compartments formed by the Cry3Aa protein of *Bacillus thuringiensis*,[18,27] plant-derived forizymes,[21] and liquid-protein condensates.[22,30,41] All abbreviations used throughout this Perspective are summarized in Table S1 of the Supporting Information.

Enzyme Immobilization by Inclusion Body Display. Bacterial IBs are dense, insoluble, submicrometer particles that form due to cellular stress, where the misfolded and partially unfolded recombinant proteins aggregate to form IBs.[42,43] In most cases, IB formation occurs due strong overexpression of recombinant genes, which puts a high load on the cell's protein quality control machinery. This is especially the case when the recombinant protein is, e.g., a large mono- or oligomer that requires assistance by chaperones and foldases to attain its native conformation. In those cases the target proteins are incorrectly folded and/or targeted within the cell (e.g., membrane proteins), or the host is unable to provide posttranslational modifications needed for native function/folding of the target. More generally, the availability of chaperones to assist the proper folding of the protein can be low due the folding/degradation machinery being titered out,

https://doi.org/10.1021/acssuschemeng.1c02045
ACS Sustainable Chem. Eng. XXXX, XXX, XXX−XXX

ACS Sustainable Chemistry & Engineering pubs.acs.org/journal/ascecg Perspective

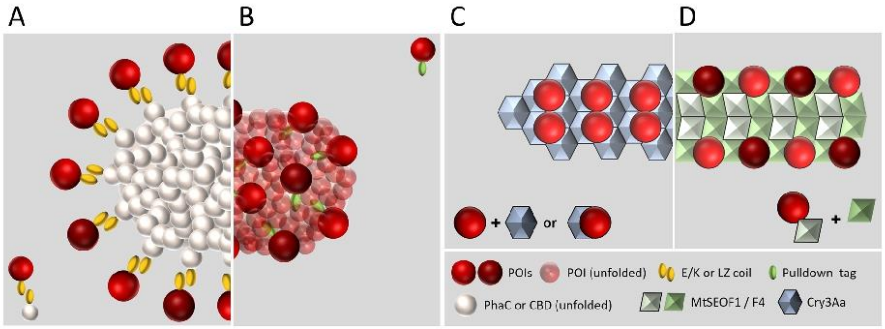

Figure 2. Inclusion body (IB) display, catalytically active IBs (CatIBs), and crystal-based immobilizates. Engineered fusion proteins required for POI immobilization as well as the resulting immobilizates are shown. Details are given in the text. (A) IB display; protein of interest (POI) linked to the surface of IBs formed by the polyhydroxybutyrate synthase PhaC or a cellulose binding domain (CBD) via E/K or LZ heterodimeric coiled coils. (B) CatIB formation is induced by the fusion of different "pull-down" tags (Table 1) to a POI. (C) POIs entrapped in crystals formed by the Cry3Aa protein of *Bacillus thuringiensis* resulting from either coexpression of Cry3Aa and a POI or fusion of a POI to Cry3Aa. (D) The POI assembled into plant-derived forisome-like crystalline structures is achieved by fusion of a POI to one forisome subunit, which is coexpressed with the same or another forisome subunit protein (e.g., POI-MtSEO-F1/MtSEO-F4).

which results in protein aggregation and deposition into IBs. IBs are formed in the cytoplasm and are typically located at the cell poles;[44] however, they can be also located in the periplasm of Gram-negative bacteria, as shown for a folding-defective variant of the maltose binding protein (MalE31), translocated to the periplasm via the Sec-secretion apparatus.[45] In addition, their presence has also been shown in yeasts[46] and mammalian cells, where they are known as aggresomes.[47] IB formation is possibly initiated from a single molecule (or a few molecules) serving as a nucleation site(s) or, rather, where smaller aggregates of proteins associate to form larger aggregates.[43] Further, the composition of IBs can vary depending on several factors such as culture conditions and the properties of the recombinant protein, and some IBs have been shown to contain amyloid-like, fibril structures, pointing toward a rather complex structure.[43,48]

Despite containing high amounts of almost pure (80−95%) target protein in a stable form that is essentially protected against proteolytic degradation,[42] IBs are generally viewed as an undesired consequence of heterologous expression as enzymes located in IBs typically lack activity (unlike enzymes that are immobilized in CatIBs, see the next section). As such, IBs are usually either discarded as waste or used for refolding studies where they are solubilized by applying denaturing agents such as urea in high concentrations, followed by slowly removing the denaturing agent from the solution to facilitate refolding of the solubilized proteins.[49]

For immobilization purposes, IBs have been used as a biological scaffold material for the immobilization of proteins of interest (POIs) (Figure 2A), which was exemplified by the aggregation of a galactose oxidase (GOase, from *Fusarium* spp.) within IBs formed by high-level expression of the polyhydroxybutyrate (PHB) synthase (PhaC) of *Cupriavidus necator* in *Escherichia coli*.[50] IB display was achieved by fusing the gene encoding the engineered, negatively charged, α-helical coil (E coil) to *phaC*, along with the fusion of the gene encoding positively charged, lysine-rich coil (K coil) to that of GOase. When coproduced in the same cell, the E coil and K coil form a heterodimer, resulting in the localization of GOase to the PhaC IBs. The loading capacity of the PhaC-IBs for GOase was estimated to exceed 200 mg of wet IBs/g, albeit with a 35% decrease in GOase activity, when compared to the activity detected in cells expressing only GOase.

In 2016, the same principle was successfully implemented using a modified PhaC-IB strategy to coimmobilize an alcohol dehydrogenase from *Rhodococcus erythropolis* and a formate dehydrogenase from *Candida boidinii*, where the formate dehydrogenase was used to regenerate NADH required by the alcohol dehydrogenase.[51] Both POIs were tagged with a K coil and cultivated as separate strains to produce the corresponding enzymes in a soluble form, using *E. coli* as a host organism. A strain producing E coil-tagged PhaC IBs was cultivated separately, and colocalization of K coil tagged alcohol dehydrogenase and formate dehydrogenase to the E coil tagged PhaC particles was achieved by mixing the appropriate fractions of the crude cell extracts together after cell lysis. In this way, an enzyme cascade was established on the surface of the PhaC IBs catalyzing the conversion of 4-chloroacetophenone to (*S*)-4-chloro-α-methylbenzyl alcohol with a 99.7% conversion rate and 99% ee, in addition to requiring NAD^+ only in catalytic amounts. The approach was also tested in a biphasic system to account for the low water solubility of the substrate, where the enzyme decorated PhaC IBs were reported to localize to the water/*n*-heptane phase boundary and catalyzed the reaction, albeit with a lowered conversion rate (67% after 72 h).

It is likewise possible to use leucine zippers (LZs) in a bait−prey strategy to localize a POI to IBs, making use of the dimerization of antiparallel LZ bait and prey domains. For instance, the cellulose binding domain (CBD) from *Cellulomonas fimi*, which was shown to form IBs when overproduced in *E. coli*,[52] was fused to a bait-LZ tag, which successfully localized the prey-LZ tagged, soluble monomeric red fluorescent protein 1 to CBD IBs.[16] Notably, an artificial 1-butanol production pathway requiring four different enzymes, namely, 3-hydroxybutyryl-CoA dehydrogenase, crotonase, and butylaldehyde/butanol dehydrogenase from *Clostridium acetobutylicum* and butyryl-CoA dehydrogenase from *Treponema*

https://doi.org/10.1021/acssuschemeng.1c02045
ACS Sustainable Chem. Eng. XXXX, XXX, XXX−XXX

denticola, has been established using LZ-mediated IB display.[39] It is worthwhile to underline that the use of E coil/K coil tagged PhaC IBs and LZ tagged CBD IBs in the above presented cases is different from the direct production of CatIBs (see the following section). Despite relying on the targeted formation of functional IBs, IB display approaches only employ the nonfunctional IB material as a scaffold onto which soluble enzymes are displayed.

Catalytically Active Inclusion Bodies (CatIBs)—Biologically Produced Enzyme Immobilizates. As outlined above, IBs are dense, insoluble aggregates of recombinant proteins that typically lack activity. However, IBs possessing catalytic activity had been reported as early as 1989, where β-galactosidase IBs were shown to be active.[53] The importance of this discovery bas been brought into more light in recent years, with the emergence of unconventional, active IBs, lately also called catalytically active inclusion bodies (CatIBs), as a targeted strategy to naturally produce novel, carrier-free enzyme immobilizates.[34,40,54−56] Unlike the more common approach employing conventional (inactive) IBs, the CatIB strategy relies on the production of the POI in a correctly folded, functional form, which is incorporated into IBs formed by the fusion protein.[40] The strategy relies on the use of aggregation-prone or aggregation-inducing tags (also called "pull-down" tags; for details see below), whose genes are fused to the gene encoding the POI at the 5′ or 3′ end, with or without linker sequences separating the tag and POI. When overproduced in the host cells, the POI folds, at least partially, into its functional conformation, while the tag provides the driving force for aggregation of the fusion protein, thereby localizing it into CatIBs (Figure 2B). Making use of the higher density pertaining to IBs, CatIBs can be easily obtained via centrifugation after cell lysis.[49] Therefore, the power of the CatIB method lies in the utilization of biologically produced enzyme immobilizates that can be directly used for biocatalysis without tedious, time-consuming, and expensive chromatographic purification and further immobilization steps. Like most immobilizates, where the substrates/products have to cross a physical barrier, CatIBs are prone to diffusional limitation,[17] which, however, was not addressed explicitly for many of the systems.

"Pull-down" tag systems available to induce CatIB formation have been reviewed extensively in recent years.[26,40] In brief, tags range from short peptides of 8−20 amino acids in length, coiled-coil tags of intermediate size (53−172 amino acids), larger aggregation-prone protein domains of up to a few hundred amino acids, to full-length proteins of more than 500 amino acids in size. Since the last published compilation of the available systems reviewed by Jäger et al. (2020) has seen a few additions, we include here a table that provides an overview over all available "pull-down" tags for CatIB formation (Table 1). Along the same lines, strategies to improve CatIB formation have also been summarized in recent reviews and are thus not covered here in detail. In summary, several factors are known that influence both CatIB formation efficiency (fraction of active POI within the insoluble IB) as well as the residual activity of the CatIBs relative to the soluble purified enzyme. In particular, the presence and nature of linker polypeptides between the tag and POI and the site of tag fusion (N- vs C-terminal), but also expression parameters such as induction strength and temperature, proved to be important.[25,40,57−59] However, systematic studies that comparatively address the properties of CatIBs produced by different means (i.e., tag and linker combinations) using the same host strain and plasmid construct as well as identical production conditions are direly needed to provide better insights into future applications of the CatIB strategy.

To illustrate the application potential of the CatIB strategy, we will, in the following paragraphs, summarize the repertoire of target proteins that have been successfully immobilized (see also Table 1). From the first discovery of β-galactosidase IBs displaying catalytic activity in the late 1980s[53] to present day, numerous POIs ranging from simple, monomeric reporter proteins to complex, cofactor requiring multimeric enzymes have been successfully immobilized within CatIBs. For instance, monomeric red fluorescent protein mCherry[25,60] and yellow fluorescent protein mYFP from *Aequorea victoria*,[25,60] weakly dimeric blue and green fluorescent proteins BFP and GFP from *A. victoria*,[24,61−65] along with DsRed from *Discosoma* sp.[52] have been aggregated in CatIBs in a functional form.

Similarly, CatIBs containing the monomeric enzymes Amadoriase II[24,62,63,67] and β-glycosidase from *Thermus caldophilus*[52] as well as the industrially relevant enzyme lipase A from *Bacillus subtilis*[17,24,62,67] have been produced. The clinically relevant, yet unstable and difficult to produce enzyme hyaluronidase from *Apis mellifera* was successfully generated as natural CatIBs (not requiring the fusion of a "pull-down" tag) in *E. coli* in a fed batch cultivation mode by the careful modification of the process parameters.[76] The resulting hyaluronidase CatIBs were used to generate hyaluronan oligosaccharides, which can be employed to stimulate angiogenesis and tumor suppression.

Dimeric enzymes that have been immobilized in CatIBs include an alkaline phosphatase from *E. coli*,[45] a β-xylosidase from *Bacillus pumilus*,[62,63] the hydroxynitrile lyase (AtHNL) from *Arabidopsis thaliana*, and the thiamine-diphosphate dependent enzyme MenD (2-succinyl-5-enol-pyruvyl-6-hydroxy-3-cyclohexene-1-carboxylate synthase) from *E. coli*, which is a promising biocatalyst for the production of functionalized α-hydroxy ketones.[17] AtHNL CatIBs were employed for the production of various chiral cyanohydrins with very high conversion rates and excellent ee values (96−99% ee), demonstrating the high stability and recyclability of CatIBs in an organic solvent-based reaction system. In addition, AtHNL CatIBs displayed a higher stability at low pH values compared to the native enzyme. Dimeric serine racemases from maize and human sources, which are dependent on pyridoxal 5′-phosphate (PLP) as a cofactor, have been recently added to the growing list of POIs that were incorporated within CatIBs.[78] It is worthwhile to note that, in the case of human and maize serine racemase CatIBs, from the two functions of these enzymes, namely, the reversible racemization of L-serine to D-serine, and the dehydration of both enantiomers to produce pyruvate and ammonia, only the first function has been retained, therefore generating CatIBs with altered substrate specificity.

More complex targets were also immobilized via the CatIB strategy. These include the tetrameric sialic acid aldolase[74] involved in the production of sialic acid Neu5Ac, which is a precursor for the synthesis of anti-influenza drugs, in addition to being a food additive,[79] and β-glucuronidase from *E. coli*.[52] Additionally, NADPH-dependent, tetrameric alcohol dehydrogenases from *Ralstonia* sp. (RADH) and *Lactobacillus brevis* (LbADH), and ThDP-dependent, tetrameric enzymes benzaldehyde lyase from *Pseudomonas fluorescens* (PfBAL)[25,69] and

https://doi.org/10.1021/acssuschemeng.1c02045
ACS Sustainable Chem. Eng. XXXX, XXX, XXX−XXX

Table 1. Overview of Different CatIB Formation-Inducing "Pull-Down" Tags[a]

name (origin)	length (no. of amino acids)	tag property	linker/*structure*	target enzyme/ protein	target origin	CatIB-formation efficiency[b] [%]	residual activity[c] [%]	ref
			(I) Artificial Peptides					
L6KD (and variants)	8	amphiphilic	PTPPTTPTPPTTPTPTP *unstructured*	lipase A	*Bacillus subtilis*	80	30*	24
			PTPPTTPTPPTTPTPTP *unstructured*	amadoriase II	*Aspergillus fumigatus*	61	93*	24
			PTPPTTPTPPTTPTPTP *unstructured*	β-xylosidase	*Bacillus pumilus*	84	26*	24
			PTPPTTPTPPTTPTPTP *unstructured*	GFP	*Aequorea victoria*	n.i.[d]	n.a.[e]	24
			PTPPTTPTPPTTPTPTP *unstructured*	lysine decarboxylase	*Escherichia coli*	n.i.	n.i.	59
			$(GGGS)_3$ *unstructured*	lysine decarboxylase	*E. coli*	n.i.	n.i.	59
			n.i.	tyrosine phenol-lyase	*Citrobacter freundii*	up to 41	n.i.	66
GFIL8 (and variants)	8	β-sheet	PTPPTTPTPPTTPTPTP *unstructured*	lipase A	*B. subtilis*	89	43*	67
			PTPPTTPTPPTTPTPTP *unstructured*	amadoriase II	*A. fumigatus*	93	54*	67
			PTPPTTPTPPTTPTPTP *unstructured*	Ulp1 protease	*Saccharomyces cerevisiae*	n.i.	40*	68
			PTPPTTPTPPTTPTPTP *unstructured*	lysine decarboxylase	*E. coli*	n.i.	n.i.	59
			$(GGGS)_3$ *unstructured*	lysine decarboxylase	*E. coli*	n.i.	n.i.	59
			n.i.	tyrosine phenol-lyase	*C. freundii*	98	n.i.	66
ELK16 (and variants)	16	β-sheet	PTPPTTPTPPTTPTPTP *unstructured*	amadoriase II	*A. fumigatus*	120	88*	63
			PTPPTTPTPPTTPTPTP *unstructured*	β-xylosidase	*B. pumilus*	94	77*	63
			PTPPTTPTPPTTPTPTP *unstructured*	GFP	*A. victoria*	n.i.	n.a.	63
			n.i.	tyrosine phenol-lyase	*C. freundii*	up to 49	n.i.	66
18A (and variants)	18	α-helical	PTPPTTPTPPTTPTPTP *unstructured*	lipase A	*B. subtilis*	90	150*	62
			PTPPTTPTPPTTPTPTP *unstructured*	amadoriase II	*A. fumigatus*	n.i.	n.i.	62
			PTPPTTPTPPTTPTPTP *unstructured*	β-xylosidase	*B. pumilus*	n.i.	n.i.	62
			PTPPTTPTPPTTPTPTP *unstructured*	GFP	*A. victoria*	n.i.	n.a.	62
			PTPPTTPTPPTTPTPTP *unstructured*	lysine decarboxylase	*E. coli*	n.i.	n.i.	59
			$(GGGS)_3$ *unstructured*	lysine decarboxylase	*E. coli*	n.i.	n.i.	59
			n.i.	tyrosine phenol-lyase	*C. freundii*	87	n.i.	66
ELP10	10	random coil/β-turn spiral[f]	n.i.	tyrosine phenol-lyase	*C. freundii*	51	n.i.	66
ELP20	20	random coil/β-turn spiral[f]	n.i.	tyrosine phenol-lyase	*C. freundii*	>20	n.i.	66
			(II) Coiled-Coil Domains/Proteins					
TDoT (*Staphylothermus marinus*)	53	tetrameric coiled coil	$(GGGS)_3$ *unstructured*	hydroxynitrile lyase	*Arabidopsis thaliana*	76	11	17
			$(GGGS)_3$ *unstructured*	MenD[g]	*E. coli*	90	n.i.	17
			$(GGGS)_3$ *unstructured*	lipase A	*B. subtilis*	114	n.i.	17
			$(GGGS)_3$ *unstructured*	alcohol dehydrogenase	*Ralstonia* sp.	88	2	25, 60
			$(GGGS)_3$ *unstructured*	alcohol dehydrogenase	*Lactobacillus brevis*	5	6	25
			$(GGGS)_3$ *unstructured*	benzaldehyde lyase	*Pseudomonas fluorescens*	88	1	25, 69
			$(GGGS)_3$ *unstructured*	benzoylformate decarboxylase	*Pseudomonas putida*	1	4	25

https://doi.org/10.1021/acssuschemeng.1c02045
ACS Sustainable Chem. Eng. XXXX, XXX, XXX−XXX

Table 1. continued

name (origin)	length (no. of amino acids)	tag property	linker/*structure*	target enzyme/protein	target origin	CatIB-formation efficiency[b] [%]	residual activity[c] [%]	ref
			(II) Coiled-Coil Domains/Proteins					
			$(GGGS)_3$ *unstructured*	lysine decarboxylase	*E. coli*	n.i.	n.i.	25, 59, 70
			$(GGGS)_3$ *unstructured*	YFP	*A. victoria*	65	n.a.	25, 60
			$(GGGS)_3$ *unstructured*	mCherry	*Discosoma* sp.	42	n.a.	25, 60
			PTPPTTPTPPTTPTPTP *unstructured*	lysine decarboxylase	*E. coli*	n.i.	n.i.	59
Jun	62	leucine zippers	SGGGSGGS *unstructured*	EGFP	*A. victoria*	53[h]	n.a.	71
Fos	93	leucine zippers	SGGGSGGS *unstructured*	EGFP	*A. victoria*	74[i]	n.a.	71
ZapB (*E. coli*)	81	dimeric coiled coil protein	SIPGA	GFP	*A. victoria*	95	n.a.	72
				mCherry	*Discosoma* sp.	55	n.a.	72
3HAMP (*Pseudomonas aeruginosa*)	172	dimeric coiled coil	$(GGGS)_3$ *unstructured*	alcohol dehyrogenase	*Ralstonia* sp.	75	12	25
			$(GGGS)_3$ *unstructured*	alcohol dehyrogenase	*L. brevis*	67	1	25
			$(GGGS)_3$ *unstructured*	benzaldehyde lyase	*P. fluorescens*	76	18	60
			$(GGGS)_3$ *unstructured*	benoylformate decarboxylase	*P. putida*	61	10	25
			$(GGGS)_3$ *unstructured*	lysine decarboxylase	*E. coli*	n.i.	n.i.	59, 70
			$(GGGS)_3$ *unstructured*	YFP	*A. victoria*	6	n.a.	25
			$(GGGS)_3$ *unstructured*	mCherry	*Discosoma* sp.	5	n.a.	25
			PTPPTTPTPPTTPTPTP *unstructured*	lysine decarboxylase	*E. coli*	n.i.	n.i.	59
			(III) Aggregation-Prone Proteins (Protein Domains)					
Aβ42(F19D) (*Homo sapiens*)	42	amyloid peptide	n.i.	BFP	*A. victoria*	61–65	31[f]	61
CBDcell (*Cellulomonas fimi*)	108	cellulose binding protein	n.i.	β-glucuronidase	*E. coli*	92	19	52
				β-glycosidase	*Thermus caldophilus*	93	n.i.	52
				DsRed	*Discosoma* sp.	n.i.	n.a.	52
CBDclos (*Clostridium cellulovorans*)	156	cellulose binding protein	43 amino acids with thrombin cleavage site, S-Tag, and cloning site	D-amino acid oxidase	*Trigonopsis variabilis*	>90	42*	73
				D-sialic acid aldolase	*E. coli K12*	100	100*	74
				maltodextrin phosphorylase	*Pyrococcus furiosus*	83	n.i.	74
				cytidylate kinase	*E. coli*	n.i.	n.i.	75
				polyphosphate kinase PPK3	*Silicibacter pomeroyi*	n.i.	n.i.	75
				GFP	*A. victoria*	n.i.	n.i.	65
				Gal1[k]	*E. coli*	n.i.	n.i.	65
VP1 capsid protein (foot-and-mouth disease virus)	209	virus capsid protein	n.i.	β-galactosidase	*E. coli*	36–46	166*	61
				GFP	*A. victoria*	n.i.	n.a.	61
GFP (*A. victoria*)	238	fluorescent protein	$(GGGS)_5$ *flexible*	acid phosphatase	*Enterobacter aerogenes*	n.i.	48	58
			$(AAAKE)_3$ *rigid*	acid phosphatase	*Enterobacter aerogenes*	n.i.	58	58

https://doi.org/10.1021/acssuschemeng.1c02045
ACS Sustainable Chem. Eng. XXXX, XXX, XXX−XXX

Table 1. continued

name (origin)	length (no. of amino acids)	tag property	linker/*structure*	target enzyme/protein	target origin	CatIB-formation efficiency[b] [%]	residual activity[c] [%]	ref
			(III) Aggregation-Prone Proteins (Protein Domains)					
MalE31 (*E. coli*)	396	maltose binding protein	RIPGG *unstructured*	alkaline phosphatase	*E. coli*	>95	n.i.	45
				β-lactamase	*E. coli*	>95	n.i.	45
PosB (*Paenibacillus polymyxa E681*)	574	pyruvate oxidase	n.i.	GFP	*A. victoria*	n.i.	n.a.	64
				α-amylase	*B. subtilis*	77	200[f]	64

[a]Cases where residual activity was compared only to cell lysate are marked with an asterisk (*). Details, like sequences, names, and originating organisms for all listed "pull-down" tags, can be found in refs 26 and 40. [b]CatIB-formation efficiency: defined as the activity, or in the case of fluorescent proteins, fluorescence, of the insoluble IBs relative to the activity/fluorescence of the crude cell extract. [c]Residual activity compared to purified enzyme. [d]n.i.: No information provided. [e]n.a.: Not applicable. [f]Tag property information obtained from ref 77. [g]MenD: 2-succinyl-5-enol-pyruvyl-6-hydroxy-3-cyclohexene-1-carboxylate synthase. [h]Construct containing both leucine zippers. [i]Coproduction of leucine zippers. [j]Residual specific fluorescence compared to cell lysate. [k]GalU: UDP-glucose pyrophosphorylase. [l]Volumetric activity.

benzoylformate decarboxylase from *Pseudomonas putida* (PpBFD),[25] have been similarly immobilized in the past. Particularly noteworthy is the successful implementation of a two-step cascade reaction, which was realized using CatIBs with colocalized PfBAL and RADH, where PfBAL converted benzaldehyde and acetaldehyde to (*R*)-2-hydroxy-1-phenylpropanone, which was further converted by RADH to benzyl alcohol and (1*R*, 2*R*)-1-phenylpropane-1,2-diol, a precursor of the calcium channel blocker diltiazem.[60] Recently, the tetrameric, PLP-dependent tyrosine phenol-lyase, which can be employed to produce enantiomerically pure *α*-deuterated (*S*)-amino acids, such as the dopamine precursor L-dihydroxyphenylalanine, has been immobilized using C-terminal fusions of nine different artificial peptide tags.[66] Notably, two of those constructs (bearing GFIL16 and 18AWT tags) yielded CatIBs with improved thermostability and half-lives, reaching 87−98% of the activity detected in the supernatant of the soluble enzyme, respectively. To the best of our knowledge, the most complex oligomeric POI that was immobilized with the CatIB strategy is the PLP-dependent, decameric L-lysine decarboxylase from *E. coli*, using TdoT and 3HAMP as tags.[25,70] The enzyme is of high industrial relevance due to its ability to produce 1,5-diaminopentane (cadaverine), which is a building block for biobased polyamides. Recently, a number of small, artificial peptide tags have also been employed for the immobilization of L-lysine decarboxylase in CatIBs as well.[59]

Enzyme Immobilization by Cry3Aa Crystal Entrapment. The Cry family of proteins, produced by the Gram-positive soil bacterium *B. thuringiensis*, comprises highly valued toxins due to their insecticidal use.[80] Cry proteins have been classified in over 70 subgroups based on their sequence identities, and in general, each class exhibits selective toxicity against specific insect orders. For instance, the Cry1 class proteins exhibit specific toxicity to larvae of Lepidoptera species; Cry2 proteins are effective against Lepidoptera and Diptera species, and Cry3 class proteins are active against Coleoptera species.[80,81] Historically, Cry formulations have been used in agriculture for pest control, and since the 1990s, genetically modified crops that heterologously produce Cry proteins have been conferred with a resistance toward certain insects.[82] Moreover, an interesting characteristic of the Cry proteins is their ability to form crystals as inclusions within their natural host, which is thought to facilitate the invasion of the insect gut tissues.[80]

Apart from their common employment as an insecticide, a novel use of Cry crystals was demonstrated in 2015, where the ability of the Cry3Aa protein to form natural crystals was exploited to deliver several POIs to macrophages and mice in a functional form.[83] The genes encoding fluorescent reporter proteins GFP and mCherry, along with the firefly luciferase as model POIs, have been fused to the *cry3Aa* gene, which facilitates the entrapment of the respective POI within the intracellularly formed Cry3Aa crystals (Figure 2C). The isolated crystals, obtained via density gradient centrifugation, were shown to exhibit GFP- and mCherry-specific fluorescence, confirming the proper folding of these POIs within the crystals. Notably, the crystals were reported to retain their fluorescence for several weeks, pointing toward high stability of the POIs within the crystalline matrix.

Cry3Aa crystal entrapment was utilized for enzyme immobilization. Here, the monomeric enzymes peptide deformylase from *Borrelia burgdorferi* along with the lipase A

https://doi.org/10.1021/acssuschemeng.1c02045
ACS Sustainable Chem. Eng. XXXX, XXX, XXX−XXX

and a *para*-nitrobenzyl esterase PnbA from *B. subtilis* were immobilized within Cry3Aa crystals, where they displayed very high activities.[27] Notably, the immobilized *para*-nitrobenzyl esterase completely retained its activity, whereas the lipase A and the peptide deformylase showed approximately 84% and 48% of the activities when compared to their purified soluble counterparts, respectively. An additional construct lacking 19 residues from the C-terminus of Cry3Aa and carrying a flexible GGGS linker between the lipase and Cry3Aa was generated in an attempt to improve substrate accessibility to the enzyme, through providing a better orientation toward the large channels of the Cry3Aa crystals. Utilizing this approach, the authors reported that the activity of immobilized lipase A within the modified Cry3Aa crystals was boosted by more than 2-fold. The authors, moreover, noted that all constructs had similar K_m values and concluded that, for Cry3Aa-based immobilizates, unlike for other immobilization strategies, internal diffusion and mass transfer limitations are not an issue. In addition, improved thermostability, tolerance to organic solvents, and recyclability have been demonstrated for the modified Cry3Aa immobilized lipase, and fatty acid methyl ester (FAME) biodiesel was produced with high conversion rates (over 80% after 10 cycles). *Proteus mirabilis* lipase (PML) and its mutant Dieselzyme 4 (DLZM4) with high methanol tolerance have been likewise immobilized using the self-crystallizing Cry3Aa protein in *B. thuringiensis*.[84] However, these fusions resulted in a 20-fold activity reduction for PML and an almost complete loss of activity for DLZM4 when compared to the purified native enzymes. According to the authors, the exact reason for the observed reduction in activity remains unclear but could be because fusion to Cry3Aa does not orient PML in an optimal position for catalysis. To counter this, the authors used a directed evolution approach, and *E. coli* colonies were screened resulting in the identification of a Cry3Aa-PML double mutant (Cry3Aa-PML^{VG}) with improved activity. Additionally, despite the positive effect of Cry3Aa immobilization on thermostability, Cry3Aa-PML incubated in methanol showed a 2-fold lower activity compared to soluble PML, indicating that tolerance toward organic solvents could not be improved in this case. Interestingly, the K_m values for both immobilized Cry3Aa-PML and Cry3Aa-PML^{VG} were only about 2-fold higher compared to their soluble counterparts, suggesting that the lower activity was not due to significantly limited substrate diffusion. In a follow-up study, it was demonstrated that enzymes can be entrapped within the Cry3Aa crystals when coproduced, without the need of generating Cry3Aa fusions[18] (Figure 2C). The previously identified double mutant PML^{VG} was entrapped within the crystals via coproduction, and washing the crystals with buffers at pH values between 4 and 9, or high concentrations of sodium chloride, did not result in substantial release of the enzyme. Furthermore, the strategy has found use in bioremediation, where a metallothionein from *Synechococcus elongatus* was fused to Cry3Aa.[85] Here, the *smtA* gene encoding the metallothionein was cloned in up to six tandem repeats for the fusion to Cry3Aa, which generated crystals with similar sizes and morphologies and bound chromium and cadmium with efficiencies positively correlating with the *smtA* copy number. Notably, when nine copies of SmtA were fused to Cry3Aa, the yield was low, and the resulting crystals were less stable, pointing toward the limitation of the approach for incorporating large POIs.

Forizymes—Scaffolding of Enzymes by Using Plant Mechanoprotein Complexes. Forisomes are mechanoprotein complexes found exclusively in the phloem of legumes.[86] When the phloem is wounded, forisomes undergo a reversible conformational change and assume a dispersed, pluglike state in an adenosine triphosphate (ATP)-independent manner, allowing them to plug the sieve tubes and therefore prevent the loss of photoassimilates.[86,87] When the sieve elements regenerate, forisomes revert to their condensed, spindlelike shape. This process is triggered by the influx of calcium ions caused by wounding of the phloem; however, other divalent ions and pH change are also shown to trigger the conformational change of forisomes *ex vivo*.[88] The size of forisomes is between approximately 10 × 1 and 55 × 5 μm depending on the plant species, and the conformational change can confer an up to 9-fold increase in volume *in vitro*.[86,87,89]

From the four genes encoding forisome subunits, MtSEO-F1−4 (SEO-F1−4: sieve element occlusion by forisome) from *Medicago truncatula*, expressing only *mtSEO-F1* or *mtSEO-F4* was shown to be sufficient in generating functional forisome bodies in yeast and plant systems.[88,90] This finding paved the way for the production of functional artificial forisomes (hereinafter referred as forizymes), where heterologously expressed forisomes were used to produce several POIs in an active form in *Saccharomyces cerevisiae*.[21] The blue fluorescent protein cerulean, enhanced yellow fluorescent protein (eYFP), dimeric glucose-6-phosphate dehydrogenase (G6PDH), and hexokinase 2 (HXK2) containing forizymes were generated via the fusion of the corresponding genes to forisome subunits MtSEO-F1 and MtSEO-F4. Fusions of eYFP to forisome subunits showed that the generation of functional forizymes is highly dependent on the fusion site. Moreover, a simple fusion of the POI to MtSEO-F1 or MtSEO-F4 subunit was not enough to trigger forizyme formation in all cases except one. Instead, a heteromeric combination approach based on the coproduction of the forisome subunit together with the POI-MtSEO-F1/MtSEO-F4 fusion was required (Figure 2D). Interestingly, C-terminal fusions of eYFP to either forisome subunit generated fluorescent IBs rather than forizymes, which were similarly observed in C-terminal fusions in heteromeric combinations. Furthermore, the activity of the G6PDH forizymes was measured at different Ca^{2+} concentrations, and the resulting conformational change was shown to have no significant effect on the enzyme activity. This demonstration highlights the suitability of forizyme-based immobilizates for the immobilization of divalent-metal-utilizing/containing enzymes, yet further studies are needed to ascertain this issue. A positive effect of the approach on stability was also reported, where 80% of the original G6PDH activity could be detected after 10 reaction cycles. Notably, the HXK2 forizymes generated in a similar manner displayed activities within the same range of the literature values as reported in the study. For colocalization analyses, the authors built constructs bearing eYFP and cerulean as fluorescent reporters fused to genes encoding G6PDH and HXK2 enzymes, respectively, with each fusion additionally containing a forisome subunit. A cascade reaction was realized using G6PDH and HXK2 forizymes coproduced in yeast cells. To this end, fusion proteins consisting of G6PDH and HXK2 fused to MtSEO-F1 were coproduced with MtSEO-F1, yielding colocalization of the enzymes in approximately 51% of the forizymes. In addition, the reaction rate of the bifunctional forizymes was 1.3-fold higher, when compared to the mixtures of forizymes of

https://doi.org/10.1021/acssuschemeng.1c02045
ACS Sustainable Chem. Eng. XXXX, XXX, XXX−XXX

Table 2. Overview of Different Systems Used for Liquid−Liquid Phase Separation (LLPS) to Form Biomolecular Condensates[a]

[name of system]:LLPS-inducing tag	architecture	LLPS by	condensate morphology	*in vivo* production *[host/cell line]*	reversibility	target recruitment by	ref
[−/−]: SH3, PRM	$(SH3)_{1-5}$	multivalent interaction	liquidlike, maturation into gel	yes, *[HeLa]*	reversible, but sol−gel hardening observed *in vitro*	fusion to droplet forming domain fusion $(SH3)_6$ and $(PRM)_5$	29
[REPS]: RGG	$(RGG)_{1-3}$; RGG-[TEV/Th]-RGG; MBP-[HRV 3C]-$(RGG)_2$	multivalent interaction of IDPs; droplet disassembly by proteolytic cleavage; droplet assembly by proteolytic cleavage of MBP	liquidlike	yes, *[HEK293, HeLa, and U2OS]*	reversible assembly and disassembly	fusion of synthetic coiled-coil peptides (SYNZIPs) to droplet forming domain fusion and POI recruitment via SYNZIP interaction	31
[iPOLYMER]: FKBP, FRB	$(FKBP)_{1-5}$ = $(YF)_{1-5}$ and $(FRB)_{1-5}$ = $(CR)_{1-5}$	multivalent interaction	hydrogel-like	yes, *[COS-7]*	irreversible	fusion to droplet forming domain fusion (e.g., $(YF)_{1-5}$ or sequestration to RNA granula formed by via TIA-1 fused to CR_5)	30
[iPOLYMER]-Li: iLID, SspB	$(iLID)_6$ and $(SspB)_6$	light-triggered multivalent interaction	likely liquid-like	yes, *[COS-7]*	reversible	fusion to droplet forming domain fusion (e.g., $(iLID)_6$ or $(SspB)_6$)	30
[optoDroplets]: FUS_N, $HNRNPA1_C$ $DDX4_N$	FUS_N-Cry-2; $HNRNPA1_C$-Cry-2; DDX4-Cry-2	light-triggered multivalent interaction of IDPs	mostly liquidlike, partially gel-like	yes, *[NIH 3T3]*	mostly reversible	fusion to droplet forming domain fusion (e.g., FUS_N-Cry-2)	32
[optoClusters]: FUS_N, $HNRNPA1_C$ $DDX4_N$	FUS_N-Cry-2Olig	light-triggered multivalent interaction of IDPs	mostly gel-like clusters	yes, *[Saccharomyces cerevisiae]*	mostly irreversible	fusion to droplet forming domain fusion (e.g., FUS_N-Cry-2Olig)	32, 102
[PixELLs]: FUS_N	FUS_N-PixE and FUS_N-PixD	light-triggered dissociation of multivalent IDP interactions	liquidlike	yes, *[NIH 3T3, Saccharomyces cerevisiae]*	reversible	fusion to droplet forming domain fusion (e.g., FUS_N-PixD or FUS_N-PixE)	102, 103
[Corelets]: IDRs: FUS_N; $DDX4_N$; $HNRNPA1_C$; $TDP\text{-}43_C$; PGL-1	iLID-FTH1 and IDP-SspB	light-triggered multivalent interaction of IDPs	liquidlike	yes, [U2OS, HEK293, *Caenorhabditis elegans, S. cerevisiae*]	reversible	fusion of POI to FTH1-iLID and/or SspB-IDR module	28
[−/−]: MaSp1-116	$(MaSp1\text{-}116)_{16}$	multivalent interaction of IDPs	liquidlike	yes, *Escherichia coli*	reversible *in vitro*	fusion to droplet forming domain fusion (e.g., $(MaSp1\text{-}116)_{16}$	22
[−/−]: artificial IDRs (A-IDPs)	$(GRGDSPYS)_{20-80}$	multivalent interaction of IDPs	liquidlike	yes, *[HEK293, E. coli]*	reversible	fusion to droplet forming domain fusion	41

[a]Abbreviations: REPS, RGG-based, enzyme-triggered, phase-separating systems; SH3, SRC homology 3 domain; PRM, proline-rich-motif ligand of SH3; RGG domain, domain of the LAF1 deadbox DDX3 RNA helicase containing closely spaced Arg-Gly-Gly (RGG) repeats; [TEV/Th], tobacco etch virus or thrombin protease cleavage site; HRV 3C, human rhinovirus protease 3C; iPOLYMER, intracellular production of ligand-yielded multivalent enhancers; FKBP, FK506 binding protein; FRB, rapamycin binding protein; $(YF)_{1-5}$, constructs containing 1−5 copies of FKBP; $(CR)_{1-5}$, constructs containing 1−5 copies of FRB; TIA-1, stress granule forming protein that binds to Poly-A containing RNAs; iPOLYMER-Li, intracellular production of light-yielded multivalent enhancers with light inducibility; iLID, optogenetic construct derived from a light, oxygen, voltage (LOV) sensory domain of *Avena sativa* Phototropin-2 fused with SsrA peptide; SspB, protein binding partner of the SsrA peptide; FUS_N, $HNRNPA1_C$ $DDX4_N$, N- or C-terminal intrinsically disordered protein regions (IDRs) of intrinsically disordered proteins (IDPs) of the fused in sarcoma protein (FUS), Heterogeneous nuclear ribonucleoprotein A1 (HNRNPA1), and the ATP-dependent RNA helicase, Deadbox Helicase 4 (DDX4); $TDP\text{-}43_C$, IDR of TAR DNA binding protein 4; PGL-1, RNA-binding IDP of *C. elegans* germ granules; FTH1, human ferritin heavy chain; MaSp1-116, IDP consisting of 16 repeats of the major ampullate spidroin 1 protein of *Nephila clavipes*; GRGDSPYS, parent motif of artificial IDRs inspired by the *Drosophila melanogaster* Rec-1 resilin.

https://doi.org/10.1021/acssuschemeng.1c02045
ACS Sustainable Chem. Eng. XXXX, XXX, XXX−XXX

corresponding individual enzymes, as well as their soluble forms.

DESIGNED SYNTHETIC ORGANELLES—LIQUID PROTEIN CONDENSATES AS IMMOBILIZATES?

Compartmentalization, the formation of intracellular compartments or organelles for separating and orchestrating biochemical reaction pathways, is an essential feature of biological systems. Classically, organelles are membrane-separated compartments such as the nucleus, mitochondria, chloroplasts, and the Golgi apparatus. However, recent studies have shown that eukaryotic cells also contain various compartments that lack such a separating membrane structure. These so-called membraneless organelles, also called biomolecular condensates, liquid protein condensates, or coacervates, are widespread in eukaryotes.[91−93] They were first identified in the form of the P granules in *Caenorhabditis elegans* embryos.[94] Other naturally present membraneless organelles are nucleoli,[95] heterochromatin,[96] stress granules,[97] Balbiani bodies in *Xenopus* oocytes, the centrosome of *C. elegans* embryos,[93] and membrane receptor signaling clusters such as the nephrin−Nck−N-WASP signaling pathway,[98] to name just a few. They are formed by liquid−liquid phase separation (LLPS), a physical phenomenon that can be described as the coexistence of a dense phase that resembles liquid droplets with a dilute phase.[99] Cellular condensates or membraneless organelles are hereby formed by a dense phase of macromolecules such as proteins and DNA/RNA that form submicrometer[36] liquidlike droplets within the dilute cytoplasm.[99] In turn, due to the liquidlike properties of LLPS protein condensates, diffusional limitation is likely much less of an issue as for the aforementioned encapsulation-based systems, where the substrate/product has to cross a liquid/solid phase boundary. This is exemplified by the observation that even POIs can be recruited to the respective condensates after they have formed (see below).

Mechanistically, one factor that is instrumental for LLPS is multivalency, a tendency of certain types of molecules to undergo inter- or intramolecular interactions to form higher-order oligomers or polymers. Those in turn have a lower solubility as compared to the dilute phase and hence tend to demix, thereby forming a separate phase from the surrounding solution.[100] In the case of folded proteins, the presence of multiple interaction sites or interacting domains, implicated in homo- or hetero-oligomerization, promotes LLPS. Similarly, for intrinsically disordered proteins (IDPs) or protein domains, multivalent weak interactions between those regions seem to drive LLPS.[100]

Sequence determinants or structure−function relationships for LLPS formation are far from understood; however, our understanding of the basic principles of LLPS now facilitates the design of synthetic membraneless organelles.[36] Please note that the (natural) building principles of membraneless organelles and their properties, biological role, and function have been expertly reviewed before (see, e.g., refs 93, 99, and 101 and references therein). Therefore, in the present Perspective we will solely focus on designed synthetic membraneless organelles and their application potential for (industrial) biocatalysis and biotechnology. All strategies for the generation of membraneless organelles/biomolecular condensates described in this Perspective are summarized in Table 2.

From Initial Approaches to Enzymatically and Chemically Triggered LLPS. In an early study, the artificial generation of membraneless organelles by LLPS was demonstrated utilizing signaling and interaction domains of multivalent signaling proteins.[101] The system presented by Li et al. hereby relied on the interaction between the SRC homology 3 (SH3) domain and its proline-rich-motif (PRM) ligand.[29] To capitalize on multivalent interactions between those molecules, they generated two types of engineered proteins consisting of 1−5 SH3 ($SH3_1$−$SH3_5$) or PRM (PRM_1−PRM_5) domains (Figure 3A). When purified proteins of higher valency ($SH3_4$ + PRM_4) were mixed together at high concentration, liquid−liquid demixing was observed resulting in the formation of spherical droplets. In addition, different experimental approaches, including dynamic light scattering, photobleaching experiments, and cryoelectron microscopy studies, suggested that the macroscopically detectable LLPS is coupled to a molecular sol−gel transition within the droplet.[29] This phenomenon is nowadays known as maturation or hardening, in some cases also reported to occur *in vivo*, with the hardened condensates likely being gels, glasses, or two-phase solids.[101,104]

Moreover, LLPS was also observed *in vivo* in HeLa cells, where the coexpression of mCherry-$SH3_5$ and EGFP-PRM_5 fusions resulted in the formation of cytoplasmic puncta showing both mCherry and EGFP fluorescence. Similarly, the authors utilized multivalent interactions of components of the nephrin−NCK−N−WASP signaling system to trigger LLPS. This study clearly demonstrated that LLPS can be engineered to yield membraneless organelles *in vivo*, which moreover can be "loaded" with cargo proteins, as demonstrated by Li et al. for the colocalization (or coimmobilization) of EGFP and mCherry. Moreover, the observation of hardened states of the condensates could be beneficial for using them as enzyme immobilizates in biocatalysis, as gels or glasses would be much more easily recoverable from the reaction system.

LLPS Droplet Assembly/Disassembly Triggered by Proteolytic Cleavage. Another artificial LLPS system, which was developed more recently, employed several strategies to make LLPS enzymatically inducible. Schuster and co-workers utilized the RGG domain (containing closely spaced Arg−Gly−Gly repeats) of the *C. elegans* LAF1 deadbox DDX3 family RNA helicase, which is found in P granules.[31] The RGG domain, located at the N-terminus of LAF1, is an IDP that shows an upper critical solution temperature (UCST): it is soluble at higher temperatures, with LLPS occurring only when the temperature is lowered below the UCST. The systems abbreviated by the authors as REPS (RGG-based, enzyme-triggered, phase-separating systems) utilized 1−3 RGG domains as single, tandem, and triple constructs. Depending on the number of RGG domains, different phase-separating properties were observed, with constructs containing a larger number of RGG domains showing an improved tendency for LLPS and an increase of the UCST (RGG: below 15 to <50 °C for RGG−RGG−RGG). To trigger droplet disassembly at a physiological temperature, the authors utilized a tandem RGG−RGG construct that contained a tobacco etch virus (TEV) or thrombin protease cleavage site between the two RGG domains (Figure 3B). While the tandem RGG−RGG construct shows LLPS at a physiological temperature for tissue culture (>15 and <40 °C), proteolytic cleavage to yield single RGG domains lowers the UCST, so that the droplets disassemble. Similarly, triggered droplet assembly was achieved

https://doi.org/10.1021/acssuschemeng.1c02045
ACS Sustainable Chem. Eng. XXXX, XXX, XXX−XXX

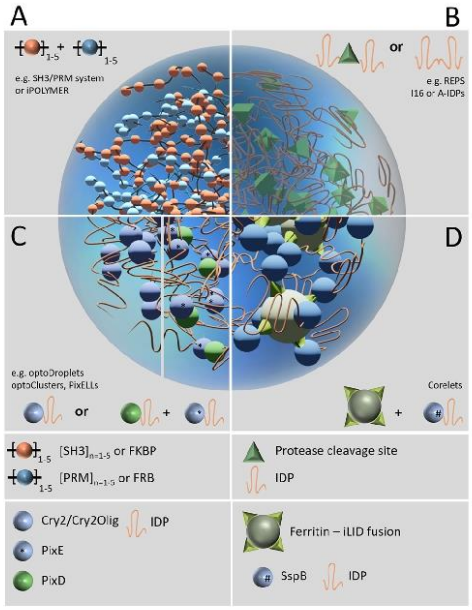

Figure 3. Liquid protein condensates as immobilizates. (A) Liquid–liquid phase separation (LLPS) due to multivalent interactions of proteins containing, e.g., multiple repeats of the SRC homology 3 domain (SH3) and its proline-rich motif (PRM) ligand (SH3/PRM system) or the FK506 binding protein (FKBP) and the rapamycin binding protein (FRB) (iPOLYMER strategy). Protein of interest (POI) recruitment by fusion to droplet/hydrogel-forming multivalent domain fusions. (B) LLPS due to fusion of multiple intrinsically disordered proteins (IDPs) such as the RGG domain of the *C. elegans* deadbox DDX3 helicase LAF1, 16 repeats of the major ampullate spidroin 1 protein of *Nephila claviceps* (116), or artificial intrinsically disordered protein regions (A-IDPs). POI recruitment via fusion of synthetic coiled-coil peptides (SYNZIPs) that interact with the correspondingly tagged droplet forming IDP-fusions or by direct fusion to the IDPs. (C) optoDroplets/optoClusters and PixELLs: light-triggered LLPS by utilizing the light-dependent homo-/hetero-oligomerization tendency of photoreceptor proteins such as cryptochromes (Cry-2/Cry-2Olig) and blue-light using flavin adenine dinucleotide (BLUF) proteins (PixE/D) fused to IDPs such as the N-terminal intrinsically disordered region (IDR) of the fused in sarcoma (FUS_N) protein, C-terminal IDR of the heterogeneous nuclear ribonucleoprotein A1 (HNRNPA1), or the N-terminal IDR of the deadbox helicase DDX4. POI recruitment by fusion of POIs to droplet/hydrogel-forming multivalent domain fusions. (D) Corelets: light-driven LLPS by utilizing the human ferritin heavy chain fused with the optogenetic tool iLID, derived from a light, oxygen, voltage (LOV) sensory domain of *Avena sativa* Phototropin-2, which upon illumination interacts with an SspB-IDP fusion, triggering LLPS. IDPs used for the Corelet strategy include FUS_N, HNRNPA1, and DDX4. POI recruitment by fusion of POIs to ferritin-iLID and/or the SspB-IDR module.

by fusing the maltose binding protein (MBP) to a tandem RGG–RGG construct, with MBP serving as a solubility enhancing tag. To allow enzyme-triggered LLPS, a cleavage site for the human rhinovirus protease 3C (HRV 3C) was inserted between MBP and RGG–RGG. While the MBP–RGG–RGG construct remained soluble at 25 °C, proteolytic cleavage of the MBP solubility enhancer yielded LLPS droplets at 25 °C. In addition, the authors demonstrated the recruitment of soluble cargo proteins to the RGG–RGG membraneless organelles by using the SYNZIP coiled-coil system,[105] which utilizes two coiled coils SYNZIP 1 and 2 (SZ1 and SZ2) to facilitate coiled-coil-mediated protein–protein interactions between the RGG–RGG compartment and the cargo protein (Figure 3B). To this end, SZ1–RGG–RGG fusion constructs were used alongside SZ2–cargo fusion constructs with either the red fluorescent protein (RFP) or the green fluorescent protein (GFP) serving as cargo model proteins. The systems were shown to work in various mammalian cells, clearly demonstrating intracellular LLPS and cargo recruitment.

Chemically Triggered Hydrogel-Formation Utilizing LLPS. The next step forward yielded the so-called iPOLYMER technique (intracellular production of ligand-yielded multivalent enhancers), which realized the chemically triggered formation of LLPS hydrogels.[30] The iPOLYMER system (Figure 3A) utilized a chemically inducible dimerizer technique, which relies on the interaction between the FK506 binding protein (FKBP) and the rapamycin binding protein (FRB), which interact upon the addition of rapamycin.[106] The authors generated fusion proteins consisting of up to five copies (n = 1–5) of FKBP (YF_1–YF_5) or FRB (CR_1–CR_5) linked via short linker polypeptides, with or without an N-terminal nuclear export signal. For easy detection of polymerization, yellow fluorescent protein (YFP) and cyan fluorescent protein (CFP) reporters were utilized, reporting simultaneously on polymerization and colocalization. The corresponding cells were shown to exhibit diffuse fluorescence signals that rapidly turned into puncta upon rapamycin addition. Depending on the valency of interactions (1–5 copies of FKBP/FRB), increased puncta formation was observed. Ultrastructural analyses by correlative electron microscopy revealed fibrillogranular structures that morphologically resembled stress granules. Further *in vitro* studies corroborated the formation of irreversible hydrogel-like materials that formed structurally stable, optically translucent materials that are able to retain water and act as a molecular sieve allowing the efficient diffusion of small molecules. Last but not least, the authors also showed the possibility of recruiting a target protein to iPOLYMER hydrogels. They fused the RNA recognition motif of TIA-1, a stress granule forming protein that binds to Poly-A containing RNAs,[107] to CR_5 and coexpressed YF_5. After the addition of rapamycin, the formed puncta were shown to contain PABP-1, which most likely binds to the Poly-A containing RNAs sequestered to the condensates via the RNA recognition motif of TIA-1 fused to CR_5. This indicates that the functionalized iPOLYMER puncta sequester Poly-A RNAs similarly to native stress granules and that, in principle, target proteins can be sequestered to iPOLYMER hydrogels by utilizing specific interaction modules. This, for example, might facilitate target recruitment via, e.g., the above-described SYNZIP coiled-coil system. The hydrogel-like properties along with the potential for target protein recruitment render the formed hydrogels an attractive platform for applications in biocatalysis, although transfer of the system to yeast or *E. coli* cells would be desirable from an application as well as sustainability perspective.

https://doi.org/10.1021/acssuschemeng.1c02045
ACS Sustainable Chem. Eng. XXXX, XXX, XXX–XXX

Overcoming Irreversibility—Light-Driven LLPS Droplet Formation. All until-now presented approaches, relying on either simple gene expression (SH3/PRM approach) or enzymatically (REPS) and chemically triggered (iPOLYMER) LLPS, are intrinsically irreversible, e.g., forming LLPS droplets under specific conditions (temperature, salt concentration), i.e., when concentrations above a critical concentration are reached. However, for the dynamic control of, e.g., metabolic processes by scavenging or scaffolding within LLPS droplets, reversible droplet assembly/disassembly is necessary. To this end, a number of light-driven, so-called optogenetic, techniques have been developed. All of the following presented systems thereby combine light-triggered protein−protein interactions with IDP-driven LLPS to allow for reversible intracellular droplet formation. While being advantageous from a metabolic engineering perspective, reversible LLPS seems less applicable for the production of *in vivo* enzyme immobilizates for biocatalytic applications.

The optoDroplets approach (Figure 3C) utilizes intrinsically disordered regions (IDRs) from proteins known to drive LLPS in living cells, fused to the *A. thaliana* cryptochrome 2 (Cry-2) photoreceptor protein, which tends to reversibly form oligomeric clusters upon blue-light illumination.[32] IDRs that were employed are the N-terminal IDR of the fused in sarcoma protein (FUS_N), the C-terminal IDR of the heterogeneous nuclear ribonucleoprotein A1 ($HNRNPA1_C$), and the N-terminal IDR of the deadbox DDX4 helicase. In addition to Cry-2, Cry-2Olig, which shows enhanced clustering, was used to drive LLPS (optoClusters[102]) (Figure 3C). Target recruitment is possible, as shown by the fusion of mCherry to the opto-IDR construct. In all cases, the use of the resulting fusion proteins allowed the intracellular formation of LLPS droplets under blue-light illumination, which in most cases fully disassembled in the dark. Only cyclic activation with high-light intensities yielded irreversible cluster formation for optoFUS. The use of the Cry-2Olig instead of Cry-2 yielded irreversible, gel-like aggregates, even under low-light activation in a single activation cycle. Interestingly, the formation of those gel-like aggregates was initially reversible, but aging processes led to the formation of irreversible aggregates. Thus, from a biocatalytic application perspective, the use of Cry-2Olig-based optoClusters seems better suited, although prokaryotic production would be desirable. Subsequently, based on the optoDroplet approach, the PixELL (Pix evaporates from liquidlike droplets in light) system (Figure 3C) was developed, which shows an inverted response (light-driven droplet dissociation) and relies on the blue light using flavin adenine dinucleotide (BLUF) photoreceptor PixE/PixD, which forms heterodimers in the dark and dissociates upon blue-light illumination.[102] All three systems were later adapted for use in yeast (*S. cerevisiae*) and used to enable light-based control of metabolic flux (see the Application of Synthetic Organelles in Metabolic Engineering and Biocatalysis section).

The later developed Corelet system (Figure 3D)[28] uses human ferritin heavy chain, a 24-mer iron storage protein that forms a spherical protein core of 12 nm in diameter, as an oligomerization hub. Each ferritin monomer is fused with the light, oxygen, voltage (LOV) domain-based optogenetic tool iLID. iLID is based on the *Avena sativa* LOV2 domain (AsLOV2) in which seven residues of the *E. coli* SsrA peptide have been incorporated within the C-terminal Jα helix (with which it shares sequence similarity).[108] Upon illumination with blue light, the SsrA-bearing Jα helix dissociates from the AsLOV2 core domain allowing for interaction with the SsrA partner protein SspB. Fusion of an IDR (FUS_N, $DDX4_N$, $HNRNPA1_C$, TAR DNA binding protein $TDP\text{-}43_C$, PGL-1) to SspB thereby facilitates light-driven LLPS droplet formation (Figure 3D). Moreover, the fusion of additional proteins to the ferritin-iLID and/or the SspB-IDP module allows for target recruitment to the LLPS droplets (exemplarily shown for EGFP and mCherry). The system, which was shown to be fully reversible over 15 cycles of activation, was also shown to work in cultured mammalian cells, in yeast (*S. cerevisiae*) and *C. elegans*, as well as in both the cytoplasm and nucleus.[28]

Similarly to the Corelet strategy, an adaptation of the above-described iPOLYMER system, coined iPOLYMER-Li (intracellular production of light-yielded multivalent enhancers),[30] utilized fusion proteins containing six iLID domains alongside a fusion protein consisting of six SspB repeats separated by short linkers. This allowed the formation of cytosolic polymer networks upon illumination, which moreover reversibly dissociated in the dark. Target recruitment was demonstrated by fusion of mCherry and YFP.[30]

LLPS in Prokaryotes—Designing Membraneless Organelles in *Escherichia coli*. While all of the above-described systems were developed for use in mammalian cells or, at best, were adapted to drive LLPS in yeast, the development of *E. coli*-produced synthetic LLPS organelles is highly desirable from a biocatalytic application and sustainability perspective. Only very recently, two studies could demonstrate that indeed IDR/IDP-driven LLPS is possible in *E. coli* using natural and artificial IDR/IDPs as fusion modules to drive POI recruitment to LLPS droplets. Both strategies rely on constructs that are architecturally similar to the RGG-based REPs system (Figure 3B) but utilize different IDPs for LLPS.[22,41] The first study, by Wei et al.,[22] showed that, e.g., the expression of a protein module consisting of 16 repeats of the consensus sequence of the major ampullate spidroin 1 protein of *Nephila clavipes* (MaSp1-I16; abbreviated as I16 by the authors) alone is sufficient to induce the formation of cellular compartments, while fusion of GFP allowed tracking in living cells, also demonstrating target recruitment. Likewise, the coexpression of two similarly tagged fluorescent proteins (GFP and mCherry) verified colocalization of the two proteins within those compartments. Finally, the authors showed that their strategy can be used for assembling a synthetic reaction cascade to produce 1,3-diaminopropane (DAP) by the coexpression of two I16-tagged enzymes (for details, see the Application of Synthetic Organelles in Metabolic Engineering and Biocatalysis section). In a second study,[41] LLPS was realized in *E. coli* by using a subset of artificial IDRs (designated by the authors as A-IDPs), inspired by the *Drosophila melanogaster* Rec-1 resilin containing multiple repeats of the parent motif $(GRGDSPYS)_x$ (with x being the number of repeats, between 20 and 80) as well as variants thereof containing rational amino acid substitutions. For a set of those variants, robust LLPS was shown in mammalian cells and in *E. coli*. Selective colocalization was demonstrated for two A-IDPs with similar phase-behavior utilizing superfolder GFP (sfGFP) and red fluorescent protein mRuby3 tagged constructs. Moreover, the authors also demonstrated that small molecules and even protein fragments (demonstrated for split GFP) can penetrate the intracellularly formed compartments opening up the possibility to generate functionalized A-IDP droplets, which was also demonstrated in proof of principle experiments using β-galactosidase[41] (see also the Application

https://doi.org/10.1021/acssuschemeng.1c02045
ACS Sustainable Chem. Eng. XXXX, XXX, XXX−XXX

ACS Sustainable Chemistry & Engineering pubs.acs.org/journal/ascecg Perspective

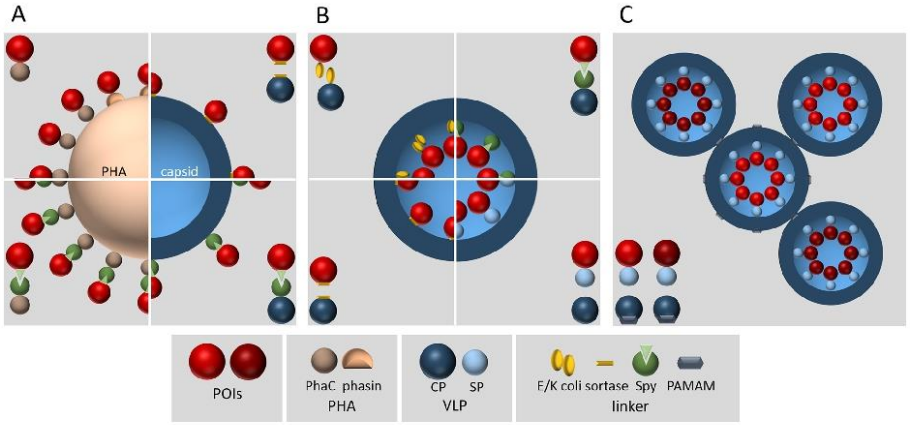

Figure 4. Polyhydroxyalkanoate (PHA) immobilizates and viruslike particles (VLPs). Engineered proteins required for respective POI immobilization as well as the resulting immobilizates are shown. Details are given in the text. (A) Carrier-based POI display. (top left) POI is covalently linked to a polyhydroxybutyrate (PHB) granule via PhaC or phasins. (bottom left) POI is covalently linked to PHB granule via the PhaC-SpyCatcher and POI-Spy tag. (top right) P22-VLP: POI is linked to capsid protein (CP) by the sortase SrtA (the yellow boxes symbolize the sorting signal peptide and the glycine-containing motif, respectively). (bottom right) T4- and B19-VLP: POI is linked to CP via the SpyCatcher/Tag system. (B) Carrier-based POI encapsulation. (top left) CCMV-VLP: POI is noncovalently linked to CP via E/K coil. (bottom left) CCMV-VLP: POI is linked to CP via SrtA. (top right) MS2-VLP: POI linked to CP via SpyCatcher/Tag. (bottom right) P22-VLP: POI covalently linked to truncated scaffolding protein (SP). (C) P22 super lattice. VLPs encapsulating different POIs were noncovalently interlinked by positively charged PAMAM dendrimers.

of Synthetic Organelles in Metabolic Engineering and Biocatalysis section). This underscores the liquidlike nature of those condensates, yet again highlighting that substrate diffusion is not a limiting factor.

Application of Synthetic Organelles in Metabolic Engineering and Biocatalysis. The ability to assemble and disassemble synthetic membraneless organelles within cells shows great potential for metabolic engineering. It could enable the on-demand compartmentalization of metabolic enzymes facilitating dynamic control of metabolic flux. The potential was demonstrated in a proof of concept study in which optogenetic clustering/LLPS tools were used in yeast to control the flux through the deoxyviolacein pathway.[103] Zhao and co-workers utilized the optoCluster and PixELL system to light-dependently enhance or suppress the metabolic flux through the deoxyviolacein pathway or control the flux through a two-enzyme metabolic branch point.[103] Similarly, first attempts were made to use the *E. coli* LLPS system, relying on enzyme fusions with the IDR I16 (*vide supra*), to realize the *de novo* synthesis of 1,3-diaminopropane within membraneless organelles.[22] The authors tagged both the L-2,4-diaminobutyrate:α-ketoglutarate 4-aminotransferase (Dat) and the L-2,4-diaminobutyrate decarboxylase (Ddc) with the I16 IDR, to facilitate the formation of membraneless organelles in *E. coli*. The corresponding cells, in turn, were utilized for the conversion of aspartate β-semialdehyde to 1,3-diaminopropane. However, the corresponding experiments did not show a clear advantage of the LLPS coimmobilized enzymes over the use of soluble expressed Dat and Ddc.[22] Second, the A-IDP approach (*vide supra*) was used to generate functionalized LLPS condensates in *E. coli* by recruiting the β-galactosidase enzyme to the droplets.[41] This was achieved by capitalizing on the widely used β-galactosidase (LacZ) blue−white screening system, in which the α peptide (αp) complements the mutated enzyme LacZΔM15, by interaction with it, to create a functional β-galactosidase enzyme. αp was therefore fused to an A-IDP−mRuby3 fragment, while inactive LacZΔM15 was coexpressed in *E. coli*. Using a fluorescein-based β-galactosidase substrate, the authors demonstrated an up to 7.5-fold increase in catalytic turnover for the droplet recruited enzyme compared to the soluble control without the A-IDP module. Based on the quantification of fluorescence production at various substrate concentrations, the authors reasoned that, while the Michaelis−Menten constant (K_m) of the enzyme for the substrate remained essentially unchanged, the colocalization of the enzyme and substrate within the droplets facilitated a better turnover by an increase in the turnover number K_{cat}.[41]

■ POLYHYDROXYALKANOATE-BASED SYSTEMS AND VIRUSLIKE PARTICLES

In addition to the strategies described in the first two parts of this Perspective, *in vivo* protein immobilization has also been achieved by attaching POIs via suited anchor proteins to natural and artificial cellular compartments offering a higher structural complexity.[19,20,109] To this end, (i) biological, often naturally occurring, membrane-separated compartments such as liposomes,[20] membrane vesicles,[110] and polymersomes;[111] or (ii) bacterial, membrane-free microcompartments such as carboxysomes,[38] metabolosomes,[19] magnetosomes,[37] bacterial bioplastic inclusions,[112,113] and viruslike particles[114−116] were rationally designed for target protein encapsulation or display. Given the diversity of nanocompartments, a comprehensive review of all available systems would exceed the scope of the present contribution. Therefore, we here describe some examples in more detail, whose applicability for *in vivo* enzyme immobilization could already be demonstrated.

https://doi.org/10.1021/acssuschemeng.1c02045
ACS Sustainable Chem. Eng. XXXX, XXX, XXX−XXX

Polyhydroxyalkanoate Granule-Based POI Immobilization. Polyhydroxyalkanoates are linear polyesters composed of (*R*)-3-hydroxy fatty acids linked by ester bonds. Under conditions of carbon excess, they are naturally produced by various Gram-positive and Gram-negative bacteria as energy storage compounds.[33,117] Depending on the chain length of the fatty acid monomers, polyhydroxyalkanoates (PHAs) are categorized into three main classes: short- (3−5 carbon atoms), medium- (6−14 carbon atoms), and long-chain-length PHAs with more than 14 carbon atoms.[118,119] The biosynthesis of polyhydroxybutyrate (PHB), one of the PHA members that is most frequently used for POI immobilization, is catalyzed by three enzymes, starting with the β-ketothiolase PhaA condensing two acetyl-CoA subunits to form acetoacetyl-CoA. Acetoacetyl-CoA is subsequently reduced to D-3-hydroxybutyryl-CoA by the acetoacetyl-CoA reductase PhaB, and finally, the polymerization reaction is catalyzed by the PHB synthase PhaC.[120−122] PHAs have been widely evaluated as an environmentally friendly surrogate for petroleum-based plastics as the bioplastic can be sustainably synthesized in natural producers or engineered bacteria and exhibits beneficial properties including good biocompatibility, high biodegradability, and nontoxicity.[123] Under appropriate growth conditions, synthesized PHA makes up up to 90% of the cell dry weight and accumulates in the cytoplasm as spherical particles with a size of 100−500 nm.[124,125] Besides the hydrophobic PHA core, the granules are surrounded by a protein layer.[126,127] This layer is composed of different PHA-associated proteins including PhaC, different phasins (e.g., PhaP or PhaF), a depolymerase, and other regulatory and structural proteins.[127−129] Based on this observation, PHA granules were further used to develop a versatile *in vivo* protein immobilization and display technology.[112,113,130−135] In most cases, accordingly engineered *E. coli* strains, harboring the essential PHB biosynthesis genes, are applied for POI *in vivo* immobilization. For this purpose, the synthase PhaC can be employed as a versatile anchor protein, because it tolerates POI fusions at its N- and C-termini. The recombinant PhaC proteins remain covalently attached to the nascent PHB chain thereby forming an amphiphilic molecule capable of self-assembling into a POI-decorated PHB sphere.[113,130,136] In addition, phasins like PhaF are applicable as alternative anchor proteins that are able to guide a POI to the PHB core via hydrophobic interactions (Figure 4A).[137] Depending on the chosen anchor protein, the distribution of POIs as well as the stability of POI−PHB conjugates can differ remarkably.[138,139] POI-decorated PHB inclusions can be easily isolated from cell extracts by centrifugation.[140−142] A linker located between the POI and the respective PHB anchor protein, harboring, e.g., a protease cleavage or intein site, can be used for subsequent (auto)catalytic POI release from the PHB carrier.[132,136,143]

Proof of concept demonstrations for the applicability of *in vitro* or *in vivo* PHB-immobilized enzymes were reported, e.g., for the production of food ingredients, commodity and fine chemicals, as well as bioremediation (e.g., reviewed in ref 112). For example, a bacterial laccase-like multicopper oxidase (CueO), suitable for the degradation of harmful synthetic dyes, was fused to PhaF, a phasin derived from *P. putida* and expressed in *E. coli*.[135] After purification of the recombinant protein, CueO-PhaF was attached *in vitro* to commercially available PHB granules resulting in enzyme immobilizates with an improved catalytic performance in comparison to unfused CueO. Here, the catalytic activity of the POI-immobilizate was up to 40-fold higher leading to a significantly increased decolorization efficiency.[135] The authors assumed that this effect is due to a preferential accumulation of some of the tested dyes at the PHB surface thereby leading to an increased substrate support.[135] In contrast to the *in vitro* assembly approach, a P450-BM3 monooxygenase was tethered to PHB granules *in vivo* via a phasin fusion using *E. coli* as the production host.[141] Here, the POI−PHB complex was assembled in one step and subsequently purified, and the enzyme activity was compared to the unfused P450-BM3. In this case, POI immobilization led to a higher stability against elevated temperatures, low pH, and increased concentrations of urea and ions. Furthermore, the simplified purification procedure of P450-BM3-PHB conducted by centrifugation enabled the use of this enzyme immobilizate to convert 7-ethoxycoumarin to the antioxidant 7-hydroxycoumarin at the preparative reactor-scale.[141] Besides the examples described above, many more enzymes were *in vivo* immobilized using PHA-based approaches (e.g., recently summarized in ref 112). For example, noncovalent PHA immobilization mediated by PhaF or PhaP was applied for the β-galactosidase from *E. coli*,[144] the D-hydantoinase D-HDT from *Agrobacterium radiobacter*,[145] the lysine decarboxylase CadA from *E. coli*,[146] or the tetrameric organophosphorus anhydride hydrolase from *Pseudoalteromonas* sp.[138] Furthermore, there are also numerous applications where the POI was covalently bound to the PHB surface via PhaC,[112] including the α-amylase from *Bacillus licheniformis*,[131] the lipase B from *Candida antarctica*,[147] the lipase M37 from *Photobacterium lipolyticum*,[142] the hexavalent chromium reductase NemA from *E. coli*,[148] the *N*-acetylglucosamine 2-epimerase Sir1975 from *Synechocystis* sp. PCC6803,[149] the carbonic anhydrase from *Desulfovibrio vulgaris*,[150] the alkaline polygalacturonate lyase from *B. subtilis*,[151] the tyrosinase from *Verrucomicrobium spinosum*,[152] or the D-tagatose-3-epimerase DTW from *Pseudomonas cichorii*.[153] In recent studies, the PhaC-mediated POI immobilization platform was further improved by combining it with the SpyTag/SpyCatcher chemistry (Figure 4A), which enables better control over PHB decoration.[23,154] In this context, the authors demonstrated that the Spy-tagged POIs can be covalently bound to the SpyCatcher-PhaC-coated PHB particles *in vitro* and *in vivo* (see below).

Taken together, PHA granules represent a promising alternative carrier material suitable for efficient enzyme scaffolding. In many cases, enzyme immobilization on PHA surfaces led to an improved tolerance against elevated temperature, low pH, or different solvents[138,145] as well as to higher catalytic performance and recyclability. PHA thus expands the large group of natural biopolymers, which also includes, e.g., chitosan, cellulose, alginate, and agarose, that are basically suitable for the immobilization of enzymes (for example, recently reviewed by ref 155). However, in contrast to immobilization strategies with these biopolymeric carrier materials, the POI can be easily immobilized to biogenic PHA granules *in vitro* and *in vivo*, using different surface proteins as anchor molecules. *In vitro* functionalization of PHA granules has some advantages, including the maintenance of tight control over particle size and density of immobilized enzymes, but requires a more tedious process. In contrast, the *in vivo* production of POI-decorated PHA nanobeads can be directly implemented in bacterial cells thereby enabling their use as artificial cellular compartments in whole-cell biocatalysis. In addition, it is a low-cost, one-step production process for

https://doi.org/10.1021/acssuschemeng.1c02045
ACS Sustainable Chem. Eng. XXXX, XXX, XXX−XXX

enzymatic active biopolymers making the *in vivo* approach convenient, efficient, and ecofriendly. However, *in vivo* formation of functionalized PHA particles intrinsically results in only limited control over POI surface coverage and particle sizes, which may restrict their applicability for flow-chemical bioprocesses. Furthermore, PHA particles tend to aggregate, and their nonporous character can further lead to high backpressure in such processes. To overcome these limitations, Rehm and co-workers recently applied a porous alginate hydrogel as a matrix for embedding enzyme-coated PHB particles.[156]

Using Viruslike Particles as POI Encapsulating and Displaying Scaffolds. Viruslike particles (VLPs) are multiprotein complexes with a size of ∼20−200 nm that resemble the structural organization of corresponding virus envelopes. In general, they consist of one or more viral capsid proteins (CPs), which can be easily synthesized *in vivo* via heterologous gene expression using different microbial hosts such as *E. coli*, *S. cerevisiae*, and *Pichia pastoris* (e.g., refs 157−159). The CPs exhibit the intrinsic property for self-assembly, and due to the lack of genetic material, the resulting VLPs are nonreplicating and noninfectious. Different VLPs were established by employing CPs from the cowpea chlorotic mottle virus (CCMV), the cowpea mosaic virus (CPMV), the parvovirus B19, as well as the bacteriophages P22, Qβ, and MS2.[112,116,159] The broad variety of structurally diverse virus capsids thus provides a molecular platform allowing the application of the genetically modifiable CPs as building blocks for generating functionalized VLPs (e.g., reviewed in refs 114, 115, 160, and 161). In the past decade, the generation of various genetically engineered VLPs was described, and these have been applied in the biomedical sector as new vaccines or drug delivery systems. Furthermore, VLPs gained increasing interest as versatile proteinaceous carrier materials that can be modularly engineered to form biocatalytically active nanomaterials. As spherical VLPs can be seen as macromolecular shells, the POIs can principally be directed to either the interior or exterior of the virus capsid. To achieve this goal, different strategies were described that are applicable for either noncovalent or covalent linkage of the POIs and the envelope of the VLP.

VLP-Mediated POI Encapsulation. In the following section, we mainly describe the application of two different VLP systems that are based on the small RNA plant virus CCMV or the *Salmonella typhimurium* bacteriophage P22 and that have been extensively studied for either *in vitro* or *in vivo* enzyme encapsulation. The CCMV-based VLP was the first virus shell system that was evaluated for POI encapsulation since its CP can be easily expressed in *E. coli*. *In vitro* VLP assembly and disassembly can be reversibly triggered by shifting the pH value, which facilitates the passive packaging of cargo molecules. Furthermore, the N-terminus of the CCMV CP is located in the shell interior, which therefore intrinsically provides a suitable site for POI attachment and subsequent directed encapsulation (e.g., reviewed in ref 114). Directed noncovalent CCMV-mediated POI encapsulation, for instance, involves the heterodimerization of suitable coiled-coil domains such as the E and K coil domains[162] that can be genetically fused to the respective VLP CP and POI thereby conferring them the ability to stably bind to each other (Figure 4B). In a pioneering work, Cornelissen and co-workers used the CCMV CP for the E/K coil-mediated encapsulation of EGFP.[163] By fusing the K coil to the N-terminus of the CP and the E coil to the C-terminus of EGFP, their heterodimerization could be facilitated by the formation of a leucine zipperlike E-K coiled-coil structure. Subsequent *in vitro* VLP self-assembly experiments revealed that up to 15 EGFP molecules were encapsulated in the interior of a CCMV capsid. This technology was further applied for the packing of the lipase CalB from *Candida antarctica*.[164] The authors could demonstrate that CCMV-encapsulated CalB exhibits increased overall reaction rates as compared to the unmodified, soluble lipase, which is presumably caused by an increased efficiency of enzyme−substrate complex formation. However, the noncovalent VLP-mediated encapsulation of POIs can be accompanied by a variable or limited POI packaging density.[114] This observation led to the development of alternative encapsulation strategies relying on covalent POI tethering, generally resulting in an improved control over site-selectivity and VLP loading efficiency. In principle, the simplest way to obtain covalent POI encapsulation is the generation of a recombinant fusion protein consisting of a CP and a POI domain. This strategy was applied, for example, for the packaging of the fluorescent marker protein TFP in CCMV-based VLPs to avoid a dissociation of the E−K coiled-coil-based heterodimers.[165] A more sophisticated strategy to achieve the covalent encapsulation was recently developed employing the sortase SrtA-catalyzed formation of peptide bonds between POIs and capsid proteins (Figure 4B).[166−170] To this end, SrtA first recognizes the sorting signal peptide (LPXTG) that can be fused, for example, to the C-terminus of POIs followed by its enzymatic cleavage. In a second catalytic reaction, the truncated signal peptide is covalently linked to a glycine-containing motif, which is fused to the N-terminus of the VLP capsid protein. The applicability was, e.g., demonstrated by using the lipase CalB as a cargo protein. It could be shown that the encapsulation in this artificial compartment affected neither enzyme activity nor substrate diffusion and additionally exerted POI protection against proteases.[167] In a similar approach, GFP, the T4 lysozyme, and a heparin binding peptide were covalently encapsulated by SrtA in CCMV capsids.[168,170,171] In addition to SrtA-mediated covalent linkage, sequestration of PLP-dependent tryptophanase TnaA and monooxygenase PMO to the interior surface of the SpyTag-MS2 capsid (Figure 4B) could be achieved by using the SpyCatcher/SpyTag system (see below).

In contrast to the CCMV VLP, formation of the bacteriophage P22 additionally relies on the assistance of a scaffolding protein (SP), which directs the CP into the procapsid structure and is subsequently located inside the VLP shell (typically ∼100−300 copies per P22 VLP).[172] Remarkably, only the last 18 amino acid residues of the respective C-terminus are needed for proper P22 shell formation. Therefore, POIs can be genetically fused to the N-terminus of the truncated SP, which in turn allows the utilization of the engineered SP as a vehicle to obtain P22 VLP encapsulated POIs. Basically, coexpression of the POI-SP fusion protein and the P22 capsid protein in the heterologous expression host *E. coli* enables the formation of POI-containing VLPs *in vivo* (Figure 4B).[173,174] Because of the robustness of the *in vivo* P22 VLP assembly, this approach can also be applied for POIs that are very large (fusion proteins with sizes ≤180 kDa have been reported so far) or rather tend to aggregation or degradation.[175,176] Moreover, sequential expression of POI-SP and CP enables the synthesis of cofactor-containing enzymes. Here, POI folding and/or cofactor loading is performed before VLP encapsulation.[177,178] The applicability of P22 VLP-based POI

https://doi.org/10.1021/acssuschemeng.1c02045
ACS Sustainable Chem. Eng. XXXX, XXX, XXX−XXX

packaging was demonstrated for various enzymes with increasing structural complexity including the monomeric alcohol dehydrogenase AdhD,[179,180] the α-galactosidase GalA,[175] the homodimeric FAD-binding NADH oxidase NOX,[181] and the homotetrameric β-glucosidase CelB from *Pyrococcus furiosus*[182,183] as well as the heme-containing P450 monooxygenase CYPBM3 (variant 21B3) from *Bacillus megaterium*,[178,184] the homodimeric, bifunctional glutathione synthase GshF from *Pasteurella multocida*,[185] and the heterodimeric [NiFe]-hydrogenase 1 (EcHyd-1) from *E. coli*.[177] The P22 VLP technology could be further used to implement multienzyme reaction cascades either via directed coencapsulation of various enzymes, whose catalytic activities are interconnected in a respective cascade reaction, or by the assembly of VLPs carrying different POIs into three-dimensional arrays (see below). For example, CelB was fused to the glucokinase GLUK and galactokinase GALK with flexible linkers to hydrolyze the disaccharide lactose into the monosaccharides galactose and glucose, which could subsequently be phosphorylated to form galactose-1-P and glucose-6-P.[176]

It can be assumed that enzyme encapsulation in P22 VLPs, which function as bacterial microcompartments, can lead to decreased enzymatic activities due to lower diffusion rates of the substrate, cofactor, or product molecules. However, so far there is no evidence that the P22 shell hampers those processes suggesting free diffusion of small molecules across the VLP wall.[180] Furthermore, colocalization of functionally coupled enzymes within the crowded interior space of VLPs may even enhance pathway kinetics via so-called diffusion channeling of intermediates.[172]

VLP-Based POI Display. Although the VLP-based POI display is mainly applied for biomedical applications as a technology platform for the generation of immunotherapeutic nanomaterials (e.g., reviewed by ref 115), some reports also describe the POI-decoration of capsid surfaces for biotechnological approaches (e.g., reviewed in ref 161). In that case, VLPs can be rationally designed to offer new catalytic or functional surface activities. In addition, functionalized surfaces can be applied for creating new VLP-based materials offering a higher three-dimensional complexity. As described for POI encapsulation, the surface display of target proteins can also be achieved by their noncovalent attachment or directed covalent linkage via SpyCatcher/SpyTag systems (see below).

In a recent approach, the encapsulation and surface display of POIs were combined to form biocatalytically active superlattices. First, the group of T. Douglas could demonstrate that the C-terminus of the P22 CP is exposed to the exterior of the VLP capsid thereby allowing the generation of surface modified P22 VLP variants.[186] Based on these findings, a strategy was developed that is based on sortase-catalyzed ligation to obtain a covalent linkage of a POI and P22 CP.[187] To this end, the authors genetically fused the above-mentioned LPXTG tag to the C-terminus of the CP and subsequently displayed GFP, offering a polyglycine peptide at its N-terminus, on the capsid surface (Figure 4A). Furthermore, by exposing the K or E coil on the capsid surface, the differently decorated virus shells could be transformed into building blocks capable of self-assembling into extended network structures.[186] This strategy was finally employed to assemble two different P22 VLPs encapsulating either the ketoisovalerate decarboxylase (KivD) or the alcohol dehydrogenase A (AdhA), which catalyze the synthesis of isobutanol from α-ketoisovalerate in a coupled two-step reaction.[188] The VLPs further display small negatively charged peptides on the capsid surfaces. Spontaneous self-assembly of the two VLP species into three-dimensional higher-order structures was subsequently facilitated by positively charged polyamidoamine (PAMAM) dendrimers (Figure 4C). Importantly, the resulting bifunctional PP2 VLP arrays could easily be recovered to enable their reuse and exhibited improved catalytic conversion *in vitro*. This result demonstrated that P22 VLP-based superlattices form porous structures allowing efficient diffusion of the substrate and product molecules.

Taken together, VLPs constitute a versatile POI immobilization platform for targeted encapsulation, scaffolding, and display of POIs *in vitro* and *in vivo* thereby providing tailor-made macromolecular assemblies where sequential biocatalytic reactions can be conducted in a concerted multienzyme reaction. Furthermore, recent advances in understanding and engineering these nanomaterials enabled the creation of new and highly functionalized synthetic nanobiological devices.

SpyCatcher SpyTag System—Covalent Functionalization of Carrier-Free and Carrier-Bound Immobilizates. Many Gram-positive bacteria including *Streptococcus pyogenes* (Spy) naturally express surface proteins that are able to spontaneously form intramolecular isopeptide bonds during folding.[189,190] One of these proteins is the fibronectin-binding adhesin FbaB,[191,192] which was shown to generate an isopeptide bond between Lys31 and Asp117 of the fibronectin binding domain CnaB2.[192] By splitting this domain into a short peptide designated as SpyTag (13 residues, contains the reactive aspartate) and the so-called SpyCatcher protein (138 residues harboring the reactive lysine), a new and powerful genetically encoded click-chemistry tool was developed that is suitable for a fast and specific covalent POI coupling with high affinity that can be applied *in vitro* and *in vivo*.[193,194] To this end, the SpyTag is fused to the N- or C-terminus of a POI or can even be inserted into internal positions.[193] To further improve this technology, the binding efficiency of both partners was enhanced by protein engineering approaches including truncations of the SpyCatcher and amino acid substitutions at selected positions of SpyCatcher and SpyTag.[195,196] For example, the amino acid sequence of the SpyCatcher002 variant starts with GAMVD instead of GAMVT, which leads to the faster formation of the covalent bond with SpyTag.[197] The removal of 23 N-terminal residues of the SpyCatcher protein (SpyCatcherΔN1) additionally enhances the ability to interact with the surface of VLPs.[195,198] Finally, SpyTag002 reacts faster with any SpyCatcher variant in comparison to SpyTag.[197] Recently, an orthologous system, without cross-reactivity to the SpyTag/SpyCatcher system, has been developed from the *Streptococcus pneumoniae* surface protein RrgA, D4 domain, which forms an isopeptide bond between Lys742 and Asp854.[199] The system consists of a so-called SnoopTag with residues 734−745 and SnoopCatcher with residues 749−860 of the D4 domain, and furthermore, mutations (G842T and D848G) were inserted to improve stability.[199] This system is also suitable for covalent binding of a POI to a reaction partner or a surface for enzyme immobilization.[200−202] To obtain a comprehensive overview of the available Spy systems and applications published so far, the group of Mark Howarth developed the SpyBank database offering more than 600 entries (https://www2.bioch.ox.ac.uk/howarth/info.htm; status, March 2021) with useful informa-

https://doi.org/10.1021/acssuschemeng.1c02045
ACS Sustainable Chem. Eng. XXXX, XXX, XXX−XXX

tion including the applied expression host and Spy system configuration in the respective experiments.[196]

The Spy-technology has been frequently used to link one or more POIs to various macromolecular carriers. For example, PHA granules and VLPs were applied as matrices as briefly described above (Figure 4A,B). As already mentioned, PHB granules constitute a promising biopolymeric-based carrier material for the generation POI scaffolds. The group of Bernd Rehm recently applied a combination of the Spy system and PHB technology for biomedical and biotechnological applications.[23,154] Therefore, PHB granules were heterologously produced in *E. coli*, using the PHB synthase PhaC as an anchor to immobilize the SpyCatcher protein on the granule surface. The SpyCatcher-decorated nanobeads were subsequently applied *in vitro* for functionalization with Spy-tagged POIs like GFP, an α-amylase (BLA), and an organophosphohydrolase (OpdA), thereby enhancing the POI's functionality, stability, and reusability (Figure 4A). Furthermore, by mixing two or three POIs, tunable coimmobilization could be achieved.[23] In a following step, the system was transferred to an *in vivo* assembly process in *E. coli*, where the SpyCatcher-PHB particles and the Spy-tagged POIs were produced in the same host cell.[154]

In addition to PHA granules, VLPs represent a promising immobilization platform for biocatalytic approaches. It is therefore appealing to likewise combine this technology with the Spy and Snoop systems. To reconstitute the two-step indigo biosynthetic pathway inside MS2 VLPs, the PLP-dependent tryptophanase TnaA and monooxygenase PMO were fused to SpyCatcher and covalently linked to the interior surface of the SpyTag-MS2 capsid (Figure 4B).[203] Remarkably, an improved conversion of L-tryptophan to indigo could be demonstrated *in vitro* as well as in living *E. coli* cells. *In vitro* studies additionally revealed that MS2 packaging of these enzymes resulted in an increased storage stability. In an analogous SpyCatcher/Tag-based approach, VLPs could also successfully be coated with POIs (Figure 4A). For example, the T4 phage capsid was used as a scaffold to immobilize an amylase, maltase, and glucokinase via *in vitro* assembly. These three enzymes are part of a four-enzyme pathway, converting maltoheptaose and 6-phosphogluconolactone.[204] The enzymes were linked to the SpyTag, and the outer capsid protein Hoc was fused to SpyCatcher.[205] By detecting the formation of the byproduct NADH, it could be demonstrated that the virus capsid-based immobilization of the enzyme cascade resulted in an 18-times higher activity as compared to the respective enzymes in solution. Furthermore, Bustos-Jaimes and coworkers described the generation of a POI nanocarrier based on the parvovirus B19 VLP, whose shell is composed of the structural protein V2. POIs such as the lipase BplA from *B. pumilus* and α-glucosidase Ima1p from *S. cerevisiae* were either genetically inserted into V2 or covalently attached to its N-terminus via the SpyCatcher/SpyTag system resulting in enzyme-displaying B19 VLPs after *in vitro* self-assembly.[206,207] In the latter case, the displayed enzymes exhibited a higher temperature optimum and increased activity. The Catcher/Tag technology was further applied to generate an enzyme complex consisting of the three enzymes isopentenyl diphosphate isomerase (Idi), farnesyl pyrophosphate (FPP) synthase (IspA), and amorpha-4,11-diene synthase (ADS) by using the *Tobacco mosaic virus* (TMV)-based VLP as a protein scaffold.[202] To this end, either the SpyTag or the SnoopTag were fused to the respective CP, and Idi- and ADS-SnoopCatcher and IspA-SpyCatcher fusions were created. The enzyme-decorated VLP was assembled in a one-step approach using *E. coli* as a heterologous production host. Remarkably, amorpha-4,11-diene only accumulated in the VLP-immobilization approach, whereas no signal was detectable when unfused enzyme variants were used.[202]

Similar to VLPs, the ethanolamine utilization bacterial microcompartment proteins are able to form hexamers which, in turn, self-assemble into large protein filaments, when overexpressed in *E. coli*.[208,209] To use this microbial microcompartment for POI immobilization, the EutM protein from *Salmonella enterica* was fused to SpyCatcher and subsequently used as an *in vitro* scaffolding system for multienzyme cascades.[210] As a proof of concept, a two-step enzyme system consisting of an alcohol dehydrogenase and an amine dehydrogenase for chiral amine synthesis was tested *in vitro*. The ADH oxidizes an alcohol to a ketone intermediate, which is further reduced by the AmDH into a chiral amine. Each of the catalytic enzymes were combined with SpyTag to build a scaffold complex with SpyCatcher-tagged EutM domains. In comparison to unfused variants, the immobilized enzymes were stabilized and able to convert the substrate more efficiently.[210] In a following step, eight EutM homologues with a different scaffold structure were fused to the SpyCatcher domain allowing the generation of a multitude of possible hybrid scaffolds.[211,212]

For the functionalization of a bacterial biofilm consisting of *E. coli* cells, a chitinase, an exo-β-D-glucosaminidase, and a deacetylase suitable for conversion of α-chitin to glucosamine were immobilized on extracellular amyloid fiber structures consisting of CsgA curli proteins.[200,213] In many Enterobacteriaceae, CsgA monomers assemble after secretion into amyloid fibers which, in turn, are promising alternative scaffolds for Spy-assisted POI immobilization. In this case, the catalytic enzymes were combined with SpyTag or SpyCatcher as well as SnoopTag or SnoopCatcher in a distinct manner. After heterologous expression, POIs are secreted by the production host *E. coli* resulting in a spontaneous assembly of the functionalized amyloid structures. This approach led to a 2-times higher activity and tolerance toward nonphysiological temperature and pH values during production of glucosamine from α-chitin in comparison to unfused variants.[200]

In contrast to applications in which biopolymeric and proteinaceous carriers serve as a framework for enzyme immobilization, all-enzyme hydrogels represent an alternative where the biocatalytically active POI itself forms the matrix.[214−216] For example, a stereoselective alcohol dehydrogenase carrying a SpyCatcher domain and a cofactor-regenerating glucose 1-dehydrogenase fused to the SpyTag were used to reduce prochiral ketones.[214] Both enzymes form homotetramers, so that ultimately, each enzyme complex contains four SpyTag or SpyCatcher domains, respectively, capable of forming a hydrogel by latticelike interconnections of the recombinant POIs. For this approach, the proteins were overexpressed in *E. coli* and subsequently purified. After *in vitro* self-assembly, the POI-hydrogel was applied in continuous flow biocatalysis to produce chiral (*R*)-configured alcohols. This application led to conversion rates of up to 99% and offered a possibility to counteract the limitations of biocatalytic flow chemistry processes, since higher enzyme concentrations can be used, and at the same time, no carrier materials increase the pressure in the reaction cell.[214,217,218]

Q

Table 3. Comparison of POI *in Vivo* Immobilization Strategies Suitable for Biocatalytic Applications

immobilization system	Engineering effort	Heterologous production host	Size of *in vivo* immobilizates	applicability for biocatalysis[a]	pros/advantages	cons/limitations
IB display	very low to low	bacteria (*E. coli*) transferrable to other pro- and eukaryotic hosts	500 nm – 1 μm	yes (but limited) yes	▪ simplest strategy for *in vivo* POI immobilization ▪ high density allowing easy separation and purification	▪ only a few cases of rational POI targeting to IBs have been reported ▪ high proportion of POI offers reduced activity or is inactive ▪ no control over scaffolding process
CatIBs	low extended toolbox available	bacteria (*E. coli*) transferrable to other hosts	500 nm – 1 μm	yes yes	▪ high POI purities (80-95%) ▪ low effort/costs for purification ▪ web tools for evaluating the aggregation tendencies available	▪ POIs in lyophilized CatIB preparations displayed activities below 15% ▪ non-porous character can lead to high back-pressure in continuous flow processes and can cause limited substrate/product diffusion
Cry3aA entrapment	low	*B. thuringiensis*	< 1 μm	no yes	▪ direct isolation of immobilizates without further purification steps ▪ immobilized enzymes with high activities	▪ only small monomeric enzymes have been successfully immobilized ▪ cascade reactions with multiple enzymes might not be feasible ▪ the crystalline nature of the immobilizates might result in limited substrate/product diffusion
Forizymes	intermediate (co-expression of F4 is needed)	yeast plant cells	10 – 55 μm	yes yes	▪ large size allows e.g. filtration of immobilizates ▪ cascade reaction has been realized	▪ approach is so far restricted to eukaryotic expression hosts ▪ large forisome subunits needs to be fused to the POI ▪ likely prone to diffusional limitation due to crystalline nature
LLPS	low to intermediate (depending on the used system co-expression of multiple constructs needed)	mammalian cells, recently *E. coli*	< 1 μm	yes yes	▪ liquid- or gel-like nature enables easy substrate diffusion and on-demand recruitment of multiple enzymes at specific time points ▪ liquid-like environment does not impair proper protein folding	▪ LLPS droplets are not stable and dissociate below a certain critical concentration ▪ irreversible aging processes resulting in the formation of gels or glasses ▪ *E. coli* is not established as host for most systems
Polyhydroxy-alkanoate granules	intermediate (requires co-expression of *phaA* and *phaB*) extended toolbox available	bacteria (*E. coli*) transferrable to other prokaryotic hosts	100 – 500 nm	yes yes	▪ non-proteinaceous carrier material ▪ low effort/costs for purification ▪ orientation of POI is determined by the used PhaC fusion (N- or C-terminal) ▪ suitable for POI co-immobilization in combination with Spy/Snoop technology	▪ potential competition of PHA biosynthesis and POI-catalyzed reactions e.g., when the precursor acetyl-CoA is needed ▪ PHA particles tend to aggregate and their non-porous character can lead to high back-pressure in continuous flow processes
Virus-like particles	low to intermediate (depending on the used system, co-expression of a scaffolding protein might be needed) extended toolbox available	bacteria (*E. coli*) transferrable to other pro- and eukaryotic hosts including yeast	20 – 200 nm	yes yes	▪ can be used for POI encapsulation and POI-display ▪ homogeneous orientation and density of immobilized POIs ▪ highly monodisperse in shape and size ▪ especially suited for POI co-immobilization in combination with Spy/Snoop technology ▪ can increase sequential enzymatic conversions via diffusional channeling ▪ creation of super lattices possible (e.g. P22)	▪ genetic fusion of POI and CP can lead to misfolding and loss of activity thereby affecting VLP ▪ endogenous assembly behavior of some CPs (e.g. instability of CCMV capsid at physiological pH) hinders *in vivo* POI immobilization without further CP modifications ▪ relative small size of VLPs can limit the POI scaffolding process and complicate its isolation

[a]Applicable for *in vivo* co-immobilization (blue) and biotransformation (green).

https://doi.org/10.1021/acssuschemeng.1c02045
ACS Sustainable Chem. Eng. XXXX, XXX, XXX−XXX

GENERAL CONCLUSIONS

The constantly growing toolbox for *in vivo* immobilization provides us with a plethora of different methods. In general, immobilization increases the operational stability (e.g., with respect to temperature, pH, ionic strength, organic solvents) as well as the shelf life of the immobilized POI and allows enzyme recycling for repetitive use. In addition, scaffolding of multiple enzymes brings them into close proximity to each other, thus providing the possibility for better substrate or intermediate channeling, e.g., allowing for cascade use. In comparison to other chemical immobilization strategies, the here described *in vivo* immobilization methods further benefit from their easy, environmentally friendly, cost-efficient, one-step production, by using sustainable feedstocks or industrial waste streams. In addition, the resulting enzyme immobilizates are nontoxic, biocompatible, and biodegradable thereby allowing their implementation into circular bioeconomy processes. However, as often is the case for emerging technologies, lab-scale applications have been shown for many of the described *in vivo* immobilization systems, but systematic studies that compare their efficacy and scalability are still missing. For many systems (forizymes, Cry3Aa immobilizates, LLPS systems), only a limited number of proof-of-concept studies are available. Thus, properties such as stability, recyclability, and even residual activity compared to the soluble, purified POI often remain undercharacterized or were simply not tested yet. A summary of advantages as well as limitations of the immobilization strategies considered in this Perspective are presented in Table 3.

In principle, only minor engineering efforts are needed for *in vivo* enzyme immobilization. In all cases, proper incorporation or display of POIs inside or on the surface of the respective biogenic carrier materials includes the genetic fusion of the POI with a protein domain that causes the self-assembly into respective immobilizate structures. For forizymes, liquid protein condensates, PHA, and VLPs, coexpression of the POI-anchor protein fusion with proteins or enzymes that are required to provide the polymeric immobilization matrix is needed. For most of the here described *in vivo* systems, engineering of fusion proteins is still a trial-and-error approach, and construct optimization might be necessary to obtain efficiently self-immobilizing catalysts. Some systems (i.e., CatIBs, PHA, and VLPs) already offer a modular immobilization toolbox allowing the comparative evaluation of different "pull down" tags, PHA anchors, or VLP capsids, whose application can result in remarkable differences of the particle properties (e.g., size, porosity, POI density, and activity). The *in vivo* production of POI immobilizates can be performed in either a narrow or a broad range of different host organisms. In most cases, the standard bacterial expression host *E. coli* is readily applicable, whereas the formation of forizymes requires yeast or plant cells. Cry3Aa immobilizates are commonly produced in *B. thuringiensis*, the natural host of the Cry3Aa protein. Liquid protein condensates are most often produced in mammalian cells, but yeast production and lately also the production in *E. coli* were shown to be feasible. Remarkably, some of the systems including CatIBs, PHA, and VLPs can be applied in various pro- and eukaryotic expression hosts including Gram-positive and Gram-negative bacteria as well as yeasts, thereby allowing the adaptation of the expression protocol to specific POI requirements, e.g., the absence of toxic LPS for biomedical applications or posttranslational modification of POIs with eukaryotic origin. Notably, the production of POI immobilizates beyond the laboratory scale requires well-established production hosts like *E. coli* or *S. cerevisiae* for which a wide range of different expression systems already exist. Depending on the respective application, the size of the POI immobilizates also matters, which can differ significantly ranging from ∼20 nm to 50 μm permitting isolation by simple centrifugation (e.g., CatIBs and PHAs) or alternatively requiring ultracentrifugation or size exclusion chromatography (e.g., some VLPs, forizymes). For *in vivo* POI coimmobilization, the presented VLP systems in combination with a "click-chemistry-like" Spy/Snoop-tag technology are particularly useful because a uniform orientation, coherent composition, and density of the immobilized POIs can be achieved. Like most enzyme immobilizates, also the here described *in vivo* generated immobilizates might suffer from suboptimal substrate turnover resulting from diffusional limitation, as they, like all immobilizates, require that substrates or products are crossing a physical barrier like a phase boundary (liquid/solid, liquid/gel, liquid/liquid) to reach the enzyme or be released from it after turnover. This, however, is in principal not the case for technologies that rely on POI-surface display such as IB display, most PHA-based strategies, and respective VLP-based protein display technologies. In those cases though, the immobilized enzymes might be more prone to inactivation by components of the reaction system as they are immobilized only on the surface of the "carrier". In contrast, most strategies that rely on POI encapsulation within microcompartment-like structures such as CatIBs-, Cry3aA-, and forisome-based immobilizates are likely to experience more severe diffusional limitation, although this issue has not been addressed empirically in all cases. In turn, due to the liquidlike properties of LLPS protein condensates, probably with the exception of those forming hydrogels, diffusional limitation should be much less of an issue as for the aforementioned encapsulation-based systems, where the substrate/product has to cross a liquid/solid phase boundary.

For future applications, expandability of the spatial structure and function, e.g., allowing the generation of multifunctionalized biomaterial, will be key. For most of the here presented immobilization systems, such expandability is limited; however, LLPS, CatIBs, PHA, and VLP systems might open up new avenues to design liquid, gel-like, or rigid supramolecular assemblies that may enable completely new biocatalytic applications.

ASSOCIATED CONTENT

Supporting Information

The Supporting Information is available free of charge at https://pubs.acs.org/doi/10.1021/acssuschemeng.1c02045.

A table of abbreviations used in the manuscript (PDF)

AUTHOR INFORMATION

Corresponding Authors

Thomas Drepper − *Institute of Molecular Enzyme Technology, Heinrich Heine University Düsseldorf, D-52425 Jülich, Germany*; Phone: ++49 2461-61-4173; Email: t.drepper@fz-juelich.de

Ulrich Krauss − *Institute of Molecular Enzyme Technology, Heinrich Heine University Düsseldorf, D-52425 Jülich, Germany; Institute of Bio- and Geosciences IBG-1: Biotechnology, Forschungszentrum Jülich GmbH, D-52425*

https://doi.org/10.1021/acssuschemeng.1c02045
ACS Sustainable Chem. Eng. XXXX, XXX, XXX−XXX

Jülich, Germany; orcid.org/0000-0003-2219-7388; Phone: ++49 2461-61-2939; Email: u.krauss@fz-juelich.de

Authors

Gizem Ölçücü – *Institute of Molecular Enzyme Technology, Heinrich Heine University Düsseldorf, D-52425 Jülich, Germany; Institute of Bio- and Geosciences IBG-1: Biotechnology, Forschungszentrum Jülich GmbH, D-52425 Jülich, Germany*

Oliver Klaus – *Institute of Molecular Enzyme Technology, Heinrich Heine University Düsseldorf, D-52425 Jülich, Germany*

Karl-Erich Jaeger – *Institute of Molecular Enzyme Technology, Heinrich Heine University Düsseldorf, D-52425 Jülich, Germany; Institute of Bio- and Geosciences IBG-1: Biotechnology, Forschungszentrum Jülich GmbH, D-52425 Jülich, Germany*

Complete contact information is available at: https://pubs.acs.org/10.1021/acssuschemeng.1c02045

Author Contributions

§G.Ö. and O.K. contributed equally.

Notes

The authors declare no competing financial interest.

Biographies

Gizem Ölçücü studied bioengineering at Montana State University, USA, and Istanbul Technical University, Turkey. She obtained her B.Sc. degrees from the bioengineering dual diploma program in 2012. In 2016, she obtained her M.Sc. degree on molecular life sciences from Friedrich Schiller University Jena, Germany. Since 2018, she has been pursuing her Ph.D. at the Institute of Molecular Enzyme Technology of the Heinrich-Heine-University Düsseldorf located at Forschungszentrum Jülich, Germany. She is interested in protein engineering and *in vivo* enzyme immobilization strategies, and her current research, within the "CLIB Competence Centre Biotechnology", is focused on catalytically active inclusion bodies and ferritin-based immobilizates for biotechnological applications.

Oliver Klaus studied biology at the Heinrich-Heine-University Düsseldorf (HHU), Germany. He finished his B.Sc. degree in 2015 and his M.Sc. degree in 2017. Since 2018, he performed his doctoral studies at the HHU Institute of Molecular Enzyme Technology, located at the Forschungszentrum Jülich, Germany. He is interested in the production of secondary metabolites in phototrophic bacteria and immobilization of biotechnologically relevant enzymes on polyhydroxybutyrate granules. His work is a part of the "CLIB Competence Centre Biotechnology" project and funded by the European Regional Development Fund.

Prof. Dr. Karl-Erich Jaeger studied biology and chemistry and obtained a Ph.D. in microbiology at Ruhr-University Bochum, Germany. From 1988 to 1989, he worked as a postdoc with Prof. Dr. Robert E.W. Hancock at the Department of Microbiology, University of British Columbia, Vancouver, B.C., Canada. In 2002, he became full professor at Heinrich-Heine-University Düsseldorf and director of the Institute of Molecular Enzyme Technology at Forschungszentrum Jülich. In 2013, the Forschungszentrum Jülich GmbH of the German Helmholtz Association additionally appointed him as director at the Institute of Bio- and Geosciences IBG-1: Biotechnology. Karl-Erich Jaeger published more than 200 research papers and 17 patent applications; he is an editorial board member of several scientific journals and serves as vice-president of the Cluster of Industrial Biotechnology—CLIB. His research interests are focused on bacterial enzymes and proteins, their identification, expression, biochemical and structural characterization, and biotechnological applications.

https://doi.org/10.1021/acssuschemeng.1c02045
ACS Sustainable Chem. Eng. XXXX, XXX, XXX−XXX

Dr. Thomas Drepper studied biology and received his diploma and Ph.D. from the Ruhr-Universität Bochum Bochum, Germany. Since 2004, he is head of the "Bacterial Photobiotechnology" group at the Institute of Molecular Enzyme Technology, Heinrich-Heine-University Düsseldorf, located at the Forschungszentrum Jülich, Germany. He published more than 70 peer-reviewed articles with an h index of 32 and more than 3000 citations (Google scholar). His current research focuses lie in synthetic biology, optogenetics, and natural product synthesis in phototrophic and nonphototrophic bacteria.

Dr. Ulrich Krauss studied applied natural sciences at the TU Bergakademie Freiberg, Germany, and obtained his Ph.D. in 2008 from the Heinrich-Heine-University Düsseldorf, Germany. From 2008 to 2010, he worked as a postdoc with Prof. Dr. Karl-Erich Jaeger and Prof. Dr. Wolfgang Gärtner at the Institute of Molecular Enzyme Technology, Heinrich-Heine-University Düsseldorf, Germany, and the Max-Planck Institute for Bioinorganic Chemistry (now MPI Chemical Energy Conversion), Mülheim an der Ruhr, Germany. Since 2009, he is heading the group "Molecular Biophotonics" at the Institute of Molecular Enzyme Technology, Heinrich-Heine-University Düsseldorf located at the Forschungszentrum Jülich, Germany. He published more than 40 peer-reviewed articles with an h index of 22 and more than 1700 citations (Google scholar). His research is focused on enzymes and photoreceptors covering the fields of photochemistry, photobiology, and optogenetics as well as biocatalysis, synthetic biology, and structural biochemistry.

■ ACKNOWLEDGMENTS

The research was financially supported by the CLIB Competence Centre Biotechnology (CKB) funded by the European Regional Development Fund ERDF (34.EFRE 0300096 and 34.EFRE 0300097).

■ REFERENCES

(1) Badenhorst, C. P. S.; Bornscheuer, U. T. Getting Momentum: From Biocatalysis to Advanced Synthetic Biology. *Trends Biochem. Sci.* **2018**, *43* (3), 180−198.
(2) Nestl, B. M.; Nebel, B. A.; Hauer, B. Recent progress in industrial biocatalysis. *Curr. Opin. Chem. Biol.* **2011**, *15* (2), 187−193.
(3) Truppo, M. D. Biocatalysis in the Pharmaceutical Industry: The Need for Speed. *ACS Med. Chem. Lett.* **2017**, *8* (5), 476−480.
(4) Liu, Z.; Wang, K.; Chen, Y.; Tan, T.; Nielsen, J. Third-generation biorefineries as the means to produce fuels and chemicals from CO_2. *Nat. Catal* **2020**, *3*, 274−288.
(5) Castro, G. R.; Knubovets, T. Homogeneous biocatalysis in organic solvents and water-organic mixtures. *Crit. Rev. Biotechnol.* **2003**, *23* (3), 195−231.
(6) Khmelnitsky, Y. L.; Rich, J. O. Biocatalysis in nonaqueous solvents. *Curr. Opin. Chem. Biol.* **1999**, *3* (1), 47−53.
(7) Sheldon, R. A. Biocatalysis and Biomass Conversion in Alternative Reaction Media. *Chem. - Eur. J.* **2016**, *22* (37), 12984−12999.
(8) Balcao, V. M.; Vila, M. M. Structural and functional stabilization of protein entities: state-of-the-art. *Adv. Drug Delivery Rev.* **2015**, *93*, 25−41.
(9) Guisan, J. M. New opportunities for immobilization of enzymes. *Methods Mol. Biol.* **2013**, *1051*, 1−13.
(10) Liese, A.; Hilterhaus, L. Evaluation of immobilized enzymes for industrial applications. *Chem. Soc. Rev.* **2013**, *42* (15), 6236−6249.
(11) Sheldon, R. A. Characteristic features and biotechnological applications of cross-linked enzyme aggregates (CLEAs). *Appl. Microbiol. Biotechnol.* **2011**, *92* (3), 467−477.
(12) Tufvesson, P.; Lima-Ramos, J.; Nordblad, M.; Woodley, J. M. Guidelines and cost analysis for catalyst production in biocatalytic processes. *Org. Process Res. Dev.* **2011**, *15*, 266−274.
(13) Homaei, A. A.; Sariri, R.; Vianello, F.; Stevanato, R. Enzyme immobilization: an update. *J. Chem. Biol.* **2013**, *6* (4), 185−205.
(14) Kress, J.; Zanaletti, R.; Amour, A.; Ladlow, M.; Frey, J. G.; Bradley, M. Enzyme accessibility and solid supports: which molecular weight enzymes can be used on solid supports? An investigation using confocal Raman microscopy. *Chem. - Eur. J.* **2002**, *8* (16), 3769−72.
(15) Bellapadrona, G.; Sinkar, S.; Sabanay, H.; Liljestrom, V.; Kostiainen, M.; Elbaum, M. Supramolecular Assembly and Coalescence of Ferritin Cages Driven by Designed Protein-Protein Interactions. *Biomacromolecules* **2015**, *16* (7), 2006−2011.
(16) Choi, S. L.; Lee, S. J.; Yeom, S. J.; Kim, H. J.; Rhee, Y. H.; Jung, H. C.; Lee, S. G. Controlled localization of functionally active proteins to inclusion bodies using leucine zippers. *PLoS One* **2014**, *9* (6), No. e97093.
(17) Diener, M.; Kopka, B.; Pohl, M.; Jaeger, K. E.; Krauss, U. Fusion of a coiled-coil domain facilitates the high-level production of catalytically active enzyme inclusion bodies. *ChemCatChem* **2016**, *8* (1), 142−152.
(18) Heater, B. S.; Yang, Z.; Lee, M. M.; Chan, M. K. In Vivo Enzyme Entrapment in a Protein Crystal. *J. Am. Chem. Soc.* **2020**, *142* (22), 9879−9883.
(19) Huber, I.; Palmer, D. J.; Ludwig, K. N.; Brown, I. R.; Warren, M. J.; Frunzke, J. Construction of Recombinant Pdu Metabolosome Shells for Small Molecule Production in *Corynebacterium glutamicum*. *ACS Synth. Biol.* **2017**, *6* (11), 2145−2156.
(20) Noireaux, V.; Libchaber, A. A vesicle bioreactor as a step toward an artificial cell assembly. *Proc. Natl. Acad. Sci. U. S. A.* **2004**, *101* (51), 17669−17674.
(21) Visser, F.; Muller, B.; Rose, J.; Prufer, D.; Noll, G. A. Forizymes - functionalised artificial forisomes as a platform for the production and immobilisation of single enzymes and multi-enzyme complexes. *Sci. Rep.* **2016**, *6*, 30839.
(22) Wei, S. P.; Qian, Z. G.; Hu, C. F.; Pan, F.; Chen, M. T.; Lee, S. Y.; Xia, X. X. Formation and functionalization of membraneless compartments in *Escherichia coli*. *Nat. Chem. Biol.* **2020**, *16* (10), 1143−1148.

https://doi.org/10.1021/acssuschemeng.1c02045
ACS Sustainable Chem. Eng. XXXX, XXX, XXX−XXX

(23) Wong, J. X.; Rehm, B. H. A. Design of Modular Polyhydroxyalkanoate Scaffolds for Protein Immobilization by Directed Ligation. *Biomacromolecules* **2018**, *19* (10), 4098−4112.
(24) Zhou, B. H.; Xing, L.; Wu, W.; Zhang, X. E.; Lin, Z. L. Small surfactant-like peptides can drive soluble proteins into active aggregates. *Microb. Cell Fact.* **2012**, *11*, 10.
(25) Jäger, V. D.; Kloss, R.; Grünberger, A.; Seide, S.; Hahn, D.; Karmainski, T.; Piqueray, M.; Embruch, J.; Longerich, S.; Mackfeld, U.; Jaeger, K. E.; Wiechert, W.; Pohl, M.; Krauss, U. Tailoring the properties of (catalytically)-active inclusion bodies. *Microb. Cell Fact.* **2019**, *18*, 18.
(26) Krauss, U.; Jäger, V. D.; Diener, M.; Pohl, M.; Jaeger, K. E. Catalytically-active inclusion bodies carrier-free protein immobilizates for application in biotechnology and biomedicine. *J. Biotechnol.* **2017**, *258*, 136−147.
(27) Heater, B. S.; Lee, M. M.; Chan, M. K. Direct production of a genetically-encoded immobilized biodiesel catalyst. *Sci. Rep.* **2018**, *8* (1), 12783.
(28) Bracha, D.; Walls, M. T.; Wei, M. T.; Zhu, L.; Kurian, M.; Avalos, J. L.; Toettcher, J. E.; Brangwynne, C. P. Mapping Local and Global Liquid Phase Behavior in Living Cells Using Photo-Oligomerizable Seeds. *Cell* **2018**, *175* (6), 1467−1480.
(29) Li, P.; Banjade, S.; Cheng, H. C.; Kim, S.; Chen, B.; Guo, L.; Llaguno, M.; Hollingsworth, J. V.; King, D. S.; Banani, S. F.; Russo, P. S.; Jiang, Q. X.; Nixon, B. T.; Rosen, M. K. Phase transitions in the assembly of multivalent signalling proteins. *Nature* **2012**, *483* (7389), 336−340.
(30) Nakamura, H.; Lee, A. A.; Afshar, A. S.; Watanabe, S.; Rho, E.; Razavi, S.; Suarez, A.; Lin, Y. C.; Tanigawa, M.; Huang, B.; DeRose, R.; Bobb, D.; Hong, W.; Gabelli, S. B.; Goutsias, J.; Inoue, T. Intracellular production of hydrogels and synthetic RNA granules by multivalent molecular interactions. *Nat. Mater.* **2018**, *17* (1), 79−89.
(31) Schuster, B. S.; Reed, E. H.; Parthasarathy, R.; Jahnke, C. N.; Caldwell, R. M.; Bermudez, J. G.; Ramage, H.; Good, M. C.; Hammer, D. A. Controllable protein phase separation and modular recruitment to form responsive membraneless organelles. *Nat. Commun.* **2018**, *9* (1), 2985.
(32) Shin, Y.; Berry, J.; Pannucci, N.; Haataja, M. P.; Toettcher, J. E.; Brangwynne, C. P. Spatiotemporal Control of Intracellular Phase Transitions Using Light-Activated optoDroplets. *Cell* **2017**, *168* (1−2), 159−171.
(33) Rehm, F. B.; Chen, S.; Rehm, B. H. Enzyme Engineering for In Situ Immobilization. *Molecules* **2016**, *21* (10), 1370.
(34) Garcia-Fruitos, E.; Vazquez, E.; Diez-Gil, C.; Corchero, J. L.; Seras-Franzoso, J.; Ratera, I.; Veciana, J.; Villaverde, A. Bacterial inclusion bodies: making gold from waste. *Trends Biotechnol.* **2012**, *30* (2), 65−70.
(35) Li, H.; Zheng, G.; Zhu, S. Construction of an organelle-like nanodevice via supramolecular self-assembly for robust biocatalysts. *Microb. Cell Fact.* **2018**, *17* (1), 26.
(36) Bracha, D.; Walls, M. T.; Brangwynne, C. P. Probing and engineering liquid-phase organelles. *Nat. Biotechnol.* **2019**, *37* (12), 1435−1445.
(37) Ginet, N.; Pardoux, R.; Adryanczyk, G.; Garcia, D.; Brutesco, C.; Pignol, D. Single-step production of a recyclable nanobiocatalyst for organophosphate pesticides biodegradation using functionalized bacterial magnetosomes. *PLoS One* **2011**, *6* (6), No. e21442.
(38) Menon, B. B.; Dou, Z.; Heinhorst, S.; Shively, J. M.; Cannon, G. C. *Halothiobacillus neapolitanus* carboxysomes sequester heterologous and chimeric RubisCO species. *PLoS One* **2008**, *3* (10), No. e3570.
(39) Han, G. H.; Seong, W.; Fu, Y.; Yoon, P. K.; Kim, S. K.; Yeom, S. J.; Lee, D. H.; Lee, S. G. Leucine zipper-mediated targeting of multi-enzyme cascade reactions to inclusion bodies in *Escherichia coli* for enhanced production of 1-butanol. *Metab. Eng.* **2017**, *40*, 41−49.
(40) Jäger, V. D.; Lamm, R.; Küsters, K.; Ölcücü, G.; Oldiges, M.; Jaeger, K. E.; Büchs, J.; Krauss, U. Catalytically-active inclusion bodies for biotechnology-general concepts, optimization, and application. *Appl. Microbiol. Biotechnol.* **2020**, *104* (17), 7313−7329.
(41) Dzuricky, M.; Rogers, B. A.; Shahid, A.; Cremer, P. S.; Chilkoti, A. De novo engineering of intracellular condensates using artificial disordered proteins. *Nat. Chem.* **2020**, *12* (9), 814−825.
(42) Baneyx, F.; Mujacic, M. Recombinant protein folding and misfolding in *Escherichia coli*. *Nat. Biotechnol.* **2004**, *22* (11), 1399−1408.
(43) Rinas, U.; Garcia-Fruitos, E.; Corchero, J. L.; Vazquez, E.; Seras-Franzoso, J.; Villaverde, A. Bacterial Inclusion Bodies: Discovering Their Better Half. *Trends Biochem. Sci.* **2017**, *42* (9), 726−737.
(44) Rokney, A.; Shagan, M.; Kessel, M.; Smith, Y.; Rosenshine, I.; Oppenheim, A. B. E. coli transports aggregated proteins to the poles by a specific and energy-dependent process. *J. Mol. Biol.* **2009**, *392* (3), 589−601.
(45) Arie, J. P.; Miot, M.; Sassoon, N.; Betton, J. M. Formation of active inclusion bodies in the periplasm of *Escherichia coli*. *Mol. Microbiol.* **2006**, *62* (2), 427−437.
(46) Cousens, L. S.; Shuster, J. R.; Gallegos, C.; Ku, L.; Stempien, M. M.; Urdea, M. S.; Sanchez-Pescador, R.; Taylor, A.; Tekamp-Olson, P. High level expression of proinsulin in the yeast, *Saccharomyces cerevisiae*. *Gene* **1987**, *61* (3), 265−275.
(47) Kopito, R. R. Aggresomes, inclusion bodies and protein aggregation. *Trends Cell Biol.* **2000**, *10* (12), 524−530.
(48) Wang, L. Towards revealing the structure of bacterial inclusion bodies. *Prion* **2009**, *3* (3), 139−145.
(49) Singh, S. M.; Panda, A. K. Solubilization and refolding of bacterial inclusion body proteins. *J. Biosci Bioeng* **2005**, *99* (4), 303−310.
(50) Steinmann, B.; Christmann, A.; Heiseler, T.; Fritz, J.; Kolmar, H. In vivo enzyme immobilization by inclusion body display. *Appl. Environ. Microbiol.* **2010**, *76* (16), 5563−5569.
(51) Spieler, V.; Valldorf, B.; Maass, F.; Kleinschek, A.; Huttenhain, S. H.; Kolmar, H. Coupled reactions on bioparticles: Stereoselective reduction with cofactor regeneration on PhaC inclusion bodies. *Biotechnol. J.* **2016**, *11* (7), 890−898.
(52) Choi, S. L.; Lee, S. J.; Ha, J. S.; Song, J.; Rhee, Y. H.; Lee, S. G. Generation of catalytic protein particles in *Escherichia coli* cells using the cellulose-binding domain from *Cellulomonas fimi* as a fusion partner. *Biotechnol. Bioprocess Eng.* **2011**, *16* (6), 1173−1179.
(53) Worrall, D. M.; Goss, N. H. The formation of biologically active beta-galactosidase inclusion bodies in *Escherichia coli*. *Aust J. Biotechnol* **1989**, *3* (1), 28−32.
(54) de Marco, A.; Ferrer-Miralles, N.; Garcia-Fruitos, E.; Mitraki, A.; Peternel, S.; Rinas, U.; Trujillo-Roldan, M. A.; Valdez-Cruz, N. A.; Vazquez, E.; Villaverde, A. Bacterial inclusion bodies are industrially exploitable amyloids. *FEMS Microbiol Rev.* **2019**, *43* (1), 53−72.
(55) Köszagová, R. Inclusion Bodies in Biotechnology. *J. Microbiol., Biotechnol. Food Sci.* **2020**, *9* (6), 1191−1196.
(56) Slouka, C.; Kopp, J.; Spadiut, O.; Herwig, C. Perspectives of inclusion bodies for bio-based products: curse or blessing? *Appl. Microbiol. Biotechnol.* **2019**, *103* (3), 1143−1153.
(57) Chen, X.; Zaro, J. L.; Shen, W. C. Fusion protein linkers: property, design and functionality. *Adv. Drug Delivery Rev.* **2013**, *65* (10), 1357−1369.
(58) Huang, Z.; Zhang, C.; Chen, S.; Ye, F.; Xing, X. H. Active inclusion bodies of acid phosphatase PhoC: aggregation induced by GFP fusion and activities modulated by linker flexibility. *Microb. Cell Fact.* **2013**, *12*, 25.
(59) Kusters, K.; Pohl, M.; Krauss, U.; Olcucu, G.; Albert, S.; Jaeger, K. E.; Wiechert, W.; Oldiges, M. Construction and comprehensive characterization of an EcLDCc-CatIB set-varying linkers and aggregation inducing tags. *Microb. Cell Fact.* **2021**, *20* (1), 49.
(60) Jäger, V. D.; Lamm, R.; Kloss, R.; Kaganovitch, E.; Grünberger, A.; Pohl, M.; Büchs, J.; Jaeger, K. E.; Krauss, U. A synthetic reaction cascade implemented by colocalization of two proteins within catalytically active inclusion bodies. *ACS Synth. Biol.* **2018**, *7* (9), 2282−2295.
(61) Garcia-Fruitos, E.; Gonzalez-Montalban, N.; Morell, M.; Vera, A.; Ferraz, R. M.; Aris, A.; Ventura, S.; Villaverde, A. Aggregation as

https://doi.org/10.1021/acssuschemeng.1c02045
ACS Sustainable Chem. Eng. XXXX, XXX, XXX−XXX

bacterial inclusion bodies does not imply inactivation of enzymes and fluorescent proteins. *Microb. Cell Fact.* **2005**, *4*, 27.
(62) Lin, Z. L.; Zhou, B. H.; Wu, W.; Xing, L.; Zhao, Q. Self-assembling amphipathic alpha-helical peptides induce the formation of active protein aggregates *in vivo*. *Faraday Discuss.* **2013**, *166*, 243−256.
(63) Wu, W.; Xing, L.; Zhou, B.; Lin, Z. Active protein aggregates induced by terminally attached self-assembling peptide ELK16 in *Escherichia coli*. *Microb. Cell Fact.* **2011**, *10* (9), 9.
(64) Park, S. Y.; Park, S. H.; Choi, S. K. Active inclusion body formation using *Paenibacillus polymyxa* PoxB as a fusion partner in *Escherichia coli*. *Anal. Biochem.* **2012**, *426* (1), 63−65.
(65) Köszagová, R.; Krajcovic, T.; Palencarova-Talafova, K.; Patoprsty, V.; Vikartovska, A.; Pospiskova, K.; Safarik, I.; Nahalka, J. Magnetization of active inclusion bodies: comparison with centrifugation in repetitive biotransformations. *Microb. Cell Fact.* **2018**, *17*, 17.
(66) Han, H.; Zeng, W.; Zhang, G.; Zhou, J. Active tyrosine phenol-lyase aggregates induced by terminally attached functional peptides in *Escherichia coli*. *J. Ind. Microbiol. Biotechnol.* **2020**, *47* (8), 563−571.
(67) Wang, X.; Zhou, B. H.; Hu, W. K.; Zhao, Q.; Lin, Z. L. Formation of active inclusion bodies induced by hydrophobic self-assembling peptide GFIL8. *Microb. Cell Fact.* **2015**, *14*, 14.
(68) Jiang, L.; Xiao, W. J.; Zhou, X.; Wang, W. Y.; Fan, J. Comparative study of the insoluble and soluble Ulp1 protease constructs as carrier free and dependent protein immobilizates. *J. Biosci Bioeng* **2019**, *127* (1), 23−29.
(69) Kloss, R.; Karmainski, T.; Jäger, V. D.; Hahn, D.; Grünberger, A.; Baumgart, M.; Krauss, U.; Jaeger, K. E.; Wiechert, W.; Pohl, M. Tailor-made catalytically active inclusion bodies for different applications in biocatalysis. *Catal. Sci. Technol.* **2018**, *8* (22), 5816−5826.
(70) Kloss, R.; Limberg, M. H.; Mackfeld, U.; Hahn, D.; Grünberger, A.; Jäger, V. D.; Krauss, U.; Oldiges, M.; Pohl, M. Catalytically active inclusion bodies of L-lysine decarboxylase from *E. coli* for 1,5-diaminopentane production. *Sci. Rep.* **2018**, *8*, 8.
(71) Roca-Pinilla, R.; Fortuna, S.; Natalello, A.; Sanchez-Chardi, A.; Ami, D.; Aris, A.; Garcia-Fruitos, E. Exploring the use of leucine zippers for the generation of a new class of inclusion bodies for pharma and biotechnological applications. *Microb. Cell Fact.* **2020**, *19* (1), 175.
(72) Gil-Garcia, M.; Navarro, S.; Ventura, S. Coiled-coil inspired functional inclusion bodies. *Microb. Cell Fact.* **2020**, *19* (1), 117.
(73) Nahalka, J.; Nidetzky, B. Fusion to a pull-down domain: A novel approach of producing *Trigonopsis variabilis* D-amino acid oxidase as insoluble enzyme aggregates. *Biotechnol. Bioeng.* **2007**, *97* (3), 454−461.
(74) Nahalka, J.; Vikartovska, A.; Hrabarova, E. A crosslinked inclusion body process for sialic acid synthesis. *J. Biotechnol.* **2008**, *134* (1−2), 146−153.
(75) Nahalka, J.; Patoprsty, V. Enzymatic synthesis of sialylation substrates powered by a novel polyphosphate kinase (PPK3). *Org. Biomol. Chem.* **2009**, *7* (9), 1778−1780.
(76) Schwaighofer, A.; Ablasser, S.; Lux, L.; Kopp, J.; Herwig, C.; Spadiut, O.; Lendl, B.; Slouka, C. Production of Active Recombinant Hyaluronidase Inclusion Bodies from *Apis mellifera* in E. coli Bl21(DE3) and characterization by FT-IR Spectroscopy. *Int. J. Mol. Sci.* **2020**, *21* (11), 3881.
(77) Pastuszka, M. K.; MacKay, J. A. Engineering structure and function using thermoresponsive biopolymers. *WIREs Nanomed Nanobiotechnol.* **2016**, *8* (1), 123−138.
(78) Wang, R.; Li, J.; Dang, D.; Hu, J.; Hu, Y.; Fan, J. Bacterial production of maize and human serine racemases as partially active inclusion bodies for d-serine synthesis. *Enzyme Microb. Technol.* **2020**, *137*, 109547.
(79) Ji, W.; Sun, W.; Feng, J.; Song, T.; Zhang, D.; Ouyang, P.; Gu, Z.; Xie, J. , Characterization of a novel N-acetylneuraminic acid lyase favoring industrial N-acetylneuraminic acid synthesis. *Sci. Rep.* **2015**, *5*, 5.
(80) Latham, J. R.; Love, M.; Hilbeck, A. The distinct properties of natural and GM cry insecticidal proteins. *Biotechnol. Genet. Eng. Rev.* **2017**, *33* (1), 62−96.
(81) Park, H.-W.; Ge, B.; Bauer, L. S.; Federici, B. A. Optimization of Cry3A Yields in *Bacillus thuringiensis* by Use of Sporulation-Dependent Promoters in Combination with the STAB-SD mRNA Sequence. *Appl. Environ. Microbiol.* **1998**, *64* (10), 3932−3938.
(82) Hammond, B. G.; Koch, M. S. A Review of the Food Safety of Bt Crops. In *Bacillus thuringiensis Biotechnology*; Sansinenea, E., Ed.; Springer: Dordrecht, 2012; pp 305−325.
(83) Nair, M. S.; Lee, M. M.; Bonnegarde-Bernard, A.; Wallace, J. A.; Dean, D. H.; Ostrowski, M. C.; Burry, R. W.; Boyaka, P. N.; Chan, M. K. Cry protein crystals: a novel platform for protein delivery. *PLoS One* **2015**, *10* (6), No. e0127669.
(84) Heater, B. S.; Chan, W. S.; Lee, M. M.; Chan, M. K. Directed evolution of a genetically encoded immobilized lipase for the efficient production of biodiesel from waste cooking oil. *Biotechnol. Biofuels* **2019**, *12*, 165.
(85) Sun, Q.; Cheng, S. W.; Cheung, K.; Lee, M. M.; Chan, M. K. Cry Protein Crystal-Immobilized Metallothioneins for Bioremediation of Heavy Metals from Water. *Crystals* **2019**, *9* (6), 287.
(86) Noll, G. A.; Müller, B.; Ernst, A. M.; Rüping, B.; Twyman, R. M.; Prüfer, D. Native and artificial forisomes: functions and applications. *Appl. Microbiol. Biotechnol.* **2011**, *89* (6), 1675−1682.
(87) Müller, B.; Groscurth, S.; Menzel, M.; Rüping, B. A.; Twyman, R. M. D.; Prüfer, D.; Noll, G. A. Molecular and ultrastructural analysis of forisome subunits reveals the principles of forisome assembly. *Ann. Bot.* **2014**, *113* (7), 1121−1137.
(88) Müller, B.; Noll, G. A.; Ernst, A. M.; Rüping, B.; Groscurth, S.; Twyman, R. M.; Kawchuk, L. M.; Prüfer, D. Recombinant artificial forisomes provide ample quantities of smart biomaterials for use in technical devices. *Appl. Microbiol. Biotechnol.* **2010**, *88* (3), 689−698.
(89) Knoblauch, M.; Stubenrauch, M.; van Bel, A. J.; Peters, W. S. Forisome performance in artificial sieve tubes. *Plant, Cell Environ.* **2012**, *35* (8), 1419−1427.
(90) Groscurth, S.; Müller, B.; Schwan, S.; Menzel, M.; Diekstall, F.; Senft, M.; Kendall, A.; Kommor, B. A.; Neumann, U.; Kalischuk, M.; Kawchuk, L. M.; Krzyzanek, V.; Heilmann, A.; Stubbs, G.; Twyman, R. M.; Prüfer, D.; Noll, G. A. Artificial Forisomes Are Ideal Models of Forisome Assembly and Activity That Allow the Development of Technical Devices. *Biomacromolecules* **2012**, *13* (10), 3076−3086.
(91) Hyman, A. A.; Weber, C. A.; Julicher, F. Liquid-liquid phase separation in biology. *Annu. Rev. Cell Dev. Biol.* **2014**, *30*, 39−58.
(92) Brangwynne, C. P.; Eckmann, C. R.; Courson, D. S.; Rybarska, A.; Hoege, C.; Gharakhani, J.; Julicher, F.; Hyman, A. A. Germline P granules are liquid droplets that localize by controlled dissolution/condensation. *Science* **2009**, *324* (5935), 1729−1732.
(93) Alberti, S. The wisdom of crowds: regulating cell function through condensed states of living matter. *J. Cell Sci.* **2017**, *130* (17), 2789−2796.
(94) Marnik, E. A.; Updike, D. L. Membraneless organelles: P granules in *Caenorhabditis elegans*. *Traffic* **2019**, *20* (6), 373−379.
(95) Latonen, L. Phase-to-Phase With Nucleoli - Stress Responses, Protein Aggregation and Novel Roles of RNA. *Front. Cell. Neurosci.* **2019**, *13*, 151.
(96) Gibson, B. A.; Doolittle, L. K.; Schneider, M. W. G.; Jensen, L. E.; Gamarra, N.; Henry, L.; Gerlich, D. W.; Redding, S.; Rosen, M. K. Organization of Chromatin by Intrinsic and Regulated Phase Separation. *Cell* **2019**, *179* (2), 470−484.
(97) Molliex, A.; Temirov, J.; Lee, J.; Coughlin, M.; Kanagaraj, A. P.; Kim, H. J.; Mittag, T.; Taylor, J. P. Phase separation by low complexity domains promotes stress granule assembly and drives pathological fibrillization. *Cell* **2015**, *163* (1), 123−133.
(98) Case, L. B.; Zhang, X.; Ditlev, J. A.; Rosen, M. K. Stoichiometry controls activity of phase-separated clusters of actin signaling proteins. *Science* **2019**, *363* (6431), 1093−1097.
(99) Alberti, S.; Gladfelter, A.; Mittag, T. Considerations and Challenges in Studying Liquid-Liquid Phase Separation and Biomolecular Condensates. *Cell* **2019**, *176* (3), 419−434.

https://doi.org/10.1021/acssuschemeng.1c02045
ACS Sustainable Chem. Eng. XXXX, XXX, XXX−XXX

(100) Feng, Z.; Chen, X.; Wu, X.; Zhang, M. Formation of biological condensates via phase separation: Characteristics, analytical methods, and physiological implications. *J. Biol. Chem.* **2019**, *294* (40), 14823−14835.
(101) Banani, S. F.; Lee, H. O.; Hyman, A. A.; Rosen, M. K. Biomolecular condensates: organizers of cellular biochemistry. *Nat. Rev. Mol. Cell Biol.* **2017**, *18* (5), 285−298.
(102) Dine, E.; Gil, A. A.; Uribe, G.; Brangwynne, C. P.; Toettcher, J. E. Protein Phase Separation Provides Long-Term Memory of Transient Spatial Stimuli. *Cell Syst* **2018**, *6* (6), 655−663.
(103) Zhao, E. M.; Suek, N.; Wilson, M. Z.; Dine, E.; Pannucci, N. L.; Gitai, Z.; Avalos, J. L.; Toettcher, J. E. Light-based control of metabolic flux through assembly of synthetic organelles. *Nat. Chem. Biol.* **2019**, *15* (6), 589−597.
(104) Zhang, H. The glassiness of hardening protein droplets. *Science* **2020**, *370* (6522), 1271−1272.
(105) Thompson, K. E.; Bashor, C. J.; Lim, W. A.; Keating, A. E. SYNZIP protein interaction toolbox: in vitro and in vivo specifications of heterospecific coiled-coil interaction domains. *ACS Synth. Biol.* **2012**, *1* (4), 118−129.
(106) Banaszynski, L. A.; Liu, C. W.; Wandless, T. J. Characterization of the FKBP.rapamycin.FRB ternary complex. *J. Am. Chem. Soc.* **2005**, *127* (13), 4715−4721.
(107) Waris, S.; Wilce, M. C.; Wilce, J. A. RNA recognition and stress granule formation by TIA proteins. *Int. J. Mol. Sci.* **2014**, *15* (12), 23377−23388.
(108) Guntas, G.; Hallett, R. A.; Zimmerman, S. P.; Williams, T.; Yumerefendi, H.; Bear, J. E.; Kuhlman, B. Engineering an improved light-induced dimer (iLID) for controlling the localization and activity of signaling proteins. *Proc. Natl. Acad. Sci. U. S. A.* **2015**, *112* (1), 112−117.
(109) Chowdhury, C.; Sinha, S.; Chun, S.; Yeates, T. O.; Bobik, T. A. Diverse bacterial microcompartment organelles. *Microbiol. Mol. Biol. Rev.* **2014**, *78* (3), 438−68.
(110) Turner, K. B.; Dean, S. N.; Walper, S. A. Bacterial bioreactors: Outer membrane vesicles for enzyme encapsulation. *Methods Enzymol.* **2019**, *617*, 187−216.
(111) De Hoog, H. P.; Arends, I. W.; Rowan, A. E.; Cornelissen, J. J.; Nolte, R. J. A hydrogel-based enzyme-loaded polymersome reactor. *Nanoscale* **2010**, *2* (5), 709−716.
(112) Wong, J. X.; Ogura, K.; Chen, S.; Rehm, B. H. A. Bioengineered Polyhydroxyalkanoates as Immobilized Enzyme Scaffolds for Industrial Applications. *Front. Bioeng. Biotechnol.* **2020**, *8*, 156.
(113) Hooks, D. O.; Venning-Slater, M.; Du, J.; Rehm, B. H. Polyhydroyxalkanoate synthase fusions as a strategy for oriented enzyme immobilisation. *Molecules* **2014**, *19* (6), 8629−8643.
(114) Wilkerson, J. W.; Yang, S. O.; Funk, P. J.; Stanley, S. K.; Bundy, B. C. Nanoreactors: Strategies to encapsulate enzyme biocatalysts in virus-like particles. *New Biotechnol.* **2018**, *44*, 59−63.
(115) Charlton Hume, H. K.; Vidigal, J.; Carrondo, M. J. T.; Middelberg, A. P. J.; Roldao, A.; Lua, L. H. L. Synthetic biology for bioengineering virus-like particle vaccines. *Biotechnol. Bioeng.* **2019**, *116* (4), 919−935.
(116) Ren, H.; Zhu, S.; Zheng, G. Nanoreactor Design Based on Self-Assembling Protein Nanocages. *Int. J. Mol. Sci.* **2019**, *20* (3), 592.
(117) Schlegel, H. G.; Gottschalk, G.; Von Bartha, R. Formation and utilization of poly-beta-hydroxybutyric acid by Knallgas bacteria (Hydrogenomonas). *Nature* **1961**, *191*, 463−465.
(118) Steinbüchel, A.; Valentin, H. E. Diversity of bacterial polyhydroxyalkanoic acids. *FEMS Microbiol. Lett.* **1995**, *128* (3), 219−228.
(119) Park, S. J.; Kim, T. W.; Kim, M. K.; Lee, S. Y.; Lim, S. C. Advanced bacterial polyhydroxyalkanoates: towards a versatile and sustainable platform for unnatural tailor-made polyesters. *Biotechnol. Adv.* **2012**, *30* (6), 1196−1206.
(120) Merrick, J. M.; Doudoroff, M. Enzymatic synthesis of poly-beta-hydroxybutyric acid in bacteria. *Nature* **1961**, *189*, 890−892.
(121) Peoples, O. P.; Sinskey, A. J. Poly-beta-hydroxybutyrate (PHB) biosynthesis in *Alcaligenes eutrophus* H16. Identification and characterization of the PHB polymerase gene (phbC). *J. Biol. Chem.* **1989**, *264* (26), 15298−15303.
(122) Jendrossek, D.; Pfeiffer, D. New insights in the formation of polyhydroxyalkanoate granules (carbonosomes) and novel functions of poly(3-hydroxybutyrate). *Environ. Microbiol.* **2014**, *16* (8), 2357−2373.
(123) Chen, G. Q. A microbial polyhydroxyalkanoates (PHA) based bio- and materials industry. *Chem. Soc. Rev.* **2009**, *38* (8), 2434−2446.
(124) Madison, L. L.; Huisman, G. W. Metabolic engineering of poly(3-hydroxyalkanoates): from DNA to plastic. *Microbiol. Mol. Biol. Rev.* **1999**, *63* (1), 21−53.
(125) Moradali, M. F.; Rehm, B. H. A. Bacterial biopolymers: from pathogenesis to advanced materials. *Nat. Rev. Microbiol.* **2020**, *18* (4), 195−210.
(126) Barnard, G. N.; Sanders, J. K. The poly-beta-hydroxybutyrate granule in vivo. A new insight based on NMR spectroscopy of whole cells. *J. Biol. Chem.* **1989**, *264* (6), 3286−3291.
(127) Gerngross, T. U.; Reilly, P.; Stubbe, J.; Sinskey, A. J.; Peoples, O. P. Immunocytochemical analysis of poly-beta-hydroxybutyrate (PHB) synthase in *Alcaligenes eutrophus* H16: localization of the synthase enzyme at the surface of PHB granules. *J. Bacteriol.* **1993**, *175* (16), 5289−5293.
(128) Prieto, M. A.; Buhler, B.; Jung, K.; Witholt, B.; Kessler, B. PhaF, a polyhydroxyalkanoate-granule-associated protein of *Pseudomonas oleovorans* GPo1 involved in the regulatory expression system for pha genes. *J. Bacteriol.* **1999**, *181* (3), 858−68.
(129) Potter, M.; Steinbuchel, A. Poly(3-hydroxybutyrate) granule-associated proteins: impacts on poly(3-hydroxybutyrate) synthesis and degradation. *Biomacromolecules* **2005**, *6* (2), 552−560.
(130) Peters, V.; Rehm, B. H. In vivo monitoring of PHA granule formation using GFP-labeled PHA synthases. *FEMS Microbiol. Lett.* **2005**, *248* (1), 93−100.
(131) Rasiah, I. A.; Rehm, B. H. One-step production of immobilized alpha-amylase in recombinant *Escherichia coli*. *Appl. Environ. Microbiol.* **2009**, *75* (7), 2012−2006.
(132) Geng, Y.; Wang, S.; Qi, Q. Expression of active recombinant human tissue-type plasminogen activator by using in vivo poly-hydroxybutyrate granule display. *Appl. Environ. Microbiol.* **2010**, *76* (21), 7226−7230.
(133) Hafizi, A.; Malboobi, M. A.; Jalali-Javaran, M.; Maliga, P.; Alizadeh, H. Covalent-display of an active chimeric-recombinant tissue plasminogen activator on polyhydroxybutyrate granules surface. *Biotechnol. Lett.* **2017**, *39* (11), 1683−1688.
(134) Stenger, B.; Gerber, A.; Bernhardt, R.; Hannemann, F. Functionalized poly(3-hydroxybutyric acid) bodies as new in vitro biocatalysts. *Biochim. Biophys. Acta, Proteins Proteomics* **2018**, *1866* (1), 52−59.
(135) Bello-Gil, D.; Roig-Molina, E.; Fonseca, J.; Sarmiento-Ferrandez, M. D.; Ferrandiz, M.; Franco, E.; Mira, E.; Maestro, B.; Sanz, J. M. An enzymatic system for decolorization of wastewater dyes using immobilized CueO laccase-like multicopper oxidase on poly-3-hydroxybutyrate. *Microb. Biotechnol.* **2018**, *11* (5), 881−892.
(136) Du, J.; Rehm, B. H. A. Purification of target proteins from intracellular inclusions mediated by intein cleavable polyhydroxyalkanoate synthase fusions. *Microb. Cell Fact.* **2017**, *16* (1), 184.
(137) Tarazona, N. A.; Machatschek, R.; Schulz, B.; Prieto, M. A.; Lendlein, A. Molecular Insights into the Physical Adsorption of Amphiphilic Protein PhaF onto Copolyester Surfaces. *Biomacromolecules* **2019**, *20* (9), 3242−3252.
(138) Li, R.; Yang, J.; Xiao, Y.; Long, L. In vivo immobilization of an organophosphorus hydrolyzing enzyme on bacterial polyhydroxyalkanoate nano-granules. *Microb. Cell Fact.* **2019**, *18* (1), 166.
(139) Dinjaski, N.; Prieto, M. A. Smart polyhydroxyalkanoate nanobeads by protein based functionalization. *Nanomedicine* **2015**, *11* (4), 885−899.
(140) Gerngross, T. U.; Snell, K. D.; Peoples, O. P.; Sinskey, A. J.; Csuhai, E.; Masamune, S.; Stubbe, J. Overexpression and purification

https://doi.org/10.1021/acssuschemeng.1c02045
ACS Sustainable Chem. Eng. XXXX, XXX, XXX−XXX

of the soluble polyhydroxyalkanoate synthase from *Alcaligenes eutrophus*: evidence for a required posttranslational modification for catalytic activity. *Biochemistry* **1994**, *33* (31), 9311−9320.
(141) Lee, J. H.; Nam, D. H.; Lee, S. H.; Park, J. H.; Park, S. J.; Lee, S. H.; Park, C. B.; Jeong, K. J. New platform for cytochrome p450 reaction combining in situ immobilization on biopolymer. *Bioconjugate Chem.* **2014**, *25* (12), 2101−4.
(142) Yang, T. H.; Kwon, M. A.; Lee, J. Y.; Choi, J. E.; Oh, J. Y.; Song, J. K. In situ immobilized lipase on the surface of intracellular polyhydroxybutyrate granules: preparation, characterization, and its promising use for the synthesis of fatty acid alkyl esters. *Appl. Biochem. Biotechnol.* **2015**, *177* (7), 1553−1564.
(143) Banki, M. R.; Gerngross, T. U.; Wood, D. W. Novel and economical purification of recombinant proteins: intein-mediated protein purification using in vivo polyhydroxybutyrate (PHB) matrix association. *Protein Sci.* **2005**, *14* (6), 1387−1395.
(144) Moldes, C.; Garcia, P.; Garcia, J. L.; Prieto, M. A. In vivo immobilization of fusion proteins on bioplastics by the novel tag BioF. *Appl. Environ. Microbiol.* **2004**, *70* (6), 3205−3212.
(145) Chen, S. Y.; Chien, Y. W.; Chao, Y. P. In vivo immobilization of D-hydantoinase in *Escherichia coli*. *J. Biosci Bioeng* **2014**, *118* (1), 78−81.
(146) Seo, H. M.; Kim, J. H.; Jeon, J. M.; Song, H. S.; Bhatia, S. K.; Sathiyanarayanan, G.; Park, K.; Kim, K. J.; Lee, S. H.; Kim, H. J.; Yang, Y. H. In situ immobilization of lysine decarboxylase on a biopolymer by fusion with phasin: Immobilization of CadA on intracellular PHA. *Process Biochem.* **2016**, *51* (10), 1413.
(147) Jahns, A. C.; Rehm, B. H. Immobilization of active lipase B from *Candida antarctica* on the surface of polyhydroxyalkanoate inclusions. *Biotechnol. Lett.* **2015**, *37* (4), 831−835.
(148) Robins, K. J.; Hooks, D. O.; Rehm, B. H.; Ackerley, D. F. *Escherichia coli* NemA is an efficient chromate reductase that can be biologically immobilized to provide a cell free system for remediation of hexavalent chromium. *PLoS One* **2013**, *8* (3), No. e59200.
(149) Hooks, D. O.; Blatchford, P. A.; Rehm, B. H. Bioengineering of bacterial polymer inclusions catalyzing the synthesis of N-acetylneuraminic acid. *Appl. Environ. Microbiol.* **2013**, *79* (9), 3116−3121.
(150) Hooks, D. O.; Rehm, B. H. Surface display of highly-stable *Desulfovibrio vulgaris* carbonic anhydrase on polyester beads for CO2 capture. *Biotechnol. Lett.* **2015**, *37* (7), 1415−20.
(151) Ran, G.; Tan, D.; Dai, W.; Zhu, X.; Zhao, J.; Ma, Q.; Lu, X. Immobilization of alkaline polygalacturonate lyase from *Bacillus subtilis* on the surface of bacterial polyhydroxyalkanoate nano-granules. *Appl. Microbiol. Biotechnol.* **2017**, *101* (8), 3247−3258.
(152) Tan, D.; Zhao, J. P.; Ran, G. Q.; Zhu, X. L.; Ding, Y.; Lu, X. Y. Highly efficient biocatalytic synthesis of L-DOPA using in situ immobilized Verrucomicrobium spinosum tyrosinase on polyhydroxyalkanoate nano-granules. *Appl. Microbiol. Biotechnol.* **2019**, *103* (14), 5663−5678.
(153) Ran, G.; Tan, D.; Zhao, J.; Fan, F.; Zhang, Q.; Wu, X.; Fan, P.; Fang, X.; Lu, X. Functionalized polyhydroxyalkanoate nano-beads as a stable biocatalyst for cost-effective production of the rare sugar d-allulose. *Bioresour. Technol.* **2019**, *289*, 121673.
(154) Wong, J. X.; Gonzalez-Miro, M.; Sutherland-Smith, A. J.; Rehm, B. H. A. Covalent Functionalization of Bioengineered Polyhydroxyalkanoate Spheres Directed by Specific Protein-Protein Interactions. *Front. Bioeng. Biotechnol.* **2020**, *8*, 44.
(155) Bilal, M.; Iqbal, H. M. N. Naturally-derived biopolymers: Potential platforms for enzyme immobilization. *Int. J. Biol. Macromol.* **2019**, *130*, 462−482.
(156) Ogura, K.; Rehm, B. H. A. Self-Assembly: Alginate Encapsulation of Bioengineered Protein-Coated Polyhydroxybutyrate Particles: A New Platform for Multifunctional Composite Materials. *Adv. Funct. Mater.* **2019**, *29* (37), 1970256.
(157) Roldao, A.; Mellado, M. C.; Castilho, L. R.; Carrondo, M. J.; Alves, P. M. Virus-like particles in vaccine development. *Expert Rev. Vaccines* **2010**, *9* (10), 1149−1176.
(158) Shirbaghaee, Z.; Bolhassani, A. Different applications of virus-like particles in biology and medicine: Vaccination and delivery systems. *Biopolymers* **2016**, *105* (3), 113−132.
(159) Diaz, D.; Care, A.; Sunna, A. Bioengineering Strategies for Protein-Based Nanoparticles. *Genes* **2018**, *9* (7), 370.
(160) Douglas, T.; Young, M. Viruses: making friends with old foes. *Science* **2006**, *312* (5775), 873−875.
(161) Aumiller, W. M.; Uchida, M.; Douglas, T. Protein cage assembly across multiple length scales. *Chem. Soc. Rev.* **2018**, *47* (10), 3433−3469.
(162) Litowski, J. R.; Hodges, R. S. Designing heterodimeric two-stranded alpha-helical coiled-coils. Effects of hydrophobicity and alpha-helical propensity on protein folding, stability, and specificity. *J. Biol. Chem.* **2002**, *277* (40), 37272−37279.
(163) Minten, I. J.; Hendriks, L. J.; Nolte, R. J.; Cornelissen, J. J. Controlled encapsulation of multiple proteins in virus capsids. *J. Am. Chem. Soc.* **2009**, *131* (49), 17771−17773.
(164) Minten, I. J.; Claessen, V. I.; Blank, K.; Rowan, A. E.; Nolte, R. J. M.; Cornelissen, J. J. L. M. Catalytic capsids: the art of confinement. *Chem. Sci.* **2011**, *2*, 358−362.
(165) Rurup, W. F.; Verbij, F.; Koay, M. S.; Blum, C.; Subramaniam, V.; Cornelissen, J. J. Predicting the loading of virus-like particles with fluorescent proteins. *Biomacromolecules* **2014**, *15* (2), 558−563.
(166) Clancy, K. W.; Melvin, J. A.; McCafferty, D. G. Sortase transpeptidases: Insights into mechanism, substrate specificity, and inhibition. *Biopolymers* **2010**, *94* (4), 385−396.
(167) Schoonen, L.; Nolte, R. J.; van Hest, J. C. Highly efficient enzyme encapsulation in a protein nanocage: towards enzyme catalysis in a cellular nanocompartment mimic. *Nanoscale* **2016**, *8* (30), 14467−14472.
(168) Schoonen, L.; Pille, J.; Borrmann, A.; Nolte, R. J.; van Hest, J. C. Sortase A-Mediated N-Terminal Modification of Cowpea Chlorotic Mottle Virus for Highly Efficient Cargo Loading. *Bioconjugate Chem.* **2015**, *26* (12), 2429−2434.
(169) Schoonen, L.; van Hest, J. C. M. Modification of CCMV Nanocages for Enzyme Encapsulation. *Methods Mol. Biol.* **2018**, *1798*, 69−83.
(170) Valimaki, S.; Liu, Q.; Schoonen, L.; Vervoort, D. F. M.; Nonappa Linko, V.; Nolte, R. J. M.; van Hest, J. C. M.; Kostiainen, M. A. Engineered protein cages for selective heparin encapsulation. *J. Mater. Chem. B* **2021**, *9* (5), 1272−1276.
(171) Schoonen, L.; Maassen, S.; Nolte, R. J. M.; van Hest, J. C. M. Stabilization of a Virus-Like Particle and Its Application as a Nanoreactor at Physiological Conditions. *Biomacromolecules* **2017**, *18* (11), 3492−3497.
(172) Schwarz, B.; Uchida, M.; Douglas, T. Biomedical and Catalytic Opportunities of Virus-Like Particles in Nanotechnology. *Adv. Virus Res.* **2017**, *97*, 1−60.
(173) Patterson, D. P. Encapsulation of Active Enzymes within Bacteriophage P22 Virus-Like Particles. *Methods Mol. Biol.* **2018**, *1798*, 11−24.
(174) McCoy, K.; Douglas, T. In Vivo Packaging of Protein Cargo Inside of Virus-Like Particle P22. *Methods Mol. Biol.* **2018**, *1776*, 295−302.
(175) Patterson, D. P.; LaFrance, B.; Douglas, T. Rescuing recombinant proteins by sequestration into the P22 VLP. *Chem. Commun. (Cambridge, U. K.)* **2013**, *49* (88), 10412−4.
(176) Patterson, D. P.; Schwarz, B.; Waters, R. S.; Gedeon, T.; Douglas, T. Encapsulation of an enzyme cascade within the bacteriophage P22 virus-like particle. *ACS Chem. Biol.* **2014**, *9* (2), 359−365.
(177) Jordan, P. C.; Patterson, D. P.; Saboda, K. N.; Edwards, E. J.; Miettinen, H. M.; Basu, G.; Thielges, M. C.; Douglas, T. Self-assembling biomolecular catalysts for hydrogen production. *Nat. Chem.* **2016**, *8* (2), 179−185.
(178) Sanchez-Sanchez, L.; Tapia-Moreno, A.; Juarez-Moreno, K.; Patterson, D. P.; Cadena-Nava, R. D.; Douglas, T.; Vazquez-Duhalt, R. Design of a VLP-nanovehicle for CYP450 enzymatic activity delivery. *J. Nanobiotechnol.* **2015**, *13*, 66.

https://doi.org/10.1021/acssuschemeng.1c02045
ACS Sustainable Chem. Eng. XXXX, XXX, XXX−XXX

(179) Patterson, D.; Edwards, E.; Douglas, T. Hybrid Nanoreactors: Coupling Enzymes and Small-Molecule Catalysts within Virus-Like Particles. *Isr. J. Chem.* **2015**, *55* (1), 96−101.
(180) Patterson, D. P.; Prevelige, P. E.; Douglas, T. Nanoreactors by programmed enzyme encapsulation inside the capsid of the bacteriophage P22. *ACS Nano* **2012**, *6* (6), 5000−5009.
(181) Patterson, D. P.; McCoy, K.; Fijen, C.; Douglas, T. Constructing catalytic antimicrobial nanoparticles by encapsulation of hydrogen peroxide producing enzyme inside the P22 VLP. *J. Mater. Chem. B* **2014**, *2* (36), 5948−5951.
(182) Patterson, D. P.; Schwarz, B.; El-Boubbou, K.; van der Oost, J.; Prevelige, P. E.; Douglas, T. Virus-like particle nanoreactors: programmed encapsulation of the thermostable CelB glycosidase inside the P22 capsid. *Soft Matter* **2012**, *8* (39), 10158−10166.
(183) Waghwani, H. K.; Uchida, M.; Fu, C. Y.; LaFrance, B.; Sharma, J.; McCoy, K.; Douglas, T. Virus-Like Particles (VLPs) as a Platform for Hierarchical Compartmentalization. *Biomacromolecules* **2020**, *21* (6), 2060−2072.
(184) Gonzalez-Davis, O.; Chauhan, K.; Zapian-Merino, S. J.; Vazquez-Duhalt, R. Bi-enzymatic virus-like bionanoreactors for the transformation of endocrine disruptor compounds. *Int. J. Biol. Macromol.* **2020**, *146*, 415−421.
(185) Wang, Y.; Uchida, M.; Waghwani, H. K.; Douglas, T. Synthetic Virus-like Particles for Glutathione Biosynthesis. *ACS Synth. Biol.* **2020**, *9* (12), 3298−3310.
(186) Servid, A.; Jordan, P.; O'Neil, A.; Prevelige, P.; Douglas, T. Location of the bacteriophage P22 coat protein C-terminus provides opportunities for the design of capsid-based materials. *Biomacromolecules* **2013**, *14* (9), 2989−95.
(187) Patterson, D.; Schwarz, B.; Avera, J.; Western, B.; Hicks, M.; Krugler, P.; Terra, M.; Uchida, M.; McCoy, K.; Douglas, T. Sortase-Mediated Ligation as a Modular Approach for the Covalent Attachment of Proteins to the Exterior of the Bacteriophage P22 Virus-like Particle. *Bioconjugate Chem.* **2017**, *28* (8), 2114−2124.
(188) Uchida, M.; McCoy, K.; Fukuto, M.; Yang, L.; Yoshimura, H.; Miettinen, H. M.; LaFrance, B.; Patterson, D. P.; Schwarz, B.; Karty, J. A.; Prevelige, P. E., Jr.; Lee, B.; Douglas, T. Modular Self-Assembly of Protein Cage Lattices for Multistep Catalysis. *ACS Nano* **2018**, *12* (2), 942−953.
(189) Kang, H. J.; Baker, E. N. Intramolecular isopeptide bonds: protein crosslinks built for stress? *Trends Biochem. Sci.* **2011**, *36* (4), 229−237.
(190) Kang, H. J.; Coulibaly, F.; Clow, F.; Proft, T.; Baker, E. N. Stabilizing isopeptide bonds revealed in gram-positive bacterial pilus structure. *Science* **2007**, *318* (5856), 1625−1628.
(191) Terao, Y.; Kawabata, S.; Nakata, M.; Nakagawa, I.; Hamada, S. Molecular characterization of a novel fibronectin-binding protein of *Streptococcus pyogenes* strains isolated from toxic shock-like syndrome patients. *J. Biol. Chem.* **2002**, *277* (49), 47428−35.
(192) Hagan, R. M.; Bjomsson, R.; McMahon, S. A.; Schomburg, B.; Braithwaite, V.; Buhl, M.; Naismith, J. H.; Schwarz-Linek, U. NMR spectroscopic and theoretical analysis of a spontaneously formed Lys-Asp isopeptide bond. *Angew. Chem., Int. Ed.* **2010**, *49* (45), 8421−8425.
(193) Zakeri, B.; Fierer, J. O.; Celik, E.; Chittock, E. C.; Schwarz-Linek, U.; Moy, V. T.; Howarth, M. Peptide tag forming a rapid covalent bond to a protein, through engineering a bacterial adhesin. *Proc. Natl. Acad. Sci. U. S. A.* **2012**, *109* (12), E690−7.
(194) Hatlem, D.; Trunk, T.; Linke, D.; Leo, J. C. Catching a SPY: Using the SpyCatcher-SpyTag and Related Systems for Labeling and Localizing Bacterial Proteins. *Int. J. Mol. Sci.* **2019**, *20* (9), 2129.
(195) Li, L.; Fierer, J. O.; Rapoport, T. A.; Howarth, M. Structural analysis and optimization of the covalent association between SpyCatcher and a peptide Tag. *J. Mol. Biol.* **2014**, *426* (2), 309−317.
(196) Keeble, A. H.; Howarth, M. Insider information on successful covalent protein coupling with help from SpyBank. *Methods Enzymol.* **2019**, *617*, 443−461.
(197) Keeble, A. H.; Banerjee, A.; Ferla, M. P.; Reddington, S. C.; Anuar, I.; Howarth, M. Evolving Accelerated Amidation by SpyTag/SpyCatcher to Analyze Membrane Dynamics. *Angew. Chem., Int. Ed.* **2017**, *56* (52), 16521−16525.
(198) Brune, K. D.; Leneghan, D. B.; Brian, I. J.; Ishizuka, A. S.; Bachmann, M. F.; Draper, S. J.; Biswas, S.; Howarth, M. Plug-and-Display: decoration of Virus-Like Particles via isopeptide bonds for modular immunization. *Sci. Rep.* **2016**, *6*, 19234.
(199) Veggiani, G.; Nakamura, T.; Brenner, M. D.; Gayet, R. V.; Yan, J.; Robinson, C. V.; Howarth, M. Programmable polyproteams built using twin peptide superglues. *Proc. Natl. Acad. Sci. U. S. A.* **2016**, *113* (5), 1202−1207.
(200) Bao, J.; Liu, N.; Zhu, L.; Xu, Q.; Huang, H.; Jiang, L. Programming a Biofilm-Mediated Multienzyme-Assembly-Cascade System for the Biocatalytic Production of Glucosamine from Chitin. *J. Agric. Food Chem.* **2018**, *66* (30), 8061−8068.
(201) Qu, J.; Cao, S.; Wei, Q.; Zhang, H.; Wang, R.; Kang, W.; Ma, T.; Zhang, L.; Liu, T.; Wing-Ngor Au, S.; Sun, F.; Xia, J. Synthetic Multienzyme Complexes, Catalytic Nanomachineries for Cascade Biosynthesis In Vivo. *ACS Nano* **2019**, *13* (9), 9895−9906.
(202) Wei, Q.; He, S.; Qu, J.; Xia, J. Synthetic Multienzyme Complexes Assembled on Virus-like Particles for Cascade Biosynthesis In Cellulo. *Bioconjugate Chem.* **2020**, *31* (10), 2413−2420.
(203) Giessen, T. W.; Silver, P. A. A Catalytic Nanoreactor Based on in Vivo Encapsulation of Multiple Enzymes in an Engineered Protein Nanocompartment. *ChemBioChem* **2016**, *17* (20), 1931−1935.
(204) Klein, W. P.; Thomsen, R. P.; Turner, K. B.; Walper, S. A.; Vranish, J.; Kjems, J.; Ancona, M. G.; Medintz, I. L. Enhanced Catalysis from Multienzyme Cascades Assembled on a DNA Origami Triangle. *ACS Nano* **2019**, *13* (12), 13677−13689.
(205) Liu, J. L.; Zabetakis, D.; Breger, J. C.; Anderson, G. P.; Goldman, E. R. Multi-Enzyme Assembly on T4 Phage Scaffold. *Front. Bioeng. Biotechnol.* **2020**, *8*, 571.
(206) Cayetano-Cruz, M.; Coffeen, C. F.; Valadez-Garcia, J.; Montiel, C.; Bustos-Jaimes, I. Decoration of virus-like particles with an enzymatic activity of biomedical interest. *Virus Res.* **2018**, *255*, 1−9.
(207) Bustos-Jaimes, I.; Soto-Roman, R. A.; Gutierrez-Landa, I. A.; Valadez-Garcia, J.; Segovia-Trinidad, C. L. Construction of protein-functionalized virus-like particles of parvovirus B19. *J. Biotechnol.* **2017**, *263*, 55−63.
(208) Takenoya, M.; Nikolakakis, K.; Sagermann, M. Crystallographic insights into the pore structures and mechanisms of the EutL and EutM shell proteins of the ethanolamine-utilizing microcompartment of *Escherichia coli*. *J. Bacteriol.* **2010**, *192* (22), 6056−63.
(209) Choudhary, S.; Quin, M. B.; Sanders, M. A.; Johnson, E. T.; Schmidt-Dannert, C. Engineered protein nano-compartments for targeted enzyme localization. *PLoS One* **2012**, *7* (3), No. e33342.
(210) Zhang, G.; Quin, M. B.; Schmidt-Dannert, C. Self-Assembling Protein Scaffold System for Easy in Vitro Coimmobilization of Biocatalytic Cascade Enzymes. *ACS Catal.* **2018**, *8* (6), 5611−5620.
(211) Schmidt-Dannert, S.; Zhang, G.; Johnston, T.; Quin, M. B.; Schmidt-Dannert, C. Building a toolbox of protein scaffolds for future immobilization of biocatalysts. *Appl. Microbiol. Biotechnol.* **2018**, *102* (19), 8373−8388.
(212) Zhang, G.; Johnston, T.; Quin, M. B.; Schmidt-Dannert, C. Developing a Protein Scaffolding System for Rapid Enzyme Immobilization and Optimization of Enzyme Functions for Biocatalysis. *ACS Synth. Biol.* **2019**, *8* (8), 1867−1876.
(213) Nguyen, P. Q.; Botyanszki, Z.; Tay, P. K.; Joshi, N. S. Programmable biofilm-based materials from engineered curli nanofibres. *Nat. Commun.* **2014**, *5*, 4945.
(214) Peschke, T.; Bitterwolf, P.; Gallus, S.; Hu, Y.; Oelschlaeger, C.; Willenbacher, N.; Rabe, K. S.; Niemeyer, C. M. Self-Assembling All-Enzyme Hydrogels for Flow Biocatalysis. *Angew. Chem., Int. Ed.* **2018**, *57* (52), 17028−17032.
(215) Yin, L.; Guo, X.; Liu, L.; Zhang, Y.; Feng, Y. Self-Assembled Multimeric-Enzyme Nanoreactor for Robust and Efficient Biocatalysis. *ACS Biomater. Sci. Eng.* **2018**, *4* (6), 2095−2099.
(216) Hammer, J. A.; Ruta, A.; Therien, A. M.; West, J. L. Cell-Compatible, Site-Specific Covalent Modification of Hydrogel

https://doi.org/10.1021/acssuschemeng.1c02045
ACS Sustainable Chem. Eng. XXXX, XXX, XXX−XXX

Scaffolds Enables User-Defined Control over Cell-Material Interactions. *Biomacromolecules* **2019**, *20* (7), 2486−2493.
(217) Bitterwolf, P.; Gallus, S.; Peschke, T.; Mittmann, E.; Oelschlaeger, C.; Willenbacher, N.; Rabe, K. S.; Niemeyer, C. M. Valency engineering of monomeric enzymes for self-assembling biocatalytic hydrogels. *Chem. Sci.* **2019**, *10* (42), 9752−9757.
(218) Mittmann, E.; Gallus, S.; Bitterwolf, P.; Oelschlaeger, C.; Willenbacher, N.; Niemeyer, C. M.; Rabe, K. S. A Phenolic Acid Decarboxylase-Based All-Enzyme Hydrogel for Flow Reactor Technology. *Micromachines (Basel)* **2019**, *10* (12), 795.

https://doi.org/10.1021/acssuschemeng.1c02045
ACS Sustainable Chem. Eng. XXXX, XXX, XXX−XXX

Table S1: Abbreviations used in the manuscript in alphabetical order.

LLPS	Liquid-liquid phase separation
AdhA	alcohol dehydrogenase A
AdhD	monomeric alcohol dehydrogenase
ADS	amorpha-4,11-diene synthase
A-IDPs	Artificial IDRs
AmDH	amine dehydrogenase
AsLOV2	LOV2 domain from *Avena sativa*
AtHNL	Hydroxynitrile lyase from *Arabidopsis thaliana*
BFP	Blue fluorescent protein
BLA	α-amylase
BlpA	lipase from *Bacillus pumilus*
Bt	*Bacillus thuringiensis*
CadA	lysine decarboxylase
CalB	lipase from *Candida antarctica*
CatIBs	Catalytically-active inclusion bodies
CBD	Cellulose binding domain
CCMV	Cowpea Chlorotic Mottle Virus
CelB	homotetrameric b-glucosidase
CFP	Cyan fluorescent protein
CnaB2	fibronectin-binding domain
CP	capsid protein
CPMV	Cowpea mosaic virus
CsgA	curli protein monomer
CueO	bacterial laccase-like multicopper oxidase
Cry1-3	Cry family of proteins *B. thuringiensis*, toxins used as insecticides
Cry-2	Cryptochrome-2 photoreceptor
Cry-2Olig	E490G variant of Cry-2, showing enhanced clustering
CYPBM3	*B. megaterium* P450 monooxygenase
DAP	1,3-diaminopropane
Dat	L-2,4-diaminobutyrate:α-ketoglutarate 4-aminotransferase
Ddc	L-2,4-diaminobutyrate decarboxylase
DDX4/3	ATP-dependent RNA helicase, Deadbox Helicase 4 or 3
D-HDT	D-hydantoinase
DLZM4	Dieselzyme 4
DTW	D-tagatose-3-epimerase
E coil	Artificial, negatively charged, α-helical coil
EcHyd-1	heterodimeric [NiFe]-hydrogenase 1
eGFP	Enhanced green fluorescent protein
EutM	ethanolamine utilization bacterial microcompartment protein
eYFP	Enhanced yellow fluorescent protein
FAME	Fatty acid methyl ester
FbaB	fibronectin-binding adhesin
FKBP	FK506 binding protein
FRB	Rapamycin binding protein
FUS	fused in sarcoma protein

FUS_N	N-terminal intrinsically disordered region of FUS
G6PDH	Glucose-6-phosphate dehydrogenase
GalA	α-galactosidase
GALK	galactosidase
GFP	Green fluorescent protein
GLUK	glucokinase
GOase	Galactose oxidase
GshF	homodimeric, bifunctional glutathione full synthase
HEK cells	Human embryonic kidney cells
HNRNPA1	Heterogeneous nuclear ribonucleoprotein A1
$HNRNPA1_C$	C-terminal intrinsically disordered region of HNRNPA1
Hoc	outer capsid protein
HRV 3C	3C protease derived from human Rhinovirus type 14
HXK2	Hexokinase 2
IBs	Inclusion bodies
Idi	isopentenyl diphosphate isomerase
IDPs	Intrinsically disordered proteins
IDRs	Intrinsically disordered regions
Ima1p	α-glucosidase
iPOLYMER	Intracellular Production Of Ligand-Yielded Multivalent Enhancers
iPOLYMER-Li	Intracellular Production of Light-Yielded Multivalent Enhancers
IspA	farnesyl pyrophosphate (FPP) synthase
K coil	Artificial, positively charged, lysine-rich coil
KivD	ketoisovalerate decarboxylase
LacZ	β-galactosidase
LbADH	Alcohol dehydrogenase from *Lactobacillus brevis*
LOV	Light, oxygen, voltage domain
LZ	Leucine zipper
MaSp1-I16	Major ampullate spidroin 1 protein from *Nephila claviceps*
MBP	Maltose binding protein
MenD	2-succinyl-5-enol-pyruvyl-6-hydroxy-3-cyclohexene-1-carboxylate synthase
MS2	bacteriophage
MtSEO-F-4	*Medicago truncatula* sieve element occlusion by forisome
NADPH	Nicotinamide adenine dinucleotide phosphate
NemA	hexavalent chromium reductase
nephrin-NCK-N-WASP	Signalling complex of the actin-regulatory pathway, which forms clusters due to LLPS
NOX	homodimeric FAD-binding NADH oxidase
OpdA	organophosphohydrolase
optoDDX4	Optgenetic construct containing the N-terminal intrinsically disordered region of DDX4
optoFUS	Optgenetic construct containing the N-terminal intrinsically disordered region of FUS
optoHNRNPA1	Optgenetic construct containing the C-terminal intrinsically disordered region of RNA binding protein HNRNPA1
P22	bacteriophage

P450-BM3	monooxygenase
PAMAM	positively charged polyamidoamine
PfBAL	Benzaldehyde lyase from *Pseudomonas fluorescens*
PHA	polyhydroxyalkanoate
PhaA	β-ketothiolase
PhaB	acetoacetyl-CoA reductase
PhaC	Polyhydroxybutyrate synthase
PhaC	PHA synthase
PhaP/PhaF	phasin (PHA-associated protein)
PhaZ	PHA depolymerase
PHB	Polyhydroxybutyrate
PixE/PixD	Photoreceptor system of the sensors of blue-light using flavin adenine dinucleotide (BLUF) family
PixELL	Pix Evaporates from Liquid-like droplets in Light
PLP	Pyridoxal 5′-phosphate
PML	Lipase from *Proteus mirabilis*
PML^{VG}	Double mutant of *Proteus mirabilis* lipase
PMO	monooxygenase
POI	Protein of interest
PpBFD	Benzoylformate decarboxylase from *Pseudomonas putida*
PRM	Proline-rich-motif
Qb	bacteriophage
RADH	Alcohol dehydrogenase from *Ralstonia sp.*
REPS	RGG-based, enzyme-triggered, phase-separating systems
RFP	Red fluorescent protein
RGG	intrinsically disordered protein domain, containing closely spaced Arg-Gly-Gly repeats, from the N-terminus of LAF1 RNA helicase from *C. elegans*
SEO-F1-4	Sieve element occlusion by forisome
sfGFP	Superfolder green fluorescent protein
SH3	SRC homology 3
Sir1975	N-acetylglucosamine 2-epimerase
SP	scaffolding protein
Spy	
SrtA	sortase
SZ1-2	SYNZIP coiled-coil 1-2
$TDP43_C$	C-terminal intrinsically disordered region of the TAR DNA-binding protein 43
TFP	teal fluorescent marker protein
TIA-1	RNA binding protein that promotes the assembly of stress granules
TnaA	PLP-dependent tryptophanase
UCST	Upper critical solution temperature
VLP	virus-like particle
YFP	Yellow fluorescent protein
αp	Alpha peptide

II.3.2 PHB-based protein immobilization in *R. capsulatus*

PUBLICATION VII

Functionalization of polyhydroxybutyrate granules in the phototrophic bacterium *Rhodobacter capsulatus* SB1003

Oliver Klaus[1], Vera Svensson[1], Karl-Erich Jaeger[1,2], Thomas Drepper[1#]

[1]Institute of Molecular Enzyme Technology, Heinrich Heine University Düsseldorf, Forschungszentrum Jülich, 52425 Jülich, Germany
[2]Institute of Bio- and Geosciences IBG-1: Biotechnology, Forschungszentrum Jülich GmbH, 52425 Jülich, Germany

[#] Corresponding author

Status: in preparation

Target Journal: *Protein Expression and Purification*

Own contribution:
Designing and performing experiments, plasmid construction, analyzing data, visualization, writing the manuscript

Functionalization of polyhydroxybutyrate granules in the phototrophic bacterium *Rhodobacter capsulatus* SB1003

Oliver Klaus[1], Vera Svensson[1], Karl-Erich Jaeger[1,2], Thomas Drepper[1]

[1]Institute of Molecular Enzyme Technology, Heinrich Heine University Düsseldorf, Forschungszentrum Jülich, Jülich, Germany

[2]Institute of Bio- and Geosciences (IBG-1: Biotechnology), Forschungszentrum Jülich GmbH, Jülich, Germany

Corresponding author: Dr. Thomas Drepper (t.drepper@fz-juelich.de)

Abstract

The *in vivo* immobilization of enzymes on the granule surface of the biopolymer polyhydroxybutyrate (PHB) represents a promising opportunity to enhance their stability and (re)usability in biotechnological and biomedical processes. However, some enzymes with specific catalytic properties may be sensitive to oxygen or require rare metallocofactors. Therefore, there is a great interest in establishing alternative bacterial hosts that are able to functionally express such proteins and to produce PHB. In this study, we aimed to implement the purple non-sulfur phototroph *Rhodobacter capsulatus* SB1003 as a new platform organism for *in vivo* coupling of target proteins to a biopolymeric surface. This facultative anaerobic organism has already been used for the sustainable production of complex membrane proteins and although intrinsic PHB biosynthesis has been well characterized, studies to functionalize the bioplastic granules are still missing. Here, as a proof-of-concept, we demonstrate the applicability of the PHB synthase PhaC as an anchor protein for the immobilization of the yellow-fluorescent protein eYFP. In addition, the *Rhodobacter* genes required for PHB biosynthesis were transferred to the non-native PHB producer *Escherichia coli* to evaluate the intrinsic enzymes without host regulatory mechanisms. Thus, *R. capsulatus* was successfully developed as an alternative host for the *in vivo* immobilization of proteins, laying the foundation for the stabilization and simple purification of difficult-to-produce enzymes for biotechnological application in future studies.

Keywords: polyhydroxybutyrate, *Rhodobacter capsulatus,* photosynthetic bacteria, protein immobilization,

Introduction

Polyhydroxybutyrate (PHB) granules are biocompatible, naturally occurring polyesters used by many bacteria as energy and carbon storage compounds [1]. In PHB biosynthesis, a β-ketothiolase (PhaA) condenses two acetyl-CoA molecules to acetoacetyl-CoA, which is reduced to D-3-hydroxybutyryl-CoA *via* an acetoacetyl-CoA reductase (PhaB) and finally polymerized by a PHB synthase (PhaC) [2–4]. This hydrophobic core is surrounded by a protein layer containing PHB synthases, PHB depolymerases, and phasins [5–7]. The PHB synthase PhaC as well as some of the phasins have already been established in engineered PHB production hosts such as *Escherichia coli* as anchor proteins for the *in vivo* immobilization of various recombinant target proteins. The display of target proteins to the surface of PHB granules were shown to enhance their stability [8] or facilitate their purification by simple PHB isolation *via* centrifugation and subsequent elution by intein- or protease-mediated cleavage [9–12]. In addition, protein-decorated bioplastic inclusions represent a promising functionalized matrix for biomedical and biotechnological applications such as immunization [13,14] or biocatalytic synthesis in flow-chemical approaches [15].

In contrast to recombinant PHB production hosts, the purple non-sulfur bacterium *Rhodobacter capsulatus* SB1003 was shown to efficiently produce PHB under nutrient-limiting conditions [16] and consequently genome sequence analysis offers genes that are homolog to the above mentioned *pha* genes, namely *phaC*, *phaB* and four copies of *phaA* [17]. PHB biosynthesis in *Rhodobacter* species has been extensively studied and could be improved by metabolic engineering [18–20]. Furthermore, *R. capsulatus* versatile metabolism allows this organism to grow either under chemotrophic conditions in the dark or phototrophically in the absence of oxygen by performing anoxygenic photosynthesis. Moreover, *R. capsulatus* is a promising alternative production host for various biotechnological relevant products including difficult-to-produce proteins [21] and secondary metabolites [22,23]. In the presented study, we therefore asked if the specific properties of *R. capsulatus* such as intrinsically high protein and PHB synthesis can be combined to develop new immobilization-based applications.

Thus, in the present study, we analyzed the suitability of the PHB synthase PhaC as a potential anchor protein for the *in vivo* immobilization of the fluorescence reporter eYFP in *R. capsulatus*. Moreover, we investigated the influence of different carbon sources as well as phototrophic growth on production of eYFP decorated PHB inclusions. To our knowledge, this is the first example of a PHB-based approach for *in vivo* protein immobilization in a purple non-sulfur phototrophic bacterium. In addition, we

transferred the *phaABC* genes from *R. capsulatus* to *E. coli* to evaluate the enzymes in the context of an environment where no host regulatory mechanisms are present.

Materials and methods

Bacterial strains and cultivation conditions

Escherichia coli strains DH5α [24] and S17-1 [25] were used for plasmid construction and conjugational transfer [26] into *Rhodobacter capsulatus*. *E. coli* cells were cultivated in LB medium (Luria/Miller, Carl Roth: 10 g/L tryptone, 5 g/L yeast extract, 10 g/L sodium chloride) or on LB agar plates containing 1.5% agar (*w/v*, Bacto agar, Difco) overnight at 37 °C. *E. coli* strain Tuner (DE3) (Novagen) was used for PHB biosynthesis and recombinant protein production. For cultivation, LB medium was supplemented with 1% (*w/v*) glucose and cells were incubated at 130 rpm and 37 °C. After an optical density OD_{580nm} of 0.5 was reached the cells were induced with 100 µL isopropyl β-D-thiogalactopyranoside (IPTG) and cultivated for further 48 h at 130 rpm and 30 °C.

R. capsulatus strain SB1003 [27] was cultivated phototrophically on PY (peptone-yeast) agar plates (10 g/L Bacto peptone, 0.5 g/L Bacto yeast extract, and 20 g/L Select Agar) or in liquid RCV minimal medium (0.1% $(NH_4)_2SO_4$, 4 g/L malate, 1 mL/L 20% $MgSO_4$ (*w/v*), 1 mL/L 7.5% $CaCl_2$ (*w/v*), 2 mL/L 1% EDTA (*w/v*), 2.4 mL 0.5% $FeSO_4$ (*w/v*) supplemented with 2 mL/L 37% HCl, 1 mL/L 0.1% thiamine (*w/v*), 1 mL/L trace element solution [0.4 g/L $MnSO_4$(x1 H_2O), 0.7 g/L H_3BO_3, 0.01 g/L $Cu(NO_3)_2$(x3 H_2O), 0.06 g/L $ZnSO_4$(x7 H_2O), 0.02 g/L $NaMoO_4$(x2 H_2O)]; pH 6.8) at 30 °C under anaerobic phototrophic conditions (bulb light, 2500 lx). Hungate glass tubes sealed with a septum and a screw cap were used to ensure airtight cultivation. For PHB production, RCV medium without malate was supplemented with 0.1% $NaHCO_3$ (*w/v*) and 50 mM acetone or 0.1% caproate (*w/v*) as alternative carbon sources, respectively [16]. Phototrophic cultivation of *R. capsulatus* on solid agar plates were performed in airtight containers with gas packs to deplete atmospheric oxygen (Microbiology Anaerocult A system, Merck KgaA, Darmstadt, Germany).

Construction of expression vectors

All oligonucleotide primers, plasmids and strains used in this study are listed in Supplementary Tables S1 & S2. The relevant genes for experiments deploying *R. capsulatus* as PHB production host were cloned into the expression vector pRhokHi-2 [21] carrying the constitutive P_{aphII} promoter. The *eyfp* gene with a DNA sequence encoding for a thrombin recognition site at the 3`-end was amplified *via* PCR

using vector pRhotHi-2-FluBO [28] as template, introducing *Nde*I and *Bam*HI sites with the respective primers 1 and 2. The *phaC* (RCAP_rcc00746) gene fragment was amplified *via* PCR from genomic DNA (*R. capsulatus* SB1003), introducing *BamH*I and *Hind*III sites at the respective 5'- and 3' ends using the primers 3 and 4. The *eyfp-phaC* fragment was inserted into pRhokHi-2 using the *Nde*I and *Hind*III sites to generate the expression vector pRhokHi-2-eyfp-phaC. For experiments performed in *E. coli*, respective genes were cloned into the expression vector pET28a(+) (Novagen) carrying the IPTG inducible P_{T7} promoter. The *eyfp-phaC* fragment was inserted using the expression vector pRhokHi-2-eyfp-phaC as template as well as the respective *Nde*I and *Hind*III sites. The *phaB1* gene (RCAP_rcc03179) was amplified *via* PCR using genomic DNA (*R. capsulatus* SB1003) as a template introducing *Not*I and *Xho*I sites at the respective 5'- and 3' ends with the primers 5 and 6. The *phaA3* gene (RCAP_rcc00518) was amplified *via* PCR using genomic DNA (*R. capsulatus* SB1003) as template introducing *BamH*I and *Not*I sites with the primers 7 and 8. The created fragments were digested using the respective restriction enzymes and ligated with a corresponding pET28a(+) backbone to construct vector pET28a-eyfp-phaCA3B.

The relevant gene sequences were verified by sequencing performed by LGC Genomics GmbH (Berlin, Germany).

PHB staining using Nile red

Nile red is a phenoxazine dye whose fluorescence spectrum changes after interaction with hydrophobic components such as lipids or biopolymers [29,30], thus enabling an indirect fluorescence-based measurement of PHB accumulation. *R. capsulatus* cultures were incubated in RCV medium under anaerobic phototrophic conditions for five days. For Nile red-based detection of PHB, cells corresponding to an OD_{660nm} of 1.0 were harvested by centrifugation (3 min, 11 000 *g*), the supernatant was discarded, and the intracellular PHB in the pellet fraction was stained for 30 min with 1 mL Nile red solution (0.5 µg/mL in 1xPBS buffer). After centrifugation (3 min, 11 000 *g*), the supernatant was discarded, and the pellet was resuspended in 1xPBS buffer. For fluorescence measurement, the samples were 1:10 diluted in a 96-well microtiter plate (Greiner Bio-One GmbH, Frickenhausen, Germany) using 1xPBS buffer and analyzed regarding their respective Nile red fluorescence (λ_{ex} = 543 nm, λ_{em} = 598 nm) [31] using a microplate reader (Infinite® M1000 Pro, Tecan Group LTD-Maennedorf, Switzerland).

Measurement of eYFP fluorescence

To detect whether expressed eYFP had attached to PHB granules or was soluble, spectroscopic studies were performed. Here, the eYFP fluorescence (λ_{ex} = 488 nm, λ_{em} = 527 nm) was measured either after cultivation with 1:10 diluted cultures (using 1xPBS buffer) or in supernatant and PHB fractions after isolation in a 96-well microtiter plate (Greiner Bio-One GmbH, Frickenhausen, Germany) using a microplate reader (Infinite® M1000 Pro, Tecan Group LTD, Maennedorf, Switzerland). Due to the anaerobic cultivation, the corresponding *R. capsulatus* samples were shaken for two hours (30 °C, 300 rpm) before fluorescent measurement to ensure subsequent maturation of the eYFP chromophore [32].

PHB isolation by ultracentrifugation

After 120 h of phototrophic cultivation, *R. capsulatus* cells corresponding to OD_{660nm}= 50 were harvested by centrifugation (10 min, 4000 *g*, 4 °C), the supernatant was discarded, and pellets were stored at -20 °C until use. The resuspended cells were passed through a French press cell disrupter (French Press Cell Disrupter, Thermo Fisher Scientific, Waltham, Massachusetts, United States) and the PHB containing fraction was separated from the crude cell fraction by ultracentrifugation (2 h, 23 400 rpm (rotor: Typ 32Ti), 4 °C, Optima XPN-80 Ultracentrifuge, Beckmann Coulter, Brea, California, United States) with a glycerol density gradient as described previously [33]. However, deviating glycerol concentrations of 20%, 40% and 90% were used to separate the PHB-containing cell fraction from cell debris and soluble proteins. The final documentation was performed under blue light illumination (λ_{max} = 470 nm, FastGene Blue/Green LED Transilluminator XL, Nippon Genetics Europe GmbH, Düren, Germany), where the fluorescent reporter protein exhibits a bright yellow-green fluorescence.

PHB isolation and elution of the target protein via protease cleavage

The subsequent PHB isolation was performed as previously described [11]. *R. capsulatus* cells corresponding to OD_{660nm}= 10 were resuspended in 1 mL TBE buffer (20 mM Tris, 500 mM NaCl, 1 mM EDTA, pH 8.6) and disrupted using a laboratory mill (10 min, precooled racks, frequency 30/s, MM 400 laboratory mill, Retsch, Haan, Germany) in combination with 0.3 mm glass beads. After glass beads removal, the suspension was centrifuged (30 min, 6000 *g*, 4 °C) and the supernatant was discarded. After two further centrifugation steps (20 min, 8000 *g*, 4 °C) with 0.5x TBE buffer and 1x TBE buffer, the samples were washed three times (4 min, 8000 *g*, 4 °C) with urea buffer (100 mM Tris, 5 mM

EDTA, 1 M urea, 2% v/v Triton X-100, pH 8.6) to remove any remaining impurities and one time with 1x PBS. To separate the eYFP protein from the PhaC-PHB slurry *via* the inserted thrombin recognition site, a protease cleavage was performed overnight at 22 °C (5 µL 10x thrombin cleavage buffer (200 mM Tris-HCl, pH 8.4, 1.5 M NaCl, 25 mM $CaCl_2$), 25 µL PHB slurry, 20 µL dH_2O, 1 Unit bovine α-thrombin native protein, Thermo Fisher Scientific, Waltham, Massachusetts, United States). Samples of the soluble protein, PHB and elution fractions were taken and analyzed for their eYFP fluorescence during the whole isolation process.

Results and Discussion

Decoration of PHB granules in R. capsulatus SB1003 using eYFP as proof of concept

The formation of PHB granules in native bacterial hosts is often triggered by a change in the nitrogen and carbon ratio caused by the usage of different carbon sources in the cultivation medium [34]. In a previous study, it could already be demonstrated that malate, acetone, and caproate have direct effects on PHB quantity and granule size composition in *R. capsulatus* under photoheterotrophic conditions [16]. Therefore, we used these carbon sources to evaluate the Nile red-based *in vivo* detection of PHB production in *R. capsulatus*. Moreover, we tested the applicability of PhaC as an anchor protein to direct eYFP to the PHB granule surface. To establish a PHB-based immobilization approach in *R. capsulatus* and evaluate the influence of medium composition on protein levels, we first constructed the expression plasmid pRhokHi-2-eyfp-phaC (Table S2, Supp. Inf.) containing the constitutive P_{aphII} promoter and a genetic fusion consisting of the *eyfp* reporter gene with a DNA sequence encoding for a thrombin recognition site at the 3`-end, and the gene for PhaC (PHB synthase). In addition, we used the plasmid pRhokHi-2_eyfp to express eYFP without the putative PHB anchor protein as respective control. The expression vectors were transferred to *R. capsulatus* SB1003 and expression cultures were incubated under phototrophic conditions using either malate, acetone or caproate as sole carbon sources. After cultivation, the Nile red fluorescence as an indirect indication for PHB accumulation as well as eYFP fluorescence were quantified (Figure 1).

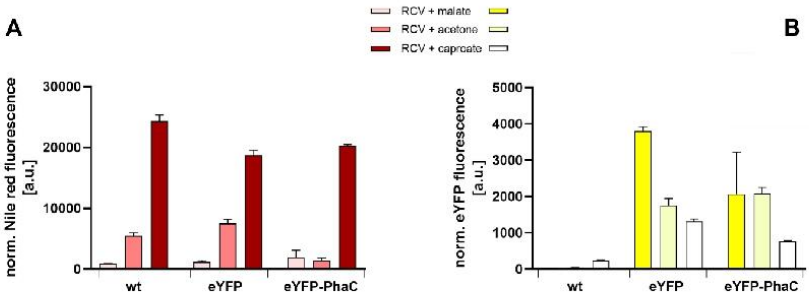

Figure 1. Influence of different carbon sources on PHB formation and eYFP production in photoheterotrophically grown *R. capsulatus* cells. The *R. capsulatus* strain SB1003 carrying either pRhokHi-2_eyfp or pRhokHi-2_eyfp-phaC was cultivated for five days photoheterotrophically in RCV minimal medium supplemented with malate, acetone or caproate, respectively. (**A**) Biomass-normalized Nile red *in vivo* fluorescence (λ_{ex} = 543 nm, λ_{em} = 598 nm). (**B**) Biomass-normalized eYFP *in vivo* fluorescence (λ_{ex} = 488 nm, λ_{em} = 527 nm). *R. capsulatus* SB1003 wildtype cells were used as negative control (wt). Values are means of individual biological triplicates. Error bars indicate the respective standard deviations.

As expected, the comparison of the Nile red fluorescence levels in the corresponding samples confirmed the effect of the used carbon sources on PHB formation in *R. capsulatus* [16]. In the case of malate, only low signals could be detected, indicating a minor among of formed PHB. These fluorescence levels were slightly enhanced when acetone was present and significantly increased using caproate as the carbon source. Not only the same trends regarding the preferred carbon source for PHB formation but also only minor impacts of the additional expression of free or fused eYFP were observed. Contrary to the PHB accumulation, the highest eYFP fluorescence signal was determined for cultures incubated with malate as carbon source, and lowest with caproate. Besides that, the fluorescence intensity of free eYFP resulted in higher intensity than that of the eYFP-PhaC fusion especially when malate was supplemented, so that the protein fusion appears to have a negative effect on eYFP activity.

We successfully demonstrated that heterologous production of the target protein eYFP can be conducted in *R. capsulatus* under PHB forming conditions and that the generation of fusion proteins of YFP with the putative PHB-anchor protein PhaC did not lead to substantial loss of protein functions. Only the addition of caproate as sole carbon source resulted in a strong PHB signal (especially in the *R. capsulatus* strain expressing the eYFP-PhaC fusion protein) that is accompanied by a sufficiently high eYFP fluorescence signal. Therefore caproate was used in the following experiment to evaluate, if PhaC can be used in *R. capsulatus* as anchor protein for the immobilization of eYFP. Therefore, in a next step, *R. capsulatus* cells expressing eYFP or eYFP-PhaC fusion proteins were cultivated

phototrophically in RCV medium containing caproate. Cells were subsequently disrupted, and cell extracts were applied to a glycerol density gradient to separate the PHB-containing cell fraction from cell debris and soluble proteins during ultracentrifugation (Figure 2).

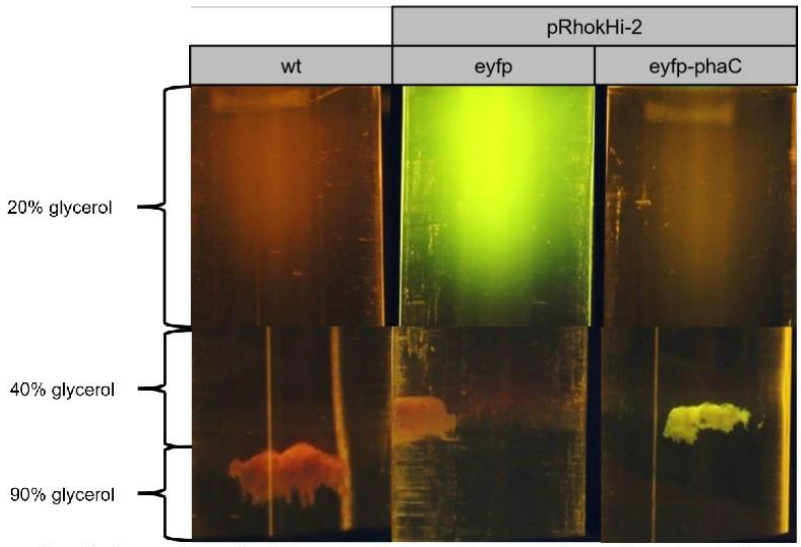

Figure 2: Photographs of different *R. capsulatus* crude cell extract fractions after ultracentrifugation. Cells cultured photoheterotrophically for five days in RCV medium containing caproate were disrupted using a French press cell disrupter. Subsequently, PHB-containing cell fractions were separated from cell debris and soluble proteins by glycerol density ultracentrifugation using a step gradient (three layers with 20%, 40% and 90% of glycerol). To detect eYFP-containing cell fractions, the complete centrifugation tube was illuminated with blue light (λ_{max} = 470 nm). PHB granules are typically enriched in the area of 40% to 90% glycerol, while soluble proteins are retained in the 20% glycerol layer [33].

As revealed by the glycerol density gradient centrifugation, the eYFP fluorescence signal could only be detected in the PHB fraction (40-90% glycerol) of *R. capsulatus* cells expressing the eYFP-PhaC fusion protein. In contrast, unfused eYFP was retained around lower glycerol concentration (20%) containing soluble cell proteins. This observation demonstrates that the eYFP-PhaC fusion proteins could predominantly located in at glycerol concentrations that are characteristic of PHB granules [33], revealing that eYFP was immobilized by PhaC to the PHBs. This was the first time that functionalization of PHB granules was successfully demonstrated in a *Rhodobacter* species.

Next, we analyzed, if eYFP which has been PHB-immobilized *via* the anchor protein PhaC, can be easily isolated from cell extracts after heterologous expression. To this end, a protocol established by Du and Rehm for the PHB isolation from *E. coli* cell extracts was accordingly applied, which is mainly based on different washing steps using a conventional centrifuge [11]. To eluate eYFP from the PHB inclusions,

a thrombin protease was used for the specific cleavage of the eYFP-PhaC fusion protein in the linker region.

To this end, the *R. capsulatus* expression cultures harboring either plasmid pRhokHi-2_eyfp or pRhokHi-2_eyfp-phaC were cultivated as described above. After cultivation, cells were disrupted, and PHB-immobilized eYFP was isolated from cell extract by repeated centrifugation and washing steps. Here, samples were taken from the soluble protein, PHB, and elution fraction, to monitor the eYFP isolation process by fluorescence measurements (Figure 3).

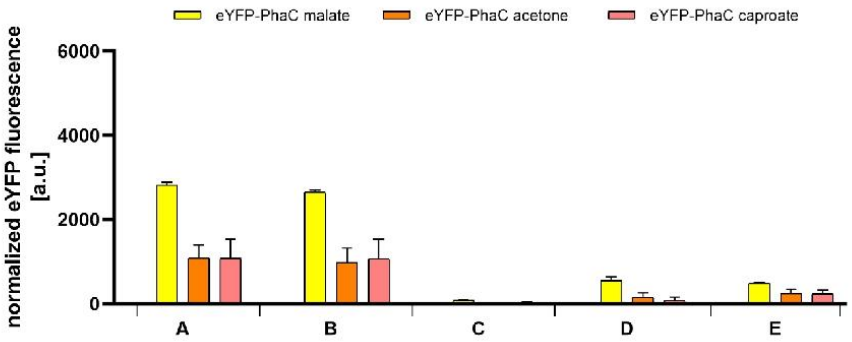

Figure 3: Isolation of PHB-immobilized eYFP from *R. capsulatus* crude cell extracts and subsequent elution. *R. capsulatus* strain SB1003 carrying pRhokHi-2_eyfp-phaC (eYFP-PhaC) was cultivated photoheterotrophically for five days in RCV minimal medium supplemented with malate, acetone or caproate, respectively. After cultivation, the *R. capsulatus* cells were harvested and disrupted using a laboratory mill. Following a PHB isolation protocol established for *E. coli* [11], biomass-normalized eYFP *in vivo* fluorescence (λ_{ex} = 488 nm, λ_{em} = 527 nm) was measured in the soluble protein, PHB, and elution fraction, respectively. To release the eYFP from PHB granules, a thrombin protease was used. Values are means of individual biological triplicates. Error bars indicate the respective standard deviations. (**A**) crude cell extract; (**B**) PHB fraction (pellet fraction after first centrifugation step); (**C**) elution fraction before addition of thrombin protease (control); (**D**) elution fraction after addition of thrombin protease; (**E**) PHB fraction after adding thrombin protease.

Similar to the previous experiment (Figure 1), the highest eYFP signal was determined for samples resulting from cultures with malate. The marginal difference between fluorescence intensity in crude cell extracts (**A**) and PHB fraction (**B**) shows, that most of the eYFP is located in the PHB fraction. To distinguish between immobilized and freely soluble eYFP in non-disrupted cells, it is necessary to analyze the supernatants before and after protease treatment (**C** & **D**). Here, the addition of thrombin protease caused higher fluorescence signals (**D**) compared to the control before enzyme addition (**C**). This suggests that the functionalized PHB granules were accessible outside of the cells and represent a feasible way to isolate target proteins using the chosen method. Nevertheless, a significant eYFP

signal is still detectable in the pellet fraction (**E**), suggesting that not the entire amount of target protein could be separated.

****

****

Transfer of the R. capsulatus phaABC genes to E. coli

After successful demonstration of PHB granule functionalization in the native host *R. capsulatus* SB1003, the next step was to establish PHB biosynthesis in the non-native PHB producer *E. coli*. In the past, genes from the PHB model organism *Cupriavidus necator* were preferentially used for recombinant PHB production [35–37], but here, the aim was to evaluate the *R. capsulatus* intrinsic PHB enzymes in the context of an environment without host regulatory mechanisms. Therefore, we constructed the expression plasmid pET28a_eyfp-phaCA3B (Table S1 & S2, Supp. Inf.) containing the IPTG-inducible P_{T7} promoter, the *eyfp* reporter gene with a DNA sequence for a thrombin recognition site directly fused to the 5`-end of the gene for PhaC and the unfused genes for PhaA3 and PhaB [17,20]. We further used the plasmid pRhokHi-2_eyfp with an unfused eYFP protein as a control. All *E. coli* expression cultures were incubated for 2 days at 30 °C in LB medium supplemented with 1% (*w/v*) glucose and induced with 100 µL IPTG as soon as an OD_{580nm} of 0.5 was reached. Consistent with the methodology used in the *R. capsulatus* experiments, samples were subjected to a PHB isolation protocol after cell disruption. After various centrifugation steps, the eYFP fluorescence of the supernatants was determined spectroscopically and the localization of the fluorescent fraction was visualized by irradiation with blue light (Figure 4).

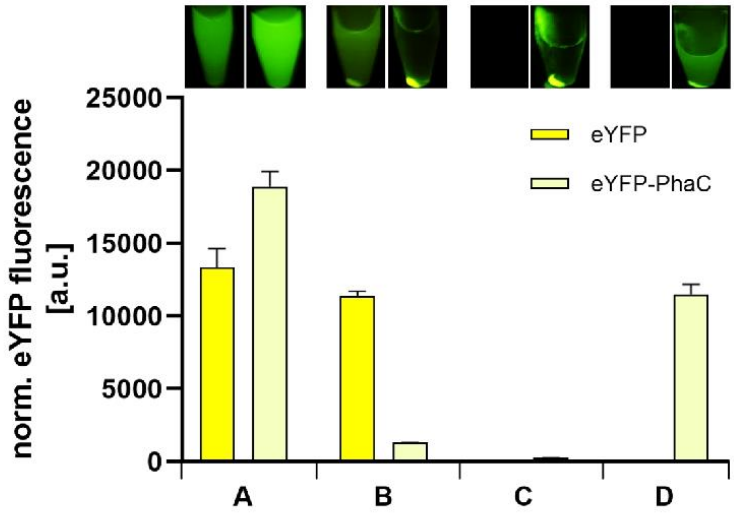

Figure 4: Isolation of eYFP from *E. coli* crude cell extract using laboratory bench centrifugation. The *E. coli* strain Tuner(DE3) carrying either pRhokHi-2_eyfp or pET28a_eyfp-phaCA3B1 was cultivated in LB medium supplemented with 1% (w/v) glucose. After cultivation, the cells were harvested and disrupted using a French Press cell disrupter. Following a PHB isolation protocol [11], biomass-normalized eYFP *in vivo* fluorescence (λ_{ex} = 488 nm, λ_{em} = 527 nm) was measured in the crude cell extract and in various supernatant fractions after centrifugation steps. (**A**) crude cell extract; (**B**) supernatant fraction after first centrifugation; (**C**) supernatant fraction after completion of all washing steps; (**D**) supernatant fraction after protease cleavage. Values are means of methodical triplicates. Error bars indicate the respective standard deviations. To detect eYFP-containing fractions, the complete centrifugation tubes were illuminated with blue light (λ_{max} = 470 nm).

As expected, the cell lysates showed significant eYFP fluorescence signals. The variation in signal intensity can be attributed to the different promoters used (constitutive P_{aphII} and inducible P_{T7}) and can be neglected. After the first centrifugation, only a low signal is detectable in the supernatant with the immobilized eYFP, while the unfused variant is still detectable (**B**). After completion of the washing protocol, no fluorescence is measurable in both samples, suggesting that all unbound protein has been removed. Upon addition of the protease, increased eYFP fluorescence was again detected in the sample with the eYFP-PhaC fusion protein, corresponding in intensity to more than 50% of the value measured in the cell lysate, indicating that protease addition could release eYFP from PHB pellets. These results show that the target protein can be clearly separated using a laboratory bench centrifugation protocol in combination with protease cleavage. Hence, it could be successfully demonstrated that the chosen *R. capsulatus pha* genes *phaA3, phaB* and *phaC* can be transferred to an alternative host to enable heterologous PHB production and furthermore a simple approach for protein isolation.

As a result, the functionalization of PHB granules using *Rhodobacter*-associated genes has now been established in both *E. coli* and *R. capsulatus*. This allows taking advantage of the different host intrinsic properties to perform a variety of applications. Especially the anaerobic growth and high supply of (metalo-) co-factors turn *Rhodobacter* into a promising alternative in the synthesis of difficult-to-express proteins, such as membrane proteins or those with a high oxygen sensitivity [21,38]. In contrast, *E. coli* offers the possibility to rapidly and simply produce PHB granules without attention to host-specific regulatory mechanisms. Therefore, this host could be suitable, for example, for the initial evaluation of new linker systems for improved binding of the target proteins [39,40].

Acknowledgements

This work was supported by grants of the European Regional Development Fund (ERDF: 34.EFRE-0300096 and 34.EFRE-0300097) within the project CLIB-Kompetenzzentrum Biotechnologie (CKB).

Author contributions

O.K. Investigation, Methodology, Data Curation, Visualization, Writing – original draft. **V.S.** Methodology. **K.-E. J.** Conceptualization, Writing – review & editing. **T.D.** Conceptualization, Writing – review & editing, Supervision.

Declaration of interest

The authors declare no conflict of interest.

References

[1] T. Palmeiro-Sánchez, V. O'Flaherty, P.N.L. Lens, Polyhydroxyalkanoate bio-production and its rise as biomaterial of the future, J Biotechnol. 348 (2022) 10–25. https://doi.org/10.1016/j.jbiotec.2022.03.001.

[2] J.M. Merrick, M. Doudoroff, Enzymatic synthesis of poly-β-hydroxybutyric acid in bacteria, Nature. 189 (1961) 890–892. https://doi.org/10.1038/189890a0.

[3] O.P. Peoples, A.J. Sinskey, Poly-P-hydroxybutyrate (PHB) Biosynthesis in *Alcaligenes eutrophus* H16 identification and characterization of the PHB polymerase gene (phbC), The Journal of Biological Chemistry (1989)

[4] D. Jendrossek, D. Pfeiffer, New insights in the formation of polyhydroxyalkanoate granules (carbonosomes) and novel functions of poly(3-hydroxybutyrate), Environ Microbiol. 16 (2014) 2357–2373. https://doi.org/10.1111/1462-2920.12356.

[5] G.N. Barnard, J.K.M. Sanders, The poly-β-hydroxybutyrate granule *in vivo*, Journal of Biological Chemistry. 264 (1989) 3286–3291. https://doi.org/10.1016/s0021-9258(18)94064-0.

[6] T.U. Gerngross, P. Reilly, J. Stubbe, A.J. Sinskey, O.P. Peoples, Immunocytochemical analysis of poly-beta-hydroxybutyrate (PHB) synthase in *Alcaligenes eutrophus* H16: localization of the synthase enzyme at the surface of PHB granules, J Bacteriol. 175 (1993) 5289–5293. https://doi.org/10.1128/jb.175.16.5289-5293.1993.

[7] M. Pötter, A. Steinbüchel, Poly(3-hydroxybutyrate) Granule-associated proteins: Impacts on poly(3-hydroxybutyrate) synthesis and degradation, Biomacromolecules. 6 (2005) 552–560. https://doi.org/10.1021/bm049401n.

[8] R. Li, J. Yang, Y. Xiao, L. Long, *In vivo* immobilization of an organophosphorus hydrolyzing enzyme on bacterial polyhydroxyalkanoate nano-granules, Microb Cell Fact. 18 (2019) 166. https://doi.org/10.1186/s12934-019-1201-2.

[9] M.R. Banki, T.U. Gerngross, D.W. Wood, Novel and economical purification of recombinant proteins: Intein-mediated protein purification using *in vivo* polyhydroxybutyrate (PHB) matrix association, Protein Science. 14 (2009) 1387–1395. https://doi.org/10.1110/ps.041296305.

[10] S.A. Doyle, ed., High throughput protein expression and purification, Humana Press, Totowa, NJ, (2009). https://doi.org/10.1007/978-1-59745-196-3.

[11] J. Du, B.H.A. Rehm, Purification of target proteins from intracellular inclusions mediated by intein cleavable polyhydroxyalkanoate synthase fusions, Microb Cell Fact. 16 (2017) 184. https://doi.org/10.1186/s12934-017-0799-1.

[12] Y. Geng, S. Wang, Q. Qi, Expression of active recombinant human tissue-type plasminogen activator by using *in vivo* polyhydroxybutyrate granule display, Appl Environ Microbiol. 76 (2010) 7226–7230. https://doi.org/10.1128/AEM.01543-10.

[13] Z.J.C. Gonzaga, S. Chen, M. Lehoux, M. Segura, B.H.A. Rehm, Engineering antigens to assemble into polymer particle vaccines for prevention of *Streptococcus suis* infection, Vaccines (Basel). 9 (2021) 1386. https://doi.org/10.3390/vaccines9121386.

[14] S. Chen, B. Evert, A. Adeniyi, M. Salla-Martret, L.H. -L. Lua, V. Ozberk, M. Pandey, M.F. Good, A. Suhrbier, P. Halfmann, Y. Kawaoka, B.H.A. Rehm, Ambient temperature stable, scalable COVID-19 polymer particle vaccines induce protective immunity, Adv Healthc Mater. 11 (2022) 2102089. https://doi.org/10.1002/adhm.202102089.

[15] G. Ölçücü, O. Klaus, K.-E. Jaeger, T. Drepper, U. Krauss, Emerging solutions for *in vivo* biocatalyst immobilization: Tailor-made catalysts for industrial biocatalysis, ACS Sustain Chem Eng. 9 (2021) 8919–8945. https://doi.org/10.1021/acssuschemeng.1c02045.

[16] R.G. Kranz, K.K. Gabbert, T.A. Locke, M.T. Madigan, Polyhydroxyalkanoate production in *Rhodobacter capsulatus*: genes, mutants, expression, and physiology, Appl Environ Microbiol. 63 (1997) 3003–3009. https://doi.org/10.1128/aem.63.8.3003-3009.1997.

[17] P. Ulbrich, J. Pačes, Genetic determination of polyhydroxyalkanoate metabolism in *Rhodobacter capsulatus* SB1003 Population genomics View project Bacterial heavy metal resistance View project, (2002). https://www.researchgate.net/publication/11194430.

[18] C. Mayet, A. Deniset-Besseau, R. Prazeres, J.-M. Ortega, A. Dazzi, Analysis of bacterial polyhydroxybutyrate production by multimodal nanoimaging, Biotechnol Adv. 31 (2013) 369–374. https://doi.org/10.1016/j.biotechadv.2012.05.003.

[19] V. Montiel Corona, S. le Borgne, S. Revah, M. Morales, Effect of light-dark cycles on hydrogen and poly-β-hydroxybutyrate production by a photoheterotrophic culture and *Rhodobacter capsulatus* using a dark fermentation effluent as substrate, Bioresour Technol. 226 (2017) 238–246. https://doi.org/10.1016/j.biortech.2016.12.021.

[20] J. Kobayashi, A. Kondo, Disruption of poly (3-hydroxyalkanoate) depolymerase gene and overexpression of three poly (3-hydroxybutyrate) biosynthetic genes improve poly (3-hydroxybutyrate) production from nitrogen rich medium by *Rhodobacter sphaeroides*, Microb Cell Fact. 18 (2019) 40. https://doi.org/10.1186/s12934-019-1088-y.

[21] N. Katzke, R. Bergmann, K.-E. Jaeger, T. Drepper, Heterologous high-level gene expression in the photosynthetic bacterium *Rhodobacter capsulatus*, in: 2012: pp. 251–269. https://doi.org/10.1007/978-1-61779-433-9_13.

[22] K. Troost, A. Loeschcke, F. Hilgers, A.Y. Özgür, T.M. Weber, B. Santiago-Schübel, V. Svensson, J. Hage-Hülsmann, S.S. Habash, F.M.W. Grundler, A.S.S. Schleker, K.-E. Jaeger, T. Drepper, Engineered *Rhodobacter capsulatus* as a phototrophic platform organism for the synthesis of plant sesquiterpenoids, Front Microbiol. 10 (2019). https://doi.org/10.3389/fmicb.2019.01998.

[23] O. Klaus, F. Hilgers, A. Nakielski, D. Hasenklever, K.-E. Jaeger, I.M. Axmann, T. Drepper, Engineering phototrophic bacteria for the production of terpenoids, Curr Opin Biotechnol. 77 (2022) 102764. https://doi.org/10.1016/j.copbio.2022.102764.

[24] D. Hanahan, Studies on transformation of *Escherichia coli* with plasmids, J Mol Biol. 166 (1983) 557–580. https://doi.org/10.1016/S0022-2836(83)80284-8.

[25] R. Simon, U. Priefer, A. Pühler, A broad host range mobilization system for *in vivo* genetic engineering: Transposon mutagenesis in Gram-negative bacteria, Bio/Technology. 1 (1983) 784–791. https://doi.org/10.1038/nbt1183-784.

[26] W. Klipp, B. Masepohl, A. Pühler, Identification and mapping of nitrogen fixation genes of *Rhodobacter capsulatus*: duplication of a nifA-nifB region, J Bacteriol. 170 (1988) 693–699. https://doi.org/10.1128/jb.170.2.693-699.1988.

[27] H. Strnad, A. Lapidus, J. Paces, P. Ulbrich, C. Vlcek, V. Paces, R. Haselkorn, Complete genome sequence of the photosynthetic purple non-sulfur bacterium *Rhodobacter capsulatus* SB1003, J Bacteriol. 192 (2010) 3545–3546. https://doi.org/10.1128/JB.00366-10.

[28] J. Potzkei, M. Kunze, T. Drepper, T. Gensch, K.-E. Jaeger, J. Büchs, Real-time determination of intracellular oxygen in bacteria using a genetically encoded FRET-based biosensor, BMC Biol. 10 (2012) 28. https://doi.org/10.1186/1741-7007-10-28.

[29] S.D. Fowler, P. Greenspan, Application of Nile red, a fluorescent hydrophobic probe, for the detection of neutral lipid deposits in tissue sections: comparison with oil red O., Journal of Histochemistry & Cytochemistry. 33 (1985) 833–836. https://doi.org/10.1177/33.8.4020099.

[30] R. Zuriani, S. Vigneswari, M.N.M. Azizan, M.I.A. Majid, A.A. Amirul, A high throughput Nile red fluorescence method for rapid quantification of intracellular bacterial polyhydroxyalkanoates, Biotechnology and Bioprocess Engineering. 18 (2013) 472–478. https://doi.org/10.1007/s12257-012-0607-z.

[31] A. Degelau, T. Scheper, J.E. Bailey, C. Guske, Fluorometric measurement of poly-β hydroxybutyrate in *Alcaligenes eutrophus* by flow cytometry and spectrofluorometry, Appl Microbiol Biotechnol. 42 (1995) 653–657. https://doi.org/10.1007/BF00171939.

[32] N. Katzke, S. Arvani, R. Bergmann, F. Circolone, A. Markert, V. Svensson, K.-E. Jaeger, A. Heck, T. Drepper, A novel T7 RNA polymerase dependent expression system for high-level protein production in the phototrophic bacterium *Rhodobacter capsulatus*, Protein Expr Purif. 69 (2010) 137–146. https://doi.org/10.1016/j.pep.2009.08.008.

[33] V. Peters, B.H.A. Rehm, *In vivo* enzyme immobilization by use of engineered polyhydroxyalkanoate synthase, Appl Environ Microbiol. 72 (2006) 1777–1783. https://doi.org/10.1128/AEM.72.3.1777-1783.2006.

[34] I. Monroy, G. Buitrón, Production of polyhydroxybutyrate by pure and mixed cultures of purple non-sulfur bacteria: A review, J Biotechnol. 317 (2020) 39–47. https://doi.org/10.1016/j.jbiotec.2020.04.012.

[35] D. Dennis, M. McCoy, A. Stangl, H.E. Valentin, Z. Wu, Formation of poly(3-hydroxybutyrate-co-3-hydroxyhexanoate) by PHA synthase from *Ralstonia eutropha*, J Biotechnol. 64 (1998) 177–186. https://doi.org/10.1016/S0168-1656(98)00110-2.

[36] J. Eggers, A. Steinbüchel, Impact of *Ralstonia eutropha's* poly(3-hydroxybutyrate) (PHB) depolymerases and phasins on PHB storage in recombinant *Escherichia coli*, Appl Environ Microbiol. 80 (2014) 7702–7709. https://doi.org/10.1128/AEM.02666-14.

[37] D. Li, L. Lv, J.-C. Chen, G.-Q. Chen, Controlling microbial PHB synthesis *via* CRISPRi, Appl Microbiol Biotechnol. 101 (2017) 5861–5867. https://doi.org/10.1007/s00253-017-8374-6.

[38] M. Erbakan, B.S. Curtis, B.T. Nixon, M. Kumar, W.R. Curtis, Advancing *Rhodobacter sphaeroides* as a platform for expression of functional membrane proteins, Protein Expr Purif. 115 (2015) 109–117. https://doi.org/10.1016/j.pep.2015.05.012.

[39] J.X. Wong, B.H.A. Rehm, Design of modular polyhydroxyalkanoate scaffolds for protein immobilization by directed ligation, Biomacromolecules. 19 (2018) 4098–4112. https://doi.org/10.1021/acs.biomac.8b01093.

[40] J.X. Wong, M. Gonzalez-Miro, A.J. Sutherland-Smith, B.H.A. Rehm, Covalent functionalization of bioengineered polyhydroxyalkanoate spheres directed by specific protein-protein interactions, Front Bioeng Biotechnol. 8 (2020). https://doi.org/10.3389/fbioe.2020.00044.

Supporting information

Functionalization of polyhydroxybutyrate granules in the anoxygenic phototrophic bacterium *Rhodobacter capsulatus* SB1003

Oliver Klaus[1], Vera Svensson[1], Karl-Erich Jaeger[1,2], Thomas Drepper[1]

[1]Institute of Molecular Enzyme Technology, Heinrich Heine University Düsseldorf, Forschungszentrum Jülich, Jülich, Germany

[2]Institute of Bio- and Geosciences IBG-1: Biotechnology, Forschungszentrum Jülich GmbH, Jülich, Germany

Content

Table S1. Bacterial strains used in this study.

Name	Characteristics	Reference
Escherichia coli		
E. coli DH5α	*F⁻Φ80lacZΔM15 Δ(lacZYA-argF) U169 recA1 endA1 hsdR17 phoA supE44 thi-1 gyrA96 relA1 deoR*	[1]
E. coli S17-1	Ec294::[RP4-2 (Tc^R::Mu)(Km^R::Tn7)] *recA, thi, pro, hsdR⁻ hsdM⁺* Tp^R Sm^R	[2]
E. coli Tuner(DE3)	*F⁻ompT hsdS*$_B$ *(*r_B^- m_B^-*) gal dcm lacY1(DE3)*	Novagen, Merck KGaA
Rhodobacter capsulatus		
R. capsulatus SB1003	wildtype, Rif^R	[3]

Table S2. Oligonucleotides and plasmids used in this study. Endonuclease restriction sites are underlined.

Oligonucleotides			
Name		Application*	Nucleotide sequence (5`->3`)
1	NdeI_YFP_fw	(PCR) amplification of *eyfp* incl. thrombin linker (pRhotHi-2-FluBO)	ATATACATATGGTGAGCAAGGGCGAGGAGC
2	BamHI_FluBo_rev	(PCR) amplification of *eyfp* incl. thrombin linker (pRhotHi-2-FluBO)	ATATATATAGGATCCGGCGCCGCTG
3	BamHI_PhaC_fw	(PCR) amplification of *phaC* (*R. capsulatus*)	ATATAGGATCCATGACAACGCCTGAAAAGGTCG
4	HindIII_PhaC_rev	(PCR) amplification of *phaC* (*R. capsulatus*)	ATATAAGCTTCTAAAGCACCACAACCTCCGAGAC
5	NotI_PhaB1_fw	(PCR) amplification of *phaB1* (*R. capsulatus*)	ATTTGCGGCCGCTTTAAGGAGATATA ATGTCCAGAGTTGCACTCGTCACCGG
6	XhoI_PhaB1_rev	(PCR) amplification of *phaB1* (*R. capsulatus*)	CCGCTCGAGCGGTCAGGTCATGTATTGGC
7	BamHI_PhaA3_fw	(PCR) amplification of *phaA3* (*R. capsulatus*)	CGGGATCCCGGGAAGCTTAGGAG ATATAATGACCGAAGCCTATATC
8	NotI_PhaA3_rev	(PCR) amplification of *phaA3* (*R. capsulatus*)	ATTTGCGGCCGCTTTATC AGACCCTCTCGATGATC

Plasmids		
Name	Characteristics	Reference
pRhotHi-2_FluBO	pBBR1mcs (*rep, mob,* Cm^R), pET22b (*mcs, pelB*), pBSL15 (*aph*II) orientation II, P_{T7}, *eyfp, FbFP*	[4]
pRhokHi-2	pBBR1mcs (*rep, mob,* Cm^R), pET22b (*mcs, pelB*), pBSL15 (*aph*II) orientation I, P_{T7}	[5]
pRhokHi-2_eyfp	pRhokHi-2 derivative, *eyfp*	
pRhokHi-2_eyfp-phaC	pRhokHi-2 derivative, translational fusion of *eyfp* & *phaC* (*R. capsulatus*)	This work

pET28a(+)	P_{T7}, his_6 tag, *mcs*, *lacI*, *bla*, Km^R, pBR322 ori, f1 ori	Novagen, Merck KGaA
pET28a_eyfp-phaCA3B	pET28a(+) derivative, translational fusion of *eyfp* & *phaC, phaA3, phaB1* (*R. capsulatus*)	This work

*The respective DNA template that have been used in the respective PCR is given in brackets; *R. capsulatus*: chromosomal DNA of this bacterium

DNA sequences of the respective expression cassettes

1. pRhokHi-2_eyfp-phaC

RBS eYFP

AAGGAGATATACATATGGTGAGCAAGGGCGAGGAGCTGTTCACCGGGGTGGTGCCCATCCTGG
TCGAGCTGGACGGCGACGTAAACGGCCACAAGTTCAGCGTGTCCGGCGAGGGCGAGGGCGATG
CCACCTACGGCAAGCTGACCCTGAAGTTCATCTGCACCACCGGCAAGCTGCCCGTGCCCTGGCC
CACCCTCGTGACCACCTTCGGCTACGGCCTGCAGTGCTTCGCCCGCTACCCCGACCACATGAAG
CAGCACGACTTCTTCAAGTCCGCCATGCCCGAAGGCTACGTCCAGGAGCGCACCATCTTCTTCA
AGGACGACGGCAACTACAAGACCCGCGCCGAGGTGAAGTTCGAGGGCGACACCCTGGTGAACC
GCATCGAGCTGAAGGGCATCGACTTCAAGGAGGACGGCAACATCCTGGGGCACAAGCTGGAGT
ACAACTACAACAGCCACAACGTCTATATCATGGCCGACAAGCAGAAGAACGGCATCAAGGTGAAC
TTCAAGATCCGCCACAACATCGAGGACGGCAGCGTGCAGCTCGCCGACCACTACCAGCAGAACA
CCCCCATCGGCGACGGCCCCGTGCTGCTGCCCGACAACCACTACCTGAGCTACCAGTCCGCCC
TGAGCAAAGACCCCAACGAGAAGCGCGATCACATGGTCCTGCTGGAGTTCGTGACCGCCGCCG

thrombine recognition site

GGATCACTCTCGGCATGGACGAGCTGTACAAGGAGCTCGCGGGCCTGGTGCCGCGCGGCAGCG

BamHI PhaC

GCGCCGGATCCATGACAACGCCTGAAAAGGTCGAATCTGCTGCATCGCAGCAAATGCGGGACAA
TCTGGCGCGGATTGAGACACTTACACAACGCATGGTTGAAGCCTTTGCGCAAAAGCGCGCGCCC
AATCCTGCGCTGGAGGGGCCGGGGCTGGATCTTTACGTCGCCTCTTCGAGCGCGCTTTTGCGC
GAGATGACGGCGAATCCGGCGAAGATCTTCGAGGCGCAGGTCAGCTATTGGGCGCAGGCGATG
ACGCATTACATCGACGCCACCCATGCCTTTGCTCAGGGCACCTTCAAGCCGCCCGCCGATCCGG
GGCCGAAGGACCGCCGCTTTTCCAACCCGCTGTGGGACAGCCATCCCTATTTCAACTTCATCAA
GCAGCAATATCTGATCGCCTCGAGCTCGATCGAGGAAGCGCTGTCGAAGATCGAGGGGCTGGA
CCCGGTCGATCGCCGCCGGCTGGAGATGTTTTCCAAGCAGATCATCGACATGATGGCGCCGACG
AATTTTCTGGCGACGAACCCGGATGCGCTGGAAAAGGCGGTGGCGACCGAGGGCGAAAGCCTG
GTGCGGGGGCTGGAAAACCTCGTGCGCGACATCGAGGCGAACCGCGGCGATCTGGTGATCACG
CTTTCGGACAAGAACGCCTTCAGCGTCGGGCACAACATCGGCACGGCGAAAGGCCAGGTGGTC
TGGCGCAACCGGCTGATGGAGATCATCCAGTACGAGCCCACCACCCCCGAGGTGCACAAGACC
CCGCTGATCATCTTTCCGCCCTGGATCAACAAGTTCTACATCCTGGATCTGAAACCGCAAAACAG
CCTGATCCGCTGGATCGTCGATCAGGGCTTCACGCTGTTCGTCGTCAGCTGGAAGAACCCGGAC
CGGTCCTATGCCGATGTGGGGATGGAGGATTACGTCCGCGACGGCTATCTGGCCGCGATCGAG
GAGGTGAAGGCGATCACCGGCGAGAAACAGGTGAATGCGGTCGGCTATTGCATCGCGGGCACG
ACGCTGAGCCTGGTCCTGTCGCTCTTGGAAAAGCGCAAGGACAAGTCGATCAAATCGGCGACCT
TTTTCACCACGCTGACCGACTTTTCCGATCAGGGCGAATTCACCCCCTTCCTGCAGGATGATTTC
GTCGACGGGATCGAGCGGCAGGTGCGGCTGGATGGCGTTCTGTCGAGCTATTACATGACGCGG
ACCTTTTCCTATCTGCGGGCGAATGACCTGATCTATCAGCCCGCGATCCGCAGCTACATGATGGG
CGAATCGCCGCCCGCCTTCGACTTGCTTTACTGGAACGGCGACAGCACCAACCTGCCGGGCAAG
ATGGCGATGGAATATCTGCGCGGGCTCTGTCAGGCCGATGCCTTCACCACCGAGGGCTTCGAGC
TGATGGGCGAGCGGCTGCATGTCTCGGGGGTCAAGGTGCCGCTCTGCGCCATCGCCTGCGAGA
CCGACCATATCGCGCCCTGGATCGTCAGCTTCAACGGCGTGGCGCAGATGGGATCGACCGACA

AGACCTTCATCCTGACGGAATCGGGCCATATCGCCGGGATCGTGAACCCGCCGAGCAAGGACAA
ATACGGCCATTACACCTCTGCGGCGCCGATTGCCGATCATCAGGTCTGGAAGGCGCAGGCCACC
TACACGAAGGGCAGCTGGTGGCCGCGCTGGGGGGAATGGCTGGCCGGGCATTCGGGCAAGAA
GATCCCCGCGCGGGCCCCGGGCGACGCGACGCATCCGCCGCTGGCCCCGGCCCCCGGCACCT

HindIII

ATGTCTCGGAGGTTGTGGTGCTTTAGAAGCTT

2. pET28a_eyfp-phaCA3B

RBS eYFP

AAGGAGATATACAT**ATG**GTGAGCAAGGGCGAGGAGCTGTTCACCGGGGTGGTGCCCATCCTGG
TCGAGCTGGACGGCGACGTAAACGGCCACAAGTTCAGCGTGTCCGGCGAGGGCGAGGGCGATG
CCACCTACGGCAAGCTGACCCTGAAGTTCATCTGCACCACCGGCAAGCTGCCCGTGCCCTGGCC
CACCCTCGTGACCACCTTCGGCTACGGCCTGCAGTGCTTCGCCCGCTACCCCGACCACATGAAG
CAGCACGACTTCTTCAAGTCCGCCATGCCCGAAGGCTACGTCCAGGAGCGCACCATCTTCTTCA
AGGACGACGGCAACTACAAGACCCGCGCCGAGGTGAAGTTCGAGGGCGACACCCTGGTGAACC
GCATCGAGCTGAAGGGCATCGACTTCAAGGAGGACGGCAACATCCTGGGGCACAAGCTGGAGT
ACAACTACAACAGCCACAACGTCTATATCATGGCCGACAAGCAGAAGAACGGCATCAAGGTGAAC
TTCAAGATCCGCCACAACATCGAGGACGGCAGCGTGCAGCTCGCCGACCACTACCAGCAGAACA
CCCCCATCGGCGACGGCCCCGTGCTGCTGCCCGACAACCACTACCTGAGCTACCAGTCCGCCC
TGAGCAAAGACCCCAACGAGAAGCGCGATCACATGGTCCTGCTGGAGTTCGTGACCGCCGCCG

thrombine recognition site

GGATCACTCTCGGCATGGACGAGCTGTACAAGGAGCTCGCGGGCCTGGTGCCGCGCGGCAGCG

BamHI PhaC

GCGCCGGATCCATGACAACGCCTGAAAAGGTCGAATCTGCTGCATCGCAGCAAATGCGGGACAA
TCTGGCGCGGATTGAGACACTTACACAACGCATGGTTGAAGCCTTTGCGCAAAAGCGCGCGCCC
AATCCTGCGCTGGAGGGGCCGGGGCTGGATCTTTACGTCGCCTCTTCGAGCGCGCTTTTGCGC
GAGATGACGGCGAATCCGGCGAAGATCTTCGAGGCGCAGGTCAGCTATTGGGCGCAGGCGATG
ACGCATTACATCGACGCCACCCATGCCTTTGCTCAGGGCACCTTCAAGCCGCCCGCCGATCCGG
GGCCGAAGGACCGCCGCTTTTCCAACCCGCTGTGGGACAGCCATCCCTATTTCAACTTCATCAA
GCAGCAATATCTGATCGCCTCGAGCTCGATCGAGGAAGCGCTGTCGAAGATCGAGGGGCTGGA
CCCGGTCGATCGCCGCCGGCTGGAGATGTTTTCCAAGCAGATCATCGACATGATGGCGCCGACG
AATTTTCTGGCGACGAACCCGGATGCGCTGGAAAAGGCGGTGGCGACCGAGGGCGAAAGCCTG
GTGCGGGGGCTGGAAAACCTCGTGCGCGACATCGAGGCGAACCGCGGCGATCTGGTGATCACG
CTTTCGGACAAGAACGCCTTCAGCGTCGGGCACAACATCGGCACGGCGAAAGGCCAGGTGGTC
TGGCGCAACCGGCTGATGGAGATCATCCAGTACGAGCCCACCACCCCCGAGGTGCACAAGACC
CCGCTGATCATCTTTCCGCCCTGGATCAACAAGTTCTACATCCTGGATCTGAAACCGCAAAACAG
CCTGATCCGCTGGATCGTCGATCAGGGCTTCACGCTGTTCGTCGTCAGCTGGAAGAACCCGGAC
CGGTCCTATGCCGATGTGGGGATGGAGGATTACGTCCGCGACGGCTATCTGGCCGCGATCGAG
GAGGTGAAGGCGATCACCGGCGAGAAACAGGTGAATGCGGTCGGCTATTGCATCGCGGGCACG
ACGCTGAGCCTGGTCCTGTCGCTCTTGGAAAAGCGCAAGGACAAGTCGATCAAATCGGCGACCT
TTTTCACCACGCTGACCGACTTTTCCGATCAGGGCGAATTCACCCCCTTCCTGCAGGATGATTTC
GTCGACGGGATCGAGCGGCAGGTGCGGCTGGATGGCGTTCTGTCGAGCTATTACATGACGCGG
ACCTTTTCCTATCTGCGGGCGAATGACCTGATCTATCAGCCCGCGATCCGCAGCTACATGATGGG
CGAATCGCCGCCCGCCTTCGACTTGCTTTACTGGAACGGCGACAGCACCAACCTGCCGGGCAAG
ATGGCGATGGAATATCTGCGCGGGCTCTGTCAGGCCGATGCCTTCACCACCGAGGGCTTCGAGC
TGATGGGCGAGCGGCTGCATGTCTCGGGGGTCAAGGTGCCGCTCTGCGCCATCGCCTGCGAGA
CCGACCATATCGCGCCCTGGATCGTCAGCTTCAACGGCGTGGCGCAGATGGGATCGACCGACA

111 GACCTTCATCCTGACGGAATCGGGCCATATCGCCGGGATCGTGAACCCGCCGAGCAAGGACAAA
112 TACGGCCATTACACCTCTGCGGCGCCGATTGCCGATCATCAGGTCTGGAAGGCGCAGGCCACCT
113 ACACGAAGGGCAGCTGGTGGCCGCGCTGGGGGGAATGGCTGGCCGGGCATTCGGGCAAGAAG
114 ATCCCCGCGCGGGCCCCGGGCGACGCGACGCATCCGCCGCTGGCCCCGGCCCCCGGCACCT

115 *HindIII* **RBS** PhaA3

116 ATGTCTCGGAGGTTGTGGTGCTTTAGAAGCTT**AGGAGA**TATAATGACCGAAGCCTATATCTATGA
117 CGCCTGCCGCACGCCGCGGGGCAAGGGGCGCGCTGACGGCAGCCTGCATGAAGTGACCTCTG
118 TCGCGCTGTCGGCGCGGCTTCTGGATGCGGTGGCGGAACGCAATGGCCTGACGGGTCCTGCGG
119 TCGAGGATGTGATCTGGGGCAATGTCACCCAGGTGGGCGAGCAGGGCGGCTGTCTGGCCCGGT
120 CTGCGGTGCTGCTTTCGGGGCTCGATGAATCGATCCCCGGTCTTTCGATCAACCGCTTTTGCGC
121 CAGCGGCATGGAGGCGGTGAACCTGGCCGCCAATCAGGTCAAGGCGGGGGCGGGCGCGGCCT
122 ATATCGCGGGCGGGGTCGAGATGATGAGCCGCGTTGCCATGGGCTCGGACGGGGCGGCGATC
123 GCCGTCGATCCGTCGCTTGCGATGAAGACCTATTTCGTGCCGCAGGGGATTTCCGCCGATATCA
124 TCGCCACCGAATACGGGTTTACCCGCGAGATGGCCGATGCGCTGGCGGTCGAAAGCCAGCGCC
125 GCGCCGCCGAGGCCTGGGCCGAGGGGCGTTTCGCGAAATCCATCGTGCCGGTGAAGGATCAGA
126 ACGGGCTGACGATTCTGGACCGCGACGAATATCTGCGCCCCGGCACGACGCTGGAGGATCTGG
127 CCAAGCTCAAGCCCGCCTTCAAGGACATGGGCGAGGTGATGCCGGGCTTCGACAAGGTGGCGA
128 TGCTGAAATATCCGCATCTGGAGCGCATCGAGCATATCCACCATGCGGGGAACTCTTCGGGCAT
129 CGTCGATGGGGCGGCGGCGGTGCTGATCGGCTCGAAGGAGTTCGGCGAGGCGCATGGGTTGA
130 AGCCGCGCGCCCGCATCCGCGCCACCGCGAAGATCGGCACCGATCCGACGATCATGCTGACCG
131 GCCCGGTGCCCGTCACCGAAAAGATCCTGCGCGACAGCGGCATGAGCATTGCCGACATCGACC
132 TTTTCGAAGTGAACGAGGCCTTTGCCGCAGTTGTTCTGCGCTTCATGCAGGCCTTTGACGTCGGT
133 CAGGACCGGGTCAACGTGAACGGCGGCGCGATGGCGCTGGGTCATCCCTTGGGCGCGACGGG
134 GGCGATCATCATCGGCACGCTGCTGGACGAGCTGGAACGCCGCGATCTGTCCACCGGGCTTGC

135 *NotI*

136 GACGCTCTGCATCGCTTCCGGCATGGGCGCGGCCACGATCATCGAGAGGGTCTGATAAAGCGG

137 **RBS** PhaB

138 CCGCTTTA**AGGAGA**TATAATGTCCAGAGTTGCACTCGTCACCGGGGGATCGCGCGGCATTGGCG
139 CCGCGATCTCGATGGCACTGAAGGACGCCGGTTACACCGTCGCCGCGAACTATGCCGGCAATG
140 ACGAAGCCGCCGCGAAATTCACCGCCGAGACCGGGATCAAGACCTACAAATGGTCGGTCGCCG
141 ATTACGACGCCTGCGCCGCGGGCATCGCCCAGGTCGAGGCCGATCTGGGCCCGGTCGACGTGC
142 TGGTGAACAATGCGGGCATCACCCGCGACGCGCCCTTCCACAAGATGACCCGCGACCAATGGG
143 ATCAGGTGATCGGCACCAACCTGAACGGCATCTTCAACATGACGCATCCGCTCTGGAACGGCAT
144 GCGCGACCGCAAATTCGGCCGGATCATCAACATTTCCTCGATCAACGGCCAAAAGGGCCAGTTC
145 GCCCAGGCGAACTATTCCGCGGCCAAGGCGGGCGACATCGGCTTCACCAAGGCGCTGGCGCAG
146 GAAGGGGCGCGGGCGGGGATCACCGTCAACGCGATCTGCCCGGGCTATATCGCCACCGAAATG
147 GTGATGGCGGTGCCCGAAAAGGTGCGCGAGCAGATCATCGCGACGATCCCGGTCGGCCGTCTG
148 GGCGAAACCGGCGATATCGCGCGCTGCGTGGTGTTCCTCGCCTCGGATGATGCGGGCTTCATC

149 *XhoI*

150 ACCGGCGCGACGCTGACCGCGAACGGCGGCCAATACATGACCTGACCGCTCGAG

151

152

153

154

155

References

[1] D. Hanahan, Studies on transformation of *Escherichia coli* with plasmids, J Mol Biol. 166 (1983) 557–580. https://doi.org/10.1016/S0022-2836(83)80284-8.

[2] R. Simon, U. Priefer, A. Pühler, A broad host range mobilization system for *in vivo* genetic engineering: Transposon mutagenesis in Gram negative bacteria, Bio/Technology. 1 (1983) 784–791. https://doi.org/10.1038/nbt1183-784.

[3] H. Strnad, A. Lapidus, J. Paces, P. Ulbrich, C. Vlcek, V. Paces, R. Haselkorn, Complete genome sequence of the photosynthetic purple non-sulfur bacterium *Rhodobacter capsulatus* SB1003, J Bacteriol. 192 (2010) 3545–3546. https://doi.org/10.1128/JB.00366-10.

[4] J. Potzkei, M. Kunze, T. Drepper, T. Gensch, K.-E. Jaeger, J. Büchs, Real-time determination of intracellular oxygen in bacteria using a genetically encoded FRET-based biosensor, BMC Biol. 10 (2012) 28. https://doi.org/10.1186/1741-7007-10-28.

[5] N. Katzke, S. Arvani, R. Bergmann, F. Circolone, A. Markert, V. Svensson, K.-E. Jaeger, A. Heck, T. Drepper, A novel T7 RNA polymerase dependent expression system for high-level protein production in the phototrophic bacterium *Rhodobacter capsulatus*, Protein Expr Purif. 69 (2010) 137–146. https://doi.org/10.1016/j.pep.2009.08.008.

II.3.3 The split GFP system as alternative linker system for protein immobilization

PUBLICATION VIII

Split GFP as a new system for facilitating and sensing *in vivo* protein immobilization

Oliver Klaus[1]*, Patrick Lenz[1]*, Thomas Gensch[2], Fabienne Hilgers[1], Andreas Knapp[1], Stephan Thies[1], Karl-Erich Jaeger[1,3], Thomas Drepper[1#]

[1]Institute of Molecular Enzyme Technology, Heinrich Heine University Düsseldorf, Forschungszentrum Jülich, 52425 Jülich, Germany
[2]Institute of Biological Information Processing (IBI-1: Molecular and Cellular Physiology), Forschungszentrum Jülich, 52425 Jülich, Germany
[3]Institute of Bio- and Geosciences IBG-1: Biotechnology, Forschungszentrum Jülich GmbH, 52425 Jülich, Germany

* These authors contributed equally
[#] Corresponding author

Status: in preparation

Target Journal: *International Journal of Molecular Sciences*

Own contribution:
Designing and performing experiments, plasmid construction, analyzing data, visualization, writing the manuscript

Split GFP as a new system for facilitating and sensing *in vivo* protein immobilization

Oliver Klaus [1,#], Patrick Lenz [1,#], Thomas Gensch [2], Fabienne Knapp [1], Andreas Knapp [1,3], Stephan Thies [1], Karl-Erich Jaeger [1,4], Thomas Drepper [1*]

[1] Institute of Molecular Enzyme Technology, Heinrich Heine University Düsseldorf, Forschungszentrum Jülich, Jülich, Germany
[2] Institute of Biological Information Processing (IBI-1: Molecular and Cellular Physiology), Forschungszentrum Jülich GmbH, Jülich, Germany
[3] present address: Castrol Germany GmbH, Mönchengladbach, Germany
[4] Institute of Bio- and Geosciences IBG-1: Biotechnology, Forschungszentrum Jülich GmbH, Jülich, Germany

* Correspondence: t.drepper@fz-juelich.de
#These authors contributed equally to this work.

Abstract: (max. 200 words)

In biotechnological processes, the immobilization of enzymes on support materials represents a promising opportunity to enhance their characteristics and (re)usability. However, *in vivo* enzyme immobilization still needs to be individually optimized for each new enzyme including the selection of appropriate production hosts, support materials, and anchor proteins. In this study, we aimed to establish split GFP as an alternative linker-biosensor system for *in vivo* coupling of target proteins to polyhydroxybutyrate (PHB) granules in *Escherichia coli*. Therefore, the ability of the two split GFP fragments GFP1-10 and GFP11 to self-assemble, a process that is accompanied by the development of a specific green fluorescence signal, was used for immobilization. As a proof-of-concept, we demonstrate the dual linker-sensor function of split GFP by using the red-fluorescent protein mCherry as well as the ester hydrolase LipD from *Alcanivorax borkumensis*. By using fluorescence microscopy and fluorescence lifetime imaging (FLIM) approaches we could demonstrate that split GFP allows *in vivo* one-step protein immobilization of proteins on biogenic carrier materials together with direct verification of the coupling process. Thus, the novel split GFP linker-sensor system can support the systematic optimization of *in vivo* enzyme immobilization and, consequently, the biotechnological application of enzyme immobilizates in future studies.

Keywords: Split GFP, Enzyme Immobilization, Polyhydroxybutyrate, Biocatalysis, Imaging

1. Introduction

The use of enzymes for biotechnological applications requires their robust and sustainable production, simple purification, and reusability [1,2]. One promising option and direct way to address these challenges is the heterologous production and simultaneous *in vivo* immobilization of enzymes on biogenic carrier materials in microbes [3]. In the past, these approaches provided increased enzyme stability within an improved temperature or solvent tolerance [4–6]. However, *in vivo* enzyme immobilization, including the selection of appropriate production hosts, carrier materials and anchor proteins, has still to be optimized on a case-to-case basis for each new enzyme, which still limits a broader applicability of such enzyme conjugates. Therefore, the development of new strategies that allow the direct and specific online monitoring of *in vivo* one-step enzyme immobilization can help to efficiently optimize this complex process in a broad variety of microbial production hosts.

In the past, polyhydroxybutyrate (PHB) granules have been successfully used as a bioplastic carrier suitable for the immobilization of enzymes [7]. PHB is a biopolymer that serves as a carbon and energy storage compound built up by many bacteria under nutrient limitation and carbon excess [8]. The biosynthesis of PHB is a three-step enzymatic process: the β-ketothiolase (PhaA) condenses two acetyl-CoA subunits to acetoacetyl-CoA, followed by a reduction to D-3-hydroxybutyryl-CoA *via* the acetoacetyl-CoA reductase (PhaB) and a final polymerization by the PHB synthase (PhaC) [9–11]. The PHB granules formed in this process accumulates in the cytoplasm as spherical inclusions of 100-500 nm and are composed of a hydrophobic core surrounded by a layer of PHB-associated proteins including PHB synthases and depolymerases as well as phasins [12]. Genetical fusions of PhaC with target proteins were successfully applied to anchor the target enzymes on the surface of PHB inclusions [13,14]. In addition to direct genetic fusion, PhaC and the target protein can also be specifically connected posttranslational by using the sophisticated SpyTag-SpyCatcher system [15,16]. By genetically fusing the SpyTag to the target protein and the SpyCatcher domain to PhaC, this versatile linker system enabled a targeted decoration of the PHB surface and assembly of multi-protein complexes on this immobilization support material [17]. However, all methods described in literature so far do not allow an *in vivo* analysis of the coupling process between the immobilization carrier and target protein. Thus, a systematic screening of the biogenic supports and optimization of *in vivo* immobilization parameters are limited.

In the presented study, we analyzed whether split GFP can be used as an alternative linker system for implementing and visualizing *in vivo* immobilization of target proteins. In the case of split GFP, the conserved β-barrel structure of superfolder GFP consisting of eleven β-sheets is separated into two non-fluorescent fragments [18,19] – one larger fragment containing the β sheets 1-10 (called GFP1-10) and one smaller fragment comprising the β-sheet 11 (GFP11 tag). After protein synthesis, both fragments can self-assemble and subsequently reconstitute a holo-split GFP whose fluorescence can be easily detected and quantified *in vivo* and *in vitro* [18,20]. In the biotechnological context, the split GFP technology was applied, e.g., for target protein detection in industrially relevant organisms such as *Escherichia coli* [21], *Bacillus subtilis* [22,23], *Corynebacterium glutamicum* [24,25] and *Pichia pastoris* [26]. In addition, split GFP was used for various *in vivo* studies, including the analysis of protein-protein interactions [27], protein localization [28], neuronal cell communication [29] and host - pathogen interactions [30].

The results presented in this work demonstrate for the first time that split GFP can further be applied as a versatile linker-sensor system that allows an efficient decoration of bioplastic granules with a protein of interest (POI) along with the *in vivo* analysis of the coupling process *via* the corresponding fluorescence signal.

2. Results and Discussion

2.1 Conceptualization of a split GFP-based linker-sensor system for in vivo enzyme immobilization.

In this work, we aimed to evaluate split GFP as a novel linker system allowing an easy-to-perform immobilization of target proteins to the surface of biogenic biopolymers together with fluorescence-based monitoring of successful coupling. Therefore, we used PHB granules as a proof-of-concept immobilization system and PhaC as the corresponding anchor protein. To perform and analyze the split GFP-mediated *in vivo* formation of PHB-POI conjugates, we chose *E. coli* as a non-natural PHB producer for expression. Hence, an expression plasmid was constructed based on the broad host range vector pBBR1mcs [31] (Figure 1A). The plasmid contains the genes for PHB biosynthesis and the split GFP system as well as the gene encoding the POI: The genes *phaA, phaB* and *phaC,* which are required for PHB biosynthesis [32,33], were placed under the control of the constitutive P_{aphII} promoter [34]. The PHB synthase PhaC was selected as anchor for protein coupling because PhaC remains covalently linked to the PHB chain [35,36]. For split GFP-mediated linkage of the POI to the PhaC-PHB complex (Figure 1 B), the *gfp11* gene was fused to the 5`-terminus of the *phaC* gene. Thus, PHB granules coated

with the GFP11-PhaC should be formed during cultivation due to the constitutive expression. In contrast, the gene encoding the POI-GFP1-10 fusion is under control of the IPTG-inducible P_{tac} promoter [37]. It should be noted that for split GFP-assisted immobilization, the POI has to be fused to the N-terminus of GFP1-10 since its C-terminus must be accessible for interaction with GFP11 [18]. After induction of P_{tac}-controlled gene expression, both split GFP fragments can self-assemble intracellularly, thereby reconstituting the holo-GFP. This process should thus result in the coupling of POI to the PHB granules, which could easily be detected by the formation of a specific fluorescence signal.

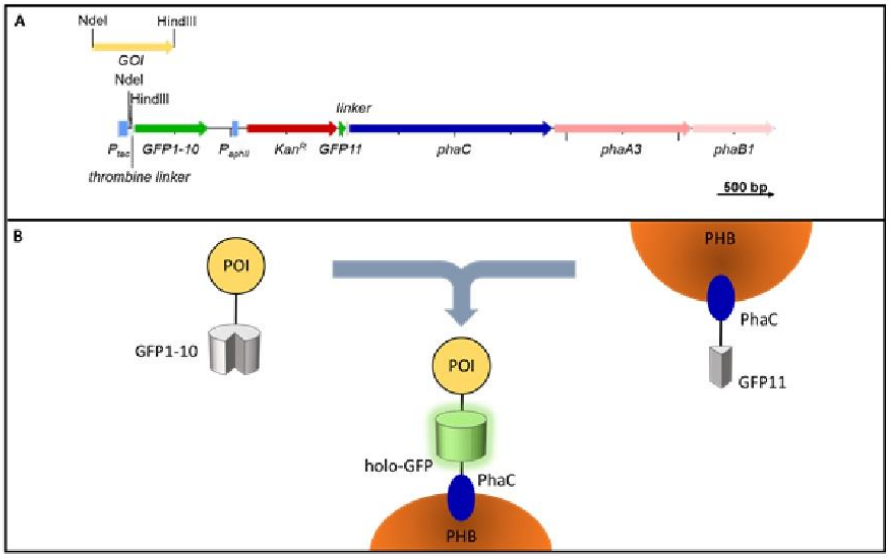

Figure 1. Concept of the split GFP-based linker-sensor system for *in vivo* protein immobilization. (**A**) Schematic overview of the genetic structure and composition of the split GFP immobilization tool. The gene of interest (GOI) is under the control of the IPTG-inducible P_{tac} promoter and is fused in frame to the *GFP1-10* gene. Genes for PHB biosynthesis (*phaA*, *phaB* and *phaC*) are organized in a tricistronic operon whose transcription is under the control of the constitutive P_{aphII} promoter. The 5`-terminus of *phaC* is fused to the GFP11 tag-encoding sequence. (**B**) After PHB synthesis, the GFP11-PhaC proteins keep covalently attached to the hydrophobic PHB chain, which can result in the intracellular self-assembly of GFP11-tagged PHB granules. The split GFP-mediated linkage of POI to the PHB granules will be detectable *in vivo via* the formation of a specific holo-split GFP fluorescence signal.

2.2. Evaluation of the linker and sensor function of split GFP-based immobilization system

To verify the proposed function of the split GFP-based *in vivo* immobilization and detection system in *E. coli*, we chose the red-fluorescent mCherry as a first target protein. To this end, the plasmid pBBR1mcs_mCherry-splitGFP, which harbors all elements necessary for the formation of mCherry-decorated PHB inclusions as well as for split GFP-mediated detection of this formation were transferred

to *E. coli* Tuner(DE3) cells. As a negative control, the plasmid pBBR1mcs_mCherrystop-splitGFP was used, carrying a stop codon at the 3'-end of the mCherry gene. Thereby, the translation of the GFP1-10 protein domain is prevented in the control strain and thus the formation of the holo-split GFP. In the resulting expression strains transcription of the mCherry-GFP1-10- and mCherry-encoding genes was induced 2 h after inoculation by adding 100 µM IPTG.

After 48 h of cultivation, the overall intensities of green and red fluorescence of both strains were quantified in corresponding cells extracts to evaluate *in vivo* immobilization of mCherry to PHB *via* holo-split GFP linkage. In case of efficient production and subsequent coupling of mCherry-GFP1-10 to PHB-GFP11, both, green and red fluorescence should be detectable in the respective samples since holo-split GFP can only be reconstituted by the assembly of both GFP-fragments [18]. As shown in Figure 2 A, the fluorescence signals confirmed the presence of both fluorescent proteins in the *E. coli* strain carrying pBBR1mcs_mCherry-splitGFP (Figure 2 A, mCherry-GFP1-10), while no GFP fluorescence was observed in cell extracts of *E. coli* expressing mCherry without the GFP1-10 fusion (Figure 2 A, mCherry). This clearly indicates that the holo-split GFP protein can be formed in *E. coli* cells offering both components of the split GFP system (i.e., mCherry-GFP1-10 and GFP11-PhaC). However, in the control strain, mCherry fluorescence showed an approximately 2.5-fold higher fluorescence intensity as compared to the mCherry-GFP1-10 expressing strain which is probably caused by a decreased expression level or activity of mCherry when fused to GFP1-10.

Next, we analyzed if the formation of holo-split GFP leads to the formation of mCherry-decorated PHB granules. The expression of mCherry-GFP1-10 can principally result in the formation of red and green fluorescing mCherry-holo-split GFP-PHB granules but also in the accumulation of soluble, red fluorescing fusion proteins if holo-split GFP-mediated PHB immobilization is incomplete. So, we examined the distribution of red and green fluorescence and the occurrence of fluorescent inclusions by fluorescence microscopy in *E. coli* cells carrying either pBBR1mcs_mCherry-splitGFP or the control plasmid pBBR1mcs_mCherrystop-splitGFP and the occurrence of fluorescent inclusions by fluorescence microscopy.

As expected, the respective fluorescence signal was homogenously distributed within the cytoplasm in cells producing the non-fused, soluble mCherry (Figure 2 B, mCherry). Remarkably, cells harboring all components that are needed for split GFP-mediated mCherry immobilization (Figure 2 B, mCherry-GFP1-10) exhibit a strong green fluorescence in the cell poles revealing globular structures that are characteristic for PHB granules [38]. In addition, split GFP signals are mostly co-localized with the red

fluorescence of mCherry (Figure 2B, mCherry-GFP-1-10 overlay). The observation of co-localized green and red fluorescence signals further supports the assumption that mCherry is mainly immobilized at PHB granules *via* successful holo-split GFP assembly. However, the detection of mCherry fluorescence outside of the granule regions indicates that mCherry-GFP-1-10 may also occur as soluble, non-coupled protein in the cytoplasm at a small extent.

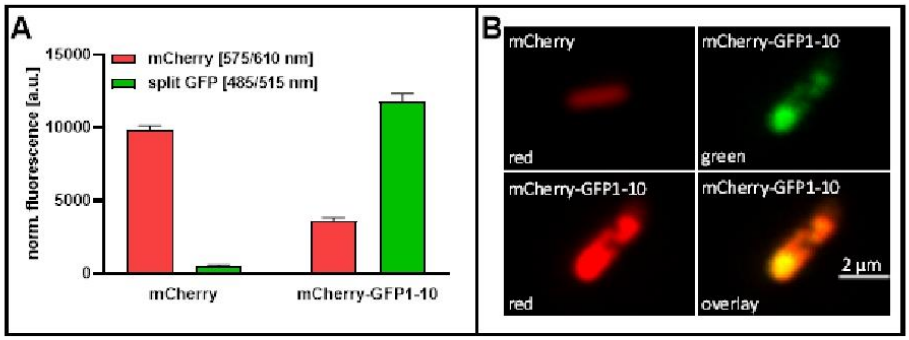

Figure 2. Analysis of split GFP-mediated *in vivo* immobilization of mCherry on PHB granules. *E. coli* Tuner(DE3) cells carrying either plasmid pBBR1mcs_mCherrystop-splitGFP (mCherry) or pBBR1mcs_mCherry-splitGFP (mCherry-GFP1-10) were cultivated for two days in LB medium supplemented with 1% (*w/v*) glucose. After cultivation, (**A**) cells were harvested and disrupted. The fluorescence of mCherry (λ_{ex} = 575 nm, λ_{em} = 610 nm) and split GFP (λ_{ex} = 485 nm, λ_{em} = 515 nm) were measured and normalized to the optical cell density (λ_{abs} = 580 nm). Measurements were performed in triplicates. Error bars indicate the respective standard deviations. (**B**) cells were analyzed by confocal fluorescence microscopy. The localization of mCherry and holo-split-GFP were analyzed using mCherry filter (562-633 nm; λ_{ex} = 561 nm) and GFP filter (490-555 nm; λ_{ex} = 488 nm). The reconstitution of holo-GFP by the assembly of both split GFP-fragments is essential for the development of the green fluorescence signal [18]. Scale bar 2 µm.

While the co-localization of the two fluorescence signals is a strong hint for only short distances between mCherry and holo-split GFP, it is no ultimate proof for direct proximity of the two proteins because the pixel width in the confocal fluorescence microscopy images is 104 nm with an optical resolution of ~200 nm in x- and y-direction and ~500 nm in z-direction. In order to unequivocally proof that immobilized mCherry is localized in very close proximity to holo-split GFP and thus is PHB immobilized in the proposed fashion in *E. coli* cells, FLIM analyses were performed. At a distance of 2-8 nm, Foerster Resonance Energy Transfer (FRET) from holo-split GFP to mCherry should occur, resulting in a significantly shorter fluorescence lifetime of the FRET donor protein compared to the fluorescence lifetime of holo-split GFP that is not fused to mCherry [39–41].

As shown in Figures 3 A and D, the average fluorescence lifetime of holo-split GFP in the presence of mCherry deduced from FLIM analysis is clearly shortened (1.11 ± 0.15 ns) as compared to holo-split GFP without mCherry (1.94 ± 0.13 ns, Figure 4 B) thereby demonstrating the occurrence of FRET between holo-split GFP and mCherry. Based on these two lifetimes, a FRET efficiency (E_{FRET}) of 0.43 can be calculated according to formula 2 (Materials and Methods section). Although the exact value of E_{FRET} is not important for our study, it can be concluded that the FRET process is very strong since typical values with GFP-like fluorescent proteins as FRET donors are in the range of 0.1 to 0.2. Based on the here presented FLIM results, the average distance between holo-split GFP and mCherry is about 5 nm [42].

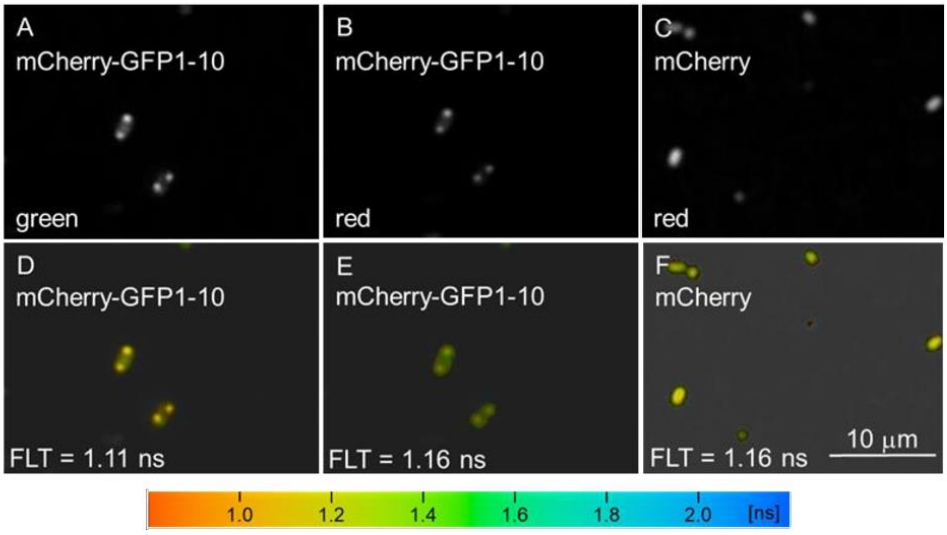

Figure 3. Split GFP-mediated PHB immobilization of mCherry as proven by FLIM-FRET analyses. Two-photon excitation (λ_{exc} = 920 nm) of holo-split GFP formed after co-expression of mCherry fused to GFP1-10 and GFP11 fused to PhaC in *E. coli* (λ_{obs} = 519-549 nm; (**A**) fluorescence intensity image; (**D**) fluorescence lifetime image). Two-photon excitation (λ_{exc} = 1080 nm) of mCherry in *E. coli* cells (same cells as in A,D) after co-expression of mCherry fused to GFP1-10 and GFP11 fused to PhaC (λ_{obs} = 575-700 nm; (**B**) fluorescence intensity image; (**E**) fluorescence lifetime image). Two-photon excitation (λ_{exc} = 1080 nm) of mCherry in *E. coli* cells after co-expression of mCherry (without GFP1-10) and GFP11 fused to PhaC (λ_{obs} = 575-700 nm; (**C**) fluorescence intensity image; (**F**) fluorescence lifetime image).

As expected, the fluorescence lifetime images of mCherry in *E. coli* expressing either mCherry-GFP1-10 (Figure 3 B and E) or mCherry (Figure 3 C and F) reveal a short fluorescence lifetime (1.16 ns) similar to that of mCherry described in literature (1.3–1.5 ns [43,44]). One has to remark that the fluorescence lifetimes for both holo-split GFP and mCherry determined in the bacterial cells are slightly shorter

compared to those from literature that have been determined for the purified proteins. This general trend is often observed for fluorescent proteins in bacterial and mammalian cells, which is attributed to differences between *in vitro* and *in vivo* measurements, including the refractive index, viscosity, and temperature [43,45,46]. In addition, GFP and mCherry have a strong spectral overlap resulting in a non-zero probability for reverse FRET process from mCherry to holo-split GFP [42]. This (often neglected) process would decrease the measured mCherry fluorescence lifetime, if the distance between the two chromophores is in the range of 3-4 nm. Taken together, the results derived from these initial PHB immobilization studies using mCherry as a proof-of-concept POI clearly demonstrate the applicability of split GFP as a novel linker-sensor system for *in vivo* POI immobilization.

2.3 The split GFP linker-sensor system is applicable for in vivo immobilization of different target proteins

To demonstrate the applicability of the newly developed split GFP-based immobilization and detection method, we replaced the model protein mCherry with the ester hydrolase LipD from *A. borkumensis*. LipD features a large substrate spectrum and considerable organic solvent tolerance rendering it valuable for numerous biotechnological applications, including the hydrolysis of water-insoluble building blocks of the chemical industry [47]. Since enzymatic catalysis often proceeds under challenging non-natural *in vitro* conditions, such as the presence of water-miscible organic solvents, enzyme immobilization on a surface might be desirable for enhanced stabilization and reusability. To analyze if the split GFP-based *in vivo* immobilization strategy is applicable for this enzyme, the corresponding expression plasmid pBBR1mcs_LipD-splitGFP was constructed and subsequently transferred to *E. coli* Tuner(DE3). After the cultivation, cells were disrupted and split GFP fluorescence as well as ester hydrolase activity towards 4-nitrophenyl butyrate (*p*NPB) as substrate were measured in the crude cell extracts (Figure 4 A).

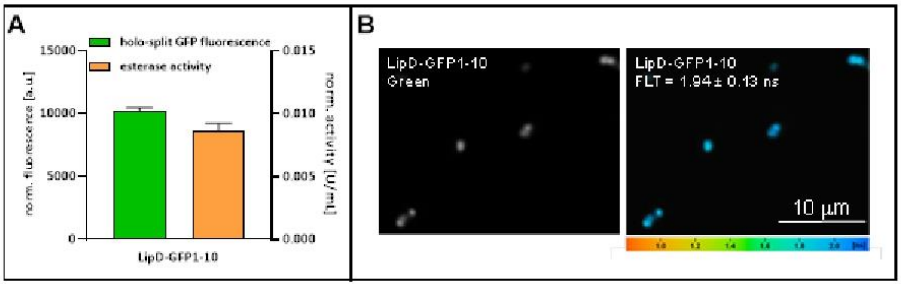

Figure 4. Analysis of *in vivo* immobilization of LipD on PHB granules. *E. coli* Tuner(DE3) carrying plasmid pBBR1mcs_LipD-splitGFP was cultivated for 2 days in LB medium supplemented with 1% (*w/v*) glucose. **A** After cultivation, cells were harvested and disrupted. The holo-split GFP fluorescence (λ_{ex} = 485 nm, λ_{em} = 515 nm) and LipD activity (λ_{abs} = 410 nm) were measured and normalized to the optical cell density (λ_{abs} = 580 nm) and corresponding background activity of *E. coli* Tuner(DE3) control extracts. Measurements were performed in triplicates. Error bars indicate the respective standard deviations. **B** Two-photon excitation (λ_{exc} = 920 nm) of holo-GFP formed after co-expression of LipD fused to GFP1-10, and GFP11 fused to PhaC in *E. coli* (λ_{obs} = 519-549 nm; left: fluorescence intensity image; right: fluorescence lifetime image).

As expected, holo-split GFP fluorescence and thus successful immobilization could also be detected when LipD was used as target protein. Moreover, PHB-immobilized LipD showed specific lipolytic activity, demonstrating that LipD remains active despite immobilization. FLIM analyses were carried out also with these cells to determine the fluorescence lifetime of holo-split GFP in a FRET-donor only situation (Figure 4 B) compared to the holo-split GFP/mCherry FRET system described above (Figure 4 D). The intrinsic, unperturbed fluorescence lifetime of holo-split GFP was 1.94 + 0.13 ns. This compares well with literature values (1.6-2.5 ns [48,49]) and confirms on the other hand the presence of mCherry-dependent FRET in the previously described experiment. It is worth mentioning that the corresponding green fluorescence signals were likewise detected in the cell poles of *E. coli*, reflecting a comparable localization of PHB-immobilized LipD. Thus, it can finally be concluded, that the here presented split GFP technology can be used as a broadly applicable linker-sensor system for *in vivo* immobilization of different target proteins.

3. Conclusions

In this study, we developed a new split GFP application for visualizable *in vivo* protein immobilization using PHB granules as biogenic carrier material. Fluorescence measurements as well as confocal fluorescent microscopy and FLIM analysis demonstrated successful coupling of GFP1-10 and GFP11, which facilitates the formation of POI-decorated PHB granules at the poles of *E. coli* cells. The novel

split GFP linker-sensor technology can be transferred to other POI as demonstrated for the esterase LipD from *A. borkumensis*.

In contrast to other linker systems, such as SpyTag/SpyCatcher [15], which is already established for the *in vivo* display of target proteins on the PHB surface [17], based on a covalent linkage of the two protein partner, the split GFP system offers the unique property to directly "**sense**" the coupling process. This approach thus allows for the first time to optimize *in vivo* POI immobilization in a process engineering approach by comparing various parameters including different carrier materials and anchor proteins as well as conditions for the optimal production of functionalized biomaterials in different production hosts. Moreover, the application of alternative split fluorescent proteins such as split eYFP and split CFP [50] may offer the possibility of co-immobilizing multi-enzyme complexes on the granule surface and to reconstitute their distribution in future studies.

4. Materials and Methods

4.1 Bacterial strains and cultivation conditions

All strains used in this study are listed in Supplementary Table S1. *Escherichia coli* strain DH5α [51] was used for plasmid cloning and *E. coli* strain Tuner(DE3) (Novagen) was applied for recombinant protein production and PHB biosynthesis. Cells were cultivated in LB medium (Luria/Miller, Carl Roth: 10 g/L tryptone, 5 g/L yeast extract, 10 g/L sodium chloride) or on LB agar plates containing 1.5% agar (*w/v*, Bacto agar, Difco) overnight at 37°C. Kanamycin was added to a final concentration of 50 µg/mL to select positive transformants. For expression experiments, LB medium was supplemented with 1% (*w/v*) glucose and cells were incubated for 48 h at 130 rpm and 30°C after induction with 100 µM IPTG (isopropyl-β-D-thiogalactopyranoside).

4.2 Construction of expression vectors

All oligonucleotide primers and plasmids used in this study are listed in Supplementary Table S2. The backbone of the expression vectors based on the pBBR1mcs vector [31]. The insert represents a synthetic DNA fragment (shown in the Supplementary Material) obtained from TwistBioscience and flanked by appropriate restriction endonuclease recognition sequences (*Bgl*II/*Xho*I). The origin of the individual gene fragments is listed below. The *lacI*^{q} gene including the ribosome binding site (RBS), promoter sequence as well as P_{tac} promoter and LacO operator region were originated from a pVLT33 expression vector. The *mCherry* gene with a C-terminal thrombin recognition site [52] was directly fused

289 to the 5`-end of the *gfp1-10* gene [18]. For PHB biosynthesis the genes for PhaC (RCAP_rcc00746),
290 PhaA3 (RCAP_rcc00518) and PhaB1 (RCAP_rcc03179) were used from *Rhodobacter capsulatus*
291 SB1003 [32,33] placed under the control of the constitutive P_{aphII} promoter [34]. Here, the corresponding
292 RBS were applied as described previously [53]. Moreover, the *gfp11* gene [18] was fused to the 5`-
293 terminus of the *phaC* gene.
294 For the construction, the *Bgl*II/*Xho*I hydrolyzed DNA fragment was inserted into likewise hydrolyzed
295 pBBR1mcs vector. The gene of interest could be exchanged using the inserted restriction endonuclease
296 recognition sequences *Nde*I and *Hind*III. For this, the *mCherry* gene was amplified *via* PCR using the
297 vector pBBR1mcs_mCherry-splitGFP as template, introducing a stop codon with the respective primers
298 1 and 2. Moreover, the *lipD* gene was also amplified *via* PCR using the vector pET22b_LipD [47] as
299 template, introducing *Nde*I and *Hind*III sites at the respective 5'- and 3' ends with the primers 3 and 4.
300 The created fragments were digested using the respective restriction enzymes and ligated with a
301 corresponding pBBR1mcs_splitGFP backbone to construct vectors pBBR1mcs_mCherrystop-splitGFP
302 and pBBR1mcs_LipD-splitGFP. The relevant nucleotide sequences of all constructs were confirmed by
303 Sanger sequencing (LGC Genomics GmbH, Berlin, Germany).
304
305 *4.3 Measurement of split GFP and mCherry fluorescence*
306 After cultivation, cells corresponding to an $OD_{580\,nm}$ = 10 were harvested, resuspended in 1xPBS buffer
307 and disrupted using an Emulsiflex cell disrupter The fluorescence was measured with 1:10 diluted
308 samples (in 1xPBS buffer) in a 96-well microtiter plate (Greiner Bio-One GmbH, Frickenhausen,
309 Germany) and analyzed regarding their respective split GFP fluorescence (λ_{ex} = 485 nm, λ_{em} = 515 nm)
310 or mCherry fluorescence (λ_{ex} = 575 nm, λ_{em} = 610 nm) using a microplate reader (Infinite® M1000 Pro,
311 Tecan Group LTD-. Maennedorf, Switzerland).
312
313 *4.4 Fluorescence microscopy and Fluorescence Lifetime Imaging (FLIM)*
314 Confocal fluorescence microscopy was performed on a LSM880 laser-scanning fluorescence
315 microscope (Zeiss, Jena, Germany) with a water immersion lens (NA 1.0) and GAsP hybrid detectors.
316 Excitation of holo-GFP and mCherry was performed with a 488 nm Ar^+-laser (holo-GFP) and a solid
317 state 561 nm DPPS laser (mCherry), respectively, where emission filters were set to 490 – 555 nm
318 (holo-GFP) and 562 – 633 nm (mCherry). Measurements were performed at 307 K.

Two-photon excitation Fluorescence Lifetime Imaging was realized with a setup described recently [54]. The heart of the setup is a LSM880 laser-scanning fluorescence microscope (Zeiss, Jena, Germany) equipped with a 20x water immersion objective (NA 1.0, WD 2.1 mm; XYZ, Zeiss). A tunable laser with near-infrared emission (InSight X3, Newport Spectra Physics, Darmstadt, output power 2.3 W at 920 nm and 2.5 W at 1080 nm, respectively), whose output is pulsed (120 fs) with a repetition frequency of 80 MHz. Fluorescence light was detected very near to the objective in descanned fashion. Fluorescence of holo-split GFP and mCherry, respectively, was separated from scattered excitation and spectrally distinguishable autofluorescence light by using suitable bandpass filters (bp534: 519 – 549 nm (Omega Optical, Brattleboro, VT, USA) and alp575: > 575 nm (Omega Optical, Brattleboro, VT, USA)) in addition to a near-infrared blocking filter (Omega Optical, Brattleboro, VT, USA). Fluorescence photons were detected with a GaAsP hybrid photodetector (HPM-100-40, Becker & Hickl, Berlin, Germany). TCSPC electronics (SPC-152; Becker & Hickl, Berlin, Germany) and acquisition software were used for FLIM as previously described [55,56].

Fluorescence lifetime images were generated using SPCImage 8.4 (Becker & Hickl, Berlin, Germany). We summed fluorescence intensity decays (FIDs) over nine pixels and assigned the resulting value to the central pixel (bin factor 1). Fluorescence decays were fitted with bi-exponential functions [41,54,57], and the average fluorescence lifetime (τ_{ave})

$$(1)\quad \tau_{ave} = \frac{a_1 \cdot \tau_1 + a_2 \cdot \tau_2}{a_1 + a_2}$$

was used to represent the fluorescence decays of mCherry and holo-split GFP in the presence of mCherry qualitatively (τ_i = lifetime of the i^{th} exponential component; a_i = respective amplitude). For holo-split GFP in the absence of mCherry a mono-exponential fit delivered satisfactorily fit results and was used for further analysis.

The probability of an excited donor molecule to deactivate *via* FRET, i.e., cause an acceptor molecule to be excited instead of deactivation *via* donor fluorescence or internal conversion, can be calculated as [39,40]:

$$(2)\quad E_{FRET} = 1 - \frac{\tau_{DA}}{\tau_D}$$

where τ_{DA} and τ_D are the donor fluorescence lifetime in the presence or absence of the acceptor, respectively. We excited holo-split GFP with a femtosecond pulsed, near-infrared laser (920 nm) and

detected the green fluorescence in a time-resolved manner relying on a time-correlated single photon counting (TCSPC) detection [58,59] setup connected to our fluorescence microscope [54,60].

4.5 Determination of LipD activity

After cultivation of PHB forming *E. coli* Tuner(DE3) and *E. coli* Tuner(DE3) wildtype, cells corresponding to an $OD_{580\ nm}$ = 10 were harvested, resuspended in 1xPBS buffer and disrupted using an Emulsiflex cell disrupter. The LipD activity was confirmed as described previously [61] using 4-nitrophenyl butyrate (*p*NPB) as substrate [47]. Here, 10 µL of the respective samples were diluted in 190 µL substrate solution (20 mM 4-nitrophenyl butyrate solved in acetonitrile and 1:20 diluted in 100 mM KPi buffer (pH 7.0)) in a 96-well microtiter plate (Greiner Bio-One GmbH, Frickenhausen, Germany). The enzyme activity was determined by measuring the product specific absorption (λ_{abs} = 410 nm) every 30 sec for 30 min using a preheated (30°C) microplate reader (Infinite® M1000 Pro, Tecan Group LTD-. Maennedorf, Switzerland).

Author Contributions

O.K. Investigation, Methodology, Data curation, Writing – original draft. **P.L.** Investigation, Methodology, Data curation, Writing – original draft. **T.G.** Investigation, Methodology, Data curation. **F.K.** Methodology. **A.K.** Conceptualization, Writing – review & editing. **S.T.** Methodology, Writing – review & editing. **K.-E. J.** Conceptualization, Writing – review & editing. **T.D.** Conceptualization, Writing – review & editing, Supervision. All authors have read and agreed to the published version of the manuscript.

Conflicts of Interest

The authors declare no competing financial interests.

ACKNOWLEDGMENTS

This work was supported by grants of the European Regional Development Fund (ERDF: 34.EFRE-0300096 and 34.EFRE-0300097) within the project CLIB-Kompetenzzentrum Biotechnologie (CKB).

REFERENCES

1. Singh, R.; Kumar, M.; Mittal, A.; Mehta, P.K. Microbial Enzymes: Industrial Progress in 21st Century. *3 Biotech* **2016**, *6*, 174, doi:10.1007/s13205-016-0485-8.
2. Sheldon, R.A.; Woodley, J.M. Role of Biocatalysis in Sustainable Chemistry. *Chem Rev* **2018**, *118*, 801–838, doi:10.1021/acs.chemrev.7b00203.
3. Ölçücü, G.; Klaus, O.; Jaeger, K.-E.; Drepper, T.; Krauss, U. Emerging Solutions for *in Vivo* Biocatalyst Immobilization: Tailor-Made Catalysts for Industrial Biocatalysis. *ACS Sustain Chem Eng* **2021**, *9*, 8919–8945, doi:10.1021/acssuschemeng.1c02045.
4. DiCosimo, R.; McAuliffe, J.; Poulose, A.J.; Bohlmann, G. Industrial Use of Immobilized Enzymes. *Chem Soc Rev* **2013**, *42*, 6437–6474, doi:10.1039/c3cs35506c.

5. Rodriguez-Abetxuko, A.; Sánchez-deAlcázar, D.; Muñumer, P.; Beloqui, A. Tunable Polymeric Scaffolds for Enzyme Immobilization. *Front Bioeng Biotechnol* **2020**, *8*, doi:10.3389/fbioe.2020.00830.

6. Balcão, V.M.; Vila, M.M.D.C. Structural and Functional Stabilization of Protein Entities: State-of-the-Art. *Adv Drug Deliv Rev* **2015**, *93*, 25–41, doi:10.1016/j.addr.2014.10.005.

7. Wong, J.X.; Ogura, K.; Chen, S.; Rehm, B.H.A. Bioengineered Polyhydroxyalkanoates as Immobilized Enzyme Scaffolds for Industrial Applications. *Front Bioeng Biotechnol* **2020**, *8*, doi:10.3389/fbioe.2020.00156.

8. McAdam, B.; Brennan Fournet, M.; McDonald, P.; Mojicevic, M. Production of Polyhydroxybutyrate (PHB) and Factors Impacting Its Chemical and Mechanical Characteristics. *Polymers (Basel)* **2020**, *12*, 2908, doi:10.3390/polym12122908.

9. Merrick, J.M.; Doudoroff, M. Enzymatic Synthesis of Poly-β-Hydroxybutyric Acid in Bacteria. *Nature* **1961**, *189*, 890–892, doi:10.1038/189890a0.

10. Peoples, O.P.; Sinskey, A.J. Poly-P-Hydroxybutyrate (PHB) Biosynthesis in *Alcaligenes eutrophus* H16 idenfification and characterization of the PHB polymerase gene (PhbC). **1989**, *J Biol Chem* Vol. 264,

11. Jendrossek, D.; Pfeiffer, D. New Insights in the Formation of Polyhydroxyalkanoate Granules (Carbonosomes) and Novel Functions of Poly(3-Hydroxybutyrate). *Environ Microbiol* **2014**, *16*, 2357–2373, doi:10.1111/1462-2920.12356.

12. Brown, B.; Immethun, C.; Wilkins, M.; Saha, R. Biotechnical Applications of Phasins: Small Proteins with Large Potential. *Renewable Sustainable Energy Rev* **2022**, *158*, 112129, doi:10.1016/j.rser.2022.112129.

13. Peters, V.; Rehm, B.H.A. In Vivo Enzyme Immobilization by Use of Engineered Polyhydroxyalkanoate Synthase. *Appl Environ Microbiol* **2006**, *72*, 1777–1783, doi:10.1128/AEM.72.3.1777-1783.2006.

14. Hooks, D.; Venning-Slater, M.; Du, J.; Rehm, B. Polyhydroyxalkanoate Synthase Fusions as a Strategy for Oriented Enzyme Immobilisation. *Molecules* **2014**, *19*, 8629–8643, doi:10.3390/molecules19068629.

15. Zakeri, B.; Fierer, J.O.; Celik, E.; Chittock, E.C.; Schwarz-Linek, U.; Moy, V.T.; Howarth, M. Peptide Tag Forming a Rapid Covalent Bond to a Protein, through Engineering a Bacterial Adhesin. *PNAS* **2012**, *109*, doi:10.1073/pnas.1115485109.

16. Wong, J.X.; Rehm, B.H.A. Design of Modular Polyhydroxyalkanoate Scaffolds for Protein Immobilization by Directed Ligation. *Biomacromolecules* **2018**, *19*, 4098–4112, doi:10.1021/acs.biomac.8b01093.

17. Wong, J.X.; Gonzalez-Miro, M.; Sutherland-Smith, A.J.; Rehm, B.H.A. Covalent Functionalization of Bioengineered Polyhydroxyalkanoate Spheres Directed by Specific Protein-Protein Interactions. *Front Bioeng Biotechnol* **2020**, *8*, doi:10.3389/fbioe.2020.00044.

18. Cabantous, S.; Terwilliger, T.C.; Waldo, G.S. Protein Tagging and Detection with Engineered Self-Assembling Fragments of Green Fluorescent Protein. *Nat Biotechnol* **2005**, *23*, 102–107, doi:10.1038/nbt1044.

19. Barondeau, D.P.; Putnam, C.D.; Kassmann, C.J.; Tainer, J.A.; Getzoff, E.D. Mechanism and Energetics of Green Fluorescent Protein Chromophore Synthesis Revealed by Trapped Intermediate Structures. *PNAS* **2003**, *100*, 12111–12116, doi:10.1073/pnas.2133463100.

20. Cabantous, S.; Waldo, G.S. In Vivo and in Vitro Protein Solubility Assays Using Split GFP. *Nat Methods* **2006**, *3*, 845–854, doi:10.1038/nmeth932.

21. Santos-Aberturas, J.; Dörr, M.; Waldo, G.S.; Bornscheuer, U.T. In-Depth High-Throughput Screening of Protein Engineering Libraries by Split GFP Direct Crude Cell Extract Data Normalization. *Chem Biol* **2015**, *22*, 1406–1414, doi:10.1016/j.chembiol.2015.08.014.

22. Knapp, A.; Ripphahn, M.; Volkenborn, K.; Skoczinski, P.; Jaeger, K.-E. Activity-Independent Screening of Secreted Proteins Using Split GFP. *J Biotechnol* **2017**, *258*, 110–116, doi:10.1016/j.jbiotec.2017.05.024.

23. Lenz, P.; Hilgers, F.; Burmeister, A.; Zimmermann, L.; Volkenborn, K.; Grünberger, A.; Kohlheyer, D.; Drepper, T.; Jaeger, K.-E.; Knapp, A. The iSplit GFP Assay Detects Intracellular Recombinant Proteins in *Bacillus subtilis*. *Microb Cell Fact* **2021**, *20*, 174, doi:10.1186/s12934-021-01663-7.

24. Bakkes, P.J.; Lenz, P.; Müller, C.; Bida, A.; Dohmen-Olma, D.; Knapp, A.; Oldiges, M.; Jaeger, K.-E.; Freudl, R. Biosensor-Based Optimization of Cutinase Secretion by *Corynebacterium glutamicum*. *Front Microbiol* **2021**, *12*, doi:10.3389/fmicb.2021.750150.

25. Müller, C.; Bakkes, P.J.; Lenz, P.; Waffenschmidt, V.; Helleckes, L.M.; Jaeger, K.-E.; Wiechert, W.; Knapp, A.; Freudl, R.; Oldiges, M. Accelerated Strain Construction and Characterization of *C. glutamicum* Protein Secretion by Laboratory Automation. *Appl Microbiol Biotechnol* **2022**, *106*, 4481–4497, doi:10.1007/s00253-022-12017-7.

26. Püllmann, P.; Knorrscheidt, A.; Münch, J.; Palme, P.R.; Hoehenwarter, W.; Marillonnet, S.; Alcalde, M.; Westermann, B.; Weissenborn, M.J. A Modular Two Yeast Species Secretion System for the Production and Preparative Application of Unspecific Peroxygenases. *Commun Biol* **2021**, *4*, 562, doi:10.1038/s42003-021-02076-3.

27. Blakeley, B.D.; Chapman, A.M.; McNaughton, B.R. Split-Superpositive GFP Reassembly Is a Fast, Efficient, and Robust Method for Detecting Protein–Protein Interactions in Vivo. *Mol Biosyst* **2012**, *8*, 2036, doi:10.1039/c2mb25130b.

28. Bader, G.; Enkler, L.; Araiso, Y.; Hemmerle, M.; Binko, K.; Baranowska, E.; de Craene, J.-O.; Ruer-Laventie, J.; Pieters, J.; Tribouillard-Tanvier, D.; et al. Assigning Mitochondrial Localization of Dual Localized Proteins Using a Yeast Bi-Genomic Mitochondrial-Split-GFP. *Elife* **2020**, *9*, doi:10.7554/eLife.56649.

29. Feinberg, E.H.; VanHoven, M.K.; Bendesky, A.; Wang, G.; Fetter, R.D.; Shen, K.; Bargmann, C.I. GFP Reconstitution Across Synaptic Partners (GRASP) Defines Cell Contacts and Synapses in Living Nervous Systems. *Neuron* **2008**, *57*, 353–363, doi:10.1016/j.neuron.2007.11.030.

30. Avilov, S. v.; Moisy, D.; Munier, S.; Schraidt, O.; Naffakh, N.; Cusack, S. Replication-Competent Influenza A Virus That Encodes a Split-Green Fluorescent Protein-Tagged PB2 Polymerase Subunit Allows Live-Cell Imaging of the Virus Life Cycle. *J Virol* **2012**, *86*, 1433–1448, doi:10.1128/JVI.05820-11.

31. Kovach, M.E.; Phillips, R.W.; Elzer, P.H.; Roop, R.M.; Peterson, K.M. PBBR1MCS: A Broad-Host-Range Cloning Vector. *Biotechniques* **1994**, *16*, 800–802.

32. Ulbrich, P.; Pačes, J. Genetic Determination of Polyhydroxyalkanoate Metabolism in *Rhodobacter capsulatus* SB1003 Population Genomics *View Project Bacterial Heavy Metal Resistance View Project*; **2002,**

33. Kobayashi, J.; Kondo, A. Disruption of Poly (3-Hydroxyalkanoate) Depolymerase Gene and Overexpression of Three Poly (3-Hydroxybutyrate) Biosynthetic Genes Improve Poly (3-Hydroxybutyrate) Production from Nitrogen Rich Medium by *Rhodobacter sphaeroides*. *Microb Cell Fact* **2019**, *18*, 40, doi:10.1186/s12934-019-1088-y.

34. Alexeyev, M.F. Three Kanamycin Resistance Gene Cassettes with Different Polylinkers. *Biotechniques* **1995**, *18*, 52, 54, 56.

35. Du, J.; Rehm, B.H.A. Purification of Target Proteins from Intracellular Inclusions Mediated by Intein Cleavable Polyhydroxyalkanoate Synthase Fusions. *Microb Cell Fact* **2017**, *16*, 184, doi:10.1186/s12934-017-0799-1.

36. Wang, Z.; Wu, H.; Chen, J.; Zhang, J.; Yao, Y.; Chen, G.-Q. A Novel Self-Cleaving Phasin Tag for Purification of Recombinant Proteins Based on Hydrophobic Polyhydroxyalkanoate Nanoparticles. *Lab Chip* **2008**, *8*, 1957, doi:10.1039/b807762b.

37. Eikmanns, B.J.; Kleinertz, E.; Liebl, W.; Sahm, H. A Family of *Corynebacterium glutamicum/Escherichia coli* Shuttle Vectors for Cloning, Controlled Gene Expression, and Promoter Probing. *Gene* **1991**, *102*, 93–98, doi:10.1016/0378-1119(91)90545-M.

38. Liu, Y.; Low, Z.J.; Ma, X.; Liang, H.; Sinskey, A.J.; Stephanopoulos, G.; Zhou, K. Using Biopolymer Bodies for Encapsulation of Hydrophobic Products in Bacterium. *Metab Eng* **2020**, *61*, 206–214, doi:10.1016/j.ymben.2020.04.006.

39. Wallrabe, H.; Periasamy, A. Imaging Protein Molecules Using FRET and FLIM Microscopy. *Curr Opin Biotechnol* **2005**, *16*, 19–27, doi:10.1016/j.copbio.2004.12.002.

40. Suhling, K.; Hirvonen, L.M.; Levitt, J.A.; Chung, P.-H.; Tregidgo, C.; le Marois, A.; Rusakov, D.A.; Zheng, K.; Ameer-Beg, S.; Poland, S.; et al. Fluorescence Lifetime Imaging (FLIM): Basic Concepts and Some Recent Developments. *Medical Photonics* **2015**, *27*, 3–40, doi:10.1016/j.medpho.2014.12.001.

41. Stölting, G.; de Oliveira, R.C.; Guzman, R.E.; Miranda-Laferte, E.; Conrad, R.; Jordan, N.; Schmidt, S.; Hendriks, J.; Gensch, T.; Hidalgo, P. Direct Interaction of CaVβ with Actin Up-Regulates L-Type Calcium Currents in HL-1 Cardiomyocytes. *Journal of Biological Chemistry* **2015**, *290*, 4561–4572, doi:10.1074/jbc.M114.573956.

42. Akrap, N.; Seidel, T.; Barisas, B.G. Förster Distances for Fluorescence Resonant Energy Transfer between mCherry and Other Visible Fluorescent Proteins. *Anal Biochem* **2010**, *402*, 105–106, doi:10.1016/j.ab.2010.03.026.

43. Seefeldt, B.; Kasper, R.; Seidel, T.; Tinnefeld, P.; Dietz, K.-J.; Heilemann, M.; Sauer, M. Fluorescent Proteins for Single-Molecule Fluorescence Applications. *J Biophotonics* **2008**, *1*, 74–82, doi:10.1002/jbio.200710024.

44. Intracellular Oxygen Mapping Using a Myoglobin-mCherry Probe with Fluorescence Lifetime Imaging. *J Biomed Opt* **2018**, *23*, 1, doi:10.1117/1.JBO.23.10.107001.

45. Festy, F.; Ameer-Beg, S.M.; Ng, T.; Suhling, K. Imaging Proteins *in vivo* Using Fluorescence Lifetime Microscopy. *Mol Biosyst* **2007**, *3*, 381, doi:10.1039/b617204k.

46. Nakabayashi, T.; Oshita, S.; Sumikawa, R.; Sun, F.; Kinjo, M.; Ohta, N. PH Dependence of the Fluorescence Lifetime of Enhanced Yellow Fluorescent Protein in Solution and Cells. *J Photochem Photobiol A Chem* **2012**, *235*, 65–71, doi:10.1016/j.jphotochem.2012.02.016.

47. Bollinger, A.; Molitor, R.; Thies, S.; Koch, R.; Coscolín, C.; Ferrer, M.; Jaeger, K.-E. Organic-Solvent-Tolerant Carboxylic Ester Hydrolases for Organic Synthesis. *Appl Environ Microbiol* **2020**, *86*, doi:10.1128/AEM.00106-20.

48. Avilov, S. v.; Moisy, D.; Naffakh, N.; Cusack, S. Influenza A Virus Progeny VRNP Trafficking in Live Infected Cells Studied with the Virus-Encoded Fluorescently Tagged PB2 Protein. *Vaccine* **2012**, *30*, 7411–7417, doi:10.1016/j.vaccine.2012.09.077.

49. Köker, T.; Fernandez, A.; Pinaud, F. Characterization of Split Fluorescent Protein Variants and Quantitative Analyses of Their Self-Assembly Process. *Sci Rep* **2018**, *8*, 5344, doi:10.1038/s41598-018-23625-7.

50. Lockard, M.A.; Waldo, G.S. Cyan and Yellow Fluorescent Color Variants of Split Gfp 2012.

51. Hanahan, D. Studies on Transformation of *Escherichia coli* with Plasmids. *J Mol Biol* **1983**, *166*, 557–580, doi:10.1016/S0022-2836(83)80284-8.

52. Potzkei, J.; Kunze, M.; Drepper, T.; Gensch, T.; Jaeger, K.-E.; Büchs, J. Real-Time Determination of Intracellular Oxygen in Bacteria Using a Genetically Encoded FRET-Based Biosensor. *BMC Biol* **2012**, *10*, 28, doi:10.1186/1741-7007-10-28.

53. Troost, K.; Loeschcke, A.; Hilgers, F.; Özgür, A.Y.; Weber, T.M.; Santiago-Schübel, B.; Svensson, V.; Hage-Hülsmann, J.; Habash, S.S.; Grundler, F.M.W.; et al. Engineered *Rhodobacter capsulatus* as a Phototrophic Platform Organism for the Synthesis of Plant Sesquiterpenoids. *Front Microbiol* **2019**, *10*, doi:10.3389/fmicb.2019.01998.

54. Engels, M.; Kalia, M.; Rahmati, S.; Petersilie, L.; Kovermann, P.; van Putten, M.J.A.M.; Rose, C.R.; Meijer, H.G.E.; Gensch, T.; Fahlke, C. Glial Chloride Homeostasis Under Transient Ischemic Stress. *Front Cell Neurosci* **2021**, *15*, doi:10.3389/fncel.2021.735300.

55. Kaneko, H.; Putzier, I.; Frings, S.; Gensch, T. Determination of Intracellular Chloride Concentration in Dorsal Root Ganglion Neurons by Fluorescence Lifetime Imaging. In; 2002; pp. 167–189.

56. Untiet, V.; Kovermann, P.; Gerkau, N.J.; Gensch, T.; Rose, C.R.; Fahlke, C. Glutamate Transporter-Associated Anion Channels Adjust Intracellular Chloride Concentrations during Glial Maturation. *Glia* **2017**, *65*, 388–400, doi:10.1002/glia.23098.

57. Kaneko, H. Chloride Accumulation in Mammalian Olfactory Sensory Neurons. *Journal of Neuroscience* **2004**, *24*, 7931–7938, doi:10.1523/JNEUROSCI.2115-04.2004.

58. Becker, W. *Advanced Time-Correlated Single Photon Counting Techniques*; Castleman, A.W., Toennies, J.P., Zinth, W., Eds.; Springer Berlin Heidelberg: Berlin, Heidelberg, 2005; Vol. 81; ISBN 978-3-540-26047-9.

59. *Advanced Time-Correlated Single Photon Counting Applications*; Becker, W., Ed.; Springer International Publishing: Cham, 2015; Vol. 111; ISBN 978-3-319-14928-8.

60. Gensch, T.; Untiet, V.; Franzen, A.; Kovermann, P.; Fahlke, C. Determination of Intracellular Chloride Concentrations by Fluorescence Lifetime Imaging. In; 2015; pp. 189–211.

548 61. Nolasco-Soria, H.; Moyano-López, F.; Vega-Villasante, F.; del Monte-Martínez, A.; Espinosa-
549 Chaurand, D.; Gisbert, E.; Nolasco-Alzaga, H.R. Lipase and Phospholipase Activity Methods for
550 Marine Organisms. In; 2018; pp. 139–167.

551

Supplementary Material

Split GFP as a new system for facilitating and sensing *in vivo* protein immobilization

Oliver Klaus [1,#], Patrick Lenz [1,#], Thomas Gensch [2], Fabienne Knapp [1], Andreas Knapp [1,3], Stephan Thies [1], Karl-Erich Jaeger [1,4], Thomas Drepper [1*]

[1] Institute of Molecular Enzyme Technology, Heinrich Heine University Düsseldorf at Forschungszentrum Jülich, Jülich, Germany
[2] Institute of Biological Information Processing (IBI-1: Molecular and Cellular Physiology), Forschungszentrum Jülich GmbH, Jülich, Germany
[3] present address: Castrol Germany GmbH, Mönchengladbach, Germany
[4] Institute of Bio- and Geosciences IBG-1: Biotechnology, Forschungszentrum Jülich GmbH, Jülich, Germany

* Correspondence: t.drepper@fz-juelich.de
#These authors contributed equally to this work.

Table of contents

Table S1. Bacterial strains used in this study.

Name	Characteristics	Reference
Escherichia coli DH5α	*F⁻Φ80lacZΔM15 Δ(lacZYA-argF) U169 recA1 endA1 hsdR17 phoA supE44 thi-1 gyrA96 relA1 deoR*	[1]
Escherichia coli Tuner(DE3)	*F⁻ompT hsdS$_B$ (r_B^- m_B^-) gal dcm lacY1(DE3)*	Novagen, Merck KGaA

Table S2. Oligonucleotides and plasmids used in this study. Endonuclease restriction sites are underlined.

Oligonucleotides			
Name		Application	Nucleotide sequence (5`->3`)
1	HindIII_mCherrystop_fw	(PCR) amplification of *mCherry* and introducing a stop codon	ATATAAGCTTTTACTTGTACAGCTCGTCCATGCC GCCGGTG
2	NdeI_mCherry_rev	(PCR) amplification of *mCherry*	ATATCATATGGTGAGCAAGGGCGAGGAG
3	NdeI_LipD_fw	(PCR) amplification of *lipD* (pET22b_LipD)[2]	GGAGATATACATATGAGCCTTCAAGCCC
4	HindIII_LipD_rev	(PCR) amplification of *lipD* (pET22b_LipD)[2]	ATATAAAGCTTGTGGTGGTGGTGGTGGTGC
Plasmids			
Name		Characteristics	Reference
pBBR1mcs_mCherry-splitGFP		pBBR1mcs (*rep, mob, Cm^R*), pET22b (*mcs, pelB*), pBSL15 (*aph*II) orientation, *mCherry*, *gfp1-10* (first 644 bp of *gfp*), *gfp11* (last 50 bp of *gfp*) *phaC, phaA3, phaB1* (*R. capsulatus*)	This work
pBBR1mcs_mCherrystop-splitGFP		pBBR1mcs (*rep, mob, Cm^R*), pET22b (*mcs, pelB*), pBSL15 (*aph*II) orientation, *mCherry*, *gfp1-10* (644 bp of *gfp*), *gfp11* (last 50 bp of *gfp*) *phaC, phaA3, phaB1* (*R. capsulatus*)	This work
pBBR1mcs_LipD-splitGFP		pBBR1mcs (*rep, mob, Cm^R*), pET22b (*mcs, pelB*), pBSL15 (*aph*II) orientation, *lipD* (*Alcanivorax borkumensis*), *gfp1-10* (644 bp of *gfp*), *gfp11* (last 50 bp of *gfp*), *phaC, phaA3, phaB1* (*R. capsulatus*)	This work

DNA sequence of the split GFP immobilization box containing all genetic elements and genes necessary for the expression of a gene of interest (here mCherry; can be substituted by using the respective *Nde*I and *Hin*dIII site), the split GFP linker-sensor system and PHB biosynthesis.

lacI

ACTGCCCGCTTTCCAGTCGGGAAACCTGTCGTGCCAGCTGCATTAATGAATCGGCCAA
CGCGCGGGGAGAGGCGGTTTGCGTATTGGGCGCCAGGGTGGTTTTTCTTTTCACCAGT
GAGACGGGCAACAGCTGATTGCCCTTCACCGCCTGGCCCTGAGAGAGTTGCAGCAAGC
GGTCCACGCTGGTTTGCCCCAGCAGGCGAAAATCCTGTTTGATGGTGGTTAACGGCGG
GATATAACATGAGCTGTCTTCGGTATCGTCGTATCCCACTACCGAGATATCCGCACCAA
CGCGCAGCCCGGACTCGGTAATGGCGCGCATTGCGCCCAGCGCCATCTGATCGTTGG
CAACCAGCATCGCAGTGGGAACGATGCCCTCATTCAGCATTTGCATGGTTTGTTGAAAA
CCGGACATGGCACTCCAGTCGCCTTCCCGTTCCGCTATCGGCTGAATTTGATTGCGAGT
GAGATATTTATGCCAGCCAGCCAGACGCAGACGCGCCGAGACAGAACTTAATGGGCCC
GCTAACAGCGCGATTTGCTGGTGACCCAATGCGACCAGATGCTCCACGCCCAGTCGCG
TACCGTCTTCATGGGAGAAAATAATACTGTTGATGGGTGTCTGGTCAGAGACATCAAGA
AATAACGCCGGAACATTAGTGCAGGCAGCTTCCACAGCAATGGCATCCTGGTCATCCAG
CGGATAGTTAATGATCAGCCCACTGACGCGTTGCGCGAGAAGATTGTGCACCGCCGCT
TTACAGGCTTCGACGCCGCTTCGTTCTACCATCGACACCACCACGCTGGCACCCAGTTG
ATCGGCGCGAGATTTAATCGCCGCGACAATTTGCGACGGCGCGTGCAGGGCCAGACTG
GAGGTGGCAACGCCAATCAGCAACGACTGTTTGCCCGCCAGTTGTTGTGCCACGCGGT
TGGGAATGTAATTCAGCTCCGCCATCGCCGCTTCCACTTTTTCCCGCGTTTTCGCAGAA
ACGTGGCTGGCCTGGTTCACCACGCGGGAAACGGTCTGATAAGAGACACCGGCATACT
CTGCGACATCGTATAACGTTACTGGTTTCA**CAT**TCACCACCCTGAATTGACTCTCTTCCG
GGCGCTATCATGCCATACCGCGAAAGGTTTTGCACCATTCGATGGTGTCAACGTAAATG
CCGCTTCGCCTTCGCGCGCGAATTGCAAGCTGATCCGGGCTTATCGACTGCACGGTGC
ACCAATGCTTCTGGCGTCAGGCAGCCATCGGAAGCTGTGGTATGGCTGTGCAGGTCGT
AAATCACTGCATAATTCGTGTCGCTCAAGGCGCACTCCCGTTCTGGATAATGTTTTTTGC
GCCGACATCATAACGGTTCTGGCAAATATTCTGAAATGAGCTGTTGACAATTAATCATCG

LacO operator NdeI

GCTCGTATAATGTGTGG**AATTGTGAGCGGATAACAATT**TCACAAGGAGGTATTTTCAT

Start *mCherry>*

ATGGTGAGCAAGGGCGAGGAGGATAACATGGCCATCATCAAGGAGTTCATGCGCTTCA
AGGTGCACATGGAGGGCTCCGTGAACGGCCACGAGTTCGAGATCGAGGGCGAGGGCG
AGGGCCGCCCCTACGAGGGCACCCAGACCGCCAAGCTGAAGGTGACCAAGGGTGGCC
CCCTGCCCTTCGCCTGGGACATCCTGTCCCCTCAGTTCATGTACGGCTCCAAGGCGTA
CGTGAAGCACCCCGCCGACATCCCCGACTACTTGAAGCTGTCCTTCCCCGAGGGCTTC
AAGTGGGAGCGCGTGATGAACTTCGAGGACGGCGGCGTGGTGACCGTGACCCAGGAC
TCCTCCTTGCAGGACGGCGAGTTCATCTACAAGGTGAAGCTGCGCGGCACCAACTTCC
CCTCCGACGGCCCCGTAATGCAGAAGAAGACGATGGGCTGGGAGGCGTCCTCCGAGC
GGATGTACCCCGAGGACGGCGCCCTGAAGGGCGAGATCAAGCAGAGGCTGAAGCTGA
AGGACGGCGGCCACTACGACGCTGAGGTCAAGACCACCTACAAGGCCAAGAAGCCCG

TGCAGCTGCCCGGCGCCTACAACGTCAACATCAAGTTGGACATCACCTCCCACAACGA
GGACTACACCATCGTGGAACAGTACGAACGCGCCGAGGGCCGCCACTCCACCGGCGG
CATGGACGAGCTGTACAAG

HindIII **thrombine linker**

AAGCTT**GCGGGCCTGGTGCCGCGCGGCAGCGGCGCC**

Start *gfp1-10*

ATGAGCAAAGGAGAAGAACTTTTCACTGGAGTTGTCCCAATTCTTGTTGAATTAGATGGT
GATGTTAATGGGCACAAATTTTCTGTCCGTGGAGAGGGTGAAGGTGATGCTACAATTGG
AAAACTCACCCTTAAATTTATTTGCACTACTGGAAAACTACCTGTTCCATGGCCAACACT
TGTCACTACTCTGACCTATGGTGTTCAATGCTTTTCCCGTTATCCGGATCACATGAAACG
GCATGACTTTTTCAAGAGTGCCATGCCCGAAGGTTATGTACAGGAACGCACTATATCTTT
CAAAGATGACGGGAAATACAAGACGCGTGCTGTTGTCAAGTTTGAAGGTGATACCCTTG
TTAATCGTATCGAGTTAAAAGGTACGGATTTTAAAGAAGATGGAAACATTCTCGGACACA
AACTCGAGTACAACTTTAACTCACACAATGTATACATCACGGCAGACAAACAAAAGAATG
GAATCAAAGCTAACTTCACGGTTCGCCACAACGTTGAAGATGGTTCCGTTCAACTAGCA
GACCATTATCAACAAAATACTCCAATTGGCGATGGCCCTGTCCTTTTACCAGACAACCAT
TACCTGTCGACACAAACGGTCCTTTCGAAAGATCCCAACGAAAAG**TGA**CGAGCTCGTTC
ACGCTGCCGCAAGCACTCAGGGCGCAAGGGCTGCTAAAGGAAGCGGAACACGTAGAA
AGCCAGTCCGCAGAAACGGTGCTGACCCCGGATGAATGTCAGCTACTGGGCTATCTGG
ACAAGGGAAAACGCAAGCGCAAAGAGAAAGCAGGTAGCTTGCAGTGGGCTTACATGGC
GATA

P_{aphII} promoter

GCTAGACTGGGCGGTTTTATGGACAGCAAGCGAACCGGAATTGCCAGCTGGGGCGCC
CTCTGGTAAGGTTGGGAAGCCCTGCAAAGTAAACTGGATGGCTTTCTTGCCGCCAAGG
ATCTGATGGCGCAGGGGATCAAGATCAGATCAAGAGACAGGATGAGGATCGTTTCGC

Start *aphII*

ATGATTGAACAAGATGGATTGCACGCAGGTTCTCCGGCCGCTTGGGTGGAGAGGCTAT
TCGGCTATGACTGGGCACAACAGACAATCGGCTGCTCTGATGCCGCCGTGTTCCGGCT
GTCAGCGCAGGGGCGCCCGGTTCTTTTTGTCAAGACCGACCTGTCCGGTGCCCTGAAT
GAACTCCAAGACGAGGCAGCGCGGCTATCGTGGCTGGCCACGACGGGCGTTCCTTGC
GCAGCTGTGCTCGACGTTGTCACTGAAGCGGGAAGGGACTGGCTGCTATTGGGCGAAG
TGCCGGGGCAGGATCTCCTGTCATCTCACCTTGCTCCTGCCGAGAAAGTATCCATCATG
GCTGATGCAATGCGGCGGCTGCATACGCTTGATCCGGCTACCTGCCCATTCGACCACC
AAGCGAAACATCGCATCGAGCGAGCACGTACTCGGATGGAAGCCGGTCTTGTCGATCA
GGATGATCTGGACGAAGAGCATCAGGGGCTCGCGCCAGCCGAACTGTTCGCCAGGCT
CAAGGCGCGGATGCCCGACGGCGAGGATCTCGTCGTGACCCATGGCGATGCCTGCTT
GCCGAATATCATGGTGGAAAATGGCCGCTTTTCTGGATTCATCGACTGTGGCCGGCTG
GGTGTGGCGGACCGCTATCAGGACATAGCGTTGGCTACCCGTGATATTGCTGAAGAGC
TTGGCGGCGAATGGGCTGACCGCTTCCTCGTGCTTTACGGTATCGCCGCTCCCGATTC
GCAGCGCATCGCCTTCTATCGCCTTCTTGACGAGTTCTTC**TGA**GCGAGCTTTGAAAGAA

Start *gfp11*

GGAGATATA**ATG**CGTGATCACATGGTTCTTCATGAATACGTTAACGCTGCTGGCATCAC

GGGGSGGGS-Linker **Start** *phaC*

AATGCGCATTATCGGCGGTGGCGGTAGCGGCGGTGGCGGTAGCATGACAACGCCTGA
AAAGGTCGAATCTGCTGCATCGCAGCAAATGCGGGACAATCTGGCGCGGATTGAGACA
CTTACACAACGCATGGTTGAAGCCTTTGCGCAAAAGCGCGCGCCCAATCCTGCGCTGG
AGGGGCCGGGGCTGGATCTTTACGTCGCCTCTTCGAGCGCGCTTTTGCGCGAGATGAC
GGCGAATCCGGCGAAAATCTTCGAGGCGCAGGTCAGCTATTGGGCGCAGGCGATGAC
GCATTACATCGACGCCACCCATGCCTTTGCTCAGGGCACCTTCAAGCCGCCCGCCGAT
CCGGGGCCGAAGGACCGCCGCTTTTCCAACCCGCTGTGGGACAGCCATCCCTATTTCA
ACTTCATCAAGCAGCAATATCTGATCGCCTCCAGCTCCATCGAGGAAGCGCTGTCGAAG
ATCGAGGGGCTGGACCCGGTCGACCGCCGCCGGCTGGAGATGTTTTCCAAGCAGATC
ATCGACATGATGGCGCCGACGAATTTTCTGGCGACGAACCCGGATGCGCTGGAAAAGG
CGGTGGCGACCGAGGGCGAAAGCCTGGTGCGGGGGCTGGAAAACCTCGTGCGCGAC
ATCGAGGCGAACCGCGGCGATCTGGTGATCACGCTTTCGGACAAGAACGCCTTCAGCG
TCGGGCACAACATCGGCACGGCGAAAGGCCAGGTGGTCTGGCGCAACCGGCTGATGG
AGATCATCCAGTACGAGCCCACCACCCCCGAGGTGCACAAGACCCCGCTGATCATCTT
TCCGCCCTGGATCAACAAGTTCTACATCCTGGATCTGAAACCGCAAAACAGCCTGATCC
GCTGGATCGTCGATCAGGGCTTCACGCTGTTCGTCGTCAGCTGGAAGAACCCGGACCG
GTCCTATGCCGATGTGGGGATGGAGGATTACGTCCGCGACGGCTATCTGGCCGCGGTC
GAGGAGGTGAAGGCGATCACCGGCGAGAAACAGGTGAATGCGGTCGGCTATTGCATC
GCGGGCACGACGCTGAGCCTGGTCCTGTCGCTCTTGGAAAAGCGCAAGGACAAGTCG
ATCAAATCGGCGACCTTTTTCACCACGCTGACCGACTTTTCCGATCAGGGCGAATTCAC
CCCCTTCCTGCAGGATGATTTCGTCCACGGGATCGAGCGGCAGGTGCGGCTGGATGG
CGTTCTGTCGAGCTATTACATGACGCGGACCTTTTCCTATCTGCGGGCGAATGACCTGA
TCTATCAGCCCGCGATCCGCAGCTACATGATGGGCGAATCGCCGCCCGCCTTCGACTT
GCTTTACTGGAACGGCGACAGCACCAACCTGCCGGGCAAGATGGCGATGGAATATCTG
CGCGGGCTCTGTCAGGCCGATGCCTTCACCACCGAGGGCTTCGAGCTGATGGGCGAG
CGGCTGCATGTCTCGGGGGTCAAGGTGCCGCTCTGCGCCATCGCCTGCGAGACCGAC
CATATCGCGCCCTGGATCGTCAGCTTCAACGGCGTGGCGCAGATGGGATCGACCGACA
AGACCTTCATCCTGACGGAATCGGGCCATATCGCCGGGATCGTGAACCCGCCGAGCAA
GGACAAATACGGCCATTACACCTCTGCGGCGCCGATTGCCGATCATCAGGTCTGGAAG
GCGCAGGCCACCTACACGAAGGGCAGCTGGTGGCCGCGCTGGGGGGAATGGCTGGC
CGGGCATTCGGGCAAGAAGATCCCCGCGCGGGCCCCGGGCGACGCGACGCATCCGC
CGCTGGCCCCGGCCCCCGGCACCTATGTCTCGGAGGTTGTGGTGCTTTAGCGAGCTC

Start *phaA3*

GGCTCTAGAGCTGAAAGAAGGAGATATACACATGACCGAAGCCTATATCTATGACGCCT
GCCGCACGCCGCGGGGCAAGGGGCGCGCTGACGGCAGCCTGCATGAAGTGACCTCT
GTCGCGCTGTCGGCGCGGCTTCTGGATGCGGTGGCGGAACGCAATGGCCTGACGGGT
CCTGCGGTCGAGGATGTGATCTGGGGCAATGTCACCCAGGTGGGCGAGCAGGGCGGC
TGTCTGGCCCGGTCTGCGGTGCTGCTTTCGGGGCTCGATGAATCGATCCCCGGTCTTT
CGATCAACCGCTTTTGCGCCAGCGGCATGGAGGCGGTGAACCTGGCCGCCAATCAGGT
CAAGGCGGGGGCGGGCGCGGCCTATATCGCGGGCGGGGTCGAGATGATGAGCCGCG
TTGCCATGGGCTCGGACGGGGCGGTGATCGCCGTCGATCCGTCGCTTGCGATGAAGA
CCTATTTCGTGCCGCAGGGGATTTCCGCCGATATCATCGCCACCGAATACGGGTTTACC
CGCGAGATGGCCGATGCGCTGGCGGTCGAAAGCCAGCGCCGCGCCGCCGAGGCCTG
GGCCGAGGGGCGTTTCGCGAAATCCATCGTGCCGGTGAAGGATCAGAACGGGCTGAC
GATTCTGGACCGCGACGAATATCTGCGCCCCGGCACGACGCTGGAGGATCTGGCCAA
GCTCAAGCCCGCCTTCAAGGACATGGGCGAGGTGATGCCGGGCTTCGACAAGGTGGC
GATGCTGAAATATCCGCATCTGGAGCGCATCGAGCATATCCACCATGCGGGGAACTCTT
CGGGCATCGTCGATGGGGCGGCGGCGGTGCTGATCGGCTCGAAGGAGTTCGGCGAG

GCGCATGGGTTGAAGCCGCGCGCCCGCATCCGCGCCACCGCGAAGATCGGCACCGAT
CCGACGATCATGCTGACCGGCCCGGTGCCCGTCACCGAAAAGATCCTGCGCGACAGC
GGCATGAGCATTGCCGACATCGACCTTTTCGAAGTGAACGAGGCCTTTGCCGCAGTTGT
TCTGCGCTTCATGCAGGCCTTTGACGTCGGTCAGGACCGGGTCAACGTGAACGGCGGC
GCGATGGCGCTGGGTCATCCCTTGGGCGCGACGGGGGCGATCATCATCGGCACGCTG
CTGGACGAGCTGGAACGCCGCGATCTGTCCACCGGGCTTGCGACGCTCTGCATCGCTT
CCGGCATGGGCGCGGCCACGATCATCGAGAGGGTC**TGA**ACGCGTATAAGGAATTGA

Start *phaB1*

ATGTCCAGAGTTGCACTCGTCACCGGGGGATCGCGCGGCATTGGCGCCGCGATCTCG
ATGGCACTGAAGGACGCCGGTTACACCGTCGCCGCGAACTATGCCGGCAATGACGAAG
CCGCCGCGAAATTCACCGCCGAGACCGGGATCAAGACCTACAAATGGTCGGTCGCCGA
TTACGACGCCTGCGCCGCGGGCATCGCCCAGGTCGAGGCCGATCTGGGCCCGGTTGA
CGTGCTGGTGAACAATGCGGGCATCACCCGCGACGCGCCCTTCCACAAGATGACCCGC
GACCAATGGGATCAGGTGATCGGCACCAACCTGAACGGCATCTTCAACATGACGCATC
CGCTCTGGAACGGCATGCGCGACCGCAAATTCGGCCGGATCATCAACATTTCCTCGAT
CAACGGCCAAAAGGGCCAGTTCGCCCAGGCGAACTATTCCGCGGCCAAGGCGGGCGA
CATCGGCTTCACCAAGGCGCTGGCGCAGGAAGGGGCGCGGGCGGGGATCACCGTCAA
CGCGATCTGCCCGGGCTATATCGCCACCGAAATGGTGATGGCGGTGCCCGAAAAGGTG
CGCGAGCAGATCATCGCGACGATCCCGGTCGGCCGTCTGGGCGAAACCGGCGATATC
GCGCGCTGCGTGGTGTTCCTCGCCTCGGATGATGCGGGCTTCATCACCGGCGCGACG
CTGACCGCGAACGGCGGCCAATACATGACC**TGA**

References

1. Hanahan, D. Studies on Transformation of *Escherichia coli* with Plasmids. *J Mol Biol* **1983**, *166*, 557–580, doi:10.1016/S0022-2836(83)80284-8.

2. Bollinger, A.; Molitor, R.; Thies, S.; Koch, R.; Coscolín, C.; Ferrer, M.; Jaeger, K.-E. Organic-Solvent-Tolerant Carboxylic Ester Hydrolases for Organic Synthesis. *Appl Environ Microbiol* **2020**, *86*, doi:10.1128/AEM.00106-20.

III. GENERAL DISCUSSION

Within this thesis, the anoxygenic phototroph *R. capsulatus* was evaluated as bacterial host for the biosynthesis of different heterologous terpene classes. Furthermore, a new P_{tac}-based vector system in combination with photocaged inducer molecules were established in this organism, and the basis for immobilization of proteins and terpene biosynthesis enzymes on PHB granules was laid.

First, existing metabolic engineering concepts such as overexpression of rate-limiting enzymes and further precursor supply were applied and their influence on the production of different terpene classes was investigated [see **Chapter II.1**]. Second, a P_{tac}-based vector system in combination with photocaged inducer molecules of different solubility was characterized in *R. capsulatus* and applied for regulation of intrinsic terpenoid biosynthesis. Afterwards, this concept was transferred to alternative biotechnologically relevant bacterial hosts [see **Chapter II.2**]. Subsequently, the immobilization of proteins on PHB granules in *R. capsulatus* was demonstrated as preliminary work. In addition, an alternative protein linker system was established enabling simple detection of successful enzyme coupling in *E. coli* [see **Chapter II.3**].

In the following section, the applied concepts of enhancing terpene production, controlling gene regulation as well as immobilization techniques will be summarized. Subsequently, the underlying metabolic engineering strategies and gene expression tools are evaluated regarding their applicability for heterologous biosynthesis in *R. capsulatus* [see **Chapter III.1.1**]. Furthermore, methods for enzyme immobilization are considered and discussed in more detail, especially in the context of possible application strategies in *R. capsulatus* [see **Chapter III.1.2**]. Finally, an outlook regarding open questions resulting from this work is given, taking into account the current state of research and guiding future studies [see **Chapter III.3**].

III.1 Terpenoid production strategies – Metabolic engineering and orchestration of gene expression

The actual state of the art in the present work is summarized below to underline the necessity of developing new fine-tunable metabolic engineering strategies for terpenoid production. Here, a special focus is set on the deployment of anoxygenic phototrophic bacteria and the transcriptional regulation of the biosynthetic genes, respectively.

III.1.1 Application of anoxygenic phototrophic bacteria for the production of plant terpenoids

The production of high-value compounds from natural material for the chemical and biotechnological industry requires the availability of stable and efficient manufacturing processes. For this purpose, engineered microbial hosts are often deployed. However, numerous potential challenges must be addressed to optimize these bioprocesses. For example, heterologous production of proteins and secondary metabolites is usually accompanied by reduced growth rates of the host and low product yields. Additionally, efforts must be made to minimize the accumulation of toxic intermediates during biosynthesis without reducing the availability of precursor molecules. This usually requires sophisticated metabolic engineering concepts as well as precise controllability of gene expression and enzyme activity. Since the natural potential of microbial hosts for efficient synthesis of bioactive compounds may differ greatly in this regard, the evaluation and establishment of new suitable alternative hosts is increasingly required. Especially in this context, phototrophic bacteria provide numerous physiological advantages for the heterologous biosynthesis of secondary metabolites, such as terpenes. For instance, these organisms can harness light as energy source, ensuring sustainable production processes. Moreover, under phototrophic conditions, these bacteria form large intracellular membrane systems that are particularly suitable for the storage of membrane-associated proteins as well as hydrophobic metabolites and they naturally offer a strong carotenoid production. Thus, the current state of research addressing terpenoid production in oxygenic as well as anoxygenic phototrophic bacteria was enlightened, especially in cyanobacteria and purple non-sulfur bacteria [see **Publication I**]. Here, an overview about established terpenoid pathway engineering strategies as well as the impact of illumination on photoproduction and bioprocess optimization was provided. Recent studies have already demonstrated the suitability of the metabolic versatile genus *Rhodobacter* as host for the heterologous biosynthesis of different terpenes (Hage-Hülsmann *et al*., 2019; Troost *et al*., 2019; X. Wu *et al*., 2021). Based on this, *R. capsulatus* was deployed to extend the possible range of heterologous products focusing on numerous biotechnologically relevant terpenes [see **Publication II & III**].

To increase the precursor supply, different metabolic engineering strategies were applied, mainly basing on the overexpression of rate-limiting enzymes. For this, the 1-deoxy-D-xylulose 5-phosphate synthase DXS, the isopentenyl diphosphate isomerase Idi and the FPP synthase IspA were overexpressed using a plasmid-based system [see **Figure 1**]. Moreover, the genes encoding the heterologous MVA pathway were genome integrated, enabling the efficient utilization of acetyl-CoA as precursor for isoprenoid biosynthesis. Interestingly, no common conclusion about metabolic engineering strategies that are generally suitable for increasing product yields could be derived for the tested terpenes. Instead, the metabolic engineering concept must be evaluated differently in context of each terpene and even, as shown for squalene, terpene synthase specific productivities play an important role for the engineering process as well. This suggests that differences regarding enzyme-specific turnover-rates and substrate inhibition may exist for each individual synthase. Therefore, a combination of certain engineering modules and co-expressed genes leading to highest product titer had to be identified in each case (Hilgers, 2021), as summarized in **Table 1**.

Table 1: Experimental setups for highest terpene yield in *R. capsulatus* within this thesis.

Product	Terpene synthase	Setup* (strain/co-expressed genes)	Product yield [mg L^{-1}]	Reference
β-caryophyllene (C_{15})	QHS1 (*Artemisia annua*)	SB1003-MVA/ *ispA*	139	(Hilgers *et al*., 2021) [see **Publication III**]
casbene (C_{20})	*Rc*CS (*Ricinus communis*)	SB1003/ *ispA-dxs-idi*	minor amounts	(Hage-Hülsmann *et al*., 2021) [see **Publication II**]
squalene (C_{30})	*At*SQS (*Arabidopsis thaliana*)	SB1003/ -	65	
	*Bb*SQS (*Botryococcus braunii*)	SB1003/ -	20	
	*Hs*SQS (*Homo sapiens*)	SB1003/ *ispA*	61	
	*Mc*SQS (*Methylococcus capsulatus*)	SB1003/ *ispA*	90	
	*Te*SQS (*Thermosynechococcus elongatus*)	SB1003-MVA/ -	20	
β-carotene (C_{40})	CrtYI (*Pantoea ananatis*)	SB1003/ *ispA-dxs-idi*	30	

* SB1003 = *R. capsulatus* SB1003; SB1003-MVA = *R. capsulatus* SB1003 with genome-integrated MVA pathway; co-expressed genes were placed on a pRhon5Hi-2 expression vector under the control of an ammonium repressed P_{nif} promotor (Troost *et al*., 2019)

In conclusion, the significance of phototrophic bacteria for the production of pharmaceutically relevant terpenoids and the current state of biotechnological research was outlined. Moreover, *R. capsulatus* was proven as a suitable host for the biosynthesis of various complex terpenoid classes by expressing terpene synthases from bacterial, mammalian and plant origin. Especially the studies focusing on the biosynthesis of various terpene synthases using a toolbox containing the underlying metabolic engineering concepts emphasize the importance of an all-encompassing evaluation of the individual experimental setups consisting of production strain and co-expressed genes. Due to the complexity of secondary metabolite pathways, a precise control over metabolic flux rates and tightly regulated gene expression of restricting enzymes might be a key feature for optimized bioproduction.

III.1.1.1 Heterologous terpene biosynthesis in the context of intrinsic regulatory mechanisms

Especially in isoprenoid biosynthesis, a variety of inhibitory effects based on intermediate accumulation are known in various organisms, representing possible intrinsic regulatory mechanisms in *R. capsulatus* [see **Figure 5**] and will be briefly discussed below.

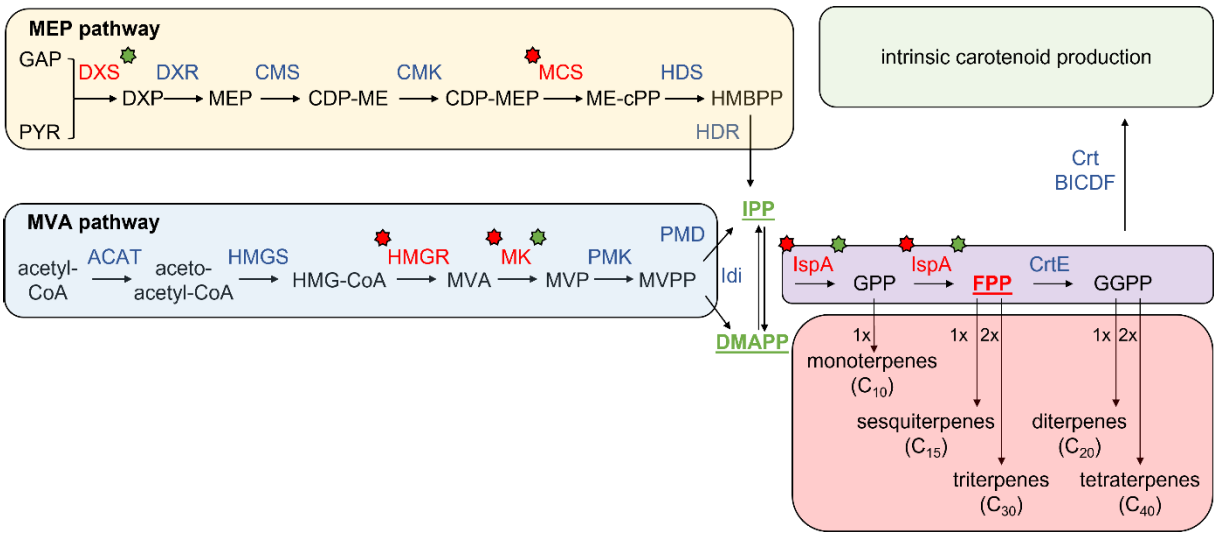

Figure 5. Schematic overview of terpenoid biosynthetic pathways and possible intrinsic regulatory mechanisms in *R. capsulatus*. The presented information is a model of putative regulatory mechanisms in *R. capsulatus* based on regulatory processes that have been described for enzymes of other microbial terpenoid production hosts. The isoprene derivatives IPP and DMAPP might inhibit DXS or the mevalonate kinase as well as a feedforward regulation of IspA, whereas FPP could negatively affect IspA, MCS and DXS as well as the mevalonate kinase and HMGR. Green symbols marked theoretical IPP and DMAPP associated inhibitory effects and red symbols marked possible FPP associated inhibitory effects. Substrates (CDP-ME: 4-diphosphocytidyl-2-methyl-D-erythritole, CDP-MEP: CDP-ME-2-phosphate, DMAPP: dimethylallylpyrophosphate, DXP: 1-desoxy-D-xylulose-5-phosphate, FPP: farnesyl pyrophosphate, GAP: glycerinaldehyde-3-phosphate, GGPP: geranylgeranyl pyrophosphate, GPP: geranyl pyrophosphate, HMBPP: (E)-4-hydroxy-3-methyl-but-2-enyl-diphosphate, HMG-CoA: β-hydroxy-β-methylglutaryl-CoA, IPP: isopentenyl pyrophosphate, Me-cPP: 2-c-methyl-D-erythritol-2,4-cyclodiphosphate, MEP: 2-c-methyl-D-erythritol-4-phosphate, MVA: mevalonate, MVP: mevalonate-5-phosphate, MVPP: mevalonate-5-pyrophosphate, PYR: pyruvate); Enzymes (ACAT: acetyl-CoA acyltransferase, CMK: cytidyl-methyl kinase, CMS: cytidyl-methylerythritol

synthase, CrtBICDF: enzymes involved in carotenoid biosynthesis, CrtE: geranylgeranyl pyrophosphate synthase, DXR: 1-desoxy-D-xylulose-5-phosphate reductase, DXS: 1-desoxy-D-xylulose-5-phosphate synthase, HDR: hydroxy-methyl-butenyl-diphosphate reductase, HDS: hydroxy-methyl-butenyl-diphosphate synthase, HMGR: hydroxy-methyl-glutaryl reductase, HMGS: hydroxy-methyl-glutaryl synthase, Idi: isopentenyl diphosphate isomerase, IspA: farnesyl pyrophosphate synthase, MCS: methyl-erythritol-cyclo-diphosphate synthase, MK: mevalonate kinase, PMD: pyrophosphate-mevalonate decarboxylase, PMK: phosphate-mevalonate kinase).

A special role in this context plays the FPP molecule, which can exert cell toxicity effects in high concentrations in *E. coli* (Dahl *et al*., 2013). Moreover, it has been shown for the human FPP synthase that FPP can bind in close proximity to the active site of the enzyme causing an allosteric conformational change, resulting in an inhibited enzyme activity (Park *et al*., 2017). Furthermore, FPP-mediated feedback inhibition is reported *in vitro* for the isolated human mevalonate kinase of the MVA pathway, which can also be blocked by GPP, GGPP as well as the isoprene derivatives IPP and DMAPP (Dorsey & Porter, 1968; Goldstein & Brown, 1990; Hinson *et al*., 1997). Similarly, the hydroxy-methyl-glutaryl reductase (HMGR) of the MVA pathway is inhibited by FPP in yeast (Donald *et al*., 1997; Paradise *et al*., 2008). Regulatory elements are also known for the MEP pathway, such as *in vitro* feedback inhibition of DXS by IPP and DMAPP (Banerjee *et al*., 2013) as well as of the methyl-erythritol-cyclo-diphosphate synthase (MCS) by FPP (Bitok & Meyers, 2012). Since feedforward inhibition by IPP and DMAPP was demonstrated for the human FPP synthase (Kavanagh *et al*., 2006), this may explain the often-observed beneficial effect of additional plasmid-based overexpression of IspA on product titers in the studies carried out here.

A more synthetic approach pursues the feeding of the two alcohol-containing homologous to DMAPP and IPP, dimethylallyl alcohol (DMAOH) and isopentenol (IOH) (Couillaud *et al*., 2021). Here, a two-step enzymatic synthesis consisting of a double phosphorylation enables the decoupling of microbial growth and terpenoid production, since an alternative pathway is used to provide the precursor molecules.

To counteract the described possible regulatory mechanisms during heterologous terpene biosynthesis in *R. capsulatus*, an optimal ratio between the supply of precursor molecules and their utilization by heterologous terpene synthases should be ensured in order to avoid the inhibition of the above mentioned enzymatic reactions as well as an improper flux of intermediates within the complex biosynthetic pathway. This could be achieved by the development of new precise expression systems, which were also addressed in the presented work.

III.1.2 Transcriptional control for regulating (intrinsic) terpenoid production in *Rhodobacter*

Highly specific regulation of the protein biosynthesis and secondary metabolite production can be achieved by precisely controlling the expression of according genes or clusters. Therefore,

two fundamental strategies can be applied. Depending on the intended aim, either genomic or plasmid-based gene expression can be selected. Here, independent from the location of incorporated genes (plasmid or genome), a distinction can be made between the use of individual promoters for targeted expression of specific genes (Kaur *et al*., 2018; Terpe, 2006) and the deployment of tools to control partial (heterologous) biosynthetic pathways (Loeschcke *et al*., 2013; Mougiakos *et al*., 2019).

In anoxygenic phototrophic bacteria, especially in *R. capsulatus* and its relatives, a wide variety of host-specific and heterologous promoter systems were evaluated and partially applied for the expression of genes encoding for terpene biosynthesis. Examples include host-specific oxygen-sensitive promoters, such as the P_{nif} system (Loeschcke *et al*., 2022), which has already been successfully applied for the heterologous biosynthesis of valencene as well as patchoulol in *R. capsulatus* (Troost *et al*., 2019) and was also used for terpenoid production in this work. Under native conditions, this promoter is engaged in the expression of nitrogenase enzyme complexes allowing this organism to metabolize atmospheric dinitrogen under nitrogen starvation (Masepohl *et al*., 2002). As a result, this system exhibits a strong expression response, which can be completely repressed by ammonium and molecular oxygen (Loeschcke *et al*., 2022). Furthermore, promoters associated with the synthesis of photosynthetic complexes show also high dependencies on the predominant oxygen availability. These include P_{puf} and P_{puc}, which were utilized for the heterologous bisabolene biosynthesis in *R. capsulatus* (Zhang *et al*., 2021) and P_{crtE} for the recombinant production of amorphadiene in *Rhodobacter sphaeroides* (Orsi *et al*., 2019). Moreover, P_{pgk} and P_{eno} originating from the glycolytic pathway in *R. capsulatus,* were also applied for bisabolene production (Zhang *et al*., 2021) and showed high expression response when glucose is used as carbon source (Piper *et al*., 1988; Toda *et al*., 2001).

In contrast, classical heterologous promoter systems, such as P_{lac} and its derivative P_{trc}, have already been widely applied as constitutive promoters (without the *lac* repressor) and as inducible variants, especially for the production of squalene and botryococcene in *R. capsulatus* (Khan *et al*., 2015) as well as pinene in *R. sphaeroides* (X. Wu *et al*., 2021). Despite this range of available expression systems [see **Table 2**], inducer uptake for controllable gene expression in *R. capsulatus* is still challenging due to its physiological properties such as an exopolysaccharide layer as well as an enlarged intracellular membrane system (Niederman, 2013).

Table 2: Overview of promoter systems utilized for heterologous terpene production in *Rhodobacter*.

Promoter	Origin*	Application	Comment	Reference
P_{nif}	nitrogenase complexes in *R. capsulatus*	valencene and patchoulol biosynthesis in *R. capsulatus*	repressed by NH_4^+ and O_2	(Troost *et al.*, 2019)
P_{puf}	light-harvesting complexes I & II from *R. capsulatus*	bisabolene biosynthesis in *R. capsulatus*	strong inhibition by O_2	(Zhang *et al.*, 2021)
P_{puc}				
P_{pgk}	encoding a phosphoglycerate kinase from *R. capsulatus*		high expression when glucose is used as carbon source	
P_{eno}	encoding a phosphoglycerate enolase from *R. capsulatus*		high expression when glucose is used as carbon source	
P_{crtE}	carotenoid biosynthesis in *R. sphaeroides*	amorphadiene biosynthesis in *R. sphaeroides*	strong inhibition by O_2	(Orsi *et al.*, 2019)
P_{lac}	*lac* operon from *E. coli*	squalene and botryococcene biosynthesis in *R. capsulatus*	applied as constitutive promoter without the *lac* repressor	(Khan *et al.*, 2015)
P_{trc}	hybrid promoter consisting of -35 region of the trp promoter and the -10 region of the lacUV5 promoter/operator from *E. coli*	pinene biosynthesis in *R. sphaeroides*	induction with IPTG	(X. Wu *et al.*, 2021)
P_{tac}	hybrid promoter consisting of -35 region of the trp promoter and the P_{lac} promoter from *E. coli*	carotenoid biosynthesis in *R. capsulatus*	gradual control as well as light regulation	(Hilgers *et al.*, 2021) [see **Publication VI**]

* The listed promoters control genes encoding for the named proteins and enzymes.

To overcome this limitation, a novel P_{tac}-based vector system was established in *R. capsulatus* using IPTG as an inducer molecule. Since light as an external stimulus represents a promising alternative to conventional methods, photocaged NP-cIPTG (Binder *et al.*, 2014; Binder, Frohwitter *et al.*, 2016) was additionally applied. To alter membrane permeability as well as water solubility, two further cIPTG derivatives with different hydrophobicity were chemically synthesized in a collaborative project by Dr. Fabian Hogenkamp, Institute of Bioorganic Chemistry (Heinrich Heine University Düsseldorf). In contrast to NP-cIPTG, BC-cIPTG

contains hydrophilic carboxylic side chains, whereas BEC-cIPTG bears additional lipophilic ester moieties.

In addition, *R. capsulatus* phototrophic growth could represent a great burden for this type of light-driven application, caused by the used light source as well as the production of photopigments. For example, bulb lights are capable for excitation of photopigments, namely the carotenoids spheroidene (λ_{max} = 454, 478, 509 nm) and spheroidenone (λ_{max} = 500 nm) as well as bacteriochlorophyll α (λ_{max} = 800, 860 nm), similar to natural daylight (Boran *et al*., 2010; Elkahlout *et al*., 2019; Katzke *et al*., 2010; Obeid *et al*., 2009). Although the UV-A light exposure (for IPTG release) was performed at 365 nm, the possibility of increased cell densities and thus enhanced absorption impairing the uncaging process remained uncertain. Additionally, the applied light sources could include a UV-A portion that already leads to an undesirable photocleavage.

So in a first step, the general inducibility of a P_{tac}-based expression system using photocaged IPTG molecules as well as an adjustability of the intrinsic carotenoid production were demonstrated in *R. capsulatus* [see **Publication IV**]. This work was realized in close cooperation with Dr. Fabienne Knapp (nèe Hilgers, Institute of Molecular Enzyme Technology, Heinrich Heine University Düsseldorf). Here, it was possible to restore the initial pigment level by plasmid-based expression of the corresponding carotenoid biosynthesis genes in an appropriate deletion strain.

To ensure the best possible exploitation, all three photocaged inducer derivatives were applied for the light-mediated control of plasmid-based gene expression under phototrophic, microaerobic, and aerobic conditions. Especially NP-cIPTG offers a sufficient as well as gradual responsiveness for all three growth behaviors and even exceeds the induction level of IPTG under microaerobic and phototrophic conditions, proving its value. Moreover, it could be shown that an enhanced absorption of the *R. capsulatus* cells in the UV-A range does not affect the uncaging process under microaerobic and anaerobic conditions [see **Publication IV**, Supplementary Material]. Even though BC- and BEC-cIPTG reached an induction level comparable to that of IPTG, severe instability effects regarding the protection groups were observed *in vivo*. Thus, both seemed inappropriate for light-mediated control of transcription in this host.

Based on these results, NP-cIPTG was identified to be the best tested inducer for intrinsic carotenoid production in *R. capsulatus*. The light impulse led to an elevated induction response in comparison to cultures induced with IPTG. Since it could be shown in this work, that the change of light source from broad-spectrum bulb light to infrared-light LED with a maximum emission wavelength of 850 nm led to 1.5-fold increased product titer of the sesquiterpene β-

caryophyllene in *R. capsulatus* [see **Publication III**], light regulation of heterologous terpene biosynthesis seems conceivable.

Besides the focus on the illumination element, further improvements could be carried out on the expression vector itself. To overcome an observed high basal *eyfp* expression level in uninduced *R. capsulatus* cultures, several modifications were conducted at the DNA level. So, the *lacI* gene was replaced by a variant with enhanced repressor activity and a DNA duplicate region of around 519 bp were deleted to avoid homologous recombination (similar to a recent publication (Bakkes *et al*., 2020)). In combination with the insertion of an *in silico* developed Shine-Dalgarno (SD) and SD-spacer sequence these measures led to an induction factor of 3.2 in comparison to 1.8 before optimization. Since ribosome binding site (RBS) adaptation in *R. sphaeroides* also resulted in a 3-fold increase in heterologous pinene biosynthesis (X. Wu *et al*., 2021), modulation of gene expression at the translational level seems to be promising in anoxygenic phototrophic bacteria in general. In this regard, a correlation between spacer length and translation initiation rate has been shown in *B. subtilis*, as this affects the mRNA secondary structure and consequently renders the RBS less accessible for ribosomes (Volkenborn *et al*., 2020). Accordingly, it cannot be excluded that such effects also have an impact in *Rhodobacter* species.

Next to selective plasmid-based gene expression, another possibility represents the genomic integration of entire recombinant genes and clusters for heterologous production of secondary metabolites. In this context, contemporary genome editing techniques such as CRISPR/Cas are already established in *R. sphaeroides* and *R. capsulatus* (Luo *et al*., 2020; Mougiakos *et al*., 2019; Zhang & Yuan, 2021). This may provide the basis for future complex modifications of the *R. capsulatus* genome facilitating the knockdown of regulatory elements and overexpression of necessary genes in terpene biosynthesis. Moreover, first attempts were made to implement a method for the transfer and expression (TREX) of biosynthetic pathways such as zeaxanthin biosynthesis to *R. capsulatus* (Loeschcke *et al*., 2013). This system allows the randomized chromosomal insertion of the gene cluster in combination with T7 RNA polymerase-mediated gene expression (Katzke *et al*., 2010).

Additionally to *R. capsulatus*, the caged inducer concept was transferred to other biotechnologically relevant bacterial hosts to verify the general applicability of the new inducer molecules in collaboration with Dr. Fabienne Knapp [see **Publication V**]. Here, NP-cIPTG remains the best suited variant in *E. coli*, whereas in *P. putida* as well as *B. subtilis* BC-cIPTG seems to be most promising. This suggests that the different solubility of tested photocaged IPTG variants seems to play only a minor role for optochemical *in vivo* applications. Thus, it could be shown that such photocaged inducer systems are very well transferable to various hosts. This distinguishes them from other light-mediated devices, such as photoreceptors,

where the cofactors needed for chromophore maturation have to be provided by the cell leading to host-specific differences regarding the applicability (Herrou & Crosson, 2011; Pudasaini *et al*., 2015).

In conclusion, a P_{tac}-based vector system combined with IPTG and various photocaged IPTG derivatives including different hydrophobic protecting groups was evaluated for its feasibility in *R. capsulatus.* The respective data showed that non-native as well as native cellular processes can be gradually controlled in a phototrophic bacterium either by adding increasing amounts of IPTG or using light as external stimulus when photocaged inducer derivatives are applied. In addition, enhancements were carried out at the DNA level of the vector such as adjustment of the SD sequence and the *lacI* gene. After demonstrating the control of intrinsic carotenoid production providing the basis for (light) regulation of heterologous terpenoid biosynthesis, the photocaged inducers were subsequently applied to several biotechnologically relevant bacteria. Thus, an alternative promoter system is now available allowing the precise expression of genes implicated in terpenoid biosynthesis.

III.2 PHB granules originating from *R. capsulatus* as a tool for protein immobilization

Besides increasing the productivity of biosynthetic pathways through metabolic engineering or the precise control of gene expression, another target for optimization is the biocatalyst itself. Here, one possibility is the immobilization of enzymes on a surface potentially leading to several improvements like increased stability or the reusability of the biocatalyst for *in vitro* applications. Moreover, co-immobilization of multi-step enzymatic cascades on a surface can reduce the spatial proximity of the enzymes to each other, resulting in substrate channeling as well as minimization of toxic intermediate accumulation within the cell. Currently, a wide range of immobilization techniques and different support materials are known. Therefore, a detailed overview of common possibilities for the *in vivo* immobilization of (industrial) biocatalysts was obtained as a first step [see **Publication VI**]. Here, a distinction was made between protein-based carrier materials like catalytically active inclusion bodies (CatIBs), synthetic organelles and natural, cellular compartments such as virus-like particles and polyhydroxybutyrate granules. In this context, biopolymeric PHB represent a promising opportunity to find application as a scaffold in heterologous terpenoid production. The hydrophobic PHB granules are surrounded by a protein layer containing the PHB synthase PhaC, a PHB depolymerase, different phasins and further regulatory and structural proteins (Gerngross *et al*., 1993; Pötter & Steinbüchel, 2005; Prieto *et al*., 1999). Especially PhaC, which catalyzes the final polymerization in PHB biosynthesis (Jendrossek & Pfeiffer, 2014), as well as phasins like PhaP are suitable as anchor proteins for the immobilization of enzymes to the granule surface [see **Figure 6 A & B**] (Du & Rehm, 2017; Tarazona *et al*., 2019).

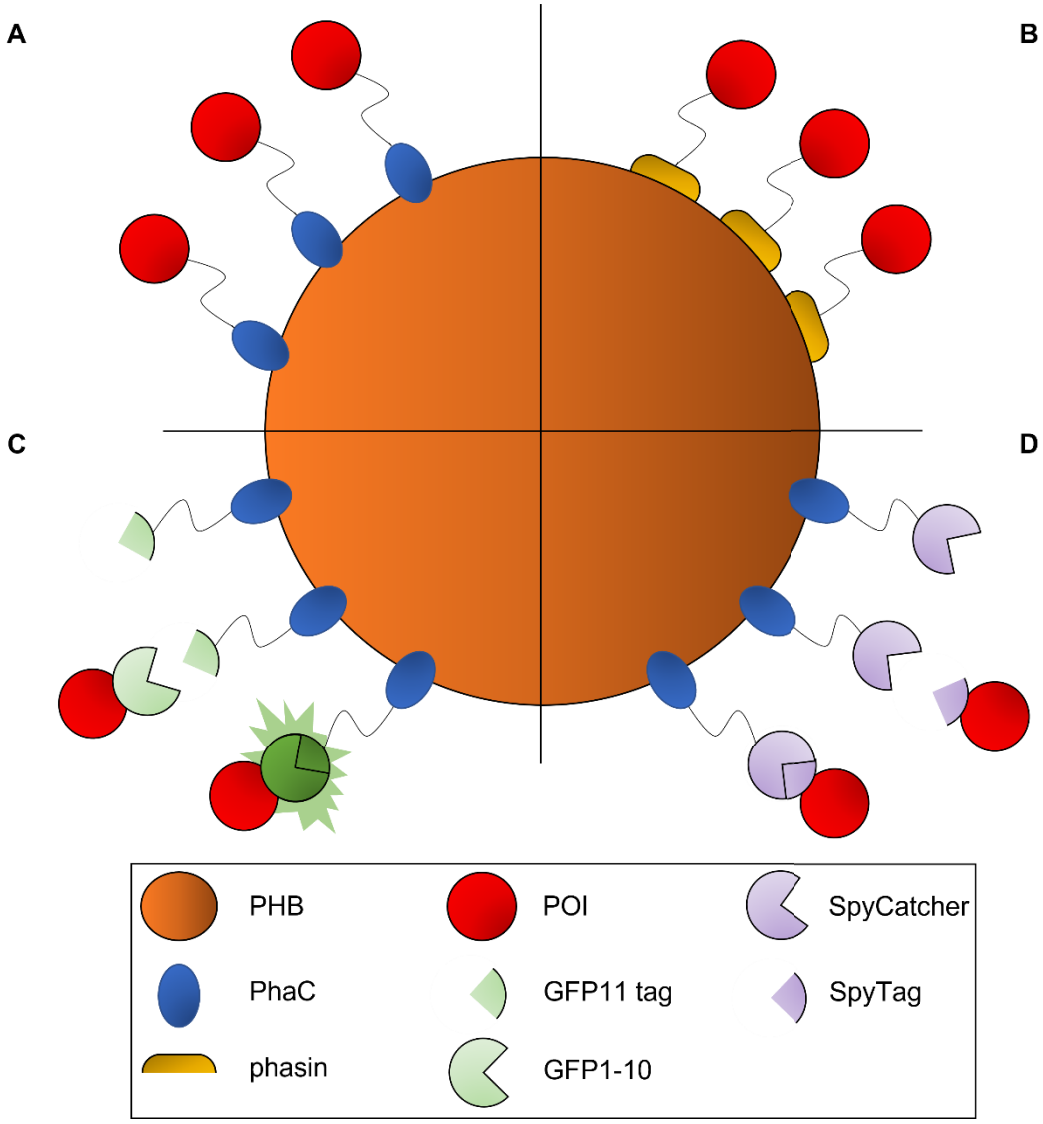

Figure 6. Different strategies to immobilize proteins on a PHB surface. Respective protein linker systems for target protein immobilization and the resulting immobilizates are shown. **A**) The POI is covalently attached to the PHB granule *via* a fusion with the PHB synthase PhaC. **B**) The POI is linked to the PHB surface *via* a fusion with a phasin protein and its hydrophobic interactions with the biopolymer core. **C**) POI is covalently attached to PHB granule *via* POI-GFP1-10 and PhaC-GFP11 tag resulting in a detectable green fluorescence signal. **D**) POI is linked to the PHB surface *via* an isopeptide bond formed by POI-SpyTag and PhaC-SpyCatcher. POI: protein of interest

PhaC remains covalently attached to the surface and represents a well-established method for *in vivo* enzyme scaffolding in biotechnological applications (Ran *et al.*, 2019; Rasiah & Rehm, 2009; T. H. Yang *et al.*, 2015). Due to the stable coupling, PhaC is also suitable as a linker in robust isolation processes to obtain the target protein in its soluble form (Du & Rehm, 2017). On the other hand, the utilization of a phasin protein such as PhaP or PhaF enables the non-covalent linkage of the target protein to the PHB surface *via* hydrophobic interactions (Dinjaski & Prieto, 2013; R. Li *et al.*, 2019; Yao *et al.*, 2008). In this context, the peptide tag BioF based

on PhaF from *P. putida* was developed, combining a shortened linker length with increased affinity and stability (Bello-Gil *et al*., 2018; Mato *et al*., 2020).
Furthermore, PHB-based applications were already implemented for production of the terpenoid lycopene in *E. coli* and, due to the hydrophobic nature of the biopolymer, PHB served as an anchor matrix for hydrophobic substrates (Bello-Gil *et al*., 2018; Y. Liu *et al*., 2020).
The bacterial host *R. capsulatus* used in this thesis is naturally capable to produce PHB under nutrient-limiting conditions [see also **Chapter II.3.1**]. Therefore, its versatile metabolism resulting in two different lifestyles and a broad range of naturally occurring cofactors in combination with high terpene production makes *R. capsulatus* a very promising platform organism for immobilization-based applications. Although PHB production in *R. capsulatus* has been previously characterized, studies about the targeted functionalization of the biopolymer granules in this host are still missing. Hence, the fluorescence protein eYFP was selected as an example for first attempts to *in vivo* immobilize a target protein on the PHB surface in *R. capsulatus* using the anchor protein PhaC [see **Publication VII**]. Herein, the attachment of eYFP to the granule surface was successfully demonstrated. Moreover, the host-specific enzymes involved in PHB biosynthesis were transferred to the non-natural PHB producer *E. coli* to characterize immobilization in an environment without the respective cellular regulatory mechanisms. Immobilization was demonstrated in this case as well, and additionally, eYFP was successfully separated *in vitro* after isolation of the PHB fraction. Thus, this work laid the foundation to study more complex *in vivo* immobilization approaches, in which enzymes could be co-immobilized on the PHB surface to produce high-value terpenoids. Interestingly, it was not possible to gradually control the decoration of PHB granules *via* the chosen methods. Likewise, immobilization process and efficiency could not be quickly and easily determined. Hence, the split GFP system was established as an alternative anchor technique for the immobilization of a target protein on the granule surface and to monitor the immobilization process readily by a green fluorescence signal [see **Publication VIII**]. In a split GFP application, GFP consisting of eleven β-sheets is divided into two non-fluorescent fragments (Barondeau *et al*., 2003; Cabantous *et al*., 2005). The larger component contained the β-sheets 1-10 (GFP1-10) and the other fragment comprised of the 11th β-sheet (GFP11 tag). After binding of the two protein partners, the chromophore maturation is initiated resulting in the formation of a holo-GFP with a detectable fluorescence signal [see **Figure 6 C**] (Cabantous *et al*., 2005; Cabantous & Waldo, 2006).

In addition to split GFP, other split fluorescent variants are known, such as yellow fluorescent split YFPs as well as blue fluorescent split CFPs (Lockard & Waldo, 2012) and red fluorescent split mCherry (Fan *et al*., 2008). The GFP family (including GFP, YFP, CFP) in particular is expanded by numerous engineered variants differing in spectral properties, quantum yield,

brightness, fluorescence lifetime, photostability, folding and chromophore maturation kinetics as well as fluorescence complementation efficiency (Köker *et al*., 2018). By transferring the split GFP principle to selected variants with different absorption and fluorescence spectra, multichromatic detection and quantification of up to three different target proteins would theoretically be thinkable. Hence, it would be possible to microscopically determine the distribution of individual enzymes of complex biosynthetic pathways on the biopolymeric surface and thus to evaluate the spatial proximity of different enzymes and its influence on production yield.

Moreover, the SpyTag/SpyCatcher system represents non-fluorescent protein-peptide interactions harnessing covalent isopeptide bond formation and enables better control over PHB decoration [see **Figure 6 D**] (Wong & Rehm, 2018). This mechanism, derived from *Streptococcus pyogenes*, is based on the binding domain CnaB2 of the fibronectin-binding adhesin FbaB, in which an isopeptide bond is formed between the amino acids Lys31 and Asp117 (Hagan *et al*., 2010; Terao *et al*., 2002). By subdividing this domain into two separate protein fragments, the SpyTag, a 13 amino acid peptide (including the reactive aspartate) and the SpyCatcher protein consisting of 139 amino acids containing the reactive lysine, a click chemistry-based system for rapid and covalent protein coupling was developed for *in vivo* as well as *in vitro* applications [see **Publication VI**] (Hatlem *et al*., 2019; Keeble & Howarth, 2019; Zakeri *et al*., 2012). In addition, other orthogonal protein ligation pairs, such as SnoopTag/SnoopCatcher derived from *Streptococcus pneumoniae* (Veggiani *et al.,* 2016) and SdyTag/SdyCatcher derived from *Streptococcus dysgalactiae* (Tan *et al.,* 2016), have already been combined with the PHB technology to create a multifunctional biopolymer platform for biotechnological applications (Wong, Gonzalez-Miro *et al*., 2020). However, the SpyTag/SpyCatcher system and its analogs have not been applied in terpene biosynthesis so far, nor tested in alternative hosts except *E. coli*.

In this thesis, GFP1-10 was fused to the C-terminus of the target protein, while the GFP11 tag was coupled to the N-terminus of the PHB synthase PhaC. Thus, it was possible to immobilize the fluorescence protein mCherry as well as the biotechnologically relevant esterase LipD on PHB granules in *E. coli* and to detect this process directly *via* a fluorescence output. In contrast to a direct genetic fusion to PhaC, a gradual decoration of the PHB granules is also enabled as the synthesis of the target protein can be regulated independently. Therefore, such systems based on “click & play” mechanics are preferable to conventional covalent fusions. Furthermore, co-localization of mCherry and split GFP could be shown microscopically, and the activity of the target proteins were determined.

All in all, it was able to anchor proteins to the PHB surface for the first time in *R. capsulatus* and to demonstrate the functionality of the PhaC-PHB system in a host-independent manner.

Finally, with split GFP, a completely new “click & play” principle for enzyme scaffolding was developed and tested in *E. coli*. Both systems are now available for application in terpene biosynthesis.

III.2.1 Regulated PHB biosynthesis in *R. capsulatus*

As mentioned above, the intrinsic PHB biosynthesis in *R. capsulatus* is triggered by nutrient limitation and by a change in the available nitrogen/carbon ratio (Kranz *et al*., 1997). In this context, altering the supplemented carbon source is a good way to produce PHB granules for protein immobilization in this host [see **Publication VII**]. However, this approach may impact cell growth as well as vitality, and the carbon source selection also affects the size and distribution of PHB granules within a cell (Kranz *et al*., 1997). To transform *R. capsulatus* into a platform organism for *in vivo*-based PHB immobilization applications, detachment from intrinsic regulatory mechanisms as well as environmental conditions would be desirable. In general, PHB biosynthesis proceeds in three enzymatic steps: First, an acetyl-CoA acetyltransferase (PhaA) condenses two molecules of acetyl-CoA to acetoacetyl-CoA. This in turn is first reduced by an NADPH-dependent acetoacetyl-CoA reductase (PhaB) to 3-hydroxyacyl-CoA. Subsequently, the final polymerization is carried out by a PHB synthase (PhaC) (Jendrossek & Pfeiffer, 2014; Merrick & Doudoroff, 1961; Peoples & Sinskey, 1989).

In *R. capsulatus* SB1003, four of the genes involved in PHB metabolism are organized in a gene cluster: These include *pha2* encoding a granule-associated phasin protein, *pha1* encoding for a transcriptional regulator for granule formation, *orfX* encoding a PHB depolymerase, and *phaC*. In contrast, the genes for PhaA and PhaB are located separately on the genome (Ulbrich & Pačes, 2002). Kranz and co-workers demonstrated that genomic deletion of *phaC* interrupts granule formation in *R. capsulatus*, whereas deletion of *phaA* or *phaB* still permits PHB production, suggesting the presence of alternative routes for substrate synthesis (Kranz *et al*., 1997). These findings were then confirmed by the presence of four different genomic copies of *phaA* (Ulbrich & Pačes, 2002). Moreover, the *phaABC* genes appear to be constitutively expressed and post-translationally regulated in *R. capsulatus* (Kranz *et al*., 1997). So, a plasmid-based overexpression of these genes could allow a disengagement of PHB biosynthesis from environmental conditions, but it is questionable whether the post-transcriptional regulatory mechanisms in place might counteract such an effect.

Here, another possibility to influence PHB formation would be the knockout or knockdown of the PHB depolymerase to avoid degradation of synthesized PHB granules. In a study of the closely related purple non-sulfur bacterium *R. sphaeroides*, PHB production was demonstrated under nitrogen-independent conditions, following the deletion of PHB depolymerase and concomitant overexpression of eight genes involved in PHB metabolism (Kobayashi & Kondo,

2019). As a result, PHB production could be increased by a factor of 2.9. However, even here the authors suspected the presence of unknown genes involved in PHB biosynthesis in purple non-sulfur bacteria in general. This complexity requires the application of advanced genomic modification tools for metabolic adaption as described previously [see **Chapter III.1.2**]. This may provide the basis to ensure PHB formation independent from nutrient availability. Therefore, an application in heterologous terpene biosynthesis would then also be conceivable, in which a part of the enzymatic cascade is immobilized on the PHB granules *in vivo* to increase enzyme stability and ensure substrate channeling [see **Chapter III.3.2**].
Additionally, Orsi *et al.* speculated, that under chemoheterotrophic conditions and nitrogen limitation in the stationary phase, PHB granules are degraded in *R. sphaeroides,* allowing sesquiterpene production under growth limitation (Orsi *et al*., 2019). In this study, an unfused variant of an amorphadiene synthase was expressed in *R. sphaeroides*, so future studies would need to consider which approach has the greatest impact on product titers: coupling the enzyme to the granule surface could be carried out (**I**) in a PhaZ-deficient strain, without the opportunity to degrade PHB, but with enlarged immobilization surfaces [see **Chapter III.2.1**] (Kobayashi & Kondo, 2019), or (**II**) in an environment with intrinsic regulatory mechanisms, enabling degradation of PHB granules as carbon source for terpene production under nutrient limiting conditions (Orsi *et al*., 2019).

III.3 Future perspectives to modulate terpenoid production

In this thesis, the heterologous production of different terpene classes was evaluated in the context of classical metabolic engineering strategies in the alternative host *R. capsulatus*. The applied concepts are mainly based on the supply of auxiliary precursor molecules by overexpressing rate-limiting enzymes. Moreover, a broad host range P_{tac}-based vector system in combination with light as external stimulus was established for the regulation of intrinsic terpene biosynthesis. In addition, PHB granules were utilized as a platform for protein immobilization for the first time in a purple non-sulfur bacterium. In the following, the knowledge acquired in this work will be combined to guide **future studies** for the optimization of terpene production in *R. capsulatus*.

III.3.1 Precise regulation of biosynthetic pathways

Secondary metabolites, including various terpenes play an important role in numerous biotechnological applications. For economic and ecological purposes, heterologous production in microorganisms is becoming increasingly attractive as compared to conventional extraction methods e.g. from plant-based material. Especially naturally occurring metabolic pathways are promising targets to channel metabolite flux rates towards the desired products and to minimize possible side effects of (toxic) intermediates (Dahl *et al*., 2013). Thus, in various

microorganisms, the knockout or knockdown of genes encoding for competing enzymes metabolizing the required precursors was performed to increase the respective product yields. Examples include the downregulation of intrinsic ergosterol biosynthesis in yeast by exchanging native promotors for weaker ones resulting in an enhanced α-santalene production (Scalcinati *et al*., 2012), the knockout of the squalene-hopene cyclase gene in *Synechocystis* sp. PCC 6803 to increase squalene accumulation (Pattanaik *et al*., 2020), or the implementation of feedback loops (Dunlop *et al*., 2010).
Especially in highly engineered microorganisms, several growth issues can be observed. Here, it can be favorable to decouple growth and production phases (Lo *et al*., 2016; Shabestary *et al*., 2021). Therefore, a versatile toolbox of regulation systems is required to enable finely tuned metabolic processes. Even though various expression systems are already present, many of them come along with side effects such as toxicity, distribution, or stability issues. In case of using salicylate as inducer, some bacteria are capable of exporting or degrading this compound resulting in an insufficient induction (Wood & Cluzel, 2012). The addition of commonly utilized inducers leading to laborious optimization for high temporal and spatial resolution to ensure the ideal induction time. As an example, induction with IPTG can show inhomogeneous distribution within the cell culture (Binder *et al*., 2014).

To overcome these limitations, an external stimulus with reduced time expenditure is required. Here, light allows the precise control over numerous cellular processes at different levels in biotechnological applications (Baumschlager & Khammash, 2021; Drepper *et al*., 2011; Klewer & Wu, 2019). Based on the accessibility, the high spatial resolution and the wide applicability, it is highly beneficial to focus on light-mediated approaches [see **Figure 7**].

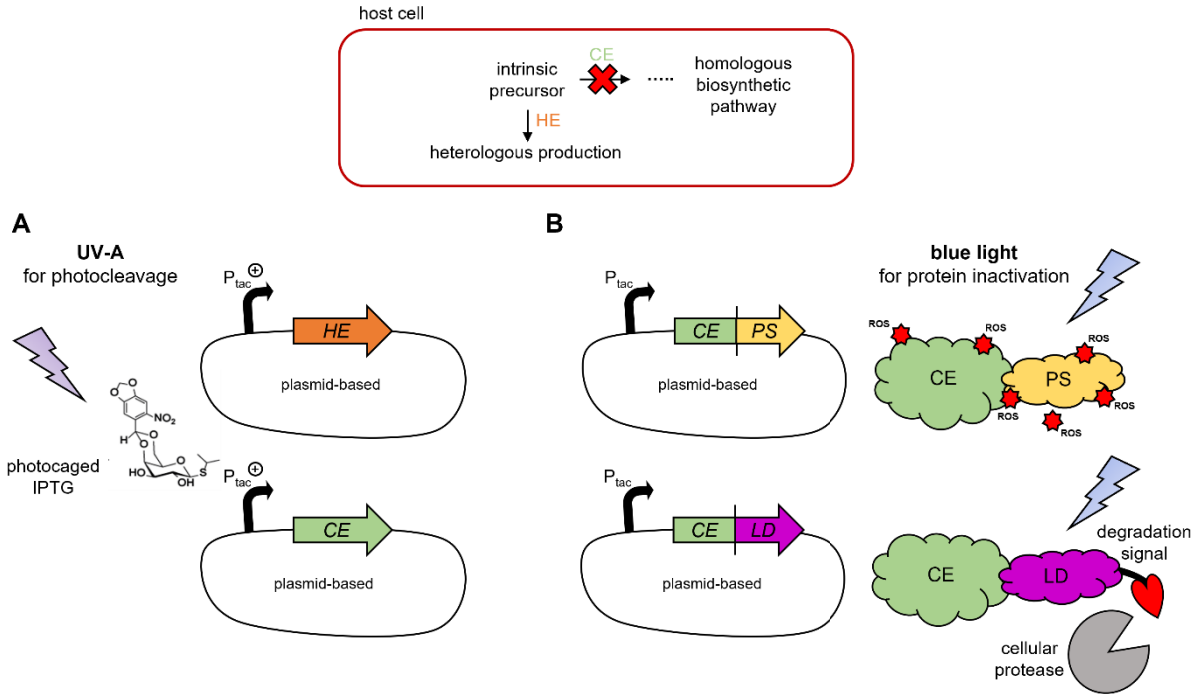

Figure 7. Different strategies to implement optogenetic control over the enzyme level for improved secondary metabolite production. In the host cell, the precursor level must be regulated to ensure an optimal link between homologous and heterologous biosynthetic pathways for improved product titers. Moreover, in various bacterial hosts, intermediates are known to cause cell toxicity effects in high concentrations. Here, light with different wavelengths was applied to control cellular processes at various levels. **A**) Photocaged IPTG-mediated expression of plasmid-based genes either for a heterologous enzyme (HE) or an intrinsic competing enzyme (CE) activated by UV-A exposure allows the optimization of precursor conversion. **B**) For post-translational regulation of homogenous biosynthesis, CE could be fused to a photosensitizer (PS). Here, illumination with blue light would lead to the production of ROS and consequently to inactivation of the CE-PS fusion protein. Another approach would be the combination of CE with a protein complex consisting of a light-sensitive protein domain and a recognition sequence for a cellular protease (LD). After light illumination and a conformational change of the photoreceptor, the recognition sequence is exposed. Thus, a cellular protease would be theoretically capable of degrading the entire fusion protein. HE: heterologous enzyme; CE: competing enzyme; UV-A: ultraviolet; PS: photosensitizer; ROS: reactive oxygen species; LD: light degron consisting of a photoreceptor and a degradation signal.

For instance, applying a light switch to precisely control gene expression could determine at which growth phase the expression of all (or parts of the) pathway genes should be initiated to obtain an optimal product yield. This may be advantageous, especially if the final product causes stress mediated cell response. This procedure is well-established in various non-optogenetic approaches and in a variety of hosts such as *E. coli* (Aguilar *et al*., 2019; Schlegel *et al*., 2013), *R. capsulatus* (Katzke *et al*., 2012) and other bacteria (Immethun & Moon, 2018; H. Yang *et al*., 2021; Zhou *et al*., 2020) enabling straightforward evaluation of multiple parameters in bioprocess development (such as induction time point or expression levels of different genes). In addition, the regulation of competing metabolic pathways may offer further advantages. Thus, in a native host, the homologous biosynthetic pathway can be interrupted at a defined step by a genomic knockout, allowing accumulation of the desired precursor

molecules. By plasmid-based expression of the deleted genes, a gradual efflux of metabolites into the native pathway can be provided, for example, to reduce toxic side effects or to enable the biosynthesis of compounds important for cell growth and viability.

However, it can be favorable as well to actively degrade produced enzymes depending on the phase of cultivation. This exceeds the regulatory possibilities deploying regular inducers, as they are designed to target the gene expression. Besides that, using UV-A light activated photocaged inducers as a non-reversible “on-switch”, the development of an “off-switch” to downregulate the substrate level is a next step to enable orchestration of metabolic pathways. One attempt would be a fusion protein composed of the consuming enzyme and a photosensitizer. Here, in a technique known as chromophore-assisted light inactivation (CALI), reactive oxygen species (ROS) are generated after excitation of a photosensitizer protein at a certain wavelength (Bulina *et al*., 2006; Riani *et al*., 2021; Wojtovich & Foster, 2014). Due to the close spatial proximity to the target protein, the enzyme will be irreversibly destroyed leading to a loss of activity. One example for an already established biotechnological application is the blue light-regulated inactivation of a pyruvate decarboxylase in a genetic fusion with the photosensitizer SOPP3 (Gerlach *et al*., 2022). Furthermore, photosensitizer susceptible for other excitation spectra such as red light (e.g. KillerRed and SuperNova) (Bulina *et al*., 2006; Gorbachev *et al*., 2020) or green light (e.g. SuperNova Green) (Riani *et al*., 2018) would enable the multi-chromatic inactivation of two or more enzymes in a shared biosynthetic pathway.

Besides inactivation *via* light-induced ROS formation, the target protein could also be degraded by an intrinsic cellular protease. Such systems for light-controlled protein degradation are already established in eukaryotic cells (Bonger *et al*., 2014; Pearce & Tucker, 2021; Ryan *et al*., 2021). Here, the protein complex is designed to consist of the target protein, a light-sensitive protein domain and a degradation signal. Therefore, various groups of flavoproteins can be considered as fusion proteins, such as blue light-sensitive flavin proteins or light oxygen voltage (LOV) domains (Gautier *et al*., 2014; Hallett *et al*., 2016; Iwata & Masuda, 2021). Thereby, the degradation signal is fused to the light-sensitive domain and obscured from intrinsic proteases. After exposure to a certain wavelength, the protein domain undergoes a conformational change resulting in the exposure of the degradation signal. This in turn is then recognized by the protease, leading to the breakdown of the entire fusion protein (Bonger *et al*., 2014). In this context it is worth mentioning that selective degradation of a competing enzyme can raise the amount of available precursor molecules and thus the desired product. This effect could already be shown, for example, in *S. cerevisiae* in a light-independent approach (Peng *et al*., 2018). Here, the fusion of a FPP synthase with an endoplasmic-reticulum-associated protein degradation signal enhanced the GPP amount within the cell, thereby increasing production of the monoterpene linalool.

In addition to the above described optochemical and optogenetic switches, light-responsive photoreceptors can be applied to reversibly control cellular processes by light. For example, a light sensor histidine kinase and its response regulator originated from cyanobacteria were used in *E. coli* for red and green light-controlled growth and methionine production (Milias-Argeitis *et al*., 2016). Furthermore, optogenetic transcription systems in yeast could be utilized to decouple the light-induced growth phase from dark-induced production phase to enhance isobutanol biosynthesis (E. M. Zhao *et al*., 2018). Additionally, light sensors can be combined with CRISPR-mediated interference (CRISPRi). Thus, in *E. coli,* transcription of guide RNA (gRNA) was placed under the control of a promoter controlled by a response regulator, which can be phosphorylated by a blue light-sensitive histidine kinase. Consequently, under strong blue-light exposure, the sensor becomes less active, resulting in decreased gRNA amount and therefore reduced repression of target gene expression by CRISPRi (H. Wu *et al*., 2014). Moreover, a related principle of this optogenetic CRISPRi technique was applied to turn off competitive pathways and to redirect the metabolic flux toward the heterologous muconic acid synthesis in *E. coli* (P. Wu *et al*., 2021).

III.3.1.1 Application of “on-” and “off-switches” for terpenoid biosynthesis in *R. capsulatus*

In advance of this work, the non-sulfur purple bacterium *R. capsulatus* was established as an alternative host for terpene production along with a developed metabolic engineering concept (Troost *et al*., 2019). In this thesis, the respective concept has been extended for the production of different terpene classes, together with the evaluation of tolerance of various terpene synthases to these strategies [see **Publications II & III**]. Moreover, preliminary work was performed to develop a novel vector system to gradually control gene expression in *R. capsulatus* and additionally regulate homogenous carotenoid biosynthesis by light-mediated *crtE* expression [see **Publication IV**]. The substrate of CrtE is the terpene precursor molecule FPP, which can be cell toxic at high concentrations (Dahl *et al*., 2013) and can cause several inhibitory effects within isoprenoid biosynthesis [see **Chapter III.1.1**]. Therefore, precise FPP regulation represents a promising target to improve both cell viability and terpene titer in heterologous production. By switching from conventional incandescent light to infrared illumination [see **Publication III**], phototrophic cultivation of *R. capsulatus* could be adapted to provide the entire remaining wavelength spectrum for optogenetic applications.

A first “on-switch” was accomplished *via* UV-A light-regulated plasmid-based expression of the *crt* genes [see **Publication IV**]. This system could be transferred to the expression of the heterologous terpene synthase in order to direct the FPP flux towards the desired product. A similar principle has already been demonstrated in *S. cerevisiae* for the production of β-carotene (Pouzet *et al*., 2022). Here, terpene synthase expression was placed under the

control of an optogenetic promoter regulated by a light-activated transcription factor leading to a β-carotene yield of 880 µg/gCDW.

Most of the “off-switches” described so far are not readily transferable to *R. capsulatus*. One reason is that photosensitizers require molecular oxygen, and the highest terpene yields in this thesis were achieved under anaerobic conditions. Therefore, it is questionable whether such an approach can be profitably realized in *R. capsulatus*. On the other hand, the described applications for light-driven protein degradation using a LOV domain are not subjected to such limitations. However, this systems are not established in bacterial hosts so far. In contrast, a general functionality of CRISPRi was demonstrated in *R. capsulatus* (Zhang & Yuan, 2021). Thus, a transfer of this technology in combination with a two-component system would be quite possible.

All in all, important milestones such as adaptation of cultivation and an “on-switch“ for precise control of gene expression have already been achieved to enable (light) control of terpene biosynthesis in *R. capsulatus*. However, especially the transfer of mainly blue light-associated “off-switches” still represents a major burden in future studies.

III.3.2 Co-immobilization of terpene biosynthetic enzymes

In this work, the cornerstone was laid to utilize PHB granules in *R. capsulatus* for immobilization of enzymes in biotechnological applications [see **Publication VII**]. Moreover, a novel system for direct *in vivo* detection of successful protein-biopolymer coupling was developed [see **Publication VIII**]. In both studies, the activity of the target enzymes was retained after coupling to the PHB surface. Especially for *in vitro* applications, enzyme immobilization is a well-established technique to enhance protein stability with regard to temperature and solvent tolerance. Moreover, the affinity of PHB granules for hydrophobic compounds has already been demonstrated in *E. coli* for the purification of dye-containing wastewater using an immobilized laccase-like multicopper oxidase (Bello-Gil *et al*., 2018). Besides that, in a recent study a lycopene synthase was fused to PhaC in *E. coli* (Y. Liu *et al*., 2020). Here, it could be shown, that the affinity for the hydrophobic FPP molecules is resulting in their increased accumulation in spatial proximity to the terpene synthase and thus in enhanced substrate supply. Hence, substrate accessibility for other terpene synthases could be enhanced as well. Therefore, it would be reasonable to combine the heterologous terpene biosynthesis with PHB immobilization techniques in *R. capsulatus*.

As shown for various terpene synthases, post-translational fusion with IspA (Baadhe *et al*., 2013; C. Wang *et al*., 2011), a cytochrome P450 enzyme (X. Wang *et al*., 2021) or genetic combination of several carotenoid biosynthesis-associated enzymes (Nogueira *et al*., 2019; Rabeharindranto *et al*., 2019) can significantly increase terpene titers in different microorganisms. The often-mentioned reason in this context is substrate channeling, i.e., the

transfer of an intermediate between two or more reaction partners without a temporary release (Spivey & Ovádi, 1999). This can improve the flow of intermediates through the reaction cascade and reduce the accumulation of toxic intermediates at certain areas within a cell, reducing possible negative effects (Kondrat & von Lieres, 2022).

Besides the coupling of single enzymes, it would be conceivable to anchor additional enzymes of an adjacent reaction step, such as IspA, to the PHB surface. Here, an alternative split fluorescence protein system could be adopted as an immobilization anchor to spectroscopically control the immobilization efficiency of both proteins [see **Figure 8**].

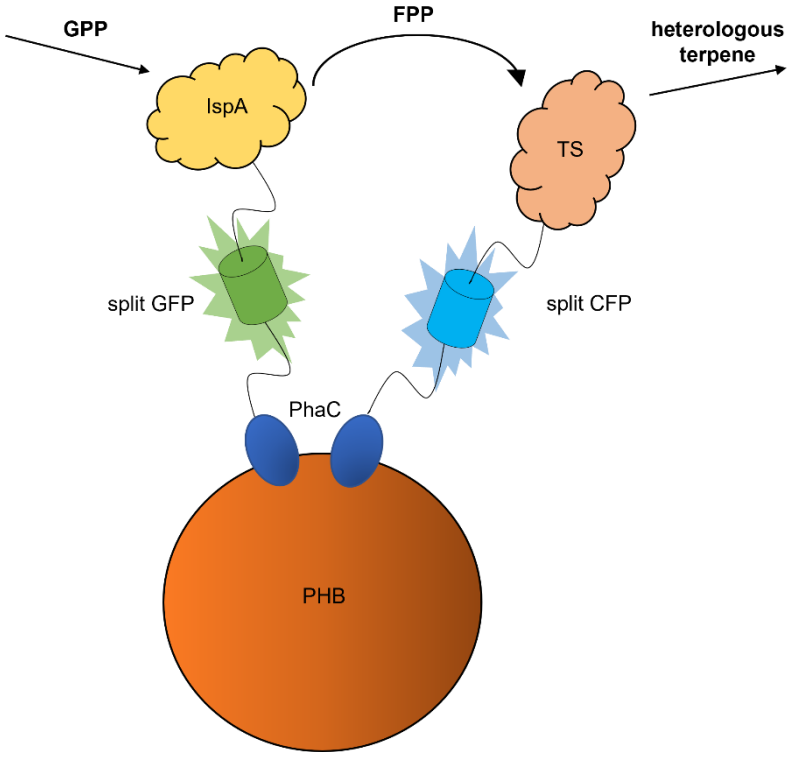

Figure 8. Display of terpene biosynthetic enzymes on a PHB surface using split fluorescence proteins. The co-immobilization of enzymes catalyzing adjacent reaction steps in terpene biosynthesis on PHB granules could lead to an improved protein stability, enhanced substrate accessibility through the hydrophobic biopolymer surface as well as substrate channeling and consequently reduced (toxic) intermediates within the cell. Here, IspA could be fused to a split GFP domain and a FPP converting terpene synthase to a split CFP domain (which is not established for PHB-based applications for enzyme immobilization so far). Successful binding of the target enzymes on the PHB surface can be then confirmed by a green or blue fluorescence signal, respectively. GPP: geranyl pyrophosphate; IspA: FPP synthase; FPP: farnesyl pyrophosphate; TS: (heterologous) terpene synthase; PhaC: PHB synthase; PHB: polyhydroxybutyrate granule.

By using two different anchor proteins emitting different fluorescence signals after successful binding to their protein partner, it would be possible to immobilize a part of an enzymatic cascade to a PHB surface and monitor the success spectroscopically. Thereby, the precise order of the individual enzymes appears to play a minor role, as demonstrated on the basis of *in vitro* violacein biosynthesis (S. Lim *et al.*, 2020). Here, there was no influence on product

titers identifiable whether the fusions consisting of the target enzymes and a catalytically inactive dCas9 nuclease were arranged on a synthetic RNA in a “scrambled” or “optimal” order relative to each other.

In the present example, the GPP-converting enzyme IspA could be fused to the already established split GFP domain, whereas a heterologous terpene synthase would be genetically combined with a split CFP domain emitting blue light after restored chromophore maturation. Other split fluorescent protein variants, such as split CFP, have already been characterized regarding their photophysical properties, but a transfer to use this system for enzyme immobilization is still missing.

Since the FPP intermediate is known for its numerous inhibitory effects as well as its toxicity at high levels [see **Chapter III.1.1.1**], substrate channeling could minimize these impacts in this case. Thus, this approach is a promising extension to the already available metabolic engineering concepts for terpene production in *R. capsulatus*.

Besides the described application for *in vivo* terpene biosynthesis, *in vitro* attempts are also possible. In this case, the individual target enzymes could be immobilized on separate biopolymers *via* different split fluorescence proteins to allow monitoring of the exact position of a PHB granule bearing the respective enzyme. However, the properties of PHB granules, specifically their non-porous structure and ability to aggregate, make them difficult to use in most industrial flow chemistry applications (Wong, Ogura *et al*., 2020). Thus, embedding the functionalized PHB granules in hydrogels would be conceivable (Nguyen & Lee, 2010). One approach describes the encapsulation of functionalized biopolymers with the anionic polysaccharide alginate using calcium ions as cross linkers (Ogura & Rehm, 2019). Here, the hydrogel porosity could be controlled by pH during the preparation. In this process, the bioengineered beads were produced in *E. coli* and encapsulated *in vitro* after isolation showing a theoretically suitability for industrial applications (Ogura & Rehm, 2019). Since this procedure should work host-independently, in the future, this technique could be applied to PHB granules produced in *R. capsulatus* in this work.

In summary, the evidence gathered in this thesis offer the possibility to establish PHB granules functionalized in *R. capsulatus* as a promising scaffold in terpene biosynthesis and the production of other high-value secondary metabolites. This may be achieved by a whole cell biocatalyst, as well as providing immobilized biocatalysts for *in vitro* flow chemistry.

IV. REFERENCES

Aalbers, F. S., & Fraaije, M. W. **(2019)**. Enzyme fusions in biocatalysis: Coupling reactions by pairing enzymes. *ChemBioChem*, *20*(1), 20–28. doi.org/10.1002/cbic.201800394

Abdallah, I. I., Xue, D., Pramastya, H., van Merkerk, R., Setroikromo, R., & Quax, W. J. **(2020)**. A regulated synthetic operon facilitates stable overexpression of multigene terpenoid pathway in *Bacillus subtilis*. *Journal of Industrial Microbiology and Biotechnology*, *47*(2), 243–249. doi.org/10.1007/s10295-019-02257-4

Abramson, J., Iwata, S., & Kaback, H. R. **(2004)**. Lactose permease as a paradigm for membrane transport proteins. *Molecular Membrane Biology*, *21*(4), 227–236. doi.org/10.1080/09687680410001716862

Aguilar, F., Scheper, T., & Beutel, S. **(2019)**. Modulating the precursor and terpene synthase supply for the whole-cell biocatalytic production of the sesquiterpene (+)-zizaene in a pathway engineered *E. coli*. *Genes*, *10*(6), 478. doi.org/10.3390/genes10060478

Albertsen, L., Chen, Y., Bach, L. S., Rattleff, S., Maury, J., Brix, S., Nielsen, J., & Mortensen, U. H. **(2011)**. Diversion of flux toward sesquiterpene production in *Saccharomyces cerevisiae* by fusion of host and heterologous enzymes. *Applied and Environmental Microbiology*, *77*(3), 1033–1040. doi.org/10.1128/AEM.01361-10

Ali, M., Ishqi, H. M., & Husain, Q. **(2020)**. Enzyme engineering: Reshaping the biocatalytic functions. *Biotechnology and Bioengineering*, *117*(6), 1877–1894. doi.org/10.1002/bit.27329

Ankenbruck, N., Courtney, T., Naro, Y., & Deiters, A. **(2018)**. Optochemical control of biological processes in cells and animals. *Angewandte Chemie International Edition*, *57*(11), 2768–2798. doi.org/10.1002/anie.201700171

Aschenbrenner, E. M., Weiss, C. K., & Landfester, K. **(2009)**. Enzymatic esterification in aqueous mini-emulsions. *Chemistry - A European Journal*, *15*(10), 2434–2444. doi.org/10.1002/chem.200801691

Atiroğlu, V., Atiroğlu, A., & Özacar, M. **(2021)**. Immobilization of α-amylase enzyme on a protein @metal–organic framework nanocomposite: A new strategy to develop the reusability and stability of the enzyme. *Food Chemistry*, *349*, 129127. doi.org/10.1016/j.foodchem.2021.129127

Baadhe, R. R., Mekala, N. K., Parcha, S. R., & Prameela Devi, Y. **(2013)**. Combination of *ERG9* repression and enzyme fusion technology for improved production of amorphadiene in *Saccharomyces cerevisiae*. *Journal of Analytical Methods in Chemistry*, 1–8. doi.org/10.1155/2013/140469

Bakkes, P. J., Ramp, P., Bida, A., Dohmen-Olma, D., Bott, M., & Freudl, R. **(2020)**. Improved pEKEx2-derived expression vectors for tightly controlled production of recombinant proteins in *Corynebacterium glutamicum*. *Plasmid*, *112*, 102540. doi.org/10.1016/j.plasmid.2020.102540

Banerjee, A., Wu, Y., Banerjee, R., Li, Y., Yan, H., & Sharkey, T. D. **(2013)**. Feedback inhibition of deoxy-d-xylulose-5-phosphate synthase regulates the methylerythritol 4-phosphate pathway. *Journal of Biological Chemistry*, *288*(23), 16926–16936. doi.org/10.1074/jbc.M113.464636

Banerjee, G., & Ray, A. K. **(2017)**. Quorum-sensing network-associated gene regulation in Gram-positive bacteria. *Acta Microbiologica et Immunologica Hungarica*, *64*(4), 439–453. doi.org/10.1556/030.64.2017.040

Barondeau, D. P., Putnam, C. D., Kassmann, C. J., Tainer, J. A., & Getzoff, E. D. **(2003)**. Mechanism and energetics of green fluorescent protein chromophore synthesis revealed by trapped intermediate structures. *Proceedings of the National Academy of Sciences*, *100*(21), 12111–12116. doi.org/10.1073/pnas.2133463100

Baumschlager, A., Aoki, S. K., & Khammash, M. **(2017)**. Dynamic blue light-inducible T7 RNA polymerases (Opto-T7RNAPs) for precise spatiotemporal gene expression control. *ACS Synthetic Biology, 6*(11), 2157-2167. doi.org/10.1101/140871

Baumschlager, A., & Khammash, M. **(2021)**. Synthetic biological approaches for optogenetics and tools for transcriptional light-control in bacteria. *Advanced Biology*, *5*(5), 2000256. doi.org/10.1002/adbi.202000256

Bello-Gil, D., Roig-Molina, E., Fonseca, J., Sarmiento-Ferrández, M. D., Ferrándiz, M., Franco, E., Mira, E., Maestro, B., & Sanz, J. M. **(2018)**. An enzymatic system for decolorization of wastewater dyes using immobilized CueO laccase-like multicopper oxidase on poly-3-hydroxybutyrate. *Microbial Biotechnology*, *11*(5), 881–892. doi.org/10.1111/1751-7915.13287

Bergman, M. E., Davis, B., & Phillips, M. A. **(2019)**. Medically useful plant terpenoids: Biosynthesis, occurrence, and mechanism of action. *Molecules*, *24*(21), 3961. doi.org/10.3390/molecules24213961

Bier, C., Binder, D., Drobietz, D., Loeschcke, A., Drepper, T., Jaeger, K.-E., & Pietruszka, J. **(2016)**. Photocaged carbohydrates: Versatile tools for controlling gene expression by light. *Synthesis*, *49*(01), 42–52. doi.org/10.1055/s-0035-1562617

Binder, D., Bier, C., Grünberger, A., Drobietz, D., Hage-Hülsmann, J., Wandrey, G., Büchs, J., Kohlheyer, D., Loeschcke, A., Wiechert, W., Jaeger, K.-E., Pietruszka, J., & Drepper, T. **(2016)**. Photocaged arabinose: A novel optogenetic switch for rapid and gradual control of microbial gene expression. *ChemBioChem*, *17*(4), 296–299. doi.org/10.1002/cbic.201500609

Binder, D., Frohwitter, J., Mahr, R., Bier, C., Grünberger, A., Loeschcke, A., Peters-Wendisch, P., Kohlheyer, D., Pietruszka, J., Frunzke, J., Jaeger, K.-E., Wendisch, V. F., & Drepper, T. **(2016)**. Light-controlled cell factories: Employing photocaged isopropyl-β-D-thiogalactopyranoside for light-mediated optimization of *lac* promoter-based gene expression and (+)-valencene biosynthesis in *Corynebacterium glutamicum*. *Applied and Environmental Microbiology*, *82*(20), 6141–6149. doi.org/10.1128/AEM.01457-16

Binder, D., Grünberger, A., Loeschcke, A., Probst, C., Bier, C., Pietruszka, J., Wiechert, W., Kohlheyer, D., Jaeger, K.-E., & Drepper, T. **(2014)**. Light-responsive control of bacterial gene expression: precise triggering of the *lac* promoter activity using photocaged IPTG. *Integr. Biol.*, *6*(8), 755–765. doi.org/10.1039/C4IB00027G

Binder, D., Probst, C., Grünberger, A., Hilgers, F., Loeschcke, A., Jaeger, K.-E., Kohlheyer, D., & Drepper, T. **(2016)**. Comparative single-cell analysis of different *E. coli* expression systems during microfluidic cultivation. *PLOS ONE*, *11*(8), e0160711. doi.org/10.1371/journal.pone.0160711

Bitok, J. K., & Meyers, C. F. **(2012)**. 2 *C*-methyl-D-erythritol 4-phosphate enhances and sustains cyclodiphosphate synthase IspF activity. *ACS Chemical Biology*, *7*(10), 1702–1710. doi.org/10.1021/cb300243w

Bollu, A., Peters, A., & Rentmeister, A. **(2022)**. Chemo-enzymatic modification of the 5′ cap to study mRNAs. *Accounts of Chemical Research*, *55*(9), 1249–1261. doi.org/10.1021/acs.accounts.2c00059

Bommarius, A. S., & Paye, M. F. **(2013)**. Stabilizing biocatalysts. *Chemical Society Reviews*, *42*(15), 6534. doi.org/10.1039/c3cs60137d

Bonger, K. M., Rakhit, R., Payumo, A. Y., Chen, J. K., & Wandless, T. J. **(2014)**. General method for regulating protein stability with light. *ACS Chemical Biology*, *9*(1), 111–115. doi.org/10.1021/cb400755b

Boran, E., Özgür, E., van der Burg, J., Yücel, M., Gündüz, U., & Eroglu, I. **(2010)**. Biological hydrogen production by *Rhodobacter capsulatus* in solar tubular photo bioreactor. *Journal of Cleaner Production*, *18*, S29–S35. doi.org/10.1016/j.jclepro.2010.03.018

Böttcher, D., & Bornscheuer, U. T. **(2010)**. Protein engineering of microbial enzymes. *Current Opinion in Microbiology*, *13*(3), 274–282. doi.org/10.1016/j.mib.2010.01.010

Brown, L., Vera Pingitore, E., Mozzi, F., Saavedra, L., M. Villegas, J., & M. Hebert, E. **(2017)**. Lactic acid bacteria as cell factories for the generation of bioactive peptides. *Protein & Peptide Letters*, *24*(2), 146–155. doi.org/10.2174/0929866524666161123111333

Bulina, M. E., Chudakov, D. M., Britanova, O. v, Yanushevich, Y. G., Staroverov, D. B., Chepurnykh, T. v, Merzlyak, E. M., Shkrob, M. A., Lukyanov, S., & Lukyanov, K. A. **(2006)**. A genetically encoded photosensitizer. *Nature Biotechnology*, *24*(1), 95–99. doi.org/10.1038/nbt1175

Busby, S., & Ebright, R. H. **(1999)**. Transcription activation by catabolite activator protein (CAP). *Journal of Molecular Biology*, *293*(2), 199–213. doi.org/10.1006/jmbi.1999.3161

Cabantous, S., Terwilliger, T. C., & Waldo, G. S. **(2005)**. Protein tagging and detection with engineered self-assembling fragments of green fluorescent protein. *Nature Biotechnology*, *23*(1), 102–107. doi.org/10.1038/nbt1044

Cabantous, S., & Waldo, G. S. **(2006)**. *In vivo* and *in vitro* protein solubility assays using split GFP. *Nature Methods*, *3*(10), 845–854. doi.org/10.1038/nmeth932

Cambridge, S. B., Geissler, D., Keller, S., & Cürten, B. **(2006)**. A caged doxycycline analogue for photoactivated gene expression. *Angewandte Chemie International Edition*, *45*(14), 2229–2231. doi.org/10.1002/anie.200503339

Camsund, D., Lindblad, P., & Jaramillo, A. **(2011)**. Genetically engineered light sensors for control of bacterial gene expression. *Biotechnology Journal*, *6*(7), 826–836. doi.org/10.1002/biot.201100091

Cantera, J. J. L. **(2002)**. Farnesyl diphosphate synthase gene of three phototrophic bacteria and its use as a phylogenetic marker. *International Journal of Systematic and Evolutionary Microbiology*, *52*(6), 1953–1960. doi.org/10.1099/ijs.0.02148-0

Carlsen, S., Ajikumar, P. K., Formenti, L. R., Zhou, K., Phon, T. H., Nielsen, M. L., Lantz, A. E., Kielland-Brandt, M. C., & Stephanopoulos, G. **(2013)**. Heterologous expression and characterization of bacterial 2-C-methyl-d-erythritol-4-phosphate pathway in *Saccharomyces cerevisiae*. *Applied Microbiology and Biotechnology*, *97*(13), 5753–5769. doi.org/10.1007/s00253-013-4877-y

Carsanba, E., Pintado, M., & Oliveira, C. **(2021)**. Fermentation strategies for production of pharmaceutical terpenoids in engineered yeast. *Pharmaceuticals*, *14*(4), 295. doi.org/10.3390/ph14040295

Chen, H.-P., & Liu, J.-K. **(2017)**. *Secondary Metabolites from Higher Fungi* (pp. 1–201). doi.org/10.1007/978-3-319-59542-9_1

Chen, X., Zaro, J. L., & Shen, W.-C. **(2013)**. Fusion protein linkers: Property, design and functionality. *Advanced Drug Delivery Reviews*, *65*(10), 1357–1369. doi.org/10.1016/j.addr.2012.09.039

Cheng, J., Wu, D., Chen, S., Chen, J., & Wu, J. **(2011)**. High-level extracellular production of α-cyclodextrin glycosyltransferase with recombinant *Escherichia coli* BL21 (DE3). *Journal of Agricultural and Food Chemistry*, *59*(8), 3797–3802. doi.org/10.1021/jf200033m

Chou, C., Young, D. D., & Deiters, A. **(2010)**. Photocaged T7 RNA polymerase for the light activation of transcription and gene function in pro- and eukaryotic cells. *ChemBioChem*, *11*(7), 972–977. doi.org/10.1002/cbic.201000041

Cirino, P. C., & Sun, L. **(2008)**. Advancing biocatalysis through enzyme, cellular, and platform engineering. *Biotechnology Progress*, *24*(3), 515–519. doi.org/10.1021/bp070387a

Clarke, L., & Kitney, R. **(2020)**. Developing synthetic biology for industrial biotechnology applications. *Biochemical Society Transactions*, *48*(1), 113–122. doi.org/10.1042/BST20190349

Collins, K. **(2006)**. The biogenesis and regulation of telomerase holoenzymes. *Nature Reviews Molecular Cell Biology*, *7*(7), 484–494. doi.org/10.1038/nrm1961

Couillaud, J., Leydet, L., Duquesne, K., & Lacazio, G. **(2021)**. The terpene mini-path, a new promising alternative for terpenoids bio-production. *Genes*, *12*(12), 1974. doi.org/10.3390/genes12121974

Cravens, A., Payne, J., & Smolke, C. D. **(2019)**. Synthetic biology strategies for microbial biosynthesis of plant natural products. *Nature Communications*, *10*, 2142. doi.org/10.1038/s41467-019-09848-w

Dahl, R. H., Zhang, F., Alonso-Gutierrez, J., Baidoo, E., Batth, T. S., Redding-Johanson, A. M., Petzold, C. J., Mukhopadhyay, A., Lee, T. S., Adams, P. D., & Keasling, J. D. **(2013)**. Engineering dynamic pathway regulation using stress-response promoters. *Nature Biotechnology*, *31*(11), 1039–1046. doi.org/10.1038/nbt.2689

Das, R., & Baker, D. **(2008)**. Macromolecular modeling with Rosetta. *Annual Review of Biochemistry*, *77*(1), 363–382. doi.org/10.1146/annurev.biochem.77.062906.171838

Dinjaski, N., & Prieto, M. A. **(2013)**. Swapping of phasin modules to optimize the *in vivo* immobilization of proteins to medium-chain-length polyhydroxyalkanoate granules in *Pseudomonas putida*. *Biomacromolecules*, *14*(9), 3285–3293. doi.org/10.1021/bm4008937

Dinjaski, N., & Prieto, M. A. **(2015)**. Smart polyhydroxyalkanoate nanobeads by protein based functionalization. *Nanomedicine: Nanotechnology, Biology and Medicine*, *11*(4), 885–899. doi.org/10.1016/j.nano.2015.01.018

Donald, K. A., Hampton, R. Y., & Fritz, I. B. **(1997)**. Effects of overproduction of the catalytic domain of 3-hydroxy-3-methylglutaryl coenzyme A reductase on squalene synthesis in *Saccharomyces cerevisiae*. *Applied and Environmental Microbiology*, *63*(9), 3341–3344. doi.org/10.1128/aem.63.9.3341-3344.1997

Donovan, R. S., Robinson, C. W., & Glick, B. R. **(1996)**. Optimizing inducer and culture conditions for expression of foreign proteins under the control of the *lac* promoter. *Journal of Industrial Microbiology*, *16*(3), 145–154. doi.org/10.1007/BF01569997

Dorsey, J. K., & Porter, J. W. **(1968)**. The inhibition of mevalonic kinase by geranyl and farnesyl pyrophosphates. *The Journal of Biological Chemistry*, *243*(18), 4667–4670. doi.org/10.1016/S0021-9258(18)93170-4

Drepper, T., Krauss, U., Meyer zu Berstenhorst, S., Pietruszka, J., & Jaeger, K.-E. **(2011)**. Lights on and action! Controlling microbial gene expression by light. *Applied Microbiology and Biotechnology*, *90*(1), 23–40. doi.org/10.1007/s00253-011-3141-6

Du, J., & Rehm, B. H. A. **(2017)**. Purification of target proteins from intracellular inclusions mediated by intein cleavable polyhydroxyalkanoate synthase fusions. *Microbial Cell Factories*, *16*(1), 184. doi.org/10.1186/s12934-017-0799-1

Dueber, J. E., Wu, G. C., Malmirchegini, G. R., Moon, T. S., Petzold, C. J., Ullal, A. v, Prather, K. L. J., & Keasling, J. D. **(2009)**. Synthetic protein scaffolds provide modular control over metabolic flux. *Nature Biotechnology*, *27*(8), 753–759. doi.org/10.1038/nbt.1557

Dumorne, K., Cordova, D. C., Astorga-Elo, M., & Renganathan, P. **(2017)**. Extremozymes: A potential source for industrial applications. *Journal of Microbiology and Biotechnology*, *27*(4), 649–659. doi.org/10.4014/jmb.1611.11006

Dunlop, M. J., Keasling, J. D., & Mukhopadhyay, A. **(2010)**. A model for improving microbial biofuel production using a synthetic feedback loop. *Systems and Synthetic Biology*, *4*(2), 95–104. doi.org/10.1007/s11693-010-9052-5

Elissawy, A., El-Shazly, M., Ebada, S., Singab, A., & Proksch, P. **(2015)**. Bioactive terpenes from marine-derived fungi. *Marine Drugs*, *13*(4), 1966–1992. doi.org/10.3390/md13041966

Elkahlout, K., Sagir, E., Alipour, S., Koku, H., Gunduz, U., Eroglu, I., & Yucel, M. **(2019)**. Long-term stable hydrogen production from acetate using immobilized *Rhodobacter capsulatus* in a panel photobioreactor. *International Journal of Hydrogen Energy*, *44*(34), 18801–18810. doi.org/10.1016/j.ijhydene.2018.10.133

Engels, B., Dahm, P., & Jennewein, S. **(2008)**. Metabolic engineering of taxadiene biosynthesis in yeast as a first step towards taxol (paclitaxel) production. *Metabolic Engineering*, *10*(3–4), 201–206. doi.org/10.1016/j.ymben.2008.03.001

Engels, J., & Schlaeger, E. J. **(1977)**. Synthesis, structure, and reactivity of adenosine cyclic 3',5'-phosphate-benzyltriesters. *Journal of Medicinal Chemistry*, *20*(7), 907–911. doi.org/10.1021/jm00217a008

Fan, J.-Y., Cui, Z.-Q., Wei, H.-P., Zhang, Z.-P., Zhou, Y.-F., Wang, Y.-P., & Zhang, X.-E. **(2008)**. Split mCherry as a new red bimolecular fluorescence complementation system for visualizing protein–protein interactions in living cells. *Biochemical and Biophysical Research Communications*, *367*(1), 47–53. doi.org/10.1016/j.bbrc.2007.12.101

Federsel, H.-J., Moody, T. S., & Taylor, S. J. C. **(2021)**. Recent trends in enzyme immobilization - Concepts for expanding the biocatalysis toolbox. *Molecules*, *26*(9), 2822. doi.org/10.3390/molecules26092822

Gardner, L., Zou, Y., Mara, A., Cropp, T. A., & Deiters, A. **(2011)**. Photochemical control of bacterial signal processing using a light-activated erythromycin. *Molecular BioSystems*, *7*(9), 2554. doi.org/10.1039/c1mb05166k

Gautier, A., Gauron, C., Volovitch, M., Bensimon, D., Jullien, L., & Vriz, S. **(2014)**. How to control proteins with light in living systems. *Nature Chemical Biology*, *10*(7), 533–541. doi.org/10.1038/nchembio.1534

George, D. M., Vincent, A. S., & Mackey, H. R. **(2020)**. An overview of anoxygenic phototrophic bacteria and their applications in environmental biotechnology for sustainable resource recovery. *Biotechnology Reports*, *28*, e00563. doi.org/10.1016/j.btre.2020.e00563

Gerlach, T., Schain, J., Söltl, S., van Schie, M. M. C. H., Hilgers, F., Bitzenhofer, N. L., Drepper, T., & Rother, D. **(2022)**. Photo-regulation of enzyme activity: The inactivation of a carboligase with genetically encoded photosensitizer fusion tags. *Frontiers in Catalysis*, *2*. doi.org/10.3389/fctls.2022.835919

Gerngross, T. U., Reilly, P., Stubbe, J., Sinskey, A. J., & Peoples, O. P. **(1993)**. Immunocytochemical analysis of poly-beta-hydroxybutyrate (PHB) synthase in *Alcaligenes eutrophus* H16: Localization of the synthase enzyme at the surface of PHB granules. *Journal of Bacteriology*, *175*(16), 5289–5293. doi.org/10.1128/jb.175.16.5289-5293.1993

Goldstein, J. L., & Brown, M. S. **(1990)**. Regulation of the mevalonate pathway. *Nature*, *343*(6257), 425–430. doi.org/10.1038/343425a0

Gomes, L., Monteiro, G., & Mergulhão, F. **(2020)**. The impact of IPTG induction on plasmid stability and heterologous protein expression by *Escherichia coli* biofilms. *International Journal of Molecular Sciences*, *21*(2), 576. doi.org/10.3390/ijms21020576

Gorbachev, D. A., Staroverov, D. B., Lukyanov, K. A., & Sarkisyan, K. S. **(2020)**. Genetically encoded red photosensitizers with enhanced phototoxicity. *International Journal of Molecular Sciences*, *21*(22), 8800. doi.org/10.3390/ijms21228800

Gorka, A. P., Yamamoto, T., Zhu, J., & Schnermann, M. J. **(2018)**. Cyanine photocages enable spatial control of inducible Cre-mediated recombination. *ChemBioChem*, *19*(12), 1239–1243. doi.org/10.1002/cbic.201800061

Gozari, M., Alborz, M., El-Seedi, H. R., & Jassbi, A. R. **(2021)**. Chemistry, biosynthesis and biological activity of terpenoids and meroterpenoids in bacteria and fungi isolated from different marine habitats. *European Journal of Medicinal Chemistry*, *210*, 112957. doi.org/10.1016/j.ejmech.2020.112957

Gruchattka, E., Hädicke, O., Klamt, S., Schütz, V., & Kayser, O. **(2013)**. *In silico* profiling of *Escherichia coli* and *Saccharomyces cerevisiae* as terpenoid factories. *Microbial Cell Factories*, *12*(1), 84. doi.org/10.1186/1475-2859-12-84

Gurung, N., Ray, S., Bose, S., & Rai, V. **(2013)**. A broader view: Microbial enzymes and their relevance in industries, medicine, and beyond. *BioMed Research International*, *2013*, 1–18. doi.org/10.1155/2013/329121

Guzik, U., Hupert-Kocurek, K., & Wojcieszyńska, D. **(2014)**. Immobilization as a strategy for improving enzyme properties - Application to oxidoreductases. *Molecules*, *19*(7), 8995–9018. doi.org/10.3390/molecules19078995

Hagan, R. M., Björnsson, R., McMahon, S. A., Schomburg, B., Braithwaite, V., Bühl, M., Naismith, J. H., & Schwarz-Linek, U. **(2010)**. NMR spectroscopic and theoretical analysis of a spontaneously formed Lys-Asp isopeptide bond. *Angewandte Chemie International Edition*, *49*(45), 8421–8425. doi.org/10.1002/anie.201004340

Hage-Hülsmann, J., Metzger, S., Wewer, V., Buechel, F., Troost, K., Thies, S., Loeschcke, A., Jaeger, K.-E., & Drepper, T. **(2019)**. Biosynthesis of cycloartenol by expression of plant and bacterial oxidosqualene cyclases in engineered *Rhodobacter capsulatus*. *Journal of Biotechnology*, *306*, 100014. doi.org/10.1016/j.btecx.2020.100014

Hahn, S. K., Chang, Y. K., & Lee, S. Y. (1995). Recovery and characterization of poly(3-hydroxybutyric acid) synthesized in *Alcaligenes eutrophus* and recombinant *Escherichia coli*. *Applied and Environmental Microbiology*, *61*(1), 34–39. doi.org/10.1128/aem.61.1.34-39.1995

Hallett, R. A., Zimmerman, S. P., Yumerefendi, H., Bear, J. E., & Kuhlman, B. **(2016)**. Correlating *in vitro* and *in vivo* activities of light-inducible dimers: A cellular optogenetics guide. *ACS Synthetic Biology*, *5*(1), 53–64. doi.org/10.1021/acssynbio.5b00119

Hansen, L. H., Knudsen, S., & Sørensen, S. J. **(1998)**. The effect of the *lacY* gene on the induction of IPTG inducible promoters, studied in *Escherichia coli* and *Pseudomonas fluorescens*. *Current Microbiology*, *36*(6), 341–347. doi.org/10.1007/s002849900320

Hartmann, D., Smith, J. M., Mazzotti, G., Chowdhry, R., & Booth, M. J. **(2020)**. Controlling gene expression with light: A multidisciplinary endeavour. *Biochemical Society Transactions*, *48*(4), 1645–1659. doi.org/10.1042/BST20200014

Hatlem, D., Trunk, T., Linke, D., & Leo, J. C. **(2019)**. Catching a SPY: Using the SpyCatcher-SpyTag and related systems for labeling and localizing bacterial proteins. *International Journal of Molecular Sciences*, *20*(9), 2129. doi.org/10.3390/ijms20092129

Heck, A., & Drepper, T. **(2017)**. Engineering photosynthetic α-proteobacteria for the production of recombinant proteins and terpenoids. In *Modern Topics in the Phototrophic Prokaryotes* (pp. 395–425). Springer International Publishing. doi.org/10.1007/978-3-319-46261-5_12

Herrou, J., & Crosson, S. **(2011)**. Function, structure and mechanism of bacterial photosensory LOV proteins. *Nature Reviews Microbiology*, *9*(10), 713–723. doi.org/10.1038/nrmicro2622

Heux, S., Meynial-Salles, I., O'Donohue, M. J., & Dumon, C. **(2015)**. White biotechnology: State of the art strategies for the development of biocatalysts for biorefining. *Biotechnology Advances*, *33*(8), 1653–1670. doi.org/10.1016/j.biotechadv.2015.08.004

Hilgers, F. **(2021)**. Optogenetic control of bio(techno)logical processes in bacteria at different cellular levels. *Dissertation*

Hinson, D. D., Chambliss, K. L., Toth, M. J., Tanaka, R. D., & Gibson, K. M. **(1997)**. Post-translational regulation of mevalonate kinase by intermediates of the cholesterol and nonsterol isoprene biosynthetic pathways. *Journal of Lipid Research*, *38*(11), 2216–2223. doi.org/10.1016/S0022-2275(20)34935-X

Hirose, Y., Shimada, T., Narikawa, R., Katayama, M., & Ikeuchi, M. **(2008)**. Cyanobacteriochrome CcaS is the green light receptor that induces the expression of phycobilisome linker protein. *Proceedings of the National Academy of Sciences*, *105*(28), 9528–9533. doi.org/10.1073/pnas.0801826105

Ho, H.-M., Huang, C.-Y., Cheng, Y.-J., Shen, K.-Y., Tzeng, T.-T., Liu, S.-J., Chen, H.-W., Huang, C.-H., & Huang, M.-H. **(2021)**. Assessment of adjuvantation strategy of lipid squalene nanoparticles for enhancing the immunogenicity of a SARS-CoV-2 spike subunit protein against COVID-19. *International Journal of Pharmaceutics*, *607*, 121024. doi.org/10.1016/j.ijpharm.2021.121024

Hogenkamp, F., Hilgers, F., Bitzenhofer, N. L., Ophoven, V., Haase, M., Bier, C., Binder, D., Jaeger, K., Drepper, T., & Pietruszka, J. **(2022)**. Optochemical control of bacterial gene expression: Novel photocaged compounds for different promoter systems. *ChemBioChem*, *23*(1). doi.org/10.1002/cbic.202100467

Hu, J.-H., Wang, F., & Liu, C.-Z. **(2015)**. Development of an efficient process intensification strategy for enhancing Pfu DNA polymerase production in recombinant *Escherichia coli*. *Bioprocess and Biosystems Engineering*, *38*(4), 651–659. doi.org/10.1007/s00449-014-1304-4

Hurme, R., & Rhen, M. **(1998)**. Temperature sensing in bacterial gene regulation - what it all boils down to. *Molecular Microbiology*, *30*(1), 1–6. doi.org/10.1046/j.1365-2958.1998.01049.x

Hyeon, J. E., Shin, S. K., & Han, S. O. **(2016)**. Design of nanoscale enzyme complexes based on various scaffolding materials for biomass conversion and immobilization. *Biotechnology Journal*, *11*(11), 1386–1396. doi.org/10.1002/biot.201600039

Immethun, C. M., & Moon, T. S. **(2018).** Synthetic gene regulation in cyanobacteria. *Advances in Experimental Medicine and Biology, 1080*, 317-355. doi.org/10.1007/978-981-13-0854-3_13

Intasian, P., Prakinee, K., Phintha, A., Trisrivirat, D., Weeranoppanant, N., Wongnate, T., & Chaiyen, P. **(2021)**. Enzymes, *in vivo* biocatalysis, and metabolic engineering for enabling a circular economy and sustainability. *Chemical Reviews*, *121*(17), 10367–10451. doi.org/10.1021/acs.chemrev.1c00121

Iturrate, L., Sánchez-Moreno, I., Doyagüez, E. G., & García-Junceda, E. **(2009)**. Substrate channeling in an engineered bifunctional aldolase/kinase enzyme confers catalytic advantage for C–C bond formation. *Chemical Communications*, *13*, 1721. doi.org/10.1039/b822345a

Iwata, T., & Masuda, S. **(2021)**. Photoreaction mechanisms of flavoprotein photoreceptors and their applications. *Advances in Experimental Medicine and Biology, 1293*, 189-206. doi.org/10.1007/978-981-15-8763-4_11

Jacob, F., & Monod, J. **(1961)**. Genetic regulatory mechanisms in the synthesis of proteins. *Journal of Molecular Biology*, *3*, 318–356. doi.org/10.1016/s0022-2836(61)80072-7

Jang, H.-J., Yoon, S.-H., Ryu, H.-K., Kim, J.-H., Wang, C.-L., Kim, J.-Y., Oh, D.-K., & Kim, S.-W. **(2011)**. Retinoid production using metabolically engineered *Escherichia coli* with a two-phase culture system. *Microbial Cell Factories*, *10*(1), 59. doi.org/10.1186/1475-2859-10-59

Jendrossek, D., & Pfeiffer, D. **(2014)**. New insights in the formation of polyhydroxyalkanoate granules (carbonosomes) and novel functions of poly(3-hydroxybutyrate). *Environmental Microbiology*, *16*(8), 2357–2373. doi.org/10.1111/1462-2920.12356

Jensen, P. R. **(2016)**. Natural products and the gene cluster revolution. *Trends in Microbiology*, *24*(12), 968–977. doi.org/10.1016/j.tim.2016.07.006

Jeon, E.-Y., Baek, A.-H., Bornscheuer, U. T., & Park, J.-B. **(2015)**. Enzyme fusion for whole-cell biotransformation of long-chain sec-alcohols into esters. *Applied Microbiology and Biotechnology*, *99*(15), 6267–6275. doi.org/10.1007/s00253-015-6392-9

Jia, H., Li, Y., Liu, Y., Yan, Q., Yang, S., & Jiang, Z. **(2012)**. Engineering a thermostable β-1,3-1,4-glucanase from *Paecilomyces thermophila* to improve catalytic efficiency at acidic pH. *Journal of Biotechnology*, *159*(1–2), 50–55. doi.org/10.1016/j.jbiotec.2012.02.007

Jiang, W., & Fang, B. **(2020)**. Synthesizing chiral drug intermediates by biocatalysis. *Applied Biochemistry and Biotechnology*, *192*(1), 146–179. doi.org/10.1007/s12010-020-03272-3

Jiang, W., Zhuang, Y., Wang, S., & Fang, B. **(2015)**. Directed evolution and resolution mechanism of 1, 3-propanediol oxidoreductase from *Klebsiella pneumoniae* toward higher activity by error-prone PCR and bioinformatics. *PLOS ONE*, *10*(11), e0141837. doi.org/10.1371/journal.pone.0141837

Jodlbauer, J., Rohr, T., Spadiut, O., Mihovilovic, M. D., & Rudroff, F. **(2021)**. Biocatalysis in green and blue: Cyanobacteria. *Trends in Biotechnology*, *39*(9), 875–889. doi.org/10.1016/j.tibtech.2020.12.009

Jordá, T., & Puig, S. **(2020)**. Regulation of ergosterol biosynthesis in *Saccharomyces cerevisiae*. *Genes*, *11*(7), 795. doi.org/10.3390/genes11070795

Joshi, R., Trinkl, J., Haugeneder, A., Härtl, K., Franz-Oberdorf, K., Giri, A., Hoffmann, T., & Schwab, W. **(2019)**. Semi-rational design and engineering of grapevine glucosyltransferases for enhanced activity and modified product selectivity. *Glycobiology*, *29*(11), 765–775. doi.org/10.1093/glycob/cwz056

Juers, D. H., Matthews, B. W., & Huber, R. E. **(2012)**. *LacZ* β-galactosidase: Structure and function of an enzyme of historical and molecular biological importance. *Protein Science*, *21*(12), 1792–1807. doi.org/10.1002/pro.2165

Kalkreuter, E., Bingham, K. S., Keeler, A. M., Lowell, A. N., Schmidt, J. J., Sherman, D. H., & Williams, G. J. **(2021)**. Computationally-guided exchange of substrate selectivity motifs in a modular polyketide synthase acyltransferase. *Nature Communications*, *12*(1), 2193. doi.org/10.1038/s41467-021-22497-2

Kang, W., Ma, T., Liu, M., Qu, J., Liu, Z., Zhang, H., Shi, B., Fu, S., Ma, J., Lai, L. T. F., He, S., Qu, J., Wing-Ngor Au, S., Ho Kang, B., Yu Lau, W. C., Deng, Z., Xia, J., & Liu, T. **(2019)**. Modular enzyme assembly for enhanced cascade biocatalysis and metabolic flux. *Nature Communications*, *10*(1). doi.org/10.1038/s41467-019-12247-w

Karlson, P. **(1969)**. Terpenoids in insects. *Biochemical Journal*, *113*(3), 26P.1. doi.org/10.1042/bj1130026Pa

Katzke, N., Arvani, S., Bergmann, R., Circolone, F., Markert, A., Svensson, V., Jaeger, K.-E., Heck, A., & Drepper, T. **(2010)**. A novel T7 RNA polymerase dependent expression system for high-level protein production in the phototrophic bacterium *Rhodobacter capsulatus*. *Protein Expression and Purification*, *69*(2), 137–146. doi.org/10.1016/j.pep.2009.08.008

Katzke, N., Bergmann, R., Jaeger, K.-E., & Drepper, T. **(2012)**. Heterologous high-level gene expression in the photosynthetic bacterium *Rhodobacter capsulatus. Methods in Molecular Biology, 824*, 251-269. doi.org/10.1007/978-1-61779-433-9_13

Kaur, J., Kumar, A., & Kaur, J. **(2018)**. Strategies for optimization of heterologous protein expression in *E. coli*: Roadblocks and reinforcements. *International Journal of Biological Macromolecules*, *106*, 803–822. doi.org/10.1016/j.ijbiomac.2017.08.080

Kavanagh, K. L., Guo, K., Dunford, J. E., Wu, X., Knapp, S., Ebetino, F. H., Rogers, M. J., Russell, R. G. G., & Oppermann, U. **(2006)**. The molecular mechanism of nitrogen-containing bisphosphonates as antiosteoporosis drugs. *Proceedings of the National Academy of Sciences*, *103*(20), 7829–7834. doi.org/10.1073/pnas.0601643103

Kavitha, G., Rengasamy, R., & Inbakandan, D. **(2018)**. Polyhydroxybutyrate production from marine source and its application. *International Journal of Biological Macromolecules*, *111*, 102–108. doi.org/10.1016/j.ijbiomac.2017.12.155

Keeble, A. H., & Howarth, M. **(2019)**. Insider information on successful covalent protein coupling with help from SpyBank. *Methods in Enzymology, 617,* 443-461. doi.org/10.1016/bs.mie.2018.12.010

Khan, N. E., Nybo, S. E., Chappell, J., & Curtis, W. R. **(2015)**. Triterpene hydrocarbon production engineered into a metabolically versatile host— *Rhodobacter capsulatus*. *Biotechnology and Bioengineering*, *112*(8), 1523–1532. doi.org/10.1002/bit.25573

Kim, T., Song, B., Cho, K. S., & Lee, I.-S. **(2020)**. Therapeutic potential of volatile terpenes and terpenoids from forests for inflammatory diseases. *International Journal of Molecular Sciences*, *21*(6), 2187. doi.org/10.3390/ijms21062187

Kirby, J., Dietzel, K. L., Wichmann, G., Chan, R., Antipov, E., Moss, N., Baidoo, E. E. K., Jackson, P., Gaucher, S. P., Gottlieb, S., LaBarge, J., Mahatdejkul, T., Hawkins, K. M., Muley, S., Newman, J. D., Liu, P., Keasling, J. D., & Zhao, L. **(2016)**. Engineering a functional 1-deoxy-D-xylulose 5-phosphate (DXP) pathway in *Saccharomyces cerevisiae*. *Metabolic Engineering*, *38*, 494–503. doi.org/10.1016/j.ymben.2016.10.017

Klewer, L., & Wu, Y. **(2019)**. Light-induced dimerization approaches to control cellular processes. *Chemistry – A European Journal*, *25*(54), 12452–12463. doi.org/10.1002/chem.201900562

Klier, A., Msadek, T., & Rapoport, G. **(1992)**. Positive regulation in the Gram-positive bacterium: *Bacillus subtilis*. *Annual Review of Microbiology*, *46*(1), 429–459. doi.org/10.1146/annurev.mi.46.100192.002241

Klipp, W., Masepohl, B., & Pühler, A. **(1988)**. Identification and mapping of nitrogen fixation genes of *Rhodobacter capsulatus*: Duplication of a nifA-nifB region. *Journal of Bacteriology*, *170*(2), 693–699. doi.org/10.1128/jb.170.2.693-699.1988

Kobayashi, J., & Kondo, A. **(2019)**. Disruption of poly (3-hydroxyalkanoate) depolymerase gene and overexpression of three poly (3-hydroxybutyrate) biosynthetic genes improve poly (3-hydroxybutyrate) production from nitrogen rich medium by *Rhodobacter sphaeroides*. *Microbial Cell Factories*, *18*(1), 40. doi.org/10.1186/s12934-019-1088-y

Kohler, A. C., Simmons, B. A., & Sale, K. L. **(2018)**. Structure-based engineering of a plant-fungal hybrid peroxidase for enhanced temperature and pH tolerance. *Cell Chemical Biology*, *25*(8), 974-983.e3. doi.org/10.1016/j.chembiol.2018.04.014

Köker, T., Fernandez, A., & Pinaud, F. **(2018)**. Characterization of split fluorescent protein variants and quantitative analyses of their self-assembly process. *Scientific Reports*, *8*(1), 5344. doi.org/10.1038/s41598-018-23625-7

Kondrat, S., & von Lieres, E. **(2022)**. Mechanisms and effects of substrate channelling in enzymatic cascades. *Methods in Molecular Biology, 2487,* 27-50 doi.org/10.1007/978-1-0716-2269-8_3

Kranz, R. G., Gabbert, K. K., Locke, T. A., & Madigan, M. T. **(1997)**. Polyhydroxyalkanoate production in *Rhodobacter capsulatus*: Genes, mutants, expression, and physiology. *Applied and Environmental Microbiology*, *63*(8), 3003–3009. doi.org/10.1128/aem.63.8.3003-3009.1997

Kschowak, M. J., Maier, F., Wortmann, H., & Buchhaupt, M. **(2020)**. Analyzing and engineering the product selectivity of a 2-methylenebornane synthase. *ACS Synthetic Biology*, *9*(5), 981–986. doi.org/10.1021/acssynbio.9b00432

Kulagina, N., Papon, N., & Courdavault, V. **(2021)**. Microbial cell factories for tetrahydroisoquinoline alkaloid production. *ChemBioChem*, *22*(4), 639–641. doi.org/10.1002/cbic.202000579

Kumar, A., Prasad, A., Sedlářová, M., Ksas, B., Havaux, M., & Pospíšil, P. **(2020)**. Interplay between antioxidants in response to photooxidative stress in *Arabidopsis*. *Free Radical Biology and Medicine*, *160*, 894–907. doi.org/10.1016/j.freeradbiomed.2020.08.027

Kummer, M. J., Lee, Y. S., Yuan, M., Alkotaini, B., Zhao, J., Blumenthal, E., & Minteer, S. D. **(2021)**. Substrate channeling by a rationally designed fusion protein in a biocatalytic cascade. *JACS Au*, *1*(8), 1187–1197. doi.org/10.1021/jacsau.1c00180

Kusen, P. M., Wandrey, G., Krewald, V., Holz, M., Berstenhorst, S. M. zu, Büchs, J., & Pietruszka, J. **(2017)**. Light-controlled gene expression in yeast using photocaged Cu 2+. *Journal of Biotechnology*, *258*, 117–125. doi.org/10.1016/j.jbiotec.2017.04.032

Kusen, P. M., Wandrey, G., Probst, C., Grünberger, A., Holz, M., Meyer zu Berstenhorst, S., Kohlheyer, D., Büchs, J., & Pietruszka, J. **(2016)**. Optogenetic regulation of tunable gene expression in yeast using

photo-labile caged methionine. *ACS Chemical Biology*, *11*(10), 2915–2922. doi.org/10.1021/acschembio.6b00462

Lalwani, M. A., Ip, S. S., Carrasco-López, C., Day, C., Zhao, E. M., Kawabe, H., & Avalos, J. L. **(2021)**. Optogenetic control of the *lac* operon for bacterial chemical and protein production. *Nature Chemical Biology*, *17*(1), 71–79. doi.org/10.1038/s41589-020-0639-1

Lancaster, L., Abdallah, W., Banta, S., & Wheeldon, I. **(2018)**. Engineering enzyme microenvironments for enhanced biocatalysis. *Chemical Society Reviews*, *47*(14), 5177–5186. doi.org/10.1039/c8cs00085a

Lauchli, R., Rabe, K. S., Kalbarczyk, K. Z., Tata, A., Heel, T., Kitto, R. Z., & Arnold, F. H. **(2013)**. High-throughput screening for terpene-synthase-cyclization activity and directed evolution of a terpene synthase. *Angewandte Chemie International Edition*, *52*(21), 5571–5574. doi.org/10.1002/anie.201301362

Lederberg, J. **(1950)**. The β-D-galactosidase of *Escherichia coli*, strain K-12. *Journal of Bacteriology*, *60*(4), 381–392. doi.org/10.1128/jb.60.4.381-392.1950

Lee, J. H., Nam, D. H., Lee, S. H., Park, J. H., Park, S. J., Lee, S. H., Park, C. B., & Jeong, K. J. **(2014)**. New platform for cytochrome P450 reaction combining *in situ* immobilization on biopolymer. *Bioconjugate Chemistry*, *25*(12), 2101–2104. doi.org/10.1021/bc500404j

Lewis, M. **(2005)**. The *lac* repressor. *Comptes Rendus Biologies*, *328*(6), 521–548. doi.org/10.1016/j.crvi.2005.04.004

Lewis, M. **(2013)**. Allostery and the *lac* operon. *Journal of Molecular Biology*, *425*(13), 2309–2316. doi.org/10.1016/j.jmb.2013.03.003

Lewis, M., Chang, G., Horton, N. C., Kercher, M. A., Pace, H. C., Schumacher, M. A., Brennan, R. G., & Lu, P. **(1996)**. Crystal structure of the lactose operon repressor and its complexes with DNA and inducer. *Science*, *271*(5253), 1247–1254. doi.org/10.1126/science.271.5253.1247

Li, K., & Gustafson, K. R. **(2021)**. Sesterterpenoids: Chemistry, biology, and biosynthesis. *Natural Product Reports*, *38*(7), 1251–1281. doi.org/10.1039/D0NP00070A

Li, M., Nian, R., Xian, M., & Zhang, H. **(2018)**. Metabolic engineering for the production of isoprene and isopentenol by *Escherichia coli*. *Applied Microbiology and Biotechnology*, *102*(18), 7725–7738. doi.org/10.1007/s00253-018-9200-5

Li, R., Yang, J., Xiao, Y., & Long, L. **(2019)**. *In vivo* immobilization of an organophosphorus hydrolyzing enzyme on bacterial polyhydroxyalkanoate nano-granules. *Microbial Cell Factories*, *18*(1), 166. doi.org/10.1186/s12934-019-1201-2

Liang, Z., Zhi, H., Fang, Z., & Zhang, P. **(2021)**. Genetic engineering of yeast, filamentous fungi and bacteria for terpene production and applications in food industry. *Food Research International*, *147*, 110487. doi.org/10.1016/j.foodres.2021.110487

Lill, R., & Mühlenhoff, U. **(2008)**. Maturation of iron-sulfur proteins in eukaryotes: Mechanisms, connected processes, and diseases. *Annual Review of Biochemistry*, *77*(1), 669–700. doi.org/10.1146/annurev.biochem.76.052705.162653

Lim, H., Park, J., & Woo, H. M. **(2020)**. Overexpression of the key enzymes in the methylerythritol 4-phosphate pathway in *Corynebacterium glutamicum* for improving farnesyl diphosphate-derived terpene production. *Journal of Agricultural and Food Chemistry*, *68*(39), 10780–10786. doi.org/10.1021/acs.jafc.0c04307

Lim, S., Kim, J., Kim, Y., Xu, D., & Clark, D. S. **(2020)**. CRISPR/Cas-directed programmable assembly of multi-enzyme complexes. *Chemical Communications*, *56*(36), 4950–4953. doi.org/10.1039/D0CC01174F

Lin, C., & Todo, T. **(2005)**. The cryptochromes. *Genome Biology*, *6*(5), 220. doi.org/10.1186/gb-2005-6-5-220

Lin, P.-C., & Pakrasi, H. B. **(2019)**. Engineering cyanobacteria for production of terpenoids. *Planta*, *249*(1), 145–154. doi.org/10.1007/s00425-018-3047-y

Lin, W., Albanese, C., Pestell, R. G., & Lawrence, D. S. **(2002)**. Spatially discrete, light-driven protein expression. *Chemistry & Biology*, *9*(12), 1347–1353. doi.org/10.1016/S1074-5521(02)00288-0

Lipson Feder, C., Cohen, O., Shapira, A., Katzir, I., Peer, R., Guberman, O., Procaccia, S., Berman, P., Flaishman, M., & Meiri, D. **(2021)**. Fertilization following pollination predominantly decreases phytocannabinoids accumulation and alters the accumulation of terpenoids in *Cannabis inflorescences*. *Frontiers in Plant Science*, *12*. doi.org/10.3389/fpls.2021.753847

Liu, C.-L., Bi, H.-R., Bai, Z., Fan, L.-H., & Tan, T.-W. **(2019)**. Engineering and manipulation of a mevalonate pathway in *Escherichia coli* for isoprene production. *Applied Microbiology and Biotechnology*, *103*(1), 239–250. doi.org/10.1007/s00253-018-9472-9

Liu, G.-S., Li, T., Zhou, W., Jiang, M., Tao, X.-Y., Liu, M., Zhao, M., Ren, Y.-H., Gao, B., Wang, F.-Q., & Wei, D.-Z. **(2020)**. The yeast peroxisome: A dynamic storage depot and subcellular factory for squalene overproduction. *Metabolic Engineering*, *57*, 151–161. doi.org/10.1016/j.ymben.2019.11.001

Liu, H., Wang, F., Deng, L., & Xu, P. **(2020)**. Genetic and bioprocess engineering to improve squalene production in *Yarrowia lipolytica*. *Bioresource Technology*, *317*, 123991. doi.org/10.1016/j.biortech.2020.123991

Liu, S., Bilal, M., Rizwan, K., Gul, I., Rasheed, T., & Iqbal, H. M. N. **(2021)**. Smart chemistry of enzyme immobilization using various support matrices – A review. *International Journal of Biological Macromolecules*, *190*, 396–408. doi.org/10.1016/j.ijbiomac.2021.09.006

Liu, Y. H., Hu, B., Xu, Y. J., Bo, J. X., Fan, S., Wang, J. L., & Lu, F. P. **(2012)**. Improvement of the acid stability of *Bacillus licheniformis* alpha amylase by error-prone PCR. *Journal of Applied Microbiology*, *113*(3), 541–549. doi.org/10.1111/j.1365-2672.2012.05359.x

Liu, Y., Hickey, D. P., Guo, J.-Y., Earl, E., Abdellaoui, S., Milton, R. D., Sigman, M. S., Minteer, S. D., & Calabrese Barton, S. **(2017)**. Substrate channeling in an artificial metabolon: A molecular dynamics blueprint for an experimental peptide bridge. *ACS Catalysis*, *7*(4), 2486–2493. doi.org/10.1021/acscatal.6b03440

Liu, Y., Hickey, D. P., Minteer, S. D., Dickson, A., & Calabrese Barton, S. **(2019)**. Markov-state transition path analysis of electrostatic channeling. *The Journal of Physical Chemistry C*, *123*(24), 15284–15292. doi.org/10.1021/acs.jpcc.9b02844

Liu, Y., Low, Z. J., Ma, X., Liang, H., Sinskey, A. J., Stephanopoulos, G., & Zhou, K. **(2020)**. Using biopolymer bodies for encapsulation of hydrophobic products in bacterium. *Metabolic Engineering*, *61*, 206–214. doi.org/10.1016/j.ymben.2020.04.006

Lo, T.-M., Chng, S. H., Teo, W. S., Cho, H.-S., & Chang, M. W. **(2016)**. A two-layer gene circuit for decoupling cell growth from metabolite production. *Cell Systems*, *3*(2), 133–143. doi.org/10.1016/j.cels.2016.07.012

Lockard, M. A., & Waldo, G. S. **(2012)**. Cyan and yellow fluorescent color variants of split GFP *Patent*

Loeschcke, A., Dienst, D., Wewer, V., Hage-Hülsmann, J., Dietsch, M., Kranz-Finger, S., Hüren, V., Metzger, S., Urlacher, V. B., Gigolashvili, T., Kopriva, S., Axmann, I. M., Drepper, T., & Jaeger, K.-E. **(2017)**. The photosynthetic bacteria *Rhodobacter capsulatus* and *Synechocystis* sp. PCC 6803 as new hosts for cyclic plant triterpene biosynthesis. *PLOS ONE*, *12*(12), e0189816. doi.org/10.1371/journal.pone.0189816

Loeschcke, A., Hage-Hülsmann, J., Troost, K., Wewer, V., Jaeger, K.-E., & Drepper, T. **(2022)**. Heterologous production of plant terpenes in the photosynthetic bacterium *Rhodobacter capsulatus*. *Methods in Molecular Biology, 2379,* 125-154 doi.org/10.1007/978-1-0716-1791-5_8

Loeschcke, A., Markert, A., Wilhelm, S., Wirtz, A., Rosenau, F., Jaeger, K.-E., & Drepper, T. **(2013)**. TREX: A universal tool for the transfer and expression of biosynthetic pathways in bacteria. *ACS Synthetic Biology*, *2*(1), 22–33. doi.org/10.1021/sb3000657

Lopez, L., Fasano, C., Perrella, G., & Facella, P. **(2021)**. Cryptochromes and the circadian clock: The story of a very complex relationship in a spinning world. *Genes*, *12*(5), 672. doi.org/10.3390/genes12050672

Lu, J., Zhao, Y., & Zhang, J. **(2018)**. High-level expression of *Aerococcus viridans* pyruvate oxidase in *Escherichia coli* by optimization of vectors and induction conditions. *Letters in Applied Microbiology*, *67*(3), 262–269. doi.org/10.1111/lam.13013

Luo, Y., Ge, M., Wang, B., Sun, C., Wang, J., Dong, Y., & Xi, J. J. **(2020)**. CRISPR/Cas9-deaminase enables robust base editing in *Rhodobacter sphaeroides* 2.4.1. *Microbial Cell Factories*, *19*(1), 93. doi.org/10.1186/s12934-020-01345-w

Madison, L. L., & Huisman, G. W. **(1999)**. Metabolic engineering of poly(3-hydroxyalkanoates): From DNA to plastic. *Microbiology and Molecular Biology Reviews*, *63*(1), 21–53. doi.org/10.1128/MMBR.63.1.21-53.1999

Marbach, A., & Bettenbrock, K. **(2012)**. *lac* operon induction in *Escherichia coli*: Systematic comparison of IPTG and TMG induction and influence of the transacetylase LacA. *Journal of Biotechnology*, *157*(1), 82–88. doi.org/10.1016/j.jbiotec.2011.10.009

Marienhagen, J., & Bott, M. **(2013)**. Metabolic engineering of microorganisms for the synthesis of plant natural products. *Journal of Biotechnology*, *163*(2), 166–178. doi.org/10.1016/j.jbiotec.2012.06.001

Markel, U., Essani, K. D., Besirlioglu, V., Schiffels, J., Streit, W. R., & Schwaneberg, U. **(2020)**. Advances in ultrahigh-throughput screening for directed enzyme evolution. *Chemical Society Reviews*, *49*(1), 233–262. doi.org/10.1039/C8CS00981C

Martin, V. J. J., Pitera, D. J., Withers, S. T., Newman, J. D., & Keasling, J. D. **(2003)**. Engineering a mevalonate pathway in *Escherichia coli* for production of terpenoids. *Nature Biotechnology*, *21*(7), 796–802. doi.org/10.1038/nbt833

Masepohl, B., Drepper, T., Paschen, A., Gross, S., Pawlowski, A., Raabe, K., Riedel, K.-U., & Klipp, W. **(2002)**. Regulation of nitrogen fixation in the phototrophic purple bacterium *Rhodobacter capsulatus*. *Journal of Molecular Microbiology and Biotechnology*, *4*(3), 243–248.

Mato, A., Blanco, F. G., Maestro, B., Sanz, J. M., Pérez-Gil, J., & Prieto, M. A. **(2020)**. Dissecting the polyhydroxyalkanoate-binding domain of the PhaF phasin: Rational design of a minimized affinity tag. *Applied and Environmental Microbiology*, *86*(12). doi.org/10.1128/AEM.00570-20

Matsumi, R., Atomi, H., Driessen, A. J. M., & van der Oost, J. **(2011)**. Isoprenoid biosynthesis in archaea – Biochemical and evolutionary implications. *Research in Microbiology*, *162*(1), 39–52. doi.org/10.1016/j.resmic.2010.10.003

Matsumoto, T., Yamada, R., & Ogino, H. **(2019)**. Chemical treatments for modification and immobilization to improve the solvent-stability of lipase. *World Journal of Microbiology and Biotechnology*, *35*(12), 193. doi.org/10.1007/s11274-019-2777-8

Mayet, C., Deniset-Besseau, A., Prazeres, R., Ortega, J.-M., & Dazzi, A. **(2013)**. Analysis of bacterial polyhydroxybutyrate production by multimodal nanoimaging. *Biotechnology Advances*, *31*(3), 369–374. doi.org/10.1016/j.biotechadv.2012.05.003

McCullum, E. O., Williams, B. A. R., Zhang, J., & Chaput, J. C. **(2010)**. Random Mutagenesis by Error-Prone PCR. *Methods in Molecular Biology, 634,* 103-109. doi.org/10.1007/978-1-60761-652-8_7

Meng, S., Ji, Y., Liu, L., Davari, M. D., & Schwaneberg, U. **(2022)**. Modulating the coupling efficiency of P450 BM3 by controlling water diffusion through access tunnel engineering. *ChemSusChem*, *15*(9):e202102434. doi.org/10.1002/cssc.202102434

Merrick, J. M., & Doudoroff, M. **(1961)**. Enzymatic synthesis of poly-β-hydroxybutyric acid in bacteria. *Nature*, *189*(4768), 890–892. doi.org/10.1038/189890a0

Mewalal, R., Rai, D. K., Kainer, D., Chen, F., Külheim, C., Peter, G. F., & Tuskan, G. A. **(2017)**. Plant-derived terpenes: A feedstock for specialty biofuels. *Trends in Biotechnology*, *35*(3), 227–240. doi.org/10.1016/j.tibtech.2016.08.003

Milias-Argeitis, A., Rullan, M., Aoki, S. K., Buchmann, P., & Khammash, M. **(2016)**. Automated optogenetic feedback control for precise and robust regulation of gene expression and cell growth. *Nature Communications*, *7*(1), 12546. doi.org/10.1038/ncomms12546

Milker, S., & Holtmann, D. **(2021)**. First time β-farnesene production by the versatile bacterium *Cupriavidus necator*. *Microbial Cell Factories*, *20*(1), 89. doi.org/10.1186/s12934-021-01562-x

Moser, S., & Pichler, H. **(2019)**. Identifying and engineering the ideal microbial terpenoid production host. *Applied Microbiology and Biotechnology*, *103*(14), 5501–5516. doi.org/10.1007/s00253-019-09892-y

Mougiakos, I., Orsi, E., Ghiffary, M. R., Post, W., de Maria, A., Adiego-Perez, B., Kengen, S. W. M., Weusthuis, R. A., & van der Oost, J. **(2019)**. Efficient Cas9-based genome editing of *Rhodobacter sphaeroides* for metabolic engineering. *Microbial Cell Factories*, *18*(1). doi.org/10.1186/s12934-019-1255-1

Mowat, C. G., Gazur, B., Campbell, L. P., & Chapman, S. K. **(2010)**. Flavin-containing heme enzymes. *Archives of Biochemistry and Biophysics*, *493*(1), 37–52. doi.org/10.1016/j.abb.2009.10.005

Nguyen, M. K., & Lee, D. S. **(2010)**. Injectable Biodegradable Hydrogels. *Macromolecular Bioscience*, *10*(6), 563–579. doi.org/10.1002/mabi.200900402

Nguyen, T. H. D. **(2021)**. Structural biology of human telomerase: Progress and prospects. *Biochemical Society Transactions*, *49*(5), 1927–1939. doi.org/10.1042/BST20200042

Niederman, R. A. **(2013)**. Membrane development in purple photosynthetic bacteria in response to alterations in light intensity and oxygen tension. *Photosynthesis Research*, *116*(2–3), 333–348. doi.org/10.1007/s11120-013-9851-0

Nirantar, S. R. **(2021)**. Directed evolution methods for enzyme engineering. *Molecules*, *26*(18), 5599. doi.org/10.3390/molecules26185599

Nogueira, M., Enfissi, E. M. A., Welsch, R., Beyer, P., Zurbriggen, M. D., & Fraser, P. D. **(2019)**. Construction of a fusion enzyme for astaxanthin formation and its characterization in microbial and plant hosts: A new tool for engineering ketocarotenoids. *Metabolic Engineering*, *52*, 243–252. doi.org/10.1016/j.ymben.2018.12.006

Obeid, J., Magnin, J., Flaus, J., Adrot, O., Willison, J., & Zlatev, R. **(2009)**. Modelling of hydrogen production in batch cultures of the photosynthetic bacterium *Rhodobacter capsulatus*. *International Journal of Hydrogen Energy*, *34*(1), 180–185. doi.org/10.1016/j.ijhydene.2008.09.081

Ogura, K., & Rehm, B. H. A. **(2019)**. Alginate encapsulation of bioengineered protein-coated polyhydroxybutyrate particles: A new platform for multifunctional composite materials. *Advanced Functional Materials*, *29*(37), 1901893. doi.org/10.1002/adfm.201901893

Ohnuma, S., Hirooka, K., Ohto, C., & Nishino, T. **(1997)**. Conversion from archaeal geranylgeranyl diphosphate synthase to farnesyl diphosphate synthase. *Journal of Biological Chemistry*, *272*(8), 5192–5198. doi.org/10.1074/jbc.272.8.5192

Oliveira, F. L., S. França, A., Castro, A. M., Alves de Souza, R. O. M., Esteves, P. M., & Gonçalves, R. S. B. **(2020)**. Enzyme immobilization in covalent organic frameworks: Strategies and applications in biocatalysis. *ChemPlusChem*, *85*(9), 2051–2066. doi.org/10.1002/cplu.202000549

Olshefsky, A., Shehata, L., & Kuldell, N. **(2016)**. Site-directed mutagenesis to improve sensitivity of a synthetic two-component signaling system. *PLOS ONE*, *11*(1), e0147494. doi.org/10.1371/journal.pone.0147494

Ong, N. T., & Tabor, J. J. **(2018)**. A miniaturized *Escherichia coli* green light sensor with high dynamic range. *ChemBioChem*, *19*(12), 1255–1258. doi.org/10.1002/cbic.201800007

Orsi, E., Folch, P. L., Monje-López, V. T., Fernhout, B. M., Turcato, A., Kengen, S. W. M., Eggink, G., & Weusthuis, R. A. **(2019)**. Characterization of heterotrophic growth and sesquiterpene production by *Rhodobacter sphaeroides* on a defined medium. *Journal of Industrial Microbiology and Biotechnology*, *46*(8), 1179–1190. doi.org/10.1007/s10295-019-02201-6

Osbourn, A. E., & Field, B. **(2009)**. Operons. *Cellular and Molecular Life Sciences*, *66*(23), 3755–3775. doi.org/10.1007/s00018-009-0114-3

Paniagua-Michel, J., Olmos-Soto, J., & Ruiz, M. A. **(2012)**. Pathways of carotenoid biosynthesis in bacteria and microalgae. *Methods in Molecular Biology, 892,* 1-12. doi.org/10.1007/978-1-61779-879-5_1

Paradise, E. M., Kirby, J., Chan, R., & Keasling, J. D. **(2008)**. Redirection of flux through the FPP branch-point in *Saccharomyces cerevisiae* by down-regulating squalene synthase. *Biotechnology and Bioengineering*, *100*(2), 371–378. doi.org/10.1002/bit.21766

Paramasivan, K., & Mutturi, S. **(2017)**. Progress in terpene synthesis strategies through engineering of *Saccharomyces cerevisiae*. *Critical Reviews in Biotechnology*, *37*(8), 974–989. doi.org/10.1080/07388551.2017.1299679

Park, J., Zielinski, M., Magder, A., Tsantrizos, Y. S., & Berghuis, A. M. **(2017)**. Human farnesyl pyrophosphate synthase is allosterically inhibited by its own product. *Nature Communications*, *8*(1), 14132. doi.org/10.1038/ncomms14132

Partow, S., Siewers, V., Daviet, L., Schalk, M., & Nielsen, J. **(2012)**. Reconstruction and evaluation of the synthetic bacterial MEP pathway in *Saccharomyces cerevisiae*. *PLoS ONE*, *7*(12), e52498. doi.org/10.1371/journal.pone.0052498

Pattanaik, B., Englund, E., Nolte, N., & Lindberg, P. **(2020)**. Introduction of a green algal squalene synthase enhances squalene accumulation in a strain of *Synechocystis* sp. PCC 6803. *Metabolic Engineering Communications*, *10*, e00125. doi.org/10.1016/j.mec.2020.e00125

Pearce, S., & Tucker, C. L. **(2021)**. Dual systems for enhancing control of protein activity through induced dimerization approaches. *Advanced Biology*, *5*(5), 2000234. doi.org/10.1002/adbi.202000234

Peng, B., Nielsen, L. K., Kampranis, S. C., & Vickers, C. E. **(2018)**. Engineered protein degradation of farnesyl pyrophosphate synthase is an effective regulatory mechanism to increase monoterpene production in *Saccharomyces cerevisiae*. *Metabolic Engineering*, *47*, 83–93. doi.org/10.1016/j.ymben.2018.02.005

Peoples, O. P., & Sinskey, A. J. **(1989)**. The journal of biological chemistry poly-p-hydroxybutyrate (PHB) biosynthesis in *Alcaligenes eutrophus* H16 identification and characterization of the PHB polymerase gene (phbC). *Journal of Biological Chemistry 26,* 15298-15303. doi.org/10.1016/S0021-9258(19)84825-1

Peters, V., & Rehm, B. H. A. **(2006)**. *In vivo* enzyme immobilization by use of engineered polyhydroxyalkanoate synthase. *Applied and Environmental Microbiology*, *72*(3), 1777–1783. doi.org/10.1128/AEM.72.3.1777-1783.2006

Pham, V. N., Kathare, P. K., & Huq, E. **(2018)**. Phytochromes and phytochrome interacting factors. *Plant Physiology*, *176*(2), 1025–1038. doi.org/10.1104/pp.17.01384

Pichersky, E., & Raguso, R. A. **(2018)**. Why do plants produce so many terpenoid compounds? *New Phytologist*, *220*(3), 692–702. doi.org/10.1111/nph.14178

Piper, P. W., Curran, B., Davies, M. W., Hirst, K., Lockheart, A., Ogden, J. E., Stanway, C. A., Kingsman, A. J., & Kingsman, S. M. **(1988)**. A heat shock element in the phosphoglycerate kinase gene promoter of yeast. *Nucleic Acids Research*, *16*(4), 1333–1348. doi.org/10.1093/nar/16.4.1333

Pitera, D. J., Paddon, C. J., Newman, J. D., & Keasling, J. D. **(2007)**. Balancing a heterologous mevalonate pathway for improved isoprenoid production in *Escherichia coli*. *Metabolic Engineering*, *9*(2), 193–207. doi.org/10.1016/j.ymben.2006.11.002

Pouzet, S., Cruz-Ramon, J., Le Bec, M., Cordier, C., Banderas, A., Barral, S., Sorre, B., Castano-Cerezo, S., Lautier, T., Truan, G., Hersen, P. **(2022)**. Optogenetic control of beta-carotene bioproduction in yeast across multiple lab-scales. *bioRxiv* doi.org/10.1101/2022.10.31.514479

Pötter, M., & Steinbüchel, A. **(2005)**. Poly(3-hydroxybutyrate) granule-associated proteins: Impacts on poly(3-hydroxybutyrate) synthesis and degradation. *Biomacromolecules*, *6*(2), 552–560. doi.org/10.1021/bm049401n

Prasad, S., & Roy, I. **(2017)**. Converting enzymes into tools of industrial importance. *Recent Patents on Biotechnology*, *12*(1). doi.org/10.2174/1872208311666170612113303

Prieto, M. A., B hler, B., Jung, K., Witholt, B., & Kessler, B. **(1999)**. PhaF, a polyhydroxyalkanoate-granule-associated protein of *Pseudomonas oleovorans* GPo1 involved in the regulatory expression system for *pha* genes. *Journal of Bacteriology*, *181*(3), 858–868. doi.org/10.1128/JB.181.3.858-868.1999

Priyanka, P., Tan, Y., Kinsella, G. K., Henehan, G. T., & Ryan, B. J. **(2019)**. Solvent stable microbial lipases: Current understanding and biotechnological applications. *Biotechnology Letters*, *41*(2), 203–220. doi.org/10.1007/s10529-018-02633-7

Pudasaini, A., El-Arab, K. K., & Zoltowski, B. D. **(2015)**. LOV-based optogenetic devices: Light-driven modules to impart photoregulated control of cellular signaling. *Frontiers in Molecular Biosciences*, *2*. doi.org/10.3389/fmolb.2015.00018

Qi, J., Malook, S. ul, Shen, G., Gao, L., Zhang, C., Li, J., Zhang, J., Wang, L., & Wu, J. **(2018)**. Current understanding of maize and rice defense against insect herbivores. *Plant Diversity*, *40*(4), 189–195. doi.org/10.1016/j.pld.2018.06.006

Qin, B., Matsuda, Y., Mori, T., Okada, M., Quan, Z., Mitsuhashi, T., Wakimoto, T., & Abe, I. **(2016)**. An unusual chimeric diterpene synthase from *Emericella variecolor* and its functional conversion into a sesterterpene synthase by domain swapping. *Angewandte Chemie International Edition*, *55*(5), 1658–1661. doi.org/10.1002/anie.201509263

Qu, G., & Sun, Z. **(2022)**. *In silico* prediction methods for site-saturation mutagenesis. *Methods in Molecular Biology, 2397*, 49–69. doi.org/10.1007/978-1-0716-1826-4_4

Quintana, A., Reinhard, J., Faure, R., Uva, P., Bagnères, A.-G., Massiot, G., & Clément, J.-L. **(2003)**. Interspecific variation in terpenoid composition of defensive secretions of European *Reticulitermes* termites. *Journal of Chemical Ecology*, *29*(3), 639–652. doi.org/10.1023/A:1022868603108

Rabeharindranto, H., Castaño-Cerezo, S., Lautier, T., Garcia-Alles, L. F., Treitz, C., Tholey, A., & Truan, G. **(2019)**. Enzyme-fusion strategies for redirecting and improving carotenoid synthesis in *S. cerevisiae*. *Metabolic Engineering Communications*, *8*, e00086. doi.org/10.1016/j.mec.2019.e00086

Raberg, M., Voigt, B., Hecker, M., & Steinbüchel, A. **(2014)**. A closer look on the polyhydroxybutyrate- (PHB-) negative phenotype of *Ralstonia eutropha* PHB-4. *PLoS ONE*, *9*(5), e95907. doi.org/10.1371/journal.pone.0095907

Ran, G., Tan, D., Zhao, J., Fan, F., Zhang, Q., Wu, X., Fan, P., Fang, X., & Lu, X. **(2019)**. Functionalized polyhydroxyalkanoate nano-beads as a stable biocatalyst for cost-effective production of the rare sugar D-allulose. *Bioresource Technology*, *289*, 121673. doi.org/10.1016/j.biortech.2019.121673

Rasiah, I. A., & Rehm, B. H. A. **(2009)**. One-step production of immobilized α-amylase in recombinant *Escherichia coli*. *Applied and Environmental Microbiology*, *75*(7), 2012–2016. doi.org/10.1128/AEM.02782-08

Raymondjean, M., Voulont, S., Cognet, M., Decaux, J. F., Puzenat, N., Bergot, M. O., & Kahn, A. **(1991)**. Positive and negative regulation of gene expression by insulin and glucagon: The model of L-type pyruvate kinase gene. *Biochimie*, *73*(1), 41–45. doi.org/10.1016/0300-9084(91)90072-9

Reddy, L. H., & Couvreur, P. **(2009)**. Squalene: A natural triterpene for use in disease management and therapy. *Advanced Drug Delivery Reviews*, *61*(15), 1412–1426. doi.org/10.1016/j.addr.2009.09.005

Riani, Y. D., Matsuda, T., & Nagai, T. **(2021)**. Genetically encoded photosensitizer for destruction of protein or cell function. *Advances in Experimental Medicine and Biology, 1293*, 265–279. doi.org/10.1007/978-981-15-8763-4_16

Riani, Y. D., Matsuda, T., Takemoto, K., & Nagai, T. **(2018)**. Green monomeric photosensitizing fluorescent protein for photo-inducible protein inactivation and cell ablation. *BMC Biology*, *16*(1), 50. doi.org/10.1186/s12915-018-0514-7

Rinaldi, M. A., Ferraz, C. A., & Scrutton, N. S. **(2022)**. Alternative metabolic pathways and strategies to high-titer terpenoid production in *Escherichia coli*. *Natural Product Reports*, *39*(1), 90–118. doi.org/10.1039/D1NP00025J

Rodriguez-Abetxuko, A., Sánchez-deAlcázar, D., Muñumer, P., & Beloqui, A. **(2020)**. Tunable polymeric scaffolds for enzyme immobilization. *Frontiers in Bioengineering and Biotechnology*, *8*. doi.org/10.3389/fbioe.2020.00830

Rohdich, F., Hecht, S., Gärtner, K., Adam, P., Krieger, C., Amslinger, S., Arigoni, D., Bacher, A., & Eisenreich, W. **(2002)**. Studies on the non-mevalonate terpene biosynthetic pathway: Metabolic role of IspH (LytB) protein. *Proceedings of the National Academy of Sciences*, *99*(3), 1158–1163. doi.org/10.1073/pnas.032658999

Ronnebaum, T. A., Eaton, S. A., Brackhahn, E. A. E., & Christianson, D. W. **(2021)**. Engineering the prenyltransferase domain of a bifunctional assembly-line terpene synthase. *Biochemistry*, *60*(42), 3162–3172. doi.org/10.1021/acs.biochem.1c00600

Rutkauskas, D., Zhan, H., Matthews, K. S., Pavone, F. S., & Vanzi, F. **(2009)**. Tetramer opening in LacI-mediated DNA looping. *Proceedings of the National Academy of Sciences*, *106*(39), 16627–16632. doi.org/10.1073/pnas.0904617106

Ruzicka, L. **(1953)**. The isoprene rule and the biogenesis of terpenic compounds. *Experientia*, *9*(10), 357–367. doi.org/10.1007/BF02167631

Ryan, A., Liu, J., & Deiters, A. **(2021)**. Targeted protein degradation through fast optogenetic activation and its application to the control of cell signaling. *Journal of the American Chemical Society*, *143*(24), 9222–9229. doi.org/10.1021/jacs.1c04324

Sato, T. **(2013)**. Unique biosynthesis of sesquarterpenes (C_{35} terpenes). *Bioscience, Biotechnology, and Biochemistry*, *77*(6), 1155–1159. doi.org/10.1271/bbb.130180

Scalcinati, G., Knuf, C., Partow, S., Chen, Y., Maury, J., Schalk, M., Daviet, L., Nielsen, J., & Siewers, V. **(2012)**. Dynamic control of gene expression in *Saccharomyces cerevisiae* engineered for the production of plant sesquitepene α-santalene in a fed-batch mode. *Metabolic Engineering*, *14*(2), 91–103. doi.org/10.1016/j.ymben.2012.01.007

Schempp, F. M., Drummond, L., Buchhaupt, M., & Schrader, J. **(2018)**. Microbial cell factories for the production of terpenoid flavor and fragrance compounds. *Journal of Agricultural and Food Chemistry*, *66*(10), 2247–2258. doi.org/10.1021/acs.jafc.7b00473

Schlegel, S., Rujas, E., Ytterberg, A. J., Zubarev, R. A., Luirink, J., & de Gier, J.-W. **(2013)**. Optimizing heterologous protein production in the periplasm of *E. coli* by regulating gene expression levels. *Microbial Cell Factories*, *12*(1), 24. doi.org/10.1186/1475-2859-12-24

Scott, W. G. **(2007)**. Ribozymes. *Current Opinion in Structural Biology*, *17*(3), 280–286. doi.org/10.1016/j.sbi.2007.05.003

Serra, S. **(2015)**. Recent advances in the synthesis of carotenoid-derived flavours and fragrances. *Molecules*, *20*(7), 12817–12840. doi.org/10.3390/molecules200712817

Shabestary, K., Hernández, H. P., Miao, R., Ljungqvist, E., Hallman, O., Sporre, E., Branco dos Santos, F., & Hudson, E. P. **(2021)**. Cycling between growth and production phases increases cyanobacteria bioproduction of lactate. *Metabolic Engineering*, *68*, 131–141. doi.org/10.1016/j.ymben.2021.09.010

Sheets, M. B., Wong, W. W., & Dunlop, M. J. **(2020)**. Light-inducible recombinases for bacterial optogenetics. *ACS Synthetic Biology*, *9*(2), 227–235. doi.org/10.1021/acssynbio.9b00395

Sheldon, R. A., & Pereira, P. C. **(2017)**. Biocatalysis engineering: The big picture. In *Chemical Society Reviews* (Vol. 46, Issue 10, pp. 2678–2691). Royal Society of Chemistry. doi.org/10.1039/c6cs00854b

Siedentop, R., & Rosenthal, K. **(2022)**. Industrially relevant enzyme cascades for drug synthesis and their ecological assessment. *International Journal of Molecular Sciences*, *23*(7), 3605. doi.org/10.3390/ijms23073605

Sivy, T. L., Fall, R., & Rosenstiel, T. N. **(2011)**. Evidence of isoprenoid precursor toxicity in *Bacillus subtilis*. *Bioscience, Biotechnology, and Biochemistry*, *75*(12), 2376–2383. doi.org/10.1271/bbb.110572

Son, H. F., & Kim, K.-J. **(2022)**. Structure based protein engineering of aldehyde dehydrogenase from *Azospirillum brasilense* to enhance enzyme activity against unnatural 3-hydroxypropionaldehyde. *Journal of Microbiology and Biotechnology*, *32*(2), 170–175. doi.org/10.4014/jmb.2110.10038

Sparagano, O., Khallaayoune, K., Duvallet, G., Nayak, S., & George, D. **(2013)**. Comparing terpenes from plant essential oils as pesticides for the poultry red mite (*Dermanyssus gallinae*). *Transboundary and Emerging Diseases*, *60*, 150–153. doi.org/10.1111/tbed.12138

Spivey, H. O., & Ovádi, J. **(1999)**. Substrate channeling. *Methods*, *19*(2), 306–321. doi.org/10.1006/meth.1999.0858

Strnad, H., Lapidus, A., Paces, J., Ulbrich, P., Vlcek, C., Paces, V., & Haselkorn, R. **(2010)**. Complete genome sequence of the photosynthetic purple non-sulfur bacterium *Rhodobacter capsulatus* SB 1003. *Journal of Bacteriology*, *192*(13), 3545–3546. doi.org/10.1128/JB.00366-10

Su, A., Shirke, A., Baik, J., Zou, Y., & Gross, R. **(2018)**. Immobilized cutinases: Preparation, solvent tolerance and thermal stability. *Enzyme and Microbial Technology*, *116*, 33–40. doi.org/10.1016/j.enzmictec.2018.05.010

Sumi, S., Suzuki, Y., Matsuki, T., Yamamoto, T., Tsuruta, Y., Mise, K., Kawamura, T., Ito, Y., Shimada, Y., Watanabe, E., Watanabe, S., Toriyabe, M., Takano (Shiratori), H., Ueda, K., & Takano, H. **(2019)**. Light-inducible carotenoid production controlled by a MarR-type regulator in *Corynebacterium glutamicum*. *Scientific Reports*, *9*(1), 13136. doi.org/10.1038/s41598-019-49384-7

Swiezewska, E., & Danikiewicz, W. **(2005)**. Polyisoprenoids: Structure, biosynthesis and function. *Progress in Lipid Research*, *44*(4), 235–258. doi.org/10.1016/j.plipres.2005.05.002

Tabita, F. R. **(1995)**. The Biochemistry and metabolic regulation of carbon metabolism and CO_2 fixation in purple bacteria. In *Anoxygenic Photosynthetic Bacteria* (pp. 885–914). Kluwer Academic Publishers. doi.org/10.1007/0-306-47954-0_41

Takano, H. **(2016)**. The regulatory mechanism underlying light-inducible production of carotenoids in non-phototrophic bacteria. *Bioscience, Biotechnology, and Biochemistry*, *80*(7), 1264–1273. doi.org/10.1080/09168451.2016.1156478

Tarazona, N. A., Machatschek, R., Schulz, B., Prieto, M. A., & Lendlein, A. **(2019)**. Molecular insights into the physical adsorption of amphiphilic protein PhaF onto copolyester surfaces. *Biomacromolecules*, *20*(9), 3242–3252. doi.org/10.1021/acs.biomac.9b00069

Tarrahi, R., Fathi, Z., Seydibeyoğlu, M. Ö., Doustkhah, E., & Khataee, A. **(2020)**. Polyhydroxyalkanoates (PHA): From production to nanoarchitecture. *International Journal of Biological Macromolecules*, *146*, 596–619. doi.org/10.1016/j.ijbiomac.2019.12.181

Terao, Y., Kawabata, S., Nakata, M., Nakagawa, I., & Hamada, S. **(2002)**. Molecular characterization of a novel fibronectin-binding protein of *Streptococcus pyogenes* strains isolated from toxic shock-like syndrome patients. *Journal of Biological Chemistry*, *277*(49), 47428–47435. doi.org/10.1074/jbc.M209133200

Terpe, K. **(2006)**. Overview of bacterial expression systems for heterologous protein production: from molecular and biochemical fundamentals to commercial systems. *Applied Microbiology and Biotechnology*, *72*(2), 211–222. doi.org/10.1007/s00253-006-0465-8

Tetali, S. D. **(2019)**. Terpenes and isoprenoids: a wealth of compounds for global use. *Planta*, *249*(1), 1–8. doi.org/10.1007/s00425-018-3056-x

Thak, E. J., Yoo, S. J., Moon, H. Y., & Kang, H. A. **(2020)**. Yeast synthetic biology for designed cell factories producing secretory recombinant proteins. *FEMS Yeast Research*, *20*(2). doi.org/10.1093/femsyr/foaa009

Tian, K., Tai, K., Chua, B. J. W., & Li, Z. **(2017)**. Directed evolution of *Thermomyces lanuginosus* lipase to enhance methanol tolerance for efficient production of biodiesel from waste grease. *Bioresource Technology*, *245*, 1491–1497. doi.org/10.1016/j.biortech.2017.05.108

Toda, T., Sano, M., Honda, M., Rimoldi, O., Yang, Y., Yamamoto, M., Takase, K., Hirozumi, K., Kitamoto, K., Minetoki, T., Gomi, K., & Machida, M. **(2001)**. Deletion analysis of the enolase gene (enoA) promoter from the filamentous fungus *Aspergillus oryzae*. *Current Genetics*, *40*(4), 260–267. doi.org/10.1007/s00294-001-0258-7

Troost, K., Loeschcke, A., Hilgers, F., Özgür, A. Y., Weber, T. M., Santiago-Schübel, B., Svensson, V., Hage-Hülsmann, J., Habash, S. S., Grundler, F. M. W., Schleker, A. S. S., Jaeger, K.-E., & Drepper, T. **(2019)**. Engineered *Rhodobacter capsulatus* as a phototrophic platform organism for the synthesis of plant sesquiterpenoids. *Frontiers in Microbiology*, *10*. doi.org/10.3389/fmicb.2019.01998

Ulbrich, P., Strnad, H., Hejkalova, V., Pačes, J. **(2002)**. Genetic determination of polyhydroxyalkanoate metabolism in *Rhodobacter capsulatus* SB 1003. *Folia Biologica, 48*(4), 157-159.

Verwaal, R., Jiang, Y., Wang, J., Daran, J.-M., Sandmann, G., van den Berg, J. A., & van Ooyen, A. J. J. **(2010)**. Heterologous carotenoid production in *Saccharomyces cerevisiae* induces the pleiotropic drug resistance stress response. *Yeast*, *27*(12), 983–998. doi.org/10.1002/yea.1807

Vespermann, K. A. C., Paulino, B. N., Barcelos, M. C. S., Pessôa, M. G., Pastore, G. M., & Molina, G. **(2017)**. Biotransformation of α- and β-pinene into flavor compounds. *Applied Microbiology and Biotechnology*, *101*(5), 1805–1817. doi.org/10.1007/s00253-016-8066-7

Volkenborn, K., Kuschmierz, L., Benz, N., Lenz, P., Knapp, A., & Jaeger, K.-E. **(2020)**. The length of ribosomal binding site spacer sequence controls the production yield for intracellular and secreted proteins by *Bacillus subtilis*. *Microbial Cell Factories*, *19*(1), 154. doi.org/10.1186/s12934-020-01404-2

Walsh, S., Gardner, L., Deiters, A., & Williams, G. J. **(2014)**. Intracellular light-activation of riboswitch activity. *ChemBioChem*, *15*(9), 1346–1351. doi.org/10.1002/cbic.201400024

Wang, C., Yoon, S.-H., Jang, H.-J., Chung, Y.-R., Kim, J.-Y., Choi, E.-S., & Kim, S.-W. **(2011)**. Metabolic engineering of *Escherichia coli* for α-farnesene production. *Metabolic Engineering*, *13*(6), 648–655. doi.org/10.1016/j.ymben.2011.08.001

Wang, K. **(2000)**. Isoprenyl diphosphate synthases. *Biochimica et Biophysica Acta (BBA) - Molecular and Cell Biology of Lipids*, *1529*(1–3), 33–48. doi.org/10.1016/S1388-1981(00)00136-0

Wang, Q., Fan, X., Jing, N., Zhao, H., Yu, L., & Tang, X. **(2021)**. Photoregulation of gene expression with ligand-modified caged siRNAs through host/guest interaction. *ChemBioChem*, *22*(11), 1901–1907. doi.org/10.1002/cbic.202000763

Wang, X., Pereira, J. H., Tsutakawa, S., Fang, X., Adams, P. D., Mukhopadhyay, A., & Lee, T. S. **(2021)**. Efficient production of oxidized terpenoids *via* engineering fusion proteins of terpene synthase and cytochrome P450. *Metabolic Engineering*, *64*, 41–51. doi.org/10.1016/j.ymben.2021.01.004

Ward, V. C. A., Chatzivasileiou, A. O., & Stephanopoulos, G. **(2018)**. Metabolic engineering of *Escherichia coli* for the production of isoprenoids. *FEMS Microbiology Letters*, *365*(10). doi.org/10.1093/femsle/fny079

Watanabe, M., Matsuzawa, T., & Yaoi, K. **(2018)**. Rational protein design for thermostabilization of glycoside hydrolases based on structural analysis. *Applied Microbiology and Biotechnology*, *102*(20), 8677–8684. doi.org/10.1007/s00253-018-9288-7

Weaver, P. F., Wall, J. D., & Gest, H. **(1975)**. Characterization of *Rhodopseudomonas capsulata*. *Archives of Microbiology*, *105*(1), 207–216. doi.org/10.1007/BF00447139

Wilson, C. J., Zhan, H., Swint-Kruse, L., & Matthews, K. S. **(2007)**. The lactose repressor system: Paradigms for regulation, allosteric behavior and protein folding. *Cellular and Molecular Life Sciences*, *64*(1), 3–16. doi.org/10.1007/s00018-006-6296-z

Wojtovich, A. P., & Foster, T. H. **(2014)**. Optogenetic control of ROS production. *Redox Biology*, *2*, 368–376. doi.org/10.1016/j.redox.2014.01.019

Wong, J. X., Gonzalez-Miro, M., Sutherland-Smith, A. J., & Rehm, B. H. A. **(2020)**. Covalent functionalization of bioengineered polyhydroxyalkanoate spheres directed by specific protein-protein interactions. *Frontiers in Bioengineering and Biotechnology*, *8*. doi.org/10.3389/fbioe.2020.00044

Wong, J. X., Ogura, K., Chen, S., & Rehm, B. H. A. **(2020)**. Bioengineered polyhydroxyalkanoates as immobilized enzyme scaffolds for industrial applications. *Frontiers in Bioengineering and Biotechnology*, *8*. doi.org/10.3389/fbioe.2020.00156

Wong, J. X., & Rehm, B. H. A. **(2018)**. Design of modular polyhydroxyalkanoate scaffolds for protein immobilization by directed ligation. *Biomacromolecules*, *19*(10), 4098–4112. doi.org/10.1021/acs.biomac.8b01093

Wong, P. T., Roberts, E. W., Tang, S., Mukherjee, J., Cannon, J., Nip, A. J., Corbin, K., Krummel, M. F., & Choi, S. K. **(2017)**. Control of an unusual photo-claisen rearrangement in coumarin caged tamoxifen through an extended spacer. *ACS Chemical Biology*, *12*(4), 1001–1010. doi.org/10.1021/acschembio.6b00999

Wood, K. B., & Cluzel, P. **(2012)**. Trade-offs between drug toxicity and benefit in the multi-antibiotic resistance system underlie optimal growth of *E. coli*. *BMC Systems Biology*, *6*(1), 48. doi.org/10.1186/1752-0509-6-48

Wu, H., Wang, Y., Wang, Y., Cao, X., Wu, Y., Meng, Z., Su, Q., Wang, Z., Yang, S., Xu, W., Liu, S., Cheng, P., Wu, J., Khan, Md. R. I., He, L., & Ma, G. **(2014)**. Quantitatively relating gene expression to light intensity *via* the serial connection of blue light sensor and CRISPRi. *ACS Synthetic Biology*, *3*(12), 979–982. doi.org/10.1021/sb500059x

Wu, P., Chen, Y., Liu, M., Xiao, G., & Yuan, J. **(2021)**. Engineering an optogenetic CRISPRi platform for improved chemical production. *ACS Synthetic Biology*, *10*(1), 125–131. doi.org/10.1021/acssynbio.0c00488

Wu, T., Ye, L., Zhao, D., Li, S., Li, Q., Zhang, B., & Bi, C. **(2018)**. Engineering membrane morphology and manipulating synthesis for increased lycopene accumulation in *Escherichia coli* cell factories. *3 Biotech*, *8*(6), 269. doi.org/10.1007/s13205-018-1298-8

Wu, X., Ma, G., Liu, C., Qiu, X., Min, L., Kuang, J., & Zhu, L. **(2021)**. Biosynthesis of pinene in purple non-sulfur photosynthetic bacteria. *Microbial Cell Factories*, *20*(1), 101. doi.org/10.1186/s12934-021-01591-6

Xie, X., Ban, X., Gu, Z., Li, C., Hong, Y., Cheng, L., & Li, Z. **(2020)**. Structure-based engineering of a maltooligosaccharide-forming amylase to enhance product specificity. *Journal of Agricultural and Food Chemistry*, *68*(3), 838–844. doi.org/10.1021/acs.jafc.9b07234

Xu, L., Han, F., Dong, Z., & Wei, Z. **(2020)**. Engineering improves enzymatic synthesis of L-tryptophan by tryptophan synthase from *Escherichia coli*. *Microorganisms*, *8*(4), 519. doi.org/10.3390/microorganisms8040519

Yang, H., Qu, J., Zou, W., Shen, W., & Chen, X. **(2021)**. An overview and future prospects of recombinant protein production in *Bacillus subtilis*. *Applied Microbiology and Biotechnology*, *105*(18), 6607–6626. doi.org/10.1007/s00253-021-11533-2

Yang, J., & Guo, L. **(2014)**. Biosynthesis of β-carotene in engineered *E. coli* using the MEP and MVA pathways. *Microbial Cell Factories*, *13*(1), 160. doi.org/10.1186/s12934-014-0160-x

Yang, J., & Nie, Q. **(2016)**. Engineering *Escherichia coli* to convert acetic acid to β-caryophyllene. *Microbial Cell Factories*, *15*(1), 74. doi.org/10.1186/s12934-016-0475-x

Yang, T. H., Kwon, M.-A., Lee, J. Y., Choi, J.-E., Oh, J. Y., & Song, J. K. **(2015)**. *In situ* immobilized lipase on the surface of intracellular polyhydroxybutyrate granules: Preparation, characterization, and its

promising use for the synthesis of fatty acid alkyl esters. *Applied Biochemistry and Biotechnology*, *177*(7), 1553–1564. doi.org/10.1007/s12010-015-1836-3

Yao, Y.-C., Zhan, X.-Y., Zhang, J., Zou, X.-H., Wang, Z.-H., Xiong, Y.-C., Chen, J., & Chen, G.-Q. **(2008)**. A specific drug targeting system based on polyhydroxyalkanoate granule binding protein PhaP fused with targeted cell ligands. *Biomaterials*, *29*(36), 4823–4830. doi.org/10.1016/j.biomaterials.2008.09.008

Young, D. D., & Deiters, A. **(2007)**. Photochemical activation of protein expression in bacterial cells. *Angewandte Chemie International Edition*, *46*(23), 4290–4292. doi.org/10.1002/anie.200700057

Zabin, I., Kepes, A., & Monod, J. **(1962)**. Thiogalactoside transacetylase. *The Journal of Biological Chemistry*, *237*, 253–257. doi.org/10.1016/s0021-9258(18)81395-3

Zakeri, B., Fierer, J. O., Celik, E., Chittock, E. C., Schwarz-Linek, U., Moy, V. T., & Howarth, M. **(2012)**. Peptide tag forming a rapid covalent bond to a protein, through engineering a bacterial adhesin. *Proceedings of the National Academy of Sciences*, *109*(12). doi.org/10.1073/pnas.1115485109

Zeng, L., & Dehesh, K. **(2021)**. The eukaryotic MEP-pathway genes are evolutionarily conserved and originated from *Chlaymidia* and cyanobacteria. *BMC Genomics*, *22*(1), 137. doi.org/10.1186/s12864-021-07448-x

Zhang, Y., Song, X., Lai, Y., Mo, Q., & Yuan, J. **(2021)**. High-yielding terpene-based biofuel production in *Rhodobacter capsulatus*. *ACS Synthetic Biology*, *10*(6), 1545–1552. doi.org/10.1021/acssynbio.1c00146

Zhang, Y., & Yuan, J. **(2021)**. CRISPR/Cas12a-mediated genome engineering in the photosynthetic bacterium *Rhodobacter capsulatus*. *Microbial Biotechnology*, *14*(6), 2700–2710. doi.org/10.1111/1751-7915.13805

Zhao, C., Kim, Y., Zeng, Y., Li, M., Wang, X., Hu, C., Gorman, C., Dai, S. Y., Ding, S.-Y., & Yuan, J. S. **(2018)**. Co-compartmentation of terpene biosynthesis and storage *via* synthetic droplet. *ACS Synthetic Biology*, *7*(3), 774–781. doi.org/10.1021/acssynbio.7b00368

Zhao, E. M., Lalwani, M. A., Chen, J.-M., Orillac, P., Toettcher, J. E., & Avalos, J. L. **(2021)**. Optogenetic amplification circuits for light-induced metabolic control. *ACS Synthetic Biology*, *10*(5), 1143–1154. doi.org/10.1021/acssynbio.0c00642

Zhao, E. M., Zhang, Y., Mehl, J., Park, H., Lalwani, M. A., Toettcher, J. E., & Avalos, J. L. **(2018)**. Optogenetic regulation of engineered cellular metabolism for microbial chemical production. *Nature*, *555*(7698), 683–687. doi.org/10.1038/nature26141

Zhao, M., Rong, J., Han, J., Zhou, Y., Li, C., Wang, L., Mao, Y., & Wang, Y. **(2019)**. Novel synthesis strategy for biocatalyst: Fast purification and immobilization of His- and ELP-tagged enzyme from fermentation broth. *ACS Applied Materials & Interfaces*, *11*(35), 31878–31888. doi.org/10.1021/acsami.9b09071

Zheng, L. **(2004)**. An efficient one-step site-directed and site-saturation mutagenesis protocol. *Nucleic Acids Research*, *32*(14), e115–e115. doi.org/10.1093/nar/gnh110

Zhou, C., Zhou, H., Li, D., Zhang, H., Wang, H., & Lu, F. **(2020)**. Optimized expression and enhanced production of alkaline protease by genetically modified *Bacillus licheniformis* 2709. *Microbial Cell Factories, 19*(1), 45. doi.org/10.1186/s12934-020-01307-2

V. ACKNOWLEDGMENTS

Ich möchte mich bei Herrn Prof. Dr. Karl-Erich Jaeger für die Überlassung des interessanten wissenschaftlichen Themas, sowie die Möglichkeit bedanken, meine Doktorarbeit am Institut für Molekulare Enzymtechnologie anfertigen zu dürfen.

Zudem möchte ich mich bei Frau Prof. Dr. Ilka Maria Axmann für die Übernahme des Korreferats bedanken, sowie für ihre Rolle als meine Mentorin während der Promotion.

Im Besonderen gilt mein Dank Herrn Dr. Thomas Drepper. Vielen Dank Tom, für die überaus engagierte Betreuung während meiner gesamten Zeit am IMET und dem großen Interesse an meinem Schaffen. Danke, dass du jederzeit ein offenes Ohr für jede Art von Problem hattest und für die familiäre Atmosphäre, die jeden Tag besonders gemacht hat.

Vielen Dank an Frau Dr. Anita Loeschcke, Herrn Dr. Achim Heck und Herrn Dr. Stephan Thies für die immer angenehme Arbeitsatmosphäre und die kleinen und großen Hilfestellungen im Laboralltag.

Ein großes Dankeschön geht an Vera für die unzähligen gemeinsamen Stunden im Büro und Labor und dafür, dass du immer da warst!

Vielen Dank an all meine Kollegen aus denen Freunde geworden sind, im Besonderen an Fabi, Robin, Nora, Andreas, Luzie, Patrick, Andrea und Alex. Danke für eure Hilfe bei jeder Art von fachlichen und vor allem persönlichen Themen. Diese Arbeit ist geschrieben, doch unsere gemeinsame Zeit wird noch viele weitere Kapitel haben.

Ich möchte mich von tiefstem Herzen bei meinen Eltern und meinem Bruder bedanken. Ich danke euch, dass ihr mich immer unterstützt, zur rechten Zeit gefordert und immer an mich geglaubt habt. Danke, dass ihr mir mein Studium ermöglicht habt und ich dadurch der Wissenschaftler und vor allem der Mensch werden konnte, der ich heute bin.

Zum Schluss möchte ich mich bei meiner Freundin bedanken. Vielen Dank Franzi, dass du in den letzten Jahren immer für mich da warst und mich bei all meinen Plänen unterstützt hast. Ich danke dir für die wertvollen Ratschläge, während der Schreibphase und das große Verständnis und die Geduld, die du mir entgegengebracht hast.

Eidesstattliche Versicherung

Ich, Herr Oliver Klaus, versichere an Eides statt, dass die vorliegende Dissertation mit dem Titel „Novel tools for the implementation of synthetic biosynthesis pathways in *Rhodobacter capsulatus*“ von mir selbstständig und ohne unzulässige fremde Hilfe angefertigt wurde. Hierbei wurden die „Grundsätze zur Sicherung guter wissenschaftlicher Praxis“ der Heinrich-Heine-Universität Düsseldorf befolgt.

Diese Arbeit wurde in der vorliegenden oder einer ähnlichen Form noch bei keiner anderen Institution eingereicht. Zudem habe ich bisher keine erfolglosen Promotionsversuche unternommen.

Krefeld, den

_____

Oliver Klaus